Brasília 2022

Latin American

Joint 5th Cubesat Workshop &
3rd Symposium on Small Satellites

http://iaa-la.org | November 7-10, 2022

5th IAA Latin American CubeSat Workshop

3rd IAA Latin American Symposium on Small Satellites

Companion Book v1.2

Organizing Committee

General chairs

Chantal Cappelletti, IAA, University of Nottingham, UK
Eduardo Augusto Bezerra, Universidade Federal de Santa Catarina, Brazil
Rainer Sandau, IAA, Germany
Livio Gratton, IAA, Universidad Nacional de San Martín, Argentina

Program chair

Laio Oriel Seman, Dr., UFSC/UNIVALI

Tutorial chair

Walter Abrahão Dos Santos, Dr., INPE

Local arrangements

Cristiano Augusto Trein, The Brazilian Space Agency (AEB), Brazil
Rodrigo Leonardi, The Brazilian Space Agency (AEB), Brazil

Welcome to the Joint 5th IAA Latin American CubeSat Workshop and 3rd IAA Latin American Symposium on Small Satellites

The IAA Latin American CubeSat Workshop and the IAA Latin American Symposium on Small Satellites bring a unique opportunity to discuss and talk about CubeSats and SmallSats technologies, which have a remarkable momentum in the space industry worldwide. Lets share experiences and knowledge on space matters among professionals, researchers, students, and companies from the Region and around the world!

Summary

Joint 5th IAA Latin American CubeSat Workshop and 3rd IAA Latin American Symposium on Small Satellites

Preliminary Program - Brasilia Time Zone (GMT -3)

7 November 2022 - Monday	
	Registration
08:45-09:00	**Opening ceremony**
09:00-09:45	Keynote: C. Cappelletti
09:45-10:15	**Coffee break**
10:15-11:15	**Panel: The Role of Small Satellites in Space**
11:15-11:30	IAA-BR-22-01-01
11:30-11:45	IAA-BR-22-01-02
11:45-12:00	IAA-BR-22-01-03
12:00-13:30	**LUNCH**
13:30-14:15	Keynote: C. Trein
14:15-14:30	IAA-BR-22-02-01
14:30-14:45	IAA-BR-22-02-02
14:45-15:00	IAA-BR-22-02-03
15:00-15:30	**Coffee break**
15:30-15:45	IAA-BR-22-03-01
15:45-16:00	IAA-BR-22-03-02
16:00-16:15	IAA-BR-22-03-03
16:15-16:30	IAA-BR-22-03-04
16:30-16:45	IAA-BR-22-03-05
16:45-17:00	IAA-BR-22-03-06
17:00-18:00	**Panel: The Next Generation in Space**
	Welcome cocktail

8 November 2022 - Tuesday	
	Registration
09:00-09:45	Keynote: A. Molinas
09:45-10:15	**Coffee break**
10:15-10:30	IAA-BR-22-04-01
10:30-10:45	IAA-BR-22-04-02
10:45-11:00	IAA-BR-22-04-03
11:00-11:15	IAA-BR-22-04-04
11:15-11:30	IAA-BR-22-05-01
11:30-11:45	IAA-BR-22-05-02
11:45-12:00	IAA-BR-22-05-03
12:00-13:30	**LUNCH**
13:30-14:15	Keynote: C. Duarte
14:15-14:30	IAA-BR-22-06-01
14:30-14:45	IAA-BR-22-06-02
14:45-15:00	Invited Talk: P. Bareš
15:00-15:30	**Coffee break**
15:30-15:45	IAA-BR-22-07-01
15:45-16:00	IAA-BR-22-07-02
16:00-16:15	IAA-BR-22-07-03
16:15-16:30	IAA-BR-22-07-04
16:30-16:45	IAA-BR-22-07-05
16:45-18:00	**Tutorial 1: A Simple Onboard Computer for Cubesats with Micropython**

9 November 2022 - Wednesday	
	Registration
09:00-09:45	Keynote: J. Spann
09:45-10:15	**Coffee break**
10:15-11:15	**Panel: Space Law**
11:15-11:30	IAA-BR-22-08-01
11:30-11:45	IAA-BR-22-08-02
11:45-12:00	IAA-BR-22-08-03
12:00-13:30	**LUNCH**
13:30-14:15	Keynote: A. Silva
14:15-14:30	IAA-BR-22-09-01
14:30-14:45	IAA-BR-22-09-02
14:45-15:00	Invited Talk: J. Wu
15:00-15:30	**Coffee break**
15:30-15:45	IAA-BR-22-10-01
15:45-16:00	IAA-BR-22-10-02
16:00-16:15	IAA-BR-22-10-03
16:15-16:30	IAA-BR-22-10-04
16:30-16:45	IAA-BR-22-11-01
16:45-18:00	**Tutorial 2: Python and Cubesats**
	Gala Dinner

10 November 2022 - Thursday	
	Registration
09:00-09:45	Keynote: L. Gratton
09:45-10:15	**Coffee break**
10:15-10:30	IAA-BR-22-12-01
10:30-10:45	IAA-BR-22-12-02
10:45-11:00	IAA-BR-22-12-03
11:00-11:15	IAA-BR-22-12-04
11:15-11:30	IAA-BR-22-13-01
11:30-11:45	IAA-BR-22-13-02
11:45-12:00	IAA-BR-22-13-03
12:00-13:30	**LUNCH**
13:30-14:15	Keynote: L. Loures
14:15-14:30	IAA-BR-22-14-01
14:30-14:45	IAA-BR-22-14-02
14:45-15:00	Invited Talk: G. Santilli
15:00-15:30	**Coffee break**
15:30-15:45	IAA-BR-22-15-01
15:45-16:00	IAA-BR-22-15-02
16:00-16:15	IAA-BR-22-15-03
16:15-16:30	IAA-BR-22-15-04
16:30-16:45	Poster Session
16:45-18:00	**Panel: Space Education**
	Closing ceremony

Day 1 - Monday, 7 November 2022
Morning

Opening ceremony

"The International Academy of Astronautics and its Activities"

Keynote Speaker: CHANTAL CAPPELLETTI IAA, University of Nottingham, UK	Keynote Speaker: JEAN-MICHEL CONTANT IAA Secretary General, France

PANEL

“The Role of Small Satellites in Space”

Rodrigo Leonardi, AEB, Brazil (Chair)
Alejandro Román Molinas, Paraguayan Space Agency, Paraguay
Carlos Roberto Duarte Muñoz, Mexican Space Agency, Mexico
Chantal Cappelletti, IAA, University of Nottingham, UK
James Spann, NASA Headquarters, USA
Livio Gratton, National University of San Martín, Argentina

Session 1 - CUBESATS AND SMALL SATELLITES ENHANCING SPACE PROGRAMS - Chair: Carlos Moura, AEB, Brazil

IAA-BR-22-01-01 [11:15-11:30]	**Small Satellites for Sustainable Science and Development in Africa: Policy Perspectives**	Anietie Ekanem and Peter Ekweozoh
IAA-BR-22-01-02 [11:30-11:45]	**Mission Design of Catarina Constellation's Fleet A: a systems engineering case study**	Damylle Cristina Xavier Donati, Rodrigo da Silva Cardozo, Ludmila Kopko, Pieter Von Tilburg Bernardes, Nicole Korres Borges, Talita Sauter Possamai, Augusto Marasca de Conto and Christopher Shneider Cerqueira
IAA-BR-22-01-03 [11:45-12:00]	**Recent Developments at INPE’s Small Satellites Division**	Walter Abrahão dos Santos, Antonio Carlos de Oliveira Pereira Junior, Lincoln Teixera, Bruno Carneiro Junqueira, Marcus Vinicius Cisotto, Antonio Cassiano Julio Filho, Auro Tikami, Luiz Antonio dos Reis Bueno, Lázaro Aparecido Pires Camargo, ngelo José Augusto Florentino, Antonio Ferreira de Brito, and Andrés Fernando Paredes Horna

Day 1 - Monday, 7 November 2022 - Afternoon

"Enabling a New Space Ecosystem in Brazil: The Role of Nano and Small Sats" - Keynote Speaker: CRISTIANO TREIN, AEB, Brazil		
Session 2 - MISSION APPLICATIONS I - Chair: Petr Bareš, Honorary President of the Czech Space Alliance, Czech Republic		
IAA-BR-22-02-01 [14:15-14:30]	Avion satellite and the physical experiments onboard	Vitaly Bogomolov, Yurii Zailko, Anatoly Iyudin, Vladimir Kalegaev, Ivan Kucherenko, Vladislav Osedlo, Oleg Peretyat'Ko, Mikhail Prokhorov and Sergey Svertilov
IAA-BR-22-02-02 [14:30-14:45]	A Payload Proposal for Lightning Flash Detection using a Nanosatellites	Lazaro Camargo, Walter Abrahao Dos Santos, Kleber Naccarato, Jhonathan Murcia Piñeros, Auro Tikami, Antonio Carlos de Oliveira Pereira Junior, Antonio Cassiano Julio Filho, Marcus Vinicius Cisotto, Luiz Antonio dos Reis Bueno, Ângelo José Augusto Florentino, Lincoln Teixeira, Bruno Carneiro Junqueira, Andres Paredes Horna and Antonio Brito
IAA-BR-22-02-03 [14:45-15:00]	Near Earth Asteroid Cubesat Mission: Selection of the Body and Discussion on the Mission Requirements	Damiana Irrera and Juan David Blanco Camargo
Session 3 - ATTITUDE DETERMINATION AND CONTROL SYSTEMS - Chair: James Spann, NASA, USA.		
IAA-BR-22-03-01 [15:30-15:45]	Magnetic parameters estimation and attitude motion reconstruction using in-flight magnetometer measurements of the AlfaCrux CubeSat	Emanuel C. Brenag, Bruno T. de Mello, Matheus L. Arruda, Renato A. Borges, Danil Ivanov, Uliana Monakhova, Yaroslav Mashtakov and Mikhail Ovchinnikov
IAA-BR-22-03-02 [15:45-16:00]	Model Predictive Control for Attitude Maneuvers of a Nanosatellite	Tomás Cardoso Miranda, Maria Cecilia Pereira Faria, Marcelo Alves Santos and Guilherme Vianna Raffo
IAA-BR-22-03-03 [16:00-16:15]	Design and simulation of a model to determine the attitude and control the orientation of a CubeSat	Johrdan Huamanchumo, Soledad Fernandez, Cristopher Rufasto, George Fajardo and Omar Blas, John Haile Abad Antialon
IAA-BR-22-03-04 [16:15-16:30]	Attitude reconstruction of the AlfaCrux CubeSat using onboard sensors and solar panels in-orbit data	Bruno T. de Mello, Renato A. Borges and Simone Battistini
IAA-BR-22-03-05 [16:30-16:45]	Ptolemy II Framework as a Tool for Analyzing Attitude Control Algorithms for Nanosatellites	Alex Alves, Luiz Silveira, Samaherni Dias and Márcio Kreutz
IAA-BR-22-03-06 [16:45-17:00]	Design of ADCS system for Earth Observation using a 3-unit CubeSat	Adolfo Chaves-Jimenez, Giancarlo Vargas-Villegas, Alberto Zamora-Mendieta, Carlos A. Fernandez-Cerdas, Jonathan Kolbeck, Mauricio Munoz-Arias
PANEL: "The Next Generation in Space", Chair: Isidora Casas del Valle, SGAC South American Regional Coordinator, Chile		

Day 2 - Tuesday, 8 November 2022
Morning

"Aerospace Development from an Emerging Country Perspective: The case of Paraguay (First CubeSat mission-GuaraniSat-1)"

Keynote Speaker: ALEJANDRO ROMÁN MOLINAS, Paraguayan Space Agency, Paraguay

Session 4 - GROUND SEGMENT - Chair: Moises Souto, IFRN, Brazil

IAA-BR-22-04-01 [10:15-10:30]	Ground and Flight Segment for tracking and transmissions for Stratospheric Balloons	João Braga, Antonio Cassiano Julio Filho, Sergio de Oliveiva and Marconi Pereira
IAA-BR-22-04-02 [10:30-10:45]	EMMN - Reports about a Multi-Mission Ground Station on Cubesats Tracking	Hilario Castro, Jefferson Silva, Manoel Carvalho, Lucio Jotha and Moises Souto
IAA-BR-22-04-03 [10:45-11:00]	A Proposal for a Space Weather Ground-Based Segment Using Software-Defined Radio and Cognitive Radio	Jaime Enrique Orduy Rodriguez, Walter Abrahao dos Santos, Claudia Maria Nicoli Candido, and Douglas Soares dos Santos, and Daniel Santiago Umaña Salinas
IAA-BR-22-04-04 [11:00-11:15]	New Challenges for Ground Segment Development: Scientific Small Satellite Missions	Antonio Cassiano Julio Filho, Antonio Carlos de Oliveira Pereira Junior, Walter Abrahao dos Santos, Marcus Vinicius Cisotto, Auro Tikami, Luiz Antonio dos Reis Bueno, Ângelo José Augusto Florentino, Antonio Ferreira de Brito, Lincoln Teixeira, Lazaro Aparecido Pires Camargo, Bruno Carneiro Junqueira and Andres Paredes Horna

Session 5 - EMBEDDED SYSTEMS RELIABILITY - Chair: Jarbas da Silveira, UFC, Brazil

IAA-BR-22-05-01 [11:15-11:30]	A Performance Evaluation of a Fault-tolerant RISC-V with Vector Instruction Support to Space Applications	Carolina Imianosky, Douglas A. dos Santos, Douglas Rossi de Melo, Luigi Dilillo, Cesar A. Zeferino, Eduardo A. Bezerra and Felipe Viel
IAA-BR-22-05-02 [11:30-11:45]	Improving Space Robustness and Reliability on Nanosatellite On-Board Equipment	Lincoln Teixeira, Bruno Junqueira, Valentino Lau, Denio Panissi, Rafael Costa, Gledson Diniz, Jose May, Jonilson Adachi, Ana Rabello, Durval Zandonadi, Antonio Pereira, Walter Abrahao, Marcus Cisotto, Antonio Filho, Auro Tikami, Luiz Bueno, Lazaro Camargo, Angelo Florentino, Antonio Brito and Andres Horna
IAA-BR-22-05-03 [11:45-12:00]	An SRAM Memory's error detector and corrector system based on FPGA for CubeSats onboard computer	Luis Claudio de Oliveira Silva, Jose de Ribamar Braga Pinheiro Junior, Carlos Alberto Rios Brito Junior, Allan Kardec Barros, Edeilson Pereira Pestana, Magalhaes Geovaana Maria de Moura Couto and Lucas Souza Azulay

Day 2 - Tuesday, 8 November 2022
Afternoon

"Best Practices for the Development of Cubesat Missions" Keynote Speaker: CARLOS DUARTE MUÑOZ, Mexican Space Agency, Mexico		
Session 6 - EDUCATIONAL SYSTEMS AND MISSIONS - Chair: Carlos Alberto Rios Brito Junior, UFMA, Brazil		
IAA-BR-22-06-01 [14:15-14:30]	Blockchain Applied in the Update the Firmware of Nanosatellites Constellations	Jose Edilson Silva Filho, José Danilo da Silva Coutinho Filho, Igor Braga Palhano and Jarbas Aryel Nunes da Silveira
IAA-BR-22-06-02 [14:30-14:45]	Enhancing STEAM Education Through Multimission Platform Development Using Stratospheric Balloon	Auro Tikami, Antonio Carlos de Oliveira Pereira Junior, Walter Abrahao dos Santos, Marcus Vinicius Cisotto, Antonio Cassiano Julio Filho, Luiz Antonio dos Reis Bueno, Ângelo José Augusto Florentino, Antonio Ferreira de Brito, Lincoln Teixeira, Lázaro Aparecido Pires Camargo, Bruno Carneiro Junqueira, Andres Paredes Horna, Jair Gustavo de Mello Torres and Marco Mammoli
Invited Talk: "Space Industry and Small Sats in Czech Republic" Petr Bareš, Honorary President of the Czech Space Alliance, Czech Republic.		
Session 7 - MISSION APPLICATIONS II - Chair: Adolfo Chaves Jiménez, TEC, Costa Rica		
IAA-BR-22-07-01 [15:30-15:45]	Lightning Events Simulation Budgeting for the RaioSat Payload On-Board Computer	Lazaro Camargo, Jhonathan Murcia Piñeros, Walter Abrahao dos Santos, Antonio Fernando Bertachini de Almeida Prado, Rodolpho Vilhena de Moraes and Kleber Naccarato
IAA-BR-22-07-02 [15:45-16:00]	A High-Level Synthesis Compressor of Hyperspectral Images based on CCSDS 123.0-B-2	Wesley Grignani, Gabriela Wisbecki, Felipe Viel and Douglas Melo
IAA-BR-22-07-03 [16:00-16:15]	CONASAT-1 Cubesat: Integration of Environmental Data Collector	Alessandra Rodrigues, Alysson Lima, Manoel Carvalho, Samaherni Dias, José Duarte and Jefferson Silva
IAA-BR-22-07-04 [16:15-16:30]	A Model-Based Mission Definition Review: the NANOSATC-BR3 CubeSat Study Case	Giulia Herdies, Nelson Schuch and Eduardo Bürger
IAA-BR-22-07-05 [16:30-16:45]	The CubeSat mission Aldebaran I	Carlos Alberto Rios Brito Junior, Edemar Morsch Filho, José Ribamar Braga Pinheiro Junior, Luis Claudio de Oliveira Silva and Geovaana Maria de Moura Couto
Tutorial 1: "A Simple Onboard Computer for Cubesats with Micropython", Lazaro Camargo and Walter Abrahao, INPE, Brazil		

Day 3 - Wednesday, 9 November 2022
Morning

"The Role and Value of Small Satellites for Research and Applications"

Keynote Speaker: JAMES SPANN, NASA Headquarters, USA

PANEL

“Space Law”

Carlos Roberto Duarte Muñoz, Mexican Space Agency, Mexico (Chair)
Chantal Cappelletti, IAA, University of Nottingham, UK
Ian Grosner, AEB, Brazil
Olavo de O. Bittencourt Neto, Universidade Católica de Santos, Brazil

Session 8 - TELECOMMUNICATIONS, TRACKING AND COMMAND - Chair: Walter Abrahao, INPE, Brazil

IAA-BR-22-08-01 [11:15-11:30]	Using Cosmos in nanosatellite testing and at the mission control center	Priscila Yamada, William Silva, Renato Borges and Wilson Yamaguti
IAA-BR-22-08-02 [11:30-11:45]	An Experimental Evaluation of Long-Range Technology in a Stratospheric Sonde for Educational CubeSat Mission Aldebaran-1	Luis Claudio de Oliveira Silva, Jose de Ribamar Braga Pinheiro Junior, Carlos Alberto Rios Brito Junior, Edemar Morsch Filho, Geovaana Maria de Moura Couto Magalhaes, Ellias Portugal Fernandes, Antonio Claudio se Sousa Dos Santos Filho, Alex Iury Vieira Almeida, Emanuel Rodrigues Valentim da Silva, Fernanda Sousa de Assuncao Vale, Isabel Silva se Araujo, Jennifer Caroline da Silva Barraza, Julio Cesar Rodrigues Machado, Leonardo Victor dos Santos Sa Menez and Rodrigo Alberto Matos de Carvalho
IAA-BR-22-08-03 [11:45-12:00]	Design and Analysis of a COTS TT&C Subsystem for a CubeSat Imaging Payload mission	Diego W. B. Arruda, Ana Carolina L. Oliveira, Carlos M. Zago and Gabriel A. Coelho

Day 3 - Wednesday, 9 November 2022 - Afternoon

"Amazonia 1 Mission – From Design to In orbit Operation – Technological and System Engineering Gains" **Keynote Speaker: ADENILSON SILVA, INPE, Brazil**		
IAA-BR-22-09-01 [14:15-14:30]	Open-Sourcing of CubeSat Bus for Capacity Building aimed to Acquire Original Space Development Capability	Tetsuhito Fuse, Mengu Cho and George Maeda
IAA-BR-22-09-02 [14:30-14:45]	Development of a Flatsat Platform for GOLDS-UFSC and Future Missions	João Cláudio Elsen Barcellos, Anderson Wedderhoff Spengler, Laio Oriel Seman and Eduardo Augusto Bezerra
Invited Talk: "Progress of Radiation Belt Exploration by a Constellation of Small Satellites TGCSS/SGRB, COSPAR" Ji Wu, National Space Science Center (NSSC) and Chinese Academy of Sciences.		
Session 10 - MISSION APPLICATIONS III - Chair: Maria Cecilia Pereira, UFMG, Brazil		
IAA-BR-22-10-01 [15:30-15:45]	UNLP's First CubeSat, USAT-I: GNSS-RO and GNSS-R Technology Demonstrator	Sonia A. Botta, Frida A. Alfaro Rodríguez, Santiago Rodríguez, Elián Hanisch, Marcos D. Actis, David O. Williams Rogers, Simón Lombardozzo, Daniel Hamann, Guillermo Garaventta, Facundo Pasquevich, Gabriel Vega Leañez, Ernesto M. López, Aldana Guilera, Adriana Barba, Santiago Ozafrain, Ezequiel Marranghelli, Mateo Salvo and Agustín Catellani
IAA-BR-22-10-02 [15:45-16:00]	BiomeSat: a Multi-Mission 6U Nanosat for Estimating Forests Health in Brazil	Walter Abrahão dos Santos, Antonio Carlos de Oliveira Pereira Junior, Lincoln Teixera, Bruno Carneiro Junqueira, Marcus Vinicius Cisotto, Antonio Cassiano Julio Filho, Auro Tikami, Luiz Antonio dos Reis Bueno, Lázaro Aparecido Pires Camargo, Ângelo José Augusto Florentino, Antonio Ferreira de Brito, Andrés Fernando Paredes Horna and Manoel Cardoso
IAA-BR-22-10-03 [16:00-16:15]	The LECX experiment onboard the nanoMIRAX satellite	Joao Braga, Otavio Durao, and Lazaro Carmago
IAA-BR-22-10-04 [16:15-16:30]	Payload-XL: A Case Study of Methodologies for Development and Documentation of Cubesat Subsystems Using ECSS Standards	Márcio Hermany Gomes de Oliveira, Edilberto Costa Neto, Kleber Reis Gouveia Junior, Felipe Viel, Miguel Boing, Gabriel Mariano Marcelino, André Martins Pio de Mattos, Laio Oriel Seman, David Merodio Codinachs and Eduardo Augusto Bezerra
Session 11 - SPACE DEBRIS - Chair: Livio Gratton, UNSM, Argentina		
IAA-BR-22-11-01 [16:30-16:45]	Space Debris: Impacts generated by the disposal of CubeSats	Fernanda Vieira and Carlos Eduardo Rosa
Tutorial 2: "Python and Cubesats", Lazaro Camargo and Walter Abrahao, INPE, Brazil		

Day 4 - Thursday, 10 November 2022
Morning

"The IAA's Handbook for Post-Mission Disposal of Satellites Less than 100 kg" **Keynote Speaker: LIVIO GRATTON, UNSM, Argentina**		
Session 12 - CONSTELLATIONS AND FORMATION FLIGHTS - Chair: Luis Eduardo Loures da Costa, ITA, Brazil		
IAA-BR-22-12-01 [10:15-10:30]	Moscow University Constellation of Nano-Satellites for Space Weather and TLE Monitoring	Svertilov Sergey, Bogomolov Vitaly, Zaiko Yurii, Zolotarev Ivan, Iyudin Anatoly, Kalegaev Vladimir, Klimov Pavel, Osedlo Vladislav, Peretyat'Ko Oleg and Petrov Vasily
IAA-BR-22-12-02 [10:30-10:45]	Orbit design analysis for a nanosatellite constellation - Constellation Catarina's case study	Nicole Korres Borges, Rodrigo da Silva Cardozo, Damylle Cristina Xavier Donati and Talita Sauter Possamai
IAA-BR-22-12-03 [10:45-11:00]	Educational and Scientific Project Monitor based on Cubesat Constellation	Vladislav Osedlo, George Antonyuk, Victor Bengin, Vitaliy Bogomolov, Ivan Zolotarev, Vladimir Kalegaev, Oleg Nechaev, Vladimir Radchenko and Sergey Svertilov
IAA-BR-22-12-04 [11:00-11:15]	Introducing SARA Constellation: Satellite for Agriculture and Remote Areas	Felipe de S. N. Coelho and Luis M. C. Acosta
Session 13 - TECHNOLOGY DEVELOPMENT FOR SPACE SYSTEMS - Chair: Paolo Gessini, UnB, Brazil		
IAA-BR-22-13-01 [11:15-11:30]	Design and implementation of DC-DC converters for CubeSat in Simulink	Germain Rosadio Vega, Kiara Micaela Rodriguez Bautista, Sheyla Claribel Lozano Burga, John Haile Abad Antialon and Omar Enrique Blas Morales
IAA-BR-22-13-02 [11:30-11:45]	Methodology for developing TT&C subsystems in academic CubeSats	Daniel Curcio Lott Guimarães, Ricardo Luiz Silva Adriano and Maria Cecilia Pereira
IAA-BR-22-13-03 [11:45-12:00]	NumPPTG: a Pulsed Plasma Thrusters Simulation Tool	Fernando Mendes and Paolo Gessini

Day 4 - Thursday, 10 November 2022
Afternoon

"Small Sat Projects of ITA Space Center" **Keynote Speaker: LUIS EDUARDO LOURES DA COSTA, ITA, Brazil**		
IAA-BR-22-14-01 [14:15-14:30]	Thermal simulation of the CubeSat Catarina-A1	Caique Sales de Miranda Gomes, Edemar Morsch Filho, Laio Oriel Seman, Eduardo Augusto Bezerra and Talita Sauter Possamai
IAA-BR-22-14-02 [14:30-14:45]	Thermal simulation of a high altitude balloon	João Gabriel Barros Marques, João Lucas Caldas dos Santos, Lucas Souza Azulay, Carlos Alberto Rios Brito Junior, Edemar Morsch Filho, José Ribamar Braga Pinheiro Junior and Luis Claudio de Oliveira Silva
Invited Talk: "ASI's Experience in Nano-Satellites", Giancarlo Santilli, UnB, Brazil		
Session 15 - ON-BOARD COMPUTER AND EPS - Chair: Alejandro Molinas, Paraguayan Space Agency, Paraguay		
IAA-BR-22-15-01 [15:30-15:45]	Simulation of CubeSat on-board computer system operating modes using MATLAB	Jesus Antonio Tapia Gallardo, Omar Enrique Blas Morales and Jhasmin Huillca Alvaro
IAA-BR-22-15-02 [15:45-16:00]	Onboard Computer for a LEO CubeSat Nanosatellite	Camila Barbosa, Samaherni Dias, Kurios Queiroz and Alex Alves
IAA-BR-22-15-03 [16:00-16:15]	Hardware-in-the-loop simulation of an on-board energy-driven scheduling algorithm for CubeSats	Vinicius Bernardo, Laio Seman, Ramon Borba and Eduardo Augusto Bezerra
IAA-BR-22-15-04 [16:15-16:30]	PdQSat Electric Power Subsystem Control using a Discrete Event Systems Model	Elder J. T. Santos, Maria Cecilia Pereira and Patrícia N. Pena
Poster Session - Chair: Moises Souto (IFRN, Brazil)		
PANEL: Space Education		
Closing ceremony		

1

Session 1 - Cubesats and Small satellites Enhancing Space Programs

MISSION DESIGN OF CATARINA CONSTELLATION'S FLEET A: A SYSTEMS ENGINEERING CASE STUDY

Damylle C. X. Donati[(1)], **Ludmila Kopko**[(2)], **Nicole K. Borges**[(3)], **Pieter von T. Bernardes**[(4)], **Rodrigo da S. Cardozo**[(5)], **Talita S. Possamai**[(6)], **Christopher S. Cerqueira**[(7)], **Augusto M. de Conto**[(8)]

[(1)] *Centro Tecnológico de Joinville, Universidade Federal de Santa Catarina; damylle.xavier@t2f.ufsc.br*
[(2)] *Centro Tecnológico de Joinville, Universidade Federal de Santa Catarina; ludmila.kopko@gmail.com*
[(3)] *Universidade do Vale do Paraíba, nicole.k.borges*
[(4)] *Centro Tecnológico de Joinville, Universidade Federal de Santa Catarina; pietervtbernardes@gmail.com*
[(5)] *Centro Tecnológico de Joinville, Universidade Federal de Santa Catarina; rodrigodasilvacardozo@gmail.com*
[(6)] *Centro Tecnológico de Joinville, Universidade Federal de Santa Catarina; talita.possamai@ufsc.br*
[(7)] *Instituto Tecnológico da Aeronáutica, christopher.cerqueira@gp.ita.br*
[(8)] *Instituto SENAI de Inovação em Sistemas Embarcados, augusto.conto@sc.senai.br*

Keywords: *Catarina Constellation, Nanosatellites Constellation, Cubesats, Mission Design, Systems Engineering.*

Catarina Constellation is a brazilian initiative to promote the aerospace industry in the state of Santa Catarina (SC) and train human resources, using the tripod involving the Brazilian Space Agency (AEB), the Federal University of Santa Catarina (UFSC) and the SENAI Institute for Inovation in Embedded Systems (ISI-SENAI). The initiative aims to launch a constellation of nanosatellites with missions defined from the survey of customer needs assigned to smaller sets called fleets. The fleet A of Catarina Constellation has as its mission the technological demonstration of a pair of nanosatellites made independently by UFSC and ISI-SENAI, respectively named Catarina-A1 space system and Catarina-A2 space system, with the objective of communicating with Data Collection Platforms (PCDs) located in SC and relay their data to the Multi-Mission station of the National Institute for Space Research located in Natal, Rio Grande do Norte (INPE-RN), in order to aggregate both the Brazilian Data Collection System (SBCD) with the nanosatellites, and the National Environmental Data System (SiNDA) with the data collected. This work presents the application of Space Systems Engineering concepts to the project, from the collection of stakeholder requirements to the definition of mission architecture and operation concepts, with specific application of the standards for space projects of the European Cooperation for Space Standardization (ECSS). Based on the results, it is identified that although CubeSats are considered low-complexity space systems, a more complete application of the Life Cycle and the ECSS-based systems engineering brings significant contributions to the development, traceability and repeatability of the CubeSats project although also resulted in an increase in the development duration of the project so far.

1. Introduction

Since the introduction of the CubeSat concept in 1999 [1] more than 1400 Cubesats were launched until the time of writing of this paper. When accounting for the total failure launch, early breakage and operational failure of these CubeSats a 40 percent failure ratio is found [2], despite this number decreased in the last years [2]. From this failures, aproximatelly 46 percent correspond to CubeSats developed by University teams [3]. If we look only at the CubeSats developed by Universities, the ratio of failure is 51 percent [4].

Various authors credit one of the reasons for this high failure rates by CubeSats developed by universities to the lack of a strong project management and low application of engineering systems during the development [4, 3]. When com pairing university-class CubeSat mission with industry-class mission the later has a higher success rate credited to the project management [4].

Regarding the university-class CubeSat missions, nearly one-third reached their full objectives [4]. This number is lower when only universities with CubeSat programs that launched less than 4 missions are considered, indicating that the lessons learned through the evolution of the program at the university is an important factor to success [4]. Lucinda et al (2019), based on a three-case study, showed that following a good reviewing system and adherence to proper documentation through the application of a space engineering system approach from the beginning of the mission are indicators to achieve success. It is well known that it can be difficult to be implemented in a university-class mission due to the nature of the participants mostly comprised of students.. This paper is focused on the mission design of Catarina Constellation´s Fleet A.

The Fleet A of the Catarina Constellation is a data collection mission composed of two CubeSats (2U and 3U) and is part of a future Constellation of nanosatellites named Catarina Constellation [5]. The Fleet A is developed by the Federal University of Santa Catarina (UFSC) and the SENAI Institute of Innovation in Embedded Systems (ISI-SE) with the support of the Brazilian Space Agency (AEB).

This article aims to present the applied engineering system with the identification of the simplifications and adaptations adopted and their repercussions found so far.

2. Methodology

This work was carried out in three stages:

1. The standardization to be followed by the project applied to the Catarina Constellation Fleet A project were tailored from the ECSS-M-ST-10C [6] standard;

2. The Fleet A's mission definition development, starting from the stakeholders identification up to the conceptual architecture definition;

3. Establishment of requirements derived from mission objectives and goals.

3. ECSS Tailoring

One of the Catarina Constellation proposed objectives is to develop human resources in space projects, in both academia and industry, focused in the State of Santa

Catarina - Brazil. In addition to the personnel involved with the space systems technical development, there is still provision for training in Systems Engineering, following official standards and regulations indicated by the project's clients.

The standard ECSS-M-ST-10C [6], developed by the European Cooperation for Space Standartization (ECSS), led by the European Space Agency (ESA), describes the steps to be followed in relation to Systems Engineering for space systems projects in the form of document packages related to revisions to be applied during the project's Life Cycle. The scope of this work is encompassed by the following reviews:

- Mission Definition Review (MDR): At this stage, the project must present the definition of the mission, which is based on the analysis of the stakeholders, the construction of the operating concepts and the definition of the initial objectives and goals of the mission;

- Preliminary Requirements Review (PRR): At this stage, the project must present the preliminary mission requirements and a more detailed analysis of the same.

For each of these revisions, the standard provides a package of deliverables (reports) referring to various topics that orbit in the development of space projects. However, since the ECSS-M-ST-10C standard was developed with a view to managing large-scale space projects, it is considered appropriate to apply tailoring to this list of revisions, as well as their respective deliverables, for better adaptation of small satellites, objects of study in the Catarina Constellation project.

Tab. 1 indicates the tailoring applied to phase A of the project based on [6]. It is possible to notice that, for this project, the PRR and SRR revisions were grouped together.

Table 1: ECSS tailoring applied to Fleet A's mission for phase A.

Branch	Document	MDR	PRR/SRR
Sustainability	Space Debris Mitigation Plan (SDMP)	X	X
Management	Product Tree		X
	Work Breakdown Structure (WBS)		X
	Schedule	X	X
	Cost Estimate Report (CER)		X
	Risk Management Policy Document	X	X
	Risk Management Plan	X	X
Product Assurance	Product Assurance Plan (PAP)		X
	Critical Items List		X
	Quality Assurance Plan (QAP)		X
Engineering	Mission Description Document	X	
	Mission Analysis	X	
	Technical Requirements Specification		X
	Technology Readiness Status List	X	X
	Technical Budget		X
	Design Definition File (DDF)		X
	Interface Control Document		X
	Design Justification File (DJF)		X
	Requirement Justification File (RJF)	X	X
	System Concept Report	X	
	Trade-off Reports	X	X

4. Stakeholders Analysis

The mission definition process begins with the definition of the project's actors, called stakeholders, which can be described as the people or entities that hold influential roles in the project.

For the project of Catarina Constellation's Fleet A, the following are defined as stakeholders:

- Mixed Parliamentary Bench;
- Federal University of Santa Catarina (UFSC);
- SENAI Institute of Innovation in Embedded Systems (ISI-SE);
- National Institute of Space Research (INPE);
- Brazillian Space Agency (AEB);
- Civil Defense of Santa Catarina state;
- Agricultural Sector.

Those who participate in the academy-industry-government tripod can be listed as primary stakeholders: UFSC as a representative of academy, ISI-SE as a representative of industry and AEB as a representative of the government.

Brazillian Space Agency has the role of client while the Mixed Parliamentary Bench is the project's funder [5]. UFSC plays a role of space system provider, as does the ISI-SE. Each will develop, test and launch a cubesat designed to achieve fleet A objectives, named Catarina-A1 and Catarina-A2 respectively. INPE will supply the ground system responsible for communication with the satellite, known as the Natal Multi-Mission Station (EMMN).

The Civil Defense of the state of Santa Catarina will provide a data collection platform (PCD) for the expected proof of concept of Fleet A. Finally, the Agricultural Sector represents the customers benefited by the data collected and relayed by satellites, available through the National System of Environmental Data (SiNDA), powered by EMMN itself.

As their own objectives, stakeholders still have intentions to develop space technology (ISI-SE), primarily Brazilian (AEB), as well as space research (UFSC) and to train human resources, both in academia (UFSC) and in industry (ISI-SE).

Fig. 1 illustrates the relationships between stakeholders in the development of Fleet A.

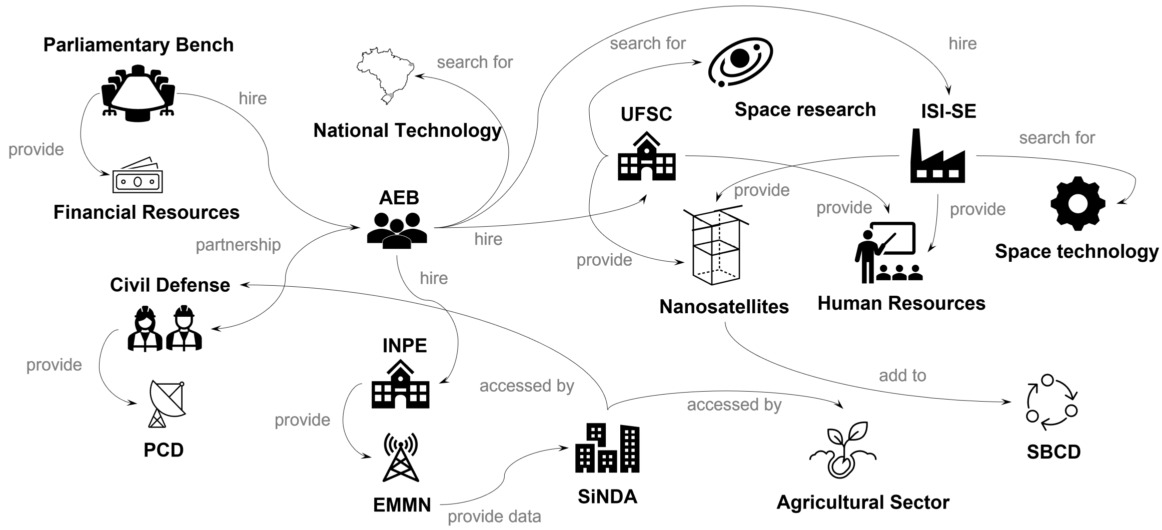

Figure 1: Stakeholders connections.

Tab. 2 lists the objectives and goals defined for the mission and derived from the needs of the stakeholders. There are three main objectives of Fleet A's mission: Collect data with national systems; Distribute data with legacy systems and empower future fleets.

In summary, it is intended to use Fleet A as a proof of concept of a data collection system so that the project team is trained satisfactorily for the course of the Catarina Constellation project and other derived space projects.

For this, already established national systems must be used, in order to add to them, such as the Brazilian Data Collection System (SBCD), which includes the Brazilian satellites of the SCD, CBERS and Amazônia families, and the National System of Environmental Data (SiNDA), which works as an environmental database fed by both the SBCD and a network of parallel instruments and can be accessed by several registered users throughout the Brazilian territory.

In order to fulfill these goals, the objectives shown in Tab. 2 were raised.

Table 2: Goals and objectives for Catarina Constellation's Fleet A mission.

ID	Goals	ID	Objectives
G.1	Collect data with national systems	O.1.1	Collect data from a platform provided by the Civil Defense and adapted by the national industry.
		O.1.2	Route the data through systems developed/adapted by the national industry, which allow the satellite data link between the platforms and the data distribution centers.
		O.1.3	Use a nanosatellite platform to perform the satellite link.
G.2	Distribute data with legacy systems	O.2.1	Integrate the data into the SBCD.
		O.2.2	Perform data distribution using SINDA.
G.3	Train for future fleets	O.3.1	Use ECSS as a basis for Space Systems Engineering.

5. Mission Description

Fig. 2 illustrates the overall mission operation concept, which encompasses the launch, commissioning, operation, and disposal steps of the space system. Since the satellites of fleet A will not communicate with each other or have different functions, the concept of operation shown is the same for both space systems.

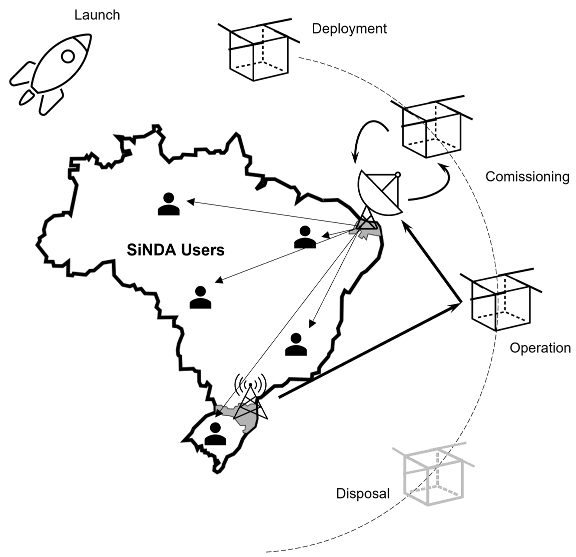

Figure 2: Fleet A's General Operation Concept

Fig. 3 illustrates two scenarios that look exclusively at the operational phase of the mission. The first scenario encompasses the collection of PCD data made by the satellites and its retransmission to the Natal Multi-Mission Station (EMMN) which has the role, in this scenario, of making the collected data available to SiNDA users.

The second scenario shows the telemetry and remote control of the satellites, to be directed from the EMMN and a secondary ground station, located in Santa Catarina.

Such scenarios help in the construction and a more refined control of interfaces, that is, in the identification of the communication interfaces between each of the elements of the mission, in its construction and in its monitoring. Such action is crucial for understanding both the mission as a whole and the flow of data during the operation.

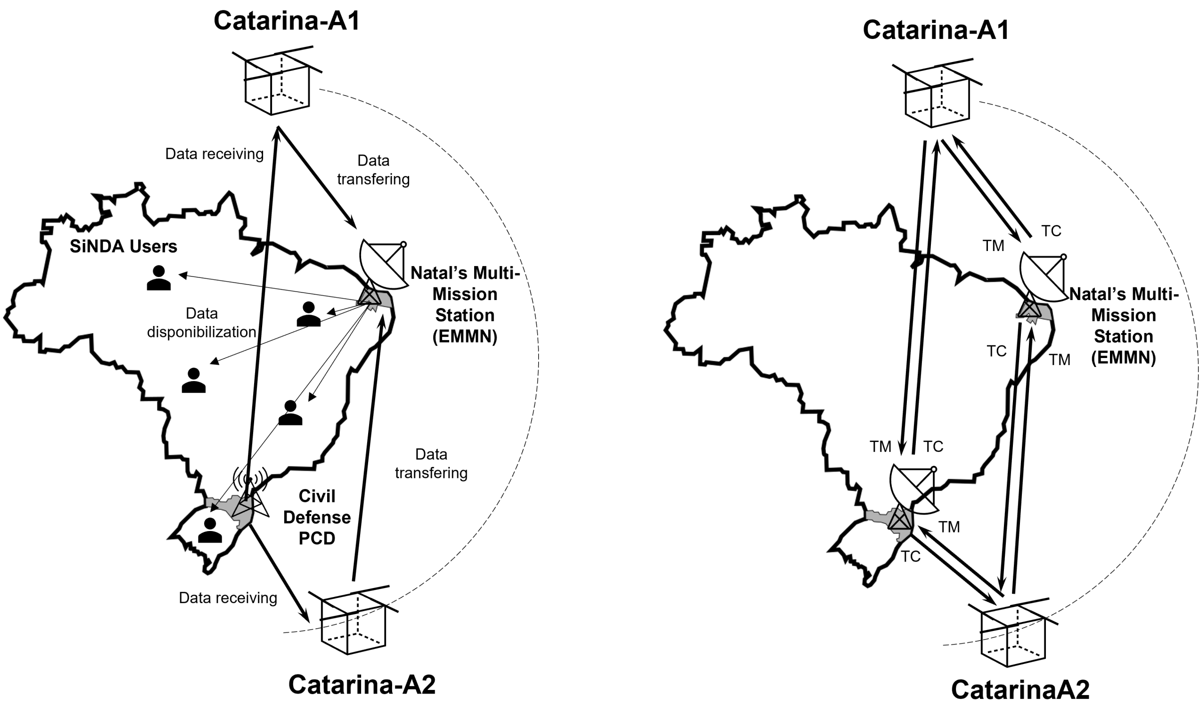

Figure 3: Fleet A's Operation Concept Scenarios

As a product of the analysis of operating concepts, a conceptual architecture of the mission is defined. In this architecture, the connections between the elements (space segment and ground segment) must be illustrated, the format of information transfer and their start and end points (if there is no feedback).

The first scenario of the concept of operations in Fig. 3 can be used as a graphical basis for the development of a conceptual architecture.

Fig. 4 shows the conceptual architecture of the mission, in which it is possible to perceive the flow of data starting from the PCD, passing through the satellites, transmitted to the ground stations and finally reaching the users.

The generalization of the number of PCDs, nanosatellites and ground stations is a defined strategy so that the mission can accommodate later upgrades without damaging its definition.

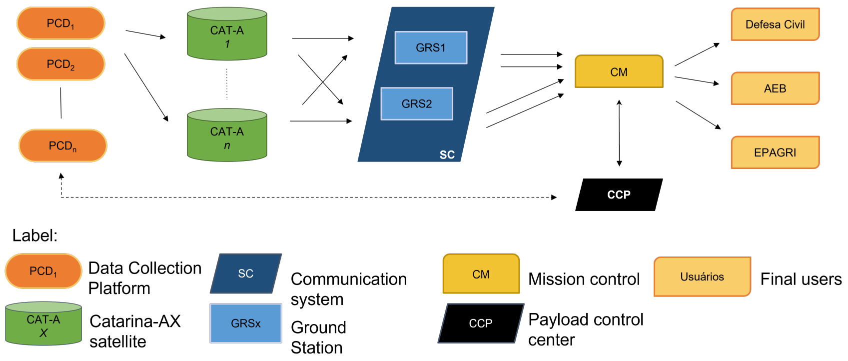

Figure 4: Fleet A's Mission Conceptual Architecture

6. Functional and Non-Functional Requirements

In order for the goals shown in Tab. 2 to be met, it is necessary to translate needs into requirements. While the needs transcribe the pains of the customers, the requirements quantify the functions to be developed by the system to supply such pains.

To define this translation, it is necessary to understand the characteristics and functions of the systems involved in the mission. Fig. 5 shows, on the left, the functions of the system, that is, the actions that the system must perform, and, on the right, its characteristics.

It is possible to generalize and indicate that functions generate functional requirements and characteristics generate non-functional requirements.

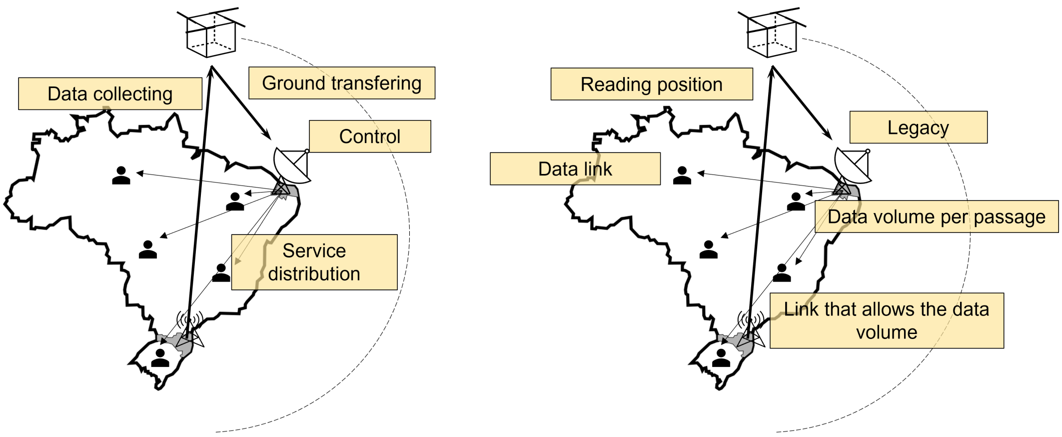

Figure 5: Architecture elements' functions and characteristics.

Functional requirements are those that define the actions to be performed on the system, while non-functional requirements define how these actions will be performed.

In Fig. 6 the blue boxes list the functional requirements of the mission, while the green ones are the non-functional ones. The functional ones are:

- FA_MISREQ_001 - Collect data from PCD;
- FA_MISREQ_002 - Send received data from PCD;
- FA_MISREQ_003 - Control space segment;

- FA_MISREQ_004 - Distribute Data.

The FA_MISREQ_001 and FA_MISREQ_002 requirements are linked to the functions of space systems for data collection and retransmission, whereas the FA_MISREQ_003 refers to the earth station and the requirement FA_MISREQ_004 to EMMN and SiNDA.

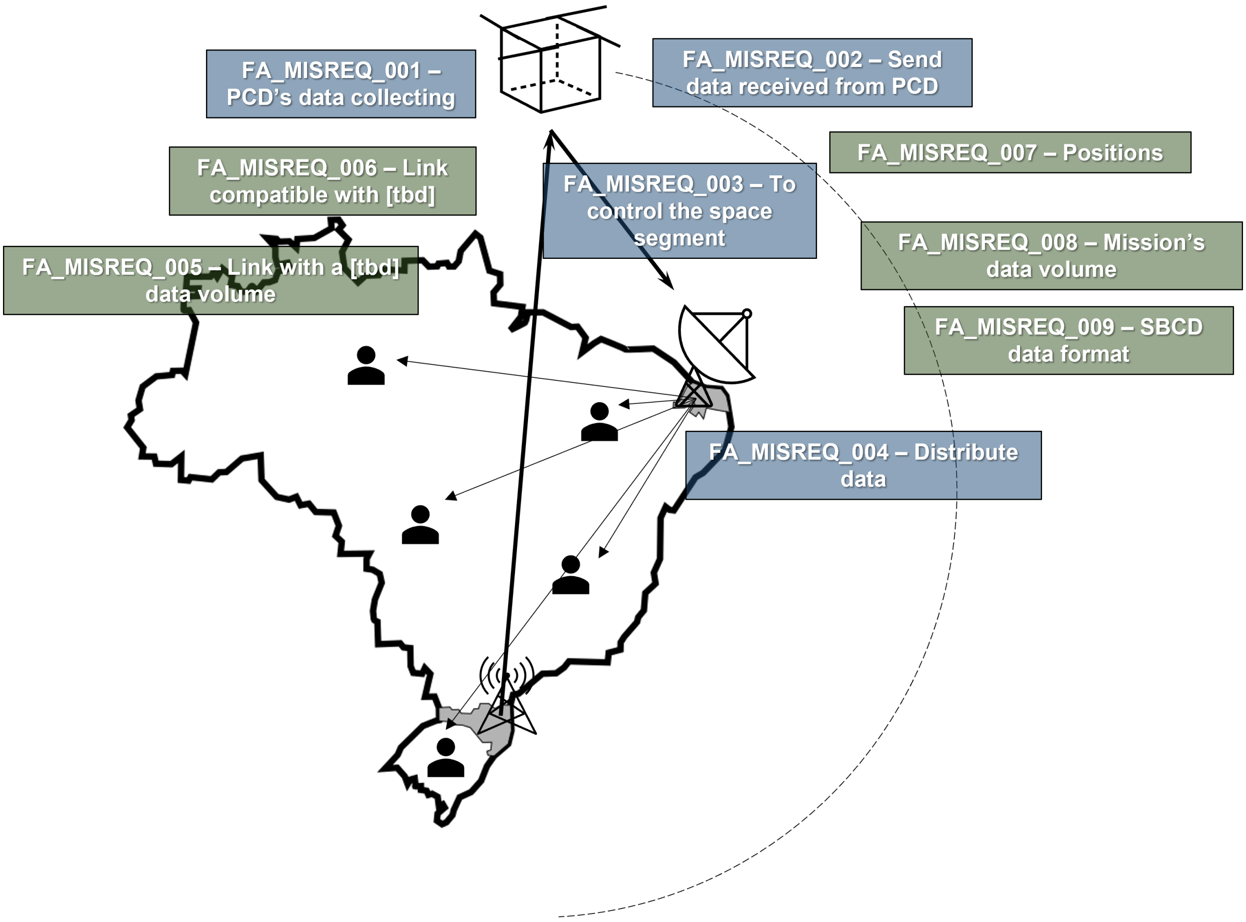

Figure 6: Functional and non-functional requirements

Non-functional requirements indicate how these actions will be carried out, with FA_MISREQ_005 and FA_MISREQ_006 relating to data collection and FA_MISREQ_007, FA_MISREQ_008 and FA_MISREQ_009 related to retransmission.

7. Conclusion

This work presented the methodology applied for the mission design of the Fleet A of the Catarina Constellation and the tailoring based on the ECSS standards for space systems defined for the reviews present in the phase A of the project.

Although not common to the nanosatellite community, the standards related to systems engineering guide the design of space missions in a clear and objective way, creating a logical path between customer needs and system operation, promoting better traceability of requirements and failures.

The application of systems engineering in the Catarina Constellation's Fleet A project made it possible to better define the needs of the stakeholders, as well as their roles, and their translation into the expected functions of the space and ground systems components of the mission.

It is important to highlight that the application of the classic review process suggested in the ECSS standard brought as positive points until the moment of the project the possibility to identify problems earlier in the project and probable greater repeatability between the fleets of the Constellation. However as negative points it was noticed an increase in the duration of the development of the project due to the time used to produce the required documents for each review.

Acknowledgments

We thank the Brazilian Space Agency for their support of the project and guidance for this work.

We thank the Santa Catarina Parliamentary Bench for the financial support for the development of Catarina Constellation.

References

[1] H. Heidt, J. Puig-Suari, A. S. Moore, S. Nakasuka, R. J. Twiggs, CubeSat: A new Generation of Picosatellite for Education and Industry Low-Cost Space Experimentation, in: 14th Annual AIAA/USU Conference on Small Satellites.

[2] T. Villela, C. A. Costa, A. M. Brandão, F. T. Bueno, R. Leonardi, Towards the Thousandth CubeSat: A Statistical Overview, International Journal of Aerospace Engineering 2019 (2019) 13.

[3] M. Swartwout, Reliving 24 Years in the Next 12 Minutes: A Statistical and Personal History of University-Class Satellites, in: 32nd Annual AIAA/USU Conference on Small Satellites.

[4] L. Berthoud, M. Swartwout, J. Cutler, D. Klumpar, J. A. Larsen, J. D. Nielsen, University CubeSat Project Management for Success, in: 33rd Annual AIAA/USU Conference on Small Satellites.

[5] C. A. T. de Moura, Ordinance No 590 - Creation of the Catarina Constellation Program and the Catarina Consortium, Ministry of Science, Technology and Innovations and Brazilian Space Agency, Palácio do Congresso Nacional - Praça dos 3 Poderes, Brasília - DF, 70160-900, 2021.

[6] ECSS-M-ST-10C - Space engineering: Project Planning and Implementation, European Cooperation for Space Standardization (ECSS), ESTEC, P.O. Box 299, 2200 AG Noordwijk, The Netherlands, 2009.

RECENT DEVELOPMENTS AT INPE´S SMALL SATELLITES DIVISION

Walter A. dos Santos[1], Antonio C.O. Pereira Jr.[2], Lincoln Teixera[3], Bruno C. Junqueira[4], Marcus V. Cisotto[5], Antonio C. Julio Filho[6], Auro Tikami[7], Luiz A. R. Bueno[8], Lázaro A. P. Camargo[9] Ângelo J. A. Florentino[10], Antonio F. De Brito[11], and Andrés F. P. Horna[12]

National Institute for Space Research (INPE)
Av. dos Astronautas, 1758, Jd.da Granja, S. José dos Campos, Brazil
Phone: +55 12 3208 7377, Mail: (1)walter.abrahao, (2)acarlos.pereira, (3)lincoln.teixera, (4)bruno.junqueira, (5)marcus.cisotto, (6)cassiano.filho, (7)auro.tikami, (8)luiz.bueno, (9)lazaro.camargo, (10)angelo.florentino, (11)antonio.brito, (12)andres.horna[@inpe.br]

Keywords: *Small satellites, Systems Engineering, Reliability, Earth Observation, Public Outreach.*

Small satellites applications nowadays are in high demand as in some cases this approach may be effective in performance and costs. INPE has recently started a series of contributions in the small satellites area and has in fact assigned a division (DIPST) on its structure to tackle just small satellites and all the concerns arising from them. This work briefly introduces a snapshot of the current activities being performed by DIPST and also where it is heading to in near future. Therefore, DIPST is assigned to: (1) Develop activities, technical consultancy and dissemination of knowledge; (2) Design cost-competitive space missions; (3) Develop of applications embedded in small satellites, suborbital flights, drones or stratospheric balloons and (4) Validate COTS com-ponents and alternatives for cost reduction. DIPST will be managing: (1) Life cycle stages, development and qualification of standard platforms and qualification of pay-loads and (2) Support the development cycle of new technologies to reach the maturity level. Finally, DIPST will participate in: (1) Actions for the Brazilian technological autonomy in the development of small satellites, their subsystems and components and (2) National and international cooperation. Concerning current projects, DIPST is taking part and supporting many nanosatellites initiatives like: (1) SPORT (Scintillation Prediction Observations Research Task) a 6U-cubesat in partnership with NASA, AEB, ITA to study the preconditions leading to equatorial plasma bubbles in the ionosphere. Mission operations will be done by INPE through its ground stations and INPE will receive, archive and distribute mission data at the Brazilian Monitoring and Study of Space Weather Program (EMBRACE) facilities and disseminate the processed data to the scientific community. (2) GOLDS-UFSC – a 2U cubesat for GOLDS Constellation (Global Open coLlecting Data System) developed by the academic sector and carrying an environmental data collecting payload from INPE´s northeast site. (3) BiomeSat – a 6-U nanosatellite for forest´s health monitoring looking at photosynthesis activity from chlorophyll fluorescence and part of a multi-mission nanosatellite platform named P10 reused in future demands. (4) BalloonSat – a balloon carrying a nanosatellite for rapid prototype developments which 1st mission is being undertaking with an educational institution as part of DIPST outreach effort. Future projects are also described like the P30 - a 30Kg small satellite, and P100 platforms - a 100Kg microsatellite bus. TuriSat, a small satellite for forests fires in Amazonia will use the first P30 platform targeted.

1. Introduction

Currently many space programs in the world have already a development on smallsats besides the traditional bigger satellites [1]. Following this trend, INPE has recently created a special division, named DIPST, dedicated to this category of satellites. DIPST is responsible for conducting the activities of development, technical support, and knowledge dissemination of technologies and capabilities for small satellites in space programs, with the academic and industrial sectors. DIPST works transversally with the other Divisions and Service of INPE´s General Coordination of Space Engineering, Technology and Science (CGCE) in order to create synergy among various areas of knowledge of this Coordination.

The main role of DIPST is the development of nanosatellites and microsatellites (up to 100kg) intended for space science and Earth science applications, including technological demonstrators. For the development, DIPST seeks to improve the quality and reliability of these satellite artifacts using INPE's experience acquired in the development of larger satellites, such as the SCD, CBERS and Amazonia-1 families. Similarly, small satellites can prototype exploratory solutions that will be used in larger missions as well as being a complement to INPE's larger remote sensing satellites like Amazonia and CBERs series.

Missions with small satellites may include several possible alternatives ranging from a single small satellite, missions with several small satellites flying in constellation or swarm, and missions together large satellites. DIPST division is gathering laboratories and qualified personnel for the development of nanosatellites and microsatellites, including initial assembly, integration and tests. As an example of contribution, INPE will provide the ground segment for the SPORT nanosat [2] to study the preconditions leading to equatorial plasma bubbles in the ionosphere, receive, archive and distribute mission data EMBRACE disseminating the processed data to the scientific community.

This paper is organized as follows: Section 2 presents some nanosat missions using the P-10 platform; Section 3 talks about prototyping missions using the BalloonSat concept; Section 4 introduces the P-30 platform and small-satellites missions derived from it; similarly, Section 5, presents micro-satellites missions in the P-100 platform; Section 6 describes some nanosatellite constellations for environmental data collection and Section 7 concludes this paper.

2. Nanosatellites Missions in the P-10 Platform

DIPST is planning two key nanosatellites mission that will use the P-10 platform [3]: (1) BiomeSat [4] - a 6U nanosatellite proposal for providing information on forest conditions in Brazil, with a level of spatial and temporal detail useful for monitoring and (2) RaioSat [5] – this mission will have, as a space segment, a prospectively 6U-cubesat with a mass of 10 kg, with an on-board computer and an attitude control system to meet the requirements for lightning flashes images.

2.1 BiomeSat Mission

Forest conservation in Brazil is important for several reasons. Forests are home to a high number of plant and animal species, and high values of water and carbon stocks and flows between the land surface and the atmosphere, thus having a substantial impact on climate, biodiversity and the availability of natural resources. Due to the large territorial extension, remote sensing is essential for monitoring forests in Brazil.

Thus, to contribute to the forest observation programs in the country and agricultural monitoring, it is intended to generate information on the conditions of these areas using the collected data. Specifically, it is intended to collect data on the state of forests and agricultural crops using vegetation indices, which can aggregate the effect of various disturbances such as droughts, deforestation and fire, and present less complexity for data acquisition and calculation.

BiomeSat will be implemented around a 6-U cubesat platform as shown in Figure 1. The proposal for mapping forest conditions and agricultural monitoring considers the use of vegetation indices based on images collected in bands of electromagnetic waves corresponding to the visible and infrared spectrum. Some examples of these indices that use data in the red (R), green (G), blue (B) and near-infrared (NIR) ranges include, among others, the Visual Normalized Difference Vegetation Index (Visual NDVI), the Green Leaf Index (GLI), the Visual Atmospheric Resistance Index (VARI), as well as the Normalized Difference Vegetation Index (NDVI) and similar ones. These indices are related to chlorophyll content, differences between plants, exposed soil and non-vegetable material and are therefore appropriate for estimating vegetation conditions and agricultural crops.

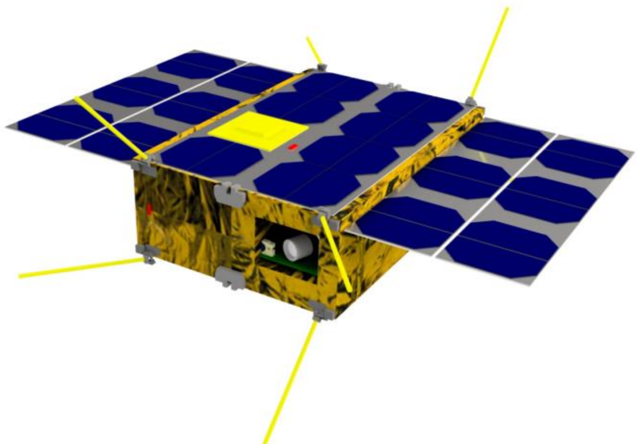

Figure 1: BiomeSat artistic view for forest health monitoring.

The BiomeSat mission intends to continue monitoring environmental changes, deforestation and forest degradation, as well as supporting applications in agriculture in order to obtain several benefits in different areas:

- Vegetation: monitoring of deforestation, degradation, and state of vigor of forests.
- Agriculture: estimate of planted area, vegetative vigor of crops, forecast of agricultural production, determination of areas of preservation of springs, forest reserves and agricultural areas, pointing out errors in fertilization, irrigation and soil preparation processes, regions with greater potential of production.
- Environment: assessment of the impact of fire, deforestation and drought on a given area, allowing a good rate of monitoring of environmental degradation, delimitation of continental water bodies, support for coastal management.

- Education: generation of material to support educational activities in geography, environmental sciences and other disciplines and generation of data and information for the development of scientific studies.

The initial conception is planned to carry a set of payloads, namely: (1) a remote sensing camera for forest health monitoring which is the primary mission, (2) a data-environmental collecting transponder (EDC) which was developed by INPE ´s Northeast site, (3) an AIS transponder for monitoring vessels in the Brazilian maritime authorities and, (4) a space-weather monitor (SEM) or tracking space environment mainly TID (Total Ionizing Dose) and SEE (Single Event Effects). The nanosatellite bus is envisaged to be a multi-mission platform for other future missions and serves as a complement to INPE's larger remote sensing satellites like Amazonia and CBERs series.

2.2 RaioSat Mission

Extreme weather events are increasingly common in Brazilian territory, and to assist in the study and generation of meteorological forecast models, the monitoring of lightning occurrences becomes extremely important [6]. The Atmospheric Electricity (ELAT) group of the Earth System Science Center (CCST) together with the Small Satellite Division (DIPST) proposed the RaioSat mission, to assist the existing ground network, for monitoring lightning occurrences.

The RaioSat mission will have, as a space segment, a 6U-cubesat as shown in Figure 2, with a mass of 10 kg, with an on-board computer and an attitude control system to meet the requirements for lightning flashes images and having the following payloads: Camera in the IR range (infrared) with sensor and optical filter, a GPS (Global Positioning System) for low orbit applications, VHF SDR (Software Defined Radio) receiver operating in the 30 - 100 MHz band, to record the electromagnetic signatures and validate the lightning detections acquired by the IR camera.

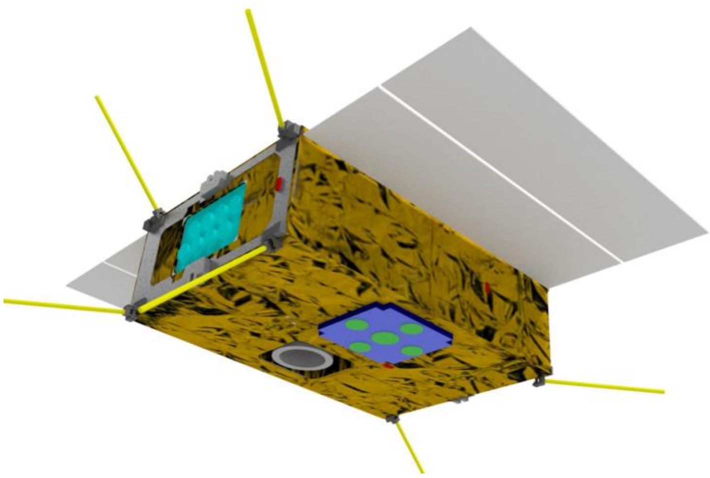

Figure 2: RaioSat artistic view for lightning events monitoring.

The RaioSat mission will complement the BrasilDat network for monitoring atmospheric electrical discharges, and assist in the Brazilian civil defense and risk and disaster management system. This mission will be fundamental for the short-term weather forecast for disaster prevention actions by storms and electrical discharges and assist in risk and disaster management and civil defense.

3. BallonSat - Multi-Mission Platform for Stratospheric Balloon

DIPST will soon launch its first experimental Multi-Mission Platform for Stratospheric Balloon (PMBE) which was developed to be used as a telemetry, remote controls and georeferencing system that, coupled to a stratospheric balloon, can help in the testing and evaluation of technological systems and scientific experiments that use stratospheric flights [7].

The stratosphere has peculiar conditions, such as low pressure and temperature, in addition to a relatively long and free link distance, which can be favorable for certain tests and experiments. The evaluation of some subsystems that are developed for nanosatellites, using CubeSat architecture or not, can use this platform, as depicted in Figure 3, since the costs would be extremely low especially when compared to those performed in orbit tests.

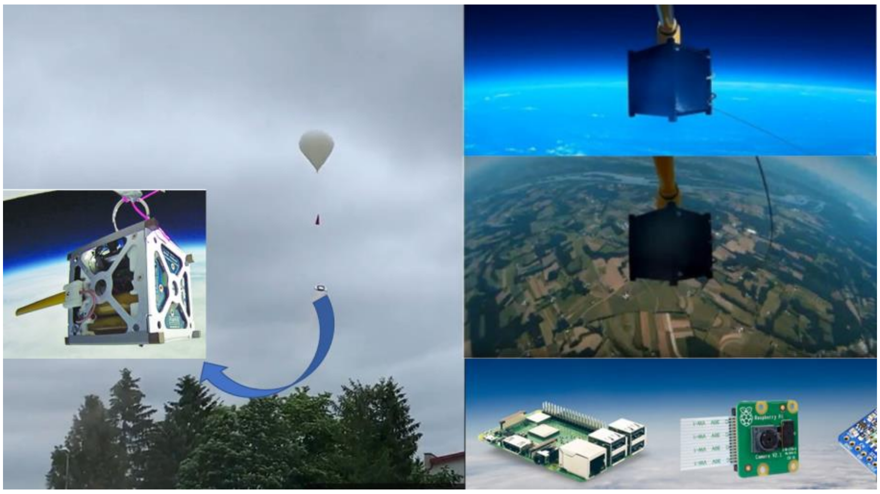

Figure 3: Multi-Mission Platform for Stratospheric Balloon (PMBE).

The PMBE is based on a CubeSat architecture. It weighs under 500g and is built with low-cost components and power consumption. Its subsystems have dimensions of 10 x 10 cm and are coupled through a PC104 connector. It consists of an on-board computer, OBDH, with integrated GPS, a subsystem for sending telemetry and receiving telecommands, TM/TC, and a power subsystem. The TM/TC is suitable for the type of mission, and its operating parameters may vary, such as transmission and reception frequencies, power, data rate and type of modulation used. It works primarily on UHF frequencies, between 400 MHz and 433 MHz, and on sub-Giga Hertz frequencies, between 900 MHz and 930 MHz. According to the configuration of the parameters of the TM/TC subsystem, it is possible to close a link of up to 900km. In addition to the subsystems mentioned, the PMBE is also composed of the structure and thermal control subsystem, for mechanical support and temperature control, containing standard analog and digital interfaces for connecting sensors, cameras and experiments.

4. Small-satellites Missions in the P-30 Platform

DIPST is designing a small satellite platform weighting 30 Kg named P-30 [8] in order to enable more demanding missions which would be instantiated into a the Turi-Sat mission. It aims to contribute to the programs of observation and preservation of forests in Brazil by generating information on the location of fires, enabling the competent authorities to act in the early stages of fires.

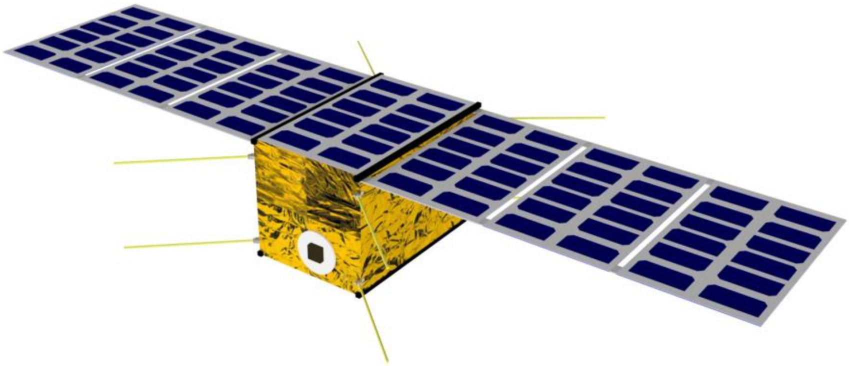

Figure 4: The TuriSat, a 30Kg small-satellite mission.

Fire fighting in forest regions has been the subject of research by several groups in international agencies. An important tool for fighting fire is the use of remote sensing techniques to identify and locate fire outbreaks, thus making it possible to extinguish the fire at an early stage, when the damage caused to the environment is still small.

The TuriSat microsatellite, class 30kg, will have three optical imagers, with appropriate characteristics, and a data collection system. It will have 3-axis control and propulsion subsystem. With this, it will be able to operate at higher altitudes and will be aligned with good practices for the rational use of space. Techniques will be used to mitigate the effects of cosmic radiation in order to extend its useful lifetime.

5. Micro-satellites Missions in the P-100 Platform

In order to meet the requirements for science mission like space weather, DIPST is envisaging a micro-satellite platform bus weighting 100 Kg named P-100 [9] which would accept another 100 Kg module for carrying the scientific payload instruments. EQUARS [10], shown in Figure 5, is the first P-100 target mission.

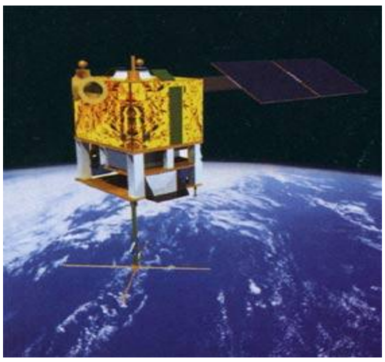

Figure 5: The EQUARS [10] mission will be using the P-100 bus platform.

6. Nanosatellite Constellations for Environmental Data Collection

Nanosatellite missions have much of their life cycle shortened as they use commercial components (COTS). The standardization achieved with nanosatellites using on the cubesat platform has allowed drastic cost reductions by enabling scientists and engineers to design small artifacts and coordinate networks of multiple cubesats (known as “cubesat constellations”) that provide a wide variety of new technologies. resources in orbit. DIPST is currently supporting of two initiatives: (1) The CONASAT Project [11] and the (2) GOLDS Constellation [12] which are described in details hereafter.

These first constellations will support mainly the Brazilian Environmental Data Collection System (SBCDA). Currently, the SBCDA is a Brazilian satellite-based environmental monitoring system developed and operated by the Brazilian Institute for Space Research (INPE). Currently, SBCDA consists of 5 Low Earth Orbit (LEO) satellites (SCD-1, SCD-2, CBERS-4, CBERS-4A and Amazonia-1); two control and data reception stations and a network of approximately 500 automated Environmental Data Collection Platforms (DCP), most of them scattered throughout the national territory and some oceanographic buoys. Today the SBCDA work as follows:

- The data are collected through sensors coupled in the DCPs that transmit them to the satellites in the frequency of 401MHz, in short-burst signal, in a unidirectional and asynchronous communication;
- LEO satellites relay the signals of the DCPs back to the Ground Receive Stations located in Alcântara and Cuiabá;
- The DCP data received at Ground Stations are sent to the mission center located in Natal, where a software-based system named SINDA (Integrated System for Environmental Data);
- SINDA processes, stores and make data available to the end users and
- The users’ access to SINDA is free through the Internet.

6.1 The CONASAT Project

The CONASAT Project (Constellation of Nanosatellites for Data Collection Environmental) [con], based on the concept of “fast and cheap access to space” using the CubeSat standard, aims to offer a technologically updated option, incorporating recent advances in microelectronics, telecommunications, embedded systems and sensors using MEMS technology. The project can be seen as an evolution of the SBCDA employing a constellation of CubeSats, aiming to improve the quality of the service, in terms of capacity, geographic coverage and shorter revisit times.

The project aims to provide the country with its own capacity in the development of the life cycle of space systems and in this context, it consolidates the application of technology from the development, operation and offer of products through a satellite system, totally designed in the country. The project operates along the following lines of Sustainable Development Goals (SDGs) - UN 2030 Agenda:

- SDG15: The project will enable effective actions in environmental management through the collection of environmental data.
- SDG14: The project may contemplate the development and immediate application through the collection of environmental data provided by oceanic buoys.

In order to ensure the continuity of the SBCDA and meet the new demands of environmental monitoring, providing new services and improving its performance, INPE, through the Northeast Spatial Coordination (COENE), is conducting the CONA-SAT project, which aims to offer an innovative solution in the space segment. The solution is based on a constellation of nanosatellites, which allows for a cost reduction while providing an improvement in the quality of service, in terms of capacity, geographic coverage and shorter revisit time.

The payload will be a transponder for collecting environmental data called EDC (Environmental Data Collector) onboard a cubesat developed and qualified by INPE. The ground and application segments will also have their capability enhanced with these missions.

Currently, CONASAT-1 is the first satellite of the CONASAT/GOLDS constellation, it is a Cubesat 1U standard satellite which objective is to test in flight the EDC transponder developed by INPE, which decodes in flight the signals received from PCDs (Platforms for Data Collection) belonging to the SBCDA. The CONA-SAT/GOLDS constellation aims to update and expand the SBCDA, which is a message forwarding system developed by INPE, in operation since 1993, based on low-orbit (LEO) satellites.

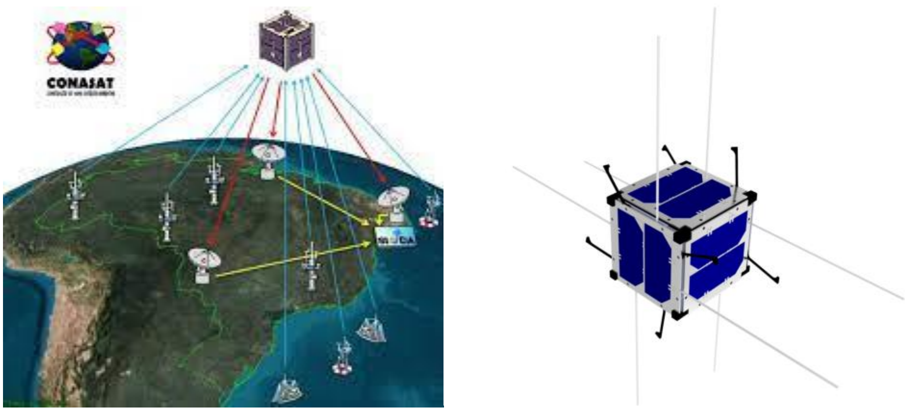

Figure 5: CONASAT-1: the 1st nanosat for data collection constellation [11].

The main results expected with CONASAT are: (1) Guaranteed operation of the SBCDA. (2) Increase in SBCDA's revisit capacity. (3) Increase in the number of SBCDA stations (PCDs) installed in the national territory and (4) Improvement of the environmental data collection service offered by the SBCDA.

6.2 The GOLDS Constellation

The GOLDS Constellation stands for “Global Open coLlecting Data System” and it is a collaborative nanosat constellation for environmental monitoring which will provide data for scientists, government institutions and private companies in the country. GOLDS gathers initiatives on the modernization of the SBCDA (Brazilian Environmental Data Collection System).

The purpose of this monitoring system is to provide data for scientists, government institutions and private companies in the country being used in a wide variety of applications, related to environmental protections, awareness, study or protecting human life, such as weather forecasting, studies of ocean currents, tides, atmospheric chemistry, agricultural planning, monitoring of the watershed, river and rain gauge data, monitoring fishing vessel route, among others.

The cubesat-2D GOLDS-UFSC will soon compose the GOLDS. The constellation will reduce the costs to provide quality of service with regards to capacity, geographic coverage and revisit times. Finally, GOLDS will support in different applications: weather forecasting, studies of ocean currents, tides, atmospheric chemistry, agricultural planning, monitoring of the watershed, river and rain gauge data, monitoring fishing vessel route, etc. It will open several possibilities for business and science cooperation in space Applications.

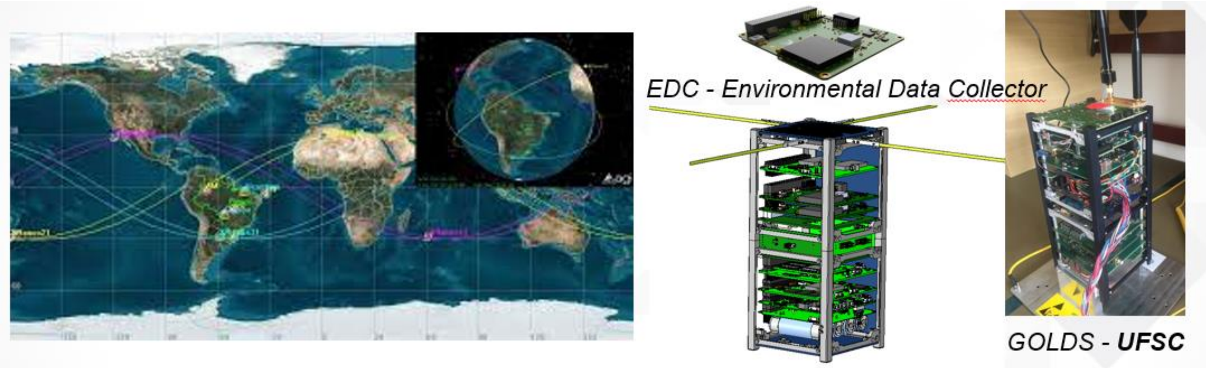

Figure 6: GOLDS Constellation [13] - "Global Open coLlecting Data System"

7 Conclusions

As the demands and opportunities for small satellites applications are increasing rapidly, INPE has decided to start a dedicated division, named DIPST, for strengthening the small satellites area as well benefitting from it towards major satellite challenges. This work presented the current and prospective projects / activities being performed by DIPST: technical consultancy and knowledge dissemination; lower the risks and costs on space missions; prototyping with stratospheric balloons flights in the BalloonSat concept and lowering the risks on COTS components. A key DIPST task is supporting the development cycle of new technologies to reach the maturity level so that they may be incorporated in larger satellites.

DIPST is involved in a myriad of initiatives such as: (a) the SPORT nanosat ground operations which launch is due very soon; (b) environmental data collection nanosats constellations like GOLDS and CONASAT; (c) climate change-related nanosatellites like BiomeSat, for monitoring forests health mainly and RaioSat, for monitoring lightning event, using a multimission platform P-10; (d) larger platforms as P-30 and P-100 which will be used in, respectively, the TuriSat for forests fires in Amazonia will use and EQUARS, a space weather science mission.

We believe if we succeed in gathering all the resources for the completion of these projects, the coming years will be quite challenging but with a singular opportunity to create new frontiers to the country´s space engineering and cater for their underlying applications.

References

[1] E.E. Areda et al., Development of Innovative CubeSat Platform for Mass Production, Appl. Sci. v. 12, 9087, 2022.
[2] J. Spann et al. The Scintillation Prediction Observations Research Task (SPORT): An International Science Mission using a CubeSat, Proceeding 31nd Annual AIIA/USU Small Satellite Conference, Logan UT, USA, 2017, SSC17-XIII-03.
[3] INPE, P-10 Platform, INPE TAP internal report, 2021.
[4] J.M. PIÑEROS et al., Preliminary analysis of a nanosat mission to integrate a lightning flashes detector with a biomass sensor in a CubeSat 3U configuration. In: Proceedings of the 4th International Academy of Astronautics Latin American Cubesat Workshop, Buenos Aires, 2020. v. 1.
[5] Carretero, M.A.; Naccarato, K.P. Detection of total lightning flashes onboard of a CubeSat satellite. In: 1st Latin American Cubesat Workshop (1st LACW), Brasilia, Brazil, 2014.
[6] K.P. Naccarato, K. P. et. al. The RaioSat project: detecting total lightning flashes from a CubeSat. In: II IAA Latin American CubeSat Workshop (IAA-2nd LACW), Florianópolis, 2016.
[7] A. S. M. Thaheer, N. A. Ismail, Mission Design and Analysis of USM High-Altitude Balloon, Journal of Mechanical Engineering, Vol 14(2), 62-92, 2017.
[8] INPE, P-30 Platform, INPE TAP internal report, 2021.
[9] INPE, P-100 Platform, INPE TAP internal report, 2021.
[10] D. Gobbi, Missão Satelital EQUARS – PRR, sid.inpe.br/mtc-m21c/2020/07.17.15.42-PRP, 2020
[11] M.J.M. Carvalho, et al., CONASAT - Constelação de Nano Satélites para Coleta de Dados Ambientais, Anais XVI Simpósio Brasileiro de Sensoriamento Remoto - SBSR, Foz do Iguaçu, PR, Brasil, 13 a 18 de abril de 2013.
[12] GOLDS, Sistema Aberto Global de Coleta de Dados, available at https://ccsl.ifrn.edu.br/portfolio-de-projetos/g-o-l-d-s-global-opena-data-collecting-system/
[13] M.F. Mattiello-Francisco et al. Fostering Environmental Data Collecting with GOLDS (Global Open CoLlecting Data System) constellation. In: United Nations/Brazil Symposium on Basic Space Tech. 'Creating Novel Opportunities with Small Satellite Space Missions', 2018, Natal, RN.

2

Session 2 - Mission Applications I

AVION SATELLITE AND THE PHYSICAL EXPERIMENTS ONBOARD

Vitaly V. Bogomolov[(1,2)], Yury K. Zaiko[(2)], Anatoly F. Iyudin[(2)], Vladimir V. Kalegaev[(2)], Ivan A. Kucherenko[(1,2)], Vladislav I. Osedlo[(2)], Oleg Yu. Peretyat'ko[(2)], Mikhail I. Prokhorov[(1,2)], Sergey I. Svertilov[(1,2)]

[(1)] M.V. Lomonosov Moscow State University, Physical Department, 1(2), Leninskie gory, GSP-1, Moscow 119991, Russia, +7 495 939-16-82, info@physics.msu.ru

[(2)] M.V. Lomonosov Moscow State University, D.V. Skobel'tsyn Institute of Nuclear Physics, 1(2), Leninskie gory, GSP-1, Moscow 119991, Russia, +7(495)939-18-18, info@sinp.msu.ru

Keywords*: CubeSat, Payload, Cosmic radiation, Gamma-ray burst, Detector*

In frame of the Moscow University space program, the Avion satellite, made in the cubesat-6U standard, is being prepared for launch into a sun-synchronous orbit. This satellite will be equipped with a payload - a complex of scientific instruments DeCoR, designed to study the temporal and spectral characteristics of electrons and gamma radiation in energy range from 20 keV to 5 MeV. The complex includes three scintillation spectrometers, whose characteristics complement each other. The subject of the study will be cosmic gamma-ray bursts, solar flares, electron precipitation, and the relationship of particle fluxes with solar activity. Data from each of the nodes of the DeCoR complex is recorded both in the form of monitoring (counting rate in several channels) and in the form of a detailed event-by-event record. The daily amount of scientific data is ~100 MB.

1. Introduction

Over the past few years, the Lomonosov Moscow University has been developing a program for conducting scientific research in the field of space physics using instruments installed on board small spacecraft of the CubeSat class [1,2]. In 2018, the SiriusSat-1 and SiriusSat-2 satellites in the 1U+ CubeSat format were launched from the International Space Station [3]. The payload of these satellites was a two-layer scintillation detector based on a combination of a CsI(Tl) crystal and a plastic scintillator designed to measure electron and gamma-ray fluxes in low orbit. One of the results of more than two years of operation of SiriusSat spacecraft in orbit was the observation of rapid variations of electron fluxes in the zone of the gap between the radiation belts.

Since better sensitivity of the equipment was required for further research, a DeCoR device with a detector area increased to 18 cm^2 was developed for future experiments. Such a device was installed on a number of scientific and educational small spacecraft launched into low polar orbit in 2019 (VDNH-80, AmurSat, both CubeSats 3U) and in 2020 (Norby, Descartes, both CubeSats 6U) [4]. All of these devices are still functioning, while the volume of transmitted scientific data and the strategy of the experiment is determined by the capabilities of the platform. One of the significant limitations is the use of a VHF ~ 435 MHz radio frequency channel for transmitting basic data, which makes it possible to transmit no more than ~ 0.5 Mb per day to one ground station.

The Avion satellite considered in this paper will have significantly better opportunities for conducting a scientific experiment than its predecessors. The CubeSat-6U platform, developed by specialists from Kaluga, will use both the traditional VHF radio channel for nanosatellites and an S-band radio transmitter that increases the daily volume of transmitted data up to ~ 200 MB. At the same time, the satellite's power system will provide continuous measurements using several scientific instruments with a total power consumption of ~ 5 watts. With this in mind, a complex of scientific equipment was developed for the Avion satellite from three devices, the characteristics of which complement each other. This significantly expands the range of cosmic phenomena that will be studied during the experiment in orbit.

2. Avion satellite payload general design

The DeCoR (Cosmic Radiation Detectors) payload complex of Avion satellite consists of three devices DeCoR-1, DeCoR-2 and DeCoR-3, differing in size and configuration of a scintillation detector that provides measurement of electron and gamma radiation fluxes and spectra in the energy range for which the device is designed. The location of the instruments in the Avion satellite body is shown in Fig. 1. One can see from the figure that the input windows of all instruments are located on one side of the Avion satellite for simultaneous observation of sources.

The electronics of the devices that are part of the DeCoR complex have a similar architecture. Electronic circuits located on one or more boards process signals and digitize them, generate secondary low-voltage power and supply voltage for photodetectors, and also accumulate and transmit data. The devices function independently of each other, their synchronization in simultaneous measurement is carried out by accurately linking the data of each of them to the onboard time.

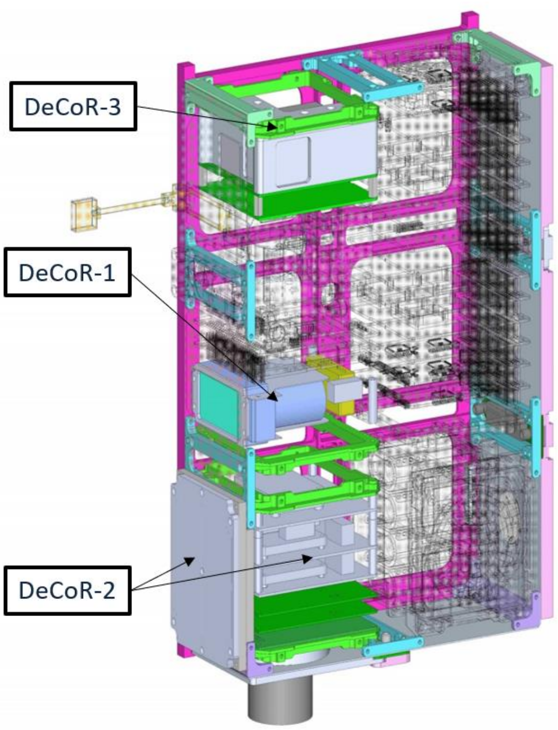

Figure 1: Sites of the instruments of DeCoR payload onboard Avion satellite.

The principle of functioning of the electronics of the devices included in the DeCoR complex is illustrated in Fig. 2. The analog part of each board receives and amplifies the output signal from two inputs to which photodetectors are connected. The chips on the electronic board generate an event processing request pulse, and form several signals to be digitized and analyzed using a microcontroller placed on the same board. To separate the cases of interaction in different scintillators with the use of their difference of the pulse shape, two signals from each input are generated and digitized in the devices: the signal of the fast component proportional to the amount of light allocated in the detector at the beginning of the pulse (in the first ~300 ns), and the signal of the slow component proportional to the amount of light allocated in the detector in the next few microseconds (~2 microseconds). The sum of these signals is used to determine the energy, and the ratio is used to determine the scintillator with which the interaction occurred.

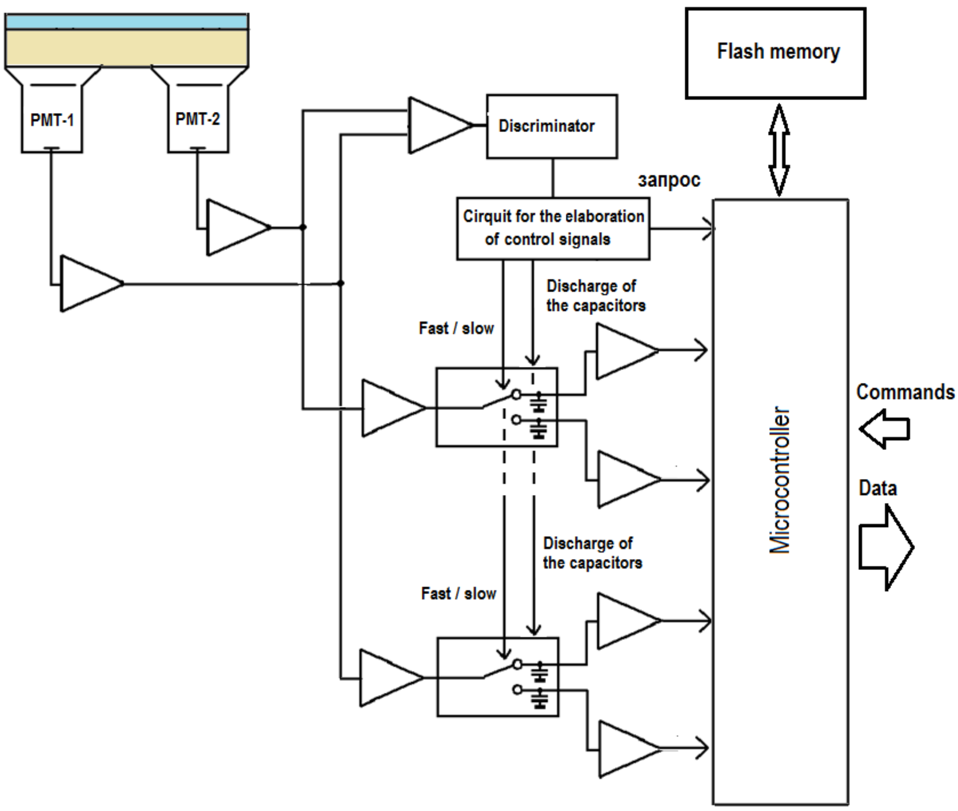

Figure 2: The design of DeCoR device electronics.

The digital part of the electronics is based on low-consumption microcontrollers. The power consumption of the digital node inside each board does not exceed 0.2 Watts. The microcontroller, by interrupting from the detector electronics, sequentially digitizes the mentioned above four signals at its inputs. Digital values are recorded in memory, at the same moment the time of the event is recorded according to the internal timer of the microcontroller. The total time of digitization and recording the event data into memory is ~ 10 microseconds.

The microcontroller analyzes the obtained values in order to measure the number of interactions with the specified parameters that occurred over a certain time interval (monitoring counting rates). The readings of 3-axe magnetometer installed on the same electronic board are added to the monitoring data. That is useful for more clear interpretation of the observed variations of the flux of cosmic electrons. Also, upon receiving the appropriate command, the digital node begins to record the initial amplitude parameters and the time of each interaction in the device's memory, making detailed measurements at the time of interest to the researcher.

Data blocks of two main types are formed from the values recorded in the device memory: "monitoring" containing the number of events of a certain type per unit of time and "array" containing primary data for a certain number of events. These data blocks are stored in the non-volatile memory of the device. On command from the satellite, data is sent via the CAN interface to the memory of the on-board computer. Scientific data are transmitted in blocks of 120 bytes on request in the form of a command indicating the type of data and the number of requested blocks.

In the main mode of operation of the equipment, all their components are turned on and function. In order to save energy, it is possible to turn on only the digital nodes of the device for transmitting already accumulated data.

2. Individual characteristics of DeCoR instruments

The complex of scientific instruments includes three scintillation spectrometers, whose characteristics complement each other. The devices differ in the sensitive area and energy range.

The DeCoR-1 node is similar to the DeCoR devices operating on the VDNH-80, Norby, and several others CubeSats launched last years. It is primarily designed to study variations of near-Earth electron fluxes such as micro-bursts similar to those observed in the experiment on the FIREBIRD-II satellite [5]. The detection element of DeCoR-1 is a combination of a 3 mm thick plastic scintillator and a 10 mm thick CsI(Tl) crystal, viewed by two PMTs. The detector has an effective area of 18 cm^2 and an energy release range of 50 keV to 2 MeV. The mass of the device is some less than 0.5 kg and its power consumption is 1.2 W for measuring mode and <0.2 W for data transfer mode when the detector electronics is turned off.

The DeCoR-2 device was optimized for the detection and study of cosmic gamma-ray bursts of various nature, so it has an effective area increased to ~65 cm^2, which is necessary both to improve the sensitivity and to increase the time resolution, which is determined primarily by the statistics of detected gamma-quanta. A composite scintillation detector consisting of a 3 mm plastic scintillator and a 9 mm CsI (Tl) is viewed by a silicon photomultiplier assembly (SiPM). The combination of mentioned scintillators allows for separate detection of gamma radiation and electrons in the energy release range from 20 keV to 1 MeV. It is important when conducting an experiment for GRB study in polar orbit.
Electronics of DeCoR-2 consists of two identical boards, operating with a half od the detector. These boards are absolutely independent. They use individual power channel, use individual set of the control commands and store data in individual part of satellite memory. Such an architecture increases the reliability of the equipment, and

also allows one to compare the readings of independent devices in order to identify significant details on the light curves of flashing sources.

The DeCoR-3 node is used to extend the range of detected gamma radiation to the high-energy region up to several MeV. Its main goal is to measure the gamma-ray spectra of solar flares and cosmic gamma-ray bursts. The detecting element of this node is a 30x30x30 mm^3 CsI(Tl) scintillation crystal. Despite the fact that this device does not have a combination of two scintillators with different illumination times, the electronics of the device, as well as for other devices of the complex, generates signals of a fast and slow component. In this case, they are used to expand the energy range of the device.

The spectrometric capabilities of the DeCoR-3 instrument can be illustrated by the energy spectrum of background gamma radiation measured during its calibration presented in Fig. 2. The emission lines of isotopes Bi-214 (609 keV), K-40 (1.46 MeV) and Tl-208 (2.6 MeV) are clearly visible on the spectrum.

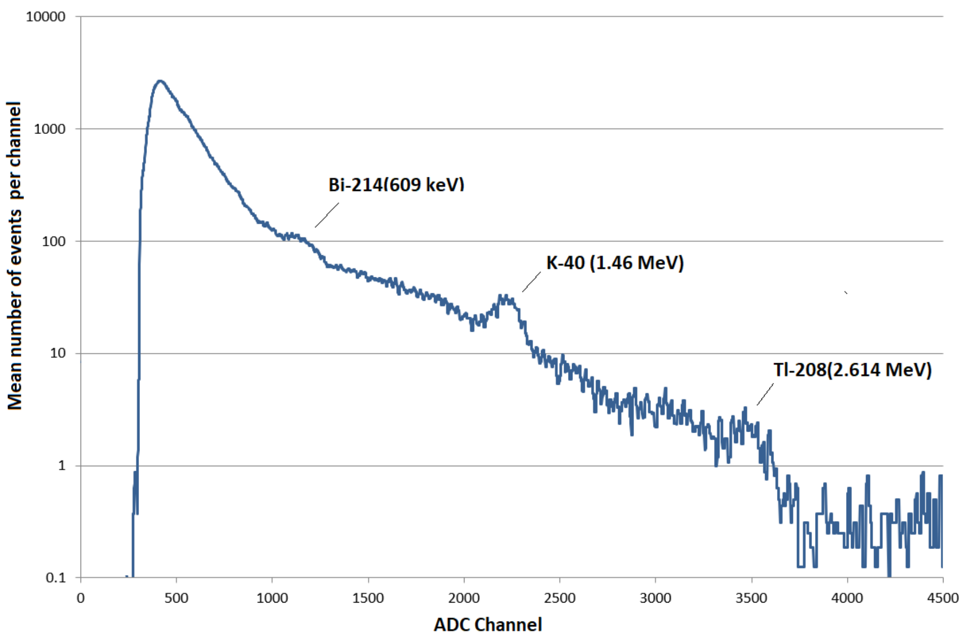

Figure 2: Background gamma-ray spectrum measured by DeCoR-3.

2. Conclusion

Currently, the Avion satellite is fully assembled, has passed a number of necessary tests and, thus, is ready for launch into a solar synchronous orbit, which is expected to be carried out in the first half of 2023. Calibrations and tests provided for the DECOR equipment confirmed its physical characteristics and readiness to conduct a space experiment to study cosmic gamma-ray bursts, the phenomena connected with the dynamics of radiation belts and solar activity. The data obtained in the space experiment will be used for the space research as well as for the practice of the university students specialized in the branch of space physics.

References

[1] Andrey V. Bogomolov, Vitaliy V. Bogomolov, Anatoly F. Iyudin, Valery E. Eremeev, Vladimir V. Kalegaev, Irina N. Myagkova, Vladislav I. Osedlo, Vasiliy L. Petrov, Oleg Y. Peretjat'ko, Mikhail I. Prokhorov, Sergey I. Svertilov, Yury K. Zaiko, Ivan V. Yashin, Vitaliy Y. Prokop'ev, Aleksey S. Styuf, Sergey V. Krasnopeev, and Aleksandr P. Papkov. Space weather effects from observations by Moscow university cubesat constellation. Universe, 8:282, 2022. DOI: 10.3390/universe8050282

[2] Sergey Svertilov, Viktor Bengin, Vitaly Bogomolov, Gali Garipov, Mikhail Dobynde, Ivan Zolotarev, Vladimir Kalegaev, Pavel Klimov, Vladislav Osedlo, Mikhail Panasyuk, Oleg Peretjat'ko, Vasily Petrov, and Mikhail Podzolko. Monitoring of radiation fields in near earth space and atmosphere in new space projects of Moscow university. E3S Web of Conferences, 196:02019, 2020, DOI: 10.1051/e3sconf/202019602019

[3] V. V. Bogomolov, A. V. Bogomolov, Yu N. Dement'ev, V. E. Eremeev, R. N. Zharkih, A. F. Iuydin, I. A. Maksimov, V. I. Osedlo, M. I. Prokhorov, and S. I. Svertilov. A scientific and educational space experiment on the siriussat-1,2 satellites. *Moscow University Physics Bulletin*, 75:665–675, 2020. DOI: 10.3103/S0027134920060077

[4] V. V. Bogomolov, A. V. Bogomolov, Yu N. Dement'ev, V. E. Eremeev, Yu K. Zaiko, V. V. Kalegaev, P. A. Klimov, V. I. Osedlo, M. I. Panasyuk, V. L. Petrov, O. Yu Peretjat'ko, M. V. Podzolko, and S. I. Svertilov. A first experience of space radiation monitoring in the multi-satelliteexperiment of moscow university in the frameworkof the universat-socrat project. Moscow University Physics Bulletin, 75:676–683, 2020. DOI: 10.3103/S0027134920060089

[5] Breneman, A. W., Crew, A., Sample, J., et al., Observations Directly Linking Relativistic Electron Microbursts to Whistler Mode Chorus: Van Allen Probes and FIREBIRD-II // Geophysical Research Letters. https://doi.org/10.1002/2017GL075001

A PAYLOAD PROPOSAL FOR LIGHTNING FLASH DETECTION USING A NANOSATELLITES

Camargo L. A. P[(1)], Dos Santos W. A.[(2)], Piñeros J. O. M[(3)], Naccarato K. [(4)] Tikami A.[(5)], Pereira A. C. O. J.[(6)], Cisotto M. V.[(7)], Julio Filho A. C.[(8)], Bueno L. A. R.[(9)], Brito A. F.[(10)], Florentino A. J. A.[(11)], Teixeira L.[(12)], Junqueira B. C.[(13)], Horna A. P.[(14)]

[(1,2,4,5,6,7,8,9,10,11,12,13,14)] National Institute for Space Research (INPE),
São José, dos Campos, São Paulo - Brasil, 55 12 3208 7164
[(1)]lazaro.camargo, [(2)]walter.abrahao, [(4)]kleber.naccarato, [(5)]auro.tikami,
[(6)]acarlos.pereira, , [(7)]marcus.cisotto,[(8)]cassiano.filho, [(9)]luiz.bueno, [(10)]antonio.brito,
[(11)]angelo.florentino, [(12)]lincoln.teixeira, [(13)]bruno.junqueira, [(14)]andres.horna
[@inpe.br],
[(3)] Institute of Sciences and Technology (ICT/UNIFESP),
jhonathan.pineros@unifesp.br

Abstract

The purpose of the RaioSat nanosatellite mission is primarily to detect both intra-cloud lightning and cloud-to-ground lightning simultaneously, the so-called total lightning data using an optical sensor and a VHF antenna to detect the radio frequency signatures of these lightnings. As RaioSat will only carry a payload to acquire this data for a time-limited mission, the nanosatellite must be launched during a window that maximizes data collection in the lightning season in Brazil, which runs from October to March. Currently, lightning detection from space is implemented with instruments such as the Lightning Imaging Sensor (LIS) on the Tropical Rainfall Measuring Mission (TRRM). Another example is the Geostationary Lightning Mapper (GLM) on Geostationary Operational Environmental Satellites (GOES). With dimensions of 20 cm x 35 cm for the LIS and 150 cm x 65 cm for the GLM, these instruments are big in terms of usability on small satellites. In this paper a proposal for enabling a hardware and software prototype of an optical lightning detection payload for the RaioSat mission is discussed where it is assumed that optical part of the payload is already provided. The current RaioSat nanosatellite prototype is planned for a 3-U-sized cubesat platform initially in a circular orbit with an inclination of approximately 25 degrees and an altitude of 650 km. This results in a complete orbit of 98 minutes with passes through Brazil of approximately 15 to 20 minutes depending on the orbit. The RaioSAT mission intends innovatively to: (i) transfer the technology of optical lightning detection to a nanosatellite platform; (ii) add VHF signal detection and recognition as an effective trigger for lightning events in order to reduce onboard processing and, consequently, payload size and power consumption; (iii) distinguish between cloud-to-ground and intra-cloud flashes using a combined optical and VHF detection technique; (iv) provide worldwide lightning detection capability at low cost and high flexibility using a prospective satellite constellation structure in the future. The payload development strategy includes various incrementing investigation steps: a) prototype the detector using an ARM microcontroller and camera; b) prototype a detector using FPGA and camera; c) development of a mini OBC for testing; d) final validation and testing. This project will be carried out by the Division of Small Satellites of INPE - National Institute for Space Research.

Keywords: *RaioSat, Lightning Flash Detection, Smallsats, Climate Change.*

1. Introduction

Severe weather phenomena are annually responsible for hundreds of deaths and billions of dollars of damage around the world. In Brazil, unlike other hydrometeorological events, severe atmospheric events are random and, therefore, do not have a socio-spatial pattern [8]. Hence, there is a significant motivation to improve the prediction techniques for this kind of events, using high resolution numerical models. A large amount of high-quality observational data is required, including lightning data in a very short-range.

In addition, the detection of lightning flashes produced by storms is important for a wide variety of applications and in some areas of scientific research, which include the understanding of the human action on the climate and how the climate change can affect the behavior of storms in long range.

Basically, the optical detection of lightning from space is measuring the radiation of light, which is emitted by the hot lightning channel and then propagates throughout the atmosphere and clouds (which mainly scatters the light), reaching finally the observer above the clouds. One method to monitor the lightning flashes is the implementation of sensors in satellites to obtain data. In this work a payload proposal for the RaioSat nanosatellite is described which is composed of a dedicated optical camera being developed abroad, a VHF radio and processing unit for data fusion of both former sensors.

2. Problem Definition

The National Institute for Space Research in Brazil (INPE) is recently envisaging Nanosatellite missions, the RaioSat [2] [3] [8] [[5] for example, as a joint work between its Earth Science and Space Engineering areas. In this sense, the objective of the RaioSat project is to develop national technology for detecting lightning flashes from the space, in order to complement the existing data from the ground detection network, BrasilDAT [8]. The RaioSat mission is designed to monitor natural phenomena like lightning flashes which have a correlation to extreme events.

The RaioSat mission is planned to be on board initially on a 3U CubeSat configuration with an operational time lower than one year in a prospective Low Earth Orbita round 650 km of altitude, with inclination between 70° to 99°. The orbit configuration allows good coverage of the interest regions and the Brazilian territory using INPE´s ground stations located in São José dos Campos, SP and Santa Maria, RS if needed. Its payloads and bus subsystems are configured to the CubeSat Standard aiming at low cost and reduced project development time.

The mission analysis has some special requirements such as orbit altitude, the region to cover, use of INPE´s ground stations, the CubeSat platform, the mission timeline, and goals to reduce cost on launch and operations if possible. Therefore, this project phase is relevant by analyzing this mission options and opens the possibility to a multi-mission nanosatellite.

Lightning observation from satellites provides a globally uniform coverage, which is very important for climatological studies. Optical detection of lightning has a long tradition of more than 10 years. On the other hand, ground-based location of lightning over large areas is better performed in the lower frequency radio bands, since the detection range is limited to the line of sight and the Earth’s curvature. A space based optical observation has the advantage of an obstructed view from above the clouds and potentially large field of views using only a single instrument. Basically, the optical detection of lightning from space is measuring the radiation of light, which is emitted by the hot lightning channel and then propagates throughout the atmosphere and clouds (which mainly scatters the light), reaching finally the observer above the clouds.

3. Proposed Solution

The proposed approach is to employ on-board sensors inside the RaioSat nanosatellite so that lightning imaging can be triggered by a VHF signal which proper signature anticipates the lightning events. The sensors on board of satellites allow a wider coverage, detecting lightning with the same efficiency, and with identical temporal and spatial resolutions. The data planned to be provided by RaioSat sensors will be made available to end users and will complement the information from the BrasilDAT network.

Therefore, there is a strong motivation to improve the forecasting techniques for severe atmospheric events using numerical weather prediction (NWP) models. A study published in the scientific literature show that the assimilation of lightning flashes data in high spatial and temporal resolutions models can provide an improved representation of convection at the beginning of the forecast [3].

The National Institute for Space Research (INPE) promotes means of technological and scientific development, meeting internal and external demands through project coordination, mission analysis, management, including the execution of the RaioSat project. The institute promotes the synergy between educational and research institutions (national and/or international) according to its mission: produce science and technology in the space areas and the terrestrial environment and offer unique products and services for the benefit of Brazil.

4. Fundamental optical feasability

When observing lightning flashes more than 50% of the flashes have a duration of at least 300 ms. [1]. However lightning flashes consists of a series of pulses, also known as strokes, which have a mean pulse width of just about 400 µs [4]. These strokes serve as optical signal source of the calculation model. A lighting stroke emits 5%-10% of the optical energy at the oxygen line of a wavelength of 777.4 nm. [4] Therefore, optical lighting detection is performed at this wavelength, the same as in the LIS and GLM detectors.

Goodman, Christian and Rust performed lightning stroke measurements above clouds using a high-altitude aircraft and found that the median radiance Ls at cloud top is ap-proximately 7x10-3Wm-2sr-1 for 777.4 nm. [4] They used a point source approach to de-scribe the total source radiances (for the hole optical spectrum) of a stroke and calculated values in single digit multiples of 108 W. [4] Respectively for the wavelength of interest a fifth to a tenth of these source radiances can be expected. For the following calculations, a source radiance PS of 30x106 W for a wavelength of 777.4 nm is used. This value is based on a conservative total source radiance of 3x108 W. The cloud top area which gets illuminated by a point source modeled stroke has an expansion of about 20x20 km2.

After describing the signal source, the number of photons reaching the satellites'optics can be calculated by using various orbit altitudes $\boldsymbol{h_o}$ and apertures $\boldsymbol{d_c}$. In this first step, no noise sources like background illumination are considered. The signal duration $\boldsymbol{t_s}$ is much smaller than the exposure time $\boldsymbol{t_e}$ when using a frame rate of 500 frames per second (fps) ($\boldsymbol{t_s}$ = 400 µs; $\boldsymbol{t_e}$ = 2 ms). Consequently, the number of photons generated by a stroke in the wavelength of interested can be estimated using the equation (4.1). To consider losses in the optics a transmission factor τ of about 0.8 is introduced.

$$N = \frac{(P_S \cdot \frac{d_C^2}{4} \cdot \pi) \cdot \tau}{(4\pi \cdot h_O^2)} \cdot \frac{\lambda}{c \cdot h \cdot t_S} \qquad (4.1)$$

In figure 1 the effect of orbit altitude and aperture on the number of photons can be seen. As expected, the numbers shrink with increasing orbit altitudes and decreasing apertures. But fundamentally the diagram shows that a decent amount of photons reaching the optics when using realistic apertures and orbit altitudes.

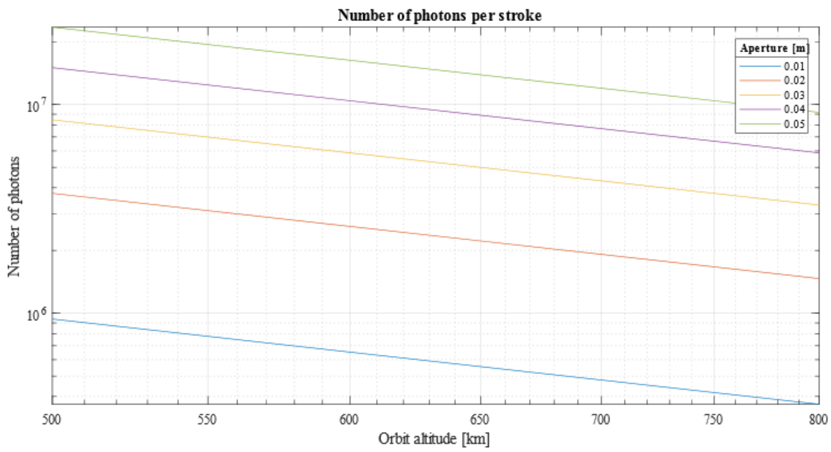

Figure 1 - Number of photons per stroke reaching the optics without noise.

To enhance the significance of the results, not the total number of photons, but the number of photons per active pixel cell of the image sensor has to be analyzed. A region of interest (RIO) of the image sensor size of 544x544 pixel and a field of view (FOV) of 600 x 600km2 seem reasonable. That means, that the FOV gets projected onto 544 x 544 pixels, consequently a stroke with an illuminated area of about 20 x 20km2 gets projected to 18x18 pixel. Therefore, every value of the calculations shown in figure 1 have to be divided by 320 to result in the number of photons per pixel of the image sensor. With typical CMOS image sensor properties like quantum efficiency (0.3), fill factor (0.4), full well capacity (20000e-) and conversion gain (25µV/e-) also the expected pixel output voltage can be evaluated.

5. Vhf trigger approach

Lighting does not just produce an optical signal, but also certain signatures in the VHF range. The possibility of using these lighting generated VHF signals to trigger the optical lighting detection shall reduce the number of frames, which have to be processed and also the computational effort in general. A processing time for an incoming VHF signal of around 200 ms is expected using a software-defined radio (SDR) with a sampling rate of 2M samples/s. Because of the duration of processing the VHF signal, a certain amount of image data always has to be cached. For better understanding, the following chapter gives a rough overview of the different components of the lighting detection payload and their communication.

Common thunderstorm/lightning discharge processes such as return strokes, leader steps, and normal intracloud discharge events have similar radio frequency (RF) spectra that roll off above about 10 MHz. Compact Intracloud Discharges (CIDs), however, radiate strongly in the HF and VHF band, with a relatively flat spectrum extending to at least 50 MHz. The VHF power of Narrow Bipolar Events (NBEs) can vary over many 48 orders of magnitude, with the largest value reaching 50 dBW [6].

One of the payloads of the RaioSat mission, will be a VHF radio receiver, to assist in the identification of the occurrence of lightning. This receiver to be implemented will be of the type SDR (software defined radio) in order to meet the mission requirements regarding energy consumption, physical size, thermal dissipation, and signal processing on board [7].

The VHF SDR receiver of the RaioSat mission will have the function of verifying the electromagnetic signature of the rays to authenticate its events. For the development of the receiver, the open-source project (hardware and software)

Tests on ground, balloons and environmental (vibration and thermal) will be carried out to check if the proposed receiver meets the requirements of the RaioSat mission.

6. Conclusion

RAIOSAT will be of great value to the Brazilian risk and disaster management system. A constellation of cubesats will allow an extension of the revisit rate compatible with the forecast of the Brazilian territory and help in the forecast of severe weather and for weather forecasting in the very short term. Because several storms are associated with the occurrence of lightning and electrical discharges and the RAIOSAT mission can contribute with measures to combat extreme events.

References

[1] Ballarotti, M. G, C. Medeiros, M. M. F. Saba, W.Schulz, O. Pinto Jr., Frequency distributions of some parameters of negative downward lightning flashes based on accurate-stroke-count studies, Journal of Geophysical Research, 2012.

[2] Carretero, M.A.; Naccarato, K.P. Detection of total lightning flashes onboard of a CubeSat satellite. In: 1st Latin American Cubesat Workshop (1st LACW), Brasilia, Brazil, 2014.

[3] Fierro A, Mansell E, Ziegler C, MacGorman D - Application of a Lightning Data Assimilation Technique in the WRF-ARW Model at Cloud-Resolving Scales for the Tornado Outbreak of 24 May 2011. Mon Wea Rev 140(8):2609-2627. https://doi.org/10.1175/MWR-D-11-00299.1, 2012.

[4] Goodman S., Mach D., Koshak W., Blakeslee R., Algorithm theoretical basis document GLM Lightning Cluster-Filter Algorithm, NOAA NESDIS Center for satellite applications and research, 2012.

[5] Julio Filho, A.C., Tikami, A., De Paula, E.S.F., Piñeros, J.M., Fernandes, G.F., Camargo, L.A.P., Santos, C.A.M.B., Dos Santos, W.A., Naccarato, K.P., CubeSat Development for Lightning Flashes Detection: RaioSat Project. JOURNAL OF AEROSPACE TECHNOLOGY AND MANAGEMENT (ONLINE), v. 1, p. 80-93, 2020.

[6] Liu, N., Dwyer, J. R., Tilles, J., Stanley, M. A., Krehbiel, P. R., Rison, W., et al. (2019). Understanding the radio spectrum of thunderstorm narrow bipolar events.

Journal of Geophysical Research: Atmospheres, 124, 10134– 10153. https://doi.org/10.1029/2019JD030439

[7] Moura, C.O. Análise de viabilidade de uma carga útil óptica em nanossatélites para detecção de raios (Master Dissertation). São José dos Campos: Instituto Nacional de Pesquisas Espaciais. In Portuguese, 2017.

[8] Naccarato KP, Pinto Junior O - Lightning detection in Southeastern Brazil from the new Brazilian Total Lightning Network (BrasilDAT). Paper presented 2012 International Conference on Lightning Protection (ICLP). IEEE; Vienna, Austria. https://doi.org/10.1109/ICLP.2012.6344294, 2012b.

NEAR EARTH ASTEROID CUBESAT MISSION: SELECTION OF THE BODY AND DISCUSSION ON THE MISSION REQUIREMENTS

Damiana Irrera(1), **Juan D. Blanco Camargo**(2)
(1) *Dipartimento di Scienze e Tecnologie Aerospaziali (DAER), Politecnico di Milano, damiana.irrera@mail.polimi.it*
(2) *Departamento de Ingeniería Aeronáutica, Fundación Universitaria Los Libertadores, jdblancoc@libertadores.edu.co*

Keywords: *Asteroid, NEA, CubeSat, deep-space, requirements*

Abstract

Nowadays, the use of planetary resources is becoming more critical, forcing humanity to deal with an environmental emergency. For this reason, the space industry is studying Near Earth Asteroids as a new solution to obtain sustainable resources, which also allows a deeper understanding of the history of our Solar System. However, space mining technology would have an unfeasible cost for the current space market. In this context, small Satellites or CubeSat's usage can reduce costs and increase the accessibility of certain investigations.In this paper, the selection of a Near Earth Asteroid is first discussed based on information about the composition, trajectory, and accessibility, as well as other properties from an extensive literature review. CubeSat's possible applications are then analyzed in order to define the mission objectives and requirements over a selected asteroid. In sum, this article may be useful in understanding the various selection criteria for a Near Earth Asteroid where CubeSat missions could be carried out in the very near future.

1. Introduction

Mineral resources have been a dependent means of human beings as they have assumed the main role as a source of manufacturing new useful tools for society. However, these elements are finite, non-renewable and some of them are rare to find on our Planet. This demand for mineral elements will not stop growing as emergeing economies and global population will have a directly proportional increase [10], therefore an alternative to obtaining resources is required. Space mining emerges as a solution thanks to the composition of Near Earth Asteroids (NEAs); it has been understood they can assume a strategic role because of their minerals that could be used on Earth. On the other hand, NEAs carry a great source of information related to the primordial phases of our solar system, having been formed in that phase [23]. They are therefore important because they contain evidence on the formation process of the Milky Way and how the Sun influences the Planets' formation [19].

Generally, asteroid mining remains hypothetical, mostly because of its high costs [28]. However, despite it, it is believed to be a worthwhile technology because of the invaluable resources offered by the asteroids, as well as the number and variety of asteroids that can be studied; according to [28], the asteroid 16 Psyche has been reported to contain US$700 quintillion worth of gold, enough for every person on earth to receive about US$93 billion.

In order to think about this type of mission in a more viable way, it is necessary to find a way to reduce mission costs. Thus, the use of small satellites like CubeSats has been proposed in this paper as an alternative use. The low-cost nature of CubeSats and their ability to accept a higher risk posture opens the opportunity provided to the mission design [6].

ESA's Hera Mission [6], proposes the use of two 6U CubeSats, which will be deployed in the vicinity of the Didymos asteroid to contribute to the composition research and mitigation assessment objectives of the mission.

However, due to the possible limitations that these types of satellites may have when operating in these environments, it is necessary to determine the different challenges that need to be faced, including radiation, limited communication opportunities, and how far small satellites can go operating in these conditions. In this paper, the first phases of the mission design are going to be discussed, in such a way to understand the major problems as well as the main objectives of these types of missions.

The selection of the asteroid (body) is a fundamental phase; the large number of possible candidates makes the optimal planning of such a mission very challenging because it has to consider scientific interest, composition, orbital dynamics, and available launch windows, among others.

2. Literature Review

In the search for long-duration deep space missions, bodies with a scientific interest have been found, and have been called Near Earth Objects (NEO's), from which the acronym for Near Earth Asteroids (NEA's). *Figure* 1, shows the accumulative number of known Near-Earth Asteroids (NEAs) versus time. Totals are shown for NEAs of all sizes, those NEAs larger than 140m in size, and those larger than 1km in size.

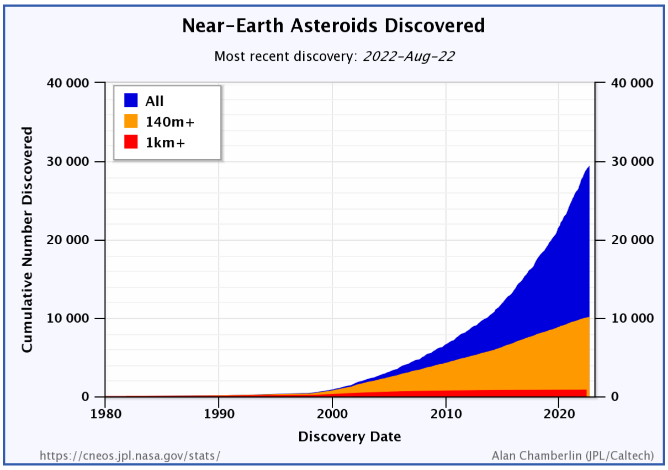

Figure 1: ***NEA's discovered to date (Aug, 2022). [15].***

2.1. Asteroids Division

NEAs are those asteroids that during their orbital motion get in proximity of our planet, their orbits span the entire region between Earth (1 AU) and Mars (1.52 AU). Particularly, to be recognized as an NEA, an asteroid needs to have its perihelion (q) less than 1.3 AU. According to the orbital elements of these asteroids, they can be divided into three groups: Amor, Apollo, and Aten. *Figure* 2 shows the orbits of these three groups of asteroids.

• **Amor**: the characteristic of this group is that the bodies have their perihelion greater than the Earth's aphelion $(q > 1.017AU)$ and they cross Mars' orbit. Because of their proximity to the Earth, they are representing one-tenth of the potentially dangerous object for our planet.

• **Apollo**: this group of asteroids has the characteristic of having their perihelion smaller than the Earth's aphelion $(q < 1.017AU)$, Apollo group is therefore crossing our planet's orbit. They represent the largest group of NEAs, and lots of them are classified as potentially hazardous objects (PHO). Some of them are as well crossing Mars' orbit.

• **Aten**: this group is as well an Earth-crossing asteroid group $(q < 1.017AU)$, but their location is limited to being inside Mars' orbit. Also in this case, many of the Atens are classified as PHO.

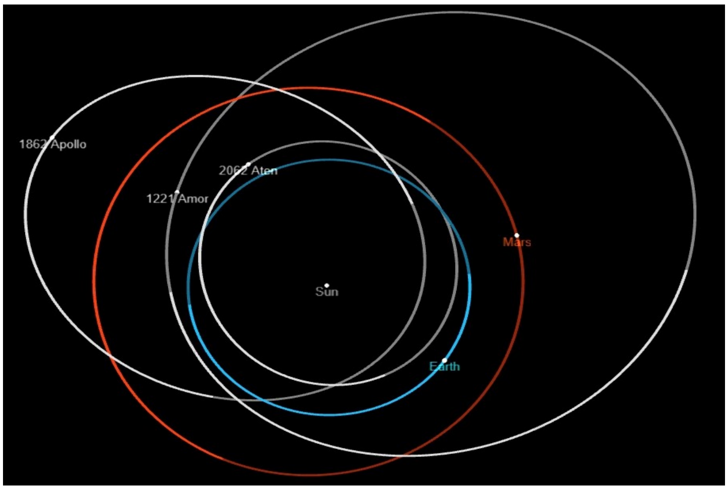

Figure 2: ***NEA's classification-orbit.***

The following table shows the number of asteroids known by type, as of September 2022 according to [16].

Table 1: ***Number of asteroids know to date (Sept, 2022).***

Asteroid type	Quantity
Amor	10757
Apollo	16559
Aten	2324

In addition to this last classification, asteroids are also divided depending on their composition and their emission spectrum, as it is shown in *Figure* 9. Particularly, only the

C, S, and M types are considered in this paper, as the ones that can have a major scientific interest in the current state of the art [18].

According to [18], the following definitions:

• **C-type (carbonaceous)**: water-bearing with very high contents of opaque, carbonaceous material. They are mainly made up of carbonaceous elements, such as rich in carbon-based compounds, this gives them the characteristic of having a very low albedo.

• **S-type (stony)**: anhydrous rocky material, consisting of silicates, sulfides, and metals.

• **M-type (metallic)**: high radar reflectivity characteristic of metals.

	Mineral	C2-type	C1-type	S-type	M-type
Free metals	Fe	10.7%	0.1%	6-19%	88%
	Ni	1.4%	—	1-2%	10%
	Co	0.11%	—	0.1%	0.5%
Volatiles	C	1.4%	1.9-3.0%	3%	—
	H_2O	5.7%	12%	0.15%	—
	S	1.3%	2%	1.5%	—
Mineral oxides	FeO	15.4%	22%	10%	—
	SiO_2	33.8%	28%	38%	—
	MgO	23.8%	20%	24%	—
	Al_2O_3	2.4%	2.1%	2.1%	—
	Na_2O	0.55%	0.3%	0.9%	—
	K_2O	0.04%	0.04%	0.1%	—
	P_2O_5	0.28%	0.23%	0.28%	—
	CaO	—	—	—	—
	TiO_2	—	—	—	—
Physical	Density (g/cm^3)	3.3	2.0-2.8	3.5-3.8	7.0-7.8

Figure 3: ***NEA's classification-type. Adopted from [18]***

2.2. Space Mining

Space mining arises as a solution to the scarcity of mineral resources on Earth, due to the high consumption of terrestrial resources, it is necessary to search for new sources of materials. However, to study the feasibility of space mining, four fundamental questions must be taken into account: where are the space minerals, what resources do they offer, how to extract them and how to make them useful [9].

This industry can bring with it many advantages, one of them is that despite the high costs that this type of mission can have, the economic benefits it generates are greater because of the value on Earth of the metals that can be extracted from the thousands of asteroids is much higher; due to a large number of asteroids another advantage is that there is a variety in the type of resources that could be exploited and on the other hand, the development of new advanced technologies improving space exploration activities.

In this regard, CubeSat mission can play a significant role on the study of the feasibility of the space mining, as it is explained in the next paragraph.

2.3. CubeSats and Applications

The use of CubeSats for deep-space exploration, particularly for asteroids, has the potential to open the door to more affordable missions, and therefore plays an essential role in a more in-depth study of NEAs.

2.3.1. Mission types

The small size of the CubeSats makes them versatile for science observation missions, for instances determining the characteristics of an asteroid, such as its shape and surface properties, internal structure, or rotational state [8]. Moreover, identifying in-situ resources present in the Asteroid is the essential step for an hypothetical future extraction.

Conducting focused science investigation around asteroids is therefore fundamental to explore our Solar System and having a better understanding about its formation and evolution. Moreover, science observation could be useful for other application, such us helping planetary defence solutions and monitoring the space weather.

2.3.2. Destination and Configuration

Considering the current situation of space exploration, the most feasible destination for CubeSats deep space mission is the Inner Solar System, which is considered affordable for Cubesats and Nanosats in free-flying as much as in mother-daughter configuration. This is the case of the asteroids considered in this work, whose orbits pass in proximity to our planet.
Particularly, it is interesting to see that the Asteroid Belt is a convenient place for interplanetary CubeSat missions; indeed, it is close enough to the Sun to use solar power generation, and sufficiently near to the Earth to communicate with it.

In the case of missions in the Outer Solar System, only the mother-daughter configuration is currently compatible. However, such a configuration turns out to be extremely expensive, so it would be advantageous to be able, at least in the case of exploring the Inner Solar System, to reach Asteroids directly via CubeSats, in this way several missions could be carried out at the same cost as the ones in a mother-daughter configuration [8]. Such a statement finds application in the M-Argo mission by ESA, the first stand-alone CubeSat mission for deep space, which demonstrated to cut the entry-level cost of deep-space exploration by about a factor of ten [4].

2.4. Mission Analysis

Mission analysis is necessary for three key aspects:

• To establish mission constraints.
• To determine how best to achieve the mission objectives
• To demonstrate the feasibility of the mission.

Since the mission taken into consideration is interplanetary, we need to expect some differences from LEO missions, for which at the moment CubeSats components are developed. The table shows the most important parameters that differ and the ones which remain comparable between deep space and LEO CubeSat mission.

Table 2: ***Parameters Cubesat Interpletary Missions vs LEO Missions. Adapted from [8]***

Differences
Operating environment (radiation tolerance-mission duration)
Telecommunications
Navigation to a variety of destinations
Instrumentation
Onboard data storage and processing
Operations autonomy
Transit as a secondary payload
Propulsion

Similarities
Structure and mechanical systems
Thermal control
Attitude determination and control

3. Asteroid Selection Criteria

The following process was adopted to select one or more asteroids for which an interplanetary, stand-alone CubeSats' mission might be suitable.

Firstly, those asteroids which, if visited, would be the most effective in terms of costs have been identified. The selection was made using the asteroid database at reference [2].

From this first classification, asteroids from Amor, Apollo, and Aten groups have been identified. They are classed as NEAs, and therefore they would be accessible by a CubeSat in free-flying. In further detail, asteroids that can scientifically impact the present society have been taken into account, and in particular C-type asteroids have been favored due to their high mineral content.

Subsequently, only those asteroids for which the incoming approach to Earth is expected to be not excessively distant from now, were considered. A time window from 2025 to 2030, considering the immediate construction of the CubeSat, is assumed as the optimal interval. However, those asteroids, which approach the Earth at least twice in one/two year period, have been advantaged; in this respect, considering that it is assumed to approach the body in the minimum possible time, the launch window which is possible to consider, results to be larger and it allows redundancy in case the launch is delayed.

Table 3 shows this first asteroids selection and respectively, *Figures* 4 and 5 shows their orbits.

Table 3: ***Selected Asteroids from [2]***

Name	Group	Type	Incoming approach years & Distance	Diameter (km)	Profit ($)
175706 (1996 FG3)	APO (PHA)	C	Mar 08, 2023: 0.398 AU Aug 06, 2023: 0.326 AU Jan 28, 2024: 0.421 AU Dec 10, 2025: 0.346 AU	1.196	181.34 billion
308635 (2005 YU55)	APO(PHA)	C	Sep 07, 2026: 0.314 AU Nov 29, 2026: 0.382 AU Sep 13, 2031: 0.298 AU Nov 22, 2031: 0.353 AU	0.4	6.23 billion
152563 (1992 BF)	ATE	Xc	Aug 18, 2023: 0.328 AU Feb 09, 2024: 0.141 AU Dec 08, 2029: 0.158 AU Jun 16, 2030: 0.348 AU Feb 27, 2031: 0.308 AU	0.272	357.67 million
136793 (1997 AQ18)	APO	C	Dec 21, 2023: 0.315 AU Aug 16, 2028: 0.412 AU Jun 14, 2033: 0.282 AU	0.465	28.82 billion

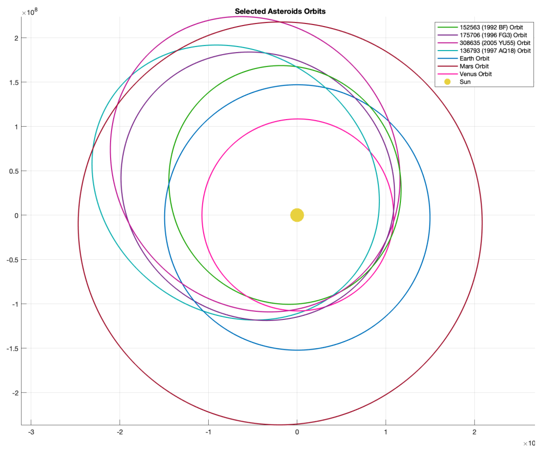

Figure 4: ***Orbits of asteroids x-y plane view***

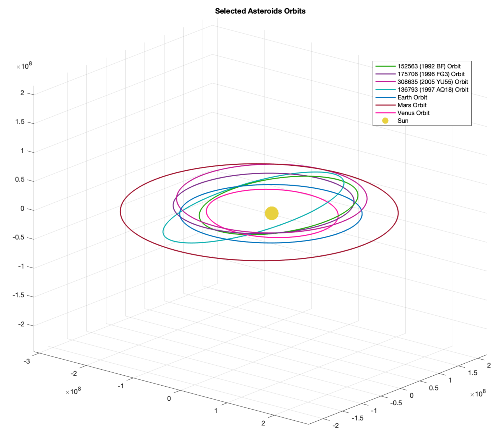

Figure 5: ***Orbits of asteroids 3D-view***

Finally, considering all of these aspects, from the four asteroids selected, the one that is taken into consideration for the study of the mission objective and requirements is 152563 (1992 BF), Xc-type asteroid from the group Aten. Particularly, additional characteristics of the asteroids were taken into account for the final selection, where the selected one stood out for:

• Larger number of the incoming Earth approaches inside the time region that was established as optimal, which allows for having more reliable launch windows.
• Smaller diameter compared to the asteroids' average. This makes it more feasible and easier for CubeSat to fulfill the mission.
• According with [20], Xc [1] type asteroids is likely to contain iron, nickel, cobalt, and platinum. Those are the primary elements for which the supply is limited on our planet [1], which make the asteroid interesting for a future exploration.

To have the choice that fit the most with our case, we have also taken into account some deeper information about the other asteroids:

• From literature review it is not able to have the same amount of data information for 08635 (2005 YU55) and 136793 (1997 AQ18), as the other two asteroids, for this reason, they have been discarded from this choice. Moreover, they are not viable for a human exploration mission [14].
• Analyzing the two asteroids, it was found that asteroid 152563 (1992 BF) has a lower delta-v (10.997 km/s), a shorter mission journey (402 days), and a higher number of potential trajectories and launch windows (2412) [20], compared to 175706 (1996 FG3) (Δv=11.274 km/s; 450 days of mission; 44 potential trajectories and launch windows)[21].

3.1. Asteroid orbital parameters

Following, at *Table* 4 the orbital elements [2] of the selected asteroid 152563 (1992 BF); *Figure* 6 and *Figure* 7shows its orbit with respect to Earth, Mars and Venus.

Table 4: ***152563 (1992 BF) Orbital Parameter***

Orbital element	Value
a	0.9076334600205421 AU
e	0.2715220060918418
i	7.257078311192453 deg
node	315.2585372927887 deg
peri	336.6004778334427 deg
M	314.759406494199 deg
period	315.8378492591373 days
Q	1.154075917881399 AU
q	0.6611910021596851 AU

[1] According to [25], X-class asteroids miss the albedos information needed to classify the asteroid correctly. However it is possible to sub-categorize this group depending on the degree of the object's reflectivity (dark, intermediate, bright). Subcategory Xc which have a spectral feature in the range of 0.55 m to 0.8 m, is allocated in the "dark" spectrum.

[2] a:semi-major axis; e:eccentricity; i:inclination; node:right ascension ascending node; peri:argument of perihelion; M:mean anomaly; period: sidereal period; Q:aphelion distance; q:perihelion distance.

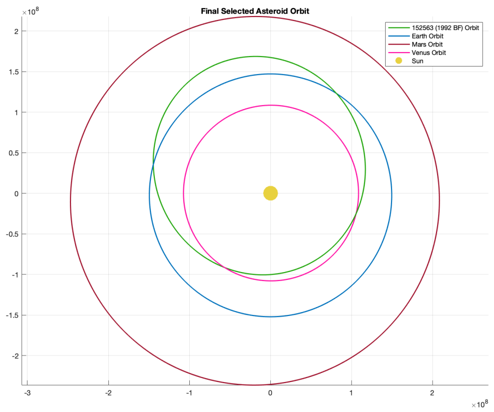

Figure 6: ***152563 (1992 BF) 2D-view Orbit***

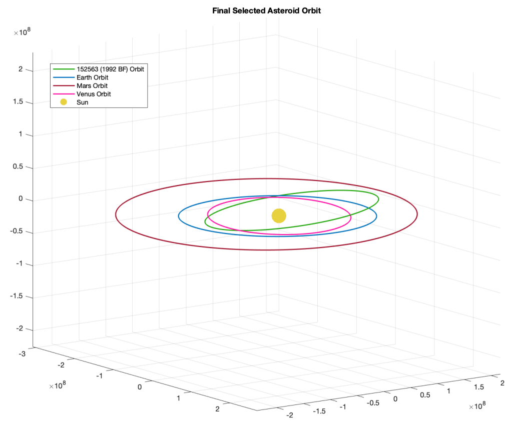

Figure 7: ***152563 (1992 BF) 3D-view Orbit***

4. Discussion of Requirements

Taking into consideration what has been discussed in *Paragraph 2.3* about the most affordable missions for a small satellite in asteroids, in the following section the general requirements for a scientific interplanetary CubeSat in a free-fly mission, with emphasis on 152563 (1992 BF), have been discussed, both the mission requirements and the spacecraft system requirements.

4.1. Mission Requirements

In the following subparagraphs, the mission requirements the team has considered the most affected by the difference between an LEO and deep-space missions have been studied, with particular attention to Performance, Reliability, Cost, and Lifetime of it.

4.1.1. Performance

Since each mission operates with a spacecraft designed specifically for it, and every spacecraft have different subsystems that work at respective quantifiable values, it is allowed to think that each mission has its specific performance requirements. These requirements will therefore always depend on the payload and how its systems and instruments should function, e.g. image quality, sensitivity, frequencies, AOCS, GNC, and structure, among others [8]. However, it is important to note that regardless of the mission, these requirements must always be verifiable, and that verification can generate requirements for testing them. Such performance verification can be found in standards such as those described in [5].

• Performance tests shall verify that the space segment equipment performances, under the specified environment, are compliant with the performances specification.

4.1.2. Reliability

Reliability is one of the most critical parameters within space systems, and the research for possible causes of in-orbit failures is always on to identify and eliminate them through various types of tests before launch. Several parameters affect the mission reliability, among them are mission type, orbit, propulsion, or spacecraft complexity.

Some specific parameters will be analyzed to understand which conditions should be reviewed and which, according to each mission, should have specific requirements, among these factors are:

• Environmental factor: it is important that such conditions be identified accurately at the beginning of the design process, in order to establish this type of requirements, it is recommended to make use of reference [12], which shows a wide variety of parameters and how they affect the reliability of this type of mission, and section 4.2.1 is more specific on this topic.

• Space Debris: This factor is determined by impact probability, depending on orbits, structural configurations, there are relations that allow to determine this statistic, for specific missions review reference [13].

• Redundancy: in the design phase it is helpful to think that none of the components will be able to function reliably on its own, so the decision to use systems with active reliability allows for guaranteeing good performance and lifetime of the system and/or mission. The use of redundancy may bring disadvantages such as higher cost, weight, and greater complexity, but greater safety and reliability are gained. This is why for each specific mission it is necessary to analyze the use of redundant systems. Reference [11], can help determine the appropriate decision to use or not this type of system.

Finally, it is recommended to follow general standards when designing CubeSat space missions, such as the FMEA (Failure Mode and Effects Analysis) method that supports RAMS (Reliability, Availability, Maintainability, Safety) allowing the engineer's understanding of the desired functional product performance through systematic and documented analyses.

4.1.3. Cost

The use of small satellites for deep space missions allows to reduce costs; this is one of the reasons for interest in the use of CubeSats for space exploration missions. The MarCO mission was a technological demonstrator of the use of CubeSats for interplanetary missions [8]; considering the costs, it was forty times less than most NASA Discovery missions and a schedule of 15 months from concept to first flight article.

According with [7], the Life Cost Cycle (LCC) of these kind of missions is USD ($500M–$1B). Generally, missions of this type have a division of costs as follows:

Table 5: *Costs*

Total Mission Costs	Satellite costs	Launch costs	Orbital operations costs over lifetime
100%	70%	20%	10%
$500M	$350M	$100M	$50M

Table 5 shows an example of a low-cost mission, particularly, the total cost $500M USD is shown [7] and the respective percentage for each variable has been calculated. However, [7] considers ”$Non - HumanSpaceFlightandScience/RoboticMissions$”, which do not specifically take into account CubeSats that have been shown to allow for differential cost reduction. Thus, references [17] and [7], show that the Satellite costs component alone represents $< 30MUSD$, therefore Table 5 could be re-estimated.

Table 6: ***CubeSatMission Costs***

Total Mission Costs	Satellite costs	Launch costs	Orbital operations costs over lifetime
100%	70%	20%	10%
$43M	$30M	$9M	$4M

The above estimation may vary somewhat depending on the mission, however, the cost reduction enables higher risks and innovations which, if proven on CubeSat missions, will then lower the costs for larger missions as well in terms of operations.

4.1.4. Lifetime

Considering the current state of the art, CubeSat's interplanetary lifetime requirements still need further development. This is evident in Figure 8, which shows the number of documents concerning the number of publications. [3]

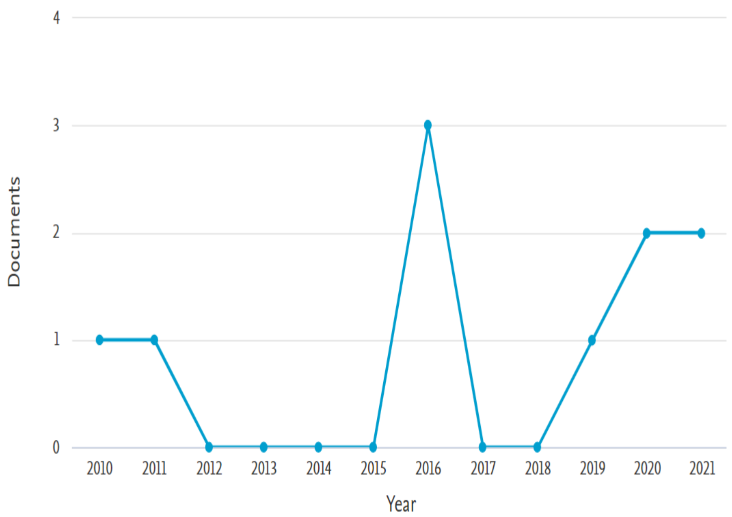

Figure 8: ***Number of documents VS number of publications (Interplanetary lifetime cubesats)***

However, some parameters can be rescued from the literature, among these:

[3]SCOPUS database has been used. Keywords: interplanetary, lifetime, cubesat

• According to the IADC[4] Space Debris Mitigation Guidelines [27] it has been found 25 years to be a reasonable and appropriate lifetime limit for these types of missions. After this period, the spacecraft should be deorbited (direct re-entry is preferred). In addition to that, it is important to mention the statement that an interplanetary CubeSat must be able to function reliably for months to years, while the lifetime of many CubeSats (in LEO) so far has been measured in days or weeks [26], however, the lifetime is for the majority less than 1 year. Generally speaking, it is admissible to consider that the operational lifetime for interplanetary CubeSats shall exceed 5 years [3].

• For an Interplanetary CubeSat, the sail film material lifetime limitation must be addressed [22]. Since aluminized KaptonTM has a much longer lifetime than other materials during solar ultraviolet exposure, it is recommended for this application.

4.2. Spacecraft System Requirements

In this section are reported the requirements related to the spacecraft system, particularly it is explained how some consideration regarding the mission influence the future design of the spacecraft.

4.2.1. Orbit and Environment

As it is now clear, the CubeSat needs to deal with deep space travel, particularly, it needs to approach the selected asteroid 152563 (1992 BF), which, as it is reported in the previous paragraph, is crossing Venus' and Earth's orbits as shown in *Figure* 6. In general, some consideration regarding the Attitude and Orbit Control System (AOCS) of the CubeSat needs to be done:

• AOCS must be able to control the spacecraft during all its deep space travel.
• AOCS must be able to perform the asteroid insertion maneuvers.
• AOCS must be able to allow to perform correction manoeuvres.

Especially, focusing on the closeness to Venus, it is necessary to consider its proximity to the Sun, and therefore the high solar radiation to which the spacecraft will be subjected; it could damage different spacecraft components, therefore some constraints are imposed:

• The scientific payload should not be disturbed by Sun radiation. In general the s/c[5] shall have a good thermal control system.
• The s/c solar arrays shall be able to resist to high temperature.
• The scientific payload and system instrumentation (as attitude sensors) should not be disturbed by the Sun light.

The proximity to Earth orbit allow to have good communication with the ground. However the mission is still interplanetary, therefore following the most significant requirements:

• The CubeSat shall have a telecommunication system able to communicate with Earth during all the cruise and the operations, as well as transmitting health status, through other spacecrafts or directly with the ground stations.

[4] Inter-Agency Space Debris Coordination Committee (IADC)
[5] s/c: spacecraft

• The CubeSat needs to have a redundancy on the antennas, in such a way it is able to communicate with Earth during the eclipses phases.

4.2.2. Power and Propulsion

The power system needs to deal with some different issues from the usual LEO CubeSat mission. Particularly, a big amount of ΔV is needed to be carried by spacecraft to achieve the goals of a deep space mission. In this instance, it is interesting to cite some propulsion systems that it is possible to take into consideration to reach the objectives of an interplanetary mission that doesn't differ to much in terms of distance with respect to the asteroid 152563 (1992 BF) case. It could be the case of cold gasses, which in general have a light system weight and can carry a high ΔV, this solution has been used for NASA/JPL's MarCO, the first interplanetary CubeSat mission around Mars [8]. It is also useful to take into account electric propulsion, which can reach a very large value of specific impulse and not requires pressurized propellants that would overload the spacecraft, however, it has smaller ΔV compared to cold gas. Particularly, two of the 13 CubeSats that will be sent to the Moon in Artemis 1, Lunar Ice-Cube and LunaH-Map, will carry a Busek RF ion propulsion system. [8] It is clear that other solutions could be taken into consideration and that a deeper and specific study should be done for each specific mission.
Following the requirements regarding the power system the team considers the most relevant for our mission type has been listed.

• The propulsion systems needs to be capable of generating enough ΔV to support trajectories from Earth escape or from GEO transfer to interplanetary destinations, and operate. Particularly, it has to taken into account the objective asteroid 152563 (1992 BF) $\Delta V = 10.997 km/s$

• The propellant shall carry enough ΔV to allow correction maneuvers, that eg. could be due to environmental disturbances. (In general, since 152563 (1992 BF) is a pretty small body, those corrections shouldn't demand a huge ΔV).

• The solar array must be able to give the right amount of energy to allow the s/c instruments to work properly.

• The solar array needs to charge the batteries during the light phases, in such a way the s/c has power during eclipse phases.

4.2.3. Operation

In this section are considered the requirements related to the operation that the CubeSat is going to take into account during the mission. Despite the fact, the mission objectives have not been discussed in this work, as mentioned in *Paragraph 2.3* the major goal of this type of mission is to study geophysical structure, dynamical state, taking images, analyze the subsurface and asteroid elements. Therefore, the only requirements taken into consideration in this section have been the following:

• The s/c must have a scientific payload capable of achieving those goals.
• When an instrument of the payload is operative should not interfere with and disturb the others.

Notice that for a deeper study, should be defined other requirements, such as the mission autonomy level, modes of operation definition, and preference operational order, taking into account the asteroid 152563 (1992 BF) properties.

4.2.4. Configuration

It is reasonable to think that based on the principal goals of the mission, the type of CubeSat that could fit the most for it is a 3U. This solution has been chosen considering other asteroid missions with a similar aim, as can be noted in the following picture [24].

name	organization	system	mission	payload
ASPECT: Asteroid Spectral Imaging	VTT, Uni. Helsinki, Aalto Uni.	single 3U CubeSat with <1° pointing, cold gas propulsion 1 m s^{-1} Δv	spectral imaging of Didymoon before/after impact from 4 km orbit	imaging spectrometer in VIS/NIR: 1–2 m GSD; SWIR spectrometer
DustCube	Uni. Vigo, Uni. Bologna, MICOS	single 3U CubeSat with cold gas propulsion 2 m s^{-1} Δv, optical IR rel. navigation	characterize ejected dust plume after impact from 3–5 km orbit, transfer to L4/L5 orbit pre-impact, DRO 280 m alt. post-impact	*in situ* nephelometer, remote nephelometer
CUBATA	GMV, Uni. La Sapienza, INTA	two 3U CubeSats with cold gas propulsion Δv 1.5 m s^{-1}, <1° pointing, optical rel. navigation	gravity field determination of Didymos system before and after impact	radio science: Cube-Cube LoS Doppler tracking with S-band transponder and ultrastable oscillator
PALS: Payload of Advanced Little Satellites	Swedish Institute of Space Physics, KTH, DLR, IEEC, AAC Microtec	two 3U CubeSats with cold gas propulsion 12.5 m s^{-1} Δv, <1° pointing, optical rel. navigation	magnetization, bulk chemical composition, presence of volatiles, super-resolution surface imaging of Didymos components impact ejecta via tour of Didymos system	narrow angle camera, volatile composition analyser, fluxgate magnetometer, video emission spectrometer
AGEX: Asteroid Geophysical Explorer	ROB, ISAE Supaero, Emxys, Antwerp Space	two 3U CubeSats: one lander, one orbiter	determination of dynamical state, geophysical surface properties, subsurface structure of Didymoon before/after impact	lander: three-axis seismometer, accelerometers, three-axis gravimeter; orbiter: 30 chipsats deployed to surface

Figure 9: ***ASPECT, DustCube, CUBATA, PALS, AGEX information from [24]***

The configuration of the payload and spacecraft subsystems choice has to take into account several consideration, such as thermal problems, high solar radiation, telecommunication.

• The subsystems and payload that are thermally sensitive, should be placed in the spacecraft faces that remain far away from the sunlight.
• The thermally sensitive sensors, should be turned off when the sunlight passes through the face where they are placed in. (eg. case of stellar attitude sensor)
• The antennas should be placed in the faces which allow them to have the best communication with the ground
• The solar arrays should be placed in the direction and angle of the sun that allow them to store the maximum energy, without damaging the array (which can be possible considering the 152563 (1992 BF) orbit).

5. Conclusion

The following paper aims to firstly give the reader an understanding of what is the purpose of a deep-space CubeSat mission, and whether it is feasible. Free-flying CubeSats usage, which economically speaking represents the best solution, is possible to reach asteroids that live in the inner solar system; especially, NEAs have considered the best options thanks to their closeness to our planet. These type of missions find their purpose in scientific studies, which is deemed to be helpful for a future deeper exploration of the asteroid.

Furthermore, this paper also intends to highlight the main differences concerning the mission's and the CubeSat systems' requirements, comparing a generic LEO mission, the most common one for small satellites, with a deep-space mission. Despite the fact it has given a focus on a mission in the asteroid 152563 (1992 BF), the main importance is given to the general family-type missions.

It has been found that the systems related to the operating environment, navigation, onboard data, and propulsion and power system are those that differ the most.

Consequently, this work open the way for new, deeper, and more precise mission design studies involving CubeSats in free-flying for asteroids and deep-space missions.

References

[1] Dana G Andrews et al. "Defining a successful commercial asteroid mining program". In: *Acta Astronautica* 108 (2015), pp. 106–118.

[2] *Asteroid Database and Mining Rankings - Asterank*. https://www.asterank.com/#upcoming-approaches.

[3] Sabrina Corpino and Fabio Nichele. "CubeSats to support Mars exploration: Three scenarios for valuable planetary science missions". In: *Proceedings of the 12th Reinventing Space Conference*. Ed. by Scott Hatton. Cham: Springer International Publishing, 2017, pp. 17–32.

[4] *ESA Website, M-Argo Mission*. https://www.esa.int/ESA_Multimedia/Images/2017/06/M_Argo. (2017).

[5] Laura Feria del Rosario et al. "Design of the mechanical structure for the CubeSat TeideSat". In: (2018).

[6] Hannah R Goldberg et al. "The juventas cubesat in support of ESA's hera mission to the asteroid didymos". In: (2019).

[7] Steven R Hirshorn, Linda D Voss, and Linda K Bromley. *Nasa systems engineering handbook*. Tech. rep. 2017.

[8] Benjamin K Malphrus et al. "Interplanetary cubesat missions". In: *Cubesat Handbook*. Elsevier, 2021, pp. 85–121.

[9] Hellen Marinho Amorim and Carlos Henrique Reis Rochael. "Minerales espaciales: cosas de nadie en beneficio de todos". In: *Derecho PUCP* 83 (2019), pp. 89–131.

[10] *Mineral Resource Governance in the 21st Century*. https://www.resourcepanel.org/reports/mineral-resource-governance-21st-century.

[11] NASA. *PREFERRED RELIABILITY PRACTICES: ACTIVE REDUNDANCY*. http://www.klabs.org/DEI/References/design_guidelines/design_series/np1216.pdf.

[12] NASA. *PREFERRED RELIABILITY PRACTICES: ENVIRONMENTAL FACTORS*. http://www.klabs.org/DEI/References/design_guidelines/environment_series/np1101.pdf.

[13] NASA. *PREFERRED RELIABILITY PRACTICES: METEOROIDS SPACE DEBRIS*. http://www.klabs.org/DEI/References/design_guidelines/environment_series/1102.pdf.

[14] *NASA Website, Accesible NEAs*. https://cneos.jpl.nasa.gov/nhats/.

[15] *NASA Website, Discovery Statistics*. https://cneos.jpl.nasa.gov/stats/totals.html.

[16] *NASA Website, Small-Body Database*. https://ssd.jpl.nasa.gov/tools/sbdb_query.html#!#results. (2022).

[17] SPACE NEWS. *MarCO shows interplanetary cubesats possible but not easy*. https://spacenews.com/marco-shows-interplanetary-cubesats-possible-but-not-easy/#:~:text=ESA%20has%20five%20deep%20space,to%20%2420%20million%2C%20Walker%20said.

[18] Shane D Ross. "Near-earth asteroid mining". In: *Space* (2001), pp. 1–24.

[19] D. Sears et al. "Near-Earth asteroid sample return missions". In: (Feb. 2001).

[20] *Spacereference Website*. https://www.spacereference.org/asteroid/152563-1992-bf.

[21] *Spacereference Website*. https://www.spacereference.org/asteroid/175706-1996-fg3.

[22] Robert L Staehle et al. *Interplanetary CubeSats: opening the solar system to a broad community at lower cost*. Tech. rep. 2012.

[23] S Tachibana et al. "Hayabusa2: Scientific importance of samples returned from C-type near-Earth asteroid (162173) 1999 JU3". In: *Geochemical Journal* 48.6 (2014), pp. 571–587.

[24] Roger Walker et al. "Deep-space CubeSats: thinking inside the box". In: *Astronomy & Geophysics* 59.5 (2018), pp. 5–24.

[25] Brian D Warner, Alan W Harris, and Petr Pravec. "The asteroid lightcurve database". In: *Icarus* 202.1 (2009), pp. 134–146.

[26] Planetary Society Weabsite. *MarCO: Planetary CubeSats Become Real*. https://www.planetary.org/articles/0708-marco-planetary-cubesats.

[27] M Yakovlev. "The "IADC Space Debris Mitigation Guidelines" and supporting documents". In: *4th European Conference on Space Debris*. Vol. 587. ESA Publications Division Noordwijk, The Netherlands. 2005, pp. 591–597.

[28] S. Yarlagadda. *Economics of the Stars: The Future of Asteroid Mining and the Global Economy*. https://hir.harvard.edu/economics-of-the-stars/. (2022).

3

Session 3 - Attitude Determination and Control Systems

MAGNETIC PARAMETERS ESTIMATION AND ATTITUDE MOTION RECONSTRUCTION USING IN-FLIGHT MAGNETOMETER MEASUREMENTS OF THE ALFACRUX CUBESAT

Emanuel Brenag[(1)], Bruno Tunes de Mello[(2)], Matheus Arruda[(3)], Renato A. Borges[(4)], Danil Ivanov[(5)], Uliana Monakhova[(6)], Yaroslav Mashtakov[(7)], Mikhail Ovchinnikov[(8)]

[(1)] *University of Brasilia, Brazil, emanuelbrenag@gmail.com*
[(2)] *University of Brasilia, Brazil,* bruno.tunesm@gmail.com
[(3)] *University of Brasilia, Brazil,* matheus.leal133@gmail.com
[(4)] *University of Brasilia, Brazil, raborges@ene.unb.br*
[(5)] *Keldysh Institute of Applied Mathematics of RAS, Miusskaya sq. 4, Moscow, Russia, +74992207929,* danilivanovs@gmail.com
[(6)] *Keldysh Institute of Applied Mathematics of RAS, Miusskaya sq. 4, Moscow, Russia, +74992207929, monakhova@phystech.edu*
[(7)] *Keldysh Institute of Applied Mathematics of RAS, Miusskaya sq. 4, Moscow, Russia, +74992207929, yarmashtakov@gmail.com*
[(8)] *Keldysh Institute of Applied Mathematics of RAS, Miusskaya sq. 4, Moscow, Russia, +74992207929, ovchinni@keldysh.ru*

Keywords*: CubeSat, satellite magnetic parameters estimation, attitude reconstruction, extended Kalman filter*

In this work, the magnetometer measurements are used to estimate the attitude motion and magnetic parameters of the satellite using the minimization technique of the sum of squared difference between the in-flight measurements and measurements estimation according to attitude motion model. The obtained magnetometer measurements are processed by extended Kalman filter in order to verify its performance and accuracy using the in-flight data. Along with the attitude quaternion and angular velocity vector, the state vector includes the magnetometer measurement bias, which is changing due to variable residual magnetic dipole. The extended Kalman filter is implemented on a simulator onboard computer, and the results of its testing using hardware-in-the-loop technique with in-flight measurements are presented in the paper.

1. Introduction

Nanosatellites of CubeSat format are frequently used for student education purposes as well as for in-flight space qualification of satellite on-board systems. Short development time of the satellite and comparatively fast launch allow to the student team to obtain skills in almost all topics of aerospace engineering – from mission design, hardware and software development to satellite in-orbit commissioning and telemetry data processing. There are many examples of such a educational

1U CubeSats, a few of them – BEESAT-3 educational CubeSat is developed by students from Berlin Technical University [1,2], FloripaSat-I is developed at the Federal University of Santa Catarina [3], SiriusSat-1&2 are constructed by school students at the Center of Gifted Education «Sirius» [4]. Most of the educational CubeSats are equipped with passive attitude control system, such as magnetic passive system, or even without any control system. In this case, the attitude motion of the satellite is affected by torques of the natural forces, in low-Earth-orbits it is mostly the gravity torque, aerodynamic torque and magnetic torque. Since 1U CubeSat has almost spherical ellipsoid of inertia and usually its center of mass is close to the geometrical center, the gravity and aerodynamic torques are much less than the magnetic torque. Even if the CubeSat is not equipped with special permanent magnet as part of the passive magnetic attitude control system, there is always a residual magnetic dipole onboard the satellite due to some amount of magnetized materials on-board or electrical currents. In case the residual magnetic dipole is constant, its direction tracks the local geomagnetic field, the magnetic torque affects the attitude motion of the satellite.

The AlfaCrux is a radio amateur and educational mission to provide a hands-on experience to students and professors in the complete process of developing and operating a space mission. The satellite is equipped with magnetometer and angular velocity sensors built into a printed circuit board with an onboard computer. Its measurements, obtained via radio communication channel, are used for attitude motion reconstruction. The satellite is not equipped with attitude actuators, so its attitude motion is affected by natural torques in orbit, particularly by gravitational torque and magnetic torque due to residual magnetic moment of the satellite. The residual magnetic moment can be produced by onboard devices during operation and it can vary in time. According to preliminary telemetry data analysis, the initial angular rotation after deployment was about 10 deg/s, and it is reduced to value of about 2-3 deg/s in two days. It shows that the satellite motion is probably affected by Foucault currents dissipating the rotational energy, or it can be the result of influence of hysteresis materials onboard.

The paper presents the first results of attitude motion reconstruction of the AlfaCrux satellite and estimation of the residual dipole. The in-flight data is used for extended Kalman fitler testing for onboard implementation for future missions.

2. AlfaCrux satellite description

The AlfaCrux nanosatellite is a 1U CubeSat, developed by the LODESTAR team at the University of Brasília and launched by the Falcon 9 Transporter-4 mission. The AlfaCrux name is inspired by the Alpha Crucis star, which appears on the Brazilian flag and coat of arms. It is a radio amateur and educational mission that aims, in addition to conducting experiments to study the impact of space weather on satellite communication in equatorial regions, also promoting a hands-on experience for students and professors on the entire process of developing and operating a space mission. The satellite has a mass of 1.065 kg and dimensions of 10 x 10 x 10 cm. A detailed description of the AlfaCrux mission can be seen at [5]. An illustrative photo is presented in Figure 1.

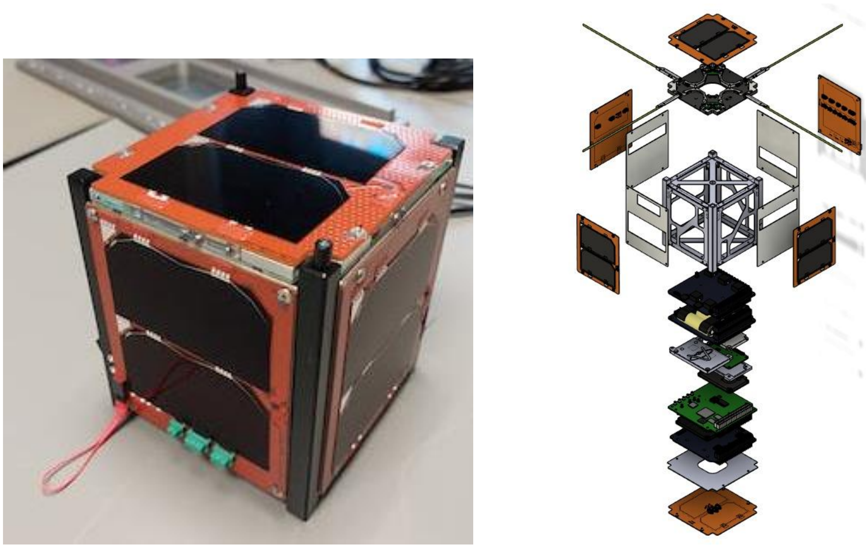

Figure 1: The AlfaCrux satellite (left) and an exploded view of its subsystems (right).

The AlfaCrux's on-board computer is based on the AVR32 MCU, a 32-bit RISC MCU ideal for applications with low power consumption requirements. Although AlfaCrux does not have an attitude control subsystem, its OBC includes a HoneyWell HMC5843 3-axis magnetometer, which allows the collection of geomagnetic field data with a sampling rate of up to 1Hz. The satellite has no attitude requirements for communication nor for the experiments.

Communication with AlfaCrux is established via radio channel. The radio subsystem in the space segment has antennas and a software-reconfigurable UHF transceiver, making it possible to change bit rate, modulation, bandwidth and even in the transmission frequency in orbit. In the ground segment, the mission has a ground station capable of transmitting and receiving data from AlfaCrux through XQuad antennas and a SDR with integrated power amplifier. The transmission of beacons with telemetry packets is performed at the frequency of 437,100 MHz with GMSK modulation.

Even without attitude actuators, the collection of magnetic field, angular velocity, temperature and current data from the solar panels allows the performance of experiments related to the AlfaCrux attitude motion, in particular, the implementation of the extended Kalman filter using measurements only of the magnetometer, which can have its results compared with the other collected data and methods.

3. Motion equations and measurement model

Attitude determination requires the motion equations of the satellite. The satellite angular motion is represented in the Earth-centered inertial (ECI) reference frame $OXYZ$. The origin of the frame is located at the Earth's centre of mass, with X-axis pointing towards the vernal equinox, Z-axis coincident with the Earth's axis of rotation, and Y-axis lies in the equatorial plane, completing the right-handed orthogonal frame. The body-fixed satellite reference frame axes are directed along the principal axes of inertia. The satellite approximate tensor of inertia is as follows

$$\mathbf{J} = \begin{bmatrix} 1.835 & -0.005 & 0.009 \\ -0.005 & 1.853 & 0.002 \\ 0.009 & 0.002 & 1.846 \end{bmatrix} \cdot 10^{-3} \text{ kg}\cdot\text{m}^2.$$

The satellite motion is described by the absolute angular velocity $\boldsymbol{\omega} = [\omega_1, \omega_2, \omega_3]^T$ and the attitude quaternion $\Lambda = (\mathbf{q}, q_0)$ of the satellite frame with respect to the inertial reference frame. Here $\mathbf{q}$ is the vector part of the quaternion and q_0 is the scalar part. The equations of motion are [5]

$$\mathbf{J}\dot{\boldsymbol{\omega}} + \boldsymbol{\omega} \times \mathbf{J}\boldsymbol{\omega} = \mathbf{M}_{mag} + \mathbf{M}_{gg} ,$$

where $\mathbf{M}_{mag}$ and $\mathbf{M}_{gg}$ are the magnetic and gravitational torques. Other disturbances are not included in the dynamical model of the satellite motion. The gravitational torque is described by

$$\mathbf{M}_{gg} = 3\omega_0^2 \left(\mathbf{A}\mathbf{e}_3\right) \times \mathbf{J}\left(\mathbf{A}\mathbf{e}_3\right) ,$$

where $\mathbf{e}_3$ is the local vertical vector in ECI, $\boldsymbol{\omega}_0$ is the orbital angular velocity vector, the rotation matrix $\mathbf{A}$ is calculated from the attitude quaternion. The magnetic torque provided by residual dipole is

$$\mathbf{M}_{mag} = \mathbf{m} \times \mathbf{B} ,$$

where $\mathbf{m}$ is the dipole moment, $\mathbf{B}$ is the local geomagnetic induction vector in the satellite reference frame.

Kinematic relations are [6]

$$\dot{\Lambda} = \frac{1}{2}\mathbf{C}\Lambda ,$$

$$\mathbf{C} = \begin{bmatrix} 0 & \omega_3 & -\omega_2 & \omega_1 \\ -\omega_3 & 0 & \omega_1 & \omega_2 \\ \omega_2 & -\omega_1 & 0 & \omega_3 \\ -\omega_1 & -\omega_2 & -\omega_3 & 0 \end{bmatrix} .$$

The magnetometer measurements model is

$$\mathbf{B}_{meas} = \mathbf{A}\mathbf{B}_{ECI} + \Delta\mathbf{B} + \delta\mathbf{B} ,$$

where $\Delta\mathbf{B}$ is a varying bias vector, $\mathbf{B}_{ECI}$ is the induction vector in ECI frame calculated using the IGRF model, $\delta\mathbf{B}$ is the Gaussian measurements error with zero mean and covariance matrix $\mathbf{R}$. The magnetometer bias dynamical model is assumed as follows

$$\frac{d(\Delta\mathbf{B})}{dt} = \boldsymbol{\eta}_{\Delta\mathbf{B}} ,$$

where $\boldsymbol{\eta}_{\Delta\mathbf{B}}$ is a vector of white noise with zero mean and covariance matrix $\mathbf{D}_{\Delta\mathbf{B}}$. The magnetometer gains and measurements axes misalignments are considered to be known in the paper. These calibration parameters were estimated on the ground before the flight using well-known calibration technique based on the geometric approach [7]. It is assumed that these parameters do not change with time. However, magnetometer bias value affected by the onboard varying magnetic dipoles cannot be considered as a constant and should be estimated in real time.

4. Attitude determination technique

Two attitude determination methods are utilized. The telemetry data is processed on the ground using the differential evolution (DE) method which is used for the attitude motion reconstruction under the assumption of constant magnetometer bias. The cost function is the difference between the values of the geomagnetic induction vector as measured in the satellite frame and the value provided in the inertial frame according to International Geomagnetic Reference Field (IGRF) model [8] for the current satellite position. The results of the DE method are also used for the evaluation of the results of the Extended Kalman filter estimation.

4.1. Differential evolution algorithm

For the reconstruction of the attitude motion, the spacecraft initial state is determined through the least squares method formulated between the magnetometer measurements and the dynamical model, constituting the minimization of the following cost function

$$\Phi(\boldsymbol{\xi}) = \sum_{k=0}^{N}(\boldsymbol{b}_{model}^{k} - \boldsymbol{b}_{meas}^{k})^2,$$

where $\boldsymbol{\xi} = [\boldsymbol{q}(t=0), \boldsymbol{\omega}(t=0),\ \boldsymbol{m}_{res}(t=0)]^T$ is the state vector formed by the attitude quaternion, the angular rates, and the residual magnetic dipole. Also, $\boldsymbol{b}_{meas}^{k}$ is the magnetometer observations vector at instant t_k and $\boldsymbol{b}_{model}^{k}$ is the geomagnetic induction vector computed from the IGRF model, $\boldsymbol{b}_{IGRF}^{k}$, rotated to the spacecraft body frame through the attitude matrix, $A^k(\boldsymbol{\xi})$, obtained from the state vector as the following

$$\boldsymbol{b}_{model}^{k} = A_k(\boldsymbol{\xi})\, \boldsymbol{b}_{IGRF}^{k}.$$

The differential evolution is utilized for the minimization of the cost function. This algorithm is a stochastic direct search method intended for global optimization [9]. The DE is comprised in four phases: initialization, mutation, crossover and selection. In the initialization phase, a population of N_P D-dimensional vectors is created, so that for the generation G such vectors are

$$x_{i,G}, i = 1, \dots, N_P,$$

and each one has its values initialized randomly to cover the state-space. The second phase is the mutation, which for each $x_{i,G}$, called target vector, a mutant vector is generated as

$$v_{i,G+1} = x_{r_1,G} + F \cdot (x_{r_2,G} - x_{r_3,G}),$$

where $r_1, r_2, r_3 \in \{1, \dots, N_P\}$ are random indexes mutually different and not equal to the current index i. The parameter $F \in [0,2]$ is the differential constant and modulates the increment of the mutation process.

In the crossover process, a trial vector is built mixing the target and mutant vectors as in the following

$$u_{ji,G+1} = \begin{cases} v_{ji,G+1} & \text{if } (randb(j) \le CR) \text{ or } j = rnbr(i) \\ x_{ji,G} & \text{if } (randb(j) > CR) \text{ or } j \ne rnbr(i) \end{cases}, j = 1, \ldots, D,$$

with j as the vector element index, $randb(\cdot)$ is a number $\in [0,1]$ generated randomly from a uniform distribution, $rnbr(\cdot)$ is an index also chosen randomly and $CR \in [0,1]$ is the crossover constant.

In the selection phase the trial vector $u_{i,G+1}$ is compared to the target vector $x_{i,G}$ in order to decide which one will become part of the $G+1$ generation vectors. The vector that yields the smaller cost function will be assigned $x_{i,G+1}$, and the DE algorithm executes again the mutation process, recursively.

4.2. Extended Kalman filter specifications

A discrete-time form of the EKF is considered. The state vector of the EKF consists of the vector part of the attitude quaternion, angular velocity vector, and the magnetometer bias vector

$$\mathbf{x} = \left[\mathbf{q}, \boldsymbol{\omega}, \mathbf{m}_{res}\right]^T .$$

The motion equations are linearized in the vicinity of the current state to propagate the covariance matrix of the state vector as

$$\delta\dot{\mathbf{x}}(t) = \mathbf{F}(\mathbf{x}, t)\delta\mathbf{x}(t),$$

where $\delta\mathbf{x}(t)$ is a small state vector increment (considering the quaternion increments features), $\mathbf{F}(\mathbf{x}, t)$ is the dynamical matrix obtained by the linearization in the vicinity of the current state. After the linearization of the attitude motion equations the dynamics matrix in discrete-time form $\mathbf{F}_k$ is

$$\mathbf{F}_k = \left.\begin{pmatrix} -\mathbf{W}_{\boldsymbol{\omega}} & \frac{1}{2}\mathbf{E} & \mathbf{0}_{3\text{x}3} \\ \mathbf{J}^{-1}\left(\mathbf{F}_{gr} + \mathbf{F}_m\right) & \mathbf{J}^{-1}\mathbf{F}_{gir} & -\mathbf{J}^{-1}\mathbf{W}_{\hat{\mathbf{B}}} \\ \mathbf{0}_{3\text{x}3} & \mathbf{0}_{3\text{x}3} & \mathbf{0}_{3\text{x}3} \end{pmatrix}\right|_{\mathbf{x}=\mathbf{x}(t_k)},$$

where t_k is the time step when the measurements are available, $\mathbf{E}$ is 3x3 identity matrix,

$$\mathbf{F}_m = 2\mathbf{W}_{\mathbf{m}}\mathbf{W}_{\hat{\mathbf{B}}},$$

$$\mathbf{F}_{gr} = 6\omega_0^2\left(\mathbf{W}_{\mathbf{Ae}_3}\mathbf{J}\mathbf{W}_{\mathbf{Ae}_3} - \mathbf{W}_{\mathbf{JAe}_3}\mathbf{W}_{\mathbf{Ae}_3}\right),$$

$$\mathbf{F}_{gir} = 2\left(\mathbf{W}_{\mathbf{J}\boldsymbol{\omega}} - \mathbf{W}_{\boldsymbol{\omega}}\mathbf{J}\right).$$

In the previous equations, $\mathbf{W}_{\mathbf{a}}$ denotes the skew-symmetric matrix of a vector $\mathbf{a} = [a_x, a_y, a_z]^T$ according to

$$\mathbf{W}_{\mathbf{a}} = \begin{bmatrix} 0 & -a_z & a_y \\ a_z & 0 & -a_x \\ -a_y & a_x & 0 \end{bmatrix}.$$

The nonlinear measurements model is also linearized in the vicinity of the current state vector as follows

$$\delta\mathbf{z}(t) = \mathbf{H}(\mathbf{x},t)\delta\mathbf{x}(t),$$

where $\delta\mathbf{z}$ is the measurements vector increment, $\mathbf{H}$ is the measurements matrix obtained by the linearization. Using the magnetometer measurements model the linearized model is as follows

$$\delta\mathbf{z} = 2\mathbf{W}_{\hat{\mathbf{b}}}\delta\mathbf{q},$$

where $\hat{\mathbf{b}}$ is a unit local geomagnetic field vector in the body-fixed reference frame calculated using the current attitude quaternion estimation $\hat{\Lambda}$ as follows

$$\hat{\mathbf{b}} = \mathbf{A}(\hat{\Lambda})\mathbf{b}_{ECI}.$$

Thus, the measurements matrix in discrete form is

$$\mathbf{H}_k = \left[2\mathbf{W}_{\hat{\mathbf{b}}} \quad \mathbf{0}_{3\text{x}3} \quad \mathbf{0}_{3\text{x}3}\right]\Big|_{\mathbf{x}=\mathbf{x}(t_k)}.$$

5. Attitude motion determination results

5.1. Results of differential evolution algorithm application

Consider an example of magnetometer measurements obtained from telemetry at August 7, 2022 at 13:20 UTC. The measurement samples are obtained each 30s during 5 min interval. The measurements are presented in Figure 2. Using TLE elements for this day, the AlfaCrux position for each time step was calculated, this data is used for the local geomagnetic field calculation using IGRF model. Using the comparison between the value of the magnetic field vector and measured magnetic field vector, the magnetometer bias is calculated, its value is as follows

$$\Delta\mathbf{B} = \left[19 \quad -14 \quad -27\right]\cdot 10^3\text{nT}.$$

This value is quite considerable, it can be explained by the onboard magnetic residual dipole. Figure 3 demonstrates the values of the magnetic field by IGRF, measured magnetic field and measured magnetic field without the bias. Fig. 4 demonstrates the magnetometer measurements without bias.

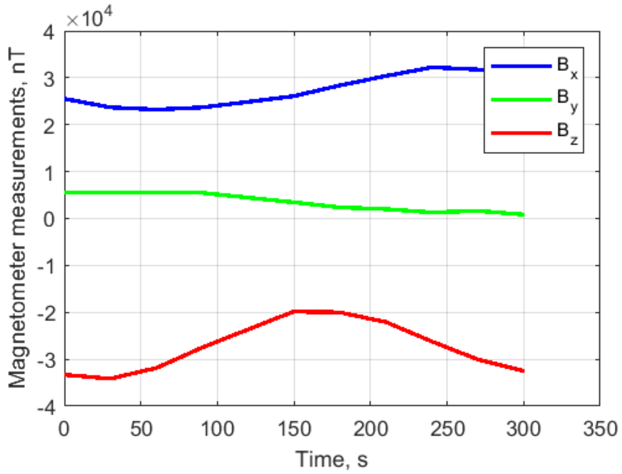

Figure 2: Magnetometer measurements from AlfaCrux obtained at August 7, 2022 at 13:20 UTC.

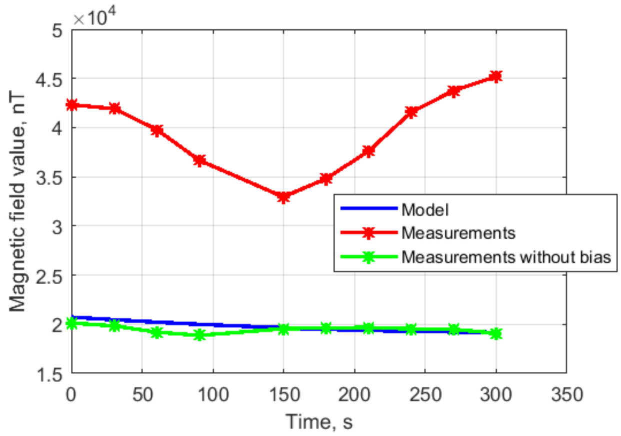

Figure 3: Magnetic field measurements with and without bias and magnetic field value given by the IGRF model.

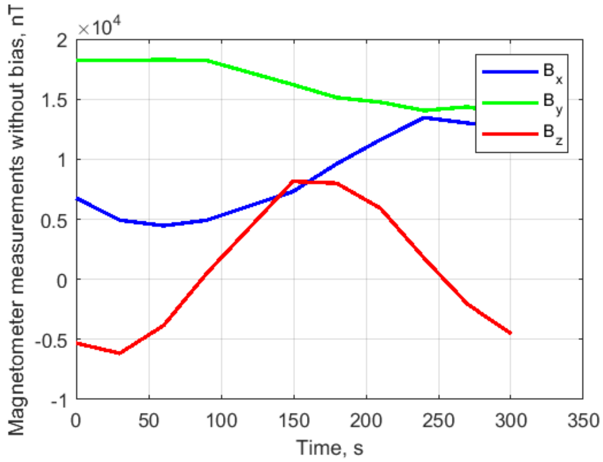

Figure 4: Magnetometer measurements without bias.

It is assumed that the magnetometer bias and residual magnetic dipole are constant during the 5 min intervals. The DE algorithm used these measurements to obtain the initial conditions and value of the residual magnetic dipole. After 300 generations (each generation consist of 100 elements) the value of the cost-function reduced to 0.014. The obtained value of the residual dipole is as follows

$$\mathbf{m}_{res} = \left[0.021 \;\; 0.003 \;\; -0.022\right] \mathrm{Am}^2 .$$

After the DE algorithm the estimated unit magnetic field vector components are close to the measured unit vector components as can be seen from Figure 5. The obtained by DE initial quaternion and angular velocity result in the attitude motion presented in Figure 6.

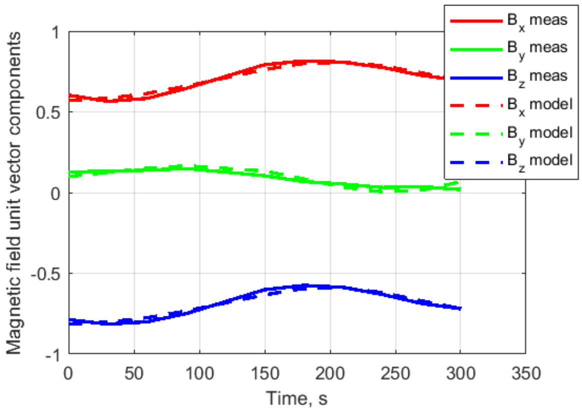

Figure 5: Comparison of the unit magnetic field vector components and the measured unit vector components.

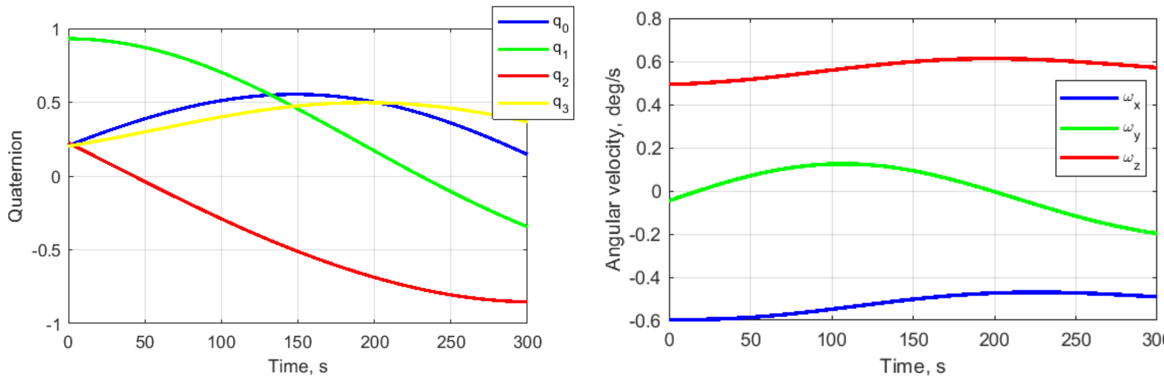

Figure 6: Quaternion and angular velocity estimations obtained with the DE method.

5.2. Extended Kalman filter application example

Using the results obtained by DE initial conditions and the estimated residual dipole, the more frequent magnetometer measurements was reproduced by the attitude motion equation numerical integration. These measurements are processed by the extended Kalman filter explained in Section 4.2. Figure 7 presents an example of the quaternion and angular velocity estimation accuracy. For the quaternion error, it does not exceed 1 deg, for the angular velocity the error is about 0.003 deg/s.

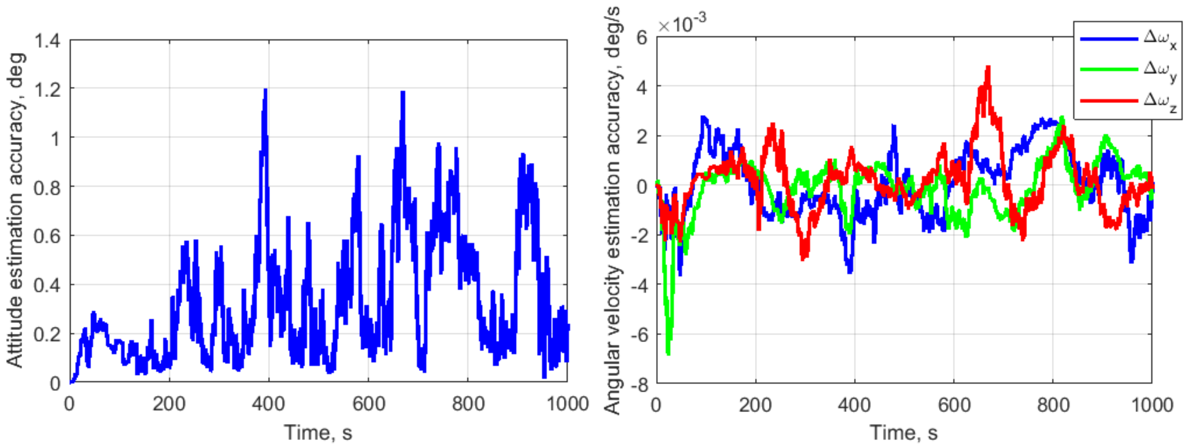

Figure 7: Attitude and angular velocity estimation accuracy

6. Conclusions

The first results of AlfaCrux magnetometer telemetry processing indicate that the CubeSat attitude motion is affected by significant residual magnetic dipole. Its value should be estimated in real-time for better onboard estimation of the attitude motion for future missions. The paper demonstrated the results of successful application of the differential evolution algorithm for motion reconstruction and extended Kalman filter for real-time attitude motion estimation.

Acknowledgments

This work is partially supported by the Russian Science Foundation (sections 3 and 4 of the paper conducted by the Russian part), grant № 22-71-10009, and by the Brazilian National Council for Scientific and Technological (CNPq) and the Brazilian Federal District Research Support Foundation (FAPDF) (sections 1,2,5,6 of the paper conducted by the Brazilian part).

References

1. Barschke M.F., Werner P., Kapitola S. BEESAT-3 commissioning – better late than never // Proceedings of 69th International Astronautical Congress. Bremen, 1-5 October 2018. Paper IAC-18.B4.3.1, 2018. P. 7.
2. Ivanov D. et al. Flight results from a passively magnetic stabilized single unit cubesat // Adv. Astronaut. Sci. Univelt Inc., 2020. Vol. 173. P. 217–233.
3. Marcelino G.M. et al. In-orbit preliminary results from the open-source educational nanosatellite FloripaSat-I // Acta Astronaut. Pergamon, 2021. Vol. 188. P. 64–80.
4. Ivanov D.S. et al. Attitude motion and sensor bias estimation onboard the SiriusSat-1 nanosatellite using magnetometer only. Acta Astronaut. Pergamon, 2021. Vol. 188. P. 295-307.
5. Borges, R. A. et al. The AlfaCrux CubeSat Mission Description and Early Results. Applied Sciences 2022, 12(19), 9764. https://doi.org/10.3390/app12199764
6. Wertz J.R. Spacecraft Attitude Determination and Control. Dordrecht/Boston, London: Acad. press, 1990. 880 p.
7. Vasconcelos J.F. et al. Geometric approach to strapdown magnetometer calibration in sensor frame // IEEE Trans. Aerosp. Electron. Syst. 2011. Vol. 47, № 2. P. 1293–1306.
8. Thébault E., Finlay C.C., Beggan C.D. et. al. International Geomagnetic Reference Field: the 12th generation // Earth, Planets Sp. Springer Berlin Heidelberg, 2015. Vol. 67, № 1. P. 79.
9. Storn R., Price K. Differential Evolution – A Simple and Efficient Heuristic for global Optimization over Continuous Spaces // J. Glob. Optim. 1997 114. Springer, 1997. Vol. 11, № 4. P. 341–359.

MODEL PREDICTIVE CONTROL FOR ATTITUDE MANEUVERS OF A NANOSATELLITE

Tomás C. Miranda[3], **Maria C. P. Faria**[1], **Marcelo A. Santos**[2], **Guilherme V. Raffo**[2]

[1] *Federal University of Minas Gerais, Department of Mechanical Engineering*
[2] *Federal University of Minas Gerais, Department of Electronic Engineering*
[3] *Federal University of Minas Gerais, Undergraduate Program in Aerospace Engineering*

Keywords: *Model predictive control, Satellite attitude control, CubeSat, Reaction wheels*

This work proposes a CubeSat attitude control system (ACS) equipped with three reaction wheels based on a Model Predictive Control (MPC) technique. The CubeSat is a nanosatellite that will be used to test a novel battery technology in space. The mission requires the ability to stabilize the spacecraft after deployment and to point its antennas to the Earth to enable communication. The spacecraft attitude dynamics are modeled using quaternions and the Newton-Euler formulation. In addition, the reaction wheels are modeled taking into account the effects of saturation. Furthermore, external environmental disturbances acting on the satellite are considered. In this context, a conventional controller might be unable to simultaneously satisfy the mission's requirements while dealing with the system's constraints. Therefore, the proposed MPC controller has the conceptual flexibility to systematically handle constraints while still providing optimized performance. Finally, numerical simulations of the closed-loop system are developed, from which it is shown that the controller is able to successfully realize the desired maneuvers.

1. Introduction

Satellite engineering is entering a new phase with the exponentially increasing participation of private enterprises and the academic community, ending the paradigmatic governmental agency as the primary driver of innovation. New and more capable launch vehicles, increased embedded computing capability, and improved materials have allowed new mission concepts and enabled low-cost development and operation. In particular, CubeSats have become a popular satellite class for scientific research due to their low development and manufacturing costs.

The control of the satellite's attitude is of particular interest, which is often necessary for detumbling and stabilizing the spacecraft, as well as pointing and orienting antennas to the Earth, payload systems, and solar panels. These requirements make the correct design of an Attitude Control System (ACS) critical for the mission success. In terms of actuators, active three-axis control using thrusters, Reaction Wheels (RW), Control Moment Gyroscope (CMG) or magnetorquers, although more expensive, allows higher accuracy and maneuverability, has no inherent constraints on pointing direction, and thus, enable greater freedom when designing mission parameters. Therefore, efficient and robust active control strategies for the ACS can lead to substantive performance gains.

Given the stringent operational demands and hostile operating environment, the ACS needs to be able to provide guarantees of constraint satisfaction, robustness, optimized performance, safety, and adaptability. To address such requirements in a systematic manner, advanced control strategies are required. Amongst them, Model Predictive Control (MPC) is particularly interesting, since it works by solving an optimization problem considering the system's predicted dynamics, constraints, and control objectives, to determine the control action at each instant.

MPC is particularly suited to attitude control due to its systematic handling of constraints, suitability for a range of system models and types, optimized performance and conceptual flexibility. A review of applications of MPC in aerospace, including but not limited to satellite attitude control, can be found in [1]. Examples include the longitudinal control of aircraft [2], path following for a quadrotor [3, 4] and for a tiltrotor [5], Guidance, Navigation and Control (GNC) for UAVs [6], and shipboard operations of helicopters [7]. Particularly for attitude control of nanosatellites, MPC has been applied to spacecraft equipped with reaction wheels [8, 9, 10, 11] as well as magnetic coils [12, 13, 14].

Therefore, this paper aims to develop a model predictive control algorithm for the attitude control of a 3U CubeSat equipped with reaction wheels. The rest of this paper is structured as follows: in section 2, the mathematical model of the satellite is obtained; in section 3, the MPC control strategy is detailed; in section 4, numerical results of simulations are shown to corroborate the proposed control strategy, including a comparison with a classical LQR controller; finally, in section 5, the work is concluded.

2. Nanosatellite Modeling

2.1. Reference Systems

For modeling purposes, three reference frames are defined [15, 16]. First, an Earth-Centered Inertial (ECI) reference frame $\mathcal{E}$ is defined by a set of orthonormal basis vectors with the origin at the Earth's center of mass, with the $X^{\mathcal{E}}$-axis aligned to the vernal equinox, the $Z^{\mathcal{E}}$-axis aligned with the Earth's axis of rotation and the $Y^{\mathcal{E}}$-axis completing the right-handed triad. The second frame is a Local-Vertical Local-Horizontal (LVLH) frame $\mathcal{L}$, with its $X^{\mathcal{L}}$-axis pointing towards Earth, the $Y^{\mathcal{L}}$-axis aligned with the orbit direction, and its $Z^{\mathcal{L}}$-axis perpendicular to the orbit plane. Finally, the third is a body-fixed reference frame $\mathcal{B}$ that is centered on the satellite's center of mass and has axes parallel to the body's principal axis of inertia. The considered reference frames are presented in Figure 1.

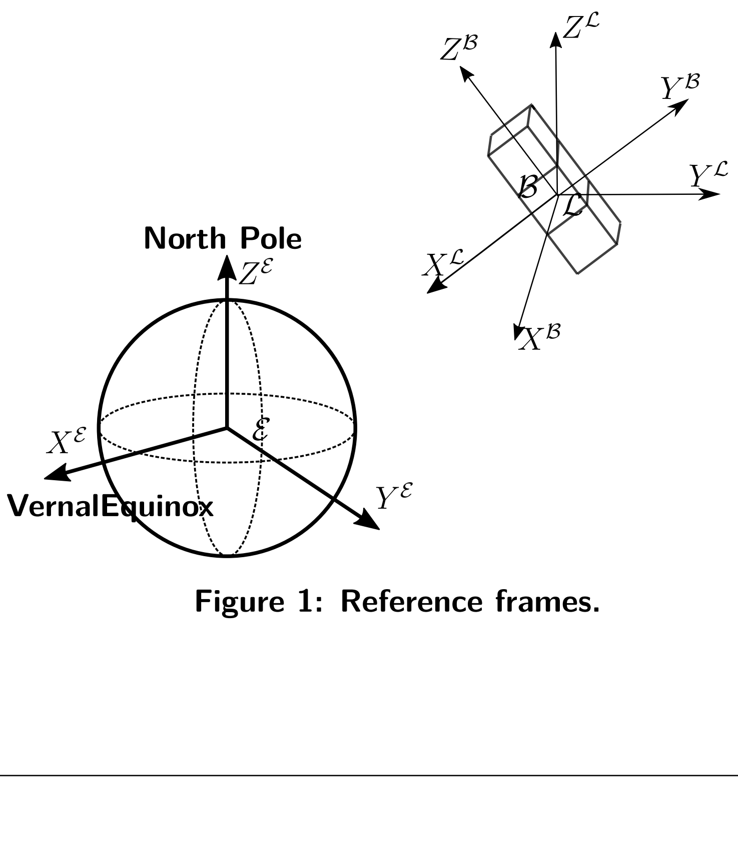

Figure 1: Reference frames.

2.2. Kinematics

To describe the orientation of $\mathcal{B}$ in relation to $\mathcal{E}$, i.e. the satellite's attitude, a suitable parametrization must be chosen. For this work, the quaternion is adopted given its lack of singularities and computational efficiency since it can represent orientation in a compact form using only four parameters. The quaternion, denoted by the group $\mathbb{H}$, is an imaginary entity that extends the complex numbers considering three imaginary units $\hat{\imath}, \hat{\jmath}, \hat{k}$. The quaternion algebra and modelling concepts can be seen with more details in [17].

In order to perform multiplication between matrices and quaternions, it is possible to define a one-by-one mapping $\mathrm{vec}_4 : \mathbb{H} \to \mathbb{R}^4$ as

$$\mathrm{vec}_4\left(\boldsymbol{h}\right) = \begin{bmatrix} h_1 & h_2 & h_3 & h_4 \end{bmatrix}^T. \tag{1}$$

Furthermore, despite the multiplication of two quaternions $\boldsymbol{h}$ and $\boldsymbol{h'}$ not being commutative, the Hamilton operator $\overset{+}{\boldsymbol{H}}_{\boldsymbol{4}}(\cdot)$ can be defined to allow commutation. Thus,

$$\mathrm{vec}_4(\boldsymbol{h}\boldsymbol{h'}) = \overset{+}{\boldsymbol{H}}_{\boldsymbol{4}}(\boldsymbol{h})\mathrm{vec}_4\left(\boldsymbol{h'}\right)$$

where

$$\overset{+}{\boldsymbol{H}}_{\boldsymbol{4}}(\boldsymbol{h}) = \begin{bmatrix} h_1 & -h_2 & -h_3 & -h_4 \\ h_2 & h_1 & -h_4 & h_3 \\ h_3 & h_4 & h_1 & -h_2 \\ h_4 & -h_3 & h_2 & h_1 \end{bmatrix}$$

Euler's eigenaxis rotation theorem states that a rigid body's attitude can be changed from any orientation to another by a rotation around a particular axis of rotation, or eigenaxis, that is fixed to the body and stationary in an inertial reference frame. Therefore, a general rotation α around an arbitrary unit norm rotation axis $\boldsymbol{t} = t_x\hat{\imath} + t_y\hat{\jmath} + t_z\hat{k}$ can be defined as [17]

$$\boldsymbol{r} = \cos(\alpha/2) + \boldsymbol{t}\sin(\alpha/2). \tag{2}$$

Thus, considering a point $\boldsymbol{p}^i$ rigidly attached to a frame $\mathcal{F}_i$, the projection of such a point in another frame $\mathcal{F}_j$ is given by

$$\boldsymbol{p}^j = \boldsymbol{r}_i^j \boldsymbol{p}^i (\boldsymbol{r}_i^j)^*, \tag{3}$$

with $\boldsymbol{r}_i^j$ being the rotation of $\mathcal{F}_i$ with respect to $\mathcal{F}_j$ and with the inverse rotation being denoted by the conjugate $\boldsymbol{r}_j^i = (\boldsymbol{r}_i^j)^*$.

In order to describe the relationship between the unit quaternion time derivative and the angular velocity, the quaternion propagation equation can be used, yielding [17]

$$\dot{\boldsymbol{r}}_i^j = \frac{1}{2}\boldsymbol{r}_i^j \boldsymbol{\omega}_{ji}^i. \tag{4}$$

with $\boldsymbol{\omega}_{ji}^j$ denoting the angular velocity of frame $\mathcal{F}_i$ with respect to $\mathcal{F}_j$, expressed in $\mathcal{F}_i$.

The Forward Kinematic Model (FKM) for rotations using quaternions provides the map between the configuration variables, $\boldsymbol{q}$, and the orientation, $\boldsymbol{r}$, i.e, $\boldsymbol{r} = f(\boldsymbol{q})$. Considering the frames defined in Figure 1, the FKM for the satellite can be obtained considering rotations ϕ, θ and ψ using the Euler convention ZYX about the local axis. Thus, for $\boldsymbol{q} = [\phi\ \theta\ \psi]^T$ it holds that

$$\boldsymbol{r}_{\mathcal{B}}^{\mathcal{E}} = \left(\cos\frac{\psi}{2} + \hat{k}\sin\frac{\psi}{2}\right)\left(\cos\frac{\theta}{2} + \hat{\jmath}\sin\frac{\theta}{2}\right)\left(\cos\frac{\phi}{2} + \hat{\imath}\sin\frac{\phi}{2}\right). \tag{5}$$

Therefore, based on equation (4), the time derivative of the orientation can be written in terms of angular velocity as

$$\mathrm{vec}_4\left(\dot{\boldsymbol{r}}_{\mathcal{B}}^{\mathcal{E}}\right) = \frac{1}{2}\overset{+}{\boldsymbol{H}}_{\boldsymbol{4}}\left(\boldsymbol{r}_{\boldsymbol{\mathcal{B}}}^{\boldsymbol{\mathcal{E}}}\right)\mathrm{vec}_4\left(\boldsymbol{\omega}_{\mathcal{E}\mathcal{B}}^{\mathcal{B}}\right). \tag{6}$$

2.3. Dynamic Modelling

The dynamic model of the satellite can be obtained considering the Newtonian mechanic's fact stating that the rate of change of angular momentum is equal to the total torque applied to the body, which is known as the Euler equation. This subsection is mostly based on [18, 19, 20, 9] and citations therein.

In order to obtain the dynamical model, the following assumptions are made: i) the satellite is a rigid body, ii) the RWs embedded in the satellite have an orthonormal configuration, iii) there is no displacement between the satellite's center of mass and its geometrical center, and iv) the RWs axes coincides with the satellite's geometrical axes.

The angular velocity of the RWs is given by

$$\boldsymbol{\omega_{tot}} = \boldsymbol{\omega} + \boldsymbol{\omega_r}, \tag{7}$$

where $\boldsymbol{\omega} = \boldsymbol{\omega}_{\mathcal{E}\mathcal{B}}^{\mathcal{B}}$ is the satellite angular velocity and $\boldsymbol{\omega_r}$ is the RW angular velocity, both expressed in the body frame. Therefore, the angular momentum of the RWs is given by

$$\boldsymbol{h_r} = \boldsymbol{I_r}\boldsymbol{\omega_{tot}}, g \tag{8}$$

with $\boldsymbol{I_r}$ being the RWs moment of inertia with respect to the body frame.

Considering that the RWs are actuated in each axis through the generalized torque $\boldsymbol{\tau_c}$, the following dynamical equation can be obtained

$$\dot{\boldsymbol{\omega}}_{\boldsymbol{r}} = \boldsymbol{I_r}^{-1}\boldsymbol{\tau_c} - \dot{\boldsymbol{\omega}}. \tag{9}$$

Similarly, the satellite's angular momentum can be written expressed in the inertial frame as

$$\boldsymbol{h_r}^{\mathcal{E}} = \boldsymbol{I}^{\mathcal{E}}\boldsymbol{\omega}^{\mathcal{E}} + \boldsymbol{I_r}^{\mathcal{E}}\boldsymbol{\omega_{tot}}^{\mathcal{E}}, \tag{10}$$

with $\boldsymbol{I}^{\mathcal{E}}$ and $\boldsymbol{I_r}^{\mathcal{E}}$ being, respectively, the satellite and the RWs moments of inertia with respect to the inertial frame. Taking the time derivative of the satellite angular momentum yields

$$\dot{\boldsymbol{h}}_{\boldsymbol{s}} = \boldsymbol{S}(\boldsymbol{\omega})\boldsymbol{I}\boldsymbol{\omega} + \boldsymbol{I}\dot{\boldsymbol{\omega}} + \boldsymbol{S}(\boldsymbol{\omega})\boldsymbol{I_r}\boldsymbol{\omega_{tot}} + \boldsymbol{I_r}\dot{\boldsymbol{\omega}}_{\boldsymbol{tot}}. \tag{11}$$

where $\boldsymbol{S} \in \mathbb{R}^{3\times 3}$ is a skew symmetric matrix such that $\boldsymbol{S}^T + \boldsymbol{S} = 0$ [19].

Considering that a generalized external torque, $\boldsymbol{\tau_{ext}}$, is applied to the satellite, it is possible to state that

$$\boldsymbol{S}(\boldsymbol{\omega})\boldsymbol{I}\boldsymbol{\omega} + \boldsymbol{I}\dot{\boldsymbol{\omega}} + \boldsymbol{S}(\boldsymbol{\omega})\boldsymbol{I_r}\boldsymbol{\omega_{tot}} + \boldsymbol{I_r}\dot{\boldsymbol{\omega}}_{\boldsymbol{tot}} = \boldsymbol{\tau_{ext}}. \tag{12}$$

Moreover, from the reaction wheel dynamic model (9), the satellite dynamics can be written as

$$\boldsymbol{S}(\boldsymbol{\omega})\boldsymbol{I}\boldsymbol{\omega} + \boldsymbol{I}\dot{\boldsymbol{\omega}} + \boldsymbol{S}(\boldsymbol{\omega})\boldsymbol{I_r}\boldsymbol{\omega_{tot}} = \boldsymbol{\tau_{ext}} - \boldsymbol{\tau_c}, \tag{13}$$

which becomes

$$\dot{\boldsymbol{\omega}} = \boldsymbol{I}^{-1}\left(-\boldsymbol{\omega} \times \boldsymbol{I}\boldsymbol{\omega} - \boldsymbol{\omega} \times \boldsymbol{I_r}\left(\boldsymbol{\omega} + \boldsymbol{\omega_r}\right) + \boldsymbol{\tau_{ext}} - \boldsymbol{\tau_c}\right). \tag{14}$$

Finally, from equations (6), (9), and (14), the dynamic model describing the satellite embedded with RWs is given by

$$\dot{\boldsymbol{x}} = f(\boldsymbol{x}, \boldsymbol{u}, \boldsymbol{d}) = \begin{bmatrix} \frac{1}{2}\overset{+}{\boldsymbol{H}}_{\boldsymbol{4}}\left(\boldsymbol{r}_{\mathcal{B}}^{\mathcal{E}}\right)\mathrm{vec}_4\left(\boldsymbol{\omega}\right) \\ \boldsymbol{I}^{-1}\left(-\boldsymbol{\omega} \times \boldsymbol{I}\boldsymbol{\omega} - \boldsymbol{\omega} \times \boldsymbol{I_r}\left(\boldsymbol{\omega} + \boldsymbol{\omega_r}\right) + \boldsymbol{\tau_{ext}} - \boldsymbol{\tau_c}\right) \\ \boldsymbol{I_r}^{-1}\boldsymbol{\tau_c} - \boldsymbol{I}^{-1}\left(-\boldsymbol{\omega} \times \boldsymbol{I}\boldsymbol{\omega} - \boldsymbol{\omega} \times \boldsymbol{I_r}\left(\boldsymbol{\omega} + \boldsymbol{\omega_r}\right) + \boldsymbol{\tau_{ext}} - \boldsymbol{\tau_c}\right) \end{bmatrix}, \tag{15}$$

where $\boldsymbol{x} = \left[\mathrm{vec}_4\left(\boldsymbol{r}_{\mathcal{B}}^{\mathcal{E}}\right)^T \ \boldsymbol{\omega}^T \ \boldsymbol{\omega_r}^T\right]^T$, $\boldsymbol{u} = \boldsymbol{\tau_c}$, and $\boldsymbol{d} = \boldsymbol{\tau_{ext}}$.

2.4. Environmental Disturbances

Increased accuracy for attitude modeling requires the use of an explicit dynamic model of the environmental disturbance torques acting on the spacecraft. Such torques can be modeled as a function of the satellite's states evolution. There are four main sources of these disturbances: Earth's gravitational field, Earth's magnetic field, solar radiation pressure, and aerodynamic drag, which are respectively described by the equations

$$\boldsymbol{\tau_{gg}} = \frac{3\mu}{\|\boldsymbol{r}_e\|^3}[\hat{\boldsymbol{r}}_e \times (\boldsymbol{J}\hat{\boldsymbol{r}}_e)], \tag{16}$$

$$\boldsymbol{\tau_{mag}} = \boldsymbol{m} \times \boldsymbol{b}, \tag{17}$$

$$\boldsymbol{\tau_{rad}} = \int \boldsymbol{r_s} \times \left(-P(1 - C_s)\hat{\boldsymbol{s}} + 2\left(C_s \cos(\eta) + \frac{1}{3}C_d\right)\hat{\boldsymbol{n}}\right)\cos(\eta) d\boldsymbol{A}, \tag{18}$$

$$\begin{aligned}\boldsymbol{\tau_{aero}} = \frac{1}{2}C_D\rho\|\boldsymbol{v_0}\|^2 \int (\hat{\boldsymbol{n}} \cdot \hat{\boldsymbol{v}}_{\boldsymbol{0}})(\hat{\boldsymbol{v}}_{\boldsymbol{0}} \times \boldsymbol{r_s}) d\boldsymbol{A} + \frac{1}{2}C_D\rho\|\boldsymbol{v_0}\|^2 \int & (\hat{\boldsymbol{n}}(\boldsymbol{\omega} \times \boldsymbol{r_s})(\hat{\boldsymbol{v}}_{\boldsymbol{0}} \times \boldsymbol{r_s}) \\ & + (\hat{\boldsymbol{n}} \cdot \hat{\boldsymbol{v}}_{\boldsymbol{0}})((\boldsymbol{\omega} \times \boldsymbol{r_s}) \times \boldsymbol{r_s}))\, d\boldsymbol{A}.\end{aligned} \tag{19}$$

In the gravity-gradient torque equation (16), μ is the gravitational parameter of the Earth, $\boldsymbol{r_e}$ is the vector between the center of mass of Earth and the center of mass of the spacecraft, and $\hat{\boldsymbol{r}}_e$ is the unit vector in the direction of $\boldsymbol{r}_e$. In the magnetic torque equation (17), $\boldsymbol{b}$ is the density of the geomagnetic flux and $\boldsymbol{m}$ is the spacecraft's magnetic moment. In the solar radiation pressure torque equation (18), P is the mean momentum flux acting on a surface normal to solar radiation, $\hat{\boldsymbol{s}}$ is the unit vector from the spacecraft to the Sun, η is the angle between $\hat{\boldsymbol{s}}$ and $\hat{\boldsymbol{n}}$, and the characteristic coefficients of the material are C_a, for absorption, C_s, for specular reflectivity, and C_d, for diffuse reflectivity. Further, in the aerodynamic torque equation (19), C_D is the drag coefficient of the surface, ρ is the atmospheric density, $\boldsymbol{v_0}$ is the velocity of the center of mass relative to the atmosphere with $\hat{\boldsymbol{v}}_{\boldsymbol{0}}$ being the unit vector in its direction, and $\hat{\boldsymbol{n}}$ is an unit vector normal to the surface element $d\boldsymbol{A}$ of the wetted area.

3. Attitude Model Predictive Control

3.1. MPC Overview

MPC is a class of optimal controllers in which the control action is found by solving a constrained finite horizon open-loop optimal control problem, at each sampling time. The measured/estimated states of the system are used as the initial condition to solve the optimization problem, yielding an optimal control sequence where the first element is applied to the system. An introduction to MPC can be found in [21] and [22].

The basic steps needed to develop a model predictive controller are

1. Derive a mathematical model of the system's dynamics;
2. Pose an optimal control problem where with the model prediction's as constraints;
3. Input the first element of the optimal control sequence as a control action;
4. Tune the weights of the cost functional until performance is satisfactory;
5. Implement the control law in the associated hardware/software.

In addition, a qualitative comparison of MPC with other control methods can be done, as summarised by the following table.

Table 1: Controller comparison.

Characteristic	PD/PID	LQR	MPC
Optimality	Sub-optimal	Optimal	Optimal
System type	Linear	Linear	Linear & Nonlinear
Constraint handling	Not-explicit	Not-explicit	Explicit
On-board computational cost	Smaller	Smaller	Greater

3.2. Prediction Process

The term prediction in the MPC acronym revolves around the propagation of the system states throughout a finite-time horizon based on a given dynamic model. For that, consider a nonlinear discrete-time system of the form

$$\boldsymbol{x}(k+1) = f(\boldsymbol{x}(k), \boldsymbol{u}(k)), \tag{20}$$

where $\boldsymbol{x} \in \mathbb{R}^n$ is the state vector, $\boldsymbol{u} \in \mathbb{R}^m$ is the control input vector, $k \in \mathbb{N}$ is the time step, and $f(\cdot) : \mathbb{R}^n \times \mathbb{R}^m \to \mathbb{R}^n$ is the state transition function that induces the successor state $\boldsymbol{x}(k+1)$ from current state $\boldsymbol{x}(k)$ and input $\boldsymbol{u}(k)$. It is assumed that the states are always accessible since attitude determination is outside of the scope of this work.

Prediction is made considering a finite number N_p of future instants, denoted as the prediction horizon, and a finite number N_c of control actions, denoted as the control horizon. This definition allows the use of a receding horizon strategy, consisting of applying the first control input of the optimal sequence to the system, then receding the prediction horizon one step forward and successively repeating this process considering at each instant the new measured or estimated states. Throughout this process, the MPC uses feedback to perform an open-loop finite optimal control problem at each time step k, giving it some degree of inherent robustness against uncertainties.

In terms of the closed-loop response, it is worthwhile mentioning that larger values of N_p lead to smoother response of the system, at the expense of greater computational cost. Meanwhile, a smaller prediction horizon may cause the system to become unstable depending on the ratio of the horizon to the system's settling time. The values of the control and prediction horizon may be different as long as $N_c < N_p$. In this case, the last control action can be held until the end of the prediction horizon.

3.3. Optimal Control Problem

The optimal control problem to be considered starts from the definition of a cost functional. For that, the performance associated with each state and control pair is evaluated using a stage cost function $\ell(\cdot) : \mathbb{R}^n \times \mathbb{R}^m \to \mathbb{R}$ at each time step. It is desired to penalize the error between the measured states and the desired ones, as well as the control effort. As such, ℓ may be written as

$$\ell(\boldsymbol{x}(j), \boldsymbol{u}(j)) = \|\boldsymbol{x}(j) - \boldsymbol{x}^r(j)\|^2_{\boldsymbol{Q}} + \|\boldsymbol{u}(j) - \boldsymbol{u}^r(j)\|^2_{\boldsymbol{R}}, \tag{21}$$

with the r superscript indicating reference values and $\boldsymbol{Q} \in \mathbb{R}^{n\times n}$ and $\boldsymbol{R} \in \mathbb{R}^{m\times m}$ being, respectively, weighting matrices for the states and control inputs. It is worthwhile mentioning that in terms of tuning, increasing the values of $\boldsymbol{Q}$ makes the controller more active in the state error minimization, leading to aggressive control actions. Likewise, increasing the values of $\boldsymbol{R}$ penalizes the control effort, leading to a slower control response.

In order to finally pose the optimal control problem for the MPC, constraints can be defined based on the characteristics of the system's states and inputs. First, considering the prediction process previously explained, constraints enforcing that each predicted state respects the dynamical model are defined together with an initial condition constraint. Second, state constraints related to physical and dynamical limitations can be added as $|\boldsymbol{x}| \leq \boldsymbol{x}_{lim}$. Likewise, input constraints related to the saturation limits of the actuators are considered as $|\boldsymbol{u}| \leq \boldsymbol{u}_{lim}$. Finally, since unit quaternions are used to model the tri-dimensional rotations of the system, the constraint $\|\boldsymbol{r}_{\boldsymbol{\mathcal{B}}}^{\boldsymbol{\mathcal{E}}}\| = 1$ is imposed for normalization.

Considering the nominal nonlinear model (20) for prediction, the cost functional (21), and the aforementioned constraints, the open-loop optimal nonlinear control problem can be stated as follows

$$
\begin{aligned}
\min_{\underset{\rightarrow}{\boldsymbol{x}}, \underset{\rightarrow}{\boldsymbol{u}}} \quad & \sum_{j=k}^{K+N_c-1} \ell(\boldsymbol{x}(j), \boldsymbol{u}(j)) + \sum_{j=k+N_c}^{K+N_p} \ell(\boldsymbol{x}(j), \boldsymbol{u}(k+N_c-1)) \\
\text{s.t. } & \boldsymbol{x}(k) = \boldsymbol{x}, \\
& \boldsymbol{x}(j+1) = f(\boldsymbol{x}(j), \boldsymbol{u}(j), \boldsymbol{d}(k)),\ j = k, \cdots, k+N_c-1 \\
& \boldsymbol{x}(j+1) = f(\boldsymbol{x}(j), \boldsymbol{u}(k+N_c-1), \boldsymbol{d}(k)),\ j = k+N_c, \cdots, k+N_p, \\
& |\boldsymbol{x}(j)| \leq \boldsymbol{x}_{lim},\ j = k, \cdots, k+N_p, \\
& |\boldsymbol{u}(j)| \leq \boldsymbol{u}_{lim},\ j = k, \cdots, k+N_c-1, \\
& \|\boldsymbol{r}_{\boldsymbol{\mathcal{B}}}^{\boldsymbol{\mathcal{E}}}(j)\| = 1,\ j = k, \cdots, k+N_p,
\end{aligned}
$$

with $\underset{\rightarrow}{\boldsymbol{x}}$ and $\underset{\rightarrow}{\boldsymbol{u}}$ denoting, respectively, the predicted state sequence and the optimal control sequence. Therefore, solving the problem (22) in a receding horizon fashion at each time step k, it can be obtained the control action to be applied to the system, which is the first element of $\underset{\rightarrow}{\boldsymbol{u}}$.

Notice that the nonlinear MPC presented in (22) can be used for regulation and tracking problems depending on how the reference are defined throughout the horizon. Particularly, if the reference value $\boldsymbol{x}^r(j)$ in (21) is constant, i.e, $\boldsymbol{x}^r(j) = \boldsymbol{x}^r(j+1)$ and $\boldsymbol{u}^r(j) = \boldsymbol{u}^r(j+1)$ for all j, the proposed controller is solving a regulation problem. Likewise, if the reference varies throughout the horizon, the proposed controller is solving a tracking control problem.

4. Numerical Results

4.1. Simulation Parameters

The sampling time must capture the fastest dynamics of the system. Thus a 10 ms interval is chosen for the discrete time step. Moreover, the discretization of the model is performed using a zero-order hold integrator over the nonlinear model for the prediction process. Although this leads to integration error, a sufficiently small time step is used so that such inaccuracies do not detract from the overall results. The nonlinear model is used for the simulation due to its accuracy throughout the whole domain, as the states vary considerably from any initial condition.

The prediction and control horizons must also be adequately chosen, so as to be able to capture the slowest dynamics of the system. Given the need to balance the stability-increasing property of larger horizons with their higher demand on computational capacity, it is decided to use a prediction and control horizon of $N_p = N_c = 30$. The weighting matrices $\boldsymbol{Q}$ and $\boldsymbol{R}$ were determined via trial and error.

The computational implementation was conducted using the Casadi toolbox [23] on MATLAB, and the optimization solver used was the Interior Point Optimizer (IPOPT) [24], which is packaged with Casadi. The orbit propagation was computed using the High Precision Orbit Propator for MATLAB [25]. The geomagnetic field was calculated using the International Geomagnetic Reference Field 13 (IGRF13) dataset [26].

Reference physical data were obtained from works dealing with similar applications, a 3U-CubeSat with reaction wheels, both for the satellite [27] and its actuators [28]. Moreover, the disturbance model detailed in subsection 2.4 also required the specification of several constants. Table 2 summarizes the values of the different parameters used in the simulations.

Item	Value	Unit	Item	Value	Unit
dt	0.01	s	$\boldsymbol{I_s}$	$diag[0.03, 0.035, 0.007]$	$kg \cdot m^2$
I_r	0.0002	$kg \cdot m^2$	$\boldsymbol{a}$	$diag[0.005\ 0.005\ 0.005]$	$-$
$\boldsymbol{u}_{lim}$	$\pm[20\ 20\ 20]$	$N \cdot m$	$\boldsymbol{m}$	$[0.0105\ 0.0105\ 0.0035]$	$A \cdot m^2$
$\boldsymbol{x}_{lim}$	$\pm[1.1\ 1.1\ 1.1\ 1.1$	$-$	C_D	2	$-$
	$50\ 50\ 50$	rad/s	ρ	$6.98 \cdot 10^{-13}$	kg/m^3
	$800\ 800\ 800]$	rad/s	μ	$3.986 \cdot 10^{14}$	m^3/s^2
C_s	0.6	$-$	C_d	0.2	$-$
P	$4.5 \cdot 10^{-6}$	Pa			

Table 2: Table of parameter values.

4.2. Simulation Scenario

In the proposed simulation scenario, the satellite initial conditions have non-null angular velocity of $[5, -6, 7]\ rad/s$. The controller must be able to bring this velocity to zero, without exceeding their actuator constraints. The evolution of the system states can be seen in Figure 2, with the state and control constraints denoted in the Figure by Max and Min.

The disturbance torques were obtained at each time step from the disturbance model and held constant during the prediction horizon. Their time evolution, along with that of the control inputs, can also be seen in Figure 2. As Table 3 shows, the largest weight was over the angular velocity states, since regulating them was the main objective.

The controller achieves the stabilization of the angular velocity even with the presence of external disturbances. However, it does not manage to achieve zero state error due to the lack of an integral action in its architecture. Moreover, as expected, it can be seen that the RWs eventually saturates, indicating the necessity to work with desaturation strategies.

Item	Values
$\boldsymbol{Q}$	$[10\ 10\ 10\ 10\ 1000\ 1000\ 1000\ 10^{-9}\ 10^{-9}\ 10^{-9}]$
$\boldsymbol{R}$	$[0.1\ 0.1\ 0.1]$

Table 3: Controller weights for scenario A.

5. Conclusion

The objective of this work was to propose a control strategy that could satisfy the requirements of the ACS for a nanosatellite mission. That is, a controller that could manage to stabilize the spacecraft. Despite the inherent challenges of the satellite attitude control problem, this was achieved.

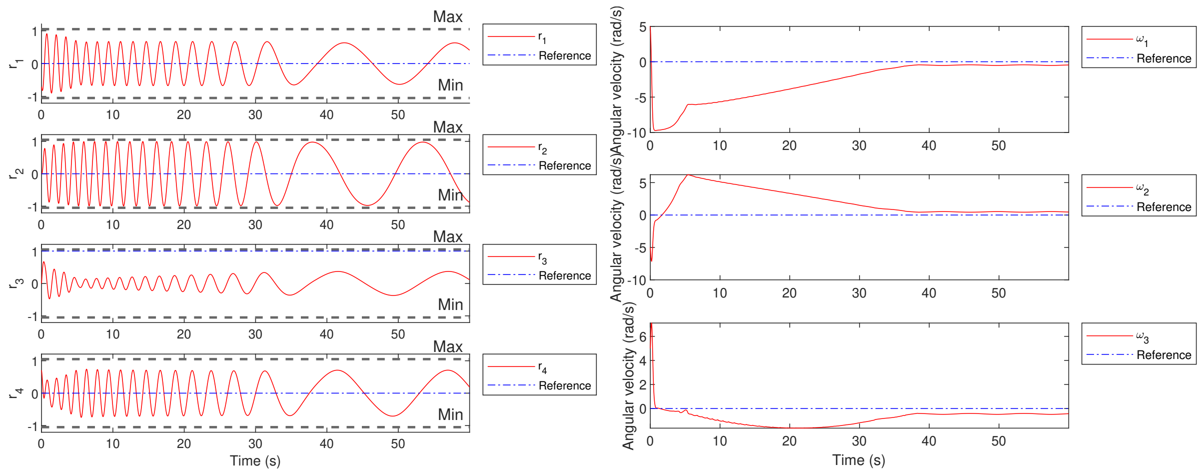

(1) Evolution of quaternion elements **(2) Evolution of satellite angular velocity**

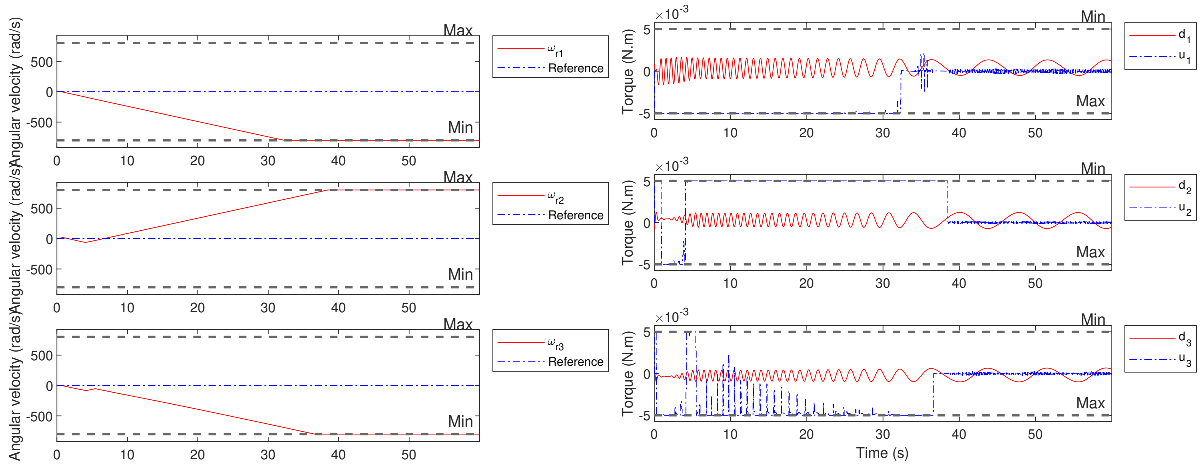

(3) Evolution of reaction wheel angular velocity **(4) Evolution of inputs and disturbances**

Figure 2: Simulation results.

The designed MPC was corroborated, through simulations, to be able to successfully compute the necessary attitude control actions of detumbling after deployment, even when affected by external disturbances, parametric uncertainties, and system constraints. These simulations also showed stability and low steady state error, which is often challenging for more conventional control strategies. However, given the employment of online optimization, the designed control law is demanding in terms of the embedded computing power needed to execute it and is dependent on the capabilities of the numerical solver algorithm that is used. Nevertheless, since spacecraft onboard computers normally have hard real-time operating capacity and given the examples of actual implementation of similar controllers in the literature, it is presumed that this control strategy will feasible to implement.

References

[1] U. Eren, A. Prach, B. B. Koçer, S. V. Rakovic, E. Kayacan, B. Açikmese, Model predictive control in aerospace systems: Current state and opportunities, Journal of Guidance, Control, and Dynamics 40 (2017) 1541–1566.

[2] P. W. Gibbens, E. D. Medagoda, Efficient model predictive control algorithm for aircraft, Journal of Guidance, Control, and Dynamics 34 (2011) 1909–1915.

[3] G. V. Raffo, M. G. Ortega, F. R. Rubio, An integral predictive/nonlinear h∞ control structure for a quadrotor helicopter, Automatica 46 (2010) 29–39.

[4] J. C. Pereira, V. J. S. Leite, G. V. Raffo, Nonlinear Model Predictive Control on SE(3) for Quadrotor Trajectory Tracking and Obstacle Avoidance*, 2019.
[5] M. A. Santos, G. V. Raffo, Path tracking model predictive control of a tilt-rotor uav carrying a suspended load, in: 2016 IEEE 19th International Conference on Intelligent Transportation Systems (ITSC), pp. 1458–1463.
[6] L. D. Filippis, G. Guglieri, F. B. Quagliotti, A novel approach for trajectory tracking of uavs, Aircraft Engineering and Aerospace Technology 86 (2014) 198–206.
[7] T. D. Ngo, C. Sultan, Model predictive control for helicopter shipboard operations in the ship airwakes, volume 39, American Institute of Aeronautics and Astronautics Inc., 2016, pp. 574–589.
[8] Øyvind Hegrenaes, J. T. Gravdahl, P. Tøndel, Attitude control by means of explicit model predictive control, via multi-parametric quadratic programming, volume 2, pp. 901–906.
[9] C. D. Petersen, F. Leve, I. Kolmanovsky, Model predictive control of an underactuated spacecraft with two reaction wheels, Journal of Guidance, Control, and Dynamics 40 (2017) 320–332.
[10] D. Y. Lee, R. Gupta, U. V. Kalabić, S. D. Cairano, A. M. Bloch, J. W. Cutler, I. V. Kolmanovsky, Geometric mechanics based nonlinear model predictive spacecraft attitude control with reaction wheels, Journal of Guidance, Control, and Dynamics 40 (2017) 309–319.
[11] M. Mammarella, D. Y. Lee, H. Park, E. Capello, M. Dentis, G. Guglieri, Attitude control of a small spacecraft via tube-based model predictive control, volume 56, American Institute of Aeronautics and Astronautics Inc., 2019, pp. 1662–1679.
[12] C. Böhm, M. Merk, W. Fichter, F. Allgöwer, Spacecraft rate damping with predictive control using magnetic actuators only, in: Nonlinear Model Predictive Control: Towards New Challenging Applications, 2009.
[13] J. Cubas, A. Farrahi, S. Pindado, Magnetic attitude control for satellites in polar or sun-synchronous orbits, Journal of Guidance, Control, and Dynamics 38 (2015) 1947–1958.
[14] K. Kondo, I. Kolmanovsky, Y. Yoshimura, M. Bando, S. Nagasaki, T. Hanada, Nonlinear model predictive detumbling of small satellites with a single-axis magnetorquer, Journal of Guidance, Control, and Dynamics 44 (2021) 1211–1218.
[15] J. R. Wertz, et al., Spacecraft attitude determination and control, 1972.
[16] B. Wie, Space vehicle dynamics and control, American Institute of Aeronautics and Astronautics, 2008.
[17] B. V. Adorno, Two-arm manipulation: from manipulators to enhanced human-robot collaboration, Ph.D. thesis, Université Montpellier 2, 2011.
[18] M. Gajamohan, M. Muehlebach, T. Widmer, R. D'andrea, The Cubli: A Reaction Wheel Based 3D Inverted Pendulum, 2013.
[19] M. W. Spong, S. Hutchinson, M. Vidyasagar, Robot Modeling and Control, John Wiley & Sons, Inc, 2006.
[20] E. Stoneking, Newton-euler dynamic equations of motion for a multi-body spacecraft, GNC-14: Spacecraft Nonlinear Attitude Dynamics and Control (2007).
[21] J. A. Rossiter, Model-based predictive control : a practical approach, CRC Press, 2003.
[22] E. Camacho, C. Bordons, Model Predictive Control - Second edition, 2007.
[23] J. Andersson, A General-Purpose Software Framework for Dynamic Optimization, PhD thesis, Arenberg Doctoral School, KU Leuven, Department of Electrical Engineering (ESAT/SCD) and Optimization in Engineering Center, Kasteelpark Arenberg 10, 3001-Heverlee, Belgium, 2013.
[24] A. Wächter, L. T. Biegler, Line search filter methods for nonlinear programming: Motivation and global convergence, SIAM Journal on Optimization 16 (2005) 1–31.
[25] M. Mahooti, High precision orbit propagator, `https://www.mathworks.com/matlabcentral/fileexchange/55167-high-precision-orbit-propagator`, 2022. [Online; accessed April 27, 2022].
[26] P. Alken, et al., International geomagnetic reference field: the thirteenth generation, Earth, Planets and Space 73 (2021).
[27] E. Bender, An Analysis of Stabilizing 3U CubeSats Using Gravity Gradient Techniques and a Low Power Reaction Wheel, Ph.D. thesis, California Polytechnic State University, 2011.
[28] S. Tkachev, Y. Mashtakov, D. Ivanov, D. Roldugin, M. Ovchinnikov, Effect of reaction wheel imbalances on attitude and stabilization accuracy, Aerospace 8 (2021).

Design and simulation of a model to determine the attitude and control the orientation of a nanosatellite for the CubeDesign contest

Johrdan Huamanchumo(1), Soledad Fernandez(2), Cristopher Rufasto(3), George Fajardo(4), Omar Blas(5), John Abad(6)

(1) National University of Engineering, 15102,+51977684471, jhuamanchumol@uni.pe
(2) National University of Engineering, 15102,+51967525572, sfernandeza@uni.pe
(3) National University of Engineering, 15102,+51932290376 cristopher.rufasto.m@uni.pe
(4) National University of Engineering, 15102,+51922689983, george.fajardo.s@uni.pe
(5) National University of Engineering, 15102,+51927966284, oblasm@uni.pe
(6) National University of Engineering, 15102,+51931274097, john.abad.a@uni.pe

***Keywords**: Attitude determination, NADIR, TRIAD.*

In this document, a model is developed to determine and control the orientation of a nanosatellite whose properties are initial values provided by the CubeDesign 2021 contest. First, a sequence was elaborated in Stateflow for the nanosatellite to activate the modes according to defined input parameters. Then, for the attitude determination, a TRIAD optimization algorithm was implemented with the values given by the sun sensor and the magnetometer. The reference model of the control system was modified so that the nanosatellite can track the NADIR point and, at the same time, keep the speed of the reaction wheels within an acceptable range. The results show that all the objectives of the contest were achieved, so the simulated nanosatellite stabilizes while in orbit.

1. Introduction

CubeSats are small satellites that have been used in low Earth orbit by commercial companies and mostly educational institutions. These satellites are conducive to carrying scientific research and technology demonstrations in space in a costeffective and relatively easy to perform manner. However, the specifications and characteristics of a cubesat-type nanosatellite restrict the development of its subsystems, in this case the study will focus on the Attitude determination control system. The main objective of this subsystem is to control the angular velocities and the gradual orientation of the satellite in the desired spatial direction, often this direction is the vector pointing towards the earth or nadir. So, ADCS system functions can be divided into attitude measurement, attitude determination and attitude control. The present report documents the work done in the CubeDesign 2021 competition. Only attitude determination and attitude control were developed in a simulator software. Three important parts were performed: the behavioral modeling using a state machine, the estimation of the pointing direction and the dynamic modeling with a velocity control [1].

2. State of art

A. Dynamic model of the ADCS sub-system

The equation for the conservation of angular momentum of a body is given by:

$$\dot{L} + \omega \times L = \tau_{ext}$$

Where L is the angular momentum of the body and τ_{ext} is the external torque. The magnitude of angular momentum in a system can only be changed by applying external torques.

A charateristic of rigid bodies is that their angular momentum depends on the angular velocity of the body. The matrix equation is given by:

$$L = J.\omega + Lr$$

Where J is the diagonal intertia matrix of positive definite shape within the principal axis and Lr is the angular momentum of the reaction wheels or gyroscope.

Finally, the vector equation representing the equations of conservation of angular momentum of a body is given by:

$$\dot{\omega} = J^{-1}[\tau_{ext} - \dot{Lr} - \omega \times (J \cdot \omega + Lr)]$$

3. System Description

A. Attitude Determination

The Simulink diagram given by the contest gives us as information the vectors from the sun sensor and the magnetometer. The four vectors are used to determine the quaternion of the CubeSat in ECI coordinates. Its attitude can be calculated with the Attitude Optimization Matrix from the optimized TRIAD algorithm. For this purpose, the following steps are followed [2]:

TRIAD-I Algorithm:

$$r_1 = \frac{w_1}{|w_1|} \qquad r_2 = \frac{r_1 \times w_2}{|r_1 \times w_2|} \qquad r_3 = r_1 \times r_2$$

$$s_1 = \frac{v_1}{|v_1|} \qquad s_2 = \frac{s_1 \times v_2}{|s_1 \times v_2|} \qquad s_3 = s_1 \times s_2$$

The matrix A1 is expressed as:

$$A_1 = r_1 \cdot s_1^T + r_2 \cdot s_2^T + r_3 \cdot s_3^T$$

TRIAD-II Algorithm:

$$r_5 = \frac{w_2}{|w_2|} \qquad r_2 = \frac{r_1 \times w_2}{|r_1 \times w_2|} \qquad r_4 = r_5 \times r_2$$

$$s_5 = \frac{v_2}{|v_2|} \qquad s_2 = \frac{s_1 \times v_2}{|s_1 \times v_2|} \qquad s_3 = s_1 \times s_2$$

The matrix A2 is expressed as:

$$A_2 = r_5 \cdot s_5^T + r_2 \cdot s_2^T + r_4 \cdot s_4^T$$

Finally, the Attitude Optimization Matrix is determined:

$$\hat{A}' = \frac{\sigma_2^2}{\sigma_1^2 + \sigma_2^2} A_1 + \frac{\sigma_1^2}{\sigma_1^2 + \sigma_2^2} A_2$$

$$A = 0.5 \left[\hat{A}' + \left(\hat{A}'^{-1} \right)^T \right]$$

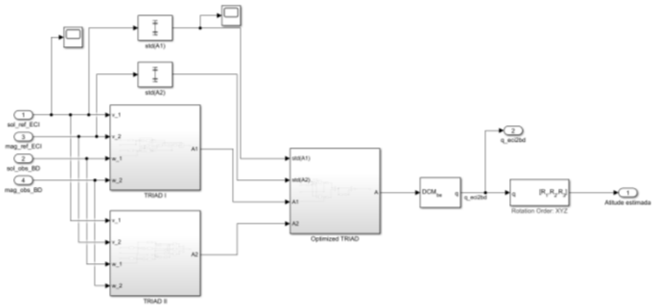

Figure 1: Diagram in Simulink to find the estimated attitude of the CubeSat using optimized TRIAD.

B. Orientation Control

Satellites normally must be pointed toward the Earth for communication missions. Therefore, the CubeSat must rotate around a vector that points towards the earth. For the contest, the vector is required to point towards the NADIR point, which is the intersection between the vertical of the observer and the celestial body. These equations are implemented in Simulink and simulated to obtain the attitude of the CubeSat in the LVLH coordinate system [3].

$$o_{3I} = -\frac{r_I}{\|r_I\|}$$

$$o_{2I} = -\frac{r_I \times v_I}{\|r_I \times v_I\|}$$

$$o_{1I} = o_{2I} \times o_{3I}$$

$$A_{IO} = [o_{1I} \quad o_{2I} \quad o_{3I}]$$

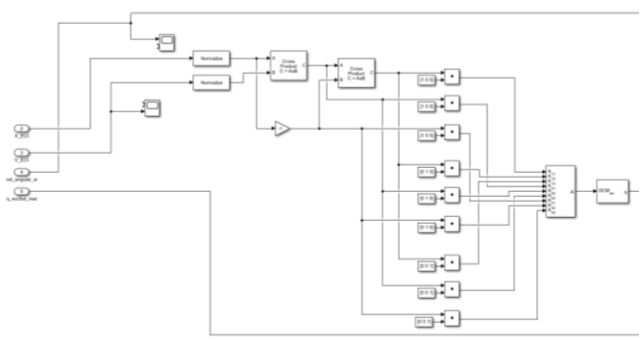

Figure 2: Simulink diagram to determine the quaternion in LVLH coordinates.

This orientation vector is used as a reference for angular position control. However, this only applies if the CubeSat is in stabilization mode. For this reason, a “Step” block was added to the diagram, which represents a signal that indicates that the ADCS system must go to stabilization mode. In this mode, the position control is activated and the CubeSat will point to the NADIR point while the angular rate controller tries to keep this variable at a value equal to zero. The outputs of both controllers are added together and serve as the torque input for the CubeSat's reaction wheel system, according to the following equation [4]:

$$L = -k_p \delta q_{1:3} - k_d \omega$$

where L is the required torque for the reaction wheels, k_p and k_d are positive scalar gains, δq is the error quaternion and ω is the angular velocity of the CubeSat.

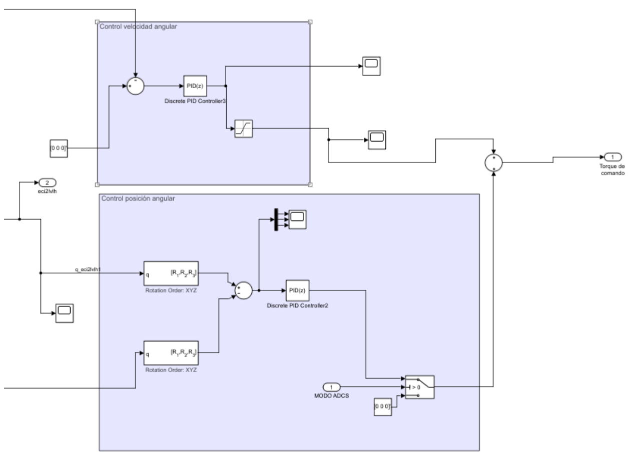

Figure 3: Simulink diagram for CubeSat position and angular velocity control.

C. Behavioral Model

The finite state machine ADCS system consists of 5 operating modes: Safety, Calibration, Pointing, IDLE (Initial) and Detumbling. These modes were extracted from the CubeDesign 2021 competition rules. The variables or inputs that affected the change of state of the subsystem are the angular velocity, orbit propagator, orientation determination, pointing error, the presence of the sun, the state of the reaction wheels and the telecommands that had the highest priority. The five modes of operation will be described below.

The IDLE mode is the nominal mode of the cubesat after launch. In addition, it is used when the cubesat in stable mode (angular velocity less than 1 rad/s) enters eclipse; at the same time, the orbit propagator, the orientation determination and the reaction wheels must be operational.

The pointing mode is used when the cubesat is exposed to sunlight. Like the IDLE mode, the cubesat must be stabilized; in addition, the orbit propagator, the orientation determination and the reaction wheels must be operational.

The safety mode is used immediately when the orbit propagator or the orientation determination is not operational. Other critical cases are when the calibration is unsuccessful, the reaction wheels fail to come out of saturation, the pointing error is out of the allowed range or the CubeSat angular velocity cannot be reduced.

The calibration mode is used in order to point the camera to the Sun after 100 seconds from the start of the simulation and remain in this mode until the calibration is successfully completed. If after a set time the calibration is not successful, the subsystem switches to safety mode.

Finally, the CubeSat will be in detumbling mode when the angular velocity passes the set limits. Additionally, the orbit propagator and orientation determination, as well as the reaction wheels, must be operational.

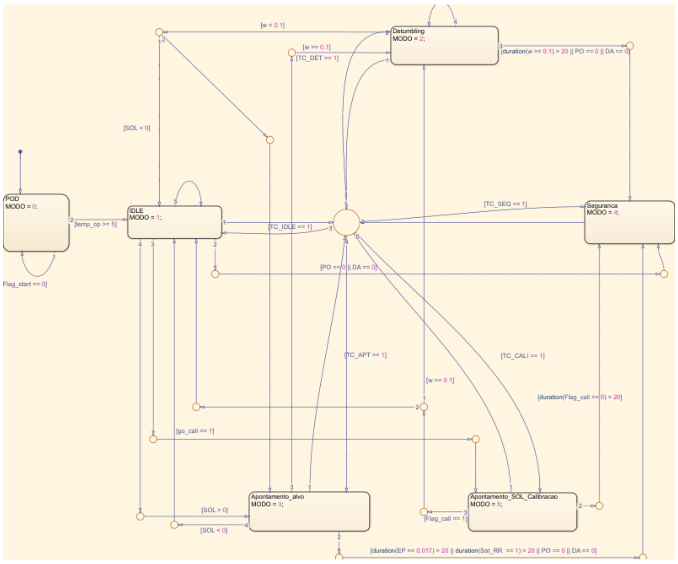

Figure 4: State Flow of compartmental design in Simulink.

4. Results

The CubeSat simulation starts with the ADCS subsystem disabled. When t = 10s, the stabilization mode is activated, and therefore the speed control is activated (see Fig. 5). The initial angular velocity of the CubeSat is [0.006 0.006 0.006] (rad/s). In a time of approximately 57s, the CubeSat stabilizes and maintains its angular velocity at zero. Then, at t = 350s, the CubeSat's pointing mode is activated, so position control is activated without deactivating velocity control (see Fig. 6). In this mode, the CubeSat tries to point towards the NADIR point while keeping its angular velocity close to zero. It is observed that, in a time of 200 seconds, the CubeSat manages to point to NADIR with pointing error values shown in the table.

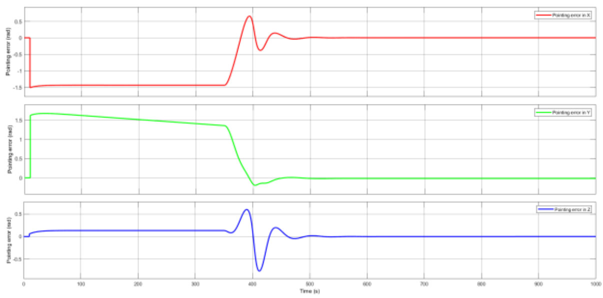

Figure 5: Pointing error of the CubeSat in X, Y and Z

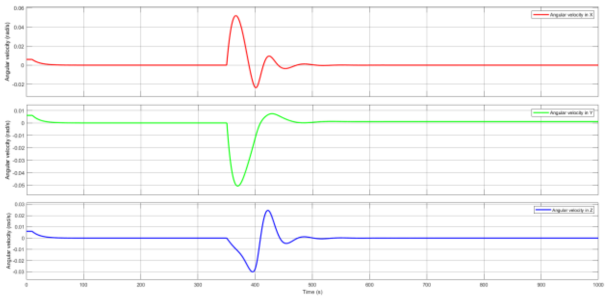

Figure 6: Angular velocity of the CubeSat in X, Y and Z

Table 1. Pointing error values after settling time

Euler Angle	Pointing error (rad)
X	1.962×10^{-5}
Y	1.597×10^{-5}
Z	3.345×10^{-5}

5. Conclusions

In this document, a model is developed to determine and control the orientation of a nanosatellite whose properties and initial conditions are provided by the organizers of the CubeDesign 2021 contest. The tests carried out with the ADCS system model for the CubeSat operating modes were satisfactory, since the nanosatellite activates the modes correctly according to the input parameters of the system. Likewise, it was possible for the CubeSat model to stabilize its angular velocity during the stabilization mode, and during the pointing mode, to point towards the NADIR point with pointing error values in the three axes within the allowed ranges. In future works, the CubeSat will be implemented and the technical data of its components will be introduced in the model to verify its operation before sending it into space.

References

[1] CUBEDESIGN II EDIÇÃO VIRTUAL (2.a ed.). (2021).

[2] MOHAMMED, M.A. & Boussadia, Halima & Bellar, A. & Adnane, Akram. (2017). Performance comparison of attitude determination, attitude estimation, and nonlinear observers algorithms. Journal of Physics: Conference Series. 783. 012017. 10.1088/1742-6596/783/1/012017.

[3] Cai, Guowei & Chen, Ben & Lee, Tong. (2011). Coordinate Systems and Transformations. Advances in Industrial Control. 10.1007/978-0-85729-635-1_2.

[4] Markley, L. F., & Crassidis, J. L. (2014). Fundamentals of Spacecraft Attitude Determination and Control: 33 (2014 ed.). Springer.

[5] STARIN, Scott R.; ETERNO, John. Spacecraft Attitude Determination and Control Systems. [S. l.: s. n.], 2011. vol. 244.

ATTITUDE RECONSTRUCTION OF THE ALFACRUX CUBESAT USING ONBOARD SENSORS AND SOLAR PANELS IN-ORBIT DATA

Bruno T. de Mello(1), **Renato A. Borges**(2), **Simone Battistini**(3)
(1) *University of Brasilia, Campus Universitário Darcy Ribeiro, Brasília, Brazil, bruno.tunesm@gmail.com*
(2) *University of Brasilia, Campus Universitário Darcy Ribeiro, Brasília, Brazil, raborges@ene.unb.br*
(3) *MBDA Italia SpA, Via Monte Flavio 45, 00131, Rome, Italy, simone.battistini@mbda.it*

Keywords: *CubeSat, Sun vector estimation, Attitude reconstruction, Unscented Kalman filter*

The deployment of nanosatellites has become the means to conduct research experiments, test new technologies concepts and improve the student qualification for the aerospace industry. Motivated by this new scenario and the range of applications, the interest in CubeSats design by Brazilian institutions has grown in the last years, resulting in successful missions. The most recent mission is the AlfaCrux, a 1U CubeSat developed by the University of Brasília that was launched into orbit on April 1st, 2022. The present work proposes to reconstruct the attitude of the AlfraCrux satellite by means of the onboard gyroscope and magnetometer data, as well as the solar panels measurements to provide information on the Sun position.The attitude is estimated using a nonlinear derivation of the Kalman Filter, called USQUE. The attitude reconstruction results are presented and discussedand future works are proposed. The results show an accuracy of 8 degrees for 3-sigma deviation in the estimated angles and filter convergence was achieved.

1. Introduction

The CubeSat standard was created for educational purposes to provide training in the field of space sciences and technologies. Due to the relative low cost and short development cycle, the CubeSats are also adopted for science missions and experiments, technology demonstrations and even commercial applications.

Brazil, as a country of vast extensions, has an increasing demand and potential opportunities in the space market. This context and the pursue for the aerospace industry's growth promoted Cubesat missions initiatives by Brazilian educational and research institutions.

The first Brazilian CubeSat launched into space was the NanoSatCBr1 in 2014 [1]. In the following year, the 1U Cubesat designed by university students AESP-14 was in orbit [2]. The ITASAT-1 6U CubeSat was launched in the end of 2018 [3]. There is also schools initiatives as the Tancredo-1 picosatellite [4]. Another mission for student education and training was the 1U CubeSat FloripaSat-1, injected into orbit in 2019 [5].

The most recent Brazilian CubeSat launched into space is the AlfaCrux, a 1U satellite developed by researchers and students from University of Brasilia (UnB), whose mission is to provide educational training and radio amateur services [6]. AlfaCrux is also the physical entity of a Digital Twin framework under development for research purposes [7].

The goal of this work is to perform the attitude reconstruction for the AlfaCrux spacecraft using in-orbit data. For this, the Unscented Quaternion Estimator (USQUE) is considered [8]. The USQUE is a filtering algorithm based on Unscented Kalman filter commonly used for spacecraft attitude estimation [9]. The attitude parameters are propagated in time through the gyroscope measurements and the correction is performed with the magnetometer and solar panels related data. First, the initial state is determined using the Triaxial Attitude Determination (TRIAD) [10]. The filtering solution consists in the use of TRIAD for the initial global attitude estimate, then, the USQUE provides the estimation of a local attitude deviation which updates the global parameters in a recursive manner. Since only the current and voltage measurements are available in the AlfaCrux for each pair of panels (opposite sides are connected in parallel), the estimation of the solar direction by taking the difference of opposite panels current cannot be carried out. Therefore, the method defined in [11] will be considered for the Sun direction estimation.

This paper is organized as follows. The AlfaCrux mission is briefly described in Section 2. Section 3 defines the spacecraft attitude motion equations and parameters, followed by the Sun direction vector estimation with solar panels data described in Section 4. In Section 5 the USQUE algorithm is presented and the results of the in-orbit flight data filtering is discussed in Section 6. Section 7 describes the conclusion and future works.

2. AlfaCrux Mission and Architecture

The AlfaCrux is a 1U Cubesat representing the space segment of a radio amateur and educational mission to provide practical learning and scientific benefits in the context of small satellite design and operations. It was launched on April 1st, 2022, and injected into a Sun-synchronous orbit (SSO) with period of 94.64 minutes, inclination of 97.39º, apogee altitude of 508 km and perigee of 494 km. Both satellite and ground station have been commissioned, and tests and verification procedures were executed in order to validate the ground station hardware and software, as well as the health of the spacecraft and its main subsystems, missing only the payload service demonstration.

Furthermore, the station telemetry data storage capabilities will allow the construction of the AlfaCrux Digital Twin, a virtual model that simulates the real satellite through the telemetry data processing along with mathematical and functional models. Within this context, the attitude reconstruction will provide the satellite pose and sensors parameters for the digital model.

2.1. Spacecraft Design

The AlfaCrux satellite is a cube with sides of 10cm length. The main subsystems are the electric power system (EPS), batteries, payload subsystem, an onboard computer (OBC) and a telemetry, tracking and Control (TTC) hardware. A deployable turnstile system with four tape springs antennas provides omnidirectional irradiation. Table 1 summarizes the subsystems description and features.

The OBC has an embedded gyroscope and magnetometer, whose data are sent in the telemetry package and will be used for the attitude reconstruction. The gyroscope

Table 1: Alfacrux subsystems description [7].

Subsystem	Features
Electric Power System	6 solar panels; voltage regulators; 3V3 and 5V buses; over-current protection; a batery of 4x Li-Ion cells
Payload	Alén Space TOTEM-SDR with UHF 437 MHZ transceiver
Onboard Computer	AVR32 32-bit MCU, clock up to 66 MHz; 128 MB Flash; 32 MB SDRAM; I2C, CAN and UART buses
TTC subsystem	UHF 435-438 MHZ transceiver; 30dBm output at 4.9/9.6 kbps; Forward error correction

is a 3-Axis MPU-3300 from InvenSense, and the magnetometer is the HMC5843 from Honeywell. Both components communicate with the microcontroller via a I2C bus.

Also, each solar panel is installed on one face of the spacecraft and provides power up to 2.4W with 4.8V and 0.5A at the maximum power point (MPP). Opposite sides panels are connected in parallel, which results in one current and voltage data for each panels pair. The temperature telemetry is individual.

3. Spacecraft Attitude Modeling

The space vehicle orientation at any time instant can be represented by a certain attitude parameterization. For this filtering problem, the chosen representation is the quaternion $\mathbf{q}$, an extension of the complex number described by four components where the first three ones constitutes a vector and the last one is a scalar. The quaternion formulation is given by

$$\mathbf{q} = \begin{bmatrix} \mathbf{e} sin(\vartheta/2) \\ cos(\vartheta/2) \end{bmatrix} = \begin{bmatrix} \varrho \\ q_4 \end{bmatrix} = \begin{bmatrix} q_1 & q_2 & q_3 & q_4 \end{bmatrix}^T, \tag{1}$$

where $\mathbf{e}$ is the rotation vector, ϑ is the rotation angle and q_i, $i = 1, \dots 4$ are the four components. Also, ϱ is the vector part of the quaternion. The only restriction regarding the quaternion attitude representation is the unit norm, in which $\mathbf{q}^T \mathbf{q} = 1$.

Besides the quaternion, another parametrization will be considered in the filter, the called Generalized Rodrigues Parameters (GRP) $\mathbf{p}$, a three-component vector related to the quaternion by

$$\mathbf{p} = f \frac{\varrho}{(a + q_4)}, \tag{2}$$

where f and a are scalars that can be arbitrarily chosen. Attitude parameters express the satellite pose in one frame with respect to a reference system.

3.1. Attitude Kinematics

Given a rigid body with rotational motion in a tridimensional space, the kinematics of the body's attitude is given by

$$\dot{\mathbf{q}}(t) = \frac{1}{2} \Xi[\mathbf{q}(t)] \omega(t), \tag{3}$$

where $\omega(t)$ is a vector composed by the angular velocity in each dimension and

$$\Xi(\mathbf{q}) = \begin{bmatrix} q_4 I_{3\times3} + [\varrho\times] \\ -\varrho^T \end{bmatrix}, \tag{4}$$

with $[\varrho\times]$ representing the cross-product matrix of ϱ, which can be defined for any tridimensional vector by

$$[\mathbf{x}\times] \equiv \begin{bmatrix} 0 & -x_3 & x_2 \\ x_3 & 0 & -x_1 \\ -x_2 & x_1 & 0 \end{bmatrix}. \tag{5}$$

The vectors considered in this work are described in three different reference frames. As shown in Figure 1, the inertial frame is fixed with respect to distant stars and its origin is located in the Earth's center, the called Earth-Centered Inertial Frame (ECI). The orbital frame is dependent of the satellite position in the orbit so that it is centered in the spacecraft center-of-mass, with components in radial direction, normal to the orbital plane and tangential to the trajectory, which results in the Local Vertical Local Horizontal Frame (LVLH). Finally, the spacecraft body frame has its origin in the CubeSat center-of-mass and its components are the structure axes.

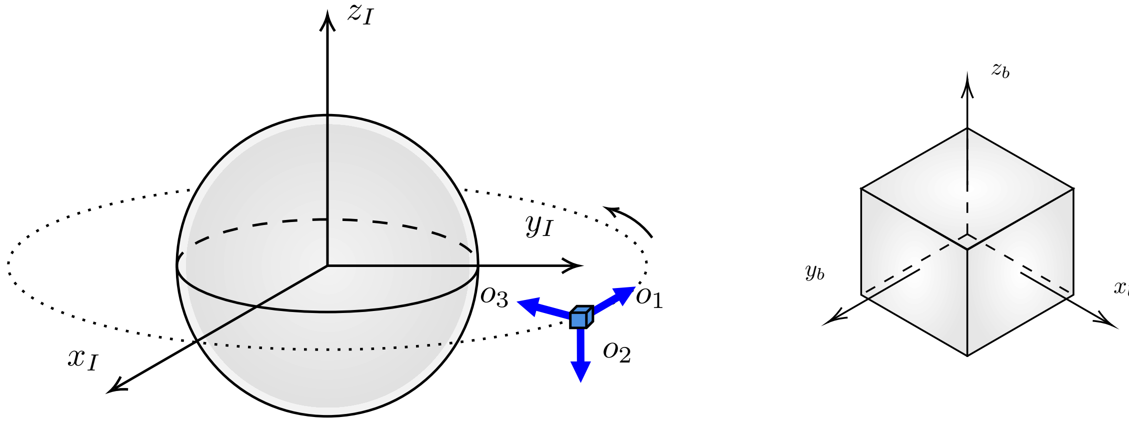

Figure 1: Inertial, orbital frames (left) and Spacecraft body frame(right).

3.2. Attitude Sensors Models

Each sensor of the AlfaCrux satellite is modeled as a true measurement with noise and error components treated as random processes. The sensor noise features are considered in the filtering process for optimizing the solution. The rate-integrating gyroscope measures a true angular velocity vector along with a bias value and a noise signal as in the following equations

$$\tilde{\omega}(t) = \omega^{true}(t) + \boldsymbol{\beta}(t) + \boldsymbol{\eta}_v(t), \quad \text{and} \quad \dot{\boldsymbol{\beta}}(t) = \boldsymbol{\eta}_u(t), \tag{6}$$

where $\omega^{true}(t)$ is the unknown true angular velocity vector, $\boldsymbol{\beta}(t)$ is the sensor bias, $\boldsymbol{\eta}_v(t)$ and $\boldsymbol{\eta}_u(t)$ are uncorrelated zero-mean Gaussian white-noise processes.

The magnetometer measures the magnetic field where the sensor is immersed in, as the geomagnetic field and electric current generated fields, along with the related noise as

$$\tilde{\mathbf{B}}(t) = \mathbf{B}^{true}(t) + \boldsymbol{\eta}_m(t), \tag{7}$$

where $\tilde{\mathbf{B}}(t)$ is the sensor output reading, $\mathbf{B}^{true}(t)$ is the true field value and $\boldsymbol{\eta}_m(t)$ is a zero-mean Gaussian random process. The true quantity can be considered as the observation computed through the environment model rotated to the sensor body frame.

4. Sun Line-of-Sight Estimation

Sun sensors are used for determining the solar radiation direction with respect to the sensors assembly. This direction can also be used for attitude determination in methods that use vector measurements, as the geomagnetic field direction vector.

In order to determine the panels configuration where the current generation occurs, the solar vector composed by the power generated by each pair is considered and the highest temperature between the opposite panels indicates which one is producing the computed power, since the CubeSat face towards the Sun will have its temperature increased, as shown in [11]. In this case the Sun direction is given by

$$\mathbf{S}_b = \begin{bmatrix} sign(T_{+X} - T_{-X})V_{\pm X}I_{\pm X} \\ sign(T_{+Y} - T_{-Y})V_{\pm Y}I_{\pm Y} \\ sign(T_{+Z} - T_{-Z})V_{\pm Z}I_{\pm Z} \end{bmatrix}, \quad (8) \quad \text{and} \quad sign(x) = \begin{cases} +1 & \text{,if } x > 0 \\ -1 & \text{,if } x < 0 \\ 0 & \text{,if } x = 0 \end{cases}, \quad (9)$$

where T is temperature of the respective panel side, V is the voltage generated by one pair and I is the current.

An important phenomenon that affects the Sun sensor accuracy is the Earth albedo, which is the solar radiation reflected by the planet surface. When such energy is captured by the onboard sensors, it can interfere in the Sun direction estimation. In order to estimate such index, [12] presents a source of measurements constituting a grid of data points, an 180x288 matrix, dividing the Earth surface into cells.

The energy reflected by a surface area cell located at latitude and longitude (ϕ_g, θ_g) that is perceived by the spacecraft is given by the equation

$$E_c(\phi_g, \theta_g) = \begin{cases} \dfrac{\rho(\phi_g, \theta_g) E_{AM0} A_c(\phi_g) \hat{\mathbf{r}}_{Sun}^T \hat{\mathbf{n}}_c \hat{\mathbf{r}}_{sat}^T \hat{\mathbf{n}}_c}{\pi \parallel \mathbf{r}_{sat} \parallel^2} & \text{if } (\phi_g, \theta_g) \in \mathbf{V}_{Sun} \cap \mathbf{V}_{sat} \\ 0 & \text{otherwise} \end{cases}, \tag{10}$$

where $\rho(\phi_g, \theta_g)$ is the reflectivity index, $A_c(\phi_g)$ is the cell area size, $\hat{\mathbf{n}}_c$ is the cell normal vector, $\hat{\mathbf{r}}_{Sun}$ is the Sun direction vector with respect to the cell and $\hat{\mathbf{r}}_{sat}$ is the satellite line of sight also with respect to the same cell. The set $\mathbf{V}_{Sun} \cap \mathbf{V}_{sat}$ is formed by all surface cells illuminated by the Sun and visible by the satellite. The scalar E_{AM0} is the solar intensity at air mass zero, which means the flux density upper the atmosphere, where the value is 1367 W/m². Figure 2 illustrates the geometry related to the albedo model. The total energy, E_a, that reaches the satellite is the sum of the radiation from all cells in the set, that is

$$E_a = \sum_{\mathbf{V}_{Sun} \cap \mathbf{V}_{sat}} E_c(\phi_g, \theta_g). \tag{11}$$

Finally, the Earth albedo resulting direction can be approximated as the radial vector according to the satellite's orbit position, that is, the satellite's nadir opposite direction [13].

5. Unscented Attitude Filter

The algorithm implemented for the attitude estimation is the Unscented Quaternion Estimator (USQUE). This method is based on the Unscented Transform (UT), which approximates a non-linear function by a set of points in the state-space according to

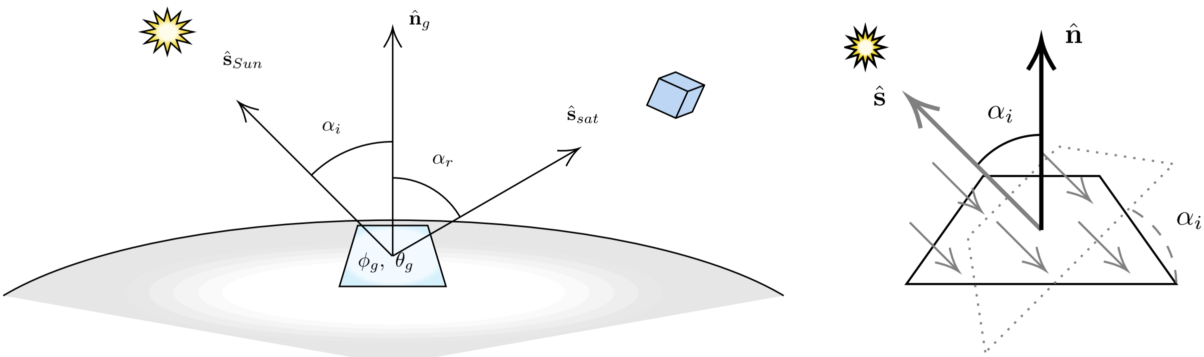

Figure 2: Solar radiation reflection geometry(left) and effective area(right).

a probability density function, usually assumed Gaussian. The system to be reconstructed is described by the following set of equations

$$\begin{aligned} \mathbf{x}_{k+1} &= \mathbf{f}(\mathbf{x}_k, k) + G_k \mathbf{w}_k, \\ \mathbf{y}_k &= \mathbf{h}(\mathbf{x}_k, k) + \mathbf{v}_k, \end{aligned} \tag{12}$$

where $\mathbf{x}$ is the state vector, $\mathbf{f}(\cdot)$ is the dynamical system non-linear function that updates the state in time, $\mathbf{w}_k$ is the model error vector, G_k is a function that maps the process errors to the state space. Besides, $\mathbf{y}$ is the output or measurement vector, $\mathbf{h}(\cdot)$ maps the state vector into the observation space and $\mathbf{v}_k$ is the measurement error vector. Both error vectors are modeled as uncorrelated Gaussian random variables.

The USQUE considers a multiplicative approach with respect to the attitude parameters. In this case, a global attitude represents the actual spacecraft pose while a local attitude parameter represents the attitude error. Such error will be estimated by the filter and it will correct the global representation after one iteration. This approach has the benefit of maintaining the quaternion unit norm. The local attitude-error quaternion, $\varrho\mathbf{q}$, is represented using a vector of GRP.

In the multiplicative approach, the new attitude quaternion is defined by the product between the error and the previous estimated one, which results in a unit quaternion. Therefore, the state vector is composed by the attitude error in GRP parameterization and the gyroscope biases, as expressed by

$$\hat{\mathbf{x}}_k^+ \equiv \begin{bmatrix} \varrho\mathbf{p}^T & \boldsymbol{\beta}^T \end{bmatrix}^T. \tag{13}$$

The $2n + 1$ σ-points are generated from the state vector for $i = 0, \ldots, 2n$, with $n = 6$ being the state dimension, as presented below

$$M = \begin{bmatrix} \mathbf{0} & S & -S \end{bmatrix}, \quad \text{where: } S = \sqrt{(n+\lambda)(P_k^+ + \bar{Q}_k)}, \tag{14}$$

$$\chi_k(i) = M_i + \hat{\mathbf{x}}_k^+, \quad \text{and} \quad \chi_k(0) = \hat{\mathbf{x}}_k^+. \tag{15}$$

Each σ-point is propagated in time. First, the GRP parameters are converted to quaternion, as a small angle in GRP can be converted to a quaternion representation such as

$$\boldsymbol{\delta}\mathbf{q} = \begin{bmatrix} \delta\varrho^T & \delta q_4 \end{bmatrix}^T. \tag{16}$$

The full σ-points quaternions are obtained by the product of the estimate $\hat{\mathbf{q}}_k^+$ and the error quaternions converted from GRP, as

$$\hat{\mathbf{q}}_k^+(i) = \boldsymbol{\delta}\mathbf{q}_k^+(i) \otimes \hat{\mathbf{q}}_k^+, \quad \text{and} \quad \hat{\mathbf{q}}_k^+(0) = \hat{\mathbf{q}}_k^+, \tag{17}$$

where $\boldsymbol{\delta}\mathbf{q}_k^+ = \begin{bmatrix}\delta\varrho_k^+ & \delta q_4^+\end{bmatrix}^T$ is the attitude-error quaternion.

The predicted state is obtained from the numeric integration of the attitude kinematic equation presented previously as $\chi_{k+1}(i) = \mathbf{f}[\chi_k(i), k]$.

The gyroscope measurements are used in the kinematic model and computed as $\hat{\omega} = \tilde{\omega} - \chi_k^\beta(i)$, where $\hat{\omega}$ is the estimated quantity, $\tilde{\omega}$ the observed one and $\chi_k^\beta(i)$ is the state vector part related to the bias estimation. After the σ-points propagation, the error quaternions are retrieved by

$$\boldsymbol{\delta}\mathbf{q}_{k+1}^-(i) = \hat{\mathbf{q}}_{k+1}^-(i) \otimes [\hat{\mathbf{q}}_{k+1}^-]^{-1}, \tag{18}$$

where $\hat{\mathbf{q}}_{k+1}^- = \hat{\mathbf{q}}_{k+1}^-(0)$. The σ-points quaternions are converted back to GRP parameters. Then, the mean state vector and mean covariance error matrix are computed as

$$\hat{\mathbf{x}}_{k+1}^- = \frac{1}{n+\lambda}\left\{\lambda\boldsymbol{\chi}_{k+1}(0) + \frac{1}{2}\sum_{i=1}^{2n}\boldsymbol{\chi}_{k+1}(i)\right\}, \tag{19}$$

$$P_{k+1}^- = \frac{1}{n+\lambda}\left\{\lambda[\boldsymbol{\chi}_{k+1}(0) - \hat{\mathbf{x}}_{k+1}^-][\boldsymbol{\chi}_{k+1}(0) - \hat{\mathbf{x}}_{k+1}^-]^T + \frac{1}{2}\sum_{i=1}^{2n}[\boldsymbol{\chi}_{k+1}(i) - \hat{\mathbf{x}}_{k+1}^-][\boldsymbol{\chi}_{k+1}(i) - \hat{\mathbf{x}}_{k+1}^-]^T\right\} + \bar{Q}_k. \tag{20}$$

The process error covariance matrix is given by

$$\bar{Q}_k = \frac{\Delta t}{2}\begin{bmatrix}(\sigma_v^2 - \frac{1}{6}\sigma_u^2)\Delta t I_{3\times3} & 0_{3\times3} \\ 0_{3\times3} & \sigma_u^2\Delta t\end{bmatrix}. \tag{21}$$

In the correction phase, the mean predicted output is computed from the observation model as

$$\hat{\mathbf{y}}_{k+1}^- = \frac{1}{n+\lambda}\left\{\lambda\boldsymbol{\gamma}_{k+1}(0) + \frac{1}{2}\sum_{i=1}^{2n}\boldsymbol{\gamma}_{k+1}(i)\right\}, \tag{22}$$

where each σ-point is transformed by the observation function $\boldsymbol{\gamma}_{k+1}(i) = \mathbf{h}[\boldsymbol{\chi}_{k+1}(i), k]$.

The observation model for any vector measurement taken by a sensor is given by

$$\tilde{\mathbf{y}}_k = \begin{bmatrix}A(\mathbf{q})\mathbf{r}_1 & A(\mathbf{q})\mathbf{r}_2 & \dots & A(\mathbf{q})\mathbf{r}_n\end{bmatrix}^T + \begin{bmatrix}\boldsymbol{\nu}_1^T & \boldsymbol{\nu}_2^T & \dots & \boldsymbol{\nu}_n^T\end{bmatrix}^T, \tag{23}$$

where $A(\mathbf{q})$ is the rotation matrix from inertial to the body frame, $\mathbf{r}_i$ are reference vectors obtained from models and $\boldsymbol{\nu}_i$ is the measurement error associated to the i-th sensor. For the predicted output, the matrix $A(\mathbf{q})$ is the attitude matrix built with the predicted quaternion from the prediction step. This is also the form of the observation function $\mathbf{h}(\cdot)$ when computing $\boldsymbol{\gamma}_{k+1}(i)$. The output covariance matrix, P_{k+1}^{yy}, the innovation covariance matrix, $P_{k+1}^{\upsilon\upsilon}$, and the cross-correlation matrix, P_{k+1}^{xy}, are computed as the equations below

$$P_{k+1}^{yy} = \frac{1}{n+\lambda}\left\{\lambda[\boldsymbol{\gamma}_{k+1}(0) - \hat{\mathbf{y}}_{k+1}][\boldsymbol{\gamma}_{k+1}(0) - \hat{\mathbf{y}}_{k+1}]^T + \frac{1}{2}\sum_{i=1}^{2n}[\boldsymbol{\gamma}_{k+1}(i) - \hat{\mathbf{y}}_{k+1}][\boldsymbol{\gamma}_{k+1}(i) - \hat{\mathbf{y}}_{k+1}]^T\right\}, \tag{24}$$

$$P_{k+1}^{\upsilon\upsilon} = P_{k+1}^{yy} + R, \tag{25}$$

$$P_{k+1}^{xy} = \frac{1}{n+\lambda}\left\{\lambda[\boldsymbol{\chi}_{k+1}(0) - \hat{\mathbf{x}}_{k+1}^-][\boldsymbol{\gamma}_{k+1}(0) - \hat{\mathbf{y}}_{k+1}]^T + \frac{1}{2}\sum_{i=1}^{2n}[\boldsymbol{\chi}_{k+1}(i) - \hat{\mathbf{x}}_{k+1}^-][\boldsymbol{\gamma}_{k+1}(i) - \hat{\mathbf{y}}_{k+1}]^T\right\}. \tag{26}$$

With the covariance matrices, the Kalman gain can be obtained as $K_k = P_k^{xy}(P_k^{\upsilon\upsilon})^{-1}$.

The innovation is computed as the difference between the sensors observations and the predicted output

$$\boldsymbol{\upsilon}_k \equiv \tilde{\mathbf{y}}_k - \hat{\mathbf{y}}_k^- = \tilde{\mathbf{y}}_k - \mathbf{h}(\hat{\mathbf{x}}_k^-, k). \tag{27}$$

The final step is the state vector update with the innovation and the gain as for the error covariance matrix

$$\hat{\mathbf{x}}_{k+1}^+ = \hat{\mathbf{x}}_k^- + K_k \boldsymbol{\upsilon}_k, \tag{28}$$

$$P_{k+1}^+ = P_k^- - K_k P_k^{\upsilon\upsilon} K_k^T. \tag{29}$$

The attitude error is transformed to a quaternion and it is used to update the global attitude representation which is the new attitude estimate, as in the equation below,

$$\hat{\mathbf{q}}_{k+1}^+ = \boldsymbol{\delta}\mathbf{q}_{k+1}^+ \otimes \hat{\mathbf{q}}_k^+. \tag{30}$$

Later, the attitude-error in the state vector is set to zero (reset) before the beginning of the next iteration.

6. Flight Data Results and Analysis

The AlfaCrux telemetry regarding the gyroscope, magnetometer and solar panels data were considered for the the attitude reconstruction and the filter assessment. Due to the spacecraft and ground station commissioning in the early operations in the first months, the telemetry report were generated using a low sample rate, and some irregular availabilities were noted in the time series of data. Therefore, for this preliminary case the sampling period is of 30 seconds and comprehends an interval of 5 minutes on August 7th 2022. The Figures 3 and 4 present the telemetry data used for the attitude reconstruction assessment.

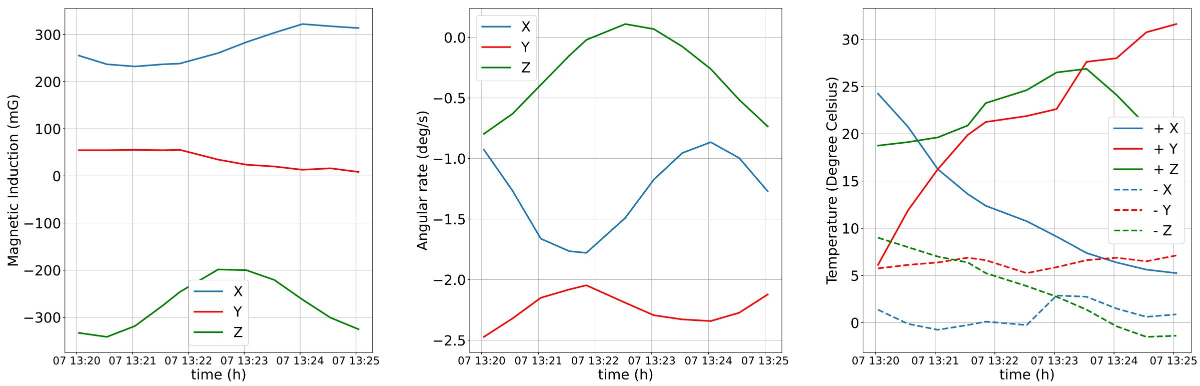

Figure 3: Magnetometer (left), gyroscope (middle) and solar panels temperature (right) measurements observations.

The USQUE is parameterized with $\sigma_u = 10^{-4}$ and $\sigma_v = 10^{-5}$, so that the process noise covariance matrix, Q_k can be computed. The measurement noise covariance matrix is $R = diag(\begin{bmatrix} 10^{-4} & 10^{-4} & 10^{-4} & 10^{-2} & 10^{-2} & 10^{-2} \end{bmatrix})$. Also, the initial state error covariance matrix is given by $P_0 = diag(\begin{bmatrix} 10^{-4} & 10^{-4} & 10^{-4} & 10^{-4} & 10^{-4} & 10^{-4} \end{bmatrix})$.

The initial spacecraft pose is obtained from the TRIAD algorithm with the magnetometer and solar panels measurements. Once the initial conditions are available, the

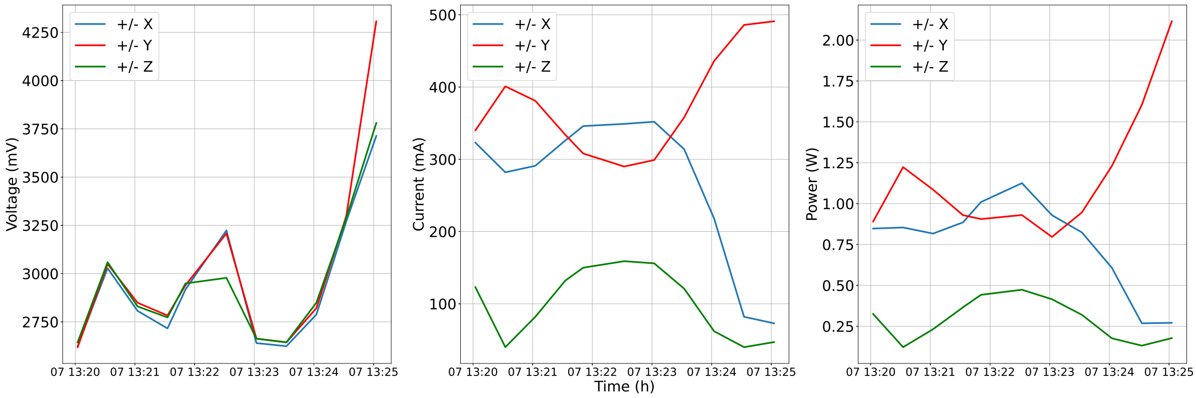

Figure 4: Solar panels output voltage, current and computed power.

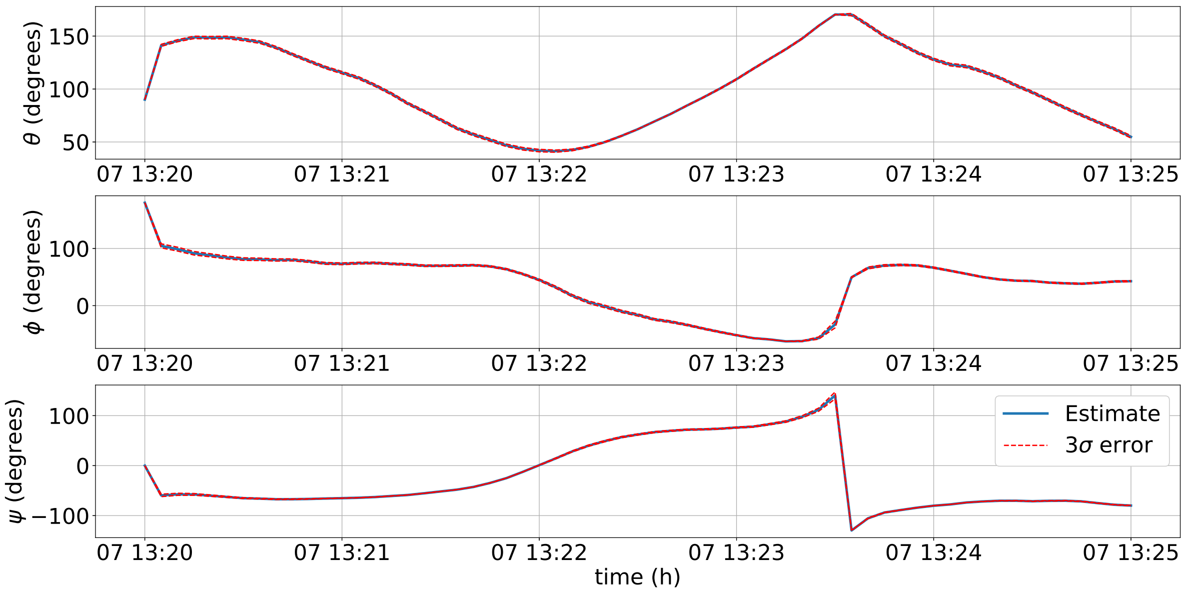

Figure 5: Euler angles described in the 3-1-3 rotation sequence.

USQUE method can be considered. Figure 5 presents the Euler angles estimated for the related time interval.

Since the AlfaCrux does not have an attitude control system, the disturbance torques are the only ones acting on the spacecraft. A spacecraft with angular rates of the same order of the ones observed in the gyroscope telemetry has the same attitude motion as the curves in the Figure 5. Also, the mean square error of the 3-sigma interval is about ± 8 degrees for each angle. For the purpose of a preliminary result, it is possible to verify that USQUE was able to estimate the attitude motion with a consistent confidence interval, as shown by the 3-sigma interval curves, which did not diverge.

In order to improve the filter performance, a deep study for the sensors characterization must be considered. The covariance matrices were chosen by the order of parameters specified in the datasheets, however a parameter assessment process may be performed. Besides, the magnetometer bias estimation and the presence of residual magnetic dipole analysis will improve the presented model, which will provide more accurate results.

7. Conclusion

This work presented preliminary results of the AlfaCrux CubeSat attitude reconstruction with in-orbit sensors measurements and solar panels related data. For this purpose, the USQUE algorithm was considered and the Sun line-of-sight was determined by means of the solar panels generated power and temperature values. The Earth albedo intensity was also accounted and its effects were also minimized.

The filtering algorithm presented an accuracy of ± 8 degrees, which can be improved if considering disturbance torques effects and sensors parameters, as bias, misalignment and so on. Such scenario is part of future works.

Acknowledgments

The authors would like to thank the Brazilian agencies National Council for Scientific and Technological (CNPq) and the Federal District Research Support Foundation (FAPDF) that supported this work.

References

[1] N. J. Schuch, O. S. C. Durão, M. R. da Silva, F. Mattiello-Francisco, J. B. dos S. Martins, A. P. Legg, A. L. da Silva, E. E. Bürguer, The NanoSatC-BR, cubesat development program - a joint cubesat program developed by UFSM and INPE/MCTIC - space geophysics mission payloads and first results, Brazilian Journal of Geophysics 37 (2019) 95–103.

[2] E. E. Bürger, G. Loureiro, P. T. Lacava, D. H. Z. Carrera, C. T. Hoffmann, The cubesat AESP14 and its systems engineering development process, in: Proceedings of the 1st Latin American IAA CubeSat WorkShop.

[3] L. H. S. Sato, L. E. V. L. da Costa, J. B. Fulindi, H. A. dos Santos, L. dos S. Paula, E. H. S. de Oliveira, J. G. de Azevedo, B. A. Crucioli, D. G. Vieira, V. Carrara, A. C. di I. Jeronymo, R. B. Januzi, D. H. Makita, W. G. dos Santos, P. K. de Albuquerque, M. de Fátima Mattiello-Francisco, The ITASAT – the lessons learned from the mission concept to the operation (2019). 33rd Annual AIAA/USU Conference on Small Satellites.

[4] A. Tikami, C. Moura, W. A. Dos-Santos, First on-orbit results from the Tancredo-1 picosat mission, in: Proceedings of the 1st IAA Latin American Symposium on Small Satellites: Advanced Technologies and Distributed Systems, Session, volume 2.

[5] G. M. Marcelino, E. M. Filho, S. V. Martinez, L. O. Seman, E. A. Bezerra, In-orbit preliminary results from the open-source educational nanosatellite FloripaSat-I, Acta Astronautica 188 (2021) 64–80.

[6] L. Reis, R. Borges, J. Leite, C. Cappelletti, S. Battistini, An overview of the AlfaCrux cubesat mission for narrowband communication, Advances in the Astronautical Sciences (2020) 245–255.

[7] R. A. Borges, A. C. dos Santos, W. R. Silva, L. Aguayo, G. A. Borges, M. M. Karam, R. B. de Sousa, B. F.-A. García, V. M. S. Botelho, J. M. Fernández-Carrillo, J. M. L. Agra, F. A. Agelet, J. V. Q. S. Borges, A. C. A. de Oliveira, B. T. de Mello, Y. C. F. Avelino, V. F. Modesto, E. C. Brenag, The AlfaCrux cubesat mission description and early results, Applied Sciences 12 (2022).

[8] J. L. Crassidis, F. L. Markley, Unscented filtering for spacecraft attitude estimation, Journal of Guidance, Control, and Dynamics 26 (2003) 536–542.

[9] S. Battistini, C. Cappelletti, F. Graziani, Results of the attitude reconstruction for the UniSat-6 microsatellite using in-orbit data, Acta Astronautica 127 (2016) 87–94.

[10] F. L. Markley, J. L. Crassidis, Fundamentals of Spacecraft Attitude Determination and Control, Space Technology Library, Springer New York, 2014.

[11] O.-J. Kim, H. Shim, S. Yu, Y. Bae, C. Kee, H. Kim, J. Lee, J. Han, S. Han, Y. Choi, In-orbit results and attitude analysis of the snuglite cube-satellite, Applied Sciences 10 (2020).

[12] D. Bhanderi, T. Bak, Modeling Earth Albedo for satellites in Earth orbit, in: AIAA Guidance, Navigation, and Control Conference and Exhibit, AIAA, 2005.

[13] D. Bhanderi, Modeling Earth Albedo currents on Sun sensors for improved vector observation, in: AIAA Guidance, Navigation, and Control Conference and Exhibit, AIAA, 2005.

[14] D. A. Vallado, Fundamentals of astrodynamics and applications, Space technology library, Microcosm Press, Hawthorne, CA, 4th ed. edition, 2013.

PTOLEMY II FRAMEWORK AS A TOOL FOR ANALYZING ATTITUDE CONTROL ALGORITHMS FOR NANOSATELLITES

Alex Alves(1), **Luiz Silveira**(1), **Samaherni Dias**(1), **Márcio Kreutz**(1)
(1) Federal University of Rio Grande do Norte, Natal/RN, Brazil, alex.alves@ufrn.br, lfelipe@dca.ufrn.br, sama@laci.ufrn.br, marcio.kreutz@ufrn.br

Keywords: *Ptolemy II, Java, CubeSat, Navigation System, Extended Kalman Filter*

Cubesat standard popularization, thanks to the advance in microelectronics, created new challenges to the design of embedded systems for space application. Considering the mass and size constraints and the radiation effects over Cubesat subsystems, it is essential to model and simulate components and algorithms that must be applied to such subsystems, which are essentially heterogeneous, before hardware and software prototyping and implementation. We believe that some open-source tools that provide environments for developing mathematical models based on the integration of pre-built software components can be useful in the design of Cubesat subsystems. An example of such tools is called Ptolemy II, which is an open-source software framework, based on Java programming language, that can be used to model, simulate, and design concurrent, real-time, embedded systems. Therefore, in this work, we investigate the use of Ptolemy II and Java to model and simulate some components of a nanosatellite navigation system. A Sun Vector Model was developed to calculate the sun vector related to an Earth-centered coordinate frame. An Earth Magnetic Field Model was created to provide the earth's magnetic field based on input information. An Orbit Propagator Model was designed to receive orbit information in the form of a Two-Line Element set and calculate latitude, longitude, and altitude using the SGP4 algorithm. The last model to be implemented was the Extended Kalman Filter (EKF) Model, which can be used for attitude estimation. These models were developed and integrated into Ptolemy II with the aid of Application Programming Interfaces (APIs) such as Hipparchus 1,7 (math library for matrix calculation) and Orekit 10.2, which is a Java library that provides basic dynamic space elements (such as orbits, dates, attitude, and frames) and various algorithms to handle them. In order to validate the developed models, simulations were run in the Ptolemy II environment, aiming at the analysis of attitude estimation using the EKF algorithm. Furthermore, this work provides results and information regarding the use of Ptolemy as an open-source framework for developing space dynamic models and simulations along with the analysis of Cubesat subsystem behavior in orbit. As future work, we cite the implementation of an embedded EKF for Hardware-in-the-Loop simulation along with Ptolemy II.

1. Introduction

At the beginning of the Space Age, access to space was restricted to large commercial entities and government organizations due to the high cost of developing satellite missions. However, the advent and popularization of microelectronics, starting in the 1980s, made it possible for physically smaller satellites to be built by small teams with modest facilities [1]. Furthermore, the technological expansion allowed the creation of a standard of picosatellites (mass between 0.1 kg and 1 kg) and nanosatellites (mass between 1 kg and 10 kg) called CubeSat.

According to the standard specification [2], a CubeSat is a 10 cm cube with a mass up to 2 kg, which is defined as 1 unit or 1U. Many units can be grouped to build larger configurations, such as 2U, 3U, and 6U. Althought CubeSats are limited in size, they are composed of all the subsystems necessary to carry out a space mission. Among these subsystems, we have Electrical Power System (EPS); Attitude and Determination Constrol System (ADCS); Telemetry, Tracking & Command System (TT&C); On-Board Computer (OBC); and payload [3]. These subsystems perform specific functions in the nanosatellite and are essential for its correct operation while in orbit. They are built on printed circuit boards and data transmission takes place via communication buses. Moreover, each subsystem may have its own processor, allowing data processing in CubeSats to be decentralized.

Since the complete behavior of the satellite in orbit is hardly predicted before launch, the modeling and simulation of hardware and software systems is an important step in the design of a nanosatellite mission. Thus, the utilization of tools that allow the implementation of mathematical models of sensors and other components of the system becomes essential. After the simulation of the modeled systems, decisions can be made regarding the components and routines executed by the embedded software in the spacecraft.

Given the specifics of a space mission, the development of embedded systems for nanosatellites may involve the integration of different components (processors, signal processing units, attitude control blocks, among others). Thus, software and hardware design must include the specification of heterogeneous systems that need more than one Model of Computation [4].

As stated by Lee [5], a model of computation contains the definitions of concurrent components of a system, as well as the way they communicate, how they relate to each other, and what information they share. There are a vast number of MoCs that deal with concurrency and time in different ways [5]. As examples of MoCs, one can cite continuous time, discrete event, finite-state machines, synchronous/reactive and dataflow models [4].

Nowadays, tools such as Ptolemy II [6], ForSyDe [7], and Simulink [8] provide MoCs combinations for heterogeneous systems specification. Furthermore, they allow the developed system to be simulated. Thus, such tools can be used as an alternative for the modeling and simulation of embedded systems for nanosatellites.

In this work, we investigate the use of the Ptolemy II open-source software framework and the Java programming language as the basis for modeling and simulating some components of a nanosatellite navigation system. This system is described in Section 2 and the methodology is presented in Section 3. The developed models that compose the system are presented in Section 4, while Section 5 includes simulation and results. Then, the conclusion and some propositions for future works are presented in Section 6.

2. Navigation System

Generally, in spacecraft dynamics problems, several reference frames are used. For example, one can fix a reference frame to the Earth ($\mathcal{F}_1$) and other to the spacecraft body ($\mathcal{F}_2$). Thus, the orientation of reference frame $\mathcal{F}_2$ with respect to $\mathcal{F}_1$ can describe the spacecraft orientation with respect to the Earth. The orientation of a spacecraft in space is called attitude [9][10].

The nanosatellite navigation system is part of the spacecraft control system and it determines the current spacecraft attitude from attitude sensor measurements [9]. However, since the sensors available in a spacecraft (such as sun sensor, star trackers, rate gyros, magnetometers) provide measurements that are corrupted by noise, it is not possible to determine the exact attitude in orbit [11]. Therefore, in order to determine the actual atittude of a spacecraft, a attitude estimation techinique must be used [9].

In Figure 1, it is presented the attitude estimation system of a spacecraft, which is assumed to be equipped with a sun sensor and a magnetometer. In order to model these sensors, it must be implemented a mathematical model that provides de sun position vector and magnetic field vector in an inertial frame (such as ECI, Earth-Centered Inertial, frame). Then, the vector coordinates in the spacecraft reference frame can be calculated by applying a rotation matrix to the coordinates obtained in the inertial frame [11].

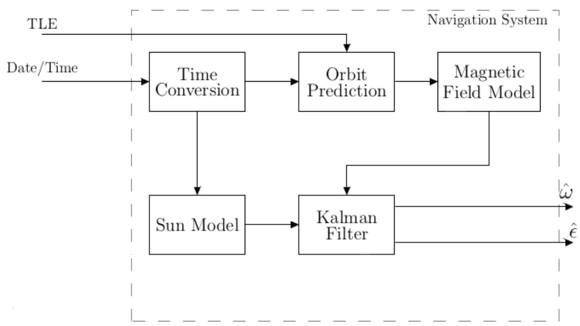

Figure 1: Navigation System (Source: Adapted from [12]).

The block diagram in Figure 1 is composed by a Sun Model and a Magnetic Field Model that provide the normalized vectors in the inertial frame. The Orbit Prediction Model is responsible for determining the spacecraft position in orbit around the Earth upon receiving a Two-Line Element set (TLE) [13]. The Kalman Filter block is used to estimate the attitude ($\hat{\epsilon}$) and angular velocity ($\hat{\omega}$) of the nanosatelite.

Kalman Filter was presented by Rudolf E. Kalman, in 1960, in his paper entitled "A New Approach to Linear Filtering and Prediction Problems" [14]. Since that time, thanks to advances in digital computing, the Kalman Filter has been widely used in research and applications, particularly in the area of assisted and autonomous navigation [15].

Given the measurements acquired over time, the Kalman Filter algorithm is able to provide estimates of unknown variables. This algorithm is divided in two stages: prediction and correction [16]. During the prediction stage, the algorithm provides the *a priori* state estimate, which is a prediction of the state given the process model and the best previous estimate. In the correction stage, the *a priori* estimate is used to improve the estimate of the state by incorporing the measurements obtained by the sensors. The corrected state estimate is also called the *a posteriori* estimate. The algorithm also incoporates process and measurement noise [9]. In nanosatellites, the process noise is related to the dynamics and kinematics of the spacecraft.

For nonlinear systems, a derivation of the filter, called Extended Kalman Filter (EKF) must be used, which is the case for the spacecraft attitude estimation. A detailed description of EKF application in nanosatellite navigation system can be found in [9], [17], and [11]. In this work, the Norm-Constrained Extended Kalman Filter described by De Ruiter et al. [9] was used as reference for modeling and simulating the attitude estimation. The mathematical specification of the norm-constrained EKF is out of the scope of this paper, but it can be accessed in one of the cited works.

3. Methodology

For the purposes of implementing the navigation system models, the following tools and API's (Application Programming Interfaces) were used:

- Eclipse IDE [18]: integrated development environment for developing models in Java programming language;
- Ptolemy II [6]: tool for simulating, modeling and design of concurrent, real-time, embedded systems;
- Hipparchus 1.7 [19]: mathematics library in Java, which has been mainly used for basic matrix operations;
- Orekit 10.2 [20]: library written in Java that provides basic elements of space dynamics (orbits, dates, attitude, frames) and handling algorithms.

The Eclipse IDE and the mentioned libraries were firstly used to write algorithms in Java that would allow the verification of Orekit and Hipparchus methods and classes. Then the libraries were integrated into a project with Ptolemy II and the models were developed.

4. Models

Ptolemy II is based on actor models, which are components that execute concurrently and share data by sending message via ports. An actor can be defined, for example, as the composite of other actors. However, the most flexible method of creating an actor is using Java programming language. Furthermore, the model of computation is specified by a component called director [21].

The interation among actors is broken into *prefire*, *fire*, and *postfire* actions. These actions are defined as Java methods. During the *fire* action, the actor tipically performs its main computation. In other words, when an actor is “fired”, it reads input data, performs computation and produces output data. *Prefire* and *postfire* methods are used, respectively, for testing preconditions for the actor to fire, and for updating an actor persistent state that evolves during execution [21].

In this work, Java models (actors) were developed for the calculation of the solar vector and the earth's magnetic field, for orbit propagation, and for attitude estimation. The EKF model was created as a composite actor from the integration of simple actors defined in Java.

4.1. Sun Vector Model

The Sun Vector was the first model to be implemented using Orekit methods that provide computation of the vector with respect to an Earth-centered reference system. Such methods receive date and time information yielding the values of the X, Y and Z components according to the chosen reference frame. In Figure 2(1), it is presented the model and the parameters that can be set.

Figure 2: Vector Models.

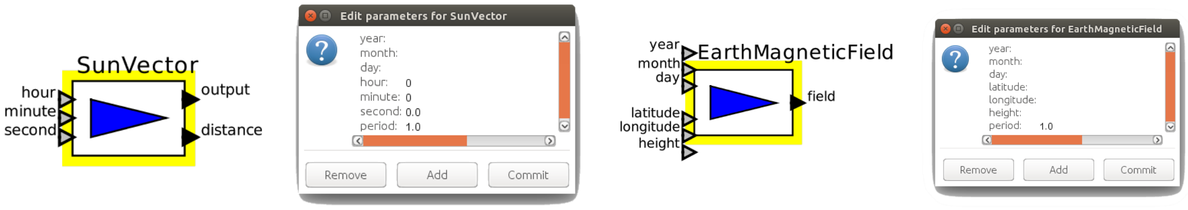

((1)) Sun Vector Model. **((2)) Earth Magnetic Field Model.**

Vector components can be observed in the port named “output” and the Earth-Sun distance can be retrieved from the “distance” port, which was used for debug purposes. The period parameter is used to define a time-step for firing the actor when no input port is connected. Thus, it was mostly used for debugging the model.

4.2. Earth Magnetic Field Model

The Earth Magnetic Field model (Figure 2(2)) was developed using Orekit methods that calculate the magnetic field based on day, month and year information. To perform such calculations, these methods rely on a set of mathematical models knows as IGRF (International Geomagnetic Reference Field) [22], which must receive latitude and longitude data in radians and the height in meters. The output of this model is the magnetic field vector in nano Tesla and the period parameter has similar behavior as the one specified in the Sun Vector Model.

4.3. Orbit Propagator Model

In order to compute latitude, longitude and height data to be retrieved by the Earth Magnetic Field Model, an Orbit Propagator was designed (Figure 3). This model receives, as parameters, the satellite orbit information TLE (.txt) [13] and date/hour references. Based on these parameters, the model calculates the latitude, the longitude, and the altitude of the nanosatellite using the SGP4 algorithm [23] available at Orekit. In this model, the parameter named “period” has the same function previously described.

4.4. Extended Kalman Filter Model

The Extended Kalman Filter is a composite actor that incorporates three main actors (Figure 4(1)): an actor responsible for generating the true system state (EkfUpdate); an actor whose role is to compute the predicted state estimate (EkfPredict); an actor that receives sensor measurements and yields the corrected state estimate (EkfCorrect).

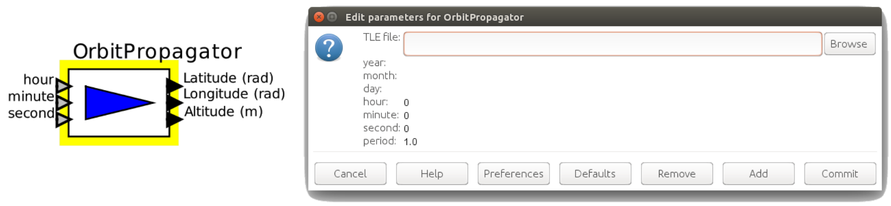

Figure 3: Orbit Propagator Model.

Figure 4: EKF Models.

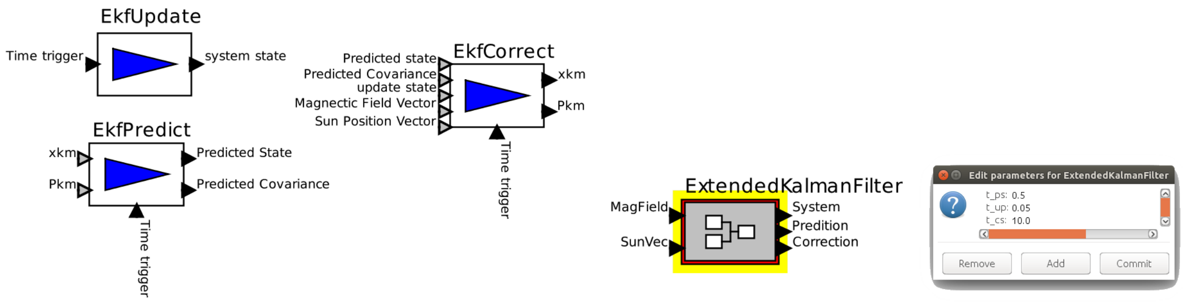

((1)) EKF main actors. **((2)) EKF composite actor.**

The EkfUpdate actor must be configured with internal parameters that are related to the spacecraft truth model, such as the moment of inertia, and the initial angular velocity and attitude. The "time trigger" input port fires the actor accordingly with a predefined time-step (t_up), which is set in the composite actor. When this actor is fired, it updates the current state (angular velocity and attitude) of the truth model. This information is latter retrieved by the EkfCorrect actor.

The EkfPredict actor has an input port that recieves the best previous estimate state (xkm) and another that represents the best previous estimate covariance (Pkm). Both data are either produced by the EkfCorrect actor or are self-updated (by making xkm and Pkm equals to the current values calculated during the predict stage) if no new output comes from EkfCorrect. The predicted data are computed in time intervals defined by a parameter of the composite actor (t_ps). This time-step is used to fire the actor through the input port "time trigger". Furthermore, the EkfPredict has internal parameters that must be set in order to calculate the outputs. Among these parameter stands out the process initial angular velocity and attitude (process initial state), the spacecraft moment of inertia, and the process noise covariance (PNC).

The correct stage of a Kalman Filter was modeled in the EkfCorrect actor, which receives as inputs the predicted state and covariance, the data produced by EkfUpdate (update state), and the normalized vectors provided by the Sun Vector and by the Earth Magnetic Field models. These normalized vectors are used by the algorithm to model a sun sensor and a magnetometer. In order to achieve that, a rotation matrix is applied to the vectors. These calculations were implemented as methods of a Java class that is instatiated in the EkfCorrect source code. EkfCorrect is fired accodingly to the time-step (t_cs) set by a parameter of the composite actor. Moreover, this actor has an internal parameter that defines the measurement noise covariance (MNC), which is used in the EKF algorithm. The algorithm described by De Ruiter et al. [9] also incorporates the disturbances, the process noise and the measurenment noises.

In Figure 4(2), it is presented the ExtendedKalmanFilter composite actor, which was created by interconnecting the previosly described actors. The way these actors were put together is out of the scope. However, it is important to notice that some Ptolemy II basic actors were used in order to ensure time synchronization between each one of the main actors.

5. Simulation and Results

Each of the models described in the previous section was simulated separately. These simulations were performed in order to validate the model behavior and computation. As an example, the SunVector model was imported into the Ptolemy II environment, and it was connect to basic actors that allowed to obtain the Earth-Sun distance in a time interval for a predefined date. This information was then compared with data avalaible in [24] in order to verify if the aphelion and perihelion time was in accordance.

For the other models, similar simulation methods were used. Once each model had been validated, the navigation system in Figure 5 was implemented in Ptolemy II. The time was computed by the TimeCounter actor starting at 00:00:00 on 28 June 2018, which was the date set as parameter of the OrbitPropagator and SunVector actors. In order to simulate the orbit propagation, the generic TLE showed in Figure 6 was set to the OrbitPropagator actor.

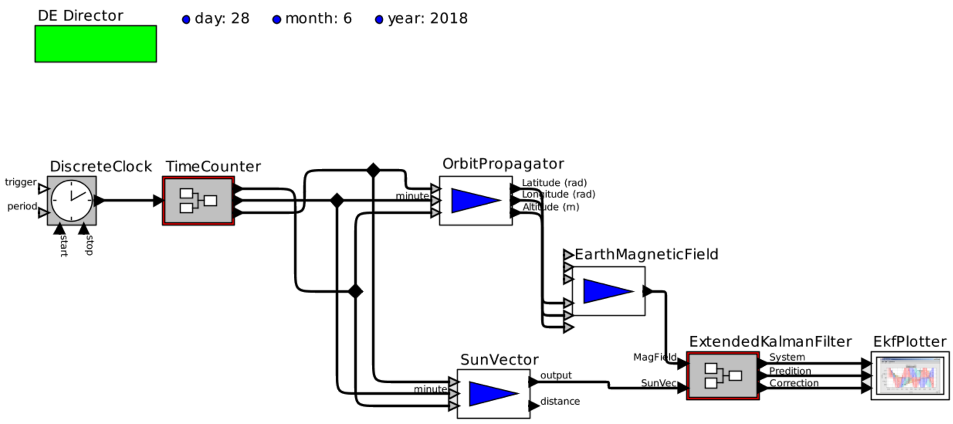

Figure 5: Navigation System Simulation.

00000U 00000000 18179.00000000 0.00000000 000000−0 00000−0 0 0000
00000 087.0000 000.0000 0000000 000.0000 00.0000 15.37599000000000

Figure 6: Generic nanosatellite TLE (Source: Adapted from [17]).

The ExtendedKalmanFilter main actors were configured with the values presented in table 1, where *diag* represents a diagonal matrix and **I** is a 3×3 identity matrix.

Simulation time parameters are presented in Table 2. The simulation total time was defined by the Discrete Event (DE) director and the time-steps were determined as parameters of the ExtendedKalmanFilter actor.

Table 1: EKF simulation parameters.

Actor	Parameter	Value
EkfUpdate	Initial angular velocity	$\begin{bmatrix} 0,05 & -0,05 & 0,05 \end{bmatrix}^T \ rad/s$
	Initial attitude	$\begin{bmatrix} \frac{\sin 0,5}{\sqrt{3}} & \frac{\sin 0,5}{\sqrt{3}} & \frac{\sin 0,5}{\sqrt{3}} & \cos 0.5 \end{bmatrix}^T$
	Moment of inertia	*diag*$\{27, 17, 25\}\ kg \cdot m^2$
EkfPredict	Process initial state	$\begin{bmatrix} 0 & 0 & 0 & 0 & 0 & 0 & 1 \end{bmatrix}$
	Initial covariance	*diag*$\{0.1, 0.1, 0.1, 0.1, 0.1, 0.1, 0.1\}$
	PNC	$0.001^2 \cdot \mathbf{I}$
EkfCorrect	MNC	*diag*$\{0.01^2, 0.01^2, 0.01^2, 0.005^2, 0.005^2, 0.005^2\}$

Table 2: Simulation time parameters.

Parameter	Value	Description
Simulation time	$300\ s$	simulation total time ruled by the DE director
t_up	$0.05\ s$	truth model timestep
t_ps	$0.5\ s$	prediction time-step
t_cs	$10\ s$	measurement acquisition time-step

In Figure 7, it is presented the simulation results produced by the EkfPlotter actor. In this figure, the red line represents the true system state, the blue dot corresponds to the predicted state estimate, and the dashed green line inlustrates the corrected state estimate. Morever, w_1, w_2 and w_3 are the angular velocities, and e_1, e_2 and e_3 are attitude components. Comparing Figure 7 with the ones presented by [17] and [9], one can observe that the behavior performed by the filter was pretty similar. However, it is important to note that due to simplicity purposes, the EKF models that were implemented in this work neglected the process and measurement noises, as well as external disturbances acting on the spacecraft. Since the models were written in Java, these characteristics can be easily incorporated in the future for a more realistic simulation.

6. Conclusions and Future Works

The use of free and open-source tools for modeling and simulating heterogeneous systems represents an alternative to overcome the challenges of developing embedded systems for space applications, such as the ones that composes nanosatellites. This is particulally interesting when the teams do not have enough finantial resources to investe in new tools.

Ptolemy II environment, along with Orekit and Hipparchus, allowed us to write models to calculate sun position and magnetic field vectors using existing algorithms, which is an advantage for developing time. Additionally, using Java can be a good alternative for those who are not familiar with programming languages like C and MATLAB. Thus, it is possible to promote the interest of those more used to software development, in order to bring them to space research areas. It is also important to note that once the models are built, integrating and simulating them in Ptolemy II environment, as shown in Figure 7, has a teaching potential of allowing to introduce some space concepts while abstracting the mathematics involved. For more complex analyses, the open-source nature of the tools provides a way to easily improve the characteristics of the models.

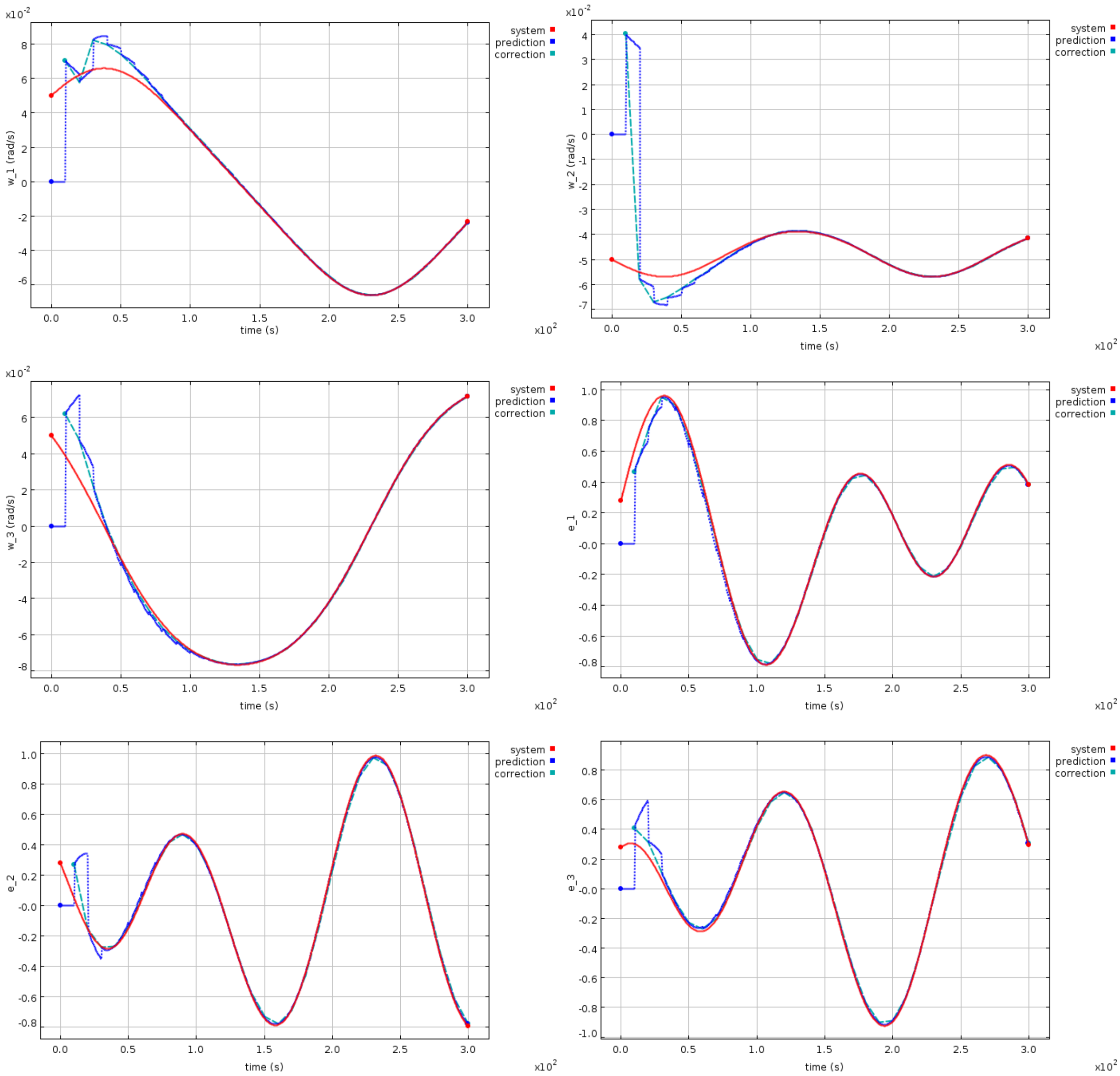

Figure 7: Simulation Results.

As the EKF model has been divided into modules, it is possible to modify any of the main actors individually, as well as quickly analyze the results of these changes. However, one can note that synchronizing all these modules may be a challenge for those not familiar with Ptolemy II. So, it may be necessary to go through a deep reading about the environment, which can be achieved, for example, by accessing the content in [21]. The main drawbacks of using the described tools may be related with understanding how actors and directors actually interates with each other. Nonetheless, there are reference documents that can help in the learning process.

In order to simulate and model a more realistic navigation system, as future work, it is proposed to run further simulations with different TLEs and spacecraft features (as moment of inertia), as well as with disturbances and noises incoporated. This is important to get rid of major bugs in the models, as well as to determine constraints and limits of the models. Furthermore, the implementation of an embedded EKF (using a microcontroller for example) for Hardware-in-the-Loop simulation along with the Sun Vector and Earth Magnectic Field models can provide a structure for embedded software validation, incorporating features of a nanosatillite in orbit (disturbances and noises).

Acknowledgments

This study was financed in part by the Coordenação de Aperfeiçoamento de Pessoal de Nível Superior - Brasil (CAPES) - Finance Code 001.

References

[1] M. N. Sweeting, Modern small satellites-changing the economics of space, Proceedings of the IEEE 106 (2018) 343–361.
[2] A. Johnstone, CubeSat Design Specification rev.14.1, Technical Report, The CubeSat Program, Cal Poly, SLO, 2022.
[3] O. Koudelka, Micro/nano/picosatellite-activities: Challenges towards space education and utilisation, in: I. Marboe (Ed.), Small Satellites: Regulatory Challenges and Chances, Studies in Space Law, Brill, 2016.
[4] X. Liu, J. Liu, J. Eker, E. A. Lee, Heterogeneous modeling and design of control systems, in: T. Samad, G. Balas (Eds.), Software-Enabled Control: Information Technology for Dynamical Systems, John Wiley & Sons, Ltd, 2005, pp. 105–122.
[5] E. A. Lee, Embedded software — an agenda for research.
[6] Ptolemy Project, Available in: https://ptolemy.berkeley.edu/, 2022. Accessed 15 Sep. 2022.
[7] ForSyDe, Available in: https://forsyde.github.io/, 2022. Accessed 15 Sep. 2022.
[8] Simulink, Available in: https://www.mathworks.com/products/simulink.html, 2022. Accessed 15 Sep. 2022.
[9] A. H. De Ruiter, C. Damaren, J. R. Forbes, Spacecraft dynamics and control: an introduction, John Wiley & Sons, 2013.
[10] J. Wertz, Spacecraft Attitude Determination and Control, Astrophysics and Space Science Library, Springer Netherlands, 2012.
[11] F. G. Soares, Estimação de Atitude e Velocidade angular em Nanossatélites Utilizando um Observador de Luenberger para Sistemas Não Lineares, Master's thesis, Technology Center, Graduate Program in Mechatronics Engineering, Federal University of Rio Grande do Norte, Brazil, 2019.
[12] E. L. Campos, K. I. P. de Melo Queiroz, United Nations / Brazil Symposium on Basic Space Technology "Creating Novel Opportunities with Small Satellite Space Mission´´, Natal/RN, Brazil. Sep., 2018.
[13] CelesTrak, title=NORAD Two-Line Element Set Format,, Available in: https://celestrak.org/NORAD/documentation/tle-fmt.php, 2022. Accessed 19 Sep. 2022.
[14] R. E. Kalman, A New Approach to Linear Filtering and Prediction Problems, Journal of Basic Engineering 82 (1960) 35–45.
[15] G. Welch, G. Bishop, An Introduction to the Kalman Filter, Technical Report TR 95-041, Department of Computer Science, University of North Carolina at Chapel Hill, 2006.
[16] Y. Kim, H. Bang, Introduction to kalman filter and its applications, in: F. Govaers (Ed.), Introduction and Implementations of the Kalman Filter, IntechOpen, Rijeka, 2019.
[17] E. L. Campos, Implementação de um Simulador para Controle de Atitude em Nanossatélites, Master's thesis, Technology Center, Graduate Program in Mechatronics Engineering, Federal University of Rio Grande do Norte, Brazil, 2019.
[18] Eclipse Foundation, Available in: https://www.eclipse.org/, 2022. Accessed 19 Sep. 2022.
[19] Hipparchus, Available in: https://hipparchus.org/, 2022. Accessed 19 Sep. 2022.
[20] Orekit, Available in: https://www.orekit.org/, 2022. Accessed 19 Sep. 2022.
[21] C. Ptolemaeus (Ed.), System Design, Modeling, and Simulation using Ptolemy II, Ptolemy.org, 2014.
[22] NOAA, Norad two-line element set format, Available in: https://www.ngdc.noaa.gov/IAGA/vmod/igrf.html, 2022. Accessed 19 Sep. 2022.
[23] D. Vallado, P. Crawford, Sgp4 orbit determination, in: AIAA/AAS Astrodynamics Specialist Conference and Exhibit, p. 6770.
[24] AstroPixels, Available in: http://www.astropixels.com/ephemeris/perap2001.html, 2022. Accessed 19 Sep. 2022.

Design of ADCS system for Earth Observation using a 3-unit CubeSat

Adolfo Chaves-Jiménez[(1)], **Giancarlo Vargas-Villegas**[(2)], **Alberto Zamora-Mendieta**[(3)], **Carlos A. Fernández-Cerdas**[(4)], **Jonathan Kolbeck**[(5)], **Mauricio Muñoz-Arias**[(6)]

[(1)] Costa Rica Institute of Technology, adchaves@itcr.ac.cr
[(2)] Costa Rica Institute of Technology, gvar97@estudiantec.cr
[(3)] Texas A&M University, albertofzamoram@tamu.edu
[(4)] Costa Rica Institute of Technology, cfercer96@gmail.com
[(5)] George Washington University, jkolbeck@gwu.edu
[(6)] University of Groningen, m.munoz.arias@rug.nl

Keywords: *CubeSat, ADCS, Earth Observation, satellite, control*

GWSat is a project led by George Washington University in collaboration with the Costa Rica Institute of Technology and the United States Naval Academy. It uses a 3U CubeSat to test GWU's Micro-Cathode Arc Thruster technology developed at GWU's Micro-Propulsion and Nanotechnology Laboratory. This CubeSat will have two advanced attitude control systems. The first system consist of a pointing mode that will allow the satellite to orientate its camera to Palo Verde National Park, Costa Rica, for remote monitoring purposes. The second system is based on a station-keeping mode that will allow the extension of the life of the mission. The attitude orbit and determination system control of GWSat is based on the combination of the thrusters and magnetometers only. In this paper, the design of the ADCS for Earth observation of GWSat is described. Here, simulations show how different control methodologies, from simple proportional-derivative controllers to a method designed using the port-Hamiltonian framework, influence the performance of the system. Perturbation, such as atmospheric drag and gravity gradient, are considered in the dynamics. This performance is of outmost importance in this mission, given that the energy efficiency is directly correlated with the use of propellant of the thrusters.

1. Introduction

GWSat is a project led by The George Washington University (GWU) in collaboration with the Costa Rica Institute of Technology (TEC) and the United States Naval Academy. It uses a 3U CubeSat to test GWU's Micro-Cathode Arc Thruster (μArc) technology that is being developed at GWU's Micro-Propulsion and Nanotechnology Laboratory.

TEC jointed GWU to develop a scientific application to the GWSat platform. The mission relates to earth environmental monitoring applied to the wetlands of Palo Verde National Park in Costa Rica. The idea is to use the satellite platform as a store and forward system of information transmitted from remote stations on the ground and remote monitoring of the wetlands using a camera on the satellite.

For this reason, GWSat will have two advanced attitude control: a pointing mode that will allow the satellite to orientate its camera to Palo Verde National Park for remote monitoring purposes, and a station keeping mode that will allow the extension of the life of the mission. This is especially important for Earth observations satellites launched from very low orbits, such as the one of the International Space Station.

GW-Sat's payload is composed by two derivate subsystems: The on-board camera system and the µCAT system. In order to take advantage of the satellite's 3-axis stabilization and to verify the pointing accuracy of the thrusters, GW-Sat would have a camera on board. The µCAT system has its main role in demonstrating full 3-axis stabilization under real conditions but there will also be additional tasks, such as characterizing its performance in space by indirect measurements.

The attitude orbit and determination system (ADCS) control of GWSat is based on the combination of the use of the thrusters and magnetometers only, allowing to evaluate the full potential of the μArc technology.

In this paper, the design of the ADCS for purposes of Earth observation of GWSat is described. First, this work assumes a configuration with both orbital and attitude dynamics been propagated and under the influence of J_2, gravitational torque and atmospheric drag force and torque, this last taking into account the coupling between orbit and attitude dynamics to calculate the influence of drag. A proportional-derivative (PD) controller is use as a base, and the mapping of the command of the controllers to the actuators is explained. Results show that the selected actuators configuration is able to stabilize the system affected by this perturbations in low-Earth orbit (LEO). The implementation of the port-Hamiltonian (pH) method to create the controller for this system are mentioned and preliminary results of these simulations are shown.

The results of this paper show the capabilities of 3U CubeSat for precise Earth observation with a efficient low-thrust propulsion system under the influence of perturbations in low-Earth orbit is shown.

The paper is structured as follows. In Section 2, the system's dynamics is introduced. Furthermore, Section 3 provides a thorough description of the GWSat. Later on, in Section 4 the proposed ADCS control for the satelitte is given, and the simulation conditions are presented in Section 5. Finally, concluding remarks and future work are shown in Section 6.

2. Dynamics Model

Consider a spacecraft orbiting the Earth. Let $\mathcal{I}$ denote a inertial geocentric Cartesian, right-handed coordinate frame, such as introduced in [1, p. 28].

Let $\boldsymbol{\omega}$ denote the angular velocity vector of the frame $\mathcal{B}$ with respect to $\mathcal{I}$ projected along $\mathcal{B}$. For any quaternion, $\boldsymbol{q}$, with vector part $\boldsymbol{e}$ and scalar part q, let $\Xi(\boldsymbol{q})$ denote the following 4×3 matrix

$$\Xi(\boldsymbol{q}) = \begin{bmatrix} \boldsymbol{e}^{\times} + q\mathbf{1}_3 \\ -\boldsymbol{e}^T \end{bmatrix} \tag{1}$$

where $\boldsymbol{e}^{\times}$ denotes the cross-product matrix

$$\boldsymbol{e}^{\times} = \begin{bmatrix} 0 & -e_3 & e_2 \\ e_3 & 0 & -e_1 \\ -e_2 & e_1 & 0 \end{bmatrix} \tag{2}$$

and $\mathbf{1}_3$ is the identity matrix in $\mathbb{R}^3$. Let $\boldsymbol{q}$, with vector part $\boldsymbol{e}$ and scalar part q, denote the quaternion of the rotation from $\mathcal{I}$ to $\mathcal{B}$.

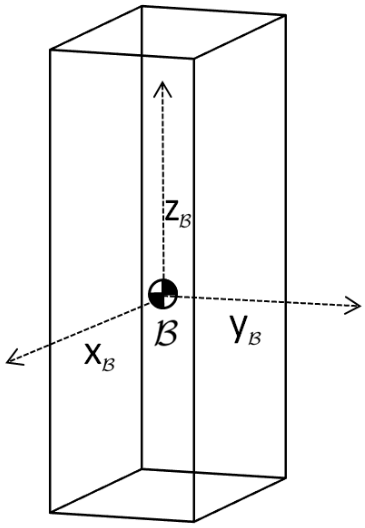

Figure 1: Definition of the Body Frame ($\mathcal{B}$).

Under the assumption of rigid body rotations around its center of mass, the orbit and attitude dynamics of a satellite is governed by the following system of equations [1, Ch. 16],

$$\dot{\boldsymbol{x}} = \begin{bmatrix} \dot{\boldsymbol{r}} \\ \dot{\boldsymbol{v}} \\ \dot{\boldsymbol{q}} \\ \boldsymbol{I}_1 \dot{\boldsymbol{\omega}} \end{bmatrix} = \begin{bmatrix} \dot{\boldsymbol{v}} \\ -\frac{\mu}{r^3}\boldsymbol{r} + \boldsymbol{a}_p \\ \frac{1}{2}\Xi(\boldsymbol{q})\boldsymbol{\omega} \\ -\boldsymbol{\omega}^{\times}\boldsymbol{I}_1\boldsymbol{\omega} + \boldsymbol{\tau}_1 \end{bmatrix} \tag{3}$$

With $\dot{\boldsymbol{r}}$ and $\dot{\boldsymbol{v}}$ the position and velocity of the center of mass of the spacecraft in $\mathcal{I}$. Here $\boldsymbol{a}_p$ and $\boldsymbol{\tau}$ represent the external force and torque perturbing the dynamics of the spacecraft.

2.1. Perturbation Model

Several physical effects existing in LEO are considered as the source of perturbations in this work. Here, the mathematical model used in this work is presented for reference. For a detail description of its simulation implementation, please refer to [2, 3].

2.1.1. Atmospheric Drag as the Source of Coupling between Attitude and Orbital Dynamics

When a satellite is in low-Earth-orbit, the interaction of the upper atmosphere particles with its surface is the cause of atmospheric drag force and torque. This atmospheric perturbation acts directly opposite to the velocity of the satellite motion with respect to the atmospheric flux, producing a deceleration of the satellite [4]. This effect constitutes the strongest non-gravitational perturbation of orbital dynamics missions working at an altitude of around 300 km [5].

Typically, the force model considering atmospheric drag use assumes a constant spacecraft effective area. Nevertheless, in reality, unless the satellite is a perfect sphere, or that spacecraft are controlled so that their effective area are constant, these effective areas change as a function of attitude, meaning that the magnitude of this perturbation on the orbit dynamics is a function of the spacecraft orientation, thus affecting both the orbit and attitude dynamics on spacecraft in flight.

The effect of the atmospheric drag, considered as the main non-gravitational force acting on the spacecraft dynamics, is described in the proper reference frames.

The acceleration due to atmospheric drag may be modeled as

$$\boldsymbol{a}_a = -\frac{1}{2}\frac{C_D\rho(\boldsymbol{r})}{m}A_{ef}\boldsymbol{v}_s^2\hat{\boldsymbol{v}}_s, \tag{4}$$

where C_D the drag coefficient of the S/C, $\rho(\boldsymbol{r})$ is the atmospheric density, m is the mass of the spacecraft, $\boldsymbol{v}_s$ the velocity of the spacecraft surface with respect to the atmosphere, $\boldsymbol{v}_s = \boldsymbol{v} - \boldsymbol{v}_a$, where $\boldsymbol{v}_a$ is the velocity of the atmosphere.

If a spacecraft is modeled as a number of plane surfaces, the effective area is given by [6]

$$A_{ef} = \sum_{i=1}^{s} A_i(\hat{\boldsymbol{n}}_i^T \cdot \hat{\boldsymbol{v}}_s), \tag{5}$$

where s is equal to the amount of plane surfaces composing the spacecraft,A_i the magnitude of area i amd $\hat{\boldsymbol{n}}_i$ a unit vector perpendicular to area i. The atmosphere is assumed to be spherical and co-rotating with the Earth [7]. In this case, its velocity projection in $\mathcal{I}$ is given by

$$\boldsymbol{v}_a = \boldsymbol{\omega_E} \times \boldsymbol{r}, \tag{6}$$

where $\boldsymbol{\omega_E}$ is the Earth rotation around its own axis. The torque produced by the atmospheric drag is then given by

$$\boldsymbol{\tau}_a = -\frac{1}{2}C_D\rho(\boldsymbol{r})\sum_{i=1}^{k} A_i(\hat{\boldsymbol{n}}_i\boldsymbol{v}_s)(\boldsymbol{d}_i \times \boldsymbol{v}_s), \tag{7}$$

with $\boldsymbol{d}_i$ the distance between the center of pressure of area i and the center of mass of the S/C.

2.1.2. J_2 Effect

The J_2 effect projected in $\mathcal{I}$, as described in [8], is given by

$$\boldsymbol{a}_{J2} = -\frac{3\mu\boldsymbol{r}_E^2}{2mr^4}J_2\left(\left(1 - 5\frac{r_z^2}{r^2}\right)\frac{\boldsymbol{r}}{r} + 2\frac{r_z}{r}\hat{\boldsymbol{z}}\right) \tag{8}$$

with m the mass of the spacecraft, $\boldsymbol{r}_E$ being the Equatorial radius of Earth, r the absolute value of the position $\boldsymbol{r}$, r_z the z-axis component of the $\boldsymbol{r}$ state, $\hat{\boldsymbol{z}} = [0, 0, 1]^T$, μ the gravity coefficient of the Earth, and J_2 the first zonal harmonic for Earth.

2.2. The Gravitational Torque Effect

Any nonsymmetrical object of finite dimensions in orbit is subject to a gravitational torque because of the variation in the Earth's gravitational object over the object [1]. If a spherical mass distribution of the Earth is assumed, this torque, projected in frame $\mathcal{B}$, is given [1] as

$$\boldsymbol{\tau}_g = 3\frac{\mu}{r^5}(\boldsymbol{r}|_{\mathcal{B}})^{\times}(\boldsymbol{I}\,\boldsymbol{r}|_{\mathcal{B}}). \tag{9}$$

Recall that in this work it has been assumed that $\boldsymbol{r} = \boldsymbol{r}|_{\mathcal{I}}$, which indicates the projection of the position in $\mathcal{I}$. This means that its projection in $\mathcal{B}$, $\boldsymbol{r}|_{\mathcal{B}} = D(\boldsymbol{q})\boldsymbol{r}$ such that

$$\boldsymbol{\tau}_g \quad = \quad 3\frac{\mu}{r^5}(D(\boldsymbol{q})\boldsymbol{r})^{\times}(\boldsymbol{I}D(\boldsymbol{q})\boldsymbol{r}). \tag{10}$$

with $D(\boldsymbol{q})$ the rotation matrix derived from $\boldsymbol{q}$. Since the perturbation model is now given by (7), (8), and (10), then we introduce in section 4 the setting of the spacecraft dynamics towards the control design strategy.

3. The GWSat CubeSat

Based on the CubeSat standard, which is a type of small satellites made of multiples of [10-10-10] cm cubic units (1U) with a mass of no more than 1.33 kg per unit, approximately, GW-Sat is a 3U CubeSat. In this case, its case dimensions are [10-10-34.05] cm, but its total dimensions could vary due to the addition of some components that could stand out from the structure, as the camera, the thrusters and some sensors. GW-Sat's maximum allowed mass is 4.5 kg, which is another change with respect to the CubeSat standard.

The attitude control is designed to allow both a station-keeping and a pointing mode, the former to perform the necessary maneuvers to increase the altitude of the orbit, the latter to point to a specific point on Earth. It is required that the control system uses the thrusters designed by The George Washington University (GWU), in combination with magnetorquers only, to be able to orientate the satellite to the desired attitude.

3.1. Actuators

GWSat attitude will be controlled mainly by μCat thrusters, but is also provided with magnetorquers for detumbrling and basic maneuvers purposes, and to complement the operation of thrusters.

3.1.1. Magnetorquers

Magnetorquers create a magnetic dipole moment, $\boldsymbol{m}$, which in turn creates a torque given by Equation 11, where $\boldsymbol{B}$ is Earth magnetic field.

$$\boldsymbol{\tau}_{MT} = \boldsymbol{m} \times \boldsymbol{B} \tag{11}$$

The most basic source of a magnetic dipole is a current loop. A current of I amperes flowing in a planar loop of area A produces a dipole moment of magnitude that can be calculated as in 12 [9].

$$m = IA \tag{12}$$

This magnetic dipole goes in the direction normal to the plane of the loop and satisfying a right-hand rule. It follows from this definition that the natural unit for the dipole moment is Am^2. When m is measured by [Am^2], the magnetic field is specified in Tesla [T], Eq. 13 gives the torque in Nm. If there are N turns of wire in the loop, the dipole moment has the magnitude that can be calculated with Equation 13 .

$$m = NIA \tag{13}$$

The dipole moment can be significantly increased by wrapping the wire loops around a ferromagnetic core. Magnetic control torques are used almost exclusively in near-Earth orbits, where the magnitude of the Earth's magnetic field is roughly in the range of 20–50 µT [9].

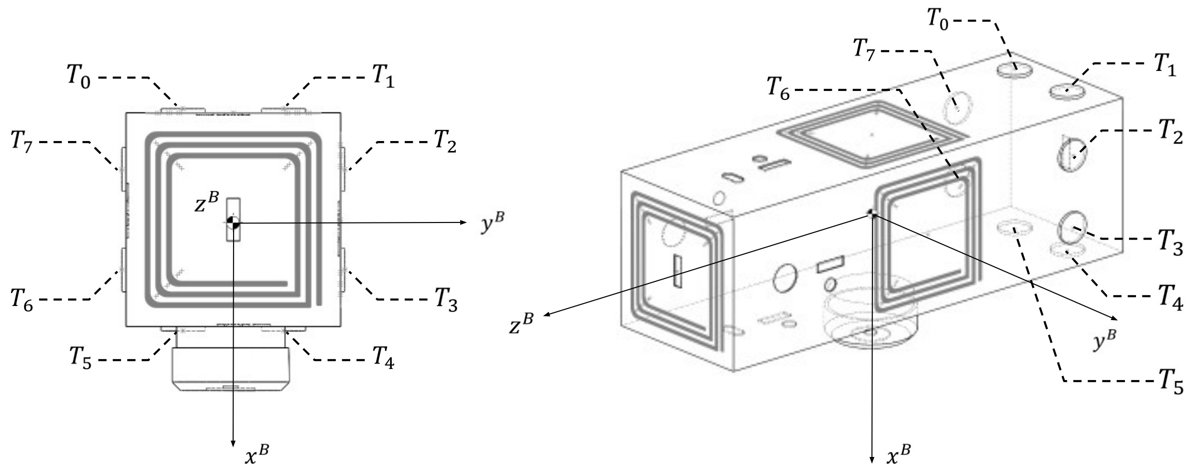

Figure 2: Assembly of µCATs in GW-Sat unit.

3.1.2. Arc micro-Catode Thrusters

Arc micro-Catode (μCat) thrusters are based on the physical phenomenon of vacuum (cathodic) arcs. The term cathodic refers to the fact that the discharge is produced on the cathode on so-called cathode spots. These are the source of electrons and ions, i.e., plasma, required to sustain the discharge. For this type of propulsion system, the cathode functions as the electrode for the discharge, and as the propellant [10].

The µCATs thusters used in this mission are produced by GWU [11, 12]. Thrusters are located symmetrically respect to its opposite satellite's face, i.e., the thrusters located at the parallel sides to xz plane are located at the same position with respect to x and z coordinates, as well as the thrusters located at the sides parallel to yz plane, with respect to y and z coordinates, as shown in Figure 2. Based on [14], the camera will be located at the center of the face parallel to yz plane, on the positive x side. There will be three magnetorquers, each one located at the center of the faces on the negative axis side. It is important to note that the selection of every component location is based on technical criteria, e.g., since µCATs work with magnetic field, which may affect the functionality of some components, the camera and magnetorquers should be located as far as possible form thrusters. Finally, throughout this document the position of the sensors will be assumed at GW-Sat's geometrical center because this simplifies the ACS model and the ADS has not been designed yet, but this does not affect the final ACS design because the processed signals from sensors (from the ADS) will match the actual model.

3.2. Sensors

In this section, the sensing technology to be used in GWSat is described for documentation purposes. In the case of this work, the results assume that the states are known, so no estimation is simulated. Future work will describe the performance of the estimation system and how does it influcence the control performance. GWSat will include the sensing technology ennumerated on Table 1

These sensors provide the needed observability to determine the orientation error for each of the advanced control modes. At the moment of writing this work, the final decision on the specific sensor devices to be used is yet to be defined. For a

Table 1: Sensors to be used in GWSat.

Sensor	Description
Gyroscope	Inertial attitude sensor, which would output the satellite's spinning rate (relative to the inertial space) directly [13]
Sun Sensor	Sun sensors are visible-light detectors that measure one or two angles between their mounting base and incident sunlight. The measured Sun direction in the body frame [14]
Star Tracker	comparing the locations of the imaged stars on the image plane to the known locations of those stars on the celestial sphere, the star tracker can estimate the satellite's attitude in a Inertial Frame [15].
Magnetometer	The magnetometer is a sensor that measures the strength and direction of the local magnetic field [14].
Global Positioning Systems (GPS)	The GPS are used to provide an accurate means of determining position for spacecrafts and autonomous navigation. They usually give the position vector from the Earth to the spacecraft.

detailed description of the principles governing each one of the sensors to be used in the mission, please refer to [3, 2].

3.3. Control Modes

In the case of the station keeping mode, the desired attitude is one where the orientation of the Z-axis of the spacecraft (where the spacecraft thrusters are located) is aligned with the velocity vector of the orbit, and it is the stage before the spacecraft turns on the thrusters to increase the orbit velocity when it is desired [3]. The desired reference frame is named Thruster Pointing Frame T and has its unit vectors defined as $[\hat{t}_1, \hat{t}_2, \hat{t}_3]$. It is chosen such a way that the second component $\hat{t}_2$ is pointing towards the radial vector of the Earth. The third component $\hat{t}_3$ is pointing towards the velocity vector direction. Then, $\hat{t}_1$ is given by right-hand rule between $\hat{t}_2$ and $\hat{t}_3$ (See Figure 3)

The Pointing Mode is a mode designed in order to verify that the system will perform well on pointing tasks and to select the components needed. For this mission, the developed solution must point GW-Sat's camera (which is centered at the x+ face of GW-Sat) to Palo Verde National Park in Costa Rica [2].

4. Spacecraft Attitude Control Design

4.1. Quaternion Feedback Regulator

The control law used to achieve the desired satellite attitude quaternion ($\boldsymbol{q}_d$) was the PD Controller based on [26]. This control law gives the necessary control torque, and Equation 14 represents it.

$$\boldsymbol{\tau}_c = -k_d \boldsymbol{I} \omega_e - k_p \boldsymbol{I} sign(q_{e4})[q_{e1}, q_{e2}, q_{e3}]^T, \tag{14}$$

with k_d, k_p the derivative and proportional constants of the proposed PD controller.

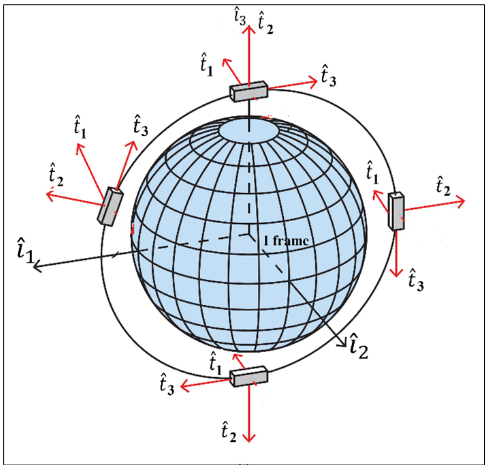

Figure 3: **Desired reference frame for station-keeping mode [16].**

Note that if the $q_{e4} < 0$, then the positive term feedback term is introduced, which provides the shorter path to reach the desired equilibrium point. For calculating the quaternion error q1:3e, Equation 15 was used.

$$q_{1:3e} = \Xi^T(\boldsymbol{q}_d)\boldsymbol{q} \tag{15}$$

Where $\Xi(\boldsymbol{q})$ can be obtained using equation 16

$$\Xi(\boldsymbol{q}_d) = \begin{bmatrix} \boldsymbol{q}_4 & \boldsymbol{q}_3 & \boldsymbol{q}_2 \\ \boldsymbol{q}_3 & \boldsymbol{q}_4 & \boldsymbol{q}_1 \\ \boldsymbol{q}_2 & \boldsymbol{q}_1 & \boldsymbol{q}_4 \\ \boldsymbol{q}_1 & \boldsymbol{q}_2 & \boldsymbol{q}_3 \end{bmatrix}, \tag{16}$$

and the fourth quaternion is given by $q_{e4} = \boldsymbol{q}^T\boldsymbol{q}_d$.

4.2. Mapping of commanded torques

In order to map the commanded torques to be applied by the magnetorquers, it is possible to derive from equation 11 that

$$\boldsymbol{\tau}_c = \begin{bmatrix} \tau_x \\ \tau_y \\ \tau_z \end{bmatrix} = \begin{bmatrix} m_y B_z - m_z B_y \\ m_x B_z - m_z B_x \\ m_x B_y - m_y B_x \end{bmatrix} \tag{17}$$

with $\boldsymbol{\tau}$ the total torque vector commanded from the control system to the satellite.

From [17] we are able to solve the value for each of the magnetic dipole commanded as

$$\boldsymbol{m} = \frac{\boldsymbol{B} \times \boldsymbol{\tau}_c}{||\boldsymbol{B}||} \tag{18}$$

From the configuration of the thrusters shown in Figure 2, it can be seen that the sumatory of torques for each axis projected in the Body frame of the spacecraft that leads to the commanded torque by the ADCS system $\boldsymbol{\tau}_c$ is

$$\boldsymbol{\tau}_c = \begin{bmatrix} \tau_x \\ \tau_y \\ \tau_z \end{bmatrix} = \begin{bmatrix} \tau_6 + \tau_7 + \tau_2 + \tau_3 \\ \tau_5 + \tau_4 + \tau_0 + \tau_1 \\ \tau_0 + \tau_2 + \tau_4 + \tau_6 + \tau_1 + \tau_3 + \tau_5 + \tau_7 \end{bmatrix} \tag{19}$$

$$\tau_i = F_{sat} r_i c_i \tag{20}$$

with τ_i, $i = [1..10]$ the torque generated by thruster i (see Figure 2), F_{sat} the maximum propulsion force of the thruster, r_i the distance from the propulsor to the center of mass of the spacecraft and c_i a pulse width modulated (PWM) signal that controls the magnitude of the total torque provided.

Due to the fact that there is more than one possible solution to generate the torque commanded by the control algorithm using GWSat thrusters, the method described in [18, 19] is used where the H matrix is defined as an array describing the equivalent torques for all the propulsion system, given by the absolute value of the distance relative to the center of mass r_i, the azimut and inclination angles (α and ϵ). In the case of an array of n thursters, H is defined as

$$\boldsymbol{H} = \begin{bmatrix} r_0 \sin(\alpha_0)\cos(\epsilon_0) - r_0 \sin(\epsilon_0) & ... & r_i \sin(\alpha_i)\cos(\epsilon_i) - r_i \sin(\epsilon_i) \\ r_0 \cos(\epsilon_0)\cos(\alpha_0) - r_0 \cos(\epsilon_0)\sin(\alpha_0) & ... & r_i \cos(\epsilon_i)\cos(\alpha_i) - r_i \cos(\epsilon_i)\sin(\alpha_i) \\ r_0 \sin(\epsilon_0) - r_0 \cos(\epsilon_0)\cos(\alpha_0) & .. & r_i \sin(\epsilon_i) - r_i \cos(\epsilon_i)\cos(\alpha_i) \end{bmatrix}. \tag{21}$$

To obtain a solution for this undertermine system, the Moore-Pensore pseudoinverse matrix is used [19]. This leads to the solution

$$\boldsymbol{F}_c = \boldsymbol{H}^{\dagger}\boldsymbol{\tau}_c, \tag{22}$$

with $\boldsymbol{H}^{\dagger}$ the Moore-Penrose pseudoinverse matrix for H, with H a $3xn$ matriz, with n the number of thrusters used by the system.

4.3. Advanced Control Algorithms Exploration: The port-Hamiltonian (pH) Approach

An advance methodology to design the control law for GWSat is currently been explored. A summary of the results given for the for the exploration presented in [20], and that constitute part of this work is presented here.

The PH framework is based on the description of systems in terms of energy variables, their interconnection structure, and power port pairs, [21, 22, 23]. PH systems include a large family of nonlinear physical systems, including satellites' dynamics as previously described by [20, 24, 25, 26]. The energy transfer between the physical system and the environment is given through energy elements, dissipation elements, and power-preserving ports.

Given a rigid body in space (satellite), we define its inner energy (Hamiltonian) function as

$$H(q, p) := \frac{1}{2} p^{\top} \boldsymbol{I}^{-1} p \tag{23}$$

with $x = \mathrm{col}(q, p)$ being the state variable that depends on the (generalized) position $q \in \mathbb{R}^3$, and generalized momenta $p \in \mathbb{R}^3$. Furthermore, the matrix $\boldsymbol{I} := \mathrm{diag}\left(\boldsymbol{I}_x, \boldsymbol{I}_y, \boldsymbol{I}_z\right)$ is the (principal) inertia matrix. Also, $p := \boldsymbol{I}\boldsymbol{\omega}$ being $\boldsymbol{\omega} \in \mathbb{R}^3$ the angular velocity vector. The dynamics of p is then given by

$$\dot{p} = p^{\times} \nabla_p H(p) + u \tag{24}$$

with $u = \boldsymbol{\tau} \in \mathbb{R}^3$ being the applied control torques to the rigid body (satellite). Based on (23) and (24), we obtain the following PH formulation

$$\Sigma_S \begin{cases} \begin{bmatrix} \dot{q} \\ \dot{p} \end{bmatrix} = \begin{bmatrix} 0_{9\times 3} & r(q) \\ -r(q)^\top & p^\times \end{bmatrix} \begin{bmatrix} \nabla_q H(q,p) \\ \nabla_p H(q,p) \end{bmatrix} + \begin{bmatrix} 0_{9\times 3} \\ G(q) \end{bmatrix} u \\ \\ y = G(q)^\top \nabla_p H(q,p) = G(q)^\top \boldsymbol{\omega} \end{cases} \tag{25}$$

where the dissipation matrix is assume zero, i.e. $\mathcal{R}(q,p) = 0$, $G(q) \in \mathbb{R}^{3\times 3}$ being the input matrix, and $r(q) : \mathbb{R}^9 \to \mathbb{R}^{9\times 3}$ is computed as

$$r(q) := \begin{bmatrix} R_x^\times \\ R_y^\times \\ R_z^\times \end{bmatrix} \tag{26}$$

with

$$q := \text{vec}\{R^\top\} = \begin{bmatrix} R_x & R_y & R_z \end{bmatrix}. \tag{27}$$

Notice from (25) that the dynamics of the generalized position q is given by

$$\dot{q} = r(q)\, p \tag{28}$$

with $r(q)$ as in (26). In [25], it is shown the full derivation of (25) with the matrix $r(q)$ as in (26), and the vector of position coordinates q as in (27).

Theorem 1. *[20]. Given a satellite dynamics represented by* (25) *with the generalized coordinate q and the generalized momenta p, we obtain asymptotic stability at the desired configuration error $\bar{q}$ with the torque input vector u as*

$$u = -\frac{1}{2}\bar{q} - K_p \bar{y} + z \tag{29}$$

with a positive constant matrix $K_p > 0$, a new system output $\bar{y} = \bar{p}$ as in (30)*, and an integral action on the extended dynamics, i.e z as in* (31) *with a positive constant matrix $K_i > 0$.*

$$\bar{p} = p + K_p \bar{q} \tag{30}$$

where $\bar{p} \in \mathbb{R}^n$, with $n > 0$ constant, positive matrix $K_p > 0$, and desired configuration error $\bar{q}$ to be defined later on, and

$$\dot{z} = -K_i \hat{y}. \tag{31}$$

The work done in this research regarding the design of a pH controller for the GWSat satellite is reported in [20] and presented here for comparison purposes. It works using an attitude matrix as the formalism to define the attitude of the system.

Table 2: **Initial Dynamic Conditions.**

Element	Value
Altitude	450 km
Inclination	51.6
Atmospheric drag density model	Harris-Priester
Initial angular position ($\boldsymbol{q}(0)$)	$[1/\sqrt{2}, 0, 1/\sqrt{2}, 0]$
Initial angular velocity ($\boldsymbol{\omega}(0)$)	[0,0,0]

Table 3: **Spacecraft Characteristics.**

Element	Value
Mass	4 kg
Inertia matrix	$\begin{bmatrix} 0.0042 & 0 & 0 \\ 0 & 0.042 & 0 \\ 0 & 0 & 0.0067 \end{bmatrix} kg\ m^2$
Thuster maximum force	10 $\mu\ N$

5. Results

For this work, the simulation conditions are given by 2 and 3. The configuration of the PD controller is given by $k_p = 2700$ and $k_d = 169 \cdot 10^4$. The desired attitude will lead the spacecraft to have a constant orientation with respect to the inertial frame. At this point of the research this gives valuable information on the stability of the system, due to the fact that the change of position changes mainly the influence of the atmospheric drag in the spacecraft. In order to give a reference of the influence of the perturbation torques, in Figure 4 their magnitude is shown. As it can be seen, not assuming a constant effective area leads to a more realistic perturbation simulation. The commands given to each one of the thrusters is shown in Figure 5, and the generated torque in each one of the axes of the body frame of the spacecraft. The latter figure show that the commanded torque is of the same order of magnitude of the perturbation, and only around double the magnitude of such perturbing effect. Nevertheless, in Figures 7 and 8 it can be seen how the presented control methodology successfully stabilizes the spacecraft after two orbits.

5.1. Advanced Mode Exploration: pH Approach

For this research, the port-Hamiltonian algorithm for attitude is under development. Preliminary results show that estabilization of a spacecraft in space is possible, and it is shown in figure 9. The response time is very low (25 s), but the algorithm is to be tested under perturbation conditions as the reported in this work, were the evaluation of its performance, specially with relation to energy usage, is to be reported.

Future work on this approach will focus on implementing this approach to use the quaternion convention for spacecraft attitude dynamics, the addition of the models of actuators to the control system model and the comparison of this approach with the classical approaches in terms of energy usage.

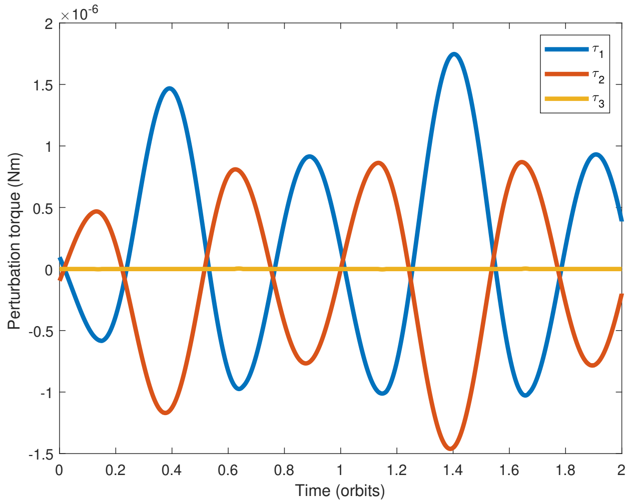

Figure 4: Perturbation torque projected on the body frame of the spacecraft

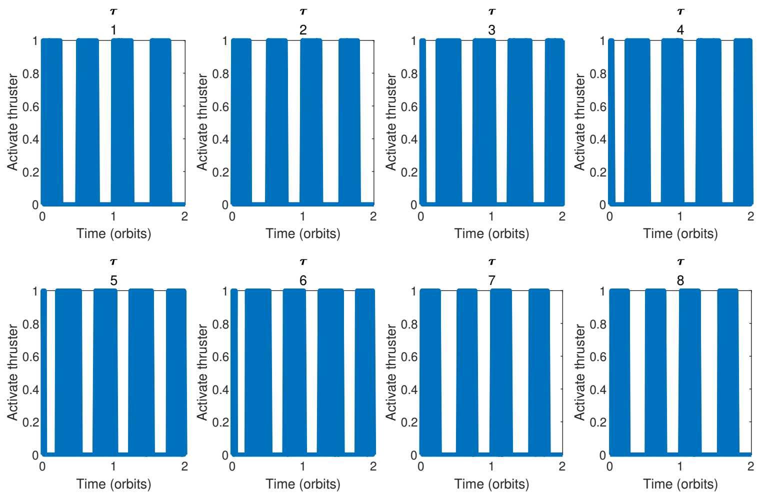

Figure 5: Commanded action for each one of the thrusters shown in Figure 2

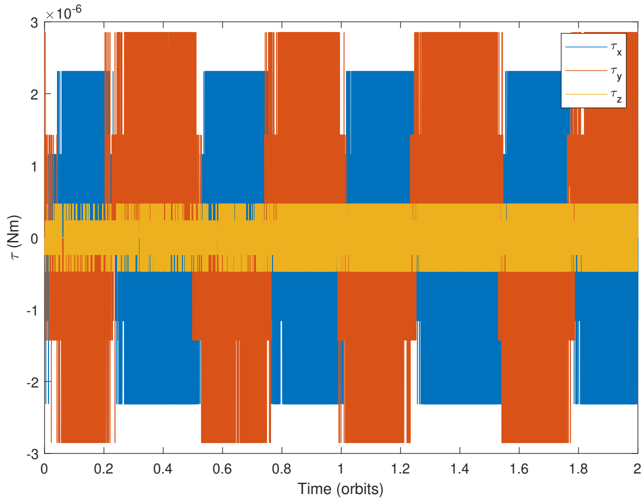

Figure 6: Torque generated by the thrusters in each of the axes of the Body frame of the spacecraft by the action of the thrusters shown in 5

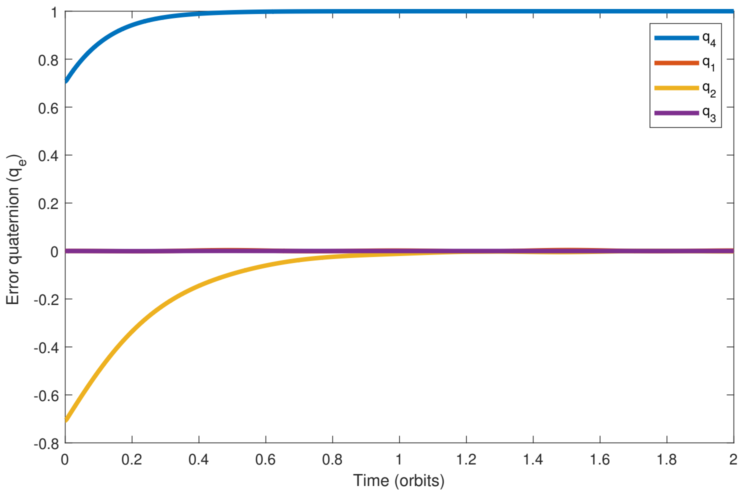

Figure 7: Quaternion error stabilization

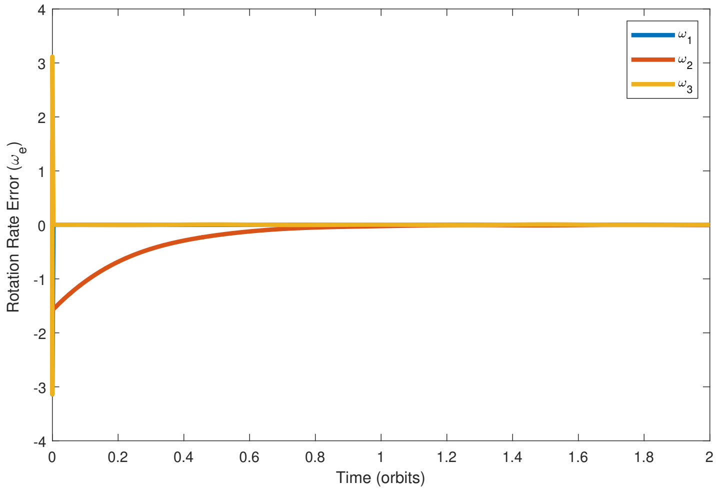

Figure 8: Rotation rate error

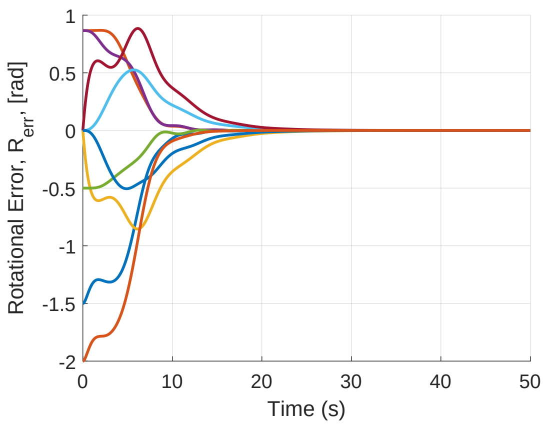

Figure 9: Simulation results of the attitude configuration with control law derived from the pH convention with nonlinear disturbances Each line represents one of the nine elements of the attitude error matrix. Asymptotic stability is obtained after $t = 25\ s$ due to the chosen gains for the controller. Taken from [20]

6. Conclusion and Future Work

In this work, it is shown that it is possible to control GWSat using the μCat thrusters under development by GWU if the system performs at its estimated thrust, even under the influence of perturbations in LEO such as atmospheric drag and the gravity gradient torque.

This stabilization is done by fixing the desired attitude to a fixed orientation with respect to the inertial frame. Given the conditions of the simulation, this implies that the torque affecting the spacecraft is in the same order of magnitude with respect to the maximum value of the torque produced by the control thrusters, in many cases leading to a perturbation of a magnitude of half the value of the control torque, with a variation of a period approximately given by 3000 s. Nevertheless, the system converges to its desired attitude after approximately one orbit, showing that the actuators are a feasible solution for attitude control if they perform correctly.

The future work of this research will include the comparison of the different control methodologies shown in this paper in terms of efficiency from the point of view of time response and energy usage. Also, future work will include implementing the estimation system for GWSat. This estimation system will provide a varying attitude error for both the pointing and the orbit maintenance modes. Both of these scenarios constitute attitude-tracking modes. This system's implementation will allow evaluation of the performance of the ADCS systems with measurement uncertainty under the conditions in which it must perform adequately.

References

[1] J. R. Wertz (Ed.), Spacecraft Attitude Determination and Control, D. Reidel, Dordrecht, The Netherlands, 1984.

[2] A. F. Zamora-Mendieta, Design of the attitude control system for the pointing mode of GW-sat satellite, 2020.

[3] C. A. Fernández-Cerdas, Attitude control design for station keeping mode in the gw-sat nanosatellite, 2020.

[4] O. Montenbruck, E. Gill, Satellite orbits: models, methods and applications, Springer, 2005.

[5] E. Gill, P. Sundaramoorthy, J. Bouwmeester, B. Zandbergen, R. Reinhard, Formation flying within a constellation of nano-satellites: The qb50 mission, Acta Astronautica (2012) –.

[6] A. Chaves Jimenez, On the Coupling of Orbit and Attitude Determination of Satellite Formations from Atmospheric Drag: Observability and Estimation Performance, Ph.D. thesis, Delft University of Technology, 2020.

[7] W. Zhong, P. Gurfil, Online estimation of mean orbital elements with control inputs, in: Proceedings of the EuroGNC 2013, 2nd CEAS Specialist Conference on Guidance, Navigation & Control, Delft University of Technology.

[8] J. L. Junkins, H. Schaub, Analytical mechanics of space systems, American Institute of Aeronautics and Astronautics, 2009.

[9] F. L. Markley, J. L. Crassidis, Fundamentals of spacecraft attitude determination and control, volume 1286, Springer, 2014.

[10] J. Kolbeck, J. Lukas, G. Teel, M. Keider, E. Hanlon, J. Pittman, M. Lange, J. Kang, μcat micropropulsion solution for autonomous mobile on-orbit diagnostic system, in: 30th Annu. AIAA/USU Conf. Small Satellite.

[11] S. E. Haque, G. Teel, M. Keidar, E. F. Agasid, O. T. Gazulla, A. D. Perez, G. T. Trinh, E. A. Uribe, Micro cathode arc thruster phonesat experiment for small satellites, in: The 33rd International Electric Propulsion Conference, The George Washington University, Washington, DC.

[12] M. Keidar, J. Schein, K. Wilson, A. Gerhan, M. Au, B. Tang, L. Idzkowski, M. Krishnan, I. I. Beilis, Magnetically enhanced vacuum arc thruster, Plasma Sources Science and Technology 14 (2005) 661.

[13] History of the cubesat, 2016.

[14] J. P. Reijneveld, Design of the Attitude Determination and Control Algorithms for the Delfi-n3Xt, Master's thesis, Space System Engineering, Delft University of Technology, 2012.
[15] A. O. Erlank, W. H. Steyn, Arcminute attitude estimation for cubesats with a novel nano star tracker, IFAC Proceedings Volumes 47 (2014) 9679–9684.
[16] A. Garzón, Y. A. Villanueva, Thermal analysis of satellite libertad 2: a guide to cubesat temperature prediction, Journal of Aerospace Technology and Management 10 (2018).
[17] W. Rafal, Satellite attitude control using only electromagnetic actuation, Ph.D. thesis, Ph. D. Thesis Aalborg Univ, 1996.
[18] M. J. Sidi, Spacecraft dynamics and control: a practical engineering approach, volume 7, Cambridge university press, 1997.
[19] E. Oland, Modeling and attitude control of satellites in elliptical orbits, in: Applied Modern Control, IntechOpen, 2018.
[20] A. Chaves-Jimenez, M. Muñoz Arias, An energy-based approach to satellite attitude control in presence of disturbances for a cubesat mission, in: 71th International Astronautical Congress, The Cyber Space Edition, International Astronautical Federation (IAF), p. 59498.
[21] V. Duindam, A. Macchelli, S. Stramigioli, H. Bruyninckx, Modeling and Control of Complex Physical Systems: The Port-Hamiltonian Approach, Springer, Berlin, Germany, 2009.
[22] A. van der Schaft, L_2-Gain and Passivity Techniques in Nonlinear Control, Springer, London, UK, 2000.
[23] A. van der Schaft, D. Jeltsema, Port-hamiltonian systems theory: An introductory overview, Foundations and Trends® in Systems and Control 1 (2014) 173–378.
[24] K. Fujimoto, T. Nishiyama, On trajectory tracking control of port-hamiltonian systems with quaternions, in: 53rd IEEE Conference on Decision and Control, IEEE, pp. 4820–4825.
[25] P. Forni, D. Jeltsema, G. A. Lopes, Port-hamiltonian formulation of rigid-body attitude control, IFAC-PapersOnLine 48 (2015) 164–169.
[26] M. Muñoz-Arias, An energy-based approach to satellite attitude control in presence of disturbances 1052 (2019).

4

Session 4 - Ground Segment

Ground and Flight Segment for tracking and transmissions for Stratospheric Balloons

João P. P. Braga [(1)], Antonio Cassiano Julio Filho [(2)], Sergio de Oliveira [(3)], Marconi Arruda [(4)]

[(1)] Federal University of São João del-Rei, joaopedropolito@aluno.ufsj.edu.br
[(2)] National Institute for Space Research (INPE), cassiano.filho@inpe.br
[(3)] Federal University of São João del-Rei, Department of Technologies (DTECH), Ouro Branco – MG – Brasil {sergiool,marconi}@ufsj.edu.br

***Keywords**: Ground Segment, Stratospheric Balloons, Space Missions, Tracking System*

The growing increase in space missions mainly in small satellites directs the development of Ground Stations with the objective to serve as a Multi Mission Platform, configurable and capable to meet different missions and operations scenarios. When analyzing the global scenario, we observe that more and more missions are validated through stratospheric balloon flights, mainly due to the agility in the testing phase and the low cost compared to a space flight. On the other hand, there is still a gap in solutions for tracking and data acquisition. This project aims to present a model of stations that perform tracking and data collection of payloads shipped in Balloons. The proposed structure combines and applies different existing methods, generating a reliable system for receiving mission data. The proposed system consists of two modules: the Flight Segment and the Ground Segment. The flight segment is composed of a hardware and software subsystem including a Payload embedded in a Balloon, being responsible for sending data to the Ground Segment, using radiofrequency in the UHF band. The Ground Segment - Ground Station - proposed consists of an omnidirectional antenna, a rotator, directional antennas, a support, a hardware subsystem and a software-defined radio (SDR), in addition to a control, storage and user interface software. The main objective of this Ground Station is to receive, through the omnidirectional antenna, the data sent by the Flight Segment, demodulate and calculate, in real time, the azimuth and elevation values of the balloon. Thus, knowing the position of the balloon, the Ground Station can control its rotator to point the directional antennas, enabling the transfer of data, according to the balloon's mission. This article describes the development process of the two segments, considering the requirements, implementation, individual tests and subsystem integration, in addition to presenting the results and future work.

1. Introduction

We are witnessing a new space race, where we have a more accessible and cheaper space. This new space race, called New Space, has brought great revolutions, mainly in terms of cheaper launches [1]. As a result, we can observe a large increase in space missions, especially those of Small Satellites.

These small satellites have taken the lead in this more accessible space. Especially when we observe that most of these satellites are developed by schools and universities.

This work aims to present a solution to facilitate tests of nanosatellites or payloads at high altitudes using stratospheric balloons, mainly in the acquisition of data from these tests, we will present a system that can be embedded in balloons, allowing the tracking of these artifacts automatically.

2. Systems Engineering

As a starting point in the development of this research we carried out bibliographic studies to analyze missions that carry out tests of their satellites or payloads using stratospheric balloons. An example of the analyzed missions is the Raiosat [2]. After this analysis we made some correlations with the techniques currently used and we propose a solution that gives greater accuracy in the reception of mission data, especially those that have a high data rate, both shown in Figure 1a and Figure 1b.

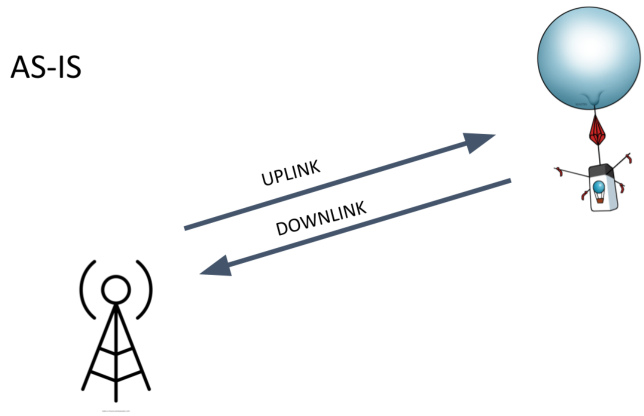

Figure 1a: How tracking is currently done.

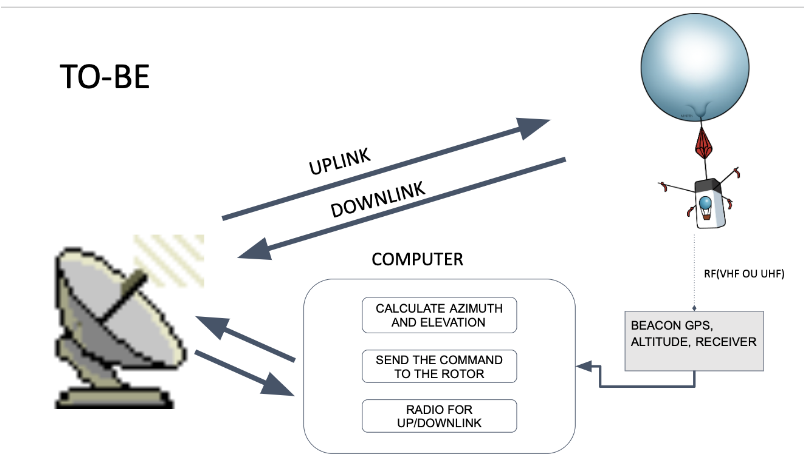

Figure 1b: First Idea of project.

From this analysis, it was then thought to develop a system divided into 3 parts: (1) the Ground Segment requirements, as shown in Table 1; (2) the Flight Segment requirements in Table 2; and (3) the Control Interface as shown in Table 3. From the definition of these three segments, requirements were raised to be met within the development of the project:

Table 1: Ground Segment Requirements.

ID	System Requirements.
RGS.1	Perform Balloon and Satellite Tracking.
RGS.2	Be a low-cost platform.
RGS.3	Possess easy adaptation for different types of mission.

Table 2: Flight Segment Requirements.

ID	System Requirements.
RFS.1	Have at least 90% off-the-shelf components.
RFS.2	Ability to send programmed beacons.
RFS.3	It has modularity for different types of mission.

Table 3: Control Interface Requirements.

ID	System Requirements.
RCI.1	Ability to perform azimuth and elevation calculations of the flight segment.
RCI.2	Ability to carry out the control of different types of rotators automatically.
RCI.3	Easy integration with different rotators.

3. Development

Based on the requirements raised, the development process of the three segments was initiated, starting with the Flight Segment. This segment is composed of the hardware and software that will be embedded onto the balloon. This segment is responsible for sending in real time the data needed to carry out the tracking of the balloon. As stated in section 2, the system has some requirements that were used during the development of the prototypes. In total, the team developed 7 hardware versions. Figure 2 shows some of the versions developed.

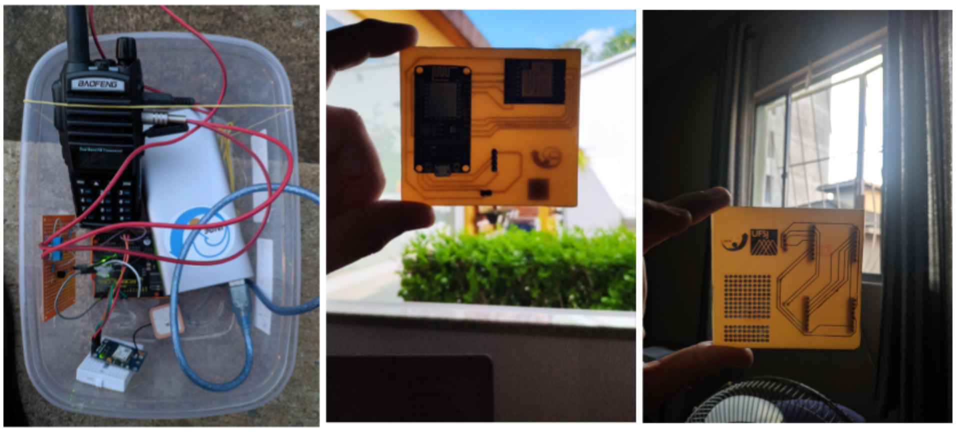

Figure 2: Project Versions.

As version 3.2 is the latest and most robust version. We chose to present it in more detail. The Flight Segment was designed to operate independently of the Stratospheric Balloon, thus giving more autonomy to the system. The version 3.2 is composed of the following components, show in table 4:

Table 4: Components list.

Components.	Quantity
Lolin D1 Mini V4.0.0 Wemos Esp8266	01
SX1278 LoRa 433MHz Ra-02 Breakout Board	01
NEO-6M GPS Module	01

Following choosing the components, the printed circuit board was developed. Which is responsible for integrating the components, on figure 3 show.

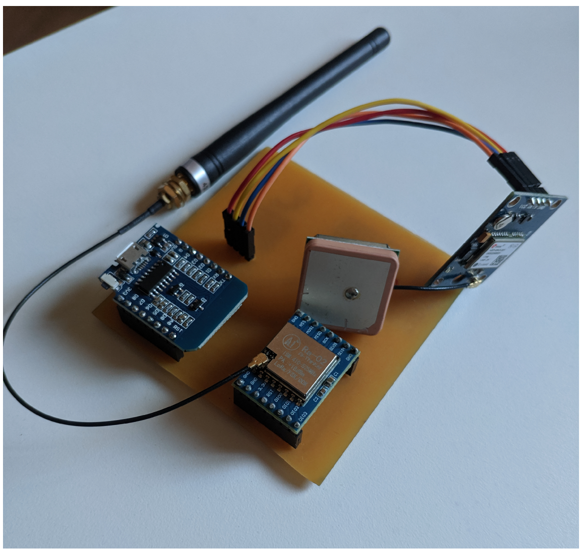

Figure 3: PCB and Components Flight Segment Version 3.2.

After the integration of the components, the development of the software was carried out, which was embedded in the Flight Segment hardware. This software was developed using the Arduino IDE platform [3], in its first version the system was able to send via RF (Radio Frequency) its location and altitude data.

Afterwards some analysis, we developed version 2.0 of the software, where we chose to add some more data needed for tracking. The final format of the packets is shown in Figure 4.

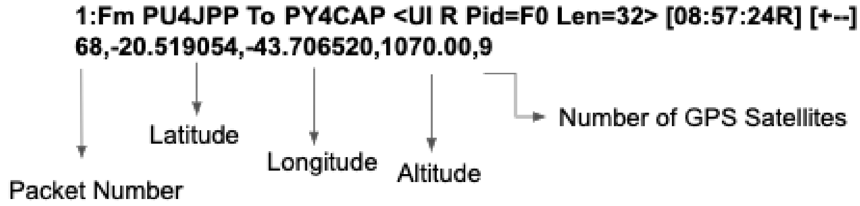

Figure 4: Packets data.

The control interface was developed to serve as an interface between the flight segment and the rotator. Being able to process the data received from the flight segment this data is used to calculate the azimuth and elevation that the rotator needs to point the antenna to downlink the data.

To calculate the azimuth, we use Haversine's Theorem, and to calculate the elevation we used as a basis the calculations performed by the Project Horus that are available on the Project's GitHub [4]. Following the calculation of the data necessary for the control of the rotator, the development of the control function was carried out.

This function has the objective to send the azimuth and elevation data via serial to the rotator connected to the control interface.

Another part that was developed by the team was Ground Segment. This segment is responsible for receiving and sending data to the balloon and its payloads on board, the system developed is composed of the following components: omnidirectional antenna, rotator, SDR (Software Defined Radio) and directional antennas.

The first components to be developed were the omnidirectional antenna and the balloon data reception system. As the flight segment sends a low amount of data, we chose to use a ground plane antenna, due to the low complexity and excellent performance in signal receptions using LoRa. To do the data decoding we developed a receiver which is responsible for sending the received from the flight segment to data to the control interface.

For the development of the rotator, it was decided to use an open-source system from SatNOGS [5], more specifically the 2.0 version of the hardware.

To assemble the system, we carry out some changes in the project to adapt the rotator to the realities of Brazil and the needs of the project. With the integrated system, as shown in Figure 6, we carried out some validations. The main validation was the tracking and reception of telemetry from the Alfacrux Satellite [6][7].

Figure 6: Ground Segment.

4. Tests

In this section we will present some tests and results obtained from this work. The first system tested and to have its validation performed was the control interface. To carry out the validation, we used data of stratospheric balloons collected by the SondeHub platform [8].

Following download of the flight data, we simulate the reception, treatment, calculations and finally the commands sent to the rotator. With this test we were able to validate the control interface and the communication with the rotator.

Then, the test was carried out to validate the reception of the data from the flight segment. Since the purpose of this test was to verify the behavior of the flight segment, we chose to use a drone in this testing phase, with 9 flights carried out. To analyze the data received, we plotted the points collected using Google Earth, as shown in the figure 7.

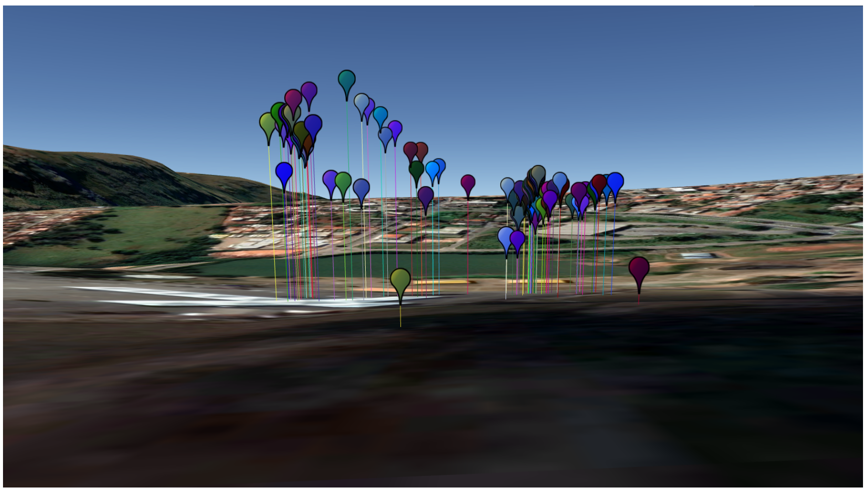

Figure 7: Flight Segment Validation

With all the parts that make up the system tested separately, we moved on to the most important test of our research: testing all three systems integrated and working together. A total of 6 flights were performed with all the integrated systems, as shown in figure 8. In this image we can see the integrated systems and the drone flying, carrying the flight segment.

Figure 8: Flight test with all integrated systems

After the flights, we can observe some problems that were not observed in the bench tests, such as the packet transmission time and the altitude variation collected by the GPS. This altitude variation can be compared from the data collected by the altimeter embedded in the drone. It is worth mentioning that for the next versions an altimeter will be added in our flight segment, to have greater accuracy with the altitude data.

5. Conclusions and Future Works

As presented at the beginning of the work, the objective of the project was to develop a tracking system for stratospheric balloons, mainly to help in collecting data from the payloads embedded in them. For this, we developed the flight segment, the control interface and the ground segment, which, when operated together, have the advantage of providing greater precision in pointing antennas for the reception of telemetry and sending telecommands for the payloads on board the balloons.

We can also highlight that this first phase of development fulfilled all the requirements presented in section 2, giving us the green light to develop the engineering model of our project. To then prepare the flight segment for the launch campaign where the system will be boarded in a stratospheric balloon. This launch is being organized by the National Institute for Space Research (INPE) which has a plan to carry out 3 launches of stratospheric balloons by the end of 2022.

Acknowledgments

We would like to thank the Federal University of São João del-Rei (UFSJ) for the institutional support and the National Institute for Space Research (INPE) for their full support in the development of this research, in addition to National Council for Scientific and Technological Development (CNPq) for funding this research, through the Scientific Initiation Scholarship Program (PIBIC-INPE).

References

[1] ODGERS BERNDTSON. (2021). New space presents new opportunities for exploration [Online]. Available:https://www.odgersberndtson.com/fr-fr/publications/new-space-presents-new-opportunities-for-exploration

[2] JÚLIO FILHO, A. C. Cubesat development for lightning flashes detection: raiosat project. Journal of Aerospace Technology and Management, v. 12, p. 80-93, 2020. DOI: <10.5028/jatm.cab.1161>. Available:: <http://doi.org/10.5028/jatm.cab.1161>.

[3] Arduino IDE. https://www.arduino.cc/en/software, Last accessed on 2022-08-30.

[4] Project Horus, 2022. https://github.com/projecthorus, Last accessed on 2022-08-31.

[5] SatNOGS, 2022. https://gitlab.com/librespacefoundation/satnogs/satnogs-rotator/-/tree/v2.0, Last accessed on 2022-08-31.

[6] The Alfacrux Project, 2022. https://lodestar.aerospace.unb.br/projects/alfacrux, Last accessed on 2022-08-31.

[7] J. Santos, J. Braga, H. Alves, J. Silva, D. Resende, A. Teixeira, and M. Kakitani, “Development of a low-cost ground segment capable of receiving data from nanosatellites: a partnership between Brazil and Portugal,” in 4th Symposium on Space Educational Activities, 2022.

[8] SondeHub, 2022. https://sondehub.org/, Last accessed on 2022-08-31.

EMMN - Reports about a Multi-Mission Ground Station on Cubesats tracking

Hilário J. S. Castro(1), **Manoel J. M. de Carvalho**(1), **Moises C. de B. Souto**(2), **Jefferson A. da Silva**(1), **Lúcio dos S. Jotha**(1)
(1) National Institute of Space Research (INPE),
2073 Carlos Serrano Street, Natal, Brazil, Phone: +55 84 3204-9100,
email: hilariojscastro@gmail.com, jeffsilva.inpe@gmail.com,
manoel.carvalho@inpe.br, lucio.jotha@inpe.br
(2) Federal Institute of Education, Science and Technology of Rio Grande do Norte,
1559 Sen. Salgado Filho Avenue, Natal, Brazil, Phone: +55 84 4005-9832,
email: moises.souto@ifrn.edu.br

Keywords: *Ground Station, Multi-Mission, TT&C, Tracking, Satellites*

Abastract

The Estação Multi-Missão de Natal (Natal Multi-Mission Station) (EMMN) resulted from the updating process of a legacy satellite tracking system, belonging to the Instituto Nacional de Pesquisas Espaciais (National Institute of Space Research) (INPE). As a ground station, the objective is to provide a secure communication link between operators and their respective orbiting satellites. To this end, the ground segment automatically acts as a broker between satellite and operator, providing the latter with an encrypted data link, using a Virtual Private Network (VPN), and reconfigurable Radio Frequency (RF) channels, in Very High Frequency (VHF), Ultra High Frequency (UHF) and S bands. EMMN's operational architecture uses Open-source software and solutions based on Distributed Systems, in an Ethernet network, which allows for better scalability and maintenance of each component of the functional complex. The services are “triggered” by an automatic system for scheduling satellite passes, whose priorities are predefined, initiating an orchestration of distributed services using the Message Queuing Telemetry Transport (MQTT) protocol. At this point, three main operations are performed in the orchestrated process, one related to the radio, another to the tracking system, and a third to communication between ground segments involved in the operation. The first task activated is made up of the collaboration between a Software Defined-Radio (SDR) and a micro-controlled set of switches, to interconnect the required antennas to signal amplifiers. This allows the channel configuration for the UHF, VHF, and/or S bands, and further configures the signal processing in SDR to modulate/demodulate the signals according to the target satellite. Another task activated is the Antenna Tracking System, formed by an electromechanical set which has been also updated to a microcontrolled scheme. It performs tracking based on an ephemeris table generated by transferring the Two-Line Element (TLE) of the satellite to be tracked, automatically obtained from the Internet. The last task is the remote communication system, which enables the external satellite operator to access the station through a secure communication channel, via Transmission Control Protocol (TCP) and VPN, providing access to Telemetry, Tracking and Command (TT&C) service and providing full compliance of mission-specified ground-to-ground communication protocols. This paper will present the report of the experiences of using the EMMN involving its multi-mission operations, with data derived from tracking some satellites.

1. Introduction

The growing number of Cubesats and Nanosats in Low Earth Orbit (LEO) has provided the emergence of demands in the space sector, such as the need to modify earth stations for the multi-mission concept. An example is the adaptation of Radio Frequency (RF) links on the ground segments to different compositions, allowing the tracking of the elements of different space missions [1].

Aiming at this context, the Instituto Nacional de Pesquisas Espaciais (Brazil's National Institute of Space Research) (INPE) updated a legacy satellite tracking system, located in the Natal city, resulting in the Estação Multi-Missão de Natal (Natal Multi-Mission Station) (EMMN). The station's new role is to cooperate in missions as a link broker, providing scheduled tracking services and reconfigurable RF Front-End link access via encrypted data channels. The abstraction of part of the Telemetry, Tracking, and Command (TT&C) tasks, allows a Satellite Operator to dedicate its efforts to the use of the communication and mission control application.

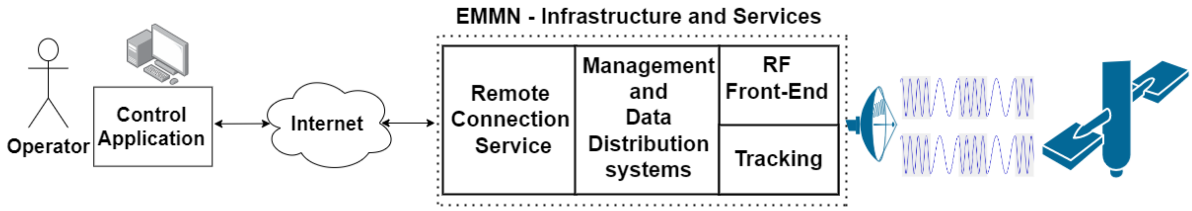

Figure 1: EMMN services' diagram of use in satellite communications.

EMMN's new architecture uses the orchestration of virtualized and networked services, which manipulate an electromechanical antenna rotation system and provide an operator with access to the station's other systems via a Virtual Private Network (VPN). With the proper permissions, the operator will be able to perform TT&C actions, with the RF Front-End acting on reconfigurable radio channels in different modulations, such as Very High Frequency (VHF), Ultra High Frequency (UHF), and S bands. The links are guaranteed by a switching system of antennas and amplifiers together with a Universal Software Radio Peripheral (USRP) [2]. To meet the multi-mission objective, the main orchestrated tasks are divided into the following systems: Management and Data Distribution, Tracking, Radio and Remote Communication. The first task acts as an activity aligner, while the other three are the main services of the station.

2. Related works

This section presents documents with information and works related to earth stations and space missions, helping in the understand the concepts of multimission and can also serve as a basis for projects in the sector.

Documents with recommendations for projects are available in the literature, addressing end-to-end communications with spatial elements. A set of standards for mission planning are the documents of the Consultative Committee for Space Data Systems (CCSDS), especially [3] and [4]. These documents present information on requirements and necessary operations for various services involved in space missions. The reference [3] informs about each segment in end-to-end communication, while the reference [4] details the content of messages between the elements involved.

In [5], some definitions of essential elements for multi-mission stations are presented, also helping in the modeling of RF links. Another reference that deals with the formation of the RF front-end and tracking system is [1], describing the architecture for stations and indicating the relationship of the multi-mission concept with the context of varied RF links and tracking of space elements in different orbits.

To establish different radio links, some solutions introduce the use of Software Defined-Radio (SDR), which allows for part of the communications to be done without the need to change hardware, through digital signal processing on computers. In [6], the use of Yagi-Uda and Helical Antennas associated with LNAs in the RF front-end stage, and the use of “RTL-SDR dongle” in the digitization and information processing stage are adopted. In [7], the concept of a multi-mission station uses VHF, UHF and S channels with Yagi antennas connected to LNAs and USRPs as SDR model. The RF elements are associated with two-axis rotation equipment.

In [8] a station concept is demonstrated using a rotation system and USRP for tracking small satellites in the S and X bands. A concept for the application of associated multi-mission receiving stations in a global network is found in [9], which describes different ways of implementing the station’s antennas and indicates the use of “Raspberry Pi” and “RTL-SDR dongle” as radio processing components.

As a concept of interaction of stations or sector activities in a local or global network, an example can be found in [10]. In this work, a VPN system is used to interconnect sectors and users, ensuring security with encrypted data. It also uses dedicated RF structures and USRP. Many efforts for network services are developed using systems virtualization, conceptually presented in [11] and in the implementation of [12].

The EMMN’s solution shares several concepts found in the literature, differing in the forms of the implementation of the services. It resembles the form of the virtualization of systems and network operations with access via VPN. It differs in the form of implementation for RF operations in multi-mission, acting not only with the use of USRP and rotation system but also in the microcontrolled connection between antennas and radios’ Uplink/Downlink channels. Another highlight is the implementation of the Message Queuing Telemetry Transport (MQTT) [13] protocol for data sharing and operations synchronization.

3. EMMN’s System

To meet the multi-mission context, EMMN had its infrastructure upgraded to provide remote access to the RF Front-end, serving TT&C activities for different missions. To this end, a solution was developed based on distributed network systems, consisting of both open-source and local solutions for software and hardware. A great advantage of this concept is the possibility of using the virtualization of the tools, which facilitates the maintenance, expansion, and distribution of the operational load of the assets.

Each element associated with the network adds an important feature to the activities, but the operations need to be aligned for the set to act in the mission’s purpose. The solution used for alignment was the application of the MQTT protocol, which uses a “broker” system as a network centralizer to distribute data between activities, helping in the task of synchronization and coordination of operations.

To provide remote access to the reconfigurable RF Front-end, the infrastructure operates in 4 main service layers, namely: Manager and Data Distribution System; Tracking System; Radio System; Remote Communication System. Figure 2 shows the connection between the layers, as well as the remote operator's access channel to the services. The next subsections describe the contribution of each service group to a trace operation.

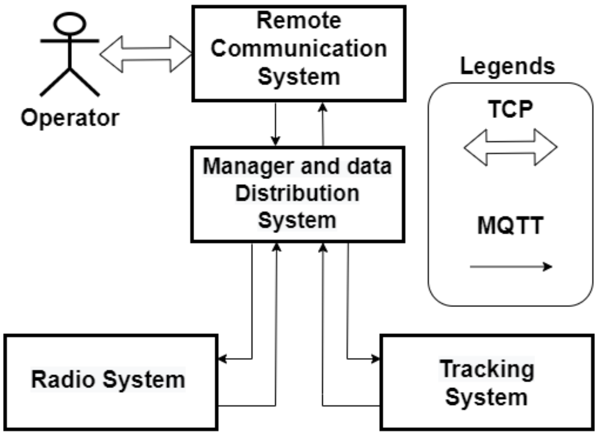

Figure 2: EMMN Summarized Architecture.

3.1. Manager and Data Distribution System

For multi-mission purposes, a necessary layer for an operation is the Manager and Data Distribution System, which will act as an event "trigger" for EMMN's main services. This layer provides the information necessary to initiate the activities of tracking, as well as to designate the configuration of the communication channels.

The block has four main tasks to ensure systems synchronization. The first application is the "Operations Manager", responsible for signaling activities to other blocks of the EMMN architecture, such as scheduling the tracking times for each satellite. These times are determined based on the Two-Line Element (TLE) provided for the mission.

Another task of the layer is the "Satellites Manager" service, which acts as the Application Programming Interface - Representational State Transfer (API-REST) for the other blocks' layers. The Station Manager is in charge of this service, by manually entering the satellites' information, such as satellite identification, Norad Number, TLE, Uplink and Downlink channel settings (frequencies, modulations, and baud rate). For TLE data, the default option is an automatic update of this parameter, via a request to CelesTrak [14].

During a tracking act, the third activity of the block is the "Orchestrator". This element acts upon receiving a call from the "Operations Manager", in order to activate the event. Faced with the request, the orchestration service collects the information necessary for the other actors to perform the desired activity, injecting the data in the proper order and intended destinations. To exemplify a trace, as shown in Figure 3, the "Operations Manager" sends data to the "Orchestrator", which collects the rest of the information in the "Satellites Manager" API, and then injects all the data into the respective "Data Distribution" (Broker MQTT) for task alignment. Continuing, the satellite's TLE will be transmitted in an MQTT topic and received by the "Tracking System" and the "Radio System"; the duration of the pass will be transmitted to the respective MQTT topic and then forwarded to the "Radio System" and "Remote Communication System".

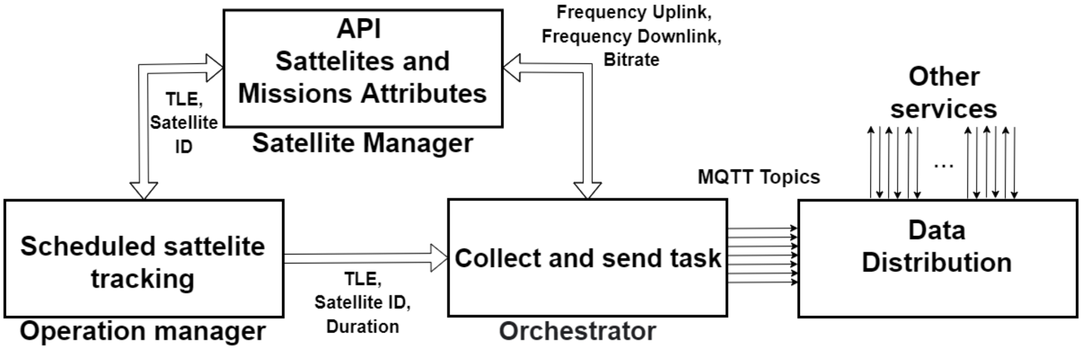

Figure 3: Flowchart of the Manager and Data Distribution System layer.

3.2. Tracking System

This complex is composed of a mechanical structure inherited from an old INPE project, which accommodates the S, UHF, and VHF band antennas, as seen in Figure 4((1)). The layer's task is to improve the performance of the RF Front-End by rotating the antennas and directing them toward the tracked element.

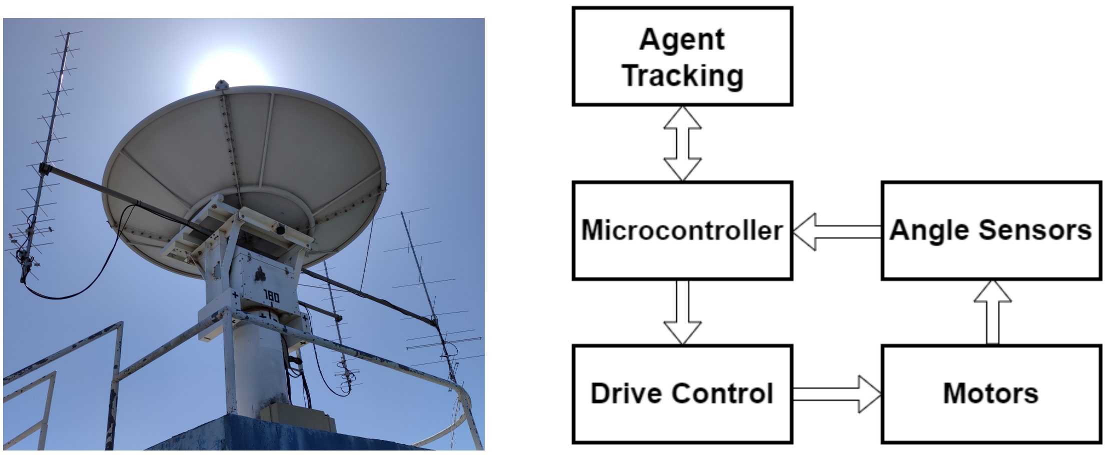

((1)) EMMN Antenna Complex.

((2)) Tracking control diagram.

Figure 4: EMMN tracking structure and its control synthesized diagram.

The mechanism positions the antennas using microcontrolled motors, with the microcontroller having a USB interface for receiving direction commands or querying the current antenna pointing. The simplified diagram of activities of the scheme can be seen in Figure 4((2)). The requests are received by the "Agent tracking" software that manages the rotations, taking decisions derived from the data received in the MQTT topics and from the readings via USB.

During a tracking event, the "Agent tracking" software receives the TLE to be used to create an ephemeris table, which indicates the antenna targeting times. The required annotation is converted by the management software into a data packet, which transfers the information via USB to the hardware that performs the action.

The piloting base is formed by microcontrolled hardware, with sensing through "resolvers" sensors for reading the azimuth and elevation angles, and signals applied to the motor rotation control drivers. The movement takes place by checking the angles by the “Resolvers”, followed by the application of the control signal to the drivers that smoothly rotate the motor axes in the desired direction. Operation is maintained until the structure is capable of the required Azimuth and Elevation.

3.3. Radio System

The layer focuses on the station’s RF Front-End configuration, selecting from the link antennas to the signal encoding and decoding scheme. In order to meet the objective, an antenna switching scheme and a signal processing script activation service were created. The general structure and its connections can be seen in Figure 5.

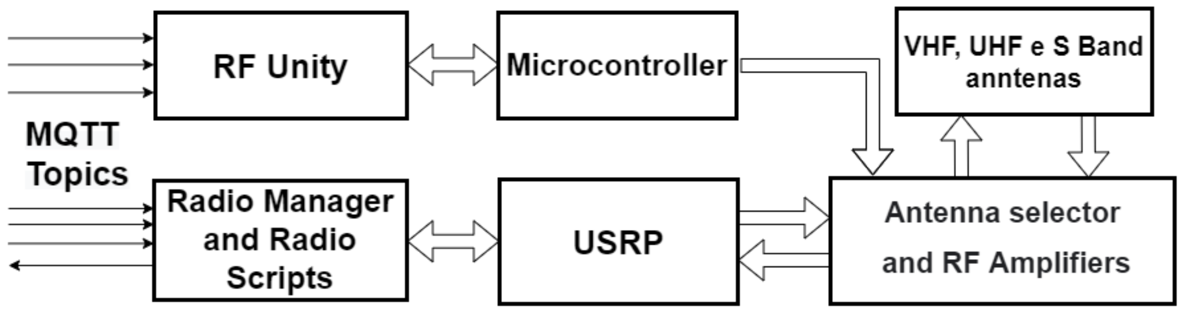

Figure 5: Diagram of the EMMN Radio System.

In Figure 5 is possible observe the antennas switching scheme. This system uses three operational blocks that control the selection of which antennas are connected to each Channel. The first block is the “RF Unity”, which interfaces the EMMN network with the second block (Microcontroller). The third block (Antenna selector and RF Amplifiers) is responsible for switching the antennas and RF amplifiers.

With the information injected by the “Orchestrator” into the link frequency topics, the “RF Unity” sends a sequence of bytes via USB to the microcontroller system. The message designates which antennas should be associated in the Uplink and Downlink. Antennas and their attributes can be viewed in the Table 1.

The bottom track of Figure 5 introduces how to execute the signal processing task. In this segment, a USRP associated with configuration scripts and signal processing generated by a GNU Radio application is used. [15]. The combination of artifices provides a radio scheme that works with different modulations and demodulations, without the need to modify the hardware.

The “Radio Manager” software interfaces radio scripts with mission radio calls. It also checks satellite ID information to activate two scripts, one for modulation and one for demodulation, which process the data together with the synchronized USRP.

The scripts use a block encoding scheme, generated by the GNU Radio application [15], whose block library provides numerous information processing options. There are blocks for interfacing with the network via the MQTT protocol, for adjusting the USRP configuration (such as frequencies and doppler shift correction), as well as for receiving telecommands to be transmitted and providing the decoded telemetry. Some blocks were developed locally.

Table 1: EMMN antennas.

Antenna	Model	Frequency range (MHz)	Gain (dBi)
VHF	YAGI-UDA 2x7 Elements	145 - 150	12.34
UHF (01)	YAGI-UDA 2x15 Elements	395 - 405	15.5
UHF (02)	YAGI-UDA 2x15 Elements	432 - 440	16.2
S	Parabolic 3m diameter	2.200 - 2.300	33.8

3.4. Remote Communication system

The last layer proposes to allow the remote user access to the services of the EMMN local network, especially the "Radio System". The task is comprised of the pfSense firewall service, the OpenVPN VPN solution, and the "Remote Module" script, developed locally for the mission. The representation of the connections and infrastructures involved in the operation can be seen in Figure 6.

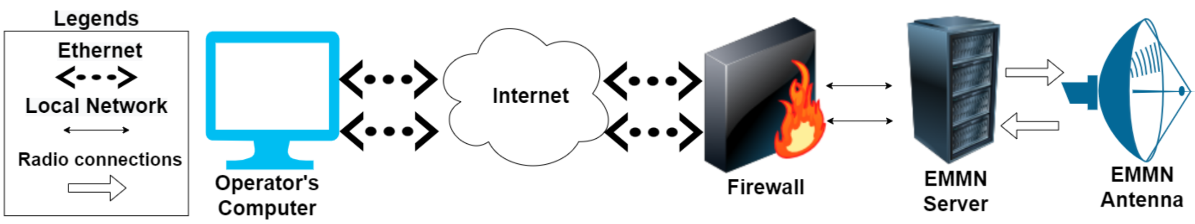

Figure 6: Network structure flowchart.

The functionalities are accessed using credentials provided to the satellite operator, generated by the firewall service, and sent to the operator in advance. Using the credentials, encrypted access is allowed by the firewall and then the connection to the "Remote Module" is established. Among the access releases, there is the connection via TCP sockets, in which two exclusive ports are previously defined in the operations of the mission: one for transmitting telecommands and another for receiving telemetry.

The execution of the communication script is performed by the "Remote Module Manager". The purpose of the management service is to measure the duration of a pass and activate the mission's "Remote Module" during the duration of the pass, in which the activated script is developed according to the mission's ground protocols.

The "Remote Module" performs two main operations. One of them is the intermediation between TCP telecommand and telemetry channels with the respective MQTT topics. The other operation, when necessary, is related to the mission protocol conference layer, normally implemented between ground segments.

4. Reports on Cubesats Trackings

This section shows data derived from executed operations by EMMN. The information derives from data collected in surveys with orbiting satellites. It aims to evaluate the performance of automated tracking, gauging the establishment of different radio links in the reception of telemetry from different sources. The approach uses two CubeSats that have different radio link configurations. They were chosen because they are in operation, according to the SatNOGS project database [9]. The link information can be seen in Table 2.

Table 2: Cubesats transceivers characteristics.

Cubesat	NORAD	Frequency	Modulation	Data rate
ITASAT	43786	148.86 MHz	BPSK	1200 bps
Platform-1	52770	400.36 MHz	GMSK	9600 bps

The records are related to the pointing angles of the antennas, on tracking events, over 30 days. The data refers to the azimuth and elevation axes during a tracking, with the acquisition of information on the pointing direction whenever telemetry is decoded by the message reception script and published in the MQTT topic of telemetry.

In Figures 7((1)) and 7((2)) histograms are shown in polar format, in which it is possible to notice the reception of telemetry in different combinations of antenna angles during the tracking of these satellites. In the Figures 7((1)) and 7((2)), concentric circles represent azimuth and radii represent elevation. Rectangular regions indicate groups of nearby angles with the occurrence of decoded signals. The darker, the more receptions occurred. In this way, it is possible to notice the change in the direction of the antennas in the most varied points, as well as the incidence of signals received from a particular satellite over several passes in the stipulated period.

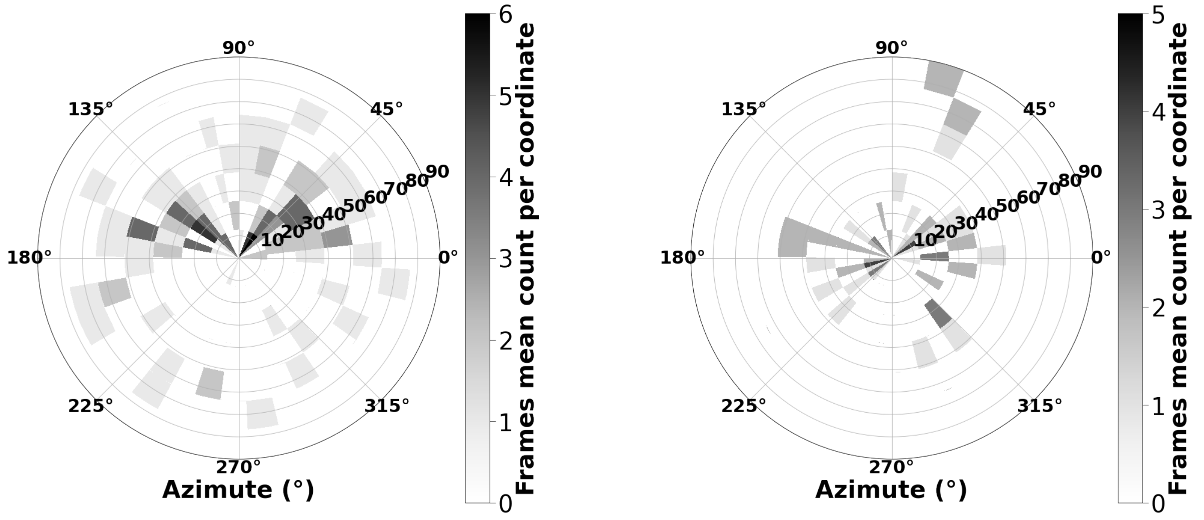

((1)) Itasat ((2)) Platform-1

Figure 7: Polar Coordinates Histograms plot from CubeSats tracking data.

The reconfigurations of the RF link and signal processing proved to be successful using the combination of automated switching of the antennas associated with the USRP and the signal processing scripts. Nevertheless, improvements are always necessary for the performance of the radio system, but the advantage of using the approach used in the EMMN scheme is that the modifications are carried out only in the processing scripts, without making it necessary to change the hardware.

During the tracking events, a computer external to the station's network executed a script for TCP connections, simulating the connection of a remote operator and establishing connections with the "Remote Modules" developed for each satellite. The simulated connection occurred as shown in Figure 6, with the reception of telemetry decoded during the passage by the operator. Using the devices and protocols used, the signals that were decoded were sent to the satellite telemetry topic, to then be transmitted to the script of the remote machine, with a delivery rate of 100% of packets to the destination application of the operator.

5. Conclusion

In this paper, the solution implemented by EMMN for Multi-Mission Ground Station tasks was presented. The application of the proposal used begins with the updating of the legacy tracking system, which allowed increasing the line of sight time of the station's UHF, VHF, and S antennas concerning the satellite in its passage. In addition to the possibility of tracking any spatial element using TLEs, the solution used the concept of reconfigurable radios using USRP and automatic antenna switching, allowing the multi-mission concept to be implemented.

The function that allows remote access has made the station's reach to other missions wider, giving other teams that have satellites access to a ground station without extra investments. Based on the reported experiments, it is possible to note the performance of the EMMN for various missions.

In general, the modularization and use of distributed systems allowed the station to act in the multi-mission task, allowing improvements, as highlighted in the tracking experiment, to be implemented without modifying hardware or the structure of the operational framework.

Acknowledgments

The authors of this article thank the Agência Espacial Brasileira (Brazilian Space Agency) (AEB) and the Conselho Nacional de Desenvolvimento Científico e Tecnológico) (National Council for Scientific and Technological Development) (CNPq) for their financial support. As well as thanks to the entire team at INPE and the Centro de Competência em Soluções Livres (Center for Competence in Free Solutions) of the Instituto Federal do Rio Grande do Norte (Federal Institute of Rio Grande do Norte) (CCSL - IFRN) for their contributions to the development of the EMMN complex.

References

[1] M. Fischer, A. L. Scholtz, Design of a multi-mission satellite ground station for education and research, in: 2010 Second International Conference on Advances in Satellite and Space Communications, pp. 58–63.

[2] M. Ettus, Universal software radio peripheral, 2022.

[3] Mission Operations Services Concept - Informational Report, Green book, CCSDS 520.0-G-2, CCSDS Secretariat, 2006.

[4] Orbit Data Messages - Recommended Standard, Blue book, CCSDS 502.0-B-2, CCSDS Secretariat, 2009.

[5] U. Ukommi, E. Ubom, I. Ikpaya, Ground station design for satellite and space technology development, American Journal of Engineering Research 10 (2022) 12 – 19.

[6] A. Saravanakumar, K. Ayyakannu, U. Manikandan, Design and development of low cost ground receiving station for leo satellite operations, International Journal of Pure and Applied Mathematics 119 (2018) 2921–2932.

[7] I. Vertat, R. LInhart, M. Pokorny, J. Masopust, P. Fiala, J. Mraz, Small satellite ground station in pilsen — experiences with vzlusat-1 commanding and future modifications toward open reference ground station solution, in: 2018 28th International Conference Radioelektronika (RADIOELEKTRONIKA), pp. 1–6.

[8] M. Boettcher, K. Leidig, S. Klinkner, R. Varatharajoo, Y.-C. Chak, S. Pätschke, A. S. Mohd Harithuddin, H. Salim, Design of a low-cost s/x dual band satellite ground station for small satellite missions.
[9] D. J. White, I. Giannelos, A. Zissimatos, E. Kosmas, D. Papadeas, P. Papadeas, M. Papamathaiou, N. Roussos, V. Tsiligiannis, I. Charitopoulos, Satnogs: Satellite networked open ground station, Engineering Faculty Publications 40 (2015).
[10] S. Hitefield, Z. Leffke, M. Fowler, R. W. McGwier, System overview of the virginia tech ground station, in: 2016 IEEE Aerospace Conference, pp. 1–13.
[11] F. Riffel, R. Gould, Satellite ground station virtualization: Secure sharing of ground stations using software defined networking, in: 2016 Annual IEEE Systems Conference (SysCon), pp. 1–8.
[12] Y. Liu, Y. Chen, Y. Jiao, H. Ma, T. Wu, A shared satellite ground station using user-oriented virtualization technology, IEEE Access 8 (2020) 63923–63934.
[13] R. A. Light, Mosquitto: server and client implementation of the MQTT protocol, The Journal of Open Source Software 2 (2017).
[14] Center for Space Standards & Innovation (CSSI), CelesTrak, 2022.
[15] E. Blossom, Exploring GNU Radio, 2022.

A PROPOSAL FOR A SPACE WEATHER GROUND-BASED SEGMENT USING SOFTWARE-DEFINED RADIO AND COGNITIVE RADIO

Jaime E. Orduy(1), Walter. Dos Santos(2), Claudia M. Cândido (3), Douglas. Dos Santos (4), Daniel S. Umaña (3)

(1)National Institute of Space Research, 12227-010, +55 (12) 3208-6000, jaime.orduy@inpe.br

(1)Fundación Universitaria Los Libertadores, 111711, +57 (1) 2544750, jaime.orduy@libertadores.edu.co

(2) National Institute of Space Research, 12227-010, +55 (12) 3208-6000, walter.abrahao@inpe.br

(3) National Institute of Space Research, 12227-010, +55 (12) 3208-6000, claudia.candido@inpe.br

(4) Aeronautics Institute of Technology, 12228900, +55 (12) 3208-6000, dsoares@ita.br

Keywords*: Global Navigation Satellite System, Software-Defined Radio, Cognitive Radio, Space Weather, Public Outreach.*

The ionosphere is a highly dynamic medium through which radio waves propagate, but also the medium that interferes with this propagation. Due to there is a weakly ionized plasma located between around 60 km and 1000 km in altitude, formed by solar radiation mainly in the UV and X-Rays range, and which has high daily variability, as well as dependence on solar activity, the season of the year, and the geomagnetic activity, and others. The large-scale plasma depletions which develop from the geomagnetic equator are generally referred to as equatorial spread F, ESF, or Equatorial Plasma Bubbles, EPBs. EPBs are seen as large-scale depletions in TEC which leads to the fluctuation in the amplitude and phase of the radio wave signal that affects radio communication and navigation systems. In South America, Brazil has monitored the Ionospheric scintillation with relatively high-cost commercial instrumentation, by contrast, Colombia does not have a highly developed system to measure scintillation or even studies about the ionosphere. This paper aims to present the proposal on software-defined radio and cognitive radio techniques for space weather studies, in which the main objective is to propose a Space Weather Low-Cost Instruments Laboratory (SWLCL) for use in space weather studies and its implementation in a campaign at two points in the equatorial regions in the longitudinal sectors of Brazil and Colombia between October 2022 and March 2023, and October 2023 and March 2024 using the digital low-cost receiver RTL-SDR and Software Radio Peripheral USRP and opensource software toolkit for the software-defined radio GNU Radio to measure the TECs between the ground receivers and Low Earth Orbit Satellites (LEOS) [1] in order to implement the cognitive radio techniques as well, the scintillation algorithm method. Such studies include probes with ground-based receivers, introducing Cognitive Radio techniques in SDR-based technology for demonstrating how reductions in the development and implementation costs while replacing hardware components could draw near the space weather public outreach, as well as miniaturization processes for application as payload to CubeSats satellites. In addition to developing these capabilities for space research, it is intended to study the feasibility of their applications in the area of accident and disaster prevention, as well as in the area of air defense and telecommunications, all of the technological, strategic, and social interest.

1. Introduction

In the Brazilian sector, where the magnetic equator presents a remarkable negative declination angle at ~20°, the climatology of EPBs is well-known, with peaks at equinoxes and December solstice. The climatology of scintillation follows the EPBs, and there are differences between distinct longitudinal sectors, which depend on local times and other factors. As mentioned previously, there is a lack of detailed information on EPBs and scintillation over Colombia, although this is of great interest for navigation and aeronautics. Scintillation processes affect the radio waves propagation in the ionosphere, which can be degraded in situations where the ionosphere is disturbed or presenting irregularities, see reducing the quality of the signal, errors in the positioning, or even loss of locking of the radio signal traveling between satellites that make up the navigation and positioning systems, such as the constellation of Global Navigation Satellite Systems, GNSS, satellites. Figure 1 represents the radio wave passing through a region with plasma irregularities (blue dots) before arriving at a ground-based receiver.

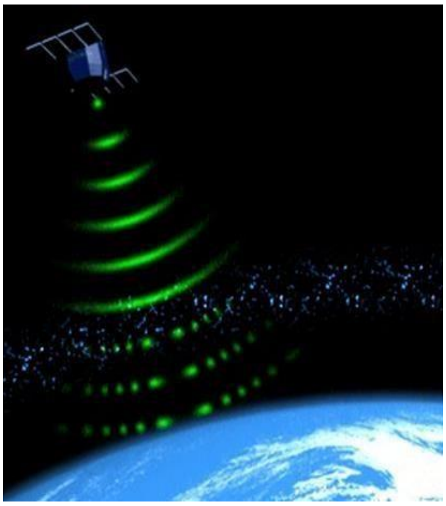

Figure 1: Radio wave through the disturbed ionosphere [2]

The process that degrades radio signals, well-known as Ionospheric scintillation, consists of fluctuations in the amplitude and phase of radio signals associated with EPB interferences. EPBs develop around post-sunset at the geomagnetic equator, move vertically and propagate simultaneously eastward and toward higher latitudes by diffusion, pressure gradient, and gravity. Therefore, an Ionospheric flicker can cause phase errors, ambiguity due to the number of cycles, increased carrier wave Doppler instability, or signal losses, which can induce errors of tens of meters or complete signal interruption. Worth mentioning that typically, the lower L band frequencies are more affected than, the higher frequencies indicating the focus of the thesis and the problem to be solved [3].

EPBs originating in the equatorial region can drastically interfere with the propagation of radio signals between satellites and ground receivers, especially in the regions where the plasma gradients are stronger, i.e., around the crests of the Equatorial Ionization Anomaly, EIA, which consists of two density crests around approximately 15 degrees of latitude north and south of the geomagnetic equator. In Brazil, one of the ionization crests is at approximately 23º S (geographic latitude). In Colombia, the north crest is around Bogota (Mag Latitude: 13.93° N). Additionally, scintillation can be strengthened or suppressed during geomagnetic activity associated with Space Weather events. Figure 2. shows the dependency of the S4 with solar activity for two solar cycles from 1998 to 2014 [4].

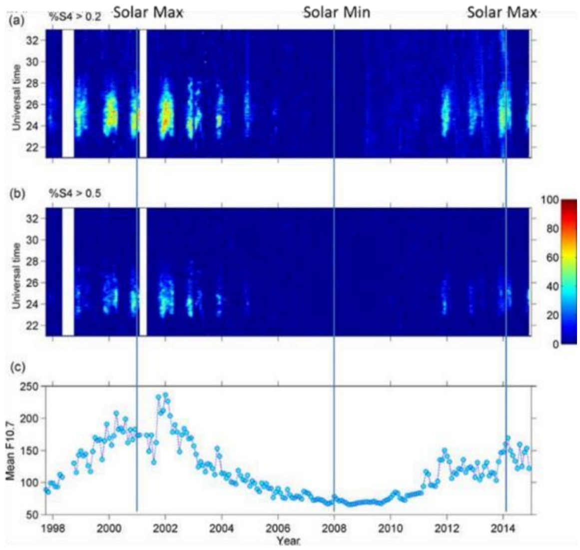

Figure 2: S4 with solar activity for two solar cycles [4]

The Ionospheric scintillation is monitored throughout the Brazilian territory, with relatively high-cost commercial instrumentation, as indicated in [5] and states the need for more complex logistics for data handling. On the other hand, in Colombia according to Ionospheric Irregularities are measured using Ground-Based GPS Networks [6]. Figure 3 show the Low-Latitude Ionospheric Sensor Network, LISN, over Latin America.

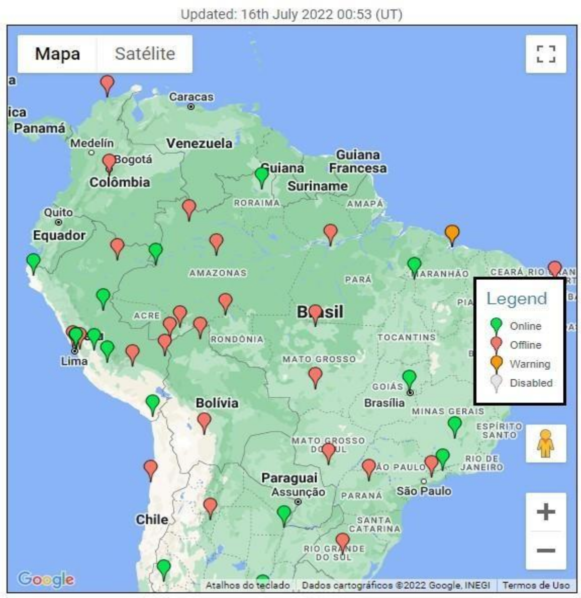

Figure 3: Low-Latitude Ionospheric Sensor Network – 2022 [7]

In this regard, the concept of Software-Defined Radio applied to Ionospheric monitoring and telecommunications technological decisions are of great interest because it can mitigate the operational difficulties of remote monitoring systems. The objective of using SDR in Ionospheric continuous sounding geomagnetically quiet periods and during space weather events has the advantage of providing higher coverage in terms of applications in the space area, using the constellation of GNSS (Global Navigation Satellite Systems) satellites and Geostationary satellites for VHF-bands. Such applications include high configurable and flexible probes with ground-based receivers. Furthermore, the SDR concept has good potential for miniaturization and application as a payload in CubeSats satellites, in addition to developing these capabilities for space research. Mitolla apud Albayrak defines Cognitive radio as an agent as software that exhibits the functional attributes of autonomy, interactivity, reactivity, goal-orientation, mobility, adaptivity; and that is capable of planning, reflection, and cooperation [8]. Besides, points out that cognitive refers to the mix of declarative and procedural knowledge in a self-aware learning system [8].

The CR inclusion is the highlight of the proposal. Bakare and Okolie declare that Cognitive Radios are intelligent devices with the ability to sense environmental conditions and can change their parameters according to the requirements to get the optimized performance at the individual nodes or the network level [9]. Thus, CR is widely regarded as one of the most promising technologies for future wireless communications, including Improve satellite communications. But, perhaps, there is no complete automation, and it requires user intervention for any changes to be implemented. It is thought to include machine learning to generate complete automation for the ground station to manage this disadvantage, and add, Adaptive Radio in which communications systems have a means of monitoring their performance and varying their parameters by closed-loop action to improve their performance. Finally, the hypothesis is that incorporating CR into SDR adds greater flexibility in handling Space weather research and monitoring. Therefore, based on the above problem, this work proposes the Software Defined Radio (SDR) platform development using a Cognitive Radio approach to simulate and replace the degraded signal-associated errors to monitor the Equatorial Plasma Bubbles having ground stations receiving signals.

3. Methodology

In this session, it is presented the general methodology and strategies to develop capabilities on detection, monitoring, prediction, warning, and decision making using cognitive radio. From the point of view of the approach to the problem, it will implement two methodologies. On the other hand, to implement the CR algorithms and techniques in the SDR, the methodology adopted is the Design Science Research Methodology (DSRM) is adopted; according to Von Brocke et al., it is a problem-solving paradigm that seeks to enhance human knowledge by creating innovative artifacts [10]. Conforming to Peffers et al., a six-step Design Science Research Methodology will be used, and the results will be published as scientific literature, as shown in Table 1 [11].

Table 1. Design Science Research Methodology

Research Step	Concerns	Output to Next Step	Entry Point?	Thesis stage methodology design
1. Identify Problem & Motivate	Define problem Show importance	Inference	ProblemCentered Initiation	Explore academic publications.
2. Define Objectives of a Solution	What would a better artifact accomplish?	Theory	Objective Centred Initiation	Define the algorithms for ionosferic scintillation detection and validation of the s4 index measurements
3. Design & Development	Artifact	How-to Knowledge	Design & Development Centred Initiation	Define the needs, requirements, and constrains of the laboratory. Modelling the ground station receiver based on the machine learning and cognitive radio techniques.
4. Demonstration	Find suitable context Use artefact to solve the problem	Metrics, Analysis Knowledge	Client/Context Initiated	Detect and monitoring of the ionosferic scintillation occurrence process in a case study.
5. Evaluation	Observe how effective, efficient Iterate back to design	Disciplinary Knowledge		Write the document.
6. Communication	Scholarly publications Professional publications			Present the results.

Source: Adapted from [11]

3.1. Hardware Proposed Prototype Development

The scintillation processes of the interest in navigation, positioning, and aeronautics occur in L-band frequencies: L1 (1575.42 MHz); L2 (1381.05 MHz), and L5 (1176.45 MHz) with more emphasis in the L1-band. VHF-band is of interest for monitoring and for strategic defense systems and will considered as one of modes of sounding. It is expected to construct an SDR prototype adding the CR techniques to mitigate the effects of the noise and errors caused by ionospheric scintillation and ensure the quality of the satellite signal troughing into the EPB. It should be noted that the mastery of such techniques with ground receivers has the potential for miniaturization processes and application as a payload in CubeSat satellites. The proposed prototype includes two stages.

The first stage defines low-cost commercial hardware: a handmade eggbeater antenna (300 MHz and 3-GHz beacon) and an RTL-SDR dongle. This stage encloses the scintillation detection and monitoring during observations, validation by comparison with conventional systems, and implementation of models over the GNU and cognitive radio plugins. It is worth mentioning that the stage in hardware is already built and installed at Bogota, Colombia in the Solar Radiometry Laboratory at Fundación Universitaria Los Libertadores, as shown in Figure 4.

Figure 4: Proposed prototype topology

The coordinates of the station are shown in Table 2

Table 2: Implemented prototype first location

Fundación Universitaria Los Libertadores Solar Radiometry Laboratory		
	Geographic	**Geomagnetic (2022)**
Latitude:	4°39′6.17′′N	13.93N
Longitude:	74°35′6.89′′ W	1.97W
Altitude	2579 M.S.N.	

This location was chosen due to it is a desire to improve the Solar Radiometry Laboratory. By 2022, this laboratory has a meteorological monitoring station and a radiometry station; with this improvement, it is predicted the consolidation of a scintillation low-cost monitoring system in Colombia. The second location was chosen due to the proximity to INPE, where conventional receivers are in operation for validation, and the possibility of using some of the facilities at the Electronic Engineering Division at ITA in Sao José dos Campos – Sao Paulo, Brazil, as shown in Table 3.

Table 3: Proposed prototype second location

Instituto Tecnológico de Aeronáutica (ITA)		
Geographic	**Geomagnetic (2022)**	
Latitude:	23°12'33"S	14.70S
Longitude:	45°52'30"W	25.39E
Altitude	597 M.S.N.	

Additionally, the use of other commercial hardware, such as Raspberry PI4, in developing the first models of the laboratory is considered to create a reliable system and to configure a portable ground station; Figure 5 establish the topology of the system; here, the software is the one that has to be developed.

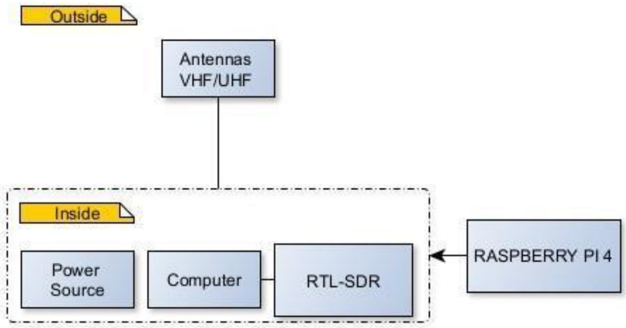

:

Figure 5: First stage topology

The second stage of the hardware proposed prototype integrates into the first model (first stage) the use of a more robust component in hardware, a USRP N210, see Figure 6 to provide more frequencies and better reliability. The ground station will be oriented by the model of [1].

Figure 6. Second stage major component in hardware
Source: [12]

According to Yamamoto GNU Radio is based on the script language Python; it is also possible to expand the capabilities of the GNU Radio by adding more signal processing codes in C++ [1].

3.2. Software Proposed Prototype Development

As mentioned previously, Cognitive Radio is a generic term used to describe a radio that is aware of its environment and can adapt its transmissions according to the interference it sees. The use of CR in this work is proposed to include an intelligence model over the GNU radio to the whole system. On the other hand, GNU Radio is the open-source software toolkit for the software-defined radio over the Linux Operating System selected to create the software prototype completely reconfigurable. In this way. It is intended to include the CR to identify the scintillation effects on radio signal propagation and over SDR software to mitigate, correct, and compensate. Figure 7 shows the functional diagram for the RTL_SDR, which has by "default" the frequency of the ATIS (Automatic Terminal Information Service) available at São José dos Campos International Airport as a use example. The Null Sink block is a simplified representation of the solution implementation for Cognitive Radio in this work. For the prototype, it will be necessary to initially specify the variables and constants that will compose this solution before starting the implementation of the block. In this way, expanding and describing the variables and constants in the final work is mandatory.

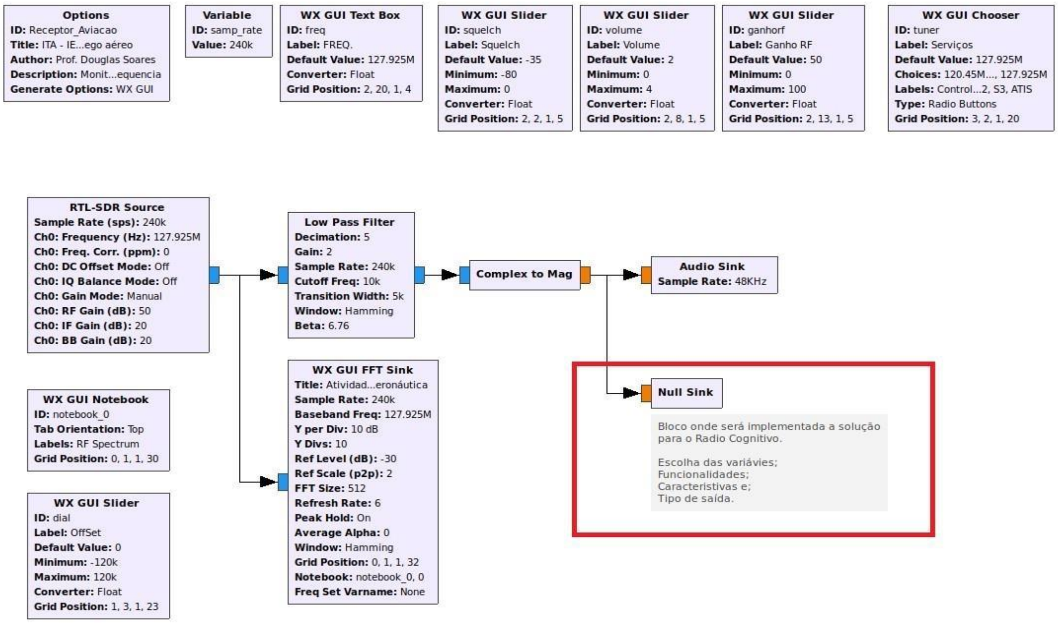

Figure 7. Implementation for Cognitive Radio

According to Biglieri, using Software-Defined Radios and Cognitive-radio protocols allows greater flexibility for new standards and concepts [13]. For example, using software radio, the devices generating multiple antenna beams can create the necessary number of beams with adjustable position and size or adapt their transmission parameters to adjust to the current propagation conditions. Narayan and Chandrasekharan in Biglieri affirm that the bands below 3.5 GHz have lower propagation loss and are sought after by all services. For this reason, one of the frequencies chosen in this document was the L-Band and VHF or even UHF [14].

4. Results

The proposal aims to generate knowledge whose central theme concerns the Cognitive Radio applied to the SDR approach to determine and mitigate the scintillation effects of navigation satellites' signals. It is expected to obtain an SDR monitoring system with high flexibility, reconfigurability, accessibility, and applicability in space weather that can monitor the Ionospheric scintillation in the L-bands and VHF bands using a case study carried out in two different areas, Brazil, and Colombia. Taking advantage of SDR represents an innovative low-cost, and flexible platform for multipath error studies, Ionospheric scintillation analysis, and, above all, GNSS reflectometry test and development. It is desired that the development of the Cognitive Radio algorithm, the design of the communication system, and its formalization in a SE process provide a proposal to be applied in mitigating the effects of scintillation in the reception of navigation and telecommunication satellites.

The main objective of the proposal is to develop a Scintillation Low-Cost Monitor System Laboratory (SLCL) based on the concept of Software-Defined Radio (SDR) for detection, monitoring, and warnings of the occurrence of Equatorial Plasma Bubbles

(EPB), as well as the Ionospheric scintillation. For this purpose, it is considered the technique of Radio Cognitive algorithms using the L-band signals (L1S: 1575.42 MHz) of the constellation of Global Navigation Satellite Systems satellites, GNSS, and VHF geostationary satellites (30 MHz to 300 MHz) available.

In order to complete the objective of the proposal: It is expected that the development of the system will agree to programmatic and regulatory restrictions, verification of the needs of the stakeholders, integration work, modeling program, simulation, and testing in order to provide a design; the simulation results on GNU RADIO will demonstrate the feasibility of using Cognitive Radio algorithms for application in problems such as the scenario presented; A campaign will demonstrate the utility of the (SWLCL) in the case study with two points over the geomagnetic equator. Bogotá, Colombia (North Latitude: 4°35'56'' and West Longitude of Greenwich: 74°04'51'') by the north side and Sao José dos Campos, Brazil, (Latitude: South, 23° 12′ 33″, Longitude: 45° 52′ 30″ West); and finally, It is expected that the system developed could aid in demonstrating its usability in the design of the multi-band communication system to monitor, detect and warn EPB and Ionospheric scintillation related to space weather.

5. Discussion

A simultaneous observation campaign in the longitudinal sectors of Brazil and Colombia will be implemented between December 2022 and March 2023 and between October 2023 and March 2024. The technology involves low-cost SDR digital receivers and the open-source software GNU Radio to measure scintillation between ground stations and GNSS satellites. Include probes with ground stations introducing machine learning and Cognitive Radio techniques into SDR-based technology to demonstrate how reductions in the development cost while replacing hardware components could draw near the space weather public outreach and could generate a new way to measure scintillation while it is learning about the ionosphere, and it is optimizing the communications channels between the ground stations and the satellites. Figure 8 shows the project purpose in general.

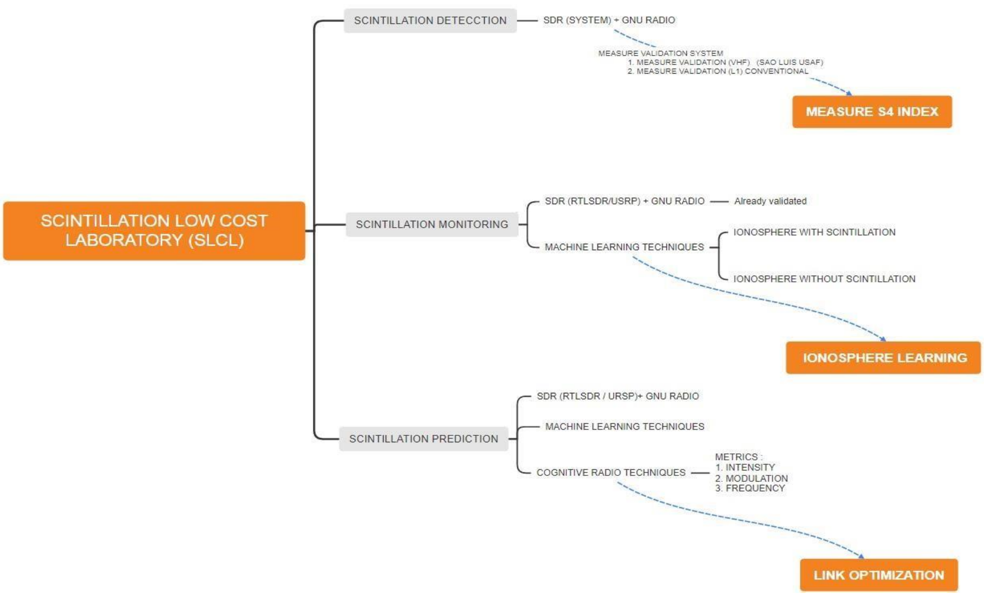

Figure 8. Project purpose in general

In fact, according to Abdu et al., in 2002, a campaign called COPEX was conducted during the October–December 2002 period in Brazil to investigate the equatorial spread F/plasma bubble irregularity (ESF) development conditions in terms of the electrodynamical state of the ionosphere along the magnetic flux tubes in which they occur [5]. In this way, it is desired to implement a similar campaign to investigate the equatorial spread F/plasma bubble irregularity over two distant and different points referenced by the geomagnetic equator with another cheaper and more flexible technology.

Acknowledgments

The authors would like to thank the National Institute for Space Research and the Fundación Universitaria Los Libertadores for their generous support and encouragement during the preparation of this manuscript.

References

[1] Yamamoto, M. (2008). Digital beacon receiver for ionospheric TEC measurement developed with GNU Radio. Earth, Planets and Space, 60(11), e21– e24. doi:10.1186/bf03353137

[2] Pinto Jayawardena, T, (2019). "Simulating ionospheric scintillation of GPS Signals for resilet PNT Testing challengues in developing a standardised test framrwork for ionospheric threats. Spirent. 2019.

[3] Acharya, R "Chapter 7 - Errors and Error Corrections," in Understanding Satellite Navigation, R. Acharya Ed. Oxford: Academic Press, 2014, pp. 243-279.

[4] Muella, M. T. A. H., Duarte-Silva, M. H., Moraes, A. O., de Paula,E. R., de Rezende, L. F. C., Alfonsi, L., and Affonso, B. J.:Climatology and modeling of ionospheric scintillations and ir-regularity zonal drifts at the equatorial anomaly crest region,Ann. Geophys., 35, 1201–1218, https://doi.org/10.5194/angeo351201-2017, 2017.

[5] Abdu, M., Batista, I., Reinisch, B., Souza, J., Sobral, J., Pedersen, T., Medeiros, A., Schuch, N., Paula, E.R., & Groves, K. (2009). Conjugate Point Equatorial Experiment (COPEX) Campaign in Brazil: Electrodynamics highlights on spread F development conditions and day-to-day variability. Journal of Geophysical Research, 114.

[6] Pi, X., Meyer, F. J., Chotoo, K., Freeman, A., Caton, R. G., & Bridgwood, C. T. (2012, September). Impact of ionospheric scintillation on spaceborne SAR observations studied using GNSS. In Proceedings of the 25th International Technical Meeting of the Satellite Division of The Institute of Navigation (ION GNSS 2012) (pp. 1998-2006).

[7] Instituto Geografico del Perú - IGP. Low Latitude Ionospheric Sensor Network. Radio Observatorio Jicamarca Chosica S/N – Lurigancho, Lima – Perú, (2022).

[8] Mitola, J. (2000). Cognitive radio. (PhD dissertation, Institutionen för teleinformatik). Retrieved from http://urn.kb.se/resolve?urn=urn:nbn:se:kth:diva2987

[9] Bakare. B.I. and Okolie. E.E. (2022) A Review of Cognitive Radio (CR) Technology Application, Prospect and Challenges. Euro. J. Adv. Engg. Tech., 2022, 9(1):1-5 [10] Vom Brocke J., Hevner A., Maedche A. (2020) Introduction to Design Science Research. In: vom Brocke J., Hevner may 24th, 2022.

[11] Peffers, K., Tuunanen, T., Rothenberger, M. A., & Chatterjee, S. (2007). A design science research methodology for information systems research. Journal of management information systems, 24(3), 45-77.

[12] Ettus Research, a National Instruments Brand. (s. f.). USRP N210 Software Defined Radio (SDR). Ettus Research. Recuperado 21 de septiembre de 2022, de https://www.ettus.com/all-products/un210kit/

[13] Biglieri, E. (2012). An overview of Cognitive Radio for satellite communications. 2012 IEEE First AESS European Conference on Satellite Telecommunications (ESTEL). doi:10.1109/estel.2012.6400078

[14] Biglieri, E., Goldsmith, A. J., Greenstein, L. J., Poor, H. V., & Mandayam, N. B. (2013). Principles of cognitive radio. Cambridge University Press.

NEW CHALLENGES FOR GROUND SEGMENT DEVELOPMENT: SCIENTIFIC SMALL SATELLITE MISSIONS.

Julio Filho A. C.[1], Pereira A. C. O. J.[2], Dos Santos W. A.[3], Cisotto M. V.[4], Tikami A.[5], Bueno L. A. R.[6], Brito A. F.[7], Florentino A. J. A.[8], Teixeira L.[9], Camargo L. A. P[10], Junqueira B. C.[11], Horna A. P.[12]

[1,2,3,4,5,6,7,8,9,10,11,12] National Institute for Space Research (INPE), São José, dos Campos, São Paulo - Brasil, 55 12 3208.6615, [1]cassiano.filho, [2]acarlos.pereira, [3]walter.abrahao, [4]marcus.cisotto, [5]auro.tikami, [6]luiz.bueno, [7]antonio.brito, [8]angelo.florentino, [9]lincoln.teixeira, [10]lazaro.camargo, [11]bruno.junqueira [@inpe.br], [12]mrandresph@gmail.com

Abstract

The National Institute for Space Research has promoted means of technological and scientific development, meeting internal and external demands through mission analysis, project coordination, management, and development, including remote sensing satellites, such as CBERS and Amazonia families, and small satellites for scientific applications, as well as the ground segment development. The ground segment must be compliant with the requirements defined by the space segment in the early stages of mission development and ensure synergy between these segments. In this scenario, the ground segment options for small satellites expand, and it is essential to consider the trade-off between data quality, data volume and cost. In the recent past, several missions relied on amateur radio ground stations to support of small satellites operation, and the amateur radio community has proven invaluable to small satellite missions. Nowadays, with increasing mission complexity and data requirements, more projects are looking at non-amateur ground stations which are part of ground segment. The ground segment for small satellites is typically based on the VHF-UHF bands, and it should meet the increasing demand for S-band and X-band telecommunications, as well as the need for reception, storage, and dissemination of high-quality scientific data. This paper presents the INPE’s ground segment development, including the Telemetry, Tracking and Command (TT&C) ground stations, the Reception and Recording Stations, the Satellite Control Center (SCC) Systems, to support scientific small satellite missions, in particular, the Scintillation Prediction Observations Research Task (SPORT). SPORT mission addresses the preconditions leading to equatorial plasma bubbles, and it is an international partnership between National Aeronautical and Space Administration (NASA) and the Brazilian Space Agency (AEB). Across NASA, American universities and the Aerospace Corporation provide the scientific instruments. Through AEB, the Technical Aeronautics Institute of the Brazilian Air Force Command Department (DCTA/ITA), and the National Institute for Space Research (INPE) contribute to the mission development. The paper also describes an overview of the spacecraft and mission objectives under the responsibility of the DCTA/ITA teams. It presents the ground segment integration, the planning for control and operation of the SPORT satellite, under the leadership of INPE's multidisciplinary teams, including the data storage and dissemination by Brazilian Monitoring and Study of Space Weather (EMBRACE). The design´s status, lessons learned, and the contributions to overcome challenges associated to development the ground segment for small satellites, and ensure the mission accomplishment are presented in this paper.

***Keywords**: Equatorial Plasma Bubbles, EMBRACE, Ground Segment, Satellite Control Center, SPORT.*

1. Introduction

The National Institute for Space Research (INPE), within its competences, can promote means of technological and scientific development by meeting internal and external demands through project coordination, mission analysis, management and development, such as remote sensing satellites (CBERS family, Amazonia-1) and the small satellites for educational and technological applications, as well as the ground segment development.

The ground segment must be compliant with the requirements defined by the space segment in the early stages of mission development and ensure synergy between these segments. In the recent past, several missions relied on amateur radio ground stations to support of small satellites operation, and the amateur radio community has proven invaluable to small satellite missions. Nowadays, with increasing mission complexity and data requirements, more projects are looking at non-amateur ground stations which are part of ground segment.

A complex mission, which based in a small satellite, is the Scintillation Prediction Observations Research Task (SPORT) [1]. SPORT mission addresses the preconditions leading to equatorial plasma bubbles, and it is an international partnership between National Aeronautical and Space Administration (NASA) and the Brazilian Space Agency (AEB).

NASA Marshall Space Flight Center coordinates this research by overseeing the launch to orbit and the scientific instruments. Aerospace Corporation, University of Texas, Utah State University, Alabama University and NASA Goddard Space Flight Center (GSFC) provide the scientific instruments.

Through AEB, the Technical Aeronautics Institute of the Brazilian Air Force Command Department (DCTA/ITA) is responsible for spacecraft development and integration; and the National Institute for Space Research (INPE) contributes with the infrastructure of the Integration and Testing Laboratory (LIT), ground segment development, mission operations, and science data management.

The science data will be distributed from and archived at the INPE Brazilian Monitoring and Study of Space Weather (EMBRACE) regional space-weather forecasting center, and mirrored at the NASA GSFC Space Physics Data Facility (SPDF).

This document is organized as follows: section 2 presents the space system and its segments; section 3 outlines the SPORT mission, instruments and platform; section 4 describes the current INPE's ground segment; section 5 presents the INPE ground segment for the SPORT mission; and section 6 the conclusions

2. Space System

A generic space system comprises the space segment and the ground segment. A **space segment** - spacecraft - consists of a service module and payloads follows ECCS [2, 3] and NASA [4] guidelines and CCSDS [5, 6] recommendations as presented in Fortescue et al. [7], Larson and Wertz [8], and ref. [9]. A **ground segment** comprises the hardware, software and human resources needed to manage and control a spacecraft, monitoring and analyzing its operation in orbit, and data distribution to the user.

The ground segment consists of (i) the Telemetry, Tracking and Command (TT&C) ground stations, (ii) the Satellite Control Centre (SCC), and (iii) the Application Segment.

TT&C ground stations [10] are in charge of establishing communication between the ground segment and the spacecraft, and SCC is responsible for the plan and executes all activities related to the spacecraft's control.

Application Segment comprises (i) the Reception and Recording Stations, (ii) the Mission Center that plans and coordinates the spacecraft data acquisition, stores the data, and makes them available to users.

Figure 1 illustrates a space system and its segments, it refers to the CBERS-4A mission, successfully launched in 2019 [10]. It is a partnership between the INPE and the China Academy of Space Technology (CAST). Another example of a space system [10] is the Amazonia-1, successfully launched in February 2021. It is the first remote sensing satellite fully designed, integrated, tested and operated by Brazil. It is a project coordinated by the Ministry of Science, Technology and Innovations (MCTI) and conducted by INPE in partnership with the AEB.

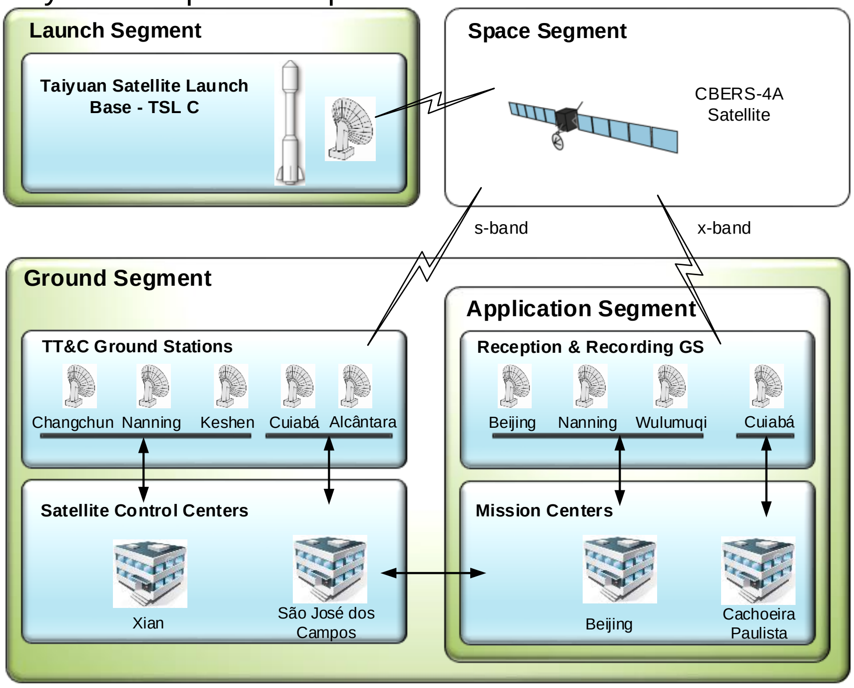

Figure 1: A typical Space System and its Segments [9, 10].

2.1. Brief of Ground Segment Evolution

Space agencies have been engaged in efforts to optimize financial resources, reduce ground segment development and deployment time. Several ground segment architectures have been proposed to meet the requirements of interoperability and cross support. In order to solve the problems associated with the large number of interfaces for exchanging services between ground stations and satellite control centers, the CCSDS, in a collaborative effort with space agencies, recommends a set of standardized services for interoperability and cross support [9, 10].

This set of standardized services, called Space Link Extension (SLE) Protocol Services [6] and their management activities provide interoperability and cross support among space agencies. Many space agencies have adopted the CCSDS recommendations of SLE Protocol Services [11], for example: ASI, CNES, DLR, ESA, ESOC, INPE, JAXA, and NASA, and by private companies.

Furthermore, cross support research and applications meet the objectives of the Interagency Operations Advisory Group (IOAG) [12]. The main goal of IOAG is the achievement of full interoperability among **member space agencies**: ASI, CNES, CSA, DLR, ESA, JAXA, NASA, and UK Space Agency.

3. SPORT Mission

The Technical Aeronautics Institute of the Brazilian Air Force Command Department (DCTA/ITA) is in charge of spacecraft development, integration, and tests [1].

The purpose of Scintillation Prediction Observations Research Task (SPORT) is to provide science data to a systematic study of the state of the pre-bubble conditions at all longitudes sectors to enhance understanding between geography and magnetic geometry. This phenomenon is the primary source of radar reflections in the equatorial F-region ionosphere and cause strong scintillations on radio signals passing through them.

SPORT will address two specific questions about these phenomena:

1) What is the state of the ionosphere that gives rise to the growth of plasma bubbles that extend into and above the F-peak at different longitudes?
2) How are plasma irregularities at satellite altitudes related to the radio scintillations observed passing through these regions?

3.1. Technical approach and instruments

SPORT, 6U CubeSat, is composed of two main systems: Payload and Platform, called Observatory.

The main characteristics are apogee and perigee of 400 km, inclination 51.64°, R.A. Ascending Node of 251.89°, Argument of Perigee 221.34°, Period of 1.54h, Orbits Numbers of 15.46, Data Storage capability of ~29GB, and nominal mission lifetime of 2 (two) years.

The **Payload** system consists of six instruments [1, 13], showed on Figure 2:

- **I**on **V**elocity **M**eter (**IVM**) to measure the velocity and direction of the íon component of ionospheric plasma at the sensor location (that collid with satellite), provided by University of Texas.
- **C**ompact **T**otal **E**lectron **C**ontent **S**ensor (**CTECS)** to obtain electron density profiles at low latitudes and to detect the presence of scintillation. CTECS is a GPS occultation sensor, provided by Aerospace Corporation.
- **E**lectrical **F**ield **P**robe (**EFP**) is used to measure only one component of both DC and AC electric fields for identifying disturbed regions of the ionosphere, provided by Utah State University (USU).
- **L**angmuir **P**robe (**LP**) to measure plasma density, as well as temperature, the floating potential, and the space potential. It is provided by USU.
- **S**wept **I**mpedance **P**robe (**SIP**) will be used to determine the absolute electron density, irrespective of the payload charging, by monitoring the changing impedance of a short cylindrical probe excited over a range radio frequency.
- **M**iniaturized **S**cience **M**agnetometer (**MSM)** will provide high-resolution measurements of the ambient magnetic field with sufficient sensitivity to potentially observe perturbations due to pressure gradients, diamagnetic cavities. Its provided by NASA Goddard Space Flight Center (GSFC).

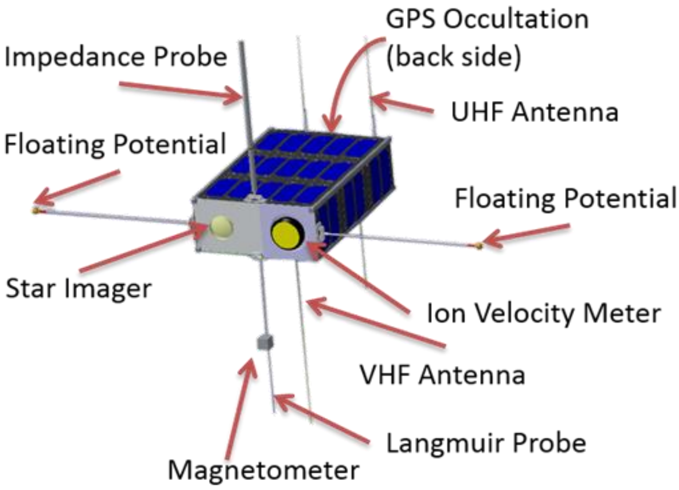

Figure 2: SPORT configuration and location of science instruments [1, 13].

The **Platform** system [1, 13] is responsible for controlling the satellite and consists of several subsystems describe below:

- **O**n**B**oard **C**omputer subsystem (**OBC**) is composed of three computers:
  - Control and Data Handler (C&DH) manages the SPORT by controlling the Attitude, VHF/UHF TT&C radio, Science Data, TM components;
  - Payload Data Handler (PLDH) interfaces with the Payloads' subsystems IVM, MSM and SIP, and send data to Data Storage Unit;
  - Data Storage Unit (DSU) stores all mission data packets to be transmitted to ground. Interfaces with CTECS for retrieving its Science Data and send to C&DH and PLDH.
- **E**lectric **P**ower **S**ubsystem (EPS) is the responsible for conditioning and distributing power to all components.
- **A**ttitude **D**etermination and **C**ontrol **S**ystem (ADCS) of the cubesat SPORT is responsible for providing stability in attitude through active control.

4. Current INPE's Ground Segment

This section presents the main systems that comprise ground segment of the INPE for space missions, (1) Reception and Recording Station, (2) Cuiabá and Alcântara TT&C INPE's Ground Stations and Satellite Control Center, (3) Natal TT&C Ground Station and (4) EMBRACE.

4.1. Reception and Recording Station

INPE, in 1973, started the activities of satellite tracking and data reception from the first remote sensing satellite, the Earth Resources Technology Satellite-1 (ERTS-1) of the Landsat Series [14].

Nowadays, the current Reception and Data Recording station - located in Cuiabá, in Mato Grosso State, Brazil) - operating in X-Band, receives and continuously records the data transmitted by Amazonia-1, CBERS satellites series, Landsat-5 and 7, SPOT-4, ERS-2, and Radarsat-1. The data are transferred to the Remote Sensing Data Center (Mission Center) in Cachoeira Paulista, in São Paulo State, for further processing and dissemination to end users, as illustrated in Figure 3.

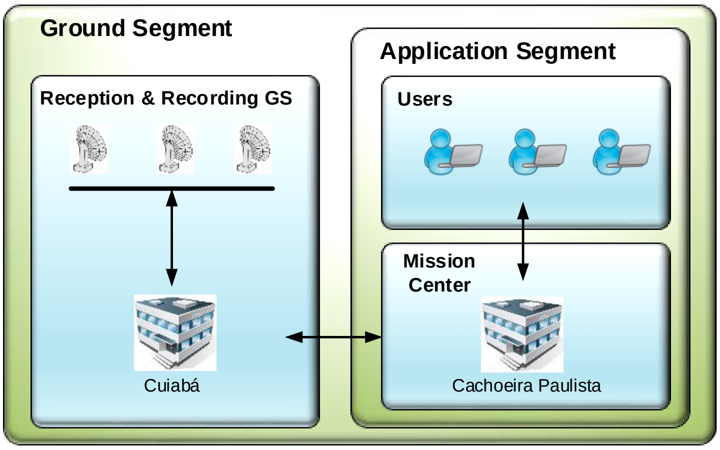

Figure 3: X-Band Reception and Recording Station.

4.2. Cuiabá and Alcântara TT&C INPE's Ground Stations and Satellite Control Center

Telemetry, Tracking and Command (TT&C) Ground Stations of INPE provide the link between the control personnel and the satellites [15, 16]. The Ground Stations operate in S-band and, are located in the cities of Cuiabá, (Mato Grosso state) and Alcântara (Maranhão state) in Brazil. This infrastructure was initially designed to support operations of the first Data Collection Satellite (SCD-1) launched in 1993. The basic infrastructure has been updated along the years.

TT&C ground station, Figure 4, comprises a RF Front End, an Antenna Control Unit, and a Time & Frequency. The functions of TM, TC, Ranging Data, Range Rate are based on Integrated Baseband System (IBS).

The IBS also enables the implementation of SLE protocol services [16] for cross support and interoperability between space agencies. In 2013, acceptance tests of the SLE protocol were performed in cooperation with the European Space Operations Centre (ESOC). On having the SLE protocol operational, INPE can rely on the support of other tracking stations distributed around the world to track its own satellites, and likewise provides tracking services to other international agencies.

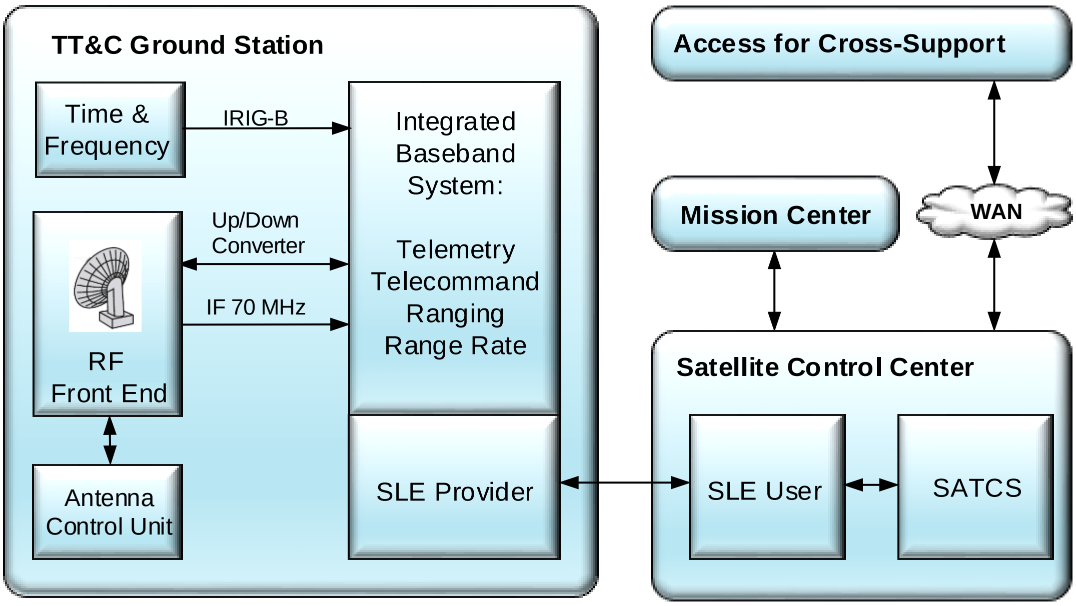

Figure 4: TT&C INPE's Ground Station and Satellite Control Center [16].

Satellite Control Center (SCC) [15], Figure 4, is located in the city of São José dos Campos, São Paulo state, Brazil. SCC is responsible for planning and executing all activities related to satellite control, and the rapid reaction in case of anomalies of a satellite. The SCC's main functions are orbit and attitude control, maneuvers calculation, operational payload configuration, and real-time monitoring of the satellite health.

The SCC structure includes a software system named **SAT**ellite **C**ontrol **S**ystems (SATCS). A specialized team from the General Coordination of Space Engineering, Technology and Science (CGCE) at INPE developed SATCS. It was designed to be an easily configurable and personalized system.

4.3. Natal TT&C Ground Station

Natal Multi-Mission Station (EMMN), Figure 5, is located at the Northeast Regional Center of the INPE, city of Natal, state of Rio Grande do Norte, Brazil. The EMMN Ground Station is designed to operate in the VHF (144 - 149 MHz), UHF (395 - 405 MHz and 432 - 440 MHz) and S-Band (2100 - 2300 MHz) frequency bands, receiving payload and telemetry data and transmitting satellite telecommands operating in low orbits [17].

The Station's radio frequency systems make use of Software Controlled Radios (SDR), which offers the flexibility of quickly reconfiguring parameters such as the type of modulation (FSK, AFSK, BPSK, GMSK, G3RUH), coding (AX-25), data rate (1200, 2400, 4800, 9600).

The station performs autonomous tracking of several satellites according to a schedule and obeying a priority scale. According to ref. [18], the missions tracked are CONASAT, FloripaSat, ITASat, NanoSatc-BR.

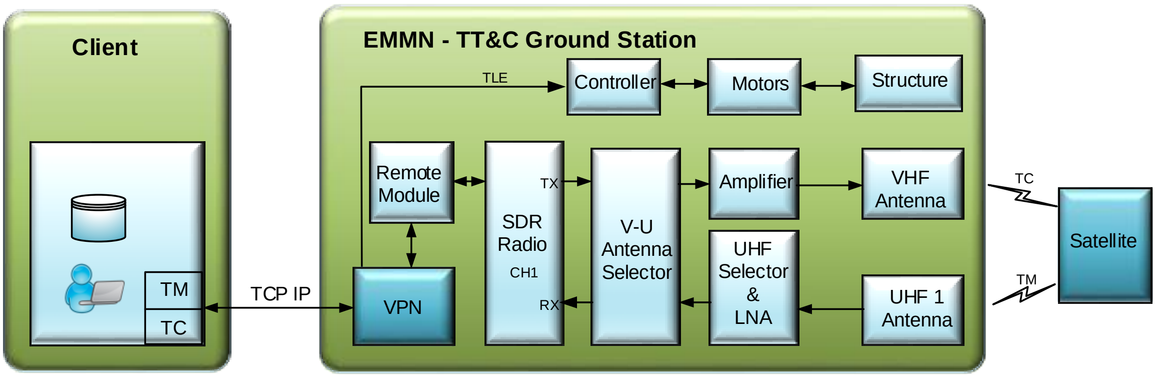

Figure 5: Natal INPE's Ground Station.

4.4. EMBRACE

EMBRACE Program [19], acronym in Portuguese "**E**studo e **M**onitoramento **BRA**sileiro de **C**lima **E**spacial" - Brazilian Space Weather Study and Monitoring, was created, in 2007 by INPE, to monitor the Sun-Earth space environment, the magnetosphere, the upper atmosphere and the effects of induced currents on the ground to predict possible influences on technological and economic activities.

Recently, EMBRACE acquired an antenna, installed in Cuiabá, Mato Grosso state, Brazil, for reception of data from the Constellation Observing System for Meteorology, Ionosphere, and Climate2 (COSMIC-2). COSMIC-2 is a network of six radio occultation observation satellites of the GNSS satellite constellation used to collect atmospheric data used in weather forecasting, and space weather monitoring and prediction.

5. INPE's Ground Segment for SPORT Mission

SPORT mission posed new challenges for the implementation of the ground segment. The ground segment will allow attending the higher rate revisits, associated the controlling, data reception, support and interoperability to all ground facilities, which requires an architecture to support them. This architecture should be attending remote sensing satellites, such as CBERS and Amazonia families; radio occultation observation satellites, COSMIC-2; and small satellites for scientific applications.

The contributions to overcoming the challenges associated with the development of the ground segment for small satellites and ensure the mission accomplishment are the integration of the ground segment, the planning for control and operation of the SPORT satellite, under the leadership of INPE's multidisciplinary teams, including data storage and dissemination by the Brazilian Space Weather Monitoring and Study (EMBRACE).

SPORT [1, 13] will use ground segment, Figure 6, comprises by INPE TT&C ground stations located at Natal (northeast) and Cuiabá (center west) with additional system for operation in UHF and VHF bands, under control of Satellite Control Center (SCC), located in São José dos Campos. For scientific data downlink (ERD), the SPORT will use two X-band antennas located at Cuiabá (center west) and Cachoeira Paulista (southeast).

The SCC at INPE headquarters in São José dos Campos will remotely operate TT&C ground stations using SATellite Control System for SPORT (SATCSport) and communication private links. The mission operations at INPE involve the support and operational teams, ground system infrastructure (hardware and software) and facilities, as well the real time (SATCSport) and non-real time flight dynamics software.

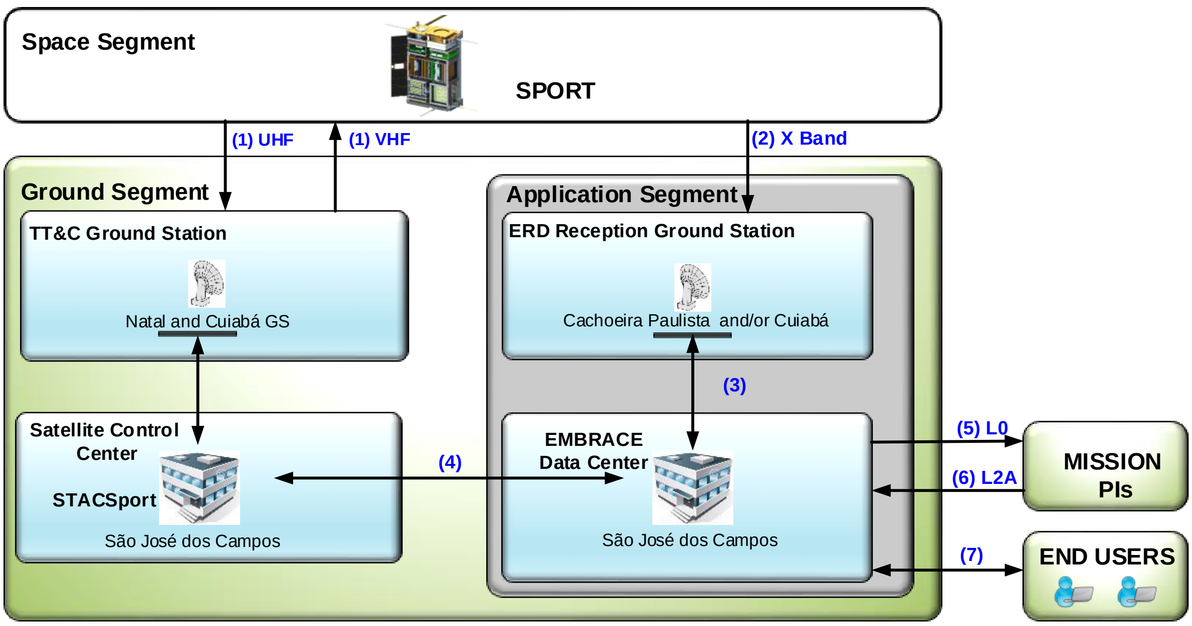

Figure 6: INPE's Ground Segment for SPORT Mission.

The data center at EMBRACE will receive the data and distribute decommutated instrument and engineering data to the instrument teams (Mission PIs) for data reduction.

The reduced instrument data will be sent back to EMBRACE from each instrument team, where it will be processed, archived, and ingested into space weather analysis models and tools [1].

SPORT has a fully open data policy consistent with NASA data policies. EMBRACE will be the SPORT mission data distribution center for the science and end user communities. The data will be mirrored and archived at the NASA Goddard Space Flight Center (GSFC) Space Physics Data Facility (SPDF).

6. Conclusions

The requirements of the INPE's different missions involve definitions as communication band; uplink and downlink rate; protocols; onboard processing; remote reconfiguration of service and payload modules, and classically, determine the design and development of missions and posed new challenges for the implementation of the ground segment.

From the Ground Segment perspective, partnerships for space systems development should follow a strong standardization of system engineering procedures, consistent and traceable documentation, management, and implementation of the ground segment and its interfaces with the space segment. Furthermore, the challenges and complexity for the development of the ground segment are the same, regardless of the satellites' dimensions and applications.

In July 2022, the Aeronautical Technical Institute of the Brazilian Air Force Command Department (DCTA/ITA) delivered the SPORT satellite to Nanoracks payload hosting services provider, https://nanoracks.com/, and its launch to the ISS is scheduled for November 2022.

TT&C stations, Reception and Data Recording stations, and EMBRACE are in the final integration and testing phase. The Satellite Control Center is in the final stages of preparation of the launch campaign, training of the tracking and operations teams.

Acknowledgments

We thank all our coworkers at the Brazilian National Institute for Space Research (INPE) for support.

References

[1] Spann J., Swenson C., Durão O., Loures L., Hellis R., Bishop R., Le G., Le G., Abdu M., Krause L., Fry C., Denardini C., Shibuya L., Casas J., S. Nazh-Stevenson S. N., Muralikrishana P., Costa J., Eberly E., Mesmer B., Padua M. B., Wrasse C. "The Scintillation Prediction Observations Research Task (SPORT): An International Science Mission using a CubeSat", Proceeding 31nd Annual AIIA/USU Small Satellite Conference, Logan UT, USA, 2017, SSC17-XIII-03, http://digitalcommons.usu.edu/cgi/viewcontent.cgi?article=3695&context=smallsat

[2] European Cooperation for Space Standardization (ECSS) (2003). "ECSS-E-70-41A. Space engineering - ground systems and operations telemetry and telecommand packet utilization". <http://www.ecss.nl/>.

[3] European Cooperation for Space Standardization (ECSS) (2008) "ECSS-E-ST-70C. Space engineering - ground systems and operations". <http://www.ecss.nl/>.

[4] National Aeronautics and Space Administration (NASA). (2013) “NASA Procedural Requirements - NPR 7123.1B. Systems Engineering Processes and Requirements”. Washington, DC.
[5] CCSDS TM Space Data Link Protocol. Recommended Standard. CCSDS 132.0-B-1. Blue Book. Issue 1. Washington, D.C., September 2003.
[6] CCSDS Cross support concept - Part 1: Space Link Extension Services - CCSDS 910.3-G-3. Washington, D.C, 2006.
[7] Fortescue, P.; Stark, J.; Swinerd, G. (2003) "Spacecraft systems engineering 3". Chichester, UK: John Wiley. ISBN: 678 ISBN 0-471-61951-5.
[8] Larson, W.J.; Wertz, J. R. (Ed). (1999) "Space mission analysis and design 3". Dordrecht, Netherlands: Kluwer Academic, 1999. ISBN: 969306936 ISBN 1-881883-10-8.
[9] Julio Filho, A. C., Ambrosio, A. M., Ferreira, M. G. V., “Model-Based System Engineering (MBSE) applied to Ground Segment Development of Space Missions: New Challenges”. In: International Astronautical Congress, 72th Online Proceedings...2021
[10] Julio Filho, A. C.; Ambrosio, A. M.; Ferreira, M. G. V. (2021) " The Ground Segment: A proposal Framework based on concepts of Dynamic Management of the Space Link Extension Protocol Services”. In: International Conference on Space Operations 16th, Cape Town, South Africa.
[11] CCSDS Space Communication Cross Support – Architecture Description Document - Informational Report. CCSDS 901.0-G-1. Green Book. Issue 1. Washington, D.C., November 2013.
[12] The Interagency Operations Advisory Group https://www.ioag.org/default.aspx. Accessed Jul 2021.
[13] https://www.nasa.gov/mission_pages/sport/index.html
[14] Julio Filho A. C., Ambrosio, A. M., Ferreira, M. G. V., Bergamini, E. W., “New Challenges for Dynamic Management of the Space Link Extension Protocol Services: The Amazonia-1 Satellite Ground Segment”. In: SPACEOPS Conference, Marseille, France. Proceedings...2018. DVD.
[15] Julio Filho, A. C., Ambrosio, A. M., Ferreira, M. G. V., Loureiro, G., “The China-Brazil Earth Resources Satellite - CBERS-4A: A proposal for Ground Segment based on the Space Link Extension Protocol Services”, in: International Astronautical Congress, 70th IAC. Washington D.C., United States, 2019.
[16] Julio Filho, A. C.; Ferreira, M. G. V.; Ambrosio, A. M. . The Ground Segment: A proposal Framework based on concepts of Dynamic Management of the Space Link Extension Protocol Services. In: 16th International Conference on Space Operations, 2021, Cape Town, South Africa.
[17] Jotha, L. S. “Estação multimissão de Natal - manual técnico.” São José dos Campos: INPE, 2020. 90 p. IBI: <8JMKD3MGP3W34R/436TMAB>. (sid.inpe.br/mtc-m21c/2020/09.02.14.30-MAN). Available in: <ibi:8JMKD3MGP3W34R/436TMAB>.
[18] https://ccsl.ifrn.edu.br/portfolio-de-projetos/emmn-estacao-multi-missao-de-natal/.
[19] http://www2.inpe.br/climaespacial/portal/wp-content/uploads/2020/08/PROGRAMA_EMBRACE.pdf

5

Session 5 - Embedded Systems Reliability

A Performance Evaluation of a Fault-tolerant RISC-V with Vector Instruction Support to Space Applications

Carolina Imianosky(1), **Douglas A. Santos**(2), **Douglas R. Melo**(1), **Luigi Dilillo**(2), **Cesar A. Zeferino**(1), **Eduardo A. Bezerra**(3), **Felipe Viel**(1),(3)
(1) LEDS, University of Vale do Itajaí, Brazil
(2) LIRMM, University of Montpellier, CNRS, France
(3) SpaceLab, Federal University of Santa Catarina, Brazil

Keywords: *RISC-V, Vector Instructions, Fault tolerance, Space Applications*

Computational systems used in space systems have constantly been evolving in several aspects, ranging from the ability of tolerate faults and failures to process large volumes of data. These aspects mainly affect the characteristics of the processing cores, ranging from microcontrollers to microprocessors, impacting in the computer architecture and organization used. One instruction set architecture under extensive study for application in the space environment is the RISC-V. This architecture has been widely used in space systems because it is simple, open, and modular, enabling the application of techniques that mitigate faults caused in a space environment. However, the application of these techniques affects the performance of the components. Thus, it affects the high-resolution data captured by the sensors, which needs to be processed before being transmitted to Earth. Therefore, it is necessary to apply techniques that accelerate the processing of this data. As a solution to the demand for an increase in processing performance, RISC-V can support vector instructions, which allow operating on a vector of data with only one instruction. This approach allows exploring levels of data parallelism and improving the acceleration of applications. Therefore, we developed support for a subset of the vector extension for an existing functional fault-tolerant RISC-V processor. We analyzed the vector instructions that are relevant to digital signal processing, since it is a time-costly type of processing, to define the instructions that constitute the subset. Thus, we implemented only sequential memory access, addition, and subtraction vector instructions. We evaluated the impact of using these instructions compared to scalar instructions, analyzing the execution time, logical resource utilization, and power consumption. The results showed a performance improvement of up to 4x when using the vector instructions relative to the scalar instructions, but, there was a hardware overhead of 1.5x for consumed Lookup Tables and 1.8x for Flip-Flop. Besides the hardware overhead, this cost is negligible compared to the acceleration offered.

1. Introduction

Space systems are affected by the harsh elements of the space environment, such as radiation, extreme temperatures, and lack of gravity. These elements may lead

Email addresses: `imianosky@edu.univali.br` (**Carolina Imianosky**), `viel@univali.br` (**Felipe Viel**)

to faults that can affect the functioning of computational systems. Thus, it is important to apply fault-tolerance techniques in spacecrafts design to improve the systems reliability [1].

The processor implemented by Santos et al. [2], also known as HARV, is an example of technology for space systems, in which the authors developed a low-cost fault-tolerant RISC-V processor. This work used fault-tolerance techniques to prevent possible errors due to its exposition to harsh environments. Also, in [3], the authors analyzed the impact of Deep Neural Networks (DNNs) for space applications. Therefore, they evaluated the use of DNNs in a RISC-V vector processor and presented a several recommendations to systematically enable OBDM with RISC-V vector processors. Thus, as it can be observed, there is a tendency to use the RISC-V ISA (Instruction Set Architecture) as processing core for space applications.

RISC-V is an ISA that has gained popularity within the past few years. This is mostly due to its simplicity, openness, and modularity, i.e., composed by a base ISA and optional extensions [4]. Among the various ISA extensions defined in the standard, there is the vector extension. With this extension, the systems can perform an instruction on multiple data elements simultaneously [5]. Thus, it is possible to explore high data parallelism levels, decreasing processing latency and power consumption. These factors are critical in space systems since they have limitations regarding energy harvesting [6].

Currently, some commercial and academic cores implement or are based on the RISC-V Vector (RVV) extension. For instance, Arrow [7] is a configurable co-processor aimed at edge machine learning inference that implements a subset of RVV version 0.9. Further, Johns and Kazmierski [8] implemented a subset of the RVV v0.8 extension instructions to a RISC-V processor to satisfy microcontrollers area and power consumption requirements. Also, Ara [9] is a parametric in-order high-performance 64-bit vector unit based on RVV version 0.5 that works in tandem with Ariane. However, although these works explore the RVV extension, to the best of our knowledge, there are no works that implement the RVV extension for a fault-tolerant processor.

Given the context above, this work has as its main contribution the support development of a vector instructions subset for a low-cost fault-tolerant RISC-V processor developed in [2]. Our primary focus was to improve the performance of signal processing applications. The experiments comprised the execution of basic arithmetic operations and memory read and write with scalar and vector instructions to compare the impact of using vector instructions.

The remainder of this paper is organized as follows. Section II presents additional concepts on hardware acceleration, RISC-V ISA, and its vector extension. Next, Section III discusses related work, and Section IV describes the materials and methods employed in this study. Following, Section V presents and discusses the experimental results, while Section VI gives the final remarks.

2. Background

2.1. Hardware Acceleration

One way to speed up computational processing is using the Data-Level Parallelism (DLP) concept, which is used to operate on multiple data elements simultaneously [5]. Single Instruction, Multiple Data (SIMD) is one class of processors exploring the DLP. This architecture became popular in the 1970s for partitioning 64-bit registers into multiple 8-, 16- or 32-bit registers and operating them in parallel. This way, a single instruction operates on several data array elements within only one instruction fetch and decode. The Operation Code (Opcode) supplied the data width and the operation [10].

Subsequently, to speed up SIMD architectures, the architects increased the width of the registers to process more elements in parallel. Once data and operation width are indicated in the instructions Opcode, expanding the SIMD registers also implies increasing the instruction set [10]. Thus, SIMD instructions operate in fixed-size registers that are generally set to 128 bits wide [11].

An alternative to SIMD architecture that explores DLP is the vector architecture, represented in Fig. 1. This architecture gathers objects from the main memory, puts them into exclusive vector registers, operates on these registers, and then scatters the results back to the main memory. However, unlike SIMD, the size of vector is determined by the implementation rather than described in the Opcode [10]. Consequently, vector architectures require a smaller instruction set and make hardware design flexible to parallelize data without affecting algorithms development.

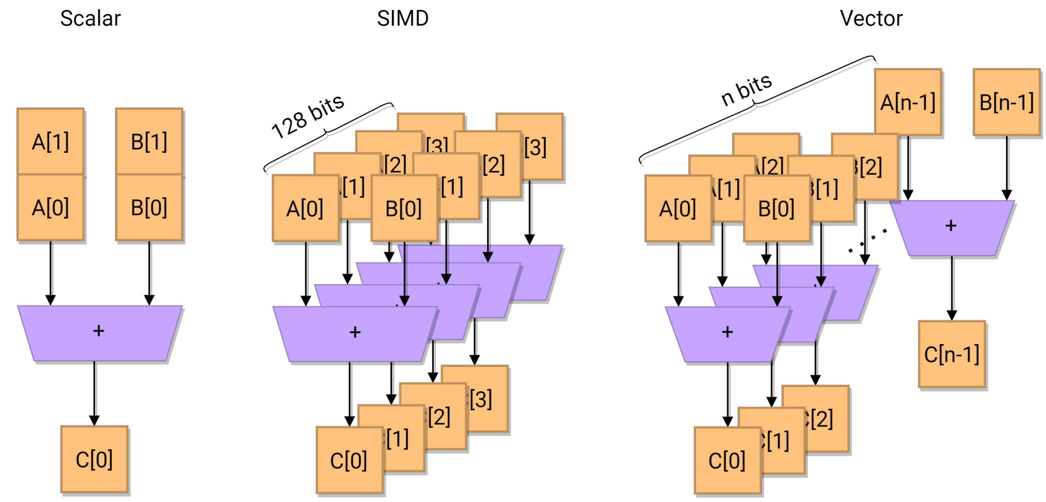

Figure 1: Addition instruction in scalar, SIMD and vector architecture [11].

2.2. RISC-V

The RISC-V ISA was developed at the University of California, Berkeley, based on the Reduced Instruction Set Computer (RISC) architecture [12]. This ISA has a highly regular instruction encoding and simple memory access instructions with a direct memory model. One of the benefits of RISC-V is the minimal size of simple cores, which are much smaller compared to Advanced RISC Machine (ARM) and x86 architectures. However, the difference is not noticeable on higher-capacity cores [13].

The RISC-V structure is modular, i.e., it comprises a base instruction set and a variety of optional extensions. The three main base instruction sets are RV32I, RV32E, and RV64I. The first one is a 32-bit set with 47 instructions, enough to fill basic requirements of the modern operational systems. The other two sets are very similar. The RV32E is a variation with only 15 registers aimed at embedded systems, and the RV64I differs only on the integer and Program Counter (PC) registers width [10]. The optional extensions can be added as needed by each application to form a more robust instruction set [12].

2.2.1. *Vector extension*

The RISC-V vector extension allows adapting the RISC-V ISA to a vector architecture. It adds 32 vector registers to the base RISC-V and enables its splitting for executing more operations simultaneously, which is configured through the seven additional CSRs [12].

The Configuration-Setting instructions change the values of CSRs. The vector arithmetic instructions operate on values stored in the vector registers, and memory read and write operations transfers a certain number of bits from memory to the vector database and back again. All instructions in this set fit into two existing instruction formats: LOAD-FP/STORE-FP from the floating-point extension, or OP-V, a vector-exclusive format [14].

3. Architecture

HARV [2] is a low-cost fault-tolerant RISC-V processor developed through cooperation between the Laboratory of Embedded and Distributed Systems from the University of Vale do Itajaí (UNIVALI) and the Laboratory of Informatics, Robotics, and Microelectronics of Montpellier (LIRMM) from the University of Montpellier. The authors focused on using the least amount of resources possible. Thus, the processor uses a single-cycle micro-architecture, reducing the required registers.

This processor has five primary units: (i) instruction fetch; (ii) instruction decode; (iii) execution; (iv) memory access; and (v) write-back. We modified the decode, execute and register HARV's units to support the vector instructions subset, highlighted at Figure 2.

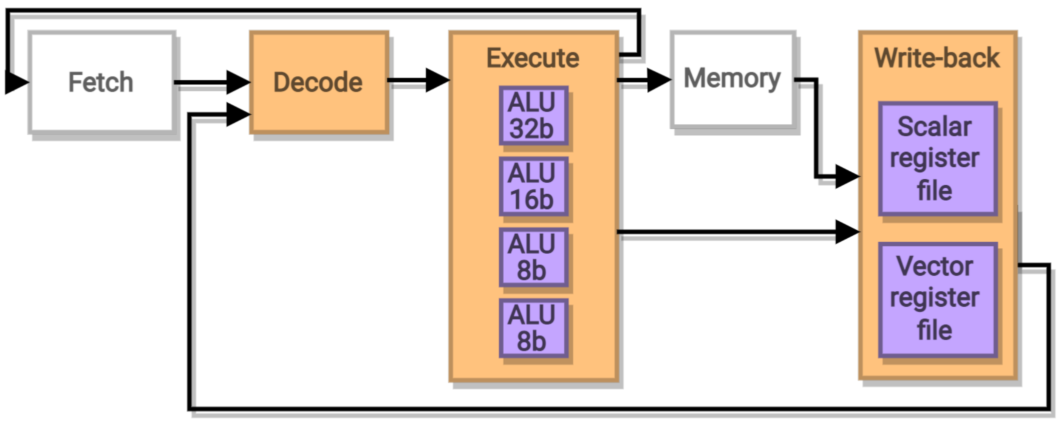

Figure 2: HARV block diagram with the modifications to support vector instructions.

This work aimed at implementing only the main vector instructions for digital signal processing to optimize these applications. Therefore, among the several possible instructions to be implemented, the subset was limited to instructions of sequential memory read and write (word, half-word, and byte) and integer arithmetic operations, such as addition and subtraction, for 32-bit architecture.

3.1. *Instruction Fetch*

The instruction fetch unit consists of a PC register, a 32-bit adder, and the required logic circuits for jumps and conditional branches. The adder increments the value stored in the PC register in case of sequential execution. Otherwise, in the case of executing a conditional branch, it adds the address offset to the PC register.

3.2. Instruction Decode

In HARV, the control unit integrates the instruction decoder, responsible for identifying the operation that will be performed. The 6 to 0 instruction bits are used as input for a combinational logic that asserts the control signals for the data path. Thus, the control unit identifies the format of the instructions according to the RISC-V ISA specification [10]. To support the vector instructions subset, we added the three instructions format defined in version 1.0 of the vector extension specification: Load-FP, Store-FP, and OP-V [14]. Subsequently, according to the format of the instructions, the output of the control unit related to the operation performed are enabled (1) or not (0).

In order to simplify the implementation, Santos et al. [2] developed the main and ALU control units as a single component. Thus, the control unit also has an output informing the ALU which operation to perform. For scalar instructions, the field *funct3* from the instruction (bits 14 to 12) defines the operation. Whereas for vector arithmetic instructions, the ALU operation is defined by the instruction field *funct6* (bits 31 to 26).

As in HARV, the processor performs the source registers reading in the decoding stage. This is done based on the addresses informed in the fields *rs1_i* and *rs2_i* of the instruction, in case of scalar registers, or *vs1_i* and *vs2_i*, in case of vector registers. For writing, the addresses fields are *rd_i*, for scalar registers and *vd_i* for vector registers.

The scalar register file was kept identical to the base processor. Thus, it can perform two registers read, and one register write simultaneously. Although, in order to write in the register, the input *write_en_i* must be enabled. The register writing is clock-synchronous, while the reading is independent of the clock, meaning that the data written in the register on the previous cycle can be read in the current cycle. The vector register file works similarly to the scalar register file, and the difference between both is that the vector register file is exclusive to vectors.

3.3. Execution

The execution unit performs operations with two 32-bit data vectors. Therefore, this unit has two data inputs, as shown in Figure 3, *data1_i* e *data2_i*. In addition, the *ALUOp_i* input, derived from the control, signals which operation to perform according to the instruction.

To develop this unit, we base on the implementation of [8]. For this reason, we used four ALUs. One of these ALUs is identical to the 32-bit ALU implemented in HARV. The arithmetic and logical operations supported by this ALU are: add, shift (left/right logical and right arithmetic), set on less than, AND, OR, and XOR. The other three are one 16-bit and two 8-bit ALUs. However, we simplified these ALUs to support only the operations used in the vector instructions subset of this work since these are useful only for vector operations.

With the width of the input vectors set to 32 bits, in just one cycle (as long as there is no pipeline and it is single-cycle), it can run either one 32-bit, two 16-bit, or four 8-bit operations. Therefore, the level of parallelization of operations depends on the vector size of elements. The inputs and outputs are mapped to their respective ALUs according to the width setting of the vector elements. The elements that are being operated on wider ALUs are zero-extended. The 32-bit ALU is selected as the only output for scalar instructions to decrease the hardware needed for vector extension.

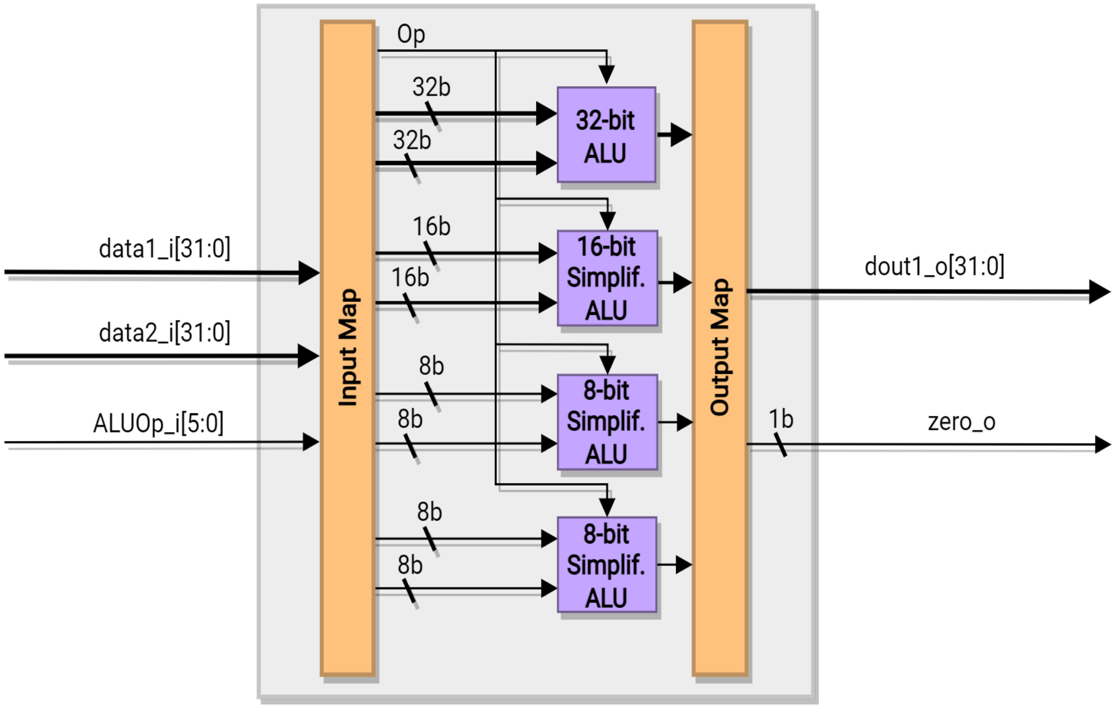

Figure 3: Execution Unit.

3.4. Memory Access

The memory access unit performs read and write operations to/from the data memory. The RISC-V specification describes that accesses with 8-, 16-, and 32-bit word widths can be performed, and all readings result in 32-bit width data. According to the instruction executed, the data signal can be extended or not. In RISC-V vector specification, there are three types of vector memory access: sequential, stride and indexed. However, we used only the sequential method in this work, which is identical to the scalar memory access implemented in HARV.

3.5. Write-back

The register write is only executed when processing instructions that write into the register file. This step is responsible for selecting the data to be written in the vector or scalar register file. The Figure 4 presents an overview of how the register writing is executed. This representation describes this operation in a simplified way. Therefore, we have abstracted the multiplexers used for other operations and the signals referring to the control outputs, immediate selection, and ALU input signals.

The inputs of the register file are connected to multiplexers, commanded by the control, and have as input the memory read and the execution results. In the case of the scalar register files, there are two additional multiplexers, also driven by the control, which inputs are the PC value and the immediate field of the instruction. The value is stored in the register at address *rd_i*, for the scalar register file, or *vd_i*, for the vector ones. These addresses are specified in the instruction, and writing to each register file is only performed if the respective write control signal is active.

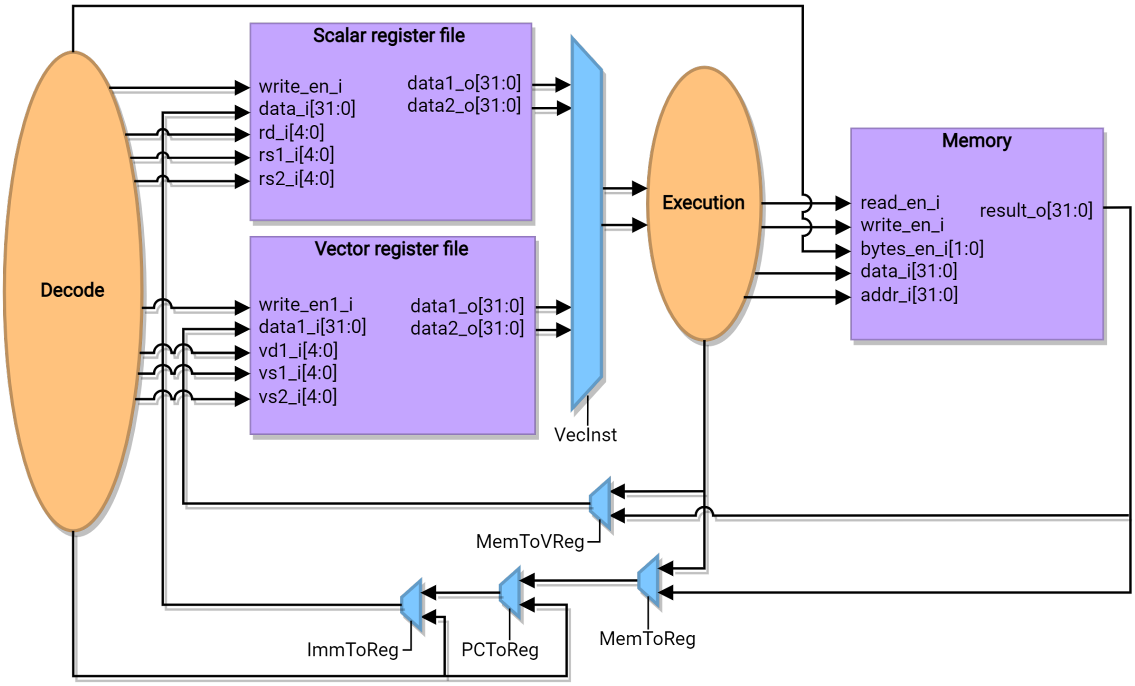

Figure 4: Write-back unit.

4. Results

4.1. Methodology

Since HARV was implemented using VHSIC Hardware Description Language (VHDL), we developed the vector instruction support using VHDL as well. We used the Xilinx Vivado 2020.2 Design Suite tool to collect the synthesis data and the Zynq ZC7020 SoC device. The metrics analyzed include the number of Look-up Tables (LUTs) and Flip-Flops (FFs), maximum operating frequency, and the estimated power dissipation.

The benchmark algorithm is a vector addition that reads two vectors from the data memory, adds the elements, and writes the result to the memory. The vectors used are 32-bits wide, but the element's width was varied among all the possibilities. This algorithm was executed in two scenarios: using only scalar instructions and using the implemented vector instructions. The programs were written in the RISC-V assembly language and optimized for vector architecture.

Therefore, it was possible to compare the read, write, and operating latency of vector elements in both scenarios with 50MHz of clock. We explored spatial memory locality in the scenario with vector instructions by storing the whole vector as a word in the memory. By this, it was possible to increase even more the performance gain.

4.2. Benchmark Performance

Table 1 presents a comparison between the number of cycles needed to execute memory access and arithmetic instructions for scalar and vector architectures. Reading and writing 16- and 8-bit memory elements with scalar instructions take two and four separate memory accesses, respectively. With vector instructions, on the other hand, it is possible to read all the elements in only one memory access, since the number of instructions required to perform the same operations is reduced. Thus, to execute memory loads and stores, the vector instructions required four and two times fewer cycles when operating on 8- and 16-bit elements, respectively.

The same happens for the arithmetic instructions since, with scalar instructions, it is necessary to operate on the elements individually. Whereas with vector instructions, the elements are operated on simultaneously. This way, when processing 8-bit data elements, as is the case of image pixels, using vector instructions decreases the number of cycles by up to four times. For 16-bit elements, the required number of cycles is two times smaller.

Table 1: Number of cycles to execute scalar and vector instructions for each possibility of vector element width.

	Operating latency (number of cycles)					
Vector elements	**Four 8-bit**		**Two 16-bit**		**One 32-bit**	
Instruction type	Scalar	Vector	Scalar	Vector	Scalar	Vector
Load / Store	32	8	16	8	8	8
Arith	20	5	10	5	5	5

4.3. Synthesis Result

The synthesis results for the original HARV processor and HARV with the vector extension are shown in Table 2. The maximum operating frequency increased 4.6%, and the power dissipation increased 6.1%.

The implementation of the extension increased the logical resources used by the processor. With the vector extension, the number of LUTs is 1.5 times higher than the original HARV, mainly due to adding the vector register file and the three ALUs. At the same time, the number of FFs is 1.8 times higher because of the 32 vector registers. However, the overhead of hardware and power are acceptable compared to the gained acceleration.

Table 2: Synthesis results.

Configuration	LUTs	FFs	F_{max}(MHz)	P(mW)
Scalar HARV	1,988	1,575	52.15	146
Vector HARV	3,158	2,826	54.72	155

5. Conclusion

This work provided support of a vector instructions subset from the RISC-V vector extension for HARV [2], which is a fault-tolerant processor. The main goal of this implementation was to accelerate signal processing applications by exploring data-level parallelism.

We evaluated the impact of using the vector instructions compared to the scalar ones in order to measure the processing acceleration. The results showed that, with the vector extension, it is possible to read and write elements from the data memory and process them four times faster.

Therefore, in future works, we intend to increase the supported vector instruction set by adding multiplication instructions. With this, it will be possible to expand the benchmark algorithms algorithm and evaluate convolution operations running with vector instructions. Also, we aim to support 64-bit width vectors to further accelerate applications.

Acknowledgments

The authors would like to thank the funding from the Foundation for Support of Research and Innovation, Santa Catarina (FAPESC-2021TR001907), Conselho Nacional de Desenvolvimento Científico e Tecnologico (CNPq) Process 140368/2021-3, and from the Region d'Occitanie and the École Doctorale I2S from the University of Montpellier (contract no. 20007368/ALDOCT-000932). The authors also thank for the support of the University Space Center of Montpellier, France.

References

[1] M. Yang, G. Hua, Y. Feng, J. Gong, Fault-tolerance techniques for spacecraft control computers, John Wiley & Sons, Singapore, 2017.
[2] D. A. Santos, L. M. Luza, C. A. Zeferino, L. Dilillo, D. R. Melo, A low-cost fault-tolerant RISC-V processor for space systems, in: 2020 15th Design Technology of Integrated Systems in Nanoscale Era (DTIS), Marrakesh, pp. 1–5.
[3] S. D. Mascio, A. Menicucci, E. Gill, G. Furano, C. Monteleone, On-board decision making in space with deep neural networks and RISC-V vector processors, Journal of Aerospace Information Systems 18 (2021) 553–570.
[4] S. D. Mascio, A. Menicucci, E. Gill, G. Furano, C. Monteleone, Leveraging the openness and modularity of RISC-V in space, Journal of Aerospace Information Systems 16 (2019) 454–472.
[5] J. L. Hennessy, D. A. Patterson, Computer Architecture: A Quantitative Approach, ISSN, Elsevier Science, Amsterdam, 2011.
[6] D. Selva, D. Krejci, A survey and assessment of the capabilities of cubesats for earth observation, Acta Astronautica 74 (2012) 50–68.
[7] I. A. Assir, M. E. Iskandarani, H. R. A. Sandid, M. A. Saghir, Arrow: A RISC-V vector accelerator for machine learning inference, arXiv preprint arXiv:2107.07169 (2021).
[8] M. Johns, T. J. Kazmierski, A minimal RISC-V vector processor for embedded systems, in: 2020 Forum for Specification and Design Languages (FDL), IEEE, Kiel, pp. 1–4.
[9] M. Cavalcante, F. Schuiki, F. Zaruba, M. Schaffner, L. Benini, Ara: A 1-ghz+ scalable and energy-efficient RISC-V vector processor with multiprecision floating-point support in 22-nm fd-soi, IEEE Transactions on Very Large Scale Integration (VLSI) Systems 28 (2019) 530–543.
[10] D. Patterson, A. Waterman, The RISC-V Reader: an open architecture Atlas, Strawberry Canyon, San Francisco, 2017.
[11] J. Gebis, D. Patterson, Embracing and extending 20th-century instruction set architectures, Computer 40 (2007) 68–75.
[12] A. Waterman, Y. Lee, D. Patterson, K. Asanovic, The RISC-V instruction set manual, Volume I: User-Level ISA', version 2 (2014).
[13] D. Kanter, RISC-V offers simple, modular ISA, Microprocessor Report (2016).
[14] RISC-V Organization, RISC-V "V" Vector Extension, `https://github.com/riscv/riscv-v-spec`, 2022. [Online; accessed 22 May 2022].

IMPROVING SPACE ROBUSTNESS AND RELIABILITY ON NANOSATELLITE ON-BOARD EQUIPMENT

Lincoln Teixera(1), Bruno Carneiro Junqueira(2), Valentino Lau(3), Denio Lemos Panissi(4), Rafael Lopes Costa(5), Gledson Hernandes Diniz(6), Jose Eduardo May(7), Jonilson Adachi(8), Ana Paula De Sa Santos Rabello(9), Durval Zandonadi Júnior(10), Antonio Carlos de Oliveira Pereira Junior(11), Walter Abrahao dos Santos(12), Marcus Vinicius Cisotto(13), Antonio Cassiano Julio Filho(14), Auro Tikami(15), Luiz Antonio dos Reis Bueno(16), Lázaro Aparecido Pires Camargo(17), Ângelo José Augusto Florentino(18), Antonio Ferreira de Brito(19) and Andrés Fernando Paredes Horna(20)

(1,2,3,4,5,6,7,8,9,10,11,12,13,14,15,16,17,18,19,20)National Institute for Space Research (INPE)
Av. dos Astronautas, 1758, Jardim da Granja, São José dos Campos, Brazil
Phone: +55 12 3208 6000, Mail: (1)lincoln.teixera, (2)bruno.junqueira, (3)valentino.lau, (4)denio.panissi, (5)rafael.costa, (6)gledson.diniz, (7)jose.may, (8)jonilson.adachi, (9)anapaula.rabello, (10)durval.zandonadi, (11)acarlos.pereira, (12)walter.abrahao, (13)marcus.cisotto, (14)cassiano.filho, (15)auro.tikami, (16)luiz.bueno, (17)lazaro.camargo, (18)angelo.florentino, (19)antonio.brito, (20)andres.horna [@inpe.br]

***Keywords**: Nanosatellites, CubeSat, Reliability, Environmental Data Collection, Space Environment.*

Small satellites allow the reduction of costs and development time, making it possible to increase access to space and encourage more frequent launches. Gradually it is being used as a resource for teaching space engineering as well as explore for the development of innovative technological and scientific solutions. In addition to universities, research and technology centers have benefited from the opportunities to improve knowledge within their projects or in partnerships. Due to nanosatellites high early mortality rates, it is necessary to constantly improve manufacturing processes in order to provide more resistance and reliability to on-board equipment. In this scenario, this work presents the experience acquired using a nanosatellite payload board for environmental data collection, named EDC for short, where good practices are introduced to the former ones in order to make it more robust to outer space. A partnership was made between the INPE´s space segment engineering located in São José dos Campos and the its Northeast regional unit in Natal, responsible for the EDC development. The EDC project was developed with the objective of expanding a prospective satellite constellation for the Brazilian Environmental Data Collection System (SBCDA) and demonstrating its feasibility on nanosatellites. Improvements to the EDC design were targeted for greater resistance to launch and life-in-orbit efforts, this included quality assurance inspections, electronic board reworks, reinforcement of the coupling between the main and daughter boards, application of resins to encapsulate and to structure components. Thermal and reliability analysis was also carried out and environmental tests performed at INPE´s Integration and Testing Laboratory (LIT) for board qualification. The payload circuitry redesign was kept out this work scope. This proposal is very much in line to the activities developed by INPE's Small Satellites Division (DIPST) for improving space mission success rate and in accordance to INPE's bylaws on fostering science and technology, human resources training and the knowledge dissemination for the benefit of Brazilian society.

1. Introduction

All satellite projects present risks, but for nanosatellites the failure rate is quite expressive, around 35% of unknown causes occur on the first day [2]. Thus, the method to increase the robustness must use several manufacturing techniques and different verification tests, to increase the probability of the flight being successful.

This article discusses a combination of methods to increase the robustness of Printed Circuit Board Assembly (PCBA), with the quality necessary to withstand the rigorous space environment. PCBAs developed for nanosatellites may have characteristics similar to commercial boards and consequently not be considered suitable for the space environment. In order for them to be used, it is necessary to adopt corrective measures to reassess whether they are suitable for being embedded in nanosatellites.

The methodology adopted in this project was applied to the EDC - Environmental Data Collecting equipment, which is a payload developed for nanosatellites to collect data from platforms spread across the Brazilian territory, the PCDs (Data Collection Platform). The data collected on the ground by the Brazilian Environmental Data Collection System (SBCDA) is used for research and climate studies, are also used by other users, who have access to data such as wind speed, solar radiation, rainfall, etc.

Preparing a PCBA for the space environment involves manufacturing issues through to environmental qualification tests. This article will not address design aspects, despite being considered extremely relevant in the space environment.

The work in [1] describes the thermal verification testing of commercial Printed-Circuit Boards for Spaceflight" exemplifies verification methods, which allow early failure detection and also verify final assembly and integration.

In order to carry out the tests, [2] describes how the test sequence was defined and also how it is possible to carry out a thermal screening of components and evaluate possible failures in the process, materials, design and workmanship.

This article presents a method for improving robustness, which was first used in EDC equipment, to qualify boards with characteristics similar to a commercial spaceflight circuit board. It is important to note that the addition of restraints and restraints was necessary for the vibration environment. Additionally, how important it is to investigate the temperatures of components operating in an environment with no convection. Verification is successful when all final components and assemblies complete the test without failure. It should be noted that at this stage the effects of radiation were not evaluated. The EDC equipment has no flight heritage, but qualification-level testing demonstrates that it will be able to withstand the launch and orbit environment.

2. Background

Although nanosatellites have certain particularities, which differentiate them from other classes of satellites, it is important to prove by various methods that the nanosatellite is fit for flight. And fitness for flight is achieved through the adoption of good engineering practices, tests and verifications at different levels of the nanosatellite. Good practices include manufacturing and analysis techniques such as EEE, FMEA, Outgassing, Radiation Resistance, Derating, Reliability in order to manage lifetime related issues.

Therefore, the success and safety of the flight depends a lot on the work of nanosatellite developers [2]. The safety aspect, for example, may involve failure issues, which can also damage the launch vehicle or a main payload or other nanosatellites.

These assumptions must be considered during the different phases of the project, such as conception, detailed design, qualification and acceptance through exhaustive functional tests, environmental tests and during the launch campaign.

The project must define the requirements for the development and qualification of equipment intended for flight, aiming at obtaining equipment, subsystems and systems, capable of functioning without failure in space, which is a hostile environment.

As the rocket also imposes restrictions [3] for launching the nanosatellite, it is also necessary to test and verify the launcher requirements such as: Mass Property Measurement, Vibration Test, Bakeout Procedure and Thermo-Vacuum Test.

Tests and verifications are essential to verify that the requirements are met. If incidents occur, the nature of the problems and the efficiency of corrective actions must also be evaluated. The objective is to increase the chances of success and improve future projects.

3. Quality Assurance

Equipment for nanosatellites tends to use COTS - Commercial off-the-shelf components with flight heritage [4], but from a manufacturing point of view it is important that the assembly and welding processes produce adequate joints, avoiding developing failures, which lead to early mortality. Therefore, it is important to adopt the best manufacturing and quality assurance practices. The IPC J-STD-001F [5] standard presents recommendations on the assembly and soldering of the components, most used by the electronics industry. The major suppliers of equipment for satellites use this standard.

The quality assurance inspection was conducted in order to verify the adherence of the mounting process with the standard requirements IPC J-STD-001F for class 3 [5]. It was identified several non-conformances which includes flux residues, solder excess, disturbed solder, poor wetting, cracks, pinholes, voids, exposed copper, solder balls/splashes, indicating fragility of the final product. These nonconformities pointed out served as guidance for the rework carried out.

3.1. Welding Rework

The batch of EDC units evaluated was manufactured without having to meet the requirements of the IPC standard [5], however the standard was used as a reference for inspections that evaluated the quality of welded joints.

It was decided to rework the joints, with the aim of correcting the problems detected. Table 1 presents some examples of electronic rework performed.

Table 1: Examples of rework performed on the EDC electronic board.

Before rework	After rework	Comments
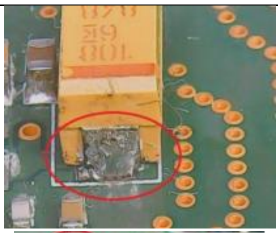		Weld with an irregular and inadequate fill. With the rework, the weld was well distributed, without excess, shiny and without major retractions.
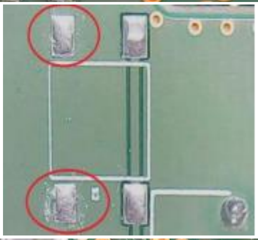	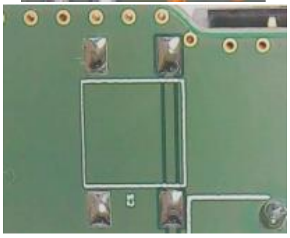	Weld with residue around the pad, grainy and opaque appearance. With the rework, the residues were removed and the weld was shiny and regular.
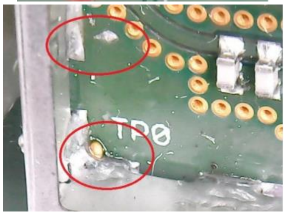	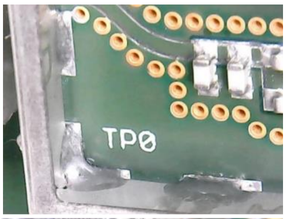	Excess solder between Shield and PCBA, fill gaps and solder spatter and other particulates. With the rework the solder was corrected and the PCBA cleaned.
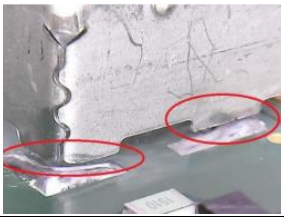	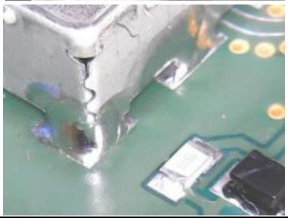	Contact interface between Shield feet and PCBA pads did not properly form a meniscus between the two parts. With the rework, this union was corrected.

Additionally, the EDC unit was rigorous cleaned with isopropyl alcohol and dried.

3.2. Mechanical Mounting

The electronic components shall withstand vibration during launch and thermal vacuum cycling in space environment. An efficient mounting of the electronic components in a PCBA reduces the mechanical efforts in the connections and improves durability. The mounting can be improved with fixtures made of epoxy resin.

The larger and heavier electronic components, which are more susceptible to damage, were selected to apply epoxy resin fixtures. Figure 1 shows some examples of these fix-tures. The EDC has a mezzanine board (daughter board). In addition to the M2.5 bolt with nut and spacer, normally used to join the daughter board, two blocks made of epoxy resin were installed to increase the points of fixture.

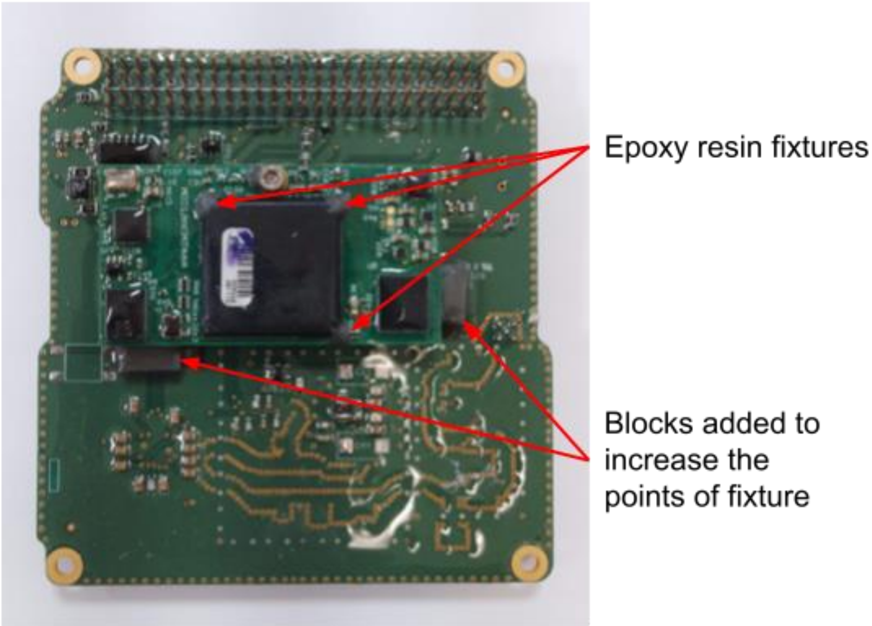

Figure 1: Improvements of electronic component fixture.

3.3. Conformal Coating

Conformal coating, a thin layer of resin applied normally with a painter spray gun, is commonly used in the industry to protect electronic components of harmful agents such as dust and moisture, and to avoid corrosion. Due to the cleanness constraints of the vacuum chamber, it was adopted a qualified resin for use in space.

Figure 2 shows the EDC board before and after applying conformal coating. The conductive parts, such as connectors and shield contacts, shall be protected with masks.

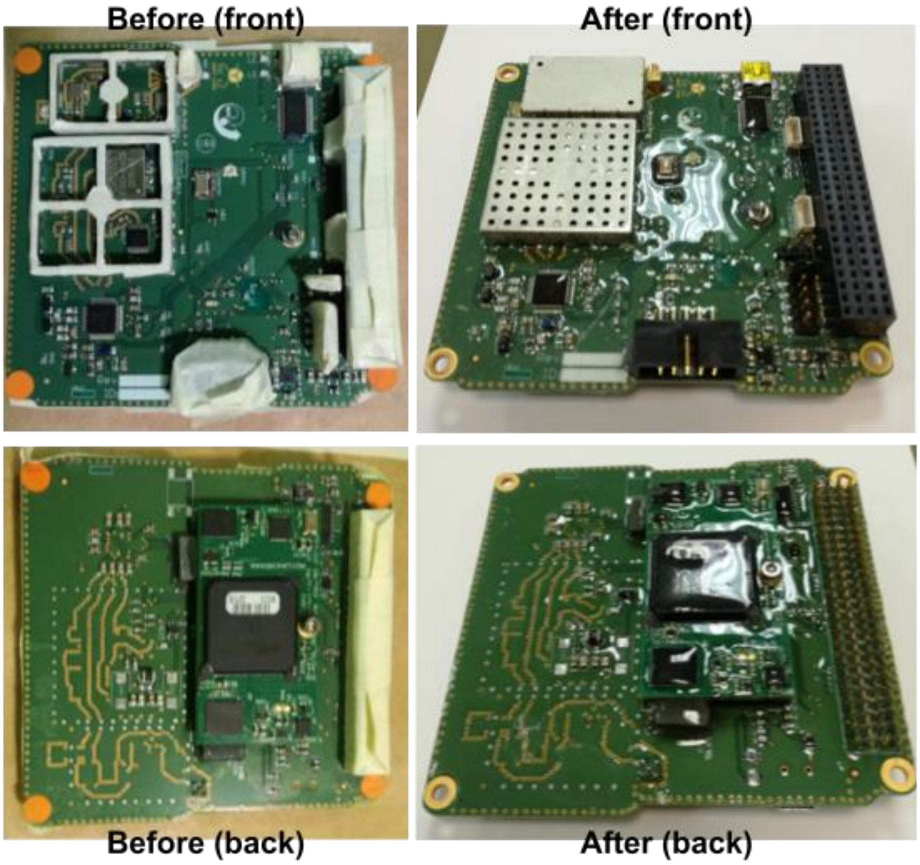

Figure 2: EDC board before and after applying conformal coating.

4. Thermal Characterization

A preliminary thermal investigation was carried out to estimate the operating temperature limits of the EDC Engineering Model PCBA. Such investigation was based on thermographic images obtained in bench tests and mathematical simulations with operating mode thermal load. This partial characterization was necessary since such limits were not specified by the PCBA developer. The results found were used to help defining the temperature limits thermal vacuum tests, preventing the PCBA from being exposed to thermal conditions beyond the limit tolerated by its components.

Figure 3 shows thermographic images of the PCBA, with dissipation in steady state operational mode and laboratory convection thermal conditions.

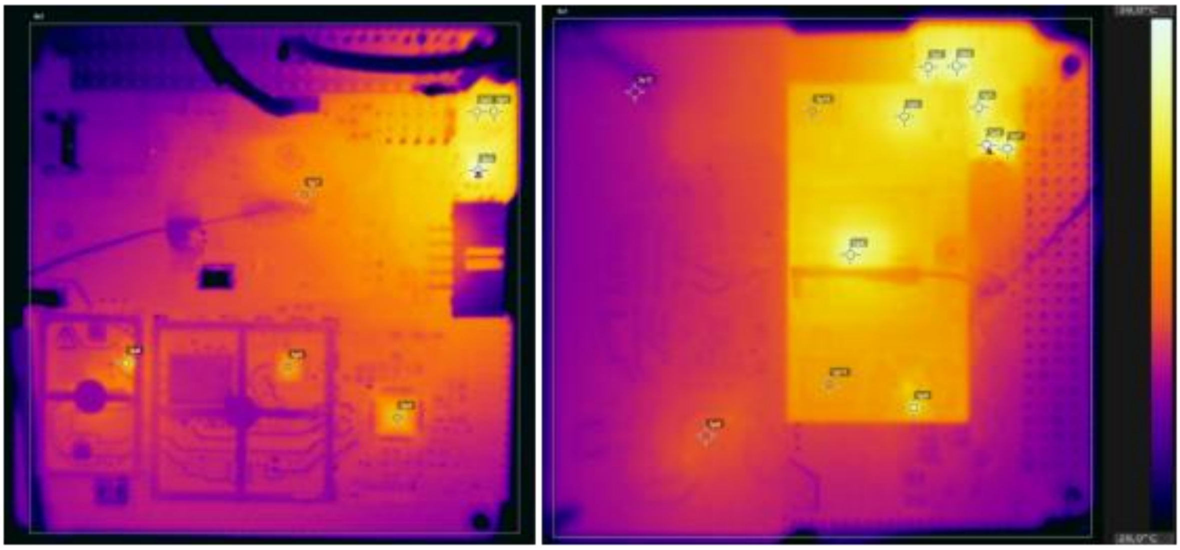

Figure 3: Thermographic image of the PCBA (front and back side).

5. Reliability Analysis

A part count reliability analysis was performed based on MIL-HDBK-217F [6], there are criticisms for being outdated, but it is still widely used [7][8], including INPE, which used the standard in its former projects, and maintains its use as a history and reference for current projects, in order to be able to compare the results between similar projects.

Due to the lack of detailed information at the time of elaboration of this reliability analysis, it was decided to use the method of counting parts, although it is known that this method is used in the initial phase of the project. However, the results obtained add significant information for the analysis of the reliability of the EDC board.

Through this analysis, it was identified that due to the characteristics of the board having relatively few components (378 in total) and being mostly passive components, the equipment failure rate resulted in a low value for a board composed of COTS components, resulting in a high MTTF (Mean Time To Failure), approximately 4 years old. Considering that the standard provides conservative results, we can conclude that despite this fact, the analysis results are satisfactory, as they meet the mission time requirement of 2 years.

6. Environmental Tests

The environmental tests simulate the critical environmental conditions the equipment will be exposed during the mission. During these tests, the equipment is tested from a functional point of view, making it possible to detect failures early and identify problems in final assembly and integration. For the EDC PCBA, vibration and thermal tests were performed.

6.1. Vibration Tests

The EDC board was vibrated as an isolated equipment, not installed to a nanosatellite. The MGSE used to fix the EDC board to the shaker is shown in Figure 4.

Figure 4: EDC Mechanical Vibration Test.

The qualification level established in GSFC-STD-7000B [9] for random vibration was adopted in the vibration test. For each direction was applied an overall of 14,1 GRMS. After the vibration test, functional tests and visual inspection were performed. No damages were detected, indicating that the mechanical mounting procedure was efficient.

6.2. Environmental Thermal Tests

After the vibration test, thermal environmental tests were performed on the EDC PCBA Engineering Model (808681) to prove the unit can minimally withstand the thermal conditions of Space. This unit was tested at the qualification level, considering the temperature limits of critical components, estimated during the pre-test of the characterization of the board. The applied test requirements provide confidence the unit can have a certain level of tolerance in relation to the space thermal environment, based on small satellites typical boundary conditions. These requirements do not include an proper margin to the maximum predicted environmental stress in Space, which depends on each satellite. Considering this equipment as an electronic unit, the test sequence applied was as follows:

1. Thermal cycling “Endurance” test;
2. Functional test;
3. Cold and hot start test;
4. Thermal vacuum test;
5. Bakeout test (although this test is recommended for system level only, it was performed here for convenience, in order to pre-check the contamination rate generated by the unit).

With the objective of optimizing resources and time, tests 2, 3, 4, and 5 were carried out in a combined way in the thermal vacuum chamber. Figure 5 shows a picture of the PCBA inside the climate chamber. The test setup in the thermal vacuum chamber can be seen in Figure 6.

Figure 5: EDC in the Climatic Chamber for the thermal cycling test.

Figure 6: EDC installed inside the thermal vacuum chamber (left). On the right, functional test setup used during the thermal vacuum test.

7. Conclusions

In order to achieve a suitable lifetime in space, satellites need to comply to a minimum list of items on Qualification and Acceptance (Q&A) testing. This work described some procedures that may help ensuring the equipment robusteness in the designs so it may meet the performance expectations required for a specific mission – from assembly and transport to launch and operation.

Manufacturing care prepares the product for the space environment. The fact that the EDC had no flight history motivated it to approach all activities with additional attention.

The screening tests performed before the vibration tests help to discover flaws at the beginning of the hardware development and allow a very assertive analysis about the product to be tested. This approach saves time in the later phases of a project. Infrared thermography of circuit boards is important to identify hot spots on boards. As most vibration test failures are not fully detectable, only thermal cycling can assess the success of the assembly and mission. The association of methods to increase PCBA robustness is considered a good practice, as it improves the ability of this PCBA not to fail under certain conditions.

This method was used in EDC to increase robustness and was designed to meet expected reliability requirements. It has proven to be a successful method to prepare products with commercial plate characteristics and increase their reliability.

Acknowledgments
We thank INPE (National Institute for Space Research), DIPST (Division of Small Satellites), DIECC (Division of Space Mechanics and Control), DISEP (Division of Space Systems), COMIT (Manufacturing, Assembly, Integration and Testing Coordination), COENE (Space Coordination of the Northeast), Technical Collaborators Carlos Alberto Bezerra Monteiro and Renata Rapuano Fernandes as well as to EDC developers Dr. José Marcelo Lima Duarte and Rafael Medeiros Araújo.

References

[1] NASA Technical Memorandum 105261, “Thermal verification testing of commercial printed-circuit boards for spaceflight”, William M. Foster II, National Aeronautics and Space Administration Lewis Research Center Cleveland, Ohio 44135.
[2] Langer, Martin and Bouwmeester, Jasper, Reliability of CubeSats – Statistical Data, Developers’ Beliefs and the Way Forward, 30th Annual AIAA/USU Conference on Small Satellites.
[3] Cal Poly- CubeSat Design Specification, Rev 14.1, San Luis Obispo, CA, 2022.
[4] TEC-SY.78.2016.REV.RW (2016) Review Objectives for ESA In-Orbit Demonstration (IOD) CubeSat Projects
[5] IPC - J-STD-001F Requirements for Soldered Electrical and Electrical Assemblies. July 2014.
[6] MILITARY HANDBOOK: RELIABILITY PREDICTION OF ELECTRONIC EQUIPMENT (MIL-HDBK-217F) (02-DEC-1991).
[7] J. W. Harms, "Revision of MIL-HDBK-217, Reliability Prediction of Electronic Equipment," 2010 Proceedings - Annual Reliability and Maintainability Symposium (RAMS), 2010, pp. 1-3, doi: 10.1109/RAMS.2010.5448046.
[8] G.P. Pandian, D. Das, C. Li, E. Zio, M. Pecht. A critique of reliability prediction techniques for avionics applications. Chinese J. Aeronaut., 31 (2018), pp. 10-20, 10.1016/j.cja.2017.11.004.
[9] GSFC-STD-7000B NASA General Environmental Verification Standard, 04/28/2021.

AN SRAM MEMORY'S ERROR DETECTOR AND CORRECTOR SYSTEM BASED ON FPGA FOR CUBESATS ONBOARD COMPUTER

Luis C. O. Silva(1), **Jose R. B. P. Junior**(2), **Carlos A. R B. Junior**(3), **Allan K. Barros**(4), **Edeilson P. Pestana**(5), **Geovaana M. M. C. Magalhaes**(7), **Lucas S. Azulay**1

(1)Federal University of Maranhão, Av. dos Portugueses, 1966 - Vila Bacanga, São Luís - MA, 65080-805, Brazil, claudio.luis@ufma.br

(2)Federal University of Maranhão, Av. dos Portugueses, 1966 - Vila Bacanga, São Luís - MA, 65080-805, Brazil, jrbp.junior@ufma.br

(3)Federal University of Maranhão, Av. dos Portugueses, 1966 - Vila Bacanga, São Luís - MA, 65080-805, Brazil, ecarlos.brito@ufma.br

(4)Federal University of Maranhão, Av. dos Portugueses, 1966 - Vila Bacanga, São Luís - MA, 65080-805, Brazil, allan.kardec@ufma.br

(5)Federal University of Maranhão, Av. dos Portugueses, 1966 - Vila Bacanga, São Luís - MA, 65080-805, Brazil, edeilsonpestana@gmail.com

(6)Federal University of Maranhão, Av. dos Portugueses, 1966 - Vila Bacanga, São Luís - MA, 65080-805, Brazil, moura.geovaana@discente.ufma.br

(7)Federal University of Maranhão, Av. dos Portugueses, 1966 - Vila Bacanga, São Luís - MA, 65080-805, Brazil, lucas.azulay@discente.ufma.br

Keywords: *CubeSat, Hamming code, VHDL, FPGA.*

The applications involving nanosats are in constant evolution and the demand for electronics components with appropriate reliability for use in hostile space environments is growing. This creates a need for greater systems designed to detect and correct errors in satellite memory elements. In this work, a method of detection and correction errors in memory for Cubesats onboard computers is proposed. The method presents and performs the Hamming code together with the parity bit method implemented in FPGA to perform the detection and correction of errors that occurred in SRAM memory. The method presented can identify and correct errors caused by single events upsets (SEUs) and double events upsets(DEUs). The algorithm was implemented in VHDL and tested from an onboard computer prototype. Comparison tests between classical Hamming code method and Hamming code together with parity bit were performed to validate the results.

1. Introduction

The environmental conditions to which an electronic component is subjected can influence its behavior and that of the entire system and other equipment. The space environment is flooded with radiation consisting of high-energy particles from the Sun, proton belts, electrons, and ions collected from the Earth's magnetic field, as well as galactic cosmic rays (GCR) arriving from beyond the Solar System. Radiation has always been a major problem for satellites and can have effects on satellite operation that can range from being unimportant to a catastrophic failure of a vital subsystem, such as the onboard computer (OBC) [1].

Most of the data corruption occurs during the satellite's passage through a region called the South Atlantic Anomaly (SAA). The South Atlantic Anomaly is a region where the earth's magnetic field has a lower intensity and, as is well known, the earth's magnetic field acts as a shield against radiation from solar winds.

The miniaturization of integrated circuits makes them even more susceptible to external interference, such as electromagnetic interference and ionizing radiation [2]. The incidence of ionizing radiation can cause a disturbance classified as SEE (Single Event Effects). Which is a phenomenon caused by the action of a single particle passing through the integrated circuit [3].

In Low Earth Orbits (LEO), it is known that one of the adverse effects of space radiation on space artifacts is a transient error known as Single Event Upset (SEU). Bit state changes (*bit-flips*) caused by SEU are a known problem in memory chips. The application of techniques using Error Detection and Correction codes (EDAC) has been an efficient solution to this problem [4].

One of the most efficient algorithms for error detection and correction is the Hamming code which was introduced by Richard Hamming in 1950. This algorithm is widely used and is capable of performing simple error detection and correction (SECSED - Single Error Correction, Single Error Detection), that is, when there is only one incorrect bit in the information, it is possible to adapt the code to be able to perform double error detection, but without changing its capacity of simple correction (SECDED - Single Error Correction Double Error Detection). [5] [6] [7].

This work aims to propose a system for error detection and correction in SRAM type of memory to be used in a CubeSat onboard computer. For this, a system will be implemented in FPGA based on the Hamming code method in conjunction with the parity method.

This paper is organized as follows: besides the introduction, this paper brings, in section II, a review of the works in the literature associated with this problem. The description of the proposed method and the FPGA implementation of the prototype for the experiments is presented in section III. In section IV, the results of the simulations and experiments performed with the developed prototype are presented. And finally, section V brings the conclusions and future work.

2. Related Works

Dug and Krstic [8], presented and implemented two methods for error detection and correction in FPGAs (Field Programmable Gate Array). The methods evaluated were: error detection and partial error correction (EDPEC) and full error detection and correction (FEDC).

Hillier and Balyan [9] evaluated three variations of Hamming's code for the application in error detection and correction in nano-satellite systems. The most efficient version of the code was Hamming[16, 11, 4]. This scheme guarantees single error correction and double error detection (SECDED), capable of protecting 11 bits against SEU in addition to performing DED (Double Error Detection).

Goerl *et al* [2] presented in their work an approach for error detection and correction (EDAC), caused by SEU due to the incidence of ionizing radiation or electromagnetic interference (EMI) in memory devices, called parity per byte and duplication PBD (Parity per Byte and Duplication), for protecting data stored in memory. The technique has been described in VHDL in conjunction with the LEON3 processor and an FPGA.

Ciani and Catelani [10] presented a fault-tolerant architecture for avoiding SEU-type errors in devices that use COTS components and are exposed to extreme environments. They focused on fault tolerance techniques in FPGA-based avionics devices in the presence of radiation disturbances induced by ionizing particle incidence.

Fauzi *et al* [11] presented a methodology for bit error detection and correction using the Hamming code algorithm. They observed that the Hamming code can correct only the SEU type of error (error in a single bit) if there is more than one bit changed in the information the classical Hamming code cannot identify the position of the incorrect bits.

Jung and Choi [12] presented an on-board processor system adopting Triple Modular Redundancy (TMR) with the concept of mitigation windows and external debugger, and also suggested a mathematical model that predicts the failure rate of the onboard processor system using only the information from the system configuration resources.

Marcelino *et al* have developed a payload for the FloripaSat-1 CubeSat, putting it into orbit in 2019 via the Chinese Long March 4A vehicle from the Taiyuan Launch Center in China. The payload is designed to be an on-orbit validation platform for a radiation tolerant FPGA, and a communication protocol called the Space Link Extension (SLE) protocol.

Benevenuti *et al* [7] developed a payload for the CubeSat NanosatC-BR2, which was put into orbit in 2021 from the Baikonour Cosmodrome, Kazakhstan, via the Soyuz 2.1a/Fregat-M launch vehicle. The payload consisted of a board named INPE-SMDH-UFRGS, containing an application based on a Xilinx Series 7 FPGA. This application, besides collecting and storing data about the occurrence of radiation particles in an SRAM inside the FPGA, performs continuously monitoring, detecting, and accounting for events of the type *bit-flips* that occurred in this memory.

3. Materials and Methods

3.1. Hamming code

The Hamming code for error detection and correction consists of adding some parity bits to the information sent The parity bits are calculated using a generator matrix that is used to shape the so-called code word . Using a parity check matrix, the scheme can detect the occurrence of an error and automatically correct the corrupted bit and thus enable the extraction of the original, error-free information. The Hamming code consists of two code blocks, the encoder, and the decoder. The encoder is the block responsible for generating the code word, that is, the union between the bits of the information to be protected and the parity bits calculated for it. The decoder, on the other hand, is the block where the information, which is the code word, is checked for errors. This checking is done through a parity check of the codeword. It is through the decoder block that it is possible to detect and correct the error that occurred. This process can be visualized in the figure 1. In this work, the evaluation of the classical method of Hamming code with 7 bits of length and containing 4 data bits, called Hamming(7,4) code, was performed to detect and correct errors caused by SEU type faults.

3.2. Hamming code + parity method

The Hamming code is widely used in systems with error detection and correction and can perform the detection and correction of simple errors, by way of explanation,

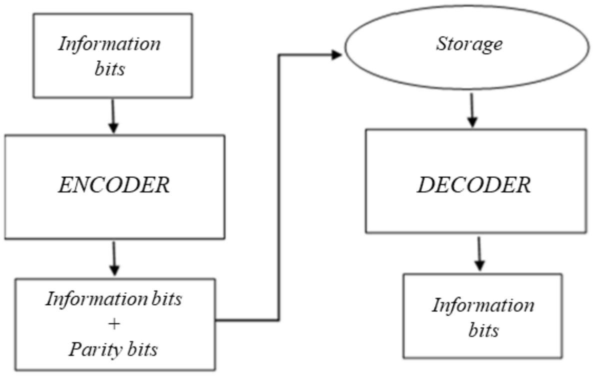

Figure 1: Information flow in Hamming's code.

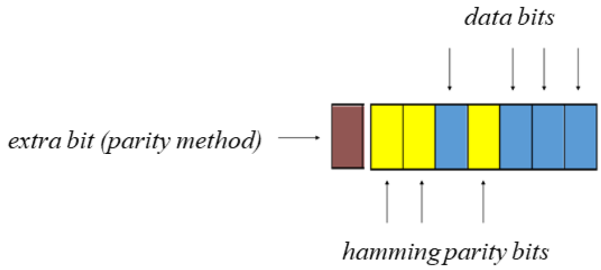

Figure 2: Organization of bits in the Hamming method + parity.

it's when there is only one incorrect bit in the information, but it is possible to adapt the code to be able to perform the detection of a double error. A way to accomplish this modification is by using the parity method in conjunction with the Hamming method. The parity method consists of the transmitter adding an extra bit to the information following the following rule: Information with odd number of bits 1, adds 1 to the word; Information with even number of bits 1, adds 0 to the word.

In the figure 2, it is possible to observe the organization of the informational bits applying the Hamming code plus a parity bit. After generating the code word it is necessary to identify the number of bits 1 in the word and subsequently add the extra bit to the information. This layout causes each column to have a unique combination of parity bits, for each bit position. This unique combination of parity bits is called the syndrome's value. Additionally, in this work, the evaluation of the Hamming(7,4) code in conjunction with the parity bit method was performed to detect and correct errors caused by failures of SEU's type.

After generating the codeword, it is necessary to identify the number of bits 1 in the word to then add the extra bit to the information. With the extra bit added to the codeword, it is necessary to evaluate 4 possible situations for the decoder result, as shown in the flowchart 3.

A From the result of the implementation in the embedded system, the decoder will be able to correct the corrupted bit and return the original information or discard the data if it is corrupted in more than one bit.

The approach here proposed aims to make FPGA devices capable of detecting and repairing SEU-induced configuration faults, in internal memory banks, without resorting to external storage circuits. The intention is that the detection and correction of SEUs will be accomplished through an SRAM memory integrity check implemented on the FPGA chip itself, using, for this purpose, an Error Detection and Correction Circuit

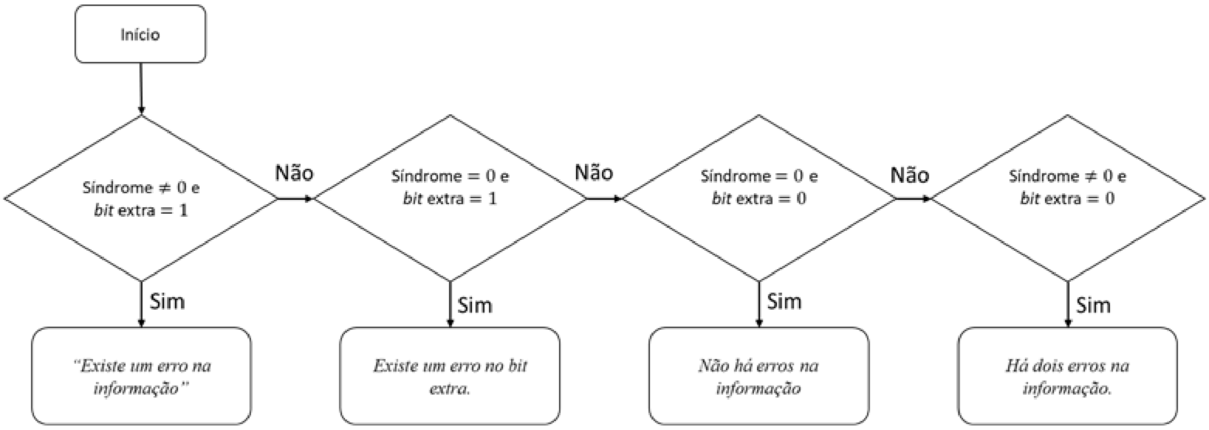

Figure 3: Decision flow of the correction code in the Hamming + parity method.

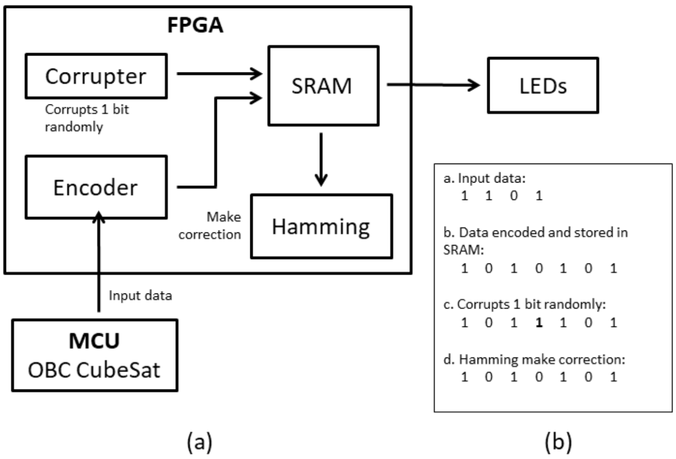

Figure 4: Basic operation of the proposed method.

(EDAC) [13] [14].

In the figure 4, the basic operation of the proposed method is presented. In the figure 4(a) It can be observed the basic building blocks of the system. The main blocks consist of a microcontroller (MCU) and an FPGA. The MCU will assume the role of the CubeSat's OBC, while the FPGA will be responsible for storing the data in an SRAM memory, besides accomodate the circuit for encoding the data sent from the MCU, along with the circuit for detecting and correcting simple errors and the circuit for corrupting the data stored in SRAM. The bit corrupting circuit will act by changing bits randomly. The content of the SRAM memory currently accessed by the MCU is displayed on the LED array so that the correction process can be verified using the Hamming code. In the figure 4(b)it is possible to see how the method works in a summarized way and through an example. After the input data is supplied from the MCU, it is encoded and stored in SRAM; then an SEU is simulated by changing one bit randomly; the circuit with the implementation of the Hamming code will act, correcting the stored bits and returning to the original information.

The error detection and correction method was developed and simulated using Altera Quartus II Web Edition software and MATLAB R2021b. The encoding and correction functions were converted to VHDL using MATLAB's HDL Coder ToolBox. Furthermore, Fixed-point data inputs were used and the exported VHDL files were

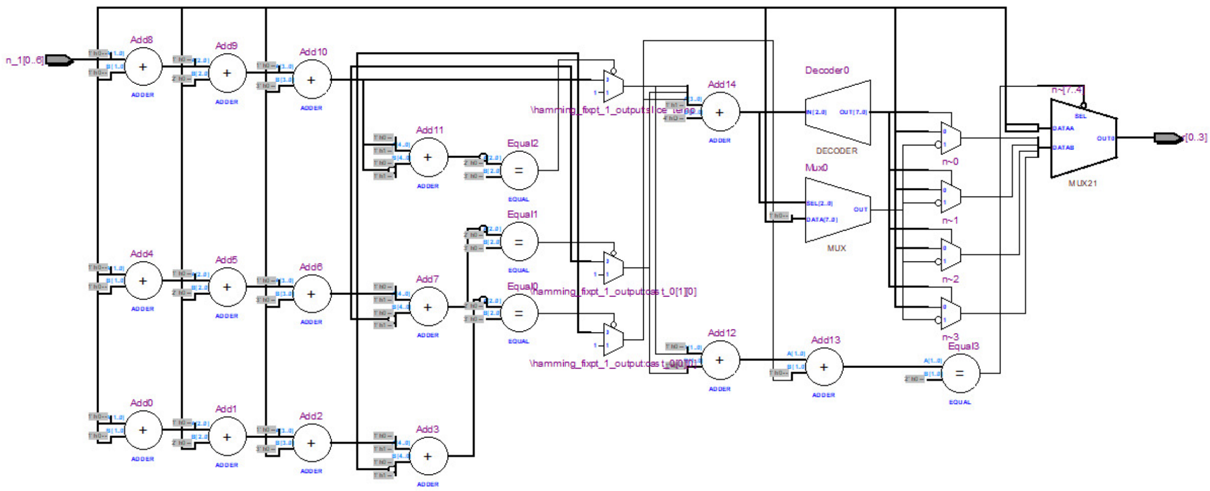

Figure 5: RTL of the correction circuit using the Hamming method.

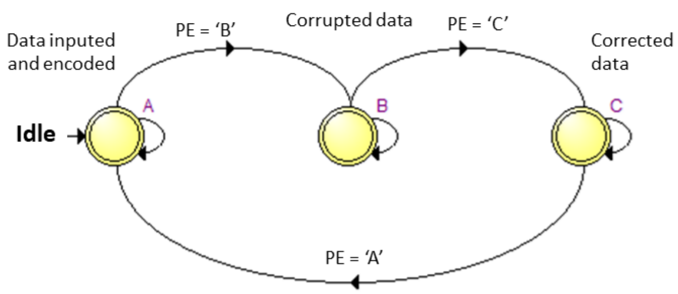

Figure 6: State machine implemented for testing.

incorporated into the design of the experiments in Altera Quartus II.

Using the RTL viewer of Altera Quartus II, it is possible to generate the RTL view of the circuit generated from the design created. It can be observed in figure 5, the RTL of the correction circuit through the Hamming code generated from MATLAB. It is possible to see in the RTL of the circuit the adding, comparing, multiplexing, and encoding components that were used in the VHDL code generation process through MATLAB. It can be seen that code generation tools have reached a level of maturity to the point of accelerating the development process of FPGA applications applied to space-based embedded systems.

A bench test was created to simulate the data input and storage of some values in SRAM memory, and the encoding, and correction of randomly generated SEU events. After compiling the digital synchronous circuit design (Register Transfer Level, RTL), an SEU was simulated on the stored input value. You can see in figure 6, the state machine implemented in VHDL, for performing the test. The system starts in the idle state (state A), in which no information is entered into memory. After data is entered and encoded, the state machine advances to the next state (state B), where corruption of one bit in the stored data occurs. Then the state machine proceeds to the last state (state C), where the circuit responsible for correcting the generated SEUs is executed to correct the errors caused. The state machine is then restarted to begin the process again.

For the physically implemented experiments, the Altera Cyclone II EP2C5T144C8 FPGA components, available on a Cyclone II EP2C5 Mini Dev Board, and the STM32

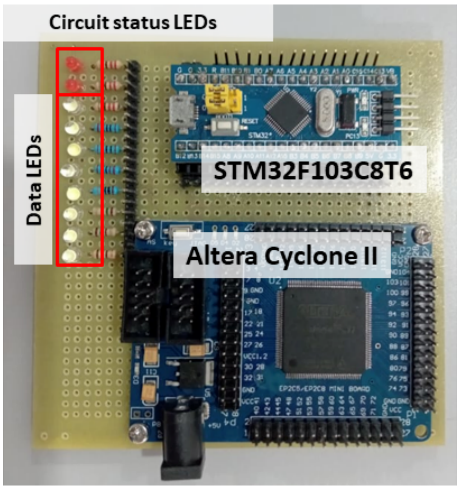

Figure 7: Integrated circuit board developed for the experiments.

microcontroller unit (MCU), model STMF103C8T6, from STMicroelectronics were used. Both the FPGA and the MCU were embedded in a universal printed circuit board, where LEDs were also attached to display system data and the circuit states stored in the FPGA. In the figure 7 it is possible to see the board developed for the experiments. It was chosen in this experimental prototype to make a universal board due to its low cost and fast development. However, the idea is to develop a standard PC/104 printed circuit board, so that it can be installed in a CubeSat.

After making the board, the FPGA pins that would be connected to the MCU, along with the pins that would be connected to the status LEDs and the data LEDs were defined. The pins connected to the MCU were used for addressing the SRAM memory on the FPGA, performing data input to the memory, performing data output after the bit correction using Hamming code, sending a clock signal, and an input signal (enable), sending a reset signal. In total, 15 MCU pins were used. The MCU pins connected to the FPGA data output had internal PULL-UP resistors enabled, preventing floating values on the pins from causing MCU to read errors. The MCU was programmed using the ST Link V2 programmer and the firmware coding was done using the Arduino IDE. The debugging of the system was done using a USB-Serial converter module connected to the USB port of a personal computer.

4. Results

Two experiments were performed to evaluate the accuracy of the proposed method and its implementation. In the first experiment, the ability to identify and correct SEU errors using only the Hamming code was evaluated. In the second experiment, the ability to identify, correct, and discard data containing SEU errors using the Hamming code in conjunction with the parity bit was evaluated. For both experiments, the same developed board was used, connected to a personal computer (PC) via the serial/USB conversion interface. A program was developed in MATLAB capable of encoding, simulating YOUR events, identifying, correcting, and discarding data using the two proposed methods.

In Figure 8 It's possible to observe the screenshot of the simulation signal diagram, run from the Simulation Waveform Editor, available in Altera Quartus II. This screenshot was obtained from one of the runned simulations for the method that identifies and

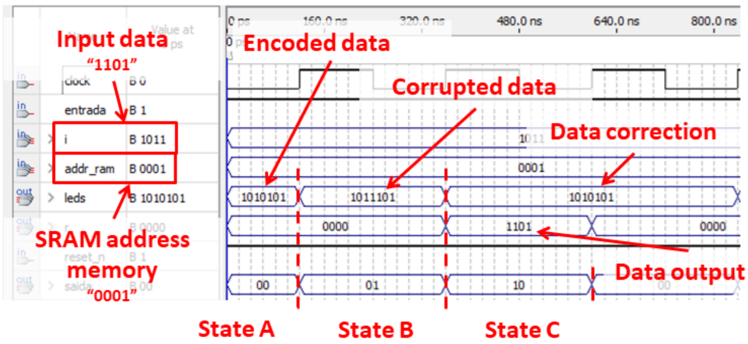

Figure 8: Signal diagram of the simulation of one of the tests performed.

corrects errors using only Hamming coding. In the screenshot, it's possible to identify the input data and the SRAM memory address of the data, inside the FPGA. In addition, you can see the encoded data, the corrupted data using SEU, the corrected data, and the output of the data after the correction process and memory read. The position of the bit that contains the error was informed as a parameter, from the microcontroller, in a random way. At the bottom of the figure, it's visible the transitions of the states, indicating the moment in which each operation of the state machine takes place

In the second experiment, in addition to the data reported in the first experiment, two bit position values containing error as a parameter were reported from the microcontroller. In this way, the system's ability to identify SEU type errors and parity errors was tested. All the tests performed were compared with the programs developed in MATLAB for checking. The AccessPort computer program was used to access the output of the experiment results through the serial/USB converter module. In the figure 9 it is possible to observe one of the several tests performed. In figure 9(a) the initial configuration of the state machine is shown, with the display of the data encoded and stored in RAM, displayed from the data LEDs. This data is supplied by the microcontroller to the FPGA and is also sent to the PC using the serial/USB converter module. In this way, the processing performed on the FPGA can be checked from the board's LEDs and also on the PC from the AccessPort program. In figure 9(b) it's possible to observe the result of processing the correction method using Hamming code combined with parity error checking.

The corrected data, the information about the existence of a syndrome error, and the existence of a parity error are perceptible. This information is passed on to the microcontroller, which can then decide whether the data can be read correctly or discarded, in the case of a syndrome and parity error simultaneously.

In figure 10(a) it is possible to observe the output sent by the microcontroller to the PC through the serial/USB converter module, on the screen of the AccessPort program. In figure 10(b) you can see the result of one of the simulations performed in MATLAB. It's perceptible in both figures that the results are equivalent, i.e., the results simulated on the PC are the same as those executed in the FPGA with the data provided by the microcontroller.

The fault detection capability of the technique was analyzed through two test batteries, one for each experiment. In each of the batteries, data was stored in the SRAM memory of the FPGA and random positions of bits that should be swapped were defined, that is, a fault injection in the data bits. In the first experiment, 100 fault injection procedures were executed, with a randomly defined position, on each of the 4 informa-

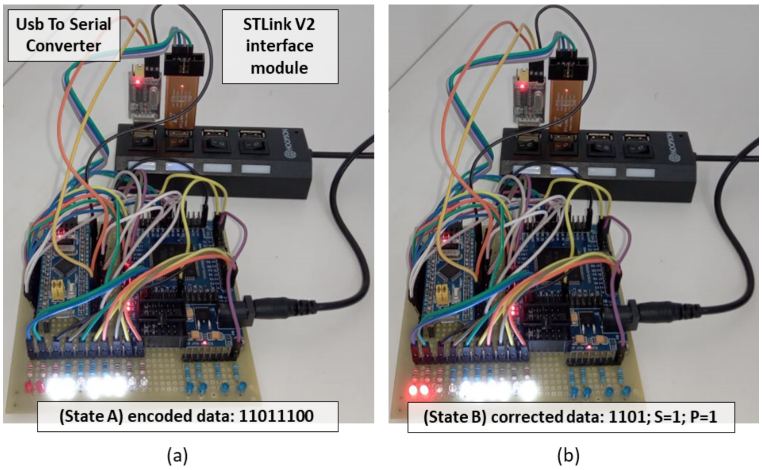

Figure 9: Result of one of the experiments performed on the LEDs on the integrated circuit board.

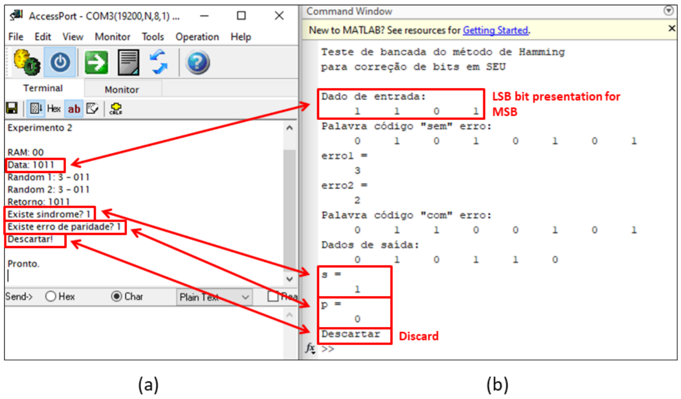

Figure 10: Output of the results sent from the microcontroller to the PC via a serial/USB converter module.

tion bits, also random. In the second experiment, 200 fault injection procedures were run with two randomly defined positions in each of the 4 information bits, also random. The results of the simulations were then compared with the simulations performed in MATLAB.

5. Conclusion

In this work, we proposed the implementation of a method for detecting and correcting errors caused by SEU events, besides being able to detect DEU events. In this way, it is possible to develop nano-satellites using off-the-shelf components and still be able to guarantee the reliability of the information collected through the use of the proposed EDAC technique. The main gain of the method developed here is in the fact that most algorithms used in the industry for the same purpose are able to detect and correct the presence of SEU events, while DEU events go unnoticed by the detection system, which results in the use of corrupted information by the nano-satellite.

Through the tests carried out, it's believed that the modeling technique and implementation of the proposed methods have made it possible to estimate and compare the efficiency of both hardware and software with regard to fault tolerance techniques in CubeSat SRAM memories.

As proposals for future works, we intend to modify the circuit synthesized in FPGA to cyclically perform constant checks and corrections in all addresses of the RAM memory available in the system. The idea is to develop an autonomous system that signalizes to the onboard computer the memory regions that are being manipulated in order to avoid access conflicts between the FPGA and the microcontroller.

Acknowledgments

The autors thanks Brazilian Space Agency (AEB) and Alcântara Launch Center (CLA) for providing financial and logistic support that contributed to development of this work.

References

[1] D. Cahyono, A. Nugroho, I. Hidayat, Design and realization on board data handling for remote sensing payload of nanosatellite fpga base, 19th Biennial Conference of the International Telecommunications Society (ITS): ”Moving Forward with Future Technologies: Opening a Platform for All”, Bangkok, Thailand, 18th-21th November 2012, International Telecommunications Society (ITS), Calgary, 2012.

[2] R. C. Goerl, An efficient edac approach for handling multiple bit upsets in memory array.

[3] J. Benfica, B. Green, B. C. Porcher, L. B. Poehls, F. Vargas, N. H. Medina, N. Added, V. A. P. de Aguiar, E. L. A. Macchione, F. Aguirre, M. A. G. Silveira, M. Perez, M. Sofo Haro, I. Sidelnik, J. Blostein, J. Lipovetzky, E. A. Bezerra, Analysis of sram-based fpga seu sensitivity to combined emi and tid-imprinted effects, IEEE Transactions on Nuclear Science 63 (2016) 1294–1300.

[4] Y. Bentoutou, E.-H. Bensikaddour, Analysis of radiation induced effects in high-density commercial memories on-board alsat-1: The impact of extreme solar particle events, Advances in Space Research 55 (2015) 2820–2832.

[5] L.-J. Saiz-Adalid, P. Gil, J.-C. Baraza-Calvo, J.-C. Ruiz, D. Gil-Tomas, J. Gracia-Moran, Modified hamming codes to enhance short burst error detection in semiconductor memories (short paper), in: 2014 Tenth European Dependable Computing Conference, IEEE, 2014.

[6] F. Benevenuti, F. L. Kastensmidt, Comparing exhaustive and random fault injection methods for configuration memory on sram-based fpgas, in: 2019 IEEE Latin American Test Symposium (LATS), pp. 1–6.

[7] F. Benevenuti, E. Chielle, J. Tonfat, L. Tambara, F. Lima Kastensmidt, C. A. Zaffari, J. B. dos Santos Martins, O. Santos Cupertino Durão, Experimental applications on sram-based fpga for the nanosatc-br2 scientific mission, in: 2019 IEEE International Parallel and Distributed Processing Symposium Workshops (IPDPSW), pp. 140–146.

[8] M. Dug, M. Krstic, D. Jokic, Implementation and analysis of methods for error detection and correction on fpga, IFAC-PapersOnLine 51 (2018) 348–353. 15th IFAC Conference on Programmable Devices and Embedded Systems PDeS 2018.

[9] C. Hillier, V. Balyan, Error detection and correction on-board nanosatellites using hamming codes, Journal of Electrical and Computer Engineering 2019 (2019) 1–15.

[10] L. Ciani, M. Catelani, A fault tolerant architecture to avoid the effects of single event upset (SEU) in avionics applications, Measurement 54 (2014) 256–263.

[11] A. Fauzi, Nurhayati, R. Rahim, Bit error detection and correction with hamming code algorithm, International journal of scientific research in science, engineering and technology 3 (2017) 76–81.

[12] S. Jung, J. P. Choi, Predicting system failure rates of SRAM-based FPGA on-board processors in space radiation environments, Reliability Engineering & System Safety 183 (2019) 374–386.

[13] M. Lanuzza, P. Zicari, F. Frustaci, S. Perri, P. Corsonello, Exploiting self-reconfiguration capability to improve sram-based fpga robustness in space and avionics applications, ACM Trans. Reconfigurable Technol. Syst. 4 (2010).

[14] Z. Ullah, M. K. Jaiswal, Y. Chan, R. C. Cheung, Fpga implementation of sram-based ternary content addressable memory, in: 2012 IEEE 26th International Parallel and Distributed Processing Symposium Workshops PhD Forum, pp. 383–389.

6

Session 6 - Educational Systems and Missions

3rd IAA Latin American Symposium on Small Satellites

IAA-LA 2022

Blockchain Applied in the Update the Firmware of Educational Nanosatellites

José Edilson Silva Filho(1), **Igor Braga Palhano**(1), **Nicolas de Araújo Moreira**(1), **Jarbas Aryel Nunes da Silveira**(1)
(1) Federal University of Ceara, edilsonfilho@lesc.ufc.br

Keywords: *Educational Nanosatellites, University, Firmware, Blockchain, Ethereum, Hyperledger Besu*

Space has increasingly attracted the attention of governments, large industries and universities. One of the most popular strategies in recent years has been the adoption of nanosatellites to fulfill different missions, which can work alone or in constellations. Among the nanosatellite launch agents, universities appear in the spotlight with more than 600 launches until 2022. The process of updating the firmware of satellites or nanosatellites that are in orbit is always a challenge, as the device needs to be visible to ground stations to receive data packets, at an average of just 10 minutes per pass. The firmware image is shredded and shipped until all the firmware can be mounted and the system completes the update. In this process, the data packet can be corrupted, either by natural phenomena or intentionally by intruders, and a new request will have to be redone. In general, universities have low financial resources to frequently access Earth Stations, and their projects are compromised if they cannot correct a firmware defect in the orbiting nanosatellite. This work presents a proposal to decentralize the process of using ground stations to update the firmware of university nanosatellites. For this, we propose a consortium between universities and institutions to create a decentralized structure for the provision of firmware updates and, for this, we propose the use of Blockchain technology and the concept of smart contracts to govern the process and diffusion of the new firmware throughout the consortium's network of satellites. We use the Hyperledger Besu Blockchain to create an Ethereum client and allow cubesats to access the servers to make firmware update requests. In practice, the nanosatellite does not make requests only to its home stations, but to any station on the network and relies on encrypted transactions to bring security to the procedure. The result is a faster propagation speed of a firmware for each cubesat. Our proposal still involves the creation of a token called GS-BC with a value of 10 percent of ETH to govern the monetization of the service. The result shows the feasibility for universities and small and medium-sized companies to access the service without incurring huge expenses. The system also allows for rewarding institutions that have earth stations, generating a new source of income.

1. Introduction

One of the satellite construction standards that has become popular in recent years is the cubesat pattern [1], cubic-shaped nanosatellites measuring 10 x 10 x 10 cm. They are divided into units, with 1 U corresponding to the smallest unit of the standard. The format is popular because its low development and launch costs, usually uses COTS (Commercial-Off-The-Shelf) parts and is lightweight. Currently, universities represent a major part of the market share of nanosatellite builders that launched in 2022. Around 640 new nanosatellites are expected by the end of 2022, which represents an increase of almost 98 percent over the previous year. In an environment where more and more governments restrict education budgets, financial resources for university and educational projects are limited. Some universities do not have their own ground stations for tracking, telemetry and control of their cubesats and need public and private partnerships to rent or use ground stations from other entities. In this scenario, solutions to reduce costs of research and space missions can increase the participation of universities in the nanosatellites ecosystem.

Like any electronic device, cubesats run over embedded software called firmware, which may need to be updated periodically [2] [3], either because of a vulnerability that needs to be fixed or because of new functions.

Figure 1((1)) shows the representation of universities as a builder of nanosatellites, and Figure 1((2)), shows the status of current missions (data from 2022).

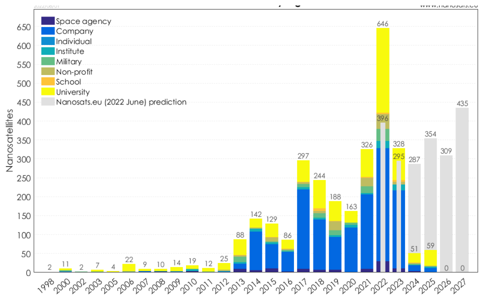

(((1))) Launchers by Category

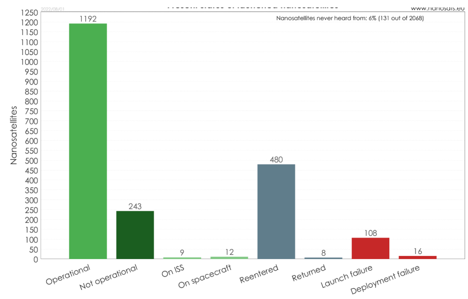

(((2))) Status Operations

Figure 1: Launchers and Status

The Figure 1((2)) shows us the status of the missions, most of which are still active, and although this work does not investigate the exact missions of each of these projects, we estimate that most of these missions perform experiments and change their firmware in orbit.

The firmware update process is quite delicate. First, during the process of transmitting and exchanging data, one of the bits may accidentally be reversed. This can occur, for example, due to environmental reasons such as a solar storm or effects on the Earth's atmosphere. Second, there is another challenge when it comes to communication between the ground station and the nanosatellites. CubeSats operating in Low Earth Orbit (LEO) take between 8 min to 10 min [4] to overpass the communication window with the ground station. Within such a short time window, the amount of data that can be transmitted is very small and the communication must be correctly done. The nanosatellite could take hours to overpass the station on Earth again. In the following sections, we will present strategies to mitigate the listed challenges.

The remainder of this paper is as follows: Section 2 discusses the state of the art of cubesats and the firmware upgrade process. Section 3 explains what is blockchain and how this decentralized infrastructure of ground stations will be built. Section 4 presents the experiments performed and their results and, finally, section 5 will present the conclusion of our work and future projects.

2. Firmware Upgrade in nanosatellites

In general, the remote firmware update procedure on space devices is divided into four very clear parts [5]: the first part is dedicated to preparing the firmware image, fragmenting [6] [7] it into small blocks and delta compressed [8] to be sent by the earth station; the second is the transfer protocol; the third part is related to storage in the nanosatellite memory and post-processing, that is, checking if the image is complete, if it has been corrupted or altered. After the verification process, the routine starts to point to the onboard computer which is the new memory address that the firmware has and initializes the system. If any errors are found, then a new request for this data packet is performed. Error Correcting Codes (ECCs) are commonly used on this step [9] [10] [11]. Figure 2 shows the representation of Software Update Protocol Timeline [5]. In our timeline, we add the identification of the satellite, and of the last captured packet. Table 1 shows some examples of missions with updates.

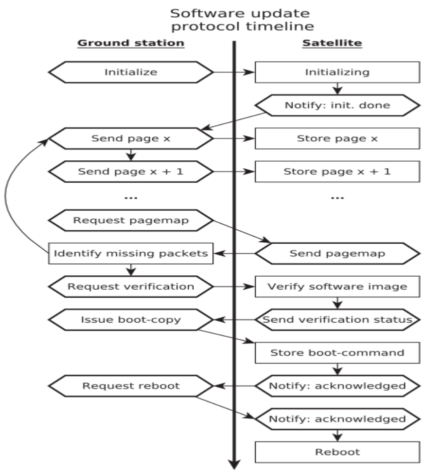

Figure 2: Software Update Protocol Timeline.

Table 1: Examples Cubesats that underwent an in-orbit firmware update

Name	Mission Time (Month)	Number of Updates
AeroCube4 [12] [13]	18	150
ESTCubete-1 [14]	Uninformed	35
STRaND-1 [14]	24 months, with many flaws	Uniformed
UWE-3 [15]	Uninformed	3

Figure 2 represents the mission of ESTCube-1, a CubeSat focused on solar sailing experiments: it was designed to be reprogrammed in orbit.

Now, we can understand not only the importance but the need for a safe procedure for updating the firmware of nanosatellites and other equipment and spacecraft.

3. Blockchain and Decentralized infrastructure of ground stations

The present section is composed by two subsections. The first is an additional exposition of the context of what has already been presented in the introduction, regarding the relevance and demand of university nanosatellites. Then, some blockchain concepts will be introduced and and explanation on how it can be a powerful tool for building consortia to create a decentralized infrastructure of ground stations is shown.

Contextualization

As already presented in the introduction to this work, the costs and expenses to carry out projects in the space sector are enormous. Universities around the world are looking for solutions to give continuity to their initiatives and one of the examples of cost sharing and research is the BIRDS Ground Station Network [16].

BIRDS is a satellite constellation project involving students from 15 countries. The constellation is composed by, usually, 1 U cubesats, equipped with cameras. They use UHF/VHF for communication and are able to run experiments.

The limitation is that it is not very clear whether there is privacy and individuality for example in the firmware update process. Our proposal goes beyond generating a shared antenna network, but in an individual, confidential and secure firmware update service, as we can foresee that in the network some cubesat developers, engineers and researchers wanted to keep their firmwares secret, but want to share resources like airtime and others. Another point is seen where it shows that the application is centralized, what we can intuit is that if there is an availability problem, the service may go down. Another interesting project is Amazon's AWS Ground Station, which rents terrestrial antennas to companies and startups. But the prices are sometimes unacceptable for educational projects or those just starting out. In the next segment we will present an important concept for our project.

Blockchain

Blockchain is basically a list chained and growing number of records. are called blocks and have encryption that protects them. In general, Blockchain has some components and they are: data, hash, previous hash and metadata (time/date stamp and block number). Let's see the what do they mean. See Figure 3 .

- Data: can be a simple string or a list of transactions;

-Hash: is a unique identifier for a block and is analogous to a fingerprint

-Previous hash: is the hash value of the previous block in the list

-Metadata: Information about the data, such as the block number, date, time etc.

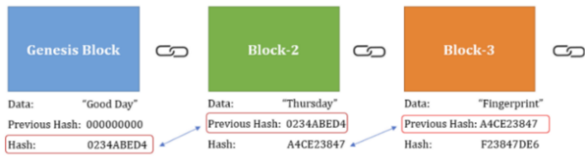

Figure 3: High-level representation of a blockchain

There are two main types of Blockchain: those without permission, that is, they are open and public, as Bitcoin and Ethereum and those allowed or with permission [17]. Another widely used concept is the Smart Contract [18]. The smart contract concept is not new, but the Ethereum Blockchain allowed him to could be implemented reliably. Are basically self-executing contracts, blocks of codes that when reaching certain markers are performed automatically. Will be the basis of transactions we will carry out. Another important concept is Web3, an idea for a new iteration of the internet based on blockchain technology, which incorporates concepts such as decentralization and token-based economy. We cannot fail to mention that ESA [19], NASA [20] have already expressed interest in the use of blockchain. Based on the fact that in the topic contextualization and Blockchain we have already laid the necessary foundations, this topic will deal with practical points of the suggested infrastructure. The process of a decentralized ground station infrastructure can be understood as follows: Each ground station is a node in the decentralized network. Each ground station has the power to write data to the Blockchain and to read the data. In section 4 this will be further detailed. Table 2 complements the reasons for our proposal

Table 2: Motivation for Decentralization Infrastructure GS wtih Blockchain

Motivation	Potential Benefit
Automation with smart contracts	-The automation of smart contracts running on the blockchain is interesting because routines and algorithms, for example, sensor calibration or orbit corrections can be executed without the need for human intervention.
Privacy with cryptographic technology	-Decentralized infrastructure with blockchain can be combined with modern cryptographic techniques to preserve the privacy of codes, binaries and transactions. Keeping each manufacturer's firmware code confidential.
Tokenization	-With the possibility of tokenizing routines and some processes, it can generate an additional source of income for the institutions that maintain the service and even attract private initiatives to invest in projects.
Service availability	-If one of the antennas stops operating for some reason, the others continue to offer the service and the firmware update process continues without stopping.
Cost Sharing	-University and other projects that will have the opportunity to share communication costs between ground stations and nanosatellites. Generating economy and cheaper space missions.

4. Experiments and Results

For Cubesat we use the PION Educational Cubesat from PIONS Labs [21]. PION's Educational CubeSat has nine sensors for space mission data collection: brightness, temperature, pressure, humidity, carbon dioxide, battery level, gyroscope, magnetometer, accelerometer. The CubeSat processor is 32-bit (ESP32) and we developed a platform for real-time data collection. See figure 4. The platform assigns a blockchain identity to Cubesat and governs other operations such as sending and requesting data. In this case, firmware.

Choosing Blockhain and Fragmentation Algorithm

In our project we chose the Hyperledger Besu blockchain [22] to implement smart contracts. The reason for the choice is a) the Besu framework allows the creation

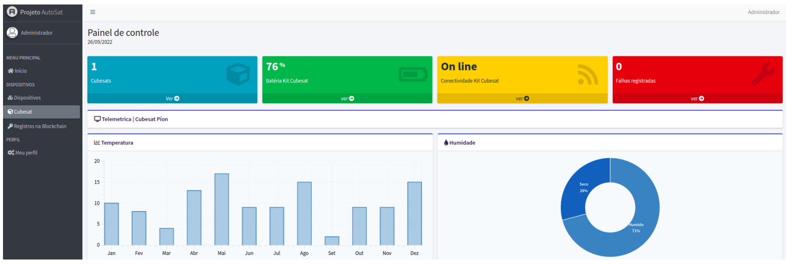

Figure 4: PION Educational Cubesat and Dashboard Web

of public and private networks b) it has several plugins and APIs for querying transactions more easily. c) It is an Ethereum client and brings together the features of the hyperledger family and d) It has several types of consensus algorithms. These characteristics allow us to develop the software artifacts that interest us faster.

We implement a fragmentation algorithm in C. It takes firmware images of any size and breaks it into 32 bytes fragments. This is because it is the size of the payload (data) that we will put in each writing transaction on the blockchain. There are several fragmentation algorithms in the literature. A very interesting document is the ”LoRaWAN Fragmented Data Block” [23] with technical explanations and example code in matlab.

Simulation

The Table 3 presents specifications used in the experiment and Figure 6 represents the decentralization of sending the firmware image. For this, each Earth Station runs a node of the private blockchain in the consortium format. In our business model the partner mission controls access a web platform that communicates with the blockchain via web3.

See Figure 5((1)) and Figure 5((2)). They upload the entire firmware image. The application backend fragments the firmware image respecting the maximum size of each packet that can be sent depending on the communication bandwidth used. For our tests we simulated UHF. Important: Each institution has its own set of public and private keys to sign the transaction. The fragment is encrypted and stored. Thus, only the cubesat of the developing institution can access the firmware fragment intended for it. The next step takes place when the cubesat passes within the range of the station. The flow in Figure 2 happens each time it enters a new range of partner stations.

Table 3: Specifications

Item	Description
Blockhain	-Hyperledger BESU 20.10.0
Used Languages	-Solidity (Smart contract) and NodeJS (API)
Consensus Algorithm	-IBFT
Frameworks	-Remix-ethereum (online) [24], Metamask (wallet), VS Code (IDE) and Docker Composer
Devices	-PION (Cubesat , with ESP32) , Notebook DELL 8 GB RAM, 2.1Ghz I3 (Ran Blockchain locally with 3 nodes and 1 rpc)

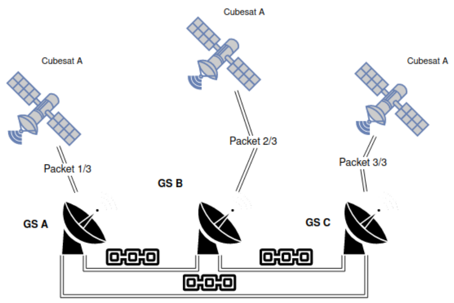

(((1))) Ground Stations Concept

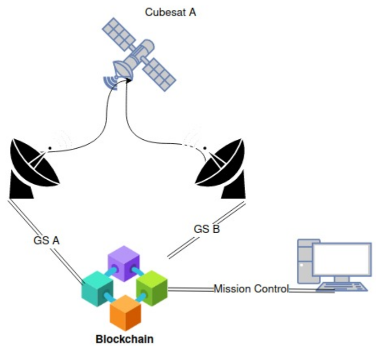

(((2))) Flow mission Control - Cubesat

Figure 5: Descentralized Infrastructure of GS in Blockchain

Although the blockchain is hosted on the servers of the ground stations, we present below some useful information about the cost and time relationship of the main smart contract methods. Note that the only transaction that generates costs is writing to the blockchain, the other methods do not generate costs. This allows it to be cheaper for institutions to carry out the maintenance process. This we defined when we created the blockchain.

Our experiment simulated the earth station server through a notebook as referenced in table 4 and the communication via antenna was replaced by requests via HTTP (using internet). We chose this to simplify our procedures. In our experiment we simulated an earth station server using a notebook (see table 4) and Cubesat PION requests were made via the web using a REST API. As each transaction on the blockchain stores in its data field 32 bytes, the fragments created obey this size. When cubesat makes requests, the backend on the server asks for the desired index. It queries the bockchain and creates a new data packet by joining all small 32bytes fragments up to a certain limit to comply with the maximum size that the channel supports to send. For our project we created a web platform that can be accessed at www.autosat.iochip.com.br. The platform allows the user to register a device, assign a cryptographic identity and even query telemetry data.

Results

A first result found is the cost in dollars to store the firmware on the blockchain. The Gas is the amount that will be charged for each transaction on Ethereum. Gas prices are indicated in Gwei, a proprietary denomination of ETH in which each Gwei is equal to 0.00000001 ETH. This value can vary according to several factors, such as the demand for the network and the type of operation. Whereas each fragment is 32bytes in size. See table 4 for some related costs. Note the matching of firmware size and transaction cost in US Dollars. Although there is variation in the price of a cryptocurrency like ETH, institutions can predict in their projects how much they will spend on firmware update processes. The price of ETH against the dollar was from September 2022.

Figure 07 represents the log of a storage transaction of a 32 bytes firmware fragment. Note that when analyzing figure 7 there is a tag called ”creator” notice that it

Table 4: Cost to Add Firmware Fragments on Blockchain

Size Firmware in Kb	Nº Fragments	Gas	ETH	USD
1	31.25	9017687.5	0.017206	22.99
2	62.50	18035375.0	0.034412	45.98
3	93.75	27053062.5	0.051618	68.97
4	125.00	36070750.0	0.068823	91.96

is the same identifier that is shown in figure 08 (Account 2). We call this the wallet address. This gives privacy to each institution and prevents firmware from being sent to the wrong cubesats. This information goes in the metadata.

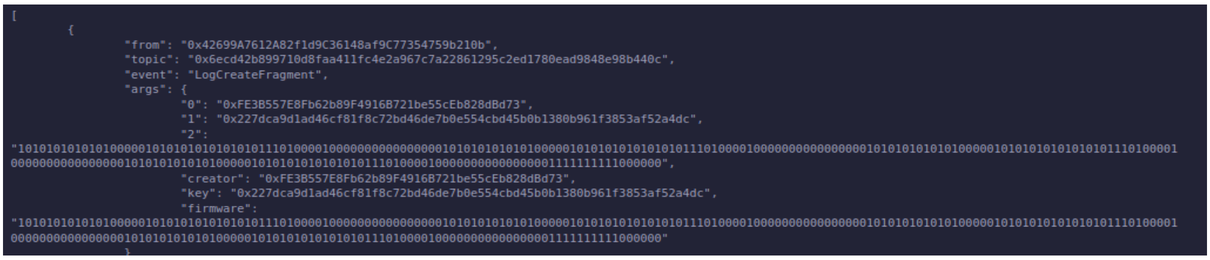

Figure 6: Log of transaction createFirmwareFragment().

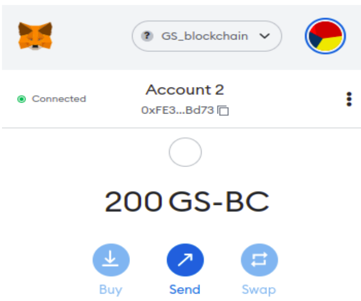

Figure 7: Wallet Metamask with Tokens GS-BC

Something that our architecture allows is the creation of tokens, i.e. digital assets, that can replace ETH. This could be interesting because the transaction prices would not be tied to the fluctuations of ETH. At the same time, it allows a new way to monetize the project and also create businesses on top of the solution. Note that in Figure 8 this portfolio has 200 GS-BC (An ERC-20 token worth 10 percent of ETH), it is an example of a token that could be used to replace ETH within the consortium of partner institutions

The Figure 9 shows the perspective of using the GS-BC Token for the private network in the consortium. Showing that economically it is more attractive to private projects, as is our target, for example Universities and small and medium-sized private companies.An additional result can be found in table 5.

A traditional VHF/UHF station used for cubesat missions costs around USD 69,7K and if we depreciate this value into the number of minutes in the time of an 18 month

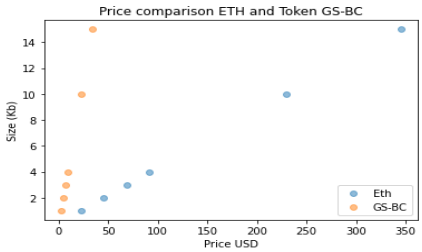

Figure 8: Cost comparison ETH x token GS-BC

Table 5: Cost Ground Station VHF/UHF

Option	Mission (month)	Cost per minute (USD)	Minutes per month	Price Final
Traditional	18	0.08	1,460	69,750.00
AWS GS	18	20	165	29,700.00
GS-BC	18	0.02	1,460	23,225.00

mission, we will arrive at how much that station cost per minute for the project. For this calculation, we do not consider technical operators, energy cost, etc. This can make some educational and even small business projects unfeasible.There are commercial alternatives for leasing earth stations, a highlight is Amazon (AWS Ground Station). It has an interesting quality standard and although at first its final cost in a 12 month package is USD 19,800.00 for an 18 month mission it was estimated at USD 29,700.00 with only 248 minutes per month. In our study, in addition to proposing the decentralized use of earth stations, we created a GS-BC token and additionally proposed offering the GS usage service at USD 1.79 per minute. Our calculations show that in an 18 month mission the cost of shared service can represent a savings of 66.7 percent of the purchase price of a VHF/UHF station. It becomes an option, as it allows better control in the management of the earth station rental resource, it is cheaper than other alternatives and can still become a source of revenue for institutions that have earth stations for rent in the consortium .

5. Conclusion

Firmware updates are an important component of successful space missions. all sizes. Bearing in mind the budgetary constraints that several university projects suffer from the dynamic and unstable world market, solutions that allow cost sharing and Missions are always welcome. Our project doesn't just offer a solution to the problem of cheaper university space missions, but also for industrial and commercial initiatives as it provides a robust and secure solution and a reliable infrastructure for uploading and firmware update for space devices, in the case studied, for cubesats. Our project proposed costs in Eth and a token we created called GS- BC with an initially fixed value of 10 percent of ETH. This can change depending on the consortium.

As a future project, we want to expand the study and implementation of technology for these other processes, such as data acquisition and sensor calibration, using centralized ground station infrastructure and blockchain. We also concluded that the The costs of registering firmware on the blockchain network are acceptable as they can be paid in cash, which facilitates the strategic planning of operators

References

[1] I.Nason, J. Puig-Suari, and R. Twiggs, Development of a family of picosatellite deployers based on the CubeSat standard , IEEE Aerospace Conference Proceedings (2002).

[2] Garrido, B. García, A. Alfaro, N and Miguel, J, On-board software maintenance, Proceedings of the DASIA '98 Conference on Data Systems in Aerospace (1998).

[3] Greco, M .E and Snyder, J. F, Operational modification of the Mars explorations rover's flight software, IEEE Systems, Man and Cybernetics, International Conference (2005).

[4] R. A. Carvalho, Optimizing the communication capacity of a ground station network, Journal Aerospace Technology and Management (2019).

[5] I. Sünter, A. Slavinskis, U. Kvell, A. Vahter, H. Kuuste, M. Noorma, J. Kutt, R. Vendt, K. Tarbe, M. Pajusalu, M. Veske, T. Ilves, Firmware updating systems for nanosatellites, IEEE Aerospace and Electronic Systems Magazine 31 (2016) 36–44.

[6] S. M. O. R. Leiner, B., B. Huber, A comparison of partitioning operating systems for integrated systems, Proceedings of 26th International Conference on Computer Safety, Reliability, and Security (SAFECOMP) (2007) 342–355.

[7] J. J. Rosa, J. Rufino, Exploiting air composability towards spacecraft onboard software update., Actas do INForum-Simpósio de Informática (2010).

[8] B. Bing, A fast secure framework for over-the-air wireless software download using reconfigurable mobile devices., IEEE Communications Magazine (2006) 58–63.

[9] L. Wood, W. Eddy, W. Ivancic, J. Mckim, C. Jackson, Saratoga: a delay-tolerant networking convergence layer with efficient link utilization, pp. 168 – 172.

[10] F. Silva, A. Muniz, J. Silveira, C. Marcon, Clc-a: An adaptive implementation of the column line code (clc) ecc, in: 2020 33rd Symposium on Integrated Circuits and Systems Design (SBCCI), pp. 1–6.

[11] R. Hamming, Error detecting and error correcting codes, The Bell System Technical Journal 29 (1950) 147–160.

[12] J. W. Gangestad, B. S. Hardy, D. Hinkley, Operations, orbit determination, and formation control of the aerocube-4 cubesats.

[13] J. W. Gangestad, D. W. Rowen, B. S. Hardy, Forest fires, sunglint, and a solar eclipse: Responsive remote sensing with aerocube-4, in: 2014 IEEE Geoscience and Remote Sensing Symposium, pp. 3622–3625.

[14] C. P. Bridges, B. Yeomans, C. Iacopino, T. E. Frame, A. Schofield, S. Kenyon, M. N. Sweeting, Smartphone qualification linux-based tools for cubesat computing payloads, in: 2013 IEEE Aerospace Conference, pp. 1–10.

[15] "UWE-3 Software Update in Space" 2014, [On Line], Accessed: 10-Nov-2022. Https://www.informatik.uni-wuerzburg.de/space/forschung/space-exploration/projects/uwe-3/uwe-3-news/single-news/news/uwe-3-software-update-in-space-1/.

[16] T. Tumenjargal, J. Members, J. Partners, M. Cho, Development status of joint global multi-nation birds cubesat constellation project.

[17] A. B. Melo, Tecnologia blockchain: Fundamentos, tecnologias de segurança e desenvolvimento de software, 2017. Https://www.cpqd.com.br.

[18] Ethereum blockchain app platform, 2013. Https://www.ethereum.org/.

[19] Blockchain and earth observation white paper, April 2019. Https://eo4society.esa.int.

[20] J. d. La Beaujardiere, R. Mital, R. Mital, Blockchain application within a multi-sensor satellite architecture, in: IGARSS 2019 - 2019 IEEE International Geoscience and Remote Sensing Symposium, pp. 5293–5296.

[21] Pion educational cubesat, 2022. Https://www.pionlabs.com.br/cubesat.

[22] Hyperledger besu blockchain, 2015. Https://www.hyperledger.org/use/besu/.

[23] Lorawan fragmented data block, 2018. Https://lora-alliance.org.

[24] Remix ethereum framework, Accessed in setember 2022. Https://remix.ethereum.org/.

ENHANCING STEAM EDUCATION THROUGH MULTIMISSION PLATFORM DEVELOPMENT USING STRATOSPHERIC BALLOON

Tikami A.[1], Pereira A. C. O. J.[2], Dos Santos W. A.[3], Cisotto M. V.[4], Julio Filho A. C.[5], Bueno L. A. R.[6], Brito A. F.[7], Florentino A. J. A.[8], Teixeira L.[9], Camargo L. A. P[10], Junqueira B. C.[11], Horna A. P.[12], Torres, J. G. M.[13], Mammoli M.[14]

[1,2,3,4,5,6,7,8,9,10,11,12] National Institute for Space Research (INPE),
São José, dos Campos, São Paulo - Brasil, 55 12 3208 6596
[1]auro.tikami, [2]acarlos.pereira, [3]walter.abrahao, [4]marcus.cisotto,
[5]cassiano.filho, [6]luiz.bueno, [7]antonio.brito, [8]angelo.florentino,
[9]lincoln.teixeira, [10]lazaro.camargo, [11]bruno.junqueira, [12]andres.horna [@inpe.br],
[13,14] National Service for Commercial Education (SENAC),
São José dos Campos, São Paulo - Brasil, 55 12 2134 9027
[13]jair.gmello, [14]marco.mammoli [@sp.senac.br]

Abstract

The small satellite programs have been successfully used as a platform for learning STEAM (Science, Technology, Engineering, Arts and Mathematics) disciplines, bringing benefits to education and research institutions. Technical schools have been considered expected candidates for hosting such programs due to their course components and infrastructure. More recently, with the dissemination of small satellite initiatives, non-technical institutions have been presented the opportunity of developing satellite design and implementation programs. In this context, the BalloonSat Stratos Senac I project, or simply BalloonSat, from SENAC, National Service for Commercial Education, aims to inspire young students to pursue knowledge in the STEAM areas stimulating technology-based entrepreneurship and improving science education in Brazil. The project, in partnership with INPE, National Institute for Space Research, consists of advising and supporting SENAC, in the development and manufacture of a platform transporting educational and scientific payloads to be launched into the stratosphere by a small meteorological balloon. The georeferenced data until the stratosphere, obtained by the platform and instruments, will be used in investigations and atmospheric phenomena studies. The development and space system prototype testing can be performed alternatively at a low cost using the stratosphere due to factors present such as low atmospheric pressure, radiation, and temperature extremes. This paper will discuss BalloonSat with some safety requirements, the helium stratospheric balloon remote station based on Arduino processor, CAM-M8 GPS module, and RFM69 transceiver. It will also discuss the ground station segment with a balloon trajectory prediction simulation map showing the launch, balloon burst, and payload impact sites. The ground station will be performing tracking, command, and data reception from the remote platform and instruments during the balloon flight to the stratosphere from the launch site till payload rescue. Preliminary functional test results without balloon launch will be presented. The BalloonSat is according to INPE´s mission of disseminating knowledge and technology to society and also aims to induce and train human resources.

***Keywords**: BalloonSat, STEAM, Stratospheric Balloon, Small Satellite, Platform.*

1. Introduction

The promotion of STEAM (Science, Technology, Engineering, Arts, and Mathematics) disciplines to foster youngsters' interest in careers in the techno-scientific fields has been a concern in our society. Recently with increasing small satellite initiative dissemination, non-technical institutions in the space segment area, such as SENAC (National Service for Commercial Education) has gotten a cooperation agreement with INPE (National Institute for Space Research to inspire young students to pursue knowledge in STEAM initiatives.

The development of space platforms like CubeSat [1] has made space science a little more accessible to educational and research institutions. To make it more accessible for everyone at a low cost, stakeholder teams working on these space platforms can conduct stratospheric balloon experiments to test their instruments in the stratosphere in a harsh environment. The extreme condition in the stratosphere can dive to as low as −56.5 °C in temperature and 2 kPa in pressure [2]. These kinds of balloons are useful platforms for various research and technology needs. In particular, they can be used for concept-proof demonstrations in preparation for new space missions.

A typical stratospheric balloon flight duration varies depending on the choice of the launch site, flight trajectory and season. Payloads can be flown at altitudes around 30 km lasting approximately 2 hours. Compared to satellites, balloons can be operated at a relatively low cost and with shorter times from the experiment conception to the flight. In this context, the BalloonSat Stratos Senac I (BalloonSat) project joins a high-altitude science experiment pursuing knowledge in the STEAM areas. In Science, the platform and balloon launch will be able to be designed by teachers and students for more engaging learning in various courses. In Technology, students will familiarize themselves with the dominant technology of balloon launch and track it online. In Engineering, students will design their payload and plan its launch. In Arts, students will utilize creative skills for their experiments and launch campaigns and rescues. In Math, at the end of each release, students will have a huge amount of data for their applications.

High altitude testing using a stratospheric balloon has been considered an effective demonstration of some features of CubeSats. For example, the hardware must be prepared for harsh thermal environments with temperatures over -50°C. Balloon satellites have lower costs than CubeSats in both development and launching. Stratospheric balloons allow access to near space around 30 km and provide a complementary and less expensive means for satellites to observe the Earth or the universe from above most of the atmosphere. Balloon launches can be carried out in very short terms with low cost and using state-of-the-art technologies. Improvements and project updates can be carried out from the data acquired with balloon launches.

2. The BalloonSat Project

Most balloon systems and payloads are recoverable and can be reused. As a stratospheric balloon ascends into the stratosphere, it expands until it ruptures whereupon a parachute is deployed to descend the balloon systems and payloads to be retrieved. The balloon envelope itself is not recycled, however, the payload platform and the elements such as the parachute and radar reflector are re-used for future flights. The total mass supported by the stratospheric balloon will be less than 1200 grams. Figure 1 shows the balloon flight system with a balloon, parachute, radar reflector, and payload.

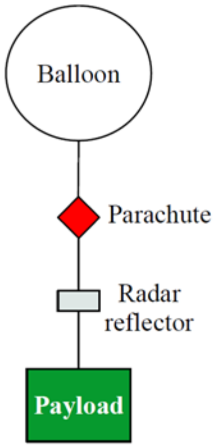

Figure 1 - Typical Balloon flight system.

The stratospheric balloon must have the following characteristics [3]:

- natural or synthetic rubber;
- homogeneous and spherical shape, uniform thickness and extensible type;
- provided with a collar of 1 to 5 cm in diameter and 10 to 20 cm in length, according to the size of the balloon;
- diameter (inflated and on the surface) of approximately 1.5 m;
- size and quality that ensure the transport of the radiosonde (from 1 to 2 kg) up to altitudes close to 30 km, with ascent rate fast enough to ensure reasonable ventilation of the measurement elements;
- it must be able to expand by at least 4 times its initial diameter and to maintain this exposure for at least one hour;
- when inflated, the balloon must have a spherical or at least circular in horizontal section.

The balloon must be inflated to perform the launch. Helium gas is considered one of the rare gases in the atmosphere and has properties such as inertness, odorless, colorless, and non-flammable. Hydrogen gas is a fuel element and the use of this gas is accompanied by a certain risk due to its highly flammable property. Factors that can cause hydrogen gas to explode, or to fire, are an unstable mixture of hydrogen and oxygen and the existence of an ignition source [3]. So the balloon launch, which involves students, helium gas must be chosen to inflate the balloon and eliminate the risk of explosion.

During the launch campaign, in order to reduce the possibility of a stratospheric balloon constituting a danger to aircraft in flight, the balloon operator must inform the local airport authority of the launch time, at least 30 minutes in advance, and other information useful for air navigation safety [3].

The BalloonSat project encompasses the balloon and ground station segments as shown in Figure 2. The balloon segment includes the balloon, inflated with Helium gas, and a radiosonde, with an Arduino processor [4], and a transmitter that sends information from the sensors and experiments to the ground station. The ground station segment receives the information sent from the balloon segment and the data processed by the Arduino are displayed on the PC. Given that Arduino processors are beginner friendly yet capable of advanced projects, Arduino is a good starting point for CubeSats built by student teams [5].

As a project development methodology, the data obtained from each launch can be used for updating and continuous improvement.

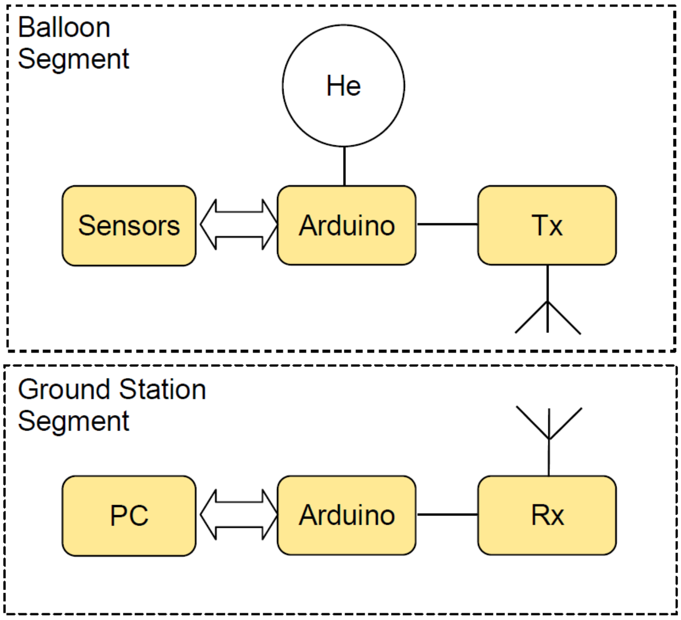

Figure 2: Balloon and Ground Station segments.

2.1. Balloon Segment

The Balloon segment block diagram is presented in Figure 3. Arduino processes time stamps, altitude, location coordinates, and altitude from the GPS CAM-M8 module [6], the sample atmospheric data, battery voltage, the internal temperature of the platform, outside temperature from the atmosphere, and payload data. The transceiver used is the RFM69HCW [7] which transmits GFSK data (4800 bps) in radio frequency (433 MHz) through an antenna to the ground station with 100 mW output power. The antenna is a monopole with an omnidirectional radiation pattern, radiating equal radio power in all directions perpendicular to the antenna's axis.

The sensors are BMP180 [8] and DS18B20 [9]. The BMP180 sensor will be used to measure atmospheric pressure, altitude, and temperature. The DS18B20 sensor is a digital thermometer with 9-bit to 12-bit Celsius temperature measurements. It communicates over a 1-wire bus. Payloads, educational and or scientific, can be embedded into the platform with data acquisition by the Arduino processor. The battery consists of a 5-volt power bank.

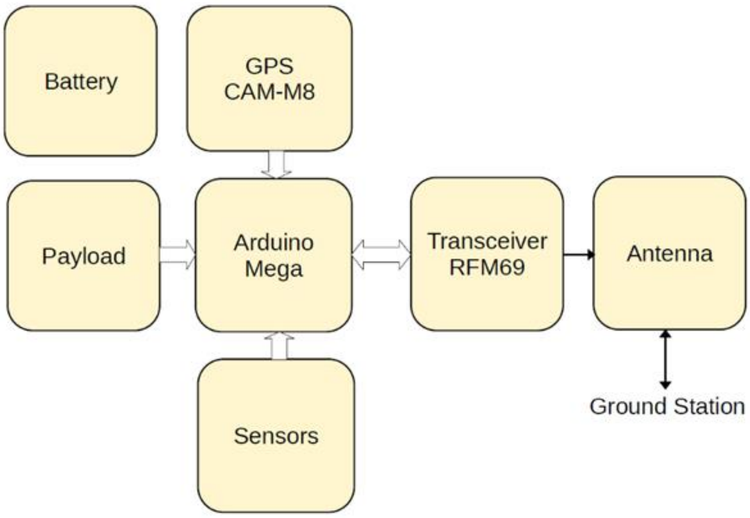

Figure 3 - The Balloon segment block diagram.

2.2. Ground Station Segment

The ground station is also based on the Arduino processor. There will be two types of the ground station, one transportable and the other mobile for the recovery of the stratospheric balloon platform. Figure 4 shows the ground station block diagram. The battery is going to use for the mobile ground station.

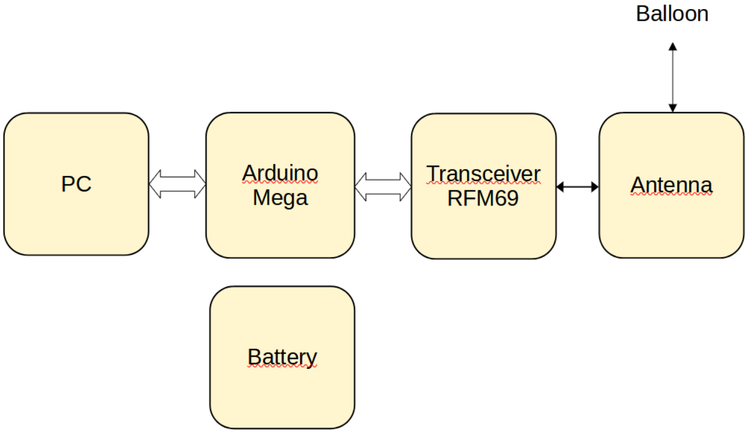

Figure 4 - Ground Station block diagram.

The visualization software was implemented using LabView [10] with Arduino processed data. Figure 5 presents the front panel view.

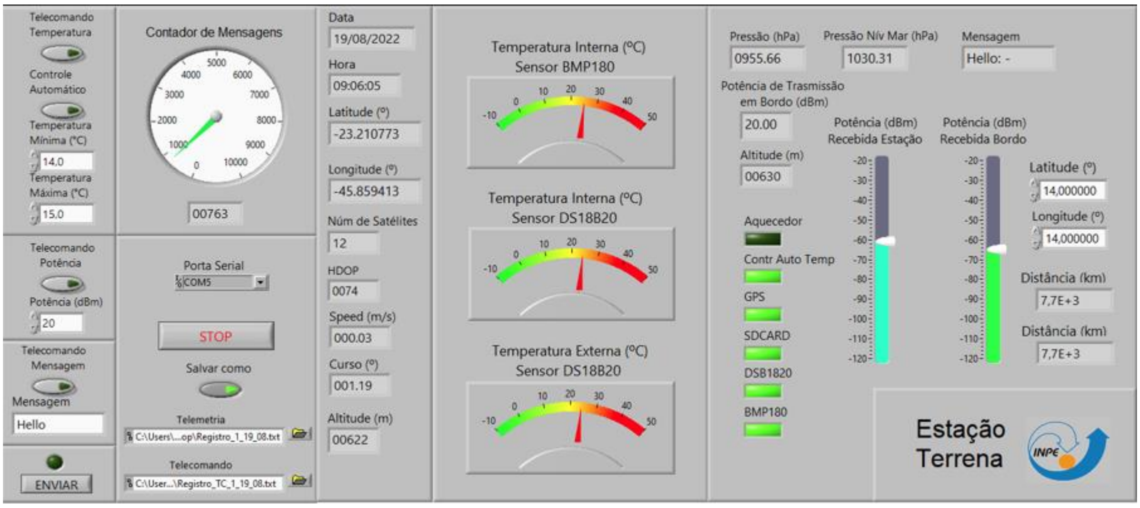

Figure 5 - Ground Station Front Panel

3. Simulation and Results

The prediction of the landing location can be enabled using a free web-based trajectory forecast tool. One of the most commonly used predictors is a CUSF [11] predictor developed by Cambridge University Spaceflight. The main advantages of this predictor are its intuitive user interface and clear trajectory maps. It also generates maps (Figure 6) and KML files directly from the predictor, allowing for easy visualization of the predicted trajectory by Google Earth (Figure 7). The simulation was performed only as an example to illustrate the predictor result. The target landing areas will preferably be open fields, away from mountains, oceans, and populated areas.

Figure 6 - Cambridge University predictor map.

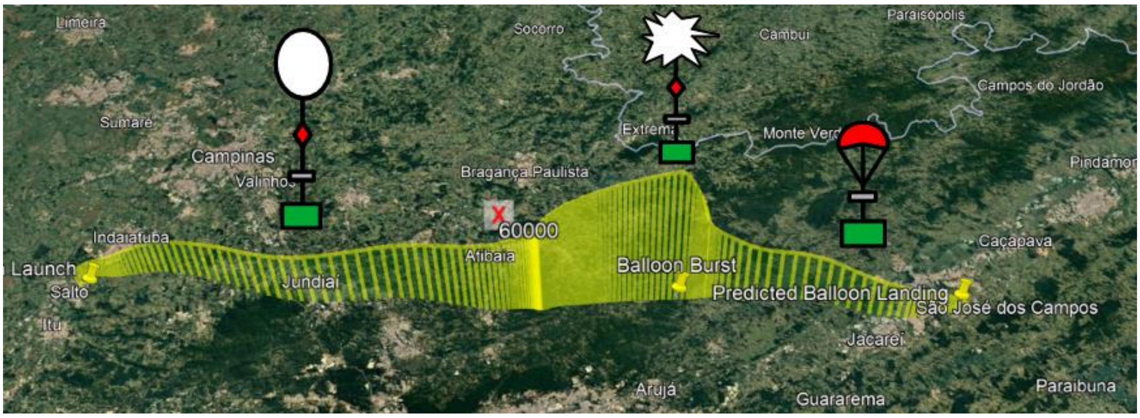

Figure.7 - Balloon trajectory forecast with Google Earth visualization.

The balloon is released and ascends to the stratosphere and during ascension, the pressure inside the balloon is bigger than the pressure of the external environment. Given the pressure difference, the balloon will start to expand up to a point at which the balloon can no longer withstand the internal pressure and will therefore burst. After bursting, the parachute will deploy and slow down the descent of the payload bus. That is significantly affected by the wind in the absence of parachute control. Finally, the search and rescue team can retrieve the payload, and the data saved onboard can be further analyzed [12].

In order to verify the general functioning of the hardware and software in development, simple tests were carried out successfully, without performing a balloon launch, between the ground station segment and the balloon transmitter located approximately 10 km away in a straight line without obstructions.

4. Conclusions

The space platform development as CubeSat has made space science accessible to educational and research institutions promoting STEAM initiatives with stratospheric balloon launches carrying satellite subsystems and experiments into the stratosphere in a harsh environment.

In this paper, we have presented the BalloonSat project with the stratospheric balloon and ground station segments based on the Arduino processor. Communication and general functioning tests between these segments were successfully carried out on the ground and the CUSF balloon trajectory prediction tool was presented with simulation.

And with the launch to be performed of the balloon into the stratosphere and their results, we can use them to improve and update the platform for future launches.

Acknowledgments

The authors would like to express gratitude to the local airport authority for the stratospheric balloon flight authorization.

References

[1] https://www.cubesat.org/

[2] J. D. Anderson Jr., (1999), "Aircraft Performance and Design", 1st ed. Boston: WCB/McGraw-Hill.

[3] Comando da Aeronáutica. Departamento de Controle do Espaço Aéreo. Manual de Estações Meteorológicas de Altitude: MCA 105-9.
[4] http://www.arduino.cc/
[5] S. L. Kenjiro, L. Li, M. Okutsu, High altitude balloon testing of Arduino and environmental sensors for CubeSat prototype, Elsevier, 2022.
[6] https://www.u-blox.com/en/product/cam-m8-series
[7] https://www.hoperf.com/modules/rf_transceiver/RFM69W.html
[8] https://www.adafruit.com/product/1603
[9] https://datasheets.maximintegrated.com/en/ds/DS18B20-PAR.pdf
[10] https://www.ni.com/pt-br/shop/labview.html
[11] https://predict.habhub.org
[12] Thaheer, A. S. M., Ismail, N. A., Mission Design and Analysis of USM High-Altitude Balloon, Journal of Mechanical Engineering, Vol 14(2), 62-92, 2017.

7

Session 7 - Mission Applications II

LIGHTNING EVENTS SIMULATION BUDGETING FOR THE RAIOSAT PAYLOAD ON-BOARD COMPUTER

Lázaro C. Camargo(1), Jhonathan O. Murcia-Piñeros(2), Walter A. Dos Santos(3), Kleber Naccarato(3), Rodolpho V. de Moraes(4)

(1) Researcher, National Institute of Space Research INPE, lazaro.camargo@inpe.br
(2) Postdoctoral researcher, ICT/UNIFESP, jhonathan.pineros@unifesp.br
(3) Researchers, National Institute of Space Research INPE, Av. Dos Astronautas 1758 Jd. Da Granja, São José dos Campos, São Paulo, Brazil.
(4) Professor, Institute of Science and Technology ICT/UNIFESP, Av. Cesare Monsueto Giulio Lattes, 1201 - Eugênio de Melo, São José dos Campos - SP, 12247-014

***Keywords**: RaioSat, lightning flash simulation, Monte Carlo simulation, small satellites.*

Extreme weather events are increasingly common in Brazilian territory, and to assist in the study and generation of meteorological forecast models, the monitoring of lightning occurrences becomes extremely important. The Atmospheric Electricity (ELAT) group of the Earth System Science Center (CCST) proposed the Cubesat RaioSat mission, to assist the existing ground network for monitoring lightning occurrences. The RaioSat mission will have, as a space segment, a CubeSat of three units (3U) with a mass of 6 kg and dimensions of 10 x 10 x 30 cm, with an on-board computer and an attitude control system to meet the requirements for imaging rays and having the following payloads: Camera in the IR range (infrared) with sensor and an optical filter, a GPS (Global Positioning System) for low orbit applications, VHF (Very High Frequency) receiver of the SDR (Software Defined Radio) type operating in the 80 - 200 MHz band, to record the electromagnetic signatures and validate the lightning detections performed by the IR camera. The objective of this work is to present a simulation of lightning events for estimating requirements to the RaioSat payload on-board computer. The methodology is to implement Monte Carlo simulations, where the random input variables are the location of the storms, the size, and duration, and the number of lightning generated, and to verify if the satellite sensor can observe the phenomenon. First, the orbit of the nanosatellite RaioSat will be simulated. Next, the coverage region of the RaioSat mission will be defined, to calculate the limits of the regions of interest. For mesh usage, the inputs are the GIS of Brazil and the mesh size, and the output is the node, latitude, and longitude. Then, to simulate the occurrence of lightning, the Monte Carlo method will be used, first using pseudo-random, then generating the storms (latitude, longitude, elliptical size, duration, and severity), and the occurrence of lightning events (latitude, longitude, and intensity). Finally, the sensor coverage of the RaioSat mission will be simulated, initializing the Field Of View of the camera (footprint), and the intersections of the sensor footprint with the simulated lightning events. In the future, the Monte Carlo method will be changed to a Machine Learning model, to develop an application like EGSE for the RaioSat mission

1. Introduction

Lightning flashes are natural phenomena described as atmospheric discharges. They describe three types of trajectories, cloud-to-ground, ground-to-cloud and, cloud-to-cloud. This natural phenomenon is related to natural disasters, being a problem for the population and the infrastructure in locations with a high incidence of storms, which is proportional to the number of cloud-to-ground discharges [1]. In Brazil as the rest of the world, a huge amount of money is estimated in damages as a consequence of the lightning strikes events [2]. To improve our knowledge about the generation of lightning flashes and to improve the forecast of these events, is necessary to collect data from the storms. Brazil has a ground network (or ground stations), named BrasilDAT, to collect meteorological data along the country. However, a larger number of stations are distributed in the south of the country, reducing the observations in the north and northeast regions, specifically in the Amazonian region [3] due to its extension. Searching to improve the coverage in these regions, and at the same time to increase the data collection of lightning flashes above Brazil, it is proposed the development of the RaioSat mission.

A Smallsat (3U nanosat) will be the space segment of the mission, which is projected to carry a CCD Camera with a UHF sensor to detect and collect the data from lightning flashes, these two instruments are the payload of the mission [4]. Due to the nature of the lightning flashes (aleatory in position and short time duration, lower than one second), it is difficult to estimate the number of lightning flashes that could be detected by the satellite during the passage above Brazil. This analysis is necessary to determine the feasibility of the mission and to select the best orbit to increase the coverage of the storms. For this reason, the aim of this paper is the lightning events simulation to analyze the number of possible events detected for the RaioSat Payload On-Board. The first part of the analysis required the model of the lightning flashes distribution or events distribution, the determination of the satellite position above Brazil, as a function of time, and the interaction between the sensor Field Of View (FOV) and the lightning flashes to detect the events. These three topics are presented in Section 2. The Monte Carlo experiment is described in Section 3, and the results from the Simulations are presented in Section 4. Finalizing the paper presented the conclusion.

2. The RaioSat Simulation Models

In this Section are presented the lighting flashes distribution, the satellite orbit, and the sensor-event interaction.

2.1. Lightning flashes distribution

The number of lightning flashes in some parts of the south and southeast Brazilian regions, was larger than 270 000 for the period 2018-2019. This data is collected and reported by the research group in atmospheric electricity (ELAT), which is part of the National Institute for Space Research (INPE) [5, 6]. The south and southeast regions of Brazil present a large incidence of lightning flashes, followed by the central-west region, the north region (which is located in the Amazonian region), and the last, with a lower incidence of flashes, is the northeast region. The quantity of lightning flashes per square kilometer per year (flashes/km^2/year) is the measurement used to present the data collected from the observations made from the passage of satellites, the measured is defined as lightning flash rate density. The mean annual flash rate in Brazil is larger than 15 flashes/km^2/year, as was reported in [7, 8]. A detailed lightning flash rate density over Brazil was presented as a map, from data analyzed by the INPE, ELAT, and the National Operator of the Electrical System (ONS), showing four regions from the period 1998-2013. A low incident region is observed in the northeast (mean of 2 flashes/km^2/year), two large incident regions, one in the central region and the other one in the south of the country (mean of 15 flashes/km^2/year), and the rest on Brazil as a median incident (mean of 8 flashes/km^2/year) [9]. From this data, it was calculated the number of lightning flashes daily inside each region. It is important to say that the data from lightning flash rate density represent a mean value uniformly distributed along the year, this means that is most probable to observe a large value of flashes daily during the rainy season (October to March), but, this data doesn't allow to determine or discretize over the time. Then, if the daily value of events is calculated from the lightning flash rate density, the most probable is a uniform distribution around this mean value. The other part is the location of the event or the lightning flash geographical coordinates (longitude and latitude), which in this case is modeled as a pseudo-random uniform distribution inside the four regions previously described. Figure 1 presents the larger (red color) and lower (blue color) regions modeled as ellipsoids. The dots represent the lightning flashes or events daily, with geographic random distribution. The horizontal axis is the longitude in degrees and the vertical axis is the latitude.

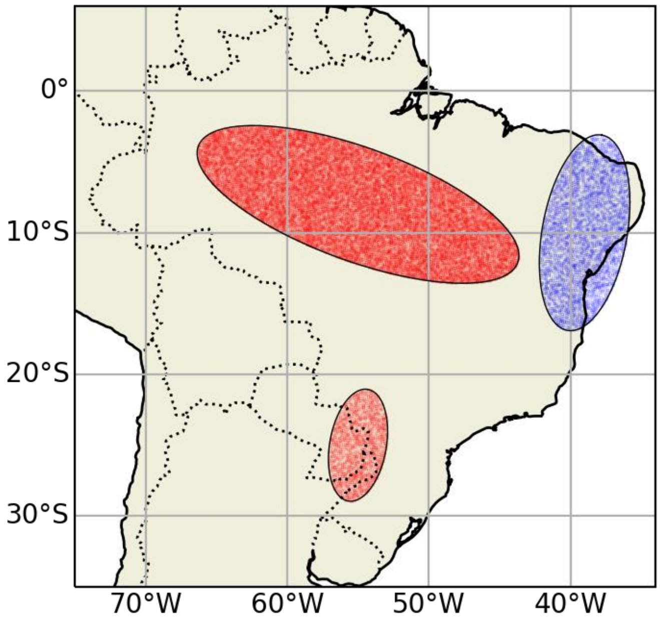

Figure 1: Daily lightning flashes simulated for high and low regions.

Table 1 presents the mean value of daily flashes calculated for the regions, a mean value of 185397 events are generated daily over Brazil. However, as was presented with the distribution along the year, in this case, the daily distribution as a function of the hour of the day is not presented in the scientific literature, which means that in mean, each 0.46 s a lightning flash is generated over Brazil.

Table 1: Daily events by region.

Region	Flashes/km^2/year	Mean daily events	Color in Figure 1
Center	15	36960	Red
South	15	3250	Red
Northeast	2	3230	Blue
Rest of Brazil	8	138557	Grey in Brazil

2.2. Modelling the satellite orbit

From the mission requirements, the space segment is projected to operate in a circular Low Earth Orbit (LEO), Sun Synchronous inclined at 98°. The geographic projection of the satellite´s orbit is presented in Figure 2 as red dots, and the blue square represents the sensor´s footprint. The orbit is modeled from the two-body problem, with the origin of the inertial at the center of the Earth. Cowell´s method is selected to propagate the orbit. The spherical perturbation of the gravitational potential (J2) is included in the dynamical equations of motion, and a numerical integrator Runge-Kutta-Felhberg 4/5 is selected to integrate numerically the equations of motion and to calculate the satellite position as a function of time. Small step sizes below 0.4 s as selected to propagate the orbit. The complete model of the orbit, perturbation, equations of motion, and numerical integrator is available in [10]. A circular orbit of 650 km of altitude and 98° of inclinations, allows the total coverage of the Brazilian territory in ten days (see Figure 3).

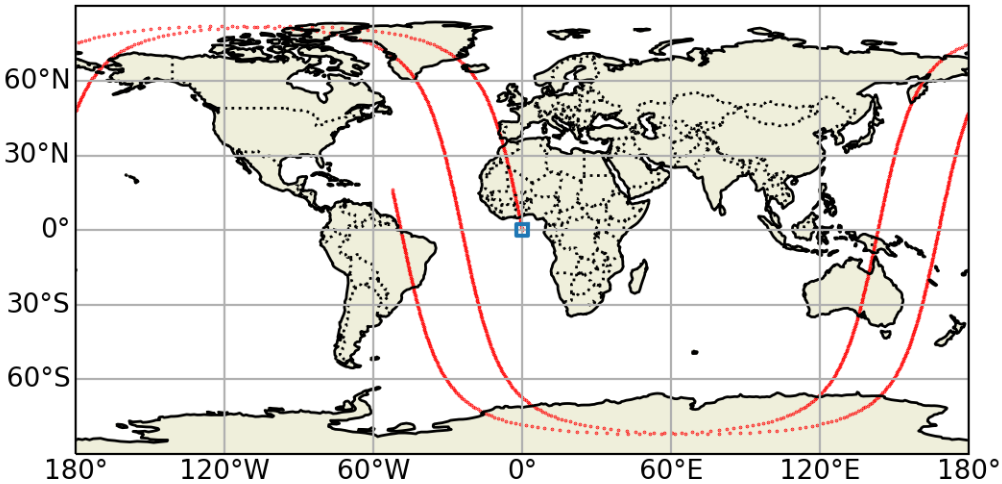

Figure 2: Satellite orbit ground track.

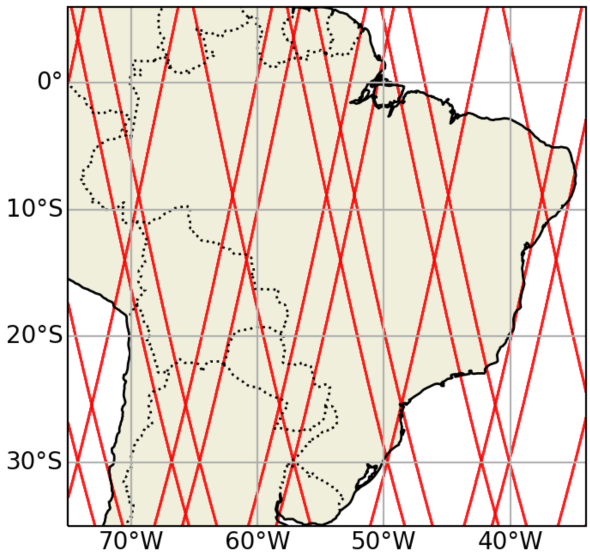

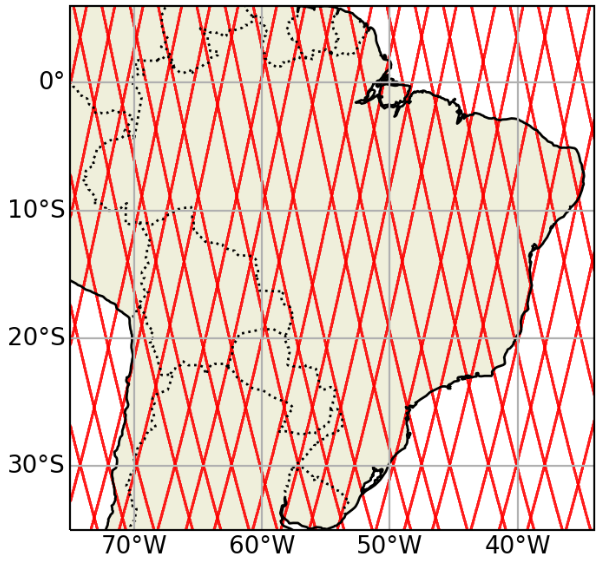

Figure 3: Satellite´s passages over Brazil for 5 days (left) and 10 days (right).

2.3. The footprint of the sensor

The last part of the model is the footprint of the sensor. The footprint is the area above the satellite, observed or sensed by the payload. This region changes as a function of time and the satellite position. The sensor is simulated with a square footprint, rotated in the direction of the orbit of the satellite. From preliminary analysis [4], it was estimated a FOV of 44°. Figure 4 presents the FOV (blue square) and one aleatory event (red dot) at the same instant of time. In this case, the aleatory is in Brazil, and at the same time, the satellite is above the south of the Indian Ocean, then the sensor does not detect the event. An event is detected when the satellite is above Brazil, and at the same time, the aleatory event is generated inside the FOV of the sensor.

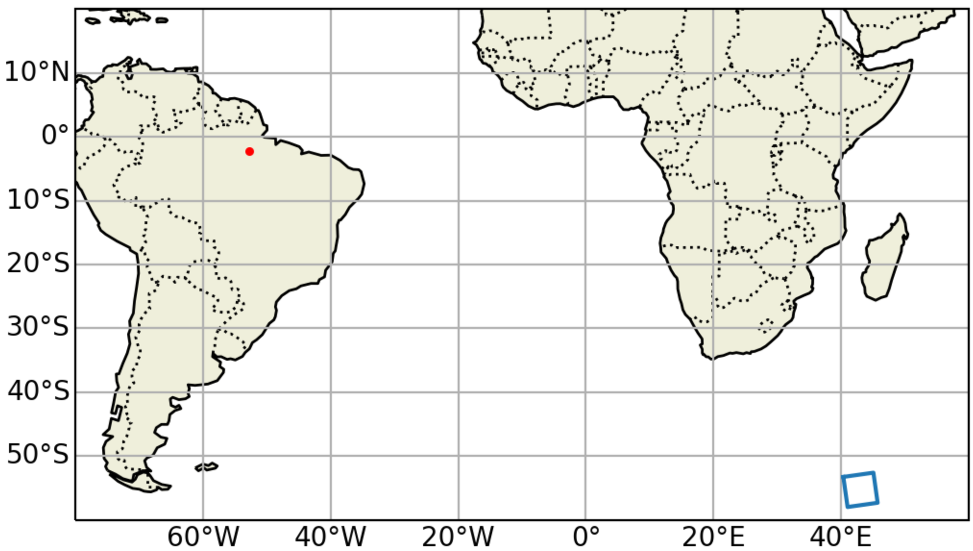

Figure 4: Footprint of the sensor and aleatory event.

3. The Monte Carlo Experiment Evaluation

Section 2 presented the models to generate the Monte Carlo simulation for aleatory events, calculate the passage of the satellite over Brazilian territory, and determine the position of the footprint of the sensor. All of the models were scripted in Python, using the Numpy, Matplotlib, and Cartopy libraries.

The first part of the experiment consists of the daily pseudo-random generation of the lightning flashes or events above Brazil, using the data from the lightning flash rate density. More than 180 000 events are generated in random locations in Brazil, and also are distributed uniformly throughout the day. The data of the events is saved, and the information on the time of the event is shared with the orbital model, to calculate the satellite position at the same instant as the time of the event. If the satellite is over Brazil, the data is saved and sent to the last module of the script, the model of the sensor. With the geospatial data of the event and the satellite position above Brazil at the same time, the last algorithm calculates the position of the event to the vertices of the FOV to determine if the event is inside or outside of the perimeter of the footprint. An event inside the FOV is classified as detected. The mean time of the passage of the satellite over Brazil in one day is above 2 500 s, and in this time more than 5 000 aleatory events are generated randomly.

The calculations of the events (quantity, time, and position) in one day, with the passage of the satellite and the calculation of the detection of these events, are defined as a simulation. At the beginning of each simulation, the pseudo-random number generator changes the total number of events, his position, and time along the day. Each lightning is instantaneous, and then the duration of the event is no longer than the step size of the propagation of the orbit. At the end of each simulation is generated a list of the events detected. The Monte Carlo method is applied over 1000 simulations, changing randomly the events.

4. Results and discussion

The Monte Carlo method was used to simulate the lightning flashes distribution. In a mean passage of the satellite with a duration of around 2 500 s more than 5 000 flashes are generated. However, the small size of the footprint and the instantaneous and random nature of the event, difficult the detection. Results of 1000 simulations show a low incidence of detections, lower than 5% of the simulations detected less than two events, and 95% of the simulations did not detect the events, even when thousands were generated at the same time of the passage, because these appear outside of the area of the sensor. Then is most probable the event occur in a large area of the Brazilian territory than in the small area of the FOV of the sensor.

There is another reason to justify the quasi-null detection of the flashes, and it is the time distribution of the event, because the model of the events is uniform, and not taken into account the possibility of having more events concentrated in specific hours of the day, nor events at the same time.

To increase the probability of detection, two technical solutions could be the increase in the FOV of the sensor, and/or the use of a smallsats constellation to increase the time of the passage over Brazil.

5. Conclusions

There was presented a method to model the random lighting flashing events, from the data of lightning flash rate density, collected by the ELAT/INPE. The model was integrated into an orbital propagator and a model of the sensor to calculate the probability of detection of the events. Monte Carlo simulations were applied, showing a low probability of detection, lower than 5% of the events detect less than two events.

The low probability of detection is attributed to the lightning flashes generation model because it is not taken into account the different distributions and/or concentration of events throughout the day. Then, it is necessary a more accurate model to generate the events and calculate the probability of detection. In addition, technical solutions could be analyzed, like a large sensor, and the use of a SmallSats constellation. The improvement of the time distribution of the lightning flashes could be used to model and configure the satellite to passage over Brazil at the same time as the larger flashes concentration, finding better orbits to the passage above the large concentration of storms.

Acknowledgments

The authors wish to express their appreciation for the support provided by Science and Technology Institute (ICT – UNIFESP) and by the National Institute for Space Research (INPE).
This work was supported by grants # 2019/26605-2 and # 2016/24561-0, from São Paulo Research Foundation (FAPESP); grants # 406841/2016-0, 301338/2016-7 and 303102/2019-5 from the National Council for Scientific and Technological Development (CNPq); grant # 88882.317514/2013-01 from the National Council for the Improvement of Higher Education (CAPES).

References

[1] INPE, Instituto Nacional de Pesquisas Espaciais. Mortes por Raios – Infográfico, São José dos Campos, 2021. Disponível em: <http://www.inpe.br/webelat/homepage/menu/el.atm/mortes.por.raios.-.infografico.php>. Acesso em: 22 ago. 2022

[2] ANEEL, Agência Nacional de Energia Elétrica. Relatório de Análise: Desligamentos Forçados do Sistema de Transmissão – Edição 2018. Brasília (2018) 685.

[3] K. P. Naccarato, et al. First performance analysis of BrasilDAT total lightning network In Southeastern Brazil. Proceedings. GROUND & LPE, 5. Bonito, (2012)

[4] A. Cassiano, et al., CubeSat Development for Lightning Flashes Detection: RaioSat Project, Journal of Aerospace Technology and management 12 (2020) 80-93.

[5] INPE/ELAT. Mapa do bienio 2018/2019, available at http://www.inpe.br/webelat/homepage/menu/infor/incidencia.de.descargas.no.pais.php, 2022.

[6] U. A. Barretto, R. L. Novais, F. J. Barbosa, Uma análise da espacialização das descargas elétricas atmosféricas e do comportamento das mortes causadas por raios no estado da Bahia, Revista Brasileira de geografia física 14 (2021) 1909-1923.

[7] D. J. Cecil, D. E. Buechler, R. J. Blakeslee, Gridded lightning climatology from TRMM-LIS and OTD: dataset description, Atmospheric research 135-136 (2014) 404-414.

[8] M. Peterson, D. Mach, D. Buechler, A global LIS/OTD Climatology of lightning flash extent density, JGR Atmospheres 126(8) (2021) 1-23.

[9] ONS. Mapa de densidade de descargas atmosféricas 1998-2013, avalible at: http://www.ons.org.br/paginas/sobre-o-sin/mapas, 2022.

[10] D. A. Vallado, Fundamentals of astrodynamics and applications 4 ed., Microcosm Press, 2013, 517-601

A High-Level Synthesis Compressor of Hyperspectral Images based on CCSDS 123.0-B-2

Wesley Grignani(1), **Gabriela Wisbecki**(1), **Felipe Viel**(1),(2), **Douglas R. Melo**(1)
(1) LEDS, University of Vale do Itajaí, Brazil
(2) SpaceLab, Federal University of Santa Catarina, Brazil

Keywords: *Systems-on-Chip, Hardware Accelerators, Image Processing.*

Abstract

Remote sensing is a technique for obtaining information from a surface through sensors that can be attached to drones, satellites, or planes. Among the most commonly used sensors are those that generate hyperspectral images. Hyperspectral images are a three-dimensional structure of pixels in which each layer is a matrix representing a single image at a given wavelength. Using hyperspectral images in industries such as agriculture and aerospace is valuable, as the massive amount of data from these images allows a deeper analysis of the scenario. In spatial systems, the processing of hyperspectral images can impact the application since such systems have processing, storage, and communication capacity limitations. Acceleration techniques have been proposed to reduce the workload from the main processor to a dedicated hardware-implemented processor for a given application. Considering these processing limitations, this work proposes implementing and analyzing a hyperspectral image compression algorithm in software and hardware using a High-Level Synthesis tool. We implemented a compressor of hyperspectral images based on the CCSDS 123.0-B-2 standard, proposed by the Consultative Committee for Space Data Systems. The implementation aims to evaluate the acceleration obtained through dedicated hardware compared to software routines on the main processor. Through software implementations and high-level synthesis, it was possible to observe that the behavior of the hardware inference resulted in the same compressed image compared to the software implementation, thus enabling the use of accelerators for this purpose. Regarding performance, the accelerator has a throughput of 13.2 MSa/s at a maximum frequency of 92 MHz, and runs 62% faster than the solution entirely in software.

1. Introduction

Over the years, the computing field has presented several technological advances, many of which have made possible the creation of smaller components with greater complexity, lower power consumption, and higher performance. Nowadays it is common to find systems that are known as Systems-on-Chip (SoCs), having several complex components on a single chip [1].

Space applications that collect data about the Earth use remote sensing techniques for this task. One of the techniques is the use of Hyperspectral Images (HSI), which can be used for applications such as Earth image collection, climate analysis and monitoring of forest environments [2].

Email addresses: `wesley.grignani@edu.univali.br` (**Wesley Grignani**), `drm@univali.br` (**Douglas R. Melo**)

Given the large volume of data present in hyperspectral images, a reduction in its size becomes desirable, aiming to minimize impacts on performance, both in transmission and in processing techniques. A well-known algorithm for compressing this type of image is CCSDS 123, developed by the Consultative Committee for Space Data Systems [3]. Its current version [4] enables lossless and near-lossless compression of hyperspectral images, where hardware design can be easily exploited to achieve high performance due to the low complexity of the algorithm.

The use of reconfigurable architectures, such as FPGAs, has seen a great increase in their adoption in the market for the creation of high-performance systems for image processing applications. However, implementing algorithms for a hardware design is a complex task when compared to implementing in software. This question is motivated since Hardware Description Languages (HDLs) demand more specific knowledge about architecture and digital circuits. Furthermore, is harder to apply software engineering techniques that increase productivity and code reliability in HDL designs. For these reasons, the adoption of High-Level Synthesis (HLS) tools has begun, allowing hardware development using programming languages [5].

The HLS aims to fill the gap between hardware and software development, mainly due to the abstraction obtained and the lower design time, because the synthesis tool is responsible for transforming the high-level code to the hardware. However, according to [5], optimizing code for hardware is drastically different from optimizing code for software, and previous knowledge to manipulate the hardware architecture employing the synthesis tool should be considered.

Thus, this work proposes the development of an HLS compressor based on the CCSDS 123.0-B-2 standard, in order to accelerate the processing of hyperspectral images in space applications.

2. Background

2.1. Hyperspectral Image

Hyperspectral images are three-dimensional structures of pixels, where each pixel is represented in an (x, y, z) coordinate system. Each layer of the z axis is a matrix representing a single image at a given electromagnetic spectrum frequency. The dimensions of this structure can be on the order of hundreds or thousands of bands in some cases [6].

The sensing through this large number of bands turns this type of image into a structure with a high volume of data, and in space systems, it affects the storage capacity, processing, and even transmission of this image to a ground station. For example, the HyspIRI sensor developed by NASA can produce up to 5 Terabytes of data per day [7]. Images such as that obtained by the HyspIRI sensor are ideal candidates for data compression.

2.2. CCSDS 123.0-B-2

CCSDS 123 is a low complexity multispectral and hyperspectral image compression standard for implementation in space systems, created by the Consultative Committee for Space Data Systems (CCSDS). The current standard has specifications for the development with the availability of lossless or near-lossless compression.

A system that follows the CCSDS 123 standard consists of two main blocks, a predictor block and an encoder block seen in Figure 1. The prediction block uses the samples of the image to be compressed and performs the prediction of the sample value, generating at the end a prediction residue, which is the difference between the actual sample and the predicted value. The encoder is responsible for encoding the residues and generating a compressed HSI at the end.

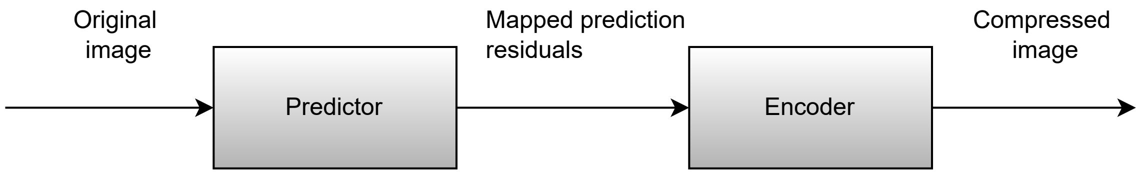

Figure 1: Overview of the compressor block.

Some compression and encoding settings can be chosen based on the available specification, which impacts how the samples are predicted and encoded. In the end, these choices can change the image compression ratio, hardware resources used, and the runtime for processing a sample.

2.3. High-level synthesis

High-level synthesis tools allow the creation of a hardware project from a high-level language, such as C/C++. The compiler in the tool is intended to perform the entire process of converting the written code to hardware [8]. The hardware creation process starts from the code specification, with the synthesis tool being responsible for the whole process of creation and resource allocation, as well as the generation of the hardware description representing the design at the register transfer level (RTL).

HLS tools automatically or semi-automatically generate a custom architecture to efficiently implement the specification. In addition to memory banks and communication interfaces, the generated architecture is described at the RTL and contains a data path (registers, multiplexers, functional units, and buses) and a controller as required by the data specification and design constraints.

3. Related works

Pereira et al. [9] present an FPGA implementation of the CCSDS 123.0-B-1 prediction stage. The architecture was developed using the reduced prediction mode. It is highlighted that the accelerator has several configurable parameters that control the compression ratio and the silicon resources used. The accelerator architecture was tested and validated on a Zynq-7000 FPGA using a hyperspectral image from AVIRIS sensor and comparing the result with the Empordá software, reporting a throughput of 20.4 MSamples/s at a frequency of 142 MHz.

Orlandić et al. [10] present the VHDL implementation of the complete compression algorithm of the CCSDS 123.0-B-1. The authors compared resource utilization and performance between different pipeline levels for compression. The tests were performed using a Zynq-7035 FPGA, where the authors highlighted their best solution with a throughput of 750 MSamples/s at a maximum frequency of 150 MHz.

Báscones et al. [11] implemented the compression algorithm of the CCSDS 123.0-B-2 standard in VHDL. The authors present an implementation with a high pipeline level between compression steps, exploring a new ordering model for the samples. The compressor was tested and verified on a Virtex-7 VC709 FPGA, highlighting that the compressor can process one sample per cycle at up to 250 MHz, ideal for meeting real-time requirements.

Barrios et al. [12] implemented the prediction and encoding steps of the CCSDS 123.0-B-2 standard, exploiting the HLS methodology. The compressor was validated on a Kintex Ultrascale FPGA. The authors report that the HLS compressor has a throughput of 12.5 MSamples/s at a maximum frequency of 125 MHz. Furthermore, the authors performed a comparison of results with another work, but implemented in HDL.

4. Implementation

The hyperspectral image compressor was based on the current version of the CCSDS compression standard(123.0-B-2). The compressor is designed to perform lossless compression and implement the prediction and coding steps.

4.1. Prediction

The calculations of the prediction process that involve part of the compression process are separated by sub-steps such as local sum, local difference, weights and local differences vector, central prediction, and mapped quantizer index, described below.

4.1.1. Local sum

The first step of the compressor consists of a local sum between samples from the same spectral band. Each sample is represented by $s_{z,y,x}$ through the coordinate system, or by the index t, defined as $(t = yN_x + x)$. It can be seen in Figure 2 that there are three options for performing the local sum, wide neighbor-oriented, narrow neighbor-oriented, and column-oriented.

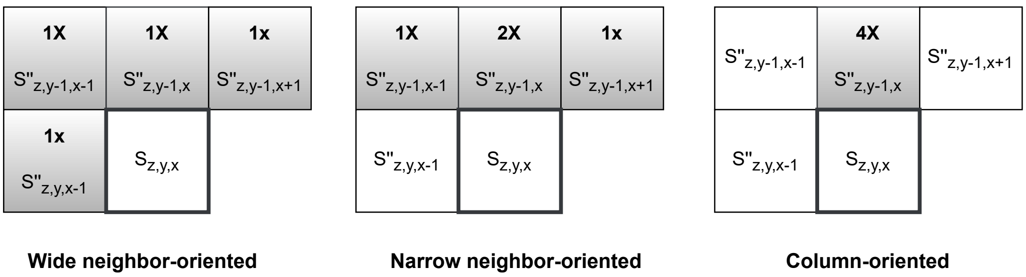

Figure 2: Local sum calculation options.

The current compression standard uses representative samples $s''_{z,y,x}$ that differ from the original sample used for the local sum calculation. However, this model is only used when lossy compression is desired, which is not the goal of this work.

4.1.2. Local difference

The local difference calculation is performed considering the local sum calculated previously. As shown in Figure 3, the local center difference considers the current center pixel and performs the local directional differences N, NW and W, but they are not used in the reduced prediction mode.

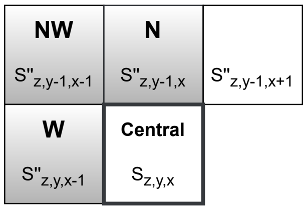

Figure 3: Local and directional center difference.

To calculate the central local difference when the chosen prediction mode is reduced, we have the result being four times the current sample minus the local sum calculated earlier.

4.1.3. Weights and local difference vectors

The local difference vector $U_z(t)$ is used to store C_z user-defined local differences, which are later used to compute the predicted value of the sample $\hat{s}_z(t)$. On the other hand, the weight vector $W_z(t)$ stores C_z values that will be used in the prediction by multiplying them by the vector of local differences.

4.1.4. Predict

For the prediction calculation, the local central difference prediction $\hat{d}_z(t)$ is first performed, being the multiplication between the weight vector $W_z(t)$ and the local difference vector $U_z(t)$. Then, the high-resolution predicted sample value $\breve{s}_z(t)$, the double-resolution predicted sample value $\tilde{s}_z(t)$, and finally, the predicted sample value $\hat{s}_z(t)$ is calculated. These calculations are necessary to get the mapped quantifier index $\delta_z(t)$, which represents the output of the predictor, and its calculations can be checked in the pattern specification.

4.1.5. Mapped quantized index

After the previous calculations, the output value of the predictor is obtained, called the mapped quantized index $\delta_z(t)$. For this, a quantized index $q_z(t)$ is used, calculated by considering the difference between the value of the current sample $s_z(t)$ and the value of the predicted sample $\hat{s}_z(t)$, called the prediction residue $\Delta_z(t)$.

At the end, each mapped quantized index is sent to the encoding block, responsible for encoding each sample of the image using some method from the specification, generating the final compressed image.

4.2. Encoding

The encoder is responsible for receiving the samples from the predictor block and encoding them using one of the methods presented in the specification. In general, the encoder should generate at the end a file that has a header and body structure of variable sizes specified by the user.

The header contains a series of information, such as the specification of the method used to perform the prediction and encoding, as well the information about the image that is being compressed.

The body of the compressed image should contain the data generated by the entropy encoder used for the implementation. In this project, the sample-adaptive entropy coder was implemented, since by specification it shows better compression results in the reduced and lossless prediction mode.

In this encoding method, each mapped quantifier index $\delta_z(t)$ must be encoded using a variable-length binary codeword. The specification standard uses variable-length words called Golomb-Power-of-2 (GPO2), represented as $\Re_k(\delta_z(t))$.

4.3. HLS Project

Figure 4 presents an overview of the prediction block implementation in HLS, where each block corresponds to a step in the described compression process. Each step was implemented in C Language using Xilinx Vitis HLS 2021.1.

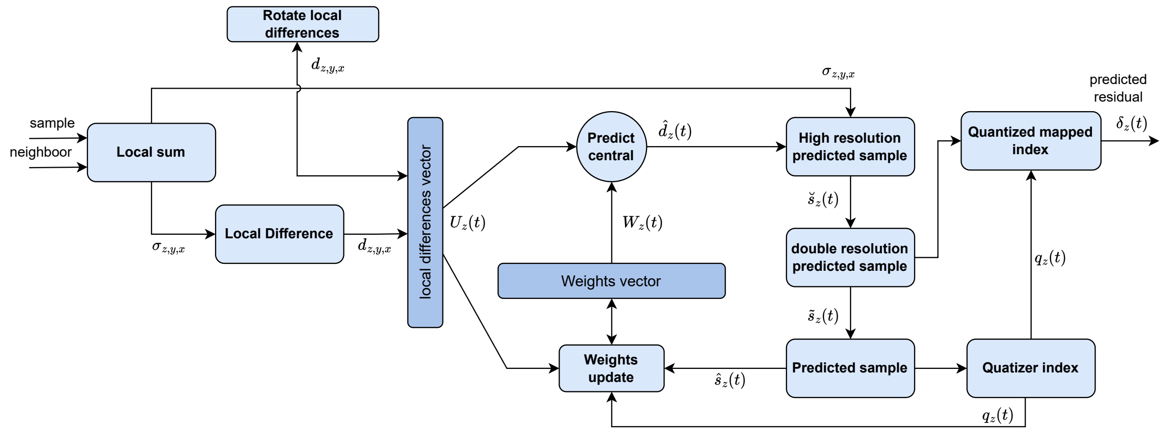

Figure 4: HLS implementation of the predictor block.

The implementation of the encoding block (Figure 5) follows the sample adaptive encoding model and receives the prediction residual calculated by the previous block as the input value. The output form of the variable length words $\Re_k(\delta_z(t))$ can change according to the calculations performed by the compressor.

The compressor implementation was aimed to reduce the implementation complexity and logic resource usage. Thus, the compressor was implemented over the reduced prediction mode and configured to perform the sample processing in Band-Interleaved by Pixel (BIP) order with the column-oriented local sum, which decreases the dependency between pixels and the complexity of the implementation. The parameter values in each step were chosen by observing the features and compression results best fitting for the observed predictor and encoder implementation model [13].

Furthermore, the HLS compressor has been implemented in two modes, with and without compiler optimization directives. The directives that were applied inform the synthesis tool on how to generate hardware in the specific parts where the directive has been inserted, which can be optimized to reduce resource usage or latency. Some of the directives used were:

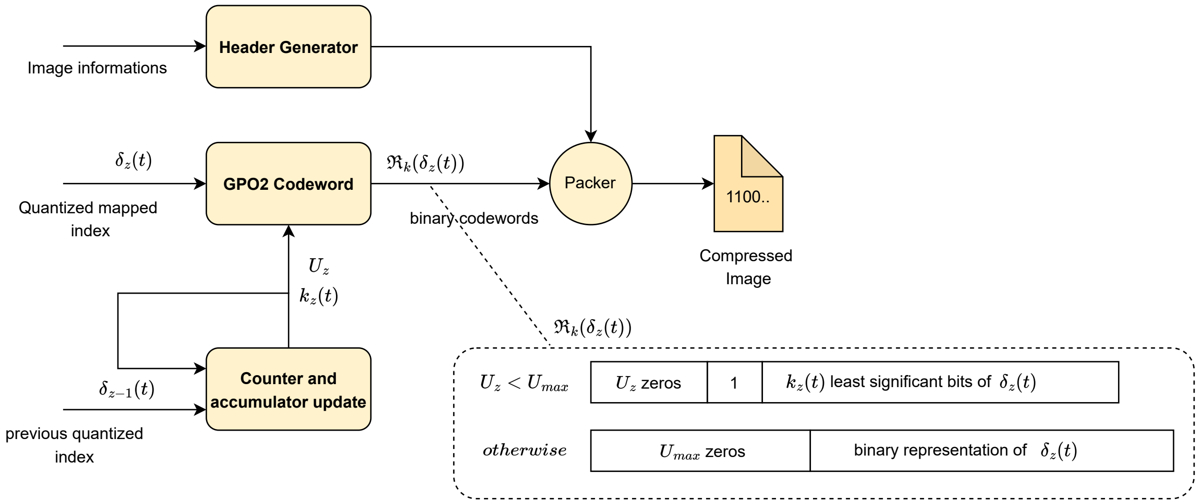

Figure 5: **HLS implementation of the encoder block.**

1. **Array Partition**: forces the compiler to partition the memory vectors into smaller blocks and allocate them in registers, allowing simultaneous access to the data.
2. **Unroll**: enables the operations contained in a repetition loop to be executed in a single clock cycle, usually using more logic resources.
3. **Pipeline**: allows you to create the hardware in parallel and with specific pipeline levels so that the startup interval of a new calculation is reduced.

4.4. Hardware Implementation

We used a Zedboard Zynq-7000 board with an ARM Cortex-A9 to prototype the developed compressor. Figure 6 illustrates the system integrated with the compressor via an AXI4-Lite communication interface. In addition, the compressor has an interrupt signal connected to the ARM processor global interrupt controller, used to inform when a sample has been compressed.

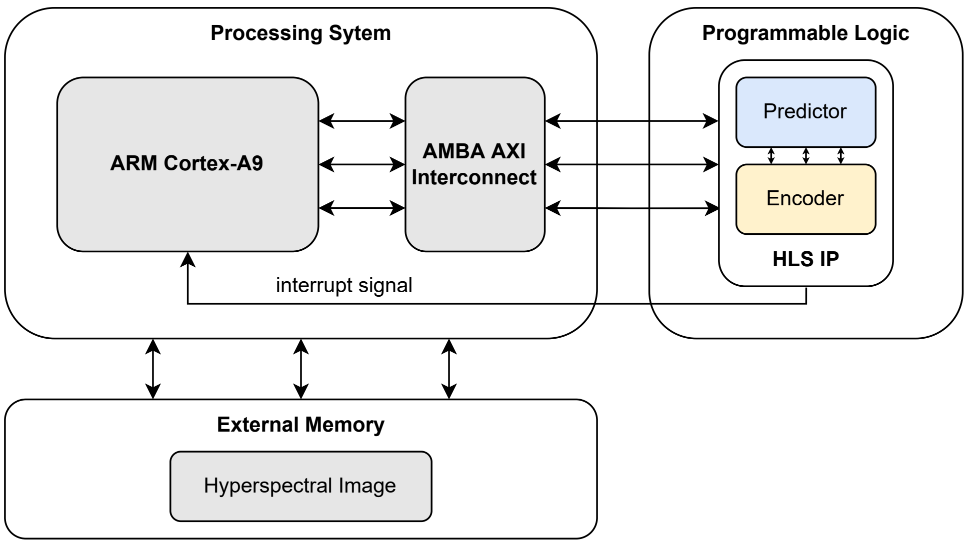

Figure 6: **Implemented system overview.**

The main processor is responsible for collecting the image from the system memory through an SD card and sending the samples to the compressor. As each sample image is processed, the interrupt signal is active informing the main processor that the compressed sample can be read.

5. Results

For the validation of the compressor, a test pattern image provided by CCSDS was used. In order to validate the application, the final compression result was compared with the reference implementation of the Empordà software, developed by the Universitat Autonoma de Barcelona [14].

The synthesis results were collected using the Xilinx Vivado 2021.1 tool. Table 1 presents the results obtained for the implementations with and without optimization directives, compared with the synthesis results obtained from the related work.

Table 1: Synthesis results comparison with related work.

Implementation	FPGA	LUTs	FFs	DSPs	BRAMs
[9]	Zynq-7000	2244	630	3	-
[10]	Zynq-7035	14709	12830	-	37
[11]	Virtex-7 VC709	16458	15707	30	187
[12]	Kintex XCKU40	17185	11915	63	85
HLS standard	Zynq-7000	3025	2625	14	1
HLS optimized	Zynq-7000	4014	3727	3	0

Among the two implemented solutions, the implementation with optimizations used about 78% less DSPs, but uses 33% more LUTs and 42% more FFs than the solution without optimizations. It is worth mentioning that the optimizations applied in the optimized solution aim to reduce the latency between the processing of the image sample, thus achieving higher throughput.

The HLS work of [12] demonstrates that the use of a HLS tool can infer a high usage of logic resources that match with [10, 11] but has a much lower performance in terms of throughput that can be seen in Table 2. The proposed compressor uses about 4x less LUTs, 3x less FFs, 21x less DSPs, and a higher throughput and energy efficiency than [12].

However, when compared to works that implement the compressor in HDL, this work has a lower performance in terms of throughput and energy. The works of [10, 11] exploits a high level of parallelism between compression steps to achieve this performance and thus has a higher logical resource utilization, except for [9] which has a lower resource utilization but implements only the prediction step.

The compressor was also tested on the Zynq-7000 SoC in a system to measure the compression application's acceleration, as shown in Figure 6. The system was initially configured to perform image compression only by the ARM Cortex-A9 processor with the same C code used to create the compressor. Then, the ARM processor is only used for sending the samples to the accelerator, which is in charge of the entire compression step.

Table 2: Performance comparison with related work.

Implementation	FPGA	Fmax (MHz)	Power (mW)	Troughtput (MSa/s)	Energy* (uJ)
[9]	Zynq-7000	142	106	20.4	5.22
[10]	Zynq-7035	150	515	750	0.68
[11]	Virtex-7 VC709	250	732	250	2.93
[12]	Kintex XCKU40	125	500	12.5	40.00
HLS standard	Zynq-7000	144	153	3.6	41.47
HLS optimized	Zynq-7000	92	138	13.2	10.45

* Energy consumed to process 1MSa.

Table 3 presents the captured execution times between the two execution modes. The image used in this test was from the AVIRIS-NG sensor in raw format, obtained from the database provided by the CCSDS Data Compression Working Group [15].

Table 3: Execution time for compression on Zynq-7000.

Implementation	Execution time* (ms)	Acceleration
Software (ARM)	56.38	-
Hardware (HLS optimized)	34.86	1.62

*Execution time to compress an AVIRIS-NG (30x50x7) image.

The obtained results seen in Table 3 make it possible to highlight that the compressor in HLS was able to accelerate the HSI compression application by 62% compared to the ARM processor running at 667 MHz. Thus, the solution is shown to be capable of accelerating such an application by moving the software routines to dedicated hardware through the HLS design.

6. Conclusion

This work performs the implementation of a lossless HSI compressor based on the CCSDS 123.0-B-2 standard using the HLS methodology. The implementation was aimed to reduce the complexity of implementation and low resource utilization for application in space systems.

We compared the achieved throughput with works developed in HDL and HLS. It was possible to observe a higher throughput and an energy efficiency compared to the HLS-related work. We also compared the compressor with a software implementation to measure the acceleration.

For future work, we intend to implement the compressor in HDL to explore higher level of data parallelism. We also intend to use an AXI4-Stream interface with a DMA system to accelerate the compression application, removing the time-consuming data read and write confirmations and transmission checks of the AXI4-Lite interface.

Acknowledgments

This work was supported in part by the Foundation for Support of Research and Innovation, Santa Catarina (FAPESC-2021TR001907), and the Brazilian National Council for Scientific and Technological Development (CNPq - processes 138179/2021-2 and 140368/2021-3).

References

[1] S. Pasricha, N. Dutt, On-Chip Communication Architectures: System on Chip Interconnect, Morgan Kaufmann Publishers Inc., San Francisco, CA, USA, 2008.

[2] L. Zhu, J. Suomalainen, J. Liu, J. Hyyppä, H. Kaartinen, H. Haggren, et al., A review: Remote sensing sensors, Multi-purposeful application of geospatial data (2018) 19–42.

[3] CCSDS, The consultative committee for space data systems, Disponível em: `https://public.ccsds.org`. Acesso em: 25 novembro 2021, 2021.

[4] CCSDS, Low-complexity lossless and near-lossless multispectral and hyperspectral image compression, Disponível em: `https://public.ccsds.org/Pubs/123x0b2c3.pdf`. Acesso em: 25 novembro 2021, 2019.

[5] J. de Fine Licht, M. Besta, S. Meierhans, T. Hoefler, Transformations of high-level synthesis codes for high-performance computing, IEEE Transactions on Parallel and Distributed Systems 32 (2020) 1014–1029.

[6] G. Lopez, E. Napoli, A. G. Strollo, Fpga implementation of the ccsds-123.0-b-1 lossless hyperspectral image compression algorithm prediction stage, in: 2015 IEEE 6th Latin American Symposium on Circuits & Systems (LASCAS), IEEE, pp. 1–4.

[7] S. J. Hook, K. Turpie, S. Veraverbeke, R. Wright, M. Anderson, A. Prakash, J. Mars, D. Quattrochi, et al., NASA 2014 the hyperspectral infrared imager (HyspIRI)–science impact of deploying instruments on separate platforms, Technical Report, Pasadena, CA: Jet Propulsion Laboratory, National Aeronautics and Space . . . , 2014.

[8] P. Coussy, D. D. Gajski, M. Meredith, A. Takach, An introduction to high-level synthesis, IEEE Design & Test of Computers 26 (2009) 8–17.

[9] L. M. Pereira, D. A. Santos, C. A. Zeferino, D. R. Melo, A low-cost hardware accelerator for ccsds 123 predictor in fpga, in: 2019 IEEE International Symposium on Circuits and Systems (ISCAS), IEEE, pp. 1–5.

[10] M. Orlandić, J. Fjeldtvedt, T. A. Johansen, A parallel fpga implementation of the ccsds-123 compression algorithm, Remote Sensing 11 (2019) 673.

[11] D. Báscones, C. Gonzalez, D. Mozos, A real-time fpga implementation of the ccsds 123.0-b-2 standard, IEEE Transactions on Geoscience and Remote Sensing 60 (2022) 1–13.

[12] Y. Barrios, A. Sánchez, R. Guerra, R. Sarmiento, Hardware implementation of the ccsds 123.0-b-2 near-lossless compression standard following an hls design methodology, Remote Sensing 13 (2021) 4388.

[13] I. Blanes, A. Kiely, M. Hernández-Cabronero, J. Serra-Sagristà, Performance impact of parameter tuning on the ccsds-123.0-b-2 low-complexity lossless and near-lossless multispectral and hyperspectral image compression standard, Remote Sensing 11 (2019) 1390.

[14] GICi, Ccsds 123.0-b-1, `http://gici.uab.cat/GiciApps/EmpordaManual.pdf`, 2011. (Accessed on 08/19/2022).

[15] CCSDS, Space Link Services Area (SLS), `https://cwe.ccsds.org/sls`, 2022. (Accessed on 09/14/2022).

CONASAT-1 Cubesat: Integration of Environmental Data Collector

Alessandra U. Rodrigues[1], **Alysson P. Lima**[1], **Manoel J. Carvalho**[1], **Samaherni M. Dias**[2], **José M. Duarte**[1], **Jefferson A. Silva**[1]
[1] National Institute for Space Research (INPE), Natal, RN, Brazil, email
[2] Federal University of Rio Grande do Norte (UFRN), Natal, RN, Brazil

Keywords: *CubeSat mission, Flight software, Environmental data collection.*

This paper describes the integration of a payload into a nanosatellite. The project that is developing this integration has the goal to renew and continue the Brazilian Environmental Data Collection System, a system that needs environmental data from all the national territories for weather forecasting and climate studies. To achieve this goal, the system needs a platform for data collection, satellites that receive environmental data and send it back to the Earth, and ground stations that receive the data sent by the satellites. This article uses the CONASAT's project, developed by INPE-Natal, which has a CubeSat, class of a nanosatellite with a square-shaped, named CONASAT-1, and to process the environmental information that came from the ground stations, the satellite has a payload named Environmental Data Collector (EDC). To make the integration and functionality of the EDC with the platform was created a flight software based on C language with an operating system, FreeRTOS, which works through tasks for keeping the satellite working. For this was developed five tasks responsible for the supervision, monitoring, and data sending, and also four modes of operation that define all the actions necessary for the satellite operation, and the sending of the environmental data back to the ground stations.

1. Introduction

In the 90s, intending to provide the country with environmental data on the national territory, started the Brazilian Environmental Data Collection System (BDCS) with the launch of the satellite SCD-1 in 1993. Over the years the BDCS has grown with the launch of a few more satellites, but currently, most of these satellites are at the end of their useful life, which makes necessary new satellites for keeping the supply of data to monitor the territory [1].

Besides the satellites, ground stations and Data Collection Platforms (DCPs) also make up the BDCS [2]. The DCPs are small stations, usually installed at remote places, that send environmental data to the satellites, among the main data are meteorological (temperature, pressure, wind direction and speed, humidity)[3]. Those data are transmitted by the satellite and used in weather forecasts, ocean currents, tides, etc. Figure 1 below, shows a configuration of the BDCS with DCPs, ground stations, and a satellite.

Currently, the BDCS is compound for two ground stations (Cuiabá and Alcântara) for control and receive data, approximately 500 DCPs spread over several regions of the country and a few satellites, among them SCD1, SCD2, CBERS1, Floripasat, and Amazonia 1.

As the number of satellites in the BDCS is small and some of them are at the end of their useful life, the project CONASAT was created as an innovative solution

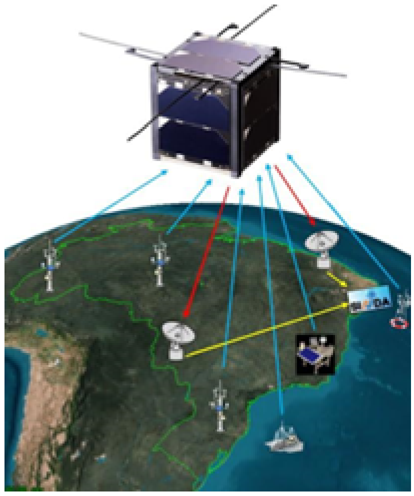

Figure 1: BDCS Illustration

for the space segment, based on a constellation of low-cost nanosatellites, to provide continuity to the BDCS[4].

The CONASAT-1, the first satellite of the constellation, is 1U CubeSat has a cubic shape, edges of 10 centimeters, and uses commercial off-the-shelf components (COTS) for its structure and electronics. The CubeSat design specification was created in the USA to provide a standard for the design of picosatellites to reduce cost and development time, increase accessibility to space, and sustain frequent launches[5]. The CONASAT has its hardware developed by the company EnduroSat and a payload developed by INPE'S (National Institute of Space Research) Northeast Space Coordination (COENE).

CubeSat can be targeted to various missions, an example is when they integrate a payload such as an image processing providing images for monitoring purposes of vast territories, borders and deforestation [6]. Another application of nanosatellites is an integration with the Global Navigation Satellite System (GNSS) which provides location and navigation but also studies the Earth's atmosphere, oceans, and land surface [7].

The CONASAT's payload is the Environment Data Collector (EDC), it is compatible with Cubesats platforms and was developed, as the satellite, as a low-cost and low-power solution to renew and expand the BDCS[8]. The EDC is a transponder of signals coming from the DCPs, with onboard decoding, capable of decoding up to 12 DCPs at the same time.

The focus of this paper is the integration and functioning of EDC with the CONASAT-1's platform, for this was developed a flight software responsible for the mission of the project. This software is based on a previous code made by EnduroSat, in which was added the entire interface communication with the EDC and a routine for its functioning, named EDC Mode. The goal of this mode is to monitor and supervise the satellite while the EDC is on, ensuring that the satellite keeps working properly and if something is not as it should take appropriate action.

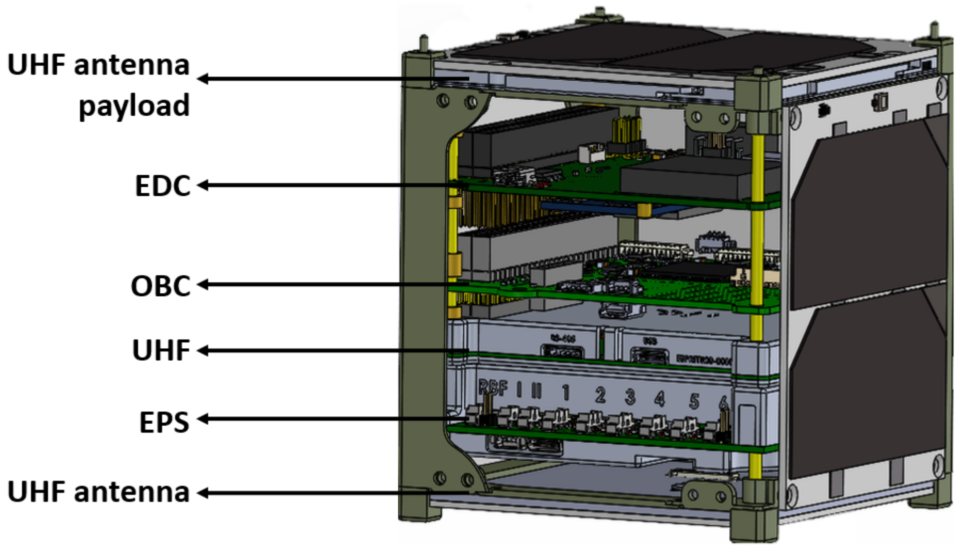

Figure 2: Architecture of CONASAT-1

2. CONASAT's Cubesat

The CONASAT-1 platform comprises the integration of antenna subsystem, power management subsystems (EPS), communications and command (UHF), data manipulation capabilities (OBC), attitude determination and control (ADCS), provided by EnduroSat, and the EDC as a payload, provided by INPE.

CONASAT-1's hardware is divided into subsystems, as in Figure 2. The communication with the satellite is established through an Ultra-High Frequency (UHF) half-duplex. This subsystem is a transceiver that uses a 2GFSK modulated signal with a typical baud rate of 9600 bps, a frequency offset of 2400 Hz, and a modulation index of 0.5. All of these communication features are controlled by EnduroSat's telemetry and telecommand protocol (ESTTC).

The entire platform is powered by the Electric Power System (EPS), which includes a battery with a capacity of 10.2 Wh and several voltage rails. Of this capacity, a typical OBC power consumption is approximately 0.2 W, for the EPS subsystem 0.08 W, UHF 1.25 W, and EDC 1.1 W.

The Onboard Computer (OBC) is the main control and data processing system on the platform, its functions are to control all other subsystems, collect and transfer data and perform attitude control-related calculations and commands. This subsystem is built on an ARM Cortex M4 microcontroller, which runs a FreeRTOS (CMSIS) instance as the basis for embedded software designed in a 4-layer structure, as shown in Figure 3. Also at the OBC runs the software of attitude determination and control, this subsystem is responsible for the satellite's orientation, it has sensors (solar sensors, magnetometers, gyroscope) to determine the satellite position and actuators (magnetorquer) to control it, this hardware it is spread over the satellite: solar sensor, gyroscope, and magnetorque are at the solar panels and the magnetorquer is on the OBC.

All embedded software was programmed in C language, and with the presence of the FreeRTOS scheduler, there are concurrent programming paradigms. The first layer presented in Figure 3 is dedicated to the software libraries for the microcontroller

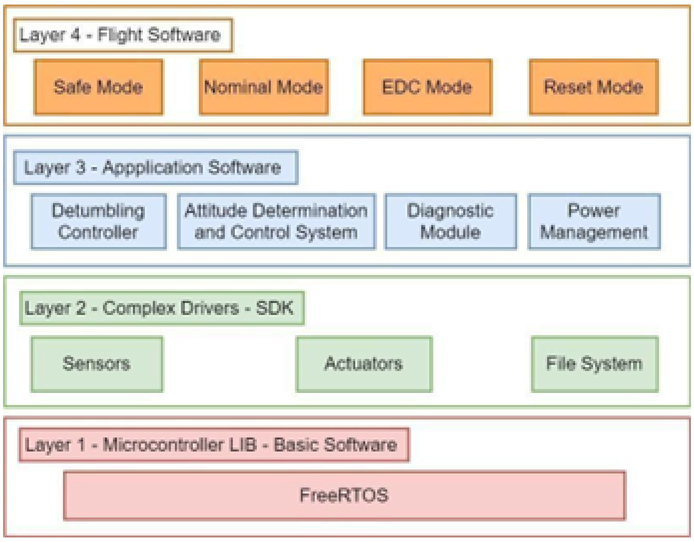

Figure 3: Layers Structure of the embedded software

peripherals, including the real-time operating system. The second layer includes the software drivers for the sensors — gyroscope, accelerometer, magnetometer, solar sensors, and actuators — magnetorquer. The third level of abstraction includes any application software for satellite stabilization and control, diagnostics, power management, etc. Finally, the focus of this work is the fourth level, which includes applications for satellite operation, integration with the payload, and manipulation of collected data.

The upper layer, shown in Figure 3, is the Flight software developed for CONASAT-1, this software layer controls the satellite and sends requests to the lower layers. Flight Software includes several tasks that are running, those tasks include, but are not limited to:

- EDCColetEnv – Linked to the payload (EDC), activate the decoding of payload signals, request collected data, and send this data to ground stations;
- Beacon - To transmit a beacon to locate the satellite and transmit specific health data from the satellite;
- Supervisor – Connected to the payload (EDC), monitor data from the sensors to guarantee, in case of a contingency, protection actions;
- StartDefaultTask – Start sensors, print on both communication channels, and monitor task crashes;
- ESTTC_UART_TASK – Check and process new commands.

In addition to the tasks, the satellite also has several modes, where each mode is a combination of certain tasks, as shown in Figure 4. In addition, the satellite can transition from one mode to another by remote controls or under certain circumstances that can be defined. There are four implemented modes:

- Nominal: satellite only emits Beacon signaling. Maintenance telemetry can be collected and downloaded to ground stations when in view.

- Safe: satellite being kept secure (only critical systems turned on).
- EDC: operations with payload activation, data request from DCPs, data manipulation, and sending to ground stations when it flies over Brazilian territory.
- Reset: satellite prepared for reset (only the task - ESTTC_UART_TASK).

CONASAT		Modes			
		Reset	Safe	EDC	Nominal
TASKS	Supervisor			✓	
	Beacon		✓	✓	✓
	SendCollect			✓	
	StartDefault		✓	✓	✓
	ESTTC Uart	✓	✓	✓	✓

Figure 4: Modes and Tasks Overview

3. Integration of Environmental Data Collector

The EDC is physically integrated into the platform by a PC-104 connector, as are all the subsystems, and it is located above OBC. Is it responsible for receiving and decoding BDCS and Argos-2 signals in the 401.635 MHz ± 30 kHz frequency range. Its receiver is capable of decoding up to 12 signals simultaneously and storing up to 64 decoded messages in its memory. However, it is important to highlight that all the reception and decoding of signals performed by the EDC is done autonomously when a telecommand is processed by the OBC activating this subsystem.

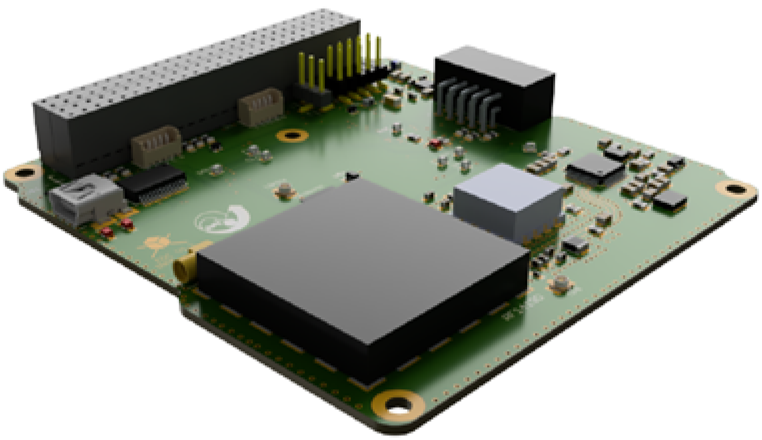

Figure 5: EDC

Furthermore, the EDC does not have a direct interface with the ground stations, it depends precisely on the OBC software, which is solely responsible for operating the EDC, requesting decoded data, handling and sending the ground stations via the UHF subsystem. The EDC has communication by I2C or RS-485, but in this project they are not used, all the communication between EDC and OBC is done by UART, as Figure 6, and using the driver development by the EDC team, some functions of this driver will be seen later, as EDC_Resume, EDC_PTT_POP, EDC_GetState, etc.

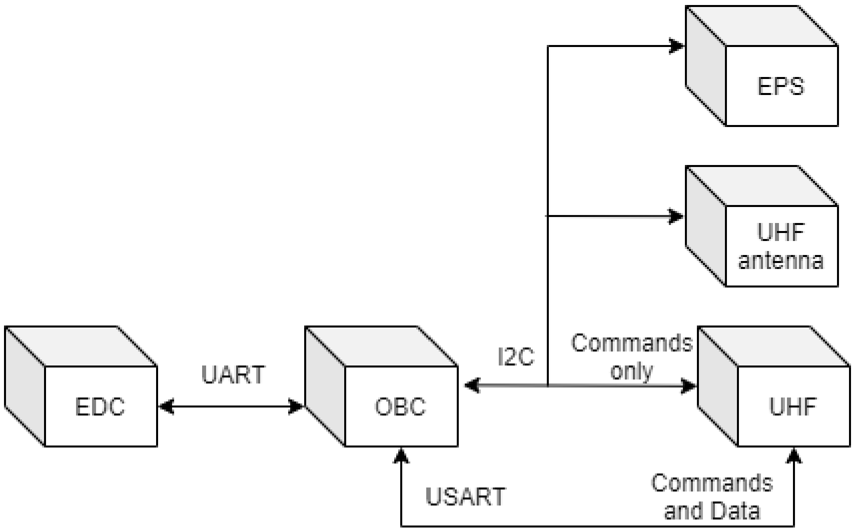

Figure 6: Communication channels between subsystems

The integration of CONASAT-1 with the EDC is fundamental to the BDCS's mission. To understand our contribution to this system it is necessary to detail the EDC mode. This mode is activated by telecommand from ground stations and governed by 4 concurrent tasks – EDCColetEnv, Supervisor, StartDefaultTask, and ESTTC_UART_TASK. The EDC's operation from its activation, by remote controls, to the transmission of its data, undergoes special characteristics. The EDC mode was programmed to operate only upon request from the stations on the ground and is automatically switched off by a 10-minute software timer after the start of the operation, in case of no change in the operating time.

3.1. Supervision task

The Supervision task aims to maintain the integrity of the EDC Hardware, by monitoring some electrical parameters provided by sensor readings present on the payload board. Among the parameters checked are voltage, currentSupplyD, currentSupplyA, and temperature. In summary, these parameters are obtained by the generation of housekeeping and compared individually with limits defined in the typical values, determined by the manufacturer, plus 25%. Whenever a violation of these limits is detected a counter variable is added and a new collection and verification is carried out, however when the failure counter reaches 5 detections, the EDC tasks are disabled, the subsystem is turned off and the Safe mode is activated.

3.2. StartDefaultTask

The StartDefaultTask task is responsible for ensuring the integrity of the software during EDC mode, ensuring that all tasks are running as planned. For this function, the independent watchdog (IWDG) was used to detect and resolve malfunctions due to software failures. It triggers a reset sequence when it is not updated within the expected time window, so it is up to the StartDefaultTask task periodically and with the lowest possible priority restarts the watchdog periodically. Therefore, in case the task scheduler error or any other task crashes the processing, the StartDefaultTask does not execute and the watchdog comes into action.

3.3. EDCColetEnv task

The main function of the payload is to receive signals from the Platform Transmitter Terminals (PTTs) belonging to the BDCS, for this, the EDC is composed of a Front End RF and a Processing Unit to facilitate its handling of internal data. The EDC can provide four types of data frames via telemetry: PTT Decoder Frame, HK Frame, System Status Frame, and ADC Sampler Frame, and OBC can select the output frame type at any time. Of these frames, the EDC Mode uses the first three, the PTT Frame is a package for every PTT signal received by EDC plus some order information such as frequency, power, and time; the HK Frame contains the most housekeeping information and the System Status Frame has information about the EDC currently status. The EDCColetEnv task, is an interaction routine between OBC and EDC focused on requesting PTT Decoder Frames, processing, and sending them to ground stations. Figure 7 illustrates its operation: when the satellite receives the command to turn on the EDC, is started the decoding of the PTTs by EDC PTT_Resume, next the OBC request to the EDC the HK Frame (EDC Housekeeping) and the state of the EDC (EDC Get_State), from the frame state is verified if the decoding is working, in the case it is not working, a PTT_Resume is done again, otherwise, the OBC asks the EDC a PTT Frame, in this step is verify the amount of PTT storage at the EDC and, existing a number higher than zero (state.pttAv), one by one they are sent to OBC and storage, to free space at the EDC is performed EDC PTT_POP, responsible for removing the oldest PTT package from the buffer in the EDC. This step of picking up the PTTs from EDC is done while the EDC has packages, until the next EDC Get_State. When there are no more PTTs, the OBC will mount a large package with all the PTTs storage and the housekeeping frame already received, to this package will be added to header information and then the package will be sent in several small packages of 128 bytes.

4. Integration Tests

To test, a test bench was set up with three sections: PCDs Emulator, Ground Station, and CONASAT Satellite. In Figure 8, it is possible to see that the first section is formed by a computer and a radio Universal Software Radio Peripheral (USRP), that is responsible for emulating the PCDs, this is made by simulating DCPs at the computer using the software GNU Radio, the USRP send the data emulated through RF antenna for the 401.635 MHz antenna at the satellite. The PCD data arrives at the satellite, is decoded by EDC, bundled in packages by EDCColetEnv, and sent back to the Earth through the UHF antenna at 462 MHz, which leads to the third section, Ground Station, that represents a real Ground Station, but in this case, is composed by an antenna and a UHF transceiver just like the one at the CONASAT's platform, for this setup, the ground station sends a telecommand and receive telemetry using the software ScripCommunicator.

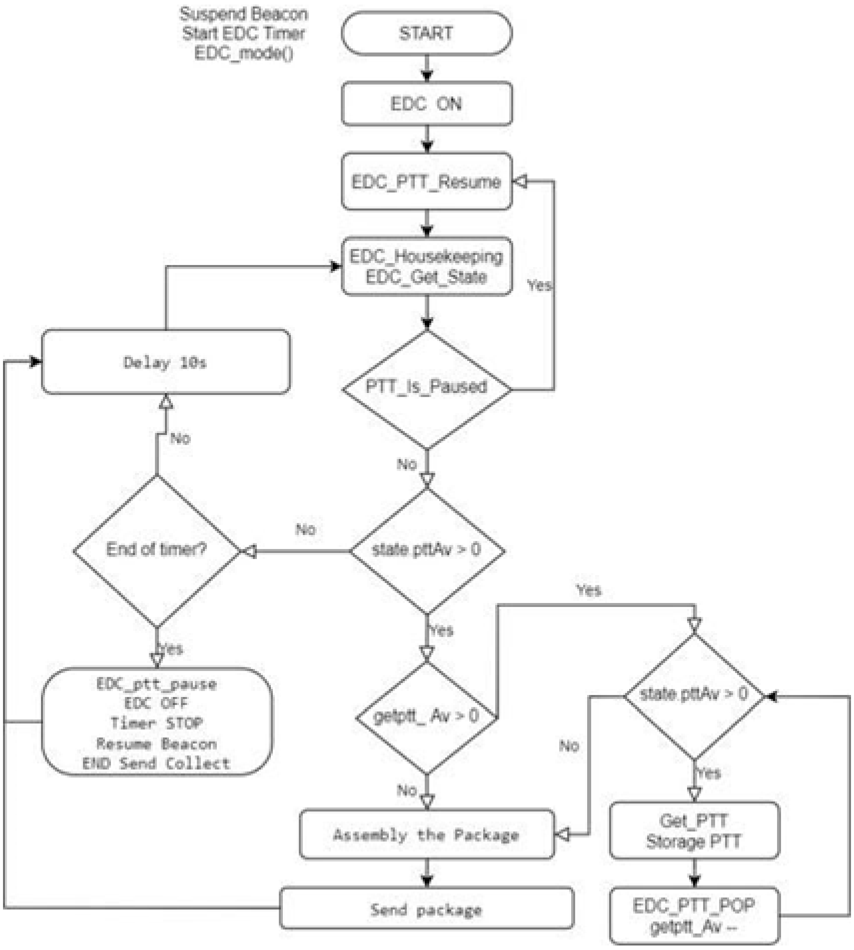

Figure 7: EDCColetEnv flowchart

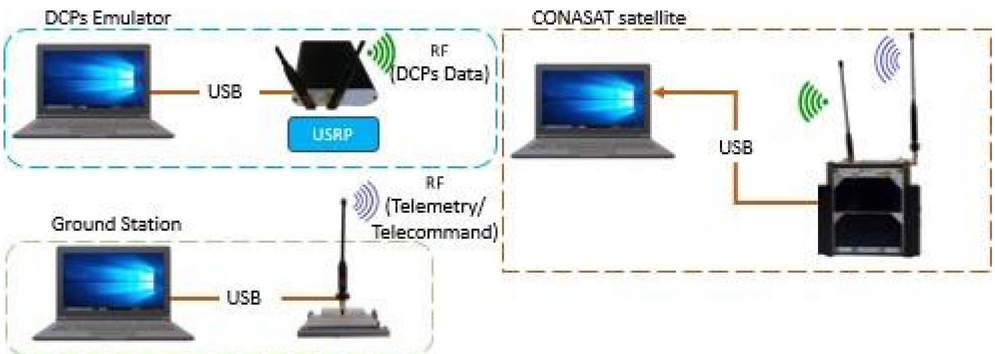

Figure 8: Test setup

4.1. EDCColetEnv test

This setup is an approximation of the BDCS made in a room of approximately 9m² in an area with 1.5 meters of distance between each section. In this room, a few tests were made to prove that the software was working as it should. The first one was in the case of normal operation, CONASAT-1 flies over Brazilian territory initially in Nominal Mode, then ground operations stations send the telecommand activating EDC mode as described in the following Figure 9, the satellite responds with a message the activation of the mode “Ok - EDC mode ON” followed by the telemetry of EDCColetEnv, the part of the message “ES+W22003323 589B0F83” it is an internal command of UHF transceiver to let it a message pass through the UHF and don’t make a part of the telemetry.

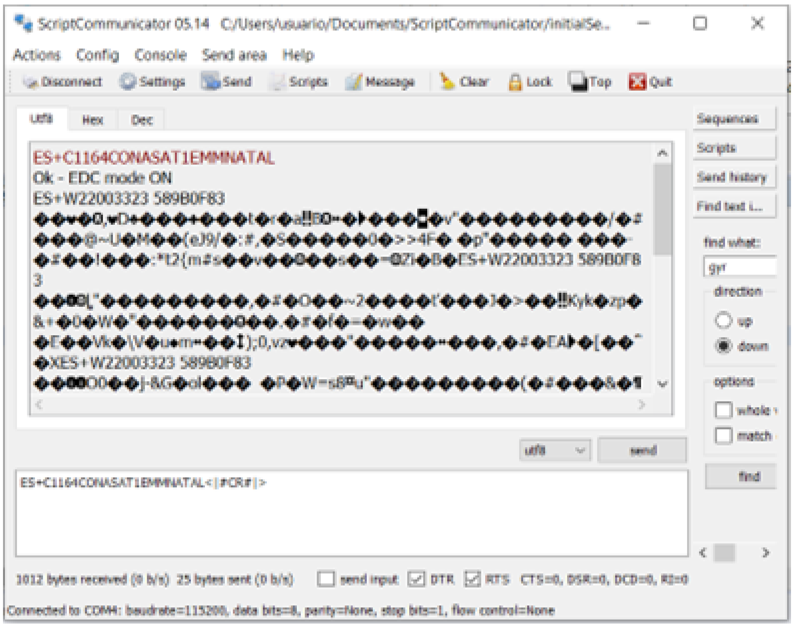

Figure 9: Reception of data collected

To check the quality of the shipment, a bit flipping was done, in 1 byte of the package, on the frames from de EDC, choose randomly. Each package has a maximum of 49 bytes, and the last of them is the checksum, which is a way to verify the frame, so the test is all about checking the checksum. The tests were made with 1000 packages and three types of tests were done, the results will be shown in the table below:

- Without bit flipping;
- With bit flipping on all packages;
- With bit flipping on 10% of the packages.

Table 1: Error identification.

Number of packages	Number of bit flipings	Identification of error(%)
	0	0
1000	1000	100
	100	10

The table above shows that the software development, for the test’s conditions (small distances and interferences), always gets right, regardless of the number of bit flipping, even in the case of inject error, the software always identifies the correct quantity of injected error, be in every package or in a few.

4.2. Supervisor task

In the same mode, for testing the StartDefaultTask task, the EDC subsystem is turned on and starts decoding the PTT signals, later the OBC requests this data releasing the EDC to collect and store new PTTs, processes and sends them to ground stations. With correct functioning, these data are requested and transmitted every 10 seconds to stations on the ground, which in turn are responsible for processing and inserting this data into SINDA. The Supervisor task periodically requests the electrical parameters of the EDC via sensors, so as soon as a violation of the tolerance limits is detected, the subsystem is turned off and its tasks are disabled, and Safe Mode is activated. The Figure 10 depicts the detection of an over voltage (listed as error 5) of 9922 mV, where the threshold is 6250 mV. To test this task, failures was simulated by increasing the value of the measurement made by the EDC's sensor measure.

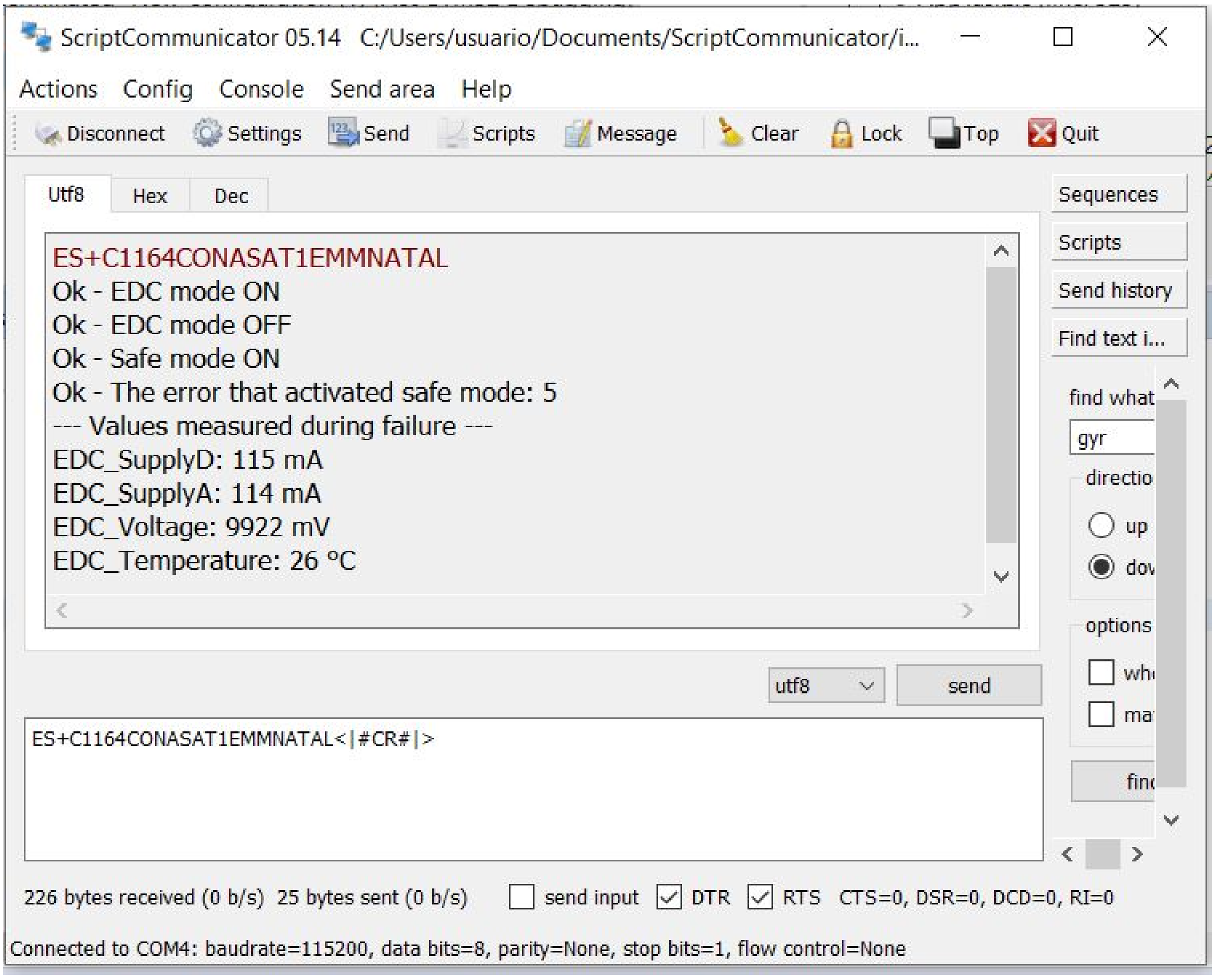

Figure 10: Supervisor Task - Result

4.3. StartDefaultTask test

For the task integrity tests, flow blocking points were inserted in order to simulate the processing crash within the tasks. One of these points is depicted in Figure 11, inserted into the EDCColetEnv task before a context switch. The fact is that as the StartDefaultTask task has the lowest execution priority, consequently these locks prevent its execution and the Watchdog refresh results in its action as shown in the following Figure 12. So if there is a lock on running tasks, platform integrity is guar-

```
        //...
        //fault injection test
        while(1){
            HAL_Delay(1000);
            fprintf(COMM, "Fault injection test \r");
        }
        HAL_Delay(5);
        osDelay(5000);//
    } // end Loop
}// end task
```

Figure 11: Fault injection test - StartDefaultTask

anteed with system reboot. During reset errors are computed, the EDC subsystem is done and tasks are disabled. Naturally, a platform reverting to Nominal Mode leads to receiving new remotes. The disadvantage of this technique is that despite avoiding blocking the platform, it is not possible to identify in which task the failure occurred. Reset is signaled for ground stations as shown in the Figure 12.

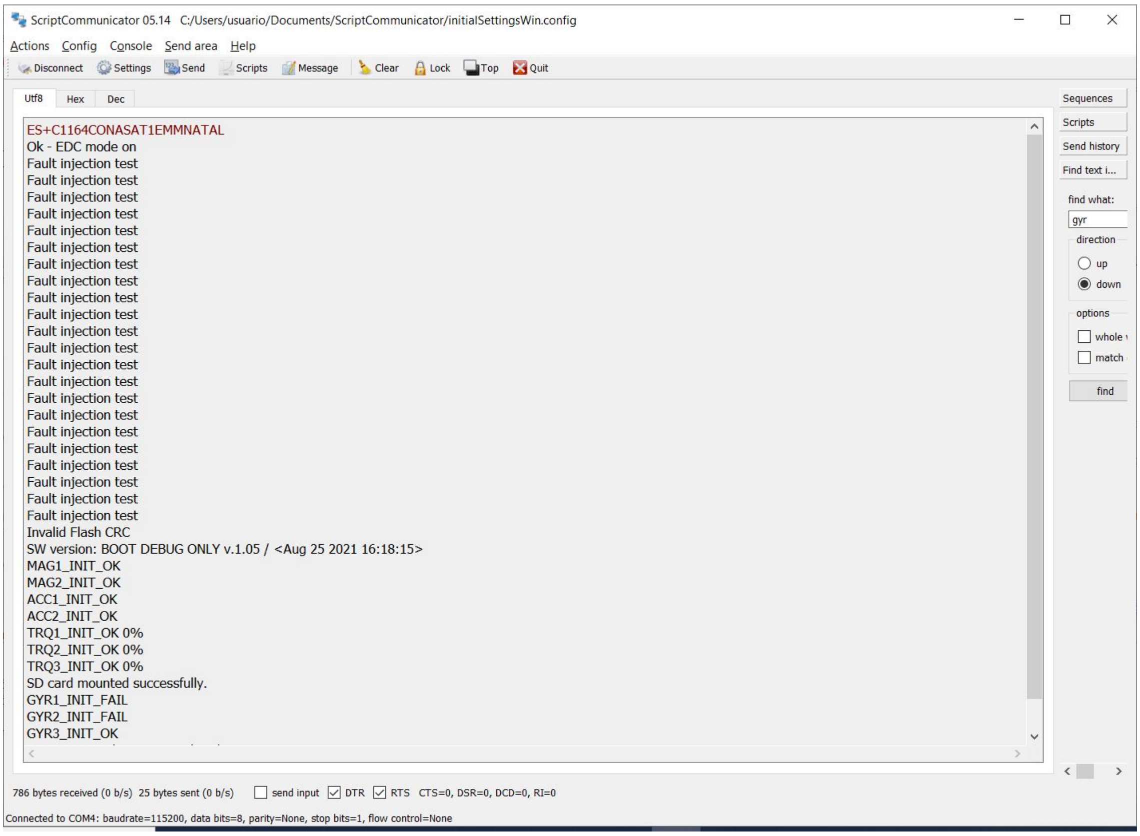

Figure 12: Fault injection test - StartDefaultTask - Result

5. Conclusion

In this article, the first version of the flight software developed for the CONASAT-1 was implemented with applications on operating modes, focusing on the integration of the platform with its payload (EDC), environmental data were received, treated, and sent to a ground station by telecommand and telemetry. Furthermore, tasks were carried out to ensure the integrity and proper functioning of the set of Hardware and Software.

The test setup intended that the design and development of the flight software meet the requirements of the platform and the mission application.

References

[1] K. P. Queiroz, S. M. Dias, J. M. Duarte, M. M. Carvalho, Uma solução para o sistema brasileiro de coleta de dados ambientais baseada em nanossatélites, HOLOS 7 (2018) 132–142.

[2] W. Y., V. O and S. P., Sistema Brasileiro de Coleta de Dados Ambientais: Status e planos futuros, in: Proceedings of the XIV Simpósio Brasileiro de Sensoriamento Remoto, Natal, RN, pp. 1633–1640. April 25-30.

[3] Instituto Nacional de Pesquisas Espaciais,INPE, Sistema nacional de dados ambientais, 2021.

[4] M. C, The New Brazilian Environmental Data Collection System, in: United Nations/South Africa Symposium on Basic Space Technology, Stellenbosch, South Africa, pp. 00–00. April 15-17.

[5] Cal Poly, Cubesat design specification cubesat design specification rev. 13 the cubesat program, 2014.

[6] D. Cahyono, A. Nugroho., Design and realization camera controller for a remote sensing payload of nanosatellite fpga (field programmable gate array) system based, in: 6th International Conference on Recent Advances in Space Technologies (RAST), Istanbul, Turkey, pp. 00–00. April 12-14.

[7] Li Qiao; E. Glennon; A. G. Dempster; S. Chaoui. , Using cubesats as platforms for remote sensing with satellite navigation signals, in: IEEE International Geoscience and Remote Sensing Symposium, IGARS, pp. 00–00. 2013.

[8] J.D. , CubeSat Payload for Environment Data Collection, in: United Nations/Brazil Symposium on Basic Space Technology, Natal, RN, pp. 00–00.

A Model-Based Mission Definition Review: the NANOSATC-BR3 CubeSat Study Case

Giulia R. Herdies(1), **Nelson J. Schuch**(2), **Eduardo E. Bürger**(3)
(1) Universidade Federal de Santa Maria - UFSM, Av. Roraima nº 1000 Cidade Universitária, Camobi, Santa Maria, Brasil, +55 12 98897-0109, giuliaherdies@gmail.com
(2) Southern Space Coordinationr - COESU/INPE-MCTI in collaboration with the Santa Maria Space Science Laboratory - LACESM/CT - UFSM, Av. Roraima, 1000 - Camobi, Santa Maria, Brasil, njschuch@gmail.com
(3) Universidade Federal de Santa Maria - UFSM,Av. Roraima nº 1000 Cidade Universitária, Camobi, Santa Maria, Brasil, +55 55 9956-6595, eduardoebrg@gmail.com

Keywords: *Model Based Systems Engineering (MBSE); Mission Definition Review (MDR);Systems Engineering; CubeSat*

The current nanosatellite from the NANOSATC-BR CubeSat Development Program, the CubeSat NANOSATC-BR3 (NCBR3), is in its concept studies phase of the development process. Being the third CubeSat developed between INPE and UFSM partnership, the NCBR3 mission has different objectives: to develop capacity building in the space sector; to study space radiation at the South Atlantic Magnetic Anomaly (SAMA) region with Brazilian data; to promote interaction between radio amateur community and small satellites, and to validate in space cutting-edge Brazilian technologies. The Project relies on the NASA life cycle phases and uses the systems engineering approach of the same space agency. According to NASA, after establishing the Concept Studies (Pre-Phase A) and as the last step of Concept and Technology Development (Phase A), it is suggested a Mission Definition Review (MDR). This review has the intention to estimate whether the proposed architecture is responsive to the performance and the functional requirements, as well as if requirements have been allocated to all functional elements of the mission. A successful and well-conducted MDR reinforces the project decisions and contributes as a baseline for the system acquisition strategy. In previous NANOSATC-BR missions, the reviews were organized through the traditional process known as document-based, which includes the use of extensive paperwork. By making the usage of documents for this type of review, revealed that several ambiguities and inconsistencies are more likely to occur. Also, it showed difficulties for configuration control in a Project involving many developers and stakeholders, such as students, professors, technicians, and scientists. With that in mind, this work proposes a method to perform Project reviews in a Model-centric approach, using the MDR of a CubeSat Project as a use case. The authors use a Model-Based Systems Engineering (MBSE) open-source software with an embedded Systems Engineering method. With the support of MBSE, the stakeholder analysis information can be broken down into operational and functional layers, allowing a global understanding of the mission. The results showed that using MBSE promotes a well-structured Review and facilitates the review process between all stakeholders with different backgrounds.

1. Introduction

The current study case is based on the development of the first review of the Project NANOSATC-BR3 (NCBR3) CubeSat. The Project takes part of a sequence of nanosatellite from the NANOSATC-BR CubeSat Development Program that aims on promoting growth in the Brazilian space area department. The NCBR3, third CubeSat, as the name suggests, is being developed by the National Institute for Space Research (INPE), through its Southern Space Coordination (COESU) in partnership with the Federal University of Santa Maria (UFSM), with support of the Brazilian Space Agency (AEB).

The NCBR3 is currently on the Concept and Technology Development, known as Phase A, by following the NASA Space Flight Project Life Cycle. As stated by [6], a small project, such as this one, may decide to combine the Mission Concept (MCR) and the System Requirements Review (SRR) with the Mission Definition Review (MDR). A MDR is a life cycle review that assesses whether the proposed mission architecture is responsive to the program functional and requirements have been allocated to all functional elements of the mission. [5] writes that the results of the reviews and measurement analysis are used to identify and record findings and discrepancies, and may lead to causal analysis and corrective or preventive action plans. These action plans are implemented, tracked, and monitored to closure.

In earlier projects the reviews were organized through the traditional process known as document-based, which includes the use of extensive paperwork. However, it was shown that several ambiguities and inconsistencies are more likely to occur, as well as, difficulties for configuration control in a Project involving many disciplines and groups. For this matter, Model-Based System Engineering (MBSE) software and systems engineering methodology is being applied. MBSE can be defined as a formalized application of modeling to assist system requirements, design, analysis, verification, and validation activities throughout all its systems engineer life cycle phases [3].

According to [2], a model-centric approach allows a easier form of traceability, more adaptability, stimulation of teamwork, and continuity to the project, in contrast to a pure document-centric approach. [1] also stated that applying MBSE since the beginning of development promotes a more consistent Project.

The main objective of this article is to promote the use of MBSE to support Project reviews contributing for a Model-centric approach, using the MDR of a CubeSat Project as a usage case.

2. Methodology

The applied methodology proposed by NASA (2016) indicates that a MDR takes place as a final review for the Phase A, component of the life cycle selected to escort the development of the NCBR3 CubeSat. This life cycle is composed by seven phases; starting with the Pre-Phase A: Concept Study and concluding with Phase F: Closeout.

The MDR, suggested by NASA, can be divided into four parts: Stakeholders Analysis and Needs Identification; Mission Analysis; Programmatic Requirements; and Concept.

To assist the review and adapt some parts in a model-centric approach, the authors, after interviewing stakeholders while focusing on the problem, documented, analyzed, and then implemented a MBSE software the operational capacities that projects stakeholders want to be able to perform.

The implemented MBSE method chosen was the Arcadia Method, stated by [7] as a structured engineering method focused on defining and validating the architecture of complex systems that are conveniently embedded into the Capella software. This method excels in comparison with other because of its unique approach, which is structured in different engineering perspectives, which establishes a clear separation between system context and needs modeling from solution modeling.

As presented in Figure 1, the method in use is divided into four different working layers: the Operational Analysis; Functional & Non-Functional Needs; Logical Architecture and Physical Architecture. Each layer may be composed of several different model views (or viewpoints). Model views may be seen as interrelated diagrams, which are different views of the same model, for example: Architectural, Hierarchical Breakdown or Scenario views.

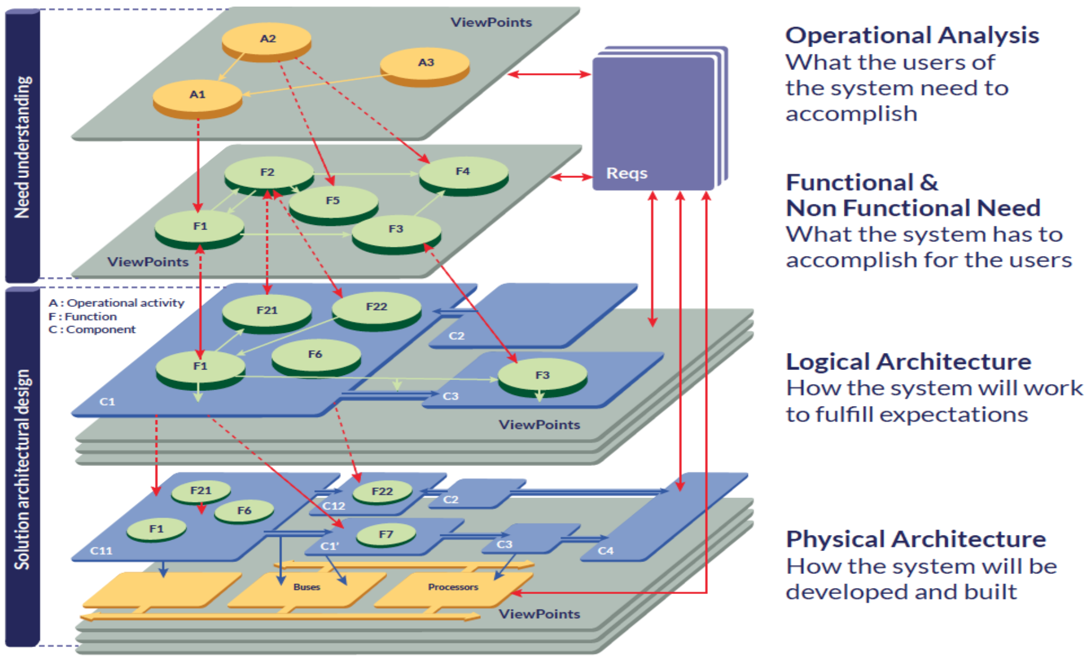

Figure 1: The Arcadia Method,[7].

Following [7] concepts, the Operational Analysis proposes a analysis of what the users and stakeholders need to achieve with the system by identifying the actors that must interact with the system, their activities and their interactions with each other. The next level is the Functional & Non-Functional Needs, that is the external functional analysis as a response to identify the system functions needed by its users, limited by the non-functional properties asked for. The Logical Architecture analyses the internal functional system, which are the sub-functions that must be carried out and put together, as well as, the identification of the logical components that carry out these internal sub-functions. For the last layer, the Physical Architecture, [7] explains that the goal of this level is the same as that of the logical architecture, except that it defines the final architecture of the system as it must be created, by adding implementation required functions and the technical choices, and highlights behavioral components that carry out these functions.

For the NCBR3 MDR, objective of this work, several model views were developed stating all of the previously mentioned modeling levels, composing the system concept. However, to meet article length size limitation, for this work it was chosen only the most comprehensive views.

3. Results and Discussion

Following the continuity of the previous missions of the NANOSATC-BR CubeSats Development Program, the NCBR3 CubeSat pre-proposed scientific mission objective is the study of space radiation and its effects on space systems. It also includes the development of capacity building in the space sector, the promotion of the interaction between radio amateur community and small satellites, and the validation of cutting-edge Brazilian technologies in space. Therefore, the group of stakeholders interviewed has needs related to these subject.

One of the first deliverables of a MDR is the Stakeholders Analysis and Needs Identification. According to [4], the stakeholder needs are transformed into a defined set of stakeholder requirements, that are able to be able to be implemented in the form of a model, a document containing textual requirement statements or both formats. In regard to the NCBR3 MDR, both forms were applied. After the primary needs from the NCBR3 stakeholders were elicited, they were analyzed and translated into stakeholders requirements through requirement analysis, and were later validated by the stakeholders.

In reference to the Arcadia Method, the first layer, Operational Analysis, pursues the stakeholders needs. The method proposes five main concepts through this level: the operational capability, operational entity, operational actor, operational activity, and operational interaction.

The Operational Capability model view, shown in Figure 2, correlates to the capabilities desired by each organization to provide a high-level objective being reached. This model view shows the interactions between stakeholders and entities with the operational capabilities. Operational capabilities can be correlated to high level stakeholders needs, actors represent stakeholders, and entities represent stakeholders organizations or external entities, such as space environment and earth. From this model view, all elements of the followings modeling levels may be traced back to these most primary needs, supporting validation process.

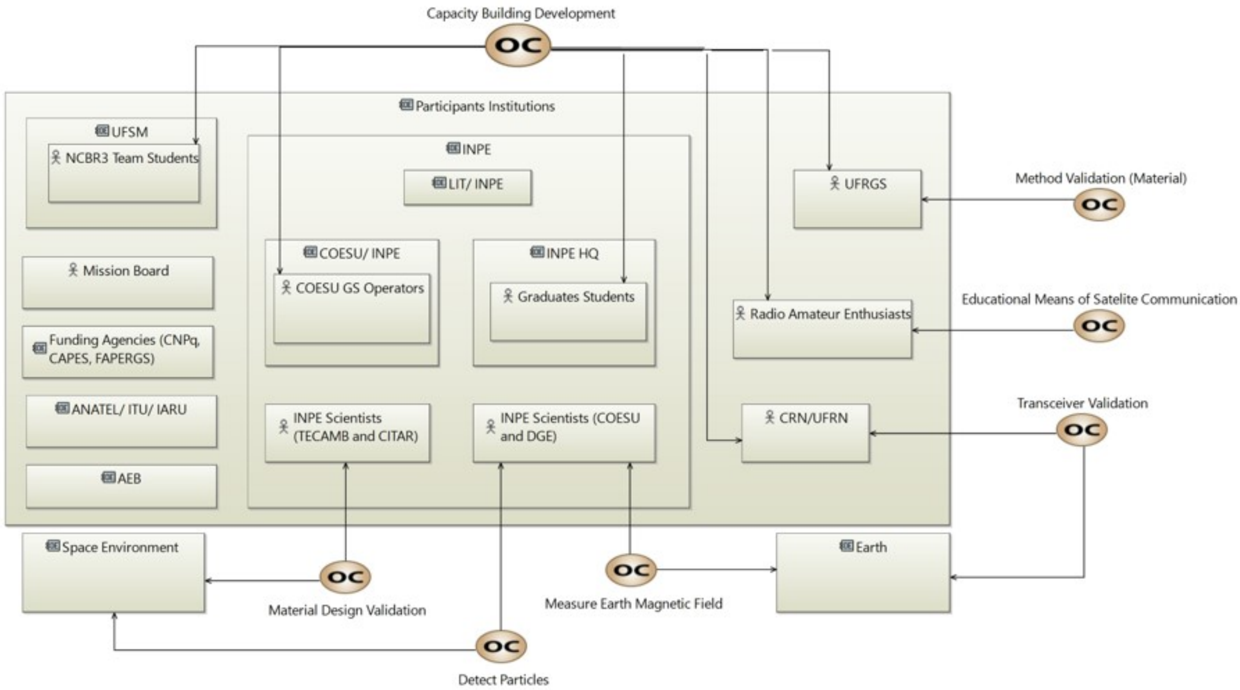

Figure 2: Operational Capabilities.

According to [7], a model has the primary objective of delivering reasonable answers for predefined questions. Therefor, for the sake of this work, the questions correspond to NCBR3 MDR deliverables.The questions of this model view are:

1. Which entities and stakeholder are involved?
2. Which are the main capabilities and their relation between the entities and stakeholders?
3. What are the educational, scientific and technological potential in a possible mission?

As it can be identified on Fig. 2, the model view highlights the most persistent operational capability evidenced by the number of its connections, which is the “Capacity Building Development”, confirming the continuity of one, if not the most important objective of the NANOSATC-BR CubeSats Development Program.

Continuing on the Operational Analysis layer, the next model view includes operational entities and actors previously identified, as well as the project’s operational activities and the interactions that connect them. Presenting a wide overview of what the users of the future system want to accomplish, the Operational Architecture, presented in Figure 3, contributes to a comprehensive visualization of which operational activities, decoupled from operational capabilities.

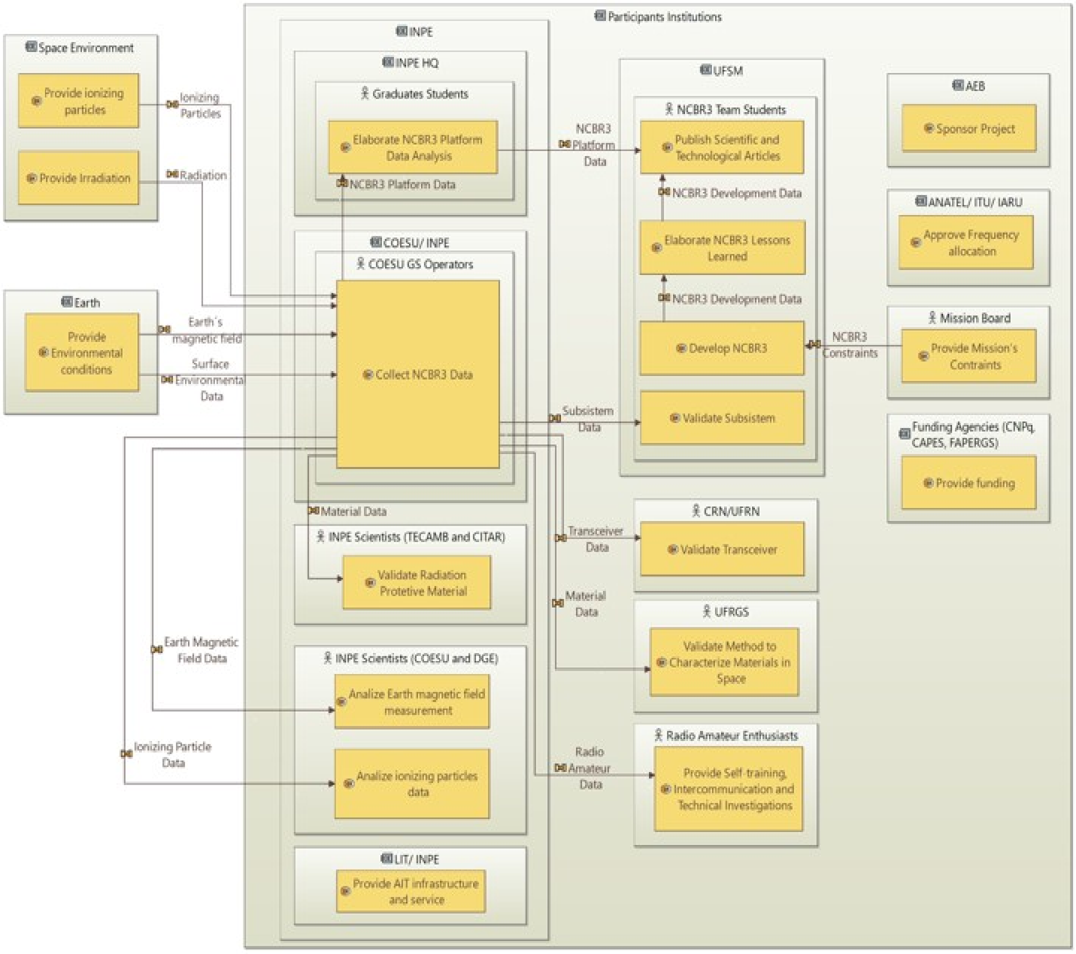

Figure 3: Operational Architecture.

The model view presented, answers the following questions considering the NCBR3 MDR:

1. What are the Needs, Goals and Objectives (NGO) of the Project?
2. Which are the main operational activities and their relation between the entities and stakeholders?

The initial assumption that can be made through this interpretation is that in future phases of the life cycle, the communication system between ground station (GS) and other entities shall be addressed with caution for an efficient and reliable transmission of mission data.

The next layer from the ARCADIA Method, known as Function & Non Functional Needs, analyzes what the system has to accomplish for the users. The main model view from this level is the System Architecture (Figure 4), the system in development is represented in dark blue, and external system in light blue. The green blocks represent the high level functions and the connections between indicates their relations.

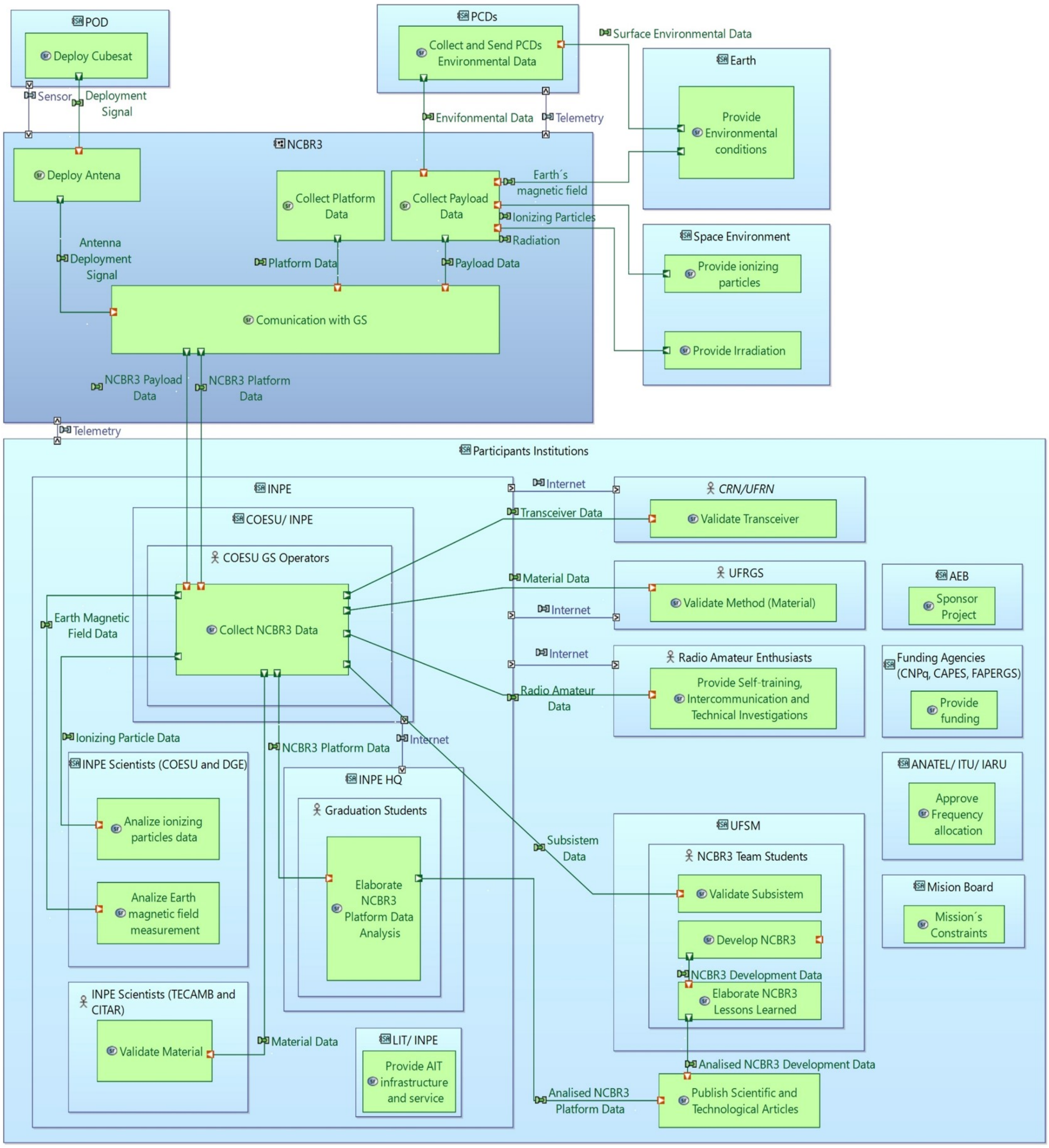

Figure 4: System Architecture.

The model view shows the relation between the system that will be developed with the entities and stakeholder, as well as the main functions of the system. This model view allows the development of the next layer, Logical Architecture.

The Logical Architecture modeling layer, as [7] describes, identify the logical components inside the system, their relations and their content, independently of any considerations of technology or implementation. The main model view from this layer is the Logical Architecture, shown in Figure 5.

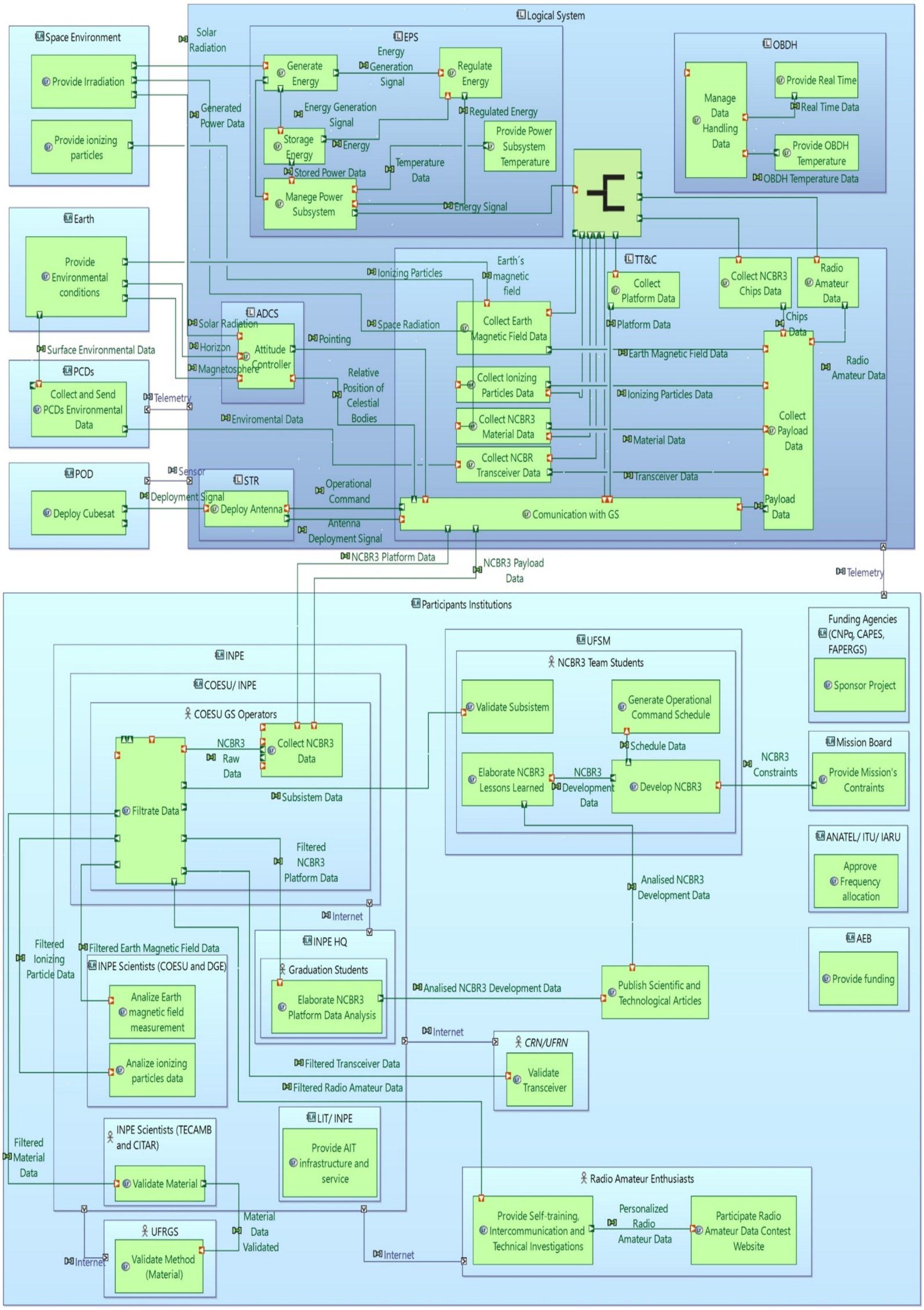

Figure 5: Logical Architecture.

The previous functions stated on the upper level, Function & Non Functional Needs, can be subdivided into internal sub-functions in this model view, while integrating the non-functional constraints that have been chosen for processing at this level. This model view allows to finely specify the responsibilities of each Logical Component elements, a structural element within the System, meaning that at this layer it can be identified the components of the work breakdown structure (WBS), a very important requirement for the MDR.

With both layers and with the help of a few external documents, the Mission Analysis part of the NCBR3 MDR can be accomplished by answering:

1. Which entities and stakeholder are involved?
2. Which are the main capabilities and their relation between the entities and stakeholders?
3. What are the educational, scientific and technological potential in a possible mission?

The last layer from the ARCADIA Method, the Physical Architecture, defines the final architecture of the system and how it is supposed to be build. The main model view developed at this layer, shown in Figure 6, is called Physical Architecture. This model view adds the functions required (identified by green blocks) for implementation, as well as the technical choices [7].

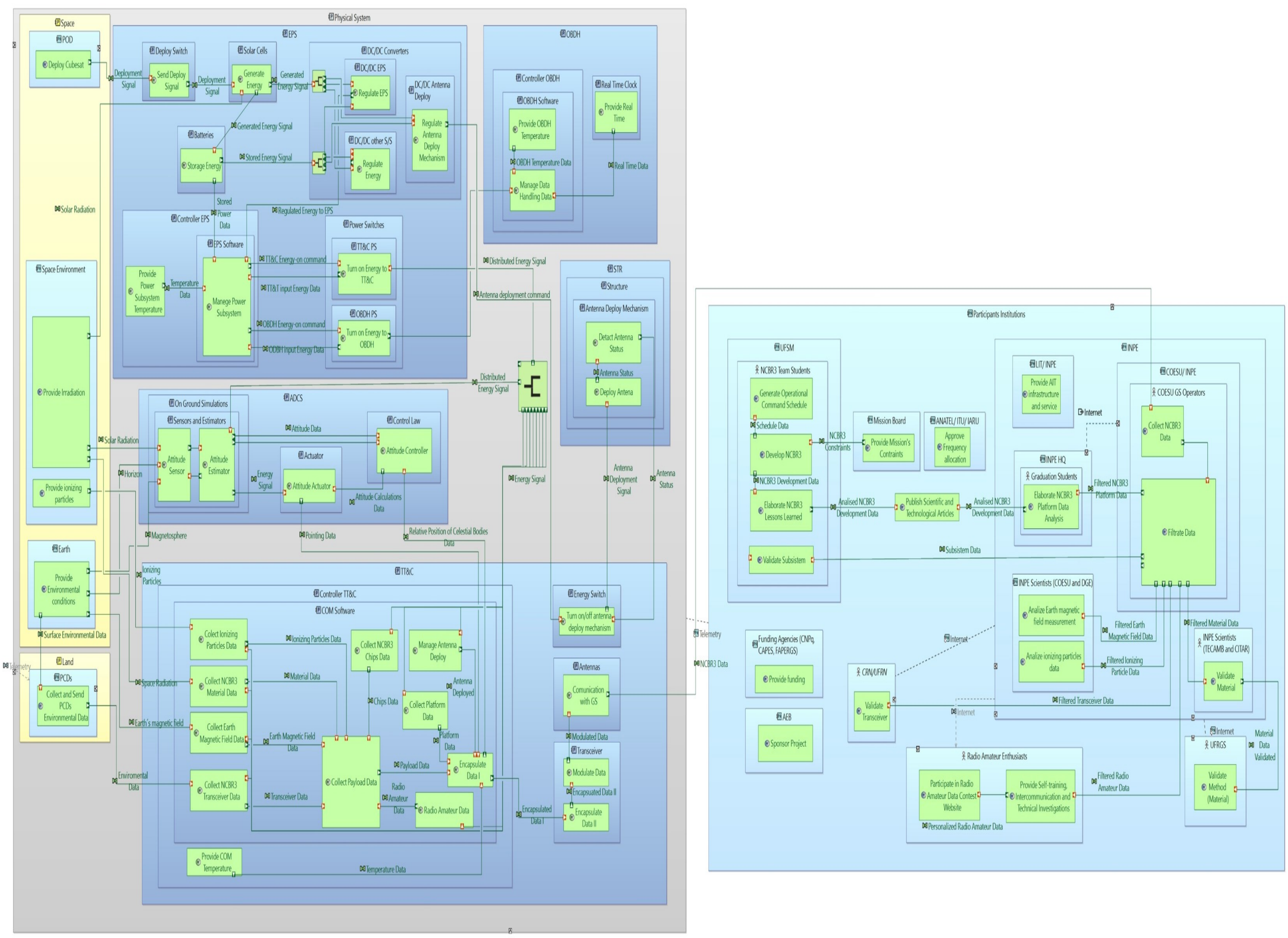

Figure 6: Physical Architecture.

In Figure 6, it can be noticed the external components of the system (yellow), such as the space environment around the nanosatellite and the surface environment, their behavior component (blue) and their functions (green). The functions presented on the physical system (gray) defines the ”real” concrete components that comprise the system.

With all layers, the last part of the NCBR3 MDR can be defined by answering:

1. What is the architecture and design of the Project?
2. What is the detailed payload?
3. What is the concept of operation of the mission?

The Table 1 show the analogy between the NCBR3 MDR deliverables and what was accomplish with modelling.

Table 1: MDR Deliverables in parallel to what was able to accomplish with the Method.

MDR	ARCADIA Method
Stakeholder Analysis	x
NGO	x
MoEs	-
Operational Activities	x
WBS/PBS	x
Mission Analysis	x
Trade-offs	x
Validate	x
Constrains	x
Cost	-
Schedule	-
Risk Analysis	x
Architecture and Design	x
Payload Details	x
Mission Objectives	x
Mission Justification	x

Many NCBR3 MDR deliverables were acquired through the use of the ARCADIA Method. However, the method does not comprehend to the extend of all NCBR3 MDR deliverables, some were structured without models, for example, the Programmatic Requirements. Still, models and Capella has the potential to assist in some Programmatic items, such as the Risk Analysis, since the software identifies critical points of the Project.

4. Conclusion

The proposed objective of this article was a study case of a Model-Based Mission Definition Review of the NANOSATC-BR3. It was shown how all layers of the ARCADIA MBSE Method through the Capella software can be applied to support the development of the MDR. Each model view created supports important deliverables suggested by NASA for this type of review. It also contributes for a less extensive paperwork, giving the first steps towards a Model-centric MDR, as a way to concentrate and unify the information, facilitating the visualization of the Project as a whole. As consequence, it eases the review process between all stakeholders with different backgrounds, as well as highlight indispensable information about the NCBR3 CubeSat system under development.

Acknowledgments

The authors value's the National Council for Scientific and Technological Development (CNPq) for the scholarship granted, as well as the Brazilian Space Agency - AEB, for the support, opportunity, and grants for the Brazilian INPE-UFSM NANOSATC-BR CubeSat Development Program. N. J. Schuch thanks CNPq for the fellowship under the number 300886/2016-0.

References

[1] BÜRGER, E. A Conceptual MBSE Framework for Satellite AIT Planning. 2018

[2] HARVEY, D. et al. Document the Model, Don't Model the Document. 2012

[3] INCOSE, INCOSE Systems Engineering Vision 2020, version 2. INCOSE Central Office, Seattle, WA 98133-9009, 2007. INCOSE-TP-2004-004-02, 2020

[4] ISO/IEC/IEEE. Systems and Software Engineering – System Life Cycle Processes. Geneva, Switzerland: International Organisation for Standardisation / International Electrotechnical Commissions / Institute of Electrical and Electronics Engineers. ISO/IEC/IEEE 15288:2015, 2015.

[5] NASA. Systems Engineering Handbook. Washington, DC, USA: National Aeronautics and Space Administration (NASA), December 2007. NASA/SP-2007-6105, 2007.

[6] NASA. NASA Systems Engineering Handbook. NASA Headquarters, Washington, D.C. 20546, 2016. NASA SP-2016-6105 Rev2. 2016.

[7] ROQUES, P. Systems Architecture Modeling with the Arcadia Method: A Practical Guide to Capella. Netherlands: Elsevier Science, 2017.

The CubeSat mission Aldebaran I

Carlos Alberto Rios Brito Junior(1), **Edemar Morsch Filho**(2), **Jose de Ribamar Braga Pinheiro Junior**(3), **Luís Claudio de Oliveira Silva**(4)
(1) Federal University of Maranhão, São Luís, Brazil, carlos.brito@ufma.br
(2) Universidade Federal do Maranhão, São Luís, Brazil, edemar.filho@ufma.br
(3) Universidade Federal do Maranhão, São Luís, Brazil, jrbp.junior@ufma.br
(4) Universidade Federal do Maranhão, São Luís, Brazil, claudio.luis@ufma.br

Keywords: *CubeSat, nanosatellite architecture, LoRa transceiver, embedded system*

The mission Aldebaran I is a CubeSat 1U under development at the Federal University of Maranhão (Universidade Federal do Maranhão - UFMA) in Brazil, with launch expected for the first semester of 2023. Except for the antenna, the design of all its subsystems as the Electric Power System - EPS, On-Board Data Handling - OBDH, Telemetry, Tracking, and Control - TT&C are from Brazil, as well as the project and manufacturing of the structure, passive attitude control, and solar panels. Primarily, the Aldebaran I aims to assist in the rescue of fishers in emergencies on the coast of Brazil by receiving alert signs from boats that face unsafe conditions on the ocean. To execute this duty, the CubeSat has a payload based on a LoRa (Long Range) transceiver. The Aldebaran I also aims to integrate undergraduate students and professors of UFMA around a real satellite mission, merging into this project the expertise of engineering courses of the institution as aerospace, electric, and computer science. The current version of the CubeSat Aldebaran I has already passed preliminary assembly and integration activities in a clean-room, and its protocol of communication is being tested using high altitude balloons. This paper presents a summary of the Aldebaran I mission context and discusses about its embedded systems and main parts.

1. Introduction

Due to the geographic characteristics of Brazil, fishing activity is abundantly present in Brazilian states, whether coastal (bathed by seas and oceans) or inland (bathed by rivers and lakes). This situation is very expressive in the state of Maranhão, which has the second longest coastline in the Northeast and has numerous rivers in its territory, being one of the largest producers of fish in the region, which is the second most important economic activity in the state [1]. In the state, 47,000 fishermen live solely from this trade and, specifically, in the city of Raposa, 80% of the population has fishing [2] as their main occupation.

The city of Raposa - MA is known as one of the most important fishing communities, participating in 12.8% of fishing production in the state. Due to the large fishing market in Raposa and the financial difficulty in equipping vessels with the most modern technologies, it is common to report fishing vessels that drift after being lost on the the sea, as in the case that occurred in June 2020, where three fishermen were unable to return after leaving Porto do Braga. Although the problem is relevant to the point of being the object of research, there are still no official updated statistics on the number of maritime accidents on the coast of Maranhão.

In cases of accidents on the seas, one of the crucial factors for carrying out a successful rescue is its execution time. Devices such as communication and tracking radios are mandatory for vessels authorized to navigate in inland and coastal waters, however, in the municipality of Raposa it is common to use small and medium-sized vessels and, usually, fishermen are unable to acquire devices that help them locate them in case of [3] accidents.

Aiming to contribute to the solution of this demand, the CubeSat Mission Aldebaran I has as its main objective to help in the rescue of fishing vessels on the coast of Maranhão through the reception and transmission of data from vessels in danger on the Brazilian coast. This nanosatellite is being developed at the Federal University of Maranhão (Universidade Federal do Maranhão - UFMA) and has the financial support of the Brazilian Space Agency (AEB). This real engineering problem mentioned above makes the Aldebaran I mission a training tool for the institution's engineering students, based on the construction and operation of a CubeSat, which corresponds to the second objective of the mission. Finally, Aldebaran I also has a scientific experiment to investigate a phenomenon called ionosphere scintillations, which is the last objective of this project. Currently, UFMA is the first university in the North-Northeast Region of Brazil to implement the Aerospace Engineering course and the Aldebaran I mission can be the first CubeSat from this region to operate in orbit.

The next sections present the main subsystems of the CubeSat 1U Aldebaran I, as well as some activities performed to test this platform.

2. Sub-systems

The mission concept for this project is based on the construction of a single satellite, from the CubeSat standard, of type 1U. In defining the subsystems, we opted for those that have a flight heritage or that, at least, have been qualified in tests in duly approved laboratories such as the Integration and Testing Laboratory (LIT) of the National Institute for Space Research (INPE). In this way, the project was based on the Brazilian CubeSat FloripaSat-I developed by the Laboratory for Research in Space Systems (SpaceLab) of the Federal University of Santa Catarina (UFSC) and launched in 2019 [4].

The CubeSat Aldebaran I payload is a LoRa-based transceiver, whose purpose is to promote the reception, processing and transmission of data referring to the location of small vessels that are in danger in the coastal region of Maranhão. As for the transmission of the vessel's location, a PTT (Platform Transmitter Terminal) will be built, which will use radio waves to share its position with the CubeSat, which in turn will transmit this signal to the ground station. Considering that this device has a high acquisition value on the market, a PTT will also be developed with low-cost, waterproof, rechargeable and easy-to-handle materials for integration into each vessel, from where it will transmit an emergency signal to the CubeSat, and it will send the location data to the ground station for rescue.

As for the objective of the scintillation studies, this will be carried out through the observation of the quality of transmission of the signals between the CubeSat and the ground station, and a modeling of ionospheric data can be carried out. Also, for telemetry reception and telecommand transmission, the implementation of a Ground Station at UFMA operating in the amateur radio range, with the AX-25 communication protocol and derivatives, is planned. However, the project is limited as a proof-of-concept, since, due to the time of revisiting the CubeSat in the coastal region of MA, a constellation of nanosatellites will be required.

2.1. Electrical Power System - EPS

The EPS includes solar panels to obtain energy, batteries to store excess energy and supply when the solar panels do not meet energy demands, and the electronic board for power control, distribution and regulation. The model adopted for the Aldebaran I operates the solar panels at their maximum power point (MPPT), and for this the board measures the current and voltage of the solar panels to perform the control.

Among the main features of the EPS are: 2 lithium-ion batteries for total supply of 7.56 V and 25 Wh; MSP430 20 MHz ultra low power microcontroller with I2C, UART and SPI interfaces; regulated voltage outputs, one 3.3V output with 1A maximum current (OBDH), two 3.3V outputs with 2A maximum current (EPS and Antenna), one 5V output with maximum current 3 A (Payload) and two 5 V outputs with a maximum current of 5 A (TT&C radios). The solar panels are bought from the Brazilian Company Orbital Engenharia, with 30% of efficiency, 60 cm^2 of solar cell's area, mounted with temperature and solar sensors on each one.

In Figure 1 is a view of the EPS module solely, without the batteries and solar panels.

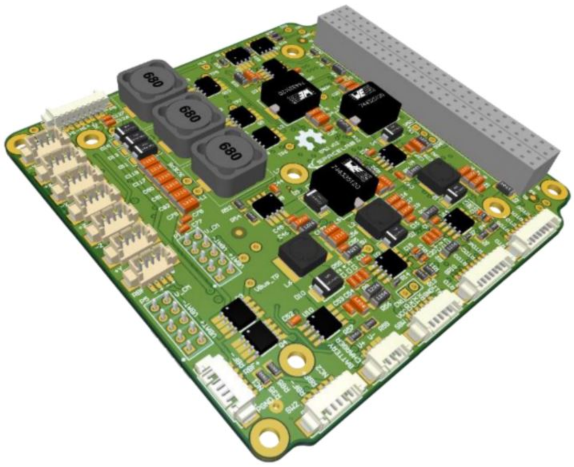

Figure 1: Virtual view of EPS.

2.2. Structure and attitude control system

The structure is based on the standard CubeSat 1U [5], as seen in Figure 2 (left). It is a commercial model purchased from the Brazilian company USIPED. The right side of Figure 2 shows the passive attitude control system assembled in the structure. This system has a magnet (pink) to align the CubeSat with the Earth's magnetic field and four hysteresis bars (green) to damp remaining oscillations.

2.3. On Board Data Handling - OBDH

This module is an on-board supervision computer system that basically implements the "command and control" and "telemetry" functions, whose main objective is to monitor the health of the other subsystems and remotely carry out their operations when necessary, as well as ensuring the temporary storage and integrity of mission data.

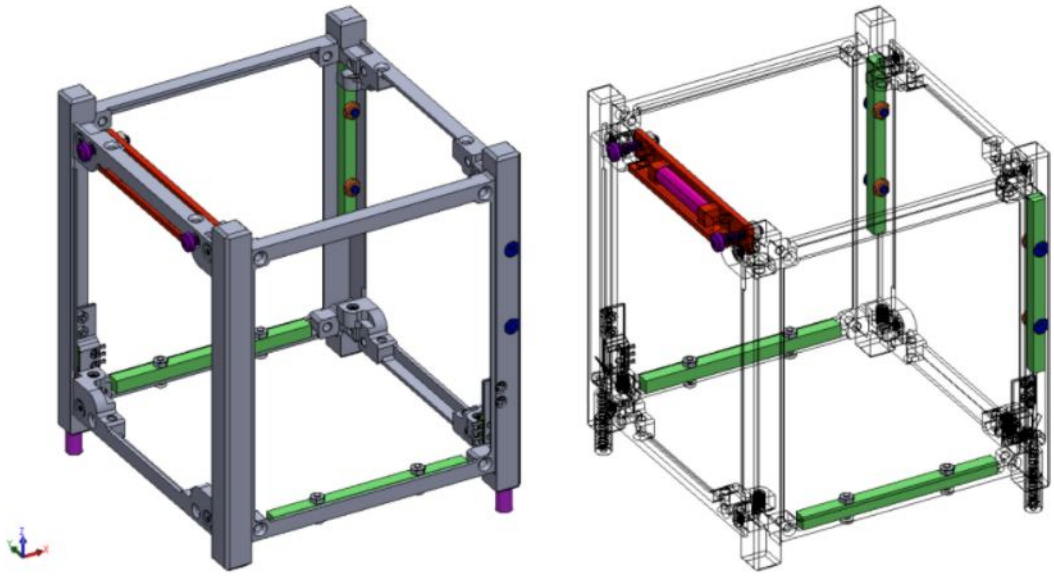

Figure 2: Virtual view of Structure and attitude control.

The functions associated with ”telemetry” on board the satellite include the real-time monitoring of the platform’s subsystems and also the payload in terms of critical parameters for the survival of the mission. Also telemetry functions in the OBDH are the packaging and temporary storage of the mission data that will be transmitted to the ground. Platform telemetry generally encompasses two categories of data, which are “housekeeping” (known as the engineering parameters that need to be monitored on the ground to check the health and operating status of onboard devices) and satellite attitude. Payload telemetry consists of the application’s dataset, that is, the mission’s scientific data.

The OBDH operation follows a sequence that starts with the initialization of the microcontroller (MSP430 20 MHz ultra low power with I2C, UART and SPI interfaces) and then reads the housekeeping data from the EPS, TT&C, the payload, antenna and the OBDH data itself. This data is stored in non-volatile memory (2G byte flash memory) and transmitted as a beacon. After that, there is a 60 second interval for the OBDH to check if a new remote has been received, and if it is true, the remote is processed, otherwise it does nothing. After this sequence, the steps begin again. Figure 3 illustrates this module.

2.4. Telemetry, telecommand and Control - TT&C

The TT&C is the system responsible for carrying out the communication between a ground station and the satellite. The configuration of the TT&C module for a satellite can have three types of links, in this case, the beacon, downlink and uplink. The beacon promotes a periodic transmission of telemetry data packets, not only from the TT&C but also from the EPS module. The downlink receives all data from the nanosatellite, ie from payload data, telemetry data and feedback from remote controls. Finally, the uplink is used to send the remote controls from a ground station to the nanosatellite. Thus, the TT&C can be divided into two submodules: (i) Submodule for Beacon; (ii) sub-module for downlink/uplink. The first is an independent sub-module that transmits a periodic signal containing satellite identification (ID) data and some

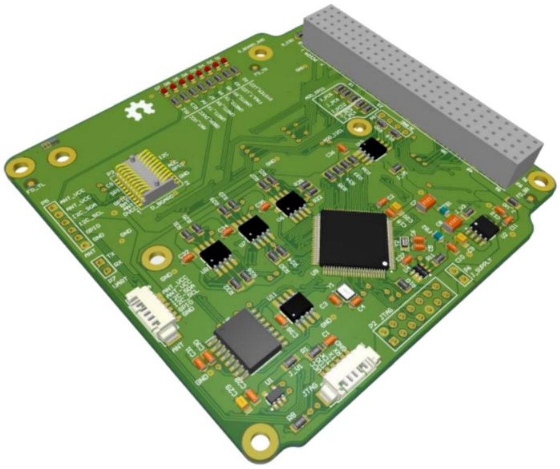

Figure 3: Virtual view of OBDH.

basic telemetry data. The second downlink/uplink submodule is the main communication device. It has a two-way data link to receive remote commands from the ground and transmit all available data back to ground.

Among its features, the following stand out:

- MSP430 20MHz ultra low power microcontroller with I2C, UART and SPI interfaces, which controls the release (ejection) of the redundant antennas with the OBDH;
- Beacon radio that transmits data packets with a baud rate of 1200 bps, through the NGHam and AX.25 protocols on a frequency in the VHF band between 145MHz and 146MHz;
- Main radio that receives remote controls and sends the data packet at a baud rate of 2400 bps to terrestrial stations in the UHF frequency band between 437MHz and 438MHz, using the NGHam protocol.
- Half-duplex communication, UHF/VHF and GFSK modulation.

This module is illustrated in Figure 4.

2.5. Antenna

The antenna used in the Aldebaran I is a ISISpace's commercial model, which already has a flight history. After reviewing the system requirements using the LoRa system, the model with 4 monopoles was adopted, with the following frequencies for each antenna:

- 1 antenna at 401 MHz: Receive signals for the EDC experiment;
- 1 antenna at 148 MHz: EDC downlink;
- 1 antenna at 437 MHz: For LoRa/Beacon/Downlink/Uplink;
- 1 antenna at 148 MHz: To be defined.

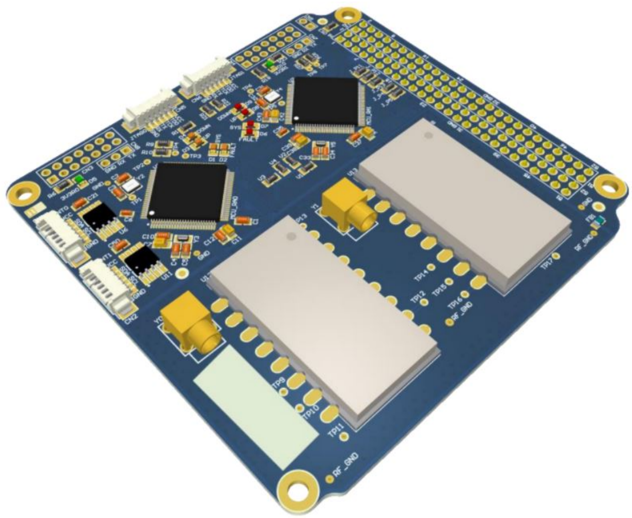

Figure 4: **Virtual view of TT&C.**

2.6. Payload

The LoRa® module that will be used in this project is a 1 W high power wireless transceiver (1278F30), which integrates the Semtech RF SX1278 transceiver chip, with the following characteristics [6, 7]:

- Frequency range: 433-460 MHz/ 470-510 MHz
- Sensitivity: above – 139 dBm;
- Maximum output power: 30 dBm;
- Modulation modes: LoRa TM, MSK, GFSK and OOK;
- Data transfer rate: in FSK 1.2 – 300 kbps, in LoRa TM 0.018–37.5 kbps;
- Operating temperature: - 40 to 85 °C.

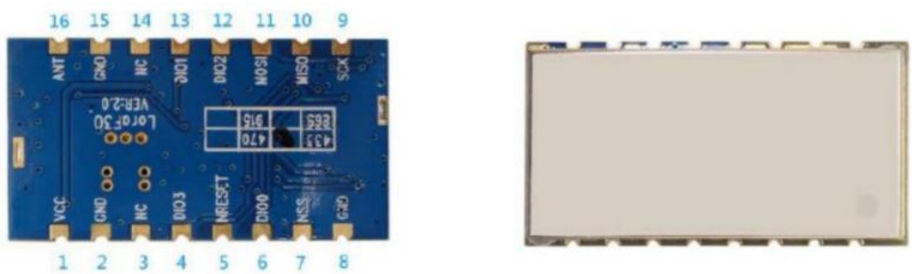

Figure 5: **LoRa used in the Aldebaran I.**

LoRa® (Long Range) is a wireless communication network technology created by Semtech Corporation and promoted through the LoRa® Alliance. A non-profit association formed by large companies with a common interest in the development and application of the Internet of Things. The LoRa®network employs a signal modulation technique that, despite being owned by Semtech, has some specifications accessible to the common user, such as the modulation derived from CSS (Chirp Spread Spectrum). This modulation maintains the same low-power characteristics as FSK modulation, but significantly increases the communication range. CSS modulation was employed for long communications applied in space and military areas. LoRa® is the first low-cost application for commercial use. Also allowing variable data rates by using orthogonal spreading factor (SF - Spread Factor), allowing the system user to change the data rate by range or power, optimizing the network depending on the application.

Briefly, the advantages of employing the LoRa communication system can be described as:

- Scalable Bandwidth - LoRa modulation is scalable in both frequency and bandwidth, so that it can be used in both narrowband and direct sequence frequency hopping mode;
- Constant Envelope/Low Power - as LoRa is similar to FSK with a constant envelope modulation scheme the same low cost high efficiency PA stages can be used without modification;
- High robustness - LoRa signals are very resistant to both in-band and out-of-band interference, with excellent immunity to pulsed AM interference;
- Multipath and Fading Resistant - signals with multiple paths or subject to the phenomenon of fading (fading) are rejected which makes the LoRa system ideal for urban and suburban locations where these problems occur;
- Doppler Resistant - the signal changes that occur by the Doppler effect Doppler does not affect the integrity of Lora signals;
- Long Range – is the main attraction of LoRa technology exceeding in much the traditional FSK.

3. Preliminary tests

3.1. High altitude balloon

The so-called stratospheric probe experiment had the support of the Alcântara CLA Launch Center to carry out telemetry and telecommand tests with 600-gram balloons used in its meteorology division. Particularly, this stratospheric probe experiment has its importance in the validation of the wireless communication protocol for long distances, known as LoRa (Long Range) that will be used in the Aldebaran-I nanosatellite and locators to perform the search and rescue mission of small vessels. Altitude communication tests were carried out with RF Wireless LoRa modules with power of 0.1 W and 1 W. Despite the excellent telemetry results, with a reception of beacons without communication failures or Doppler shift, the maximum altitude reached was between 16 to 18 km. This is because the balloon's rise in the atmosphere is limited to its weight and the weight of the experiment. Technically, a balloon with greater weight (between 1000 and 1200 grams) could reach higher altitudes for communication testing with the artifact designed with LoRa module and weight of approximately 400 grams. More details about this experiment will be described and discussed in another article.

3.2. Integration in a clean room

In December of 2021 the CubeSat Aldebaran I was partially integrated in a clean room of the Innovation SENAI Institution, at the city of Florianópolis in the Santa Catarina state. In that occasion, a mechanical integration was conducted with the flight model of structure and solar panels, also with engineering models of EPS, OBDH and TT&C to check the main dimensions, the connections among these parts and the occurrence of interference.

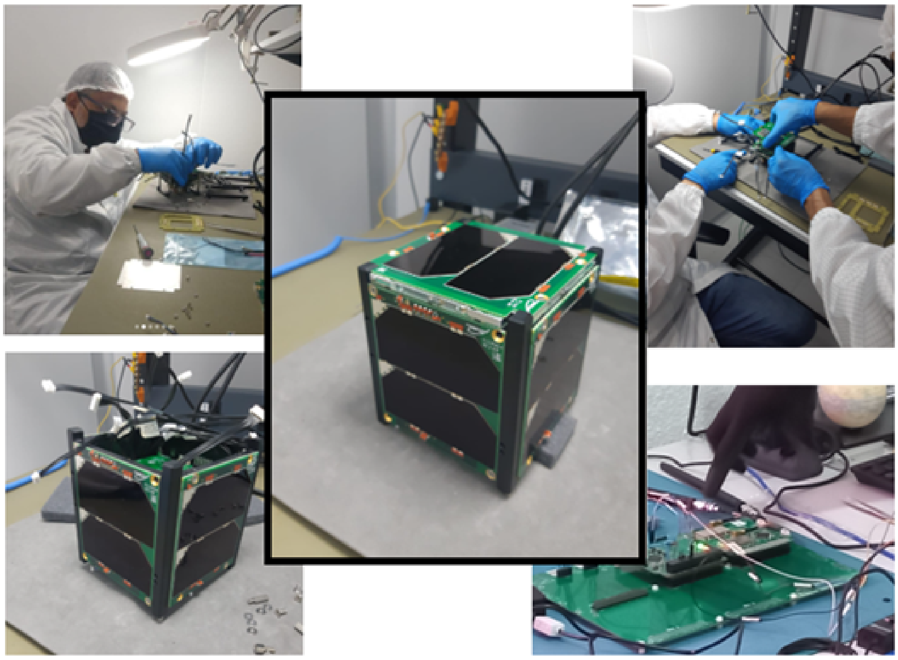

Figure 6: The integration of Aldebaran I.

4. Conclusions

The CubeSat Aldebaran I under development at the Federal University of Maranhão aims to assist the rescue of fishers exposed to dangerous situations in the ocean. When requested, the CubeSat will receive a sign from the boat and the satellite sends the vessel's position to the ground station, where authorities can be contacted.

This project is an example of problem based learning, where the students are exposed to a complex challenge and they can apply the acquired knowledge along the classes to solve problems and propose solutions.

Its orbit is not yet defined, but preliminary simulations show that the typical inclination around 98° (sun-synchronous) with 550 km of altitude or 51.5° at 430 km (deployment from the International Space Station) are appropriate to the expected lifetime and operation in orbit of this proof of concept.

It is understood that before launching a CubeSat, several scenarios must be simulated in order to predict the expected behavior in orbit. Validating simulations in the context of satellites is not always a simple task, since a laboratory environment capable of replicating the main conditions of space is in many cases unfeasible. Therefore, monitoring the operation of the satellite in orbit, such as the temperatures, currents and voltages of the solar panels and plates, is essential to prove the hypotheses adopted in the simulations. This also allows to refine the models and the elaboration of new solutions for the application in space. Also, after the launch of CubeSat, it is expected to receive its data at the radio amateur station that is in the pre-installation phase at UFMA.

Acknowledgments

We would like to thank the support from the Brazilian Space Agency, the Ministry of Science Technology and Innovation (MCTI), the Laboratory of Space Electronics and Embedded Systems (LABESEE) from the Federal University of Maranhão (UFMA), and the Space and Technology Research Laboratory (SpaceLab) from the Federal University of Santa Catarina (UFSC).

References

[1] T. J. F. Pereira, L. K. S. Ferreira, F. A. Everton, F. B. Frazão, M. de Fátima Viégas Lima, Comercialização de pescado no portinho em são luís, estado do maranhão, Brasil: uma abordagem socioeconômica dos trabalhadores, 2010. Rev. Bras. Eng. Pesca 5(3): I-VIII.

[2] P. Santos, I. Almeida-Funo, F. Piga, V. França, S. Torres, C. Melo, Perfil socioeconômico de pescadores do município da raposa, estado do maranhão, 2021. Technical report. Rev. Bras. Eng. Pesca 6(1): I-XIV, 2011. Acessed on May 3th, 2021.

[3] MARINHA DO BRASIL, Normas e procedimentos para a capitania dos portos do Maranhão, ncpc, 2020. Available on: https://www.marinha.mil.br/cpma/sites/www.marinha.mil.br.cpma/files/NPCP_2020_-_CPMA_0.pdf.

[4] G. M. Marcelino, S. Vega-Martinez, L. O. Seman, L. Kessler Slongo, E. A. Bezerra, A critical embedded system challenge: The floripasat-1 mission, IEEE Latin America Transactions 18 (2020) 249–256.

[5] The CubeSat Program, Cal Poly SLO, Cubesat design specification (CDS) rev 13, 2014. Acessed on March 29th, 2022.

[6] R. Sinha, W. Yiqiao, S.-H. Hwang, A survey on LPWA technology: LoRa and NB-IoT, ICT Express 3 (2017).

[7] S. Devalal, A. Karthikeyan, LoRa Technology - An Overview, 2018. 10.1109/ICECA.2018.8474715.

8

Session 8 - Telecommunications, Tracking and Command

Validating Cosmos to Operate as a Nanosatellite Ground Software

Priscila Y. Yamada(1), **William R. Silva**(2), **Renato A. Borges**(3), **Wilson Yamaguti**(4)
(1) *Visiona Space Technology, São José dos Campos - SP, Brazil, (61) 99835-8206, priyamada25@gmail.com*
(2) *University of Brasilia, Brasília - DF, Brazil, (61) 99632-0060, reis.william@unb.br*
(3) *University of Brasilia, Brasília - DF, Brazil, (61) 98262-0152, raborges@ene.unb.br*
(4) *Visiona Space Technology, São José dos Campos - SP, Brazil, (12) 2138-5814, wilson.yamaguti@visionaespacial.com.br*

Keywords: *Cosmos, cFS, Nanosatellites, Graduation, Software Development*

Each satellite, regardless of its mission, to perform its monitoring and control, a communication subsystem is used with the objective of sending telemetry to and receiving telecommands from a ground station. This information sent by and received from the satellite needs to be monitored and/or controlled by the operators in a Satellite Control Center. Since most satellites have a limited communication time with the ground station, viewing telemetry, especially those critical to the satellite's health, needs to be organized and easy to interpret so that the operator can send telecommands according to mission status. Ball Aerospace Cosmos' framework allows to create graphical interfaces in an efficient way for viewing telemetry, using graphics, colors to indicate boundary violations, and conversion of measurements into engineering units. It can be used for both during satellite assembly, integration and testing (AIT), and during operations in the Satellite Control Center. Thus, this work proposes a simple software development environment for real time command and control subsystem at a Satellite Control Center. To validate Cosmos applications and configurations a simple satellite simulator software can be used for telemetry transmission and telecommand reception. To further enhance satellite simulation capability, a flight software framework can be used, such as NASA's Core Flight System with mission specific applications or even by a high fidelity dynamic satellite simulator providing a very realistic satellite behavior including its orbit and attitude data. A simple satellite simulator software was used to generate telemetry and to receive telecommand messages considering its use for the University of Brasilia's CubeSat AlfaCrux mission. With this simulator, Cosmos configuration could be tested, as well as its TCP/IP interface with the simulator. The visualization of telemetry from a real mission provided by the AlfaCrux satellite as the main project, with the objective of encouraging studies and research on small satellites at universities, so that in the future students and professors can develop their own satellite control center and on-board software.

1. Introduction

Technological advancement has made achievements in the space business possible. The major milestone is the reduction in size, cost, and time in the development of satellites [1]. This new nanosatellite concept makes it easier for the university community to access space.

In recent years the number of nanosatellite competition teams has grown considerably, in 2019, one can mention the emergence of the Sirius team (UFABC), Gama

CubeDesign (UnB), Czar Space (UFMG) and others. In addition, there are university initiatives in partnership with the Brazilian Space Agency, such as the ITASAT mission (ITA) and the AlfaCrux mission (UnB).

Each satellite performs a function in a space mission, but all of them need communication between the ground segment and the space segment, for their monitoring and control by means of telecommands and telemetry functions, in addition to locating them in orbit [2]. This communication is a critical activity for the success of a missions, which makes testing and simulation necessary.

The objective of this paper is to present tools to undergraduate students that facilitate these software development for satellite AIT, and that can be used latter during the mission operations. There are tools with a well-defined basic structure, which does not depend on the satellite mission, requiring the user to develop only the specific functions of the project.

For the satellite control center command and control software, the proposal is to use the Cosmos framework, and for the space part, one can start with simple satellite simulation software for sending telemetry and receiving telecommand messages, to first test the communication between the ground segment and the space segment, and then advance to more complex tools, such as reusable flight software or even a high fidelity satellite simulator with flight on-board software, providing realistic sensors and actuators behavior in orbit.

Not having to develop software from scratch means time savings and is consistent with the purpose of nanosatellite mission. In addition, the students themselves can develop the entire control system and the on-board data handling subsystem (OBDH) in a simple Linux environment.

Cosmos is a framework used to control embedded systems, with an interface to send telecommands and receive telemetry. Within this tool there are applications with specific functions, such as execution of a telecommand script, telemetry display through graphics, and storing telemetry in a database [3].

The Cosmos configuration for a specific mission is done by configuration text files with keywords, as this framework is all open source, the user can find the code on GitHub and instructions for use on the site (https://ballaerospace.github.io/cosmos-website/). The test scripts and those for sending telecommands are written in Ruby.

Ball Aerospace, the developer of Cosmos, provides a Demo version of this tool. This version has several script examples, showing almost all the features of Cosmos. The user can use this demo version to start the project.

For the Cosmos testing, in this article, we start with a simple satellite simulation software, with the purpose of validating the Cosmos applications, sending telecommands, receiving, displaying and storing telemetry. This simulation software can be developed in any language, besides generating telemetry messages and receiving telecommand messages, requires a communication interface with Cosmos, e.g. TCP/IP.

However, reusable flight software concept can be another way to replace the simple satellite simulator software, that is, this software framework contains a layer with functions that are platform and project independent, and another layer that contains a configurable set of requirements and codes, being adaptable for any mission.

The emergence of this concept is due to the combination of making flight software more complex and reliable and reducing its development time. Technological advances have allowed the satellite to perform some on-board tasks autonomously without the need of interaction with the ground, however, more advanced software would require more time, which is contradictory to the objectives of a nanosatellite [4].

According to [5], comparative research was done between six flight software frameworks for nanosatellite missions. In this study 14 criteria were evaluated, in which, in the end, the NASA cFS (core Flight System) software that best suits projects with shorter development times was chosen.

The cFS is a reusable flight software designed by NASA, with the goal of reducing implementation time and simplifying the maintenance process. Its code is open source, made available on GitHub, and technical documentation and training is provided at [6]. The ease of access to information and training encourages undergraduates to develop their own on-board software.

This article presents in detail how to configure Cosmos, from the communication interface to viewing telemetry. In order to show that this tool works for real nanosatellite missions, telemetry from the AlfaCrux mission was used.

2. Cosmos

Cosmos is a command and control system that includes data visualization capabilities for on-board systems and can be used during the satellite assembly, integration and testing phases and during in-orbit operation.

The Cosmos architecture is implemented as a client-server. The Command and Telemetry Server connects to other tools, such as the core Flight System, to send commands and receive telemetry. Communication between these two tools can be over TPC/IP, serial, UDP or a custom interface.

Cosmos contains 18 applications, all of which rely on the Command and Telemetry Server to send commands or receive telemetry. The purpose of these applications is to facilitate operations during the mission by organizing command sequence or scripts, presenting telemetry in graphical or custom layouts, and storing telemetry in a database.

The organization of Cosmos is done in a directory structure, in which all files have a well defined location [7]. Its operation depends on all the files. However, the main configuration for creating a communication interface and customizing the applications is done by the ”config” folder.

The ”Gemfile” directory can be changed if the user wants to define other gems in his project. All files generated by Cosmos, such as logs or command sequences are stored in the ”outputs” directory. Test procedures and operations are stored in the ”procedures” folder.

3. Core Flight System

The core Flight System was designed to facilitate the development of flight software for space missions, so its architecture is flexible and layered. The libraries, applications, and functions common to each mission are all already developed in the lower layers of the cFS, requiring the engineer to develop only the mission-specific functions in the upper layer of the architecture [8].

The architecture of the layers is designed so that each layer hides its implementation details from the other layers, so changing the internals of one layer does not affect the internals of another layer. In addition, it is possible to work in desktop environments, so there is no need for specialized labs.

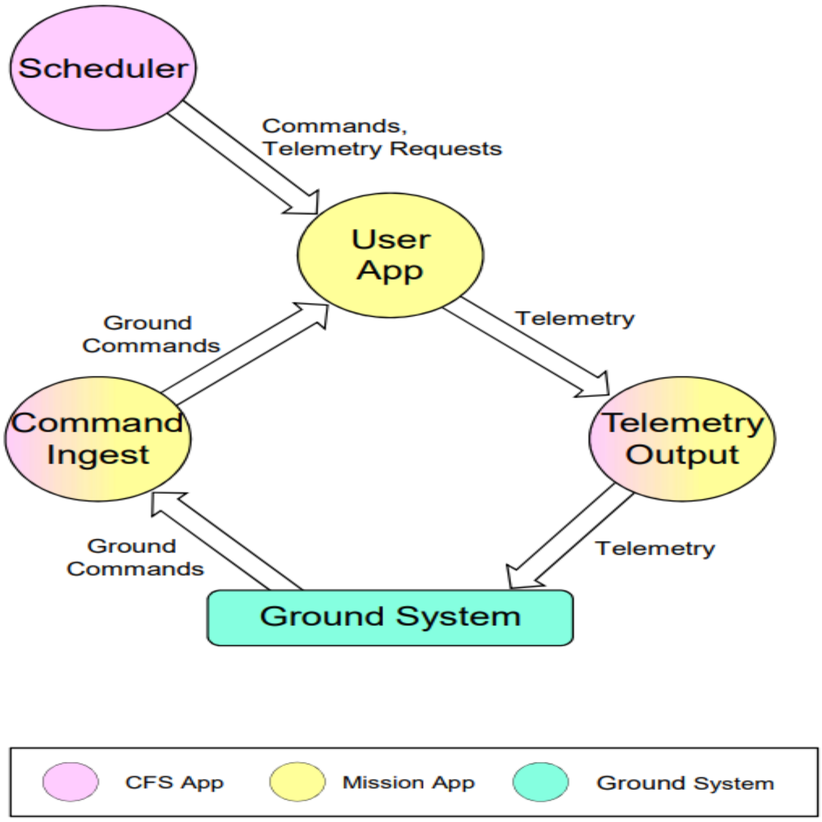

Figure 1: Communication between the cFS and the Ground Station.
Source: [11]

There are three main layers: Platform Layer, Reusable cFS Layer and Mission Specific Layer. The first provides the interface to the hardware and the real-time operating system. The second contains the Core Flight Executive (cFE), which hosts the flight software available for reuse. And the last layer allows the developer to configure the mission-specific parameters [9].

The cFS was certified in 2009 with the launch of the Constellation Programs Lunar Reconnaissance Orbiter (LRO) and has been used in other missions, such as the Lunar Atmosphere and Dust Environment Explorer (LADEE), Morpheus, the Global Precipitation Measurement Mission (GPM), Magnetospheric Multiscale Mission (MMS), Radiation Belt Storm Probe (RBSP) and others [10].

The interface between Cosmos and cFS is provided by the Cosmos Command and Telemetry Server, and the cFS Command Ingest (CI) and the Telemetry Output (TO) application. The Command and Telemetry Server communicates between Cosmos and the target, in this case the cFS, sending the commands previously prepared in the Command applications and receiving the target's telemetry, to be further processed and visualized in the Telemetry applications.

The CI and the TO are part of the cFS, in which the CI is responsible for receiving the command packets and the TO to send the telemetry packets. The Figure 1 shows a diagram of how this communication between the cFS and the ground segment works, in which the Scheduler (SCH) sends messages by software bus at predefined intervals.

4. Methodology

4.1. Installation

Cosmos can be installed on both Docker (https://github.com/BallAerospace/cosmos-docker) and host machines. On host machines, it can be installed on Windows, Linux or Mac OS, however, not all versions support this tool. Further details of limitations and documentation are described in [12].

For the development of this article, Cosmos was installed on the Ubuntu Linux operating system. It was tested on distributions 16.04, 18.04 and their variants. The installation may work on other Linux versions, but it was not tested. The Table 1 presents the step-by-step how to install Cosmos by terminal commands.

Table 1: Commands to install Cosmos on ubuntu linux.

Install Cosmos dependencies	sudo apt-get update -y && sudo apt-get install -y cmake freeglut3 freeglut3-dev gcc g++ git iproute2 libffi-dev libgdbm-dev libgdbm5 libgstreamer-plugins-base1.0-dev libgstreamer1.0-dev libncurses5-dev libreadline6-dev libsmokeqt4-dev libssl-dev libyaml-dev net-tools qt4-default qt4-dev-tools ruby2.5 ruby2.5-dev vim zlib1g-dev
Install Postgresql dependencies	sudo apt-get install -y gnome-terminal libpq-dev postgresql postgresql-contrib nodejs
Install general system dependencies 1	sudo gem install rake –no-document
Install general system dependencies 2	sudo gem install cosmos -v 4.5.2 –no-document
Clone de repository	Choose a version in https://github.com/BallAerospace/COSMOS/releases
Run inside Cosmos folder	sudo bundle install

During the Cosmos installation, there may be versioning problems with the Linux gems, making it necessary to change the Linux version. Another difficulty seen during this phase of development was the incorrect installation of Cosmos dependencies, making it necessary to uninstall and restart the process again.

4.2. Creating the target

Inside the ”config” folder there are three main folders that need to be edited to configure Cosmos: system, targets and tools. The ”system” folder contains ”system.txt”, a file in which the user needs to define the target. The ”target” folder contains the settings for each target that should be commanded or should receive telemetry. The ”tools” folder contains the configuration files for each Cosmos application.

The ”system.txt” file is the first to be modified. In it the target is declared using the keyword ”DECLARE_TARGET TARGETNAME”. The TARGETNAME must be in uppercase. It is not necessary to modify or delete the rest of the keywords in this folder.

Next a folder must be criated that will contains all the settings for this new target. In the ”config/targets” directory a new folder must be created with the same name as declared in ”system.txt”, also in uppercase.

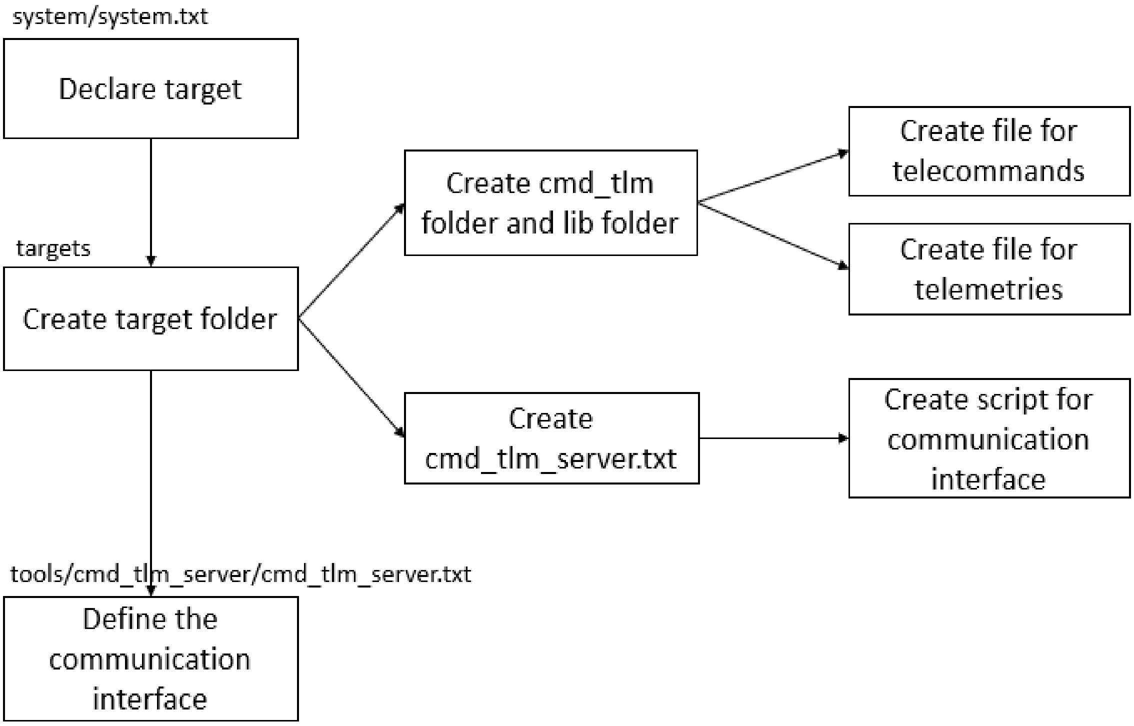

Figure 2: Cosmos configuration flowchart.

In the folder of the new target created, the folders ”cmd_tlm” and ”lib” and the file ”cmd_tlm_server.txt” are needed. In the ”cmd_tlm” folder contains files that define the commands and telemetry for the target. In the ”lib” folder contains custom codes required by the target. And in the file ”cmd_tlm_server.txt” contains a part of the configuration of the communication interface between the cosmos and the target.

In the directory that defines the commands and telemetries a file needs to be created for each one. The file that contains the telecommands settings is named ”targetname_cmds.txt” and the file to define the telemetries is called ”targetname_tlm.txt”. In which ”targetname” is the name given to the target.

The main code need to have in the ”lib” folder is the script for initializing the communication with the target. This script uses the Cosmos module, inherits the TcpipClientInterface class, and calls the functions initialize and connect.

In the file ”cmd_tlm_server.txt” the communication interface is declared. To declare the interface using the keyword ”INTERFACE” containing seven arguments: interface name (in capital letters), lib folder code, IP, write port, read port, write timeout and read timeout. This definition is made for the TCP/IP interface.

All the above settings are mandatory within the ”config” folder, however, it can create custom directories for its project, for example, folders that contain procedures, screens, tables, and other functionality.

The last mandatory configuration for Cosmos is in the ”tools/cmd_tlm_server” directory. This directory contains the file ”tools/cmd_tlm_server.txt” which defines the communication interface. This definition follows the same pattern as the ”cmd_tlm_server.txt” file. The flowchart in Figure 2 shows the steps mentioned above.

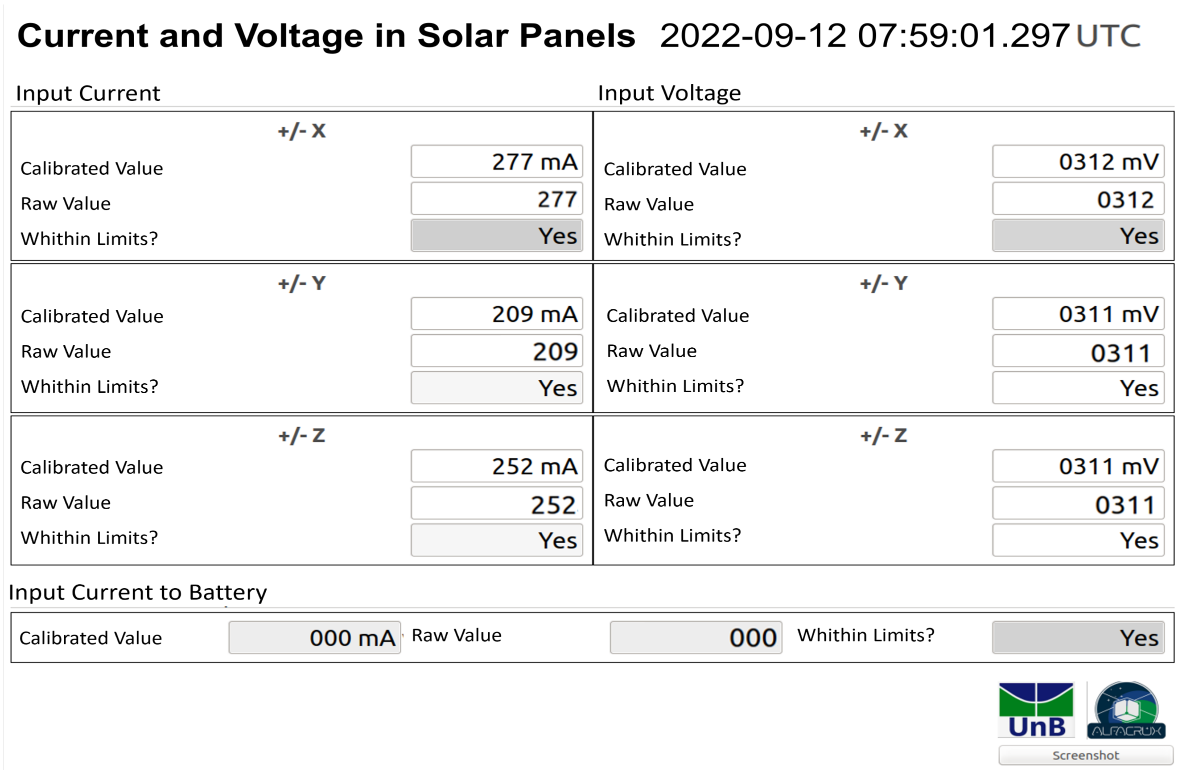

Figure 3: Viewing the telemetry of the Solar Panels packet.

5. Results

The validation of the Cosmos development was done with data from the AlfaCrux mission, launched in April 2022. Mission critical data is generated in a csv file. In a script, this file is read and a telemetry packet message is generated simulating AlfaCrux satellite telemetry to Cosmos using the TCP/IP protocol.

The telemetry from the AlphaCrux mission is separated into four packets and for each packet screens have been created to show the receipt of this telemetry. The SOLAR_PANEL packet contains the voltage and current information on the solar panels in all axes (+/-X, +/-Y and +/-Z) and the input current from the solar panel to the battery, as shown in Fig. 3.

The EPS packet receives the information of the output current from the EPS to the AlfaCrux subsystems (Fig. 4). The TEMP EPS packet contains the telemetry related to the internal temperatures of the AlfaCrux (Fig. 5) and the TEMP PAINEL SOLAR packet receives the data from the external temperatures, i.e. the temperatures of the solar panels (Fig. 6).

In [13] contain more information about the results obtained using Cosmos as a software for receiving telemetry and sending telecommands.

6. Conclusion

Cosmos is a tool that has resources to be used during the satellite AIT phase and during the satellite in orbit operations, and can be a resource that facilitates the development of ground segment software by university students, since it is open source

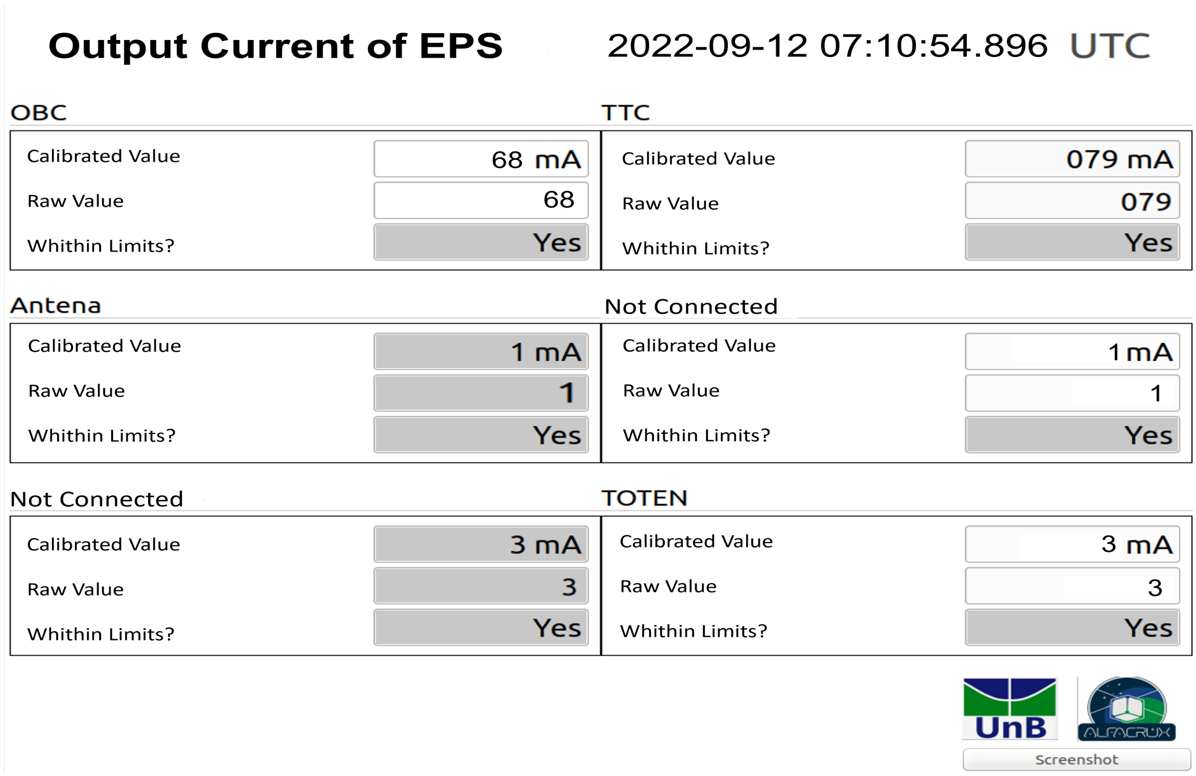

Figure 4: Viewing the telemetry of the Output Current of EPS packet.

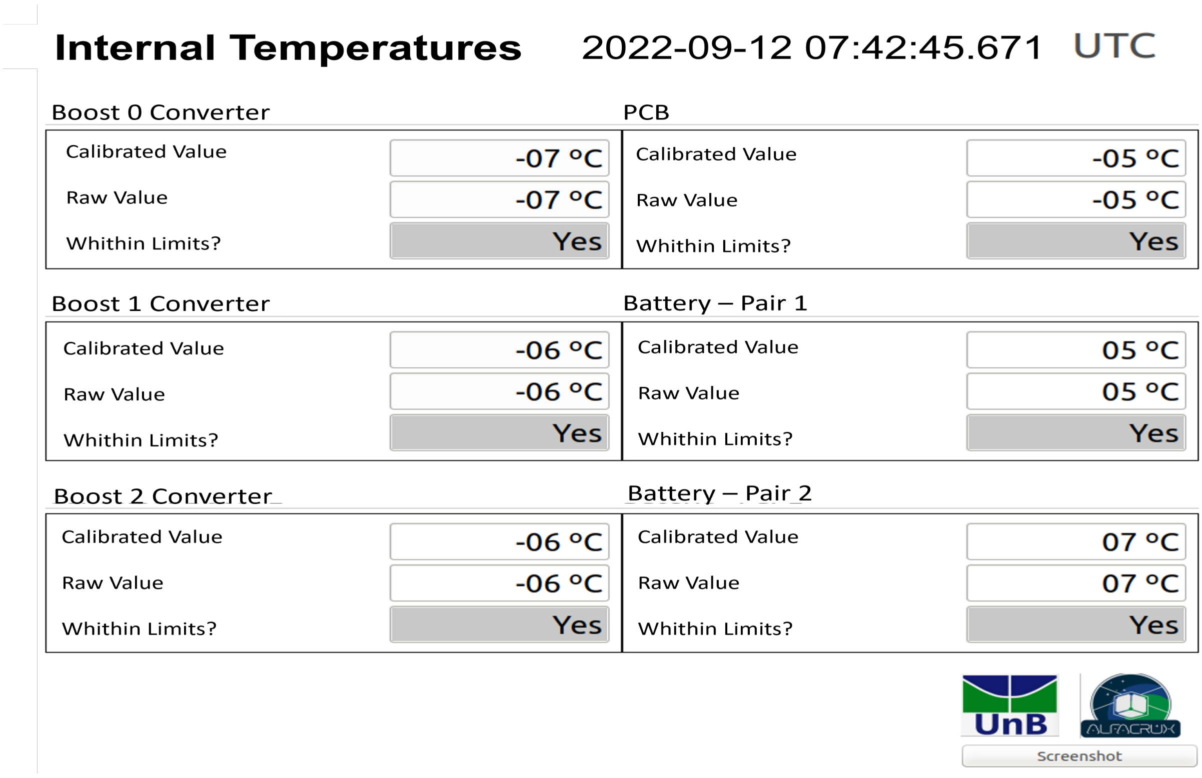

Figure 5: Viewing the telemetry of the Internal Temperatures packet.

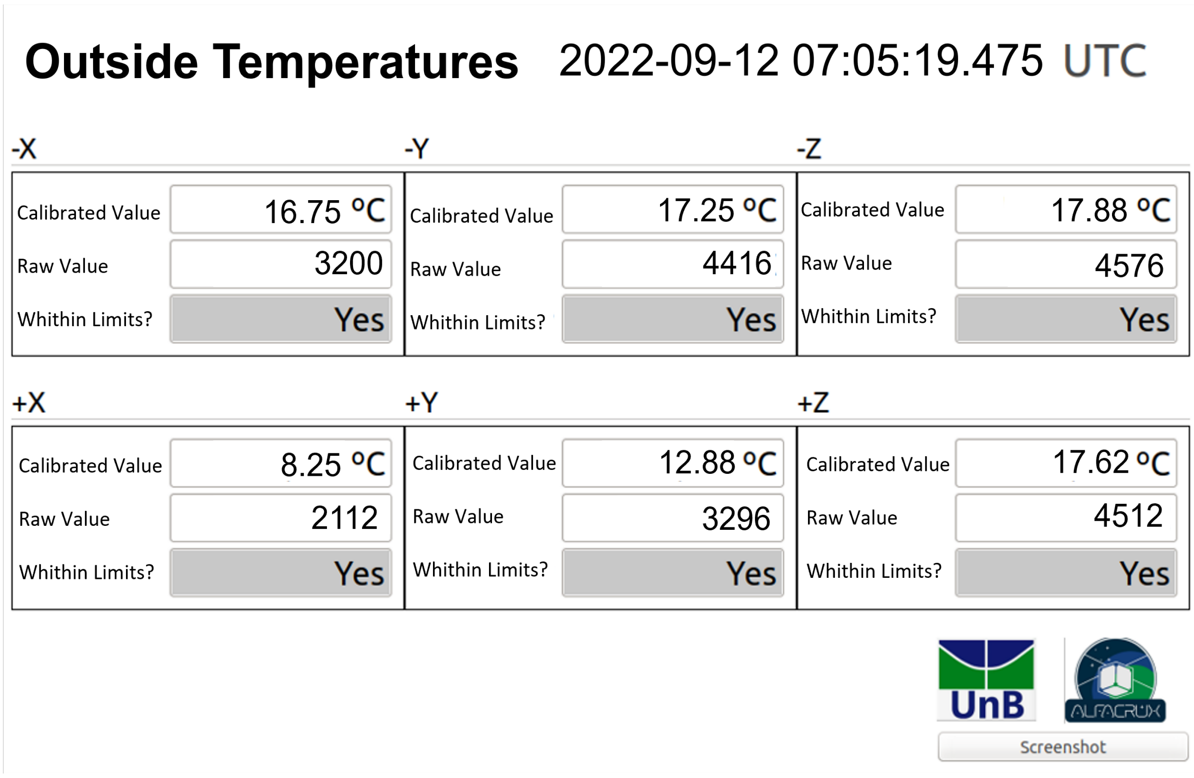

Figure 6: Viewing the telemetry of the Outside Temperatures packet.

software, with documentation explaining how it works and validated in several missions.

During the use of this tool some difficulties were seen. Problems installing Cosmos on a Linux system, limitations in the visualization layouts of telemetry, in which, version 5 brings improvements to these limitations and restrictions in the processing of telemetry through the Cosmos keywords, being necessary to create scripts for simple functions, such as adding a constant in the data received.

Since the difficulties mentioned above do not prevent the use of Cosmos for a nanosatellite operation, Cosmos is an option that students can use to facilitate the development of a ground software, both for testing and for operations.

cFS is another open source software that can be used by students to decrease the development time for flight software. NASA provides training, documentation, and source code to facilitate access to this technology.

Acknowledgments

The authors would like to thank the Brazilian agencies National Council for Scientific and Technological (CNPq) and the Federal District Research Support Foundation (FAPDF) that supported this work.

References

[1] A. Toorian, K. Diaz, S. Lee, The cubesat approach to space access, in: 2008 IEEE Aerospace Conference.

[2] A. J. Rohling, A reference architecture for satellite systems operations, Ph.D. thesis, Instituto de Pesquisas Espaciais, 2018.
[3] Ball Aerospace, The user interface for command and control of embedded systems, https://ballaerospace.github.io/cosmos-website/, 2022. Accessed in: May 12^{th}, 2022.
[4] F. de Novaes Kucinskis, M. G. V. Ferreira, On-board satellite software architecture for the goal-based Brazilian mission operations, IEEE Aerospace and Electronic Systems Magazine 28 (2013).
[5] D. J. F. Miranda, M. Ferreira, F. Kucinskis, D. McComas, A comparative survey on flight software frameworks for 'new space' nanosatellite missions, Journal of Aerospace Technology and Management 11 (2019).
[6] NASA, nasa/cfs-101, https://github.com/nasa/CFS-101, 2019. Accessed in: August 19^{th}, 2022.
[7] Ball Aerospace, Directory structure, https://ballaerospace.github.io/cosmos-website/docs/v4/structure, 2022. Accessed in: May 14^{th}, 2022.
[8] NASA, core flight system, https://cfs.gsfc.nasa.gov/, 2021. Accessed in: August 19^{th}, 2022.
[9] NASA, Features - core flight system, https://cfs.gsfc.nasa.gov/Introduction.html, 2021. Accessed in: August 19^{th}, 2022.
[10] NASA, Introduction - core flight system, https://cfs.gsfc.nasa.gov/Features.html, 2021. Accessed in: August 19^{th}, 2022.
[11] Core Flight System (cFS)Training, NASA, 2021.
[12] B. Aerospace, Installation, https://ballaerospace.github.io/cosmos-website/docs/v4/installation, 2022. Accessed in: May 14^{th}, 2022.
[13] P. Y. Yamada, Sistema de Visualização de Telemetria e Envio de Telecomando para o CubeSat AlfaCrux, Trabalho de conclusão de curso, University of Brazilian, 2022.

AN EXPERIMENTAL EVALUATION OF LONG-RANGE TECHNOLOGY IN A STRATOSPHERIC SONDE FOR EDUCATIONAL CUBESAT MISSION ALDEBARAN-1

Luis C. O. Silva[(1)], **Jose R. B. P. Junior**[1], **Carlos A. R B. Junior**[1], **Edemar M. Filho**[1], **Geovaana M. M. C. Magalhaes**[1], **Ellias P. Fernandes**[1], **Antonio C. S. Santos Filho**[1], **Alex I. V. Almeida**[1], **Emanuel R. V. Silva**[1], **Fernanda S. A. Vale**[1], **Jennifer C. S. Barraza**[1], **Julio C. R. Machado**[1], **Leonardo V. S. S. Menez**[1], **Rodrigo A. M. Carvalho**[1]

[(1)]*Federal University of Maranhão, Av. dos Portugueses, 1966 - Vila Bacanga, São Luís - MA, 65080-805, Brazil*

Keywords: *Stratospheric Sonde, LoRa, CubeSat, Aeroespace Engineering*

Long Range (LoRa) technology has been used in CubeSats because of the characteristics that make it immune to noise interference and the Doppler effect. The configuration settings such as signal power, transmission rate, spreading factor, and bandwidth can be important for the success of the space mission based on this technology. Testing involving stratospheric balloons assists in the right choice from telemetry parameters, besides them allowing long-range data collection. This work approaches some experiments performed using LoRa technology in stratospheric balloons, during the Aldebaran mission whose objective is to develop the CubeSat Aldebaran-1. Two sondes have been developed and launched containing several sensors and a 2-megapixel camera. Temperature sensors, humidity, ultraviolet, ozone, and GPS were used. In each launch, a weather balloon 600g was used with helium gas, supplied by Alcantara Space Center. These experiments verify the proposed LoRa as a solution for Aldebaran Mission and spatial applications.

1. Introduction

This work aims to present the development and results of the construction process of two stratospheric sondes, which made it possible to test radio frequency components that will be used in the Aldebaran Mission. This mission aims to build the Aldebaran-1 nano-satellite, developed by professors and students from the Aerospace Engineering course and other courses.

The stratospheric sonde consists of a balloon capable of reaching high altitudes and carrying a payload attached to it. The high-altitude balloon is a large latex balloon, inflated with helium or hydrogen, that can carry a small sonde or satellite into

Email addresses: claudio.luis@ufma.br (**Luis C. O. Silva**), jrbp.junior@ufma.br (**Jose R. B. P. Junior**), ecarlos.brito@ufma.br (**Carlos A. R B. Junior**), edemar.filho@ufma.br (**Edemar M. Filho**), moura.geovaana@discente.ufma.br (**Geovaana M. M. C. Magalhaes**), ellias.portugal@discente.ufma.br (**Ellias P. Fernandes**), claudio.antonio@discente.ufma.br (**Antonio C. S. Santos Filho**), alex.iury@discente.ufma.br (**Alex I. V. Almeida**), emanuel.valentim@discente.ufma.br (**Emanuel R. V. Silva**), fernanda.sav@discente.ufma.br (**Fernanda S. A. Vale**), jennifer.barraza@discente.ufma.br (**Jennifer C. S. Barraza**), machado.julio@discente.ufma.br (**Julio C. R. Machado**), leonardo.menez@discente.ufma.br (**Leonardo V. S. S. Menez**), rodrigo.amc@discente.ufma.br (**Rodrigo A. M. Carvalho**)

the stratosphere. After reaching its apogee, a parachute is used to cushion the fall, bringing the sonde back to the ground slowly after the balloon breaks.

The construction of the sondes was made in the Laboratory of Electronics and Space Embedded Systems (LABESEE) of the Federal University of Maranhão (UFMA) and was conducted by the professors who coordinated the Mission, with the collaboration of the Alcantara Space Center (CEA). The developed activities allowed the practical applications of antenna construction, software-defined radio (SDR), LoRa radio technology, image processing, use of communication protocols, making and assembling embedded systems, and project management.

This paper is organized as follows: besides the introduction, this paper brings, in section II, a review of literature works associated with this problem. The description of the proposed methodology and the implementation of the sondes are presented in section III. In section IV, the results of the experiments performed with the launches are presented. Finally, section V brings the conclusions.

2. Related Works

The study of planet Earth has progressively advanced after the first natural satellite was launched into space in 1957. From this event on, numerous projects in various fields of science have been developed, among them the study of climate and weather. However, there are several ways to investigate atmospheric phenomena, their properties, and their characteristics, such as, for example, the use of weather balloons. These artifacts, also known as high-altitude balloons, perform tests and measurements of the atmospheric layers.

The stratospheric balloons carry in their structure hardware, software, sensors, and cameras to the edges of space. [1]. heir analyses take place more precisely in the Troposphere and Stratosphere, which are the first layers of the Earth's surface [2].Various events happen at these levels and in the Tropopause - the intermediate zone between both [3].

High-altitude balloons have been used for decades to conduct scientific studies. According to [4], qwhich has maintained a Balloon Platform for 30 years, these artifacts allow beyond these investigations, the demonstration of spacecraft-oriented technologies. Their launch sites depend on several factors such as cost, the collection to be made, or the duration of the mission which can be hours, days, or weeks. [5].

The use of stratospheric balloons has the benefit of low cost, fast execution of activities, and easy accessibility that allows the integration of educators and students in the realization of these activities. Another benefit is that the balloons have access to various levels of the atmosphere, enabling the collection of data and the effects caused at each level. [6]. For NASA, in addition to these benefits, balloons have also conducted critical space research [7].

3. Materials and Method

The mission to qualify the LoRa radio as the communication device for the Aldebaran-1 satellite was divided into two launch operations: the first, with the objective of preparing the team and allowing, chose the parameters for data transmission to the ground segment, and the second, for testing a higher power radio, power consumption, and image transmission along with sensor data.

3.1. Data telemetry using LoRA

In the experiments performed, two LoRa radio models from different manufacturers and different powers were used. Both radios were used in the 433MHz frequency, in the ISM band, ideal for amateur radio frequency transmission experiments.

In the first experiment, a LoRa module from Chengdu Ashining Technology, AS32-TTL-100 model, based on Semtech's SX1278 controller, was used. This radio has a power of 100 mW power. In the second experiment, a LoRa module from manufacturer EBYTE, model E32-433T30D, based on Semtech's SX1278 controller, was used. This radio has a power of 1000 mW.

To facilitate the understanding of the experiments performed, in the following sections, the details of each sonde, launch, and telemetry performed will be addressed.

3.2. Structure and Parachute

The structure of the sondes for both experiments were made using Styrofoam boxes with the following dimensions: First sonde, external measures are length 15.3 cm, width 12.3 cm, and height 7.5 cm, internal measures are length 13.3 cm, width 10.3 cm, and depth 5.5 cm; case width 1 cm; Second sonde, external measures are length 16.7 cm, width 15 cm, and height 11 cm, internal measures are length 14.3 cm, width 12.6 cm, and depth 8.6 cm; case width 1.2 cm.

After reaching its apogee, a parachute is used to cushion the fall, bringing the sonde back to the ground slowly after the balloon breaks. In both experiments, a functional endurance training parachute used in sports activities was used. The approximate size diameter of the parachute used is 120 cm with material made of nylon. Launch tests were conducted to evaluate the descent speed of the parachute, at a height of approximately 10 meters, using a 400 g ballast. The time of arrival on the ground was recorded, and the final speed was determined when the parachute and ballast assembly reached the ground. Thus, it was realized that the proposed parachute could be used in the experiments in such a way as not to offer risks during descent.

3.3. Data receiving ground station

The ground station is of particular importance for the experiments. Due to its correct operation, it was possible to perform the reception and storage of the data collected by the sonde. The basic structure of the receiving station used involved antennas, some software-defined radios (SDR), LoRa radios connected to Arduino NANO microcontrollers, and computers. The station was set up in the external facilities of the Meteorology sector of the Alcantara Launch Center, where the helium balloons were filled and the sondes launched.

To receive the LoRa radio signals transmitted by the sondes, protoboard circuits were assembled containing LoRa E32-433T30D 100 mW radios connected to the antennas used in telemetry. The radios, in turn, were connected to Arduino NANO boards which, meanwhile, were connected to computers via USB cables. On the computers, software that received the telemetry data sent by the Arduino NANO boards through the computer serial ports and stored it in ASCII text files was installed. In figure 1-(a) it is possible to see one of the circuits assembled in the protoboard used in the experiments. In the picture 1-(b) it is possible to see the ground station structure assembled, in the premises of CLA's Meteorology Sector, during the launch, tracking, and telemetry operation of the first sonde.

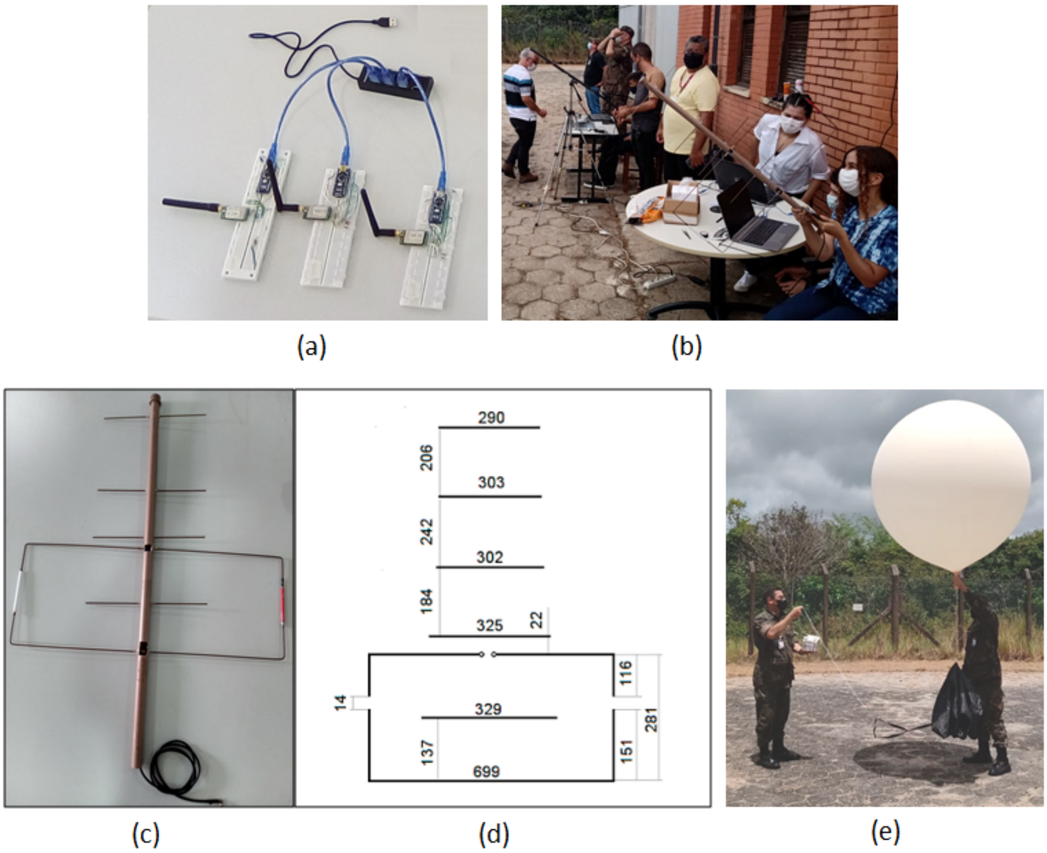

Figure 1: Data receiving ground station: (a) Protoboard circuit used in the experiments. (b) Ground station structure assembled. (c) Antenna used in experiments. (d) Measurements of the antenna elements. (e) Sonde launch.

The antennas used in the experiments were made by the students themselves who participated in the sonde launching campaigns. Workshops were held before the start of the experiments, with the objective of training the students in the operation and making of the Moxon-Yagi antennas, used in the telemetry of the data transmitted by the sondes. The model of the antennas used can be seen in figure 1-(c), and the measurements of the antenna elements in figure 1-(d). The antennas were designed to be used at the 433 MHz frequency.

3.4. First sonde

The first sonde was launched on September 22, 2021, at the Meteorology Section of the Alcantara Launch Center (CLA), with the participation of five students and four professors, as well as some meteorology personnel. The launch occurred at 11:03 am local time, after filling and tying the balloon to the parachute and sonde. From this moment on the team started receiving the telemetry data and the tracking operation of the sonde.

Both the weather balloon and the helium gas used in the operation were provided by CLA's Meteorology Sector. A 600 g balloon was used, which is normally used to launch RS41 weather radiosondes. In the picture 1-(e) it is possible to see the sonde launch being carried out, after signaling for favorable launch conditions.

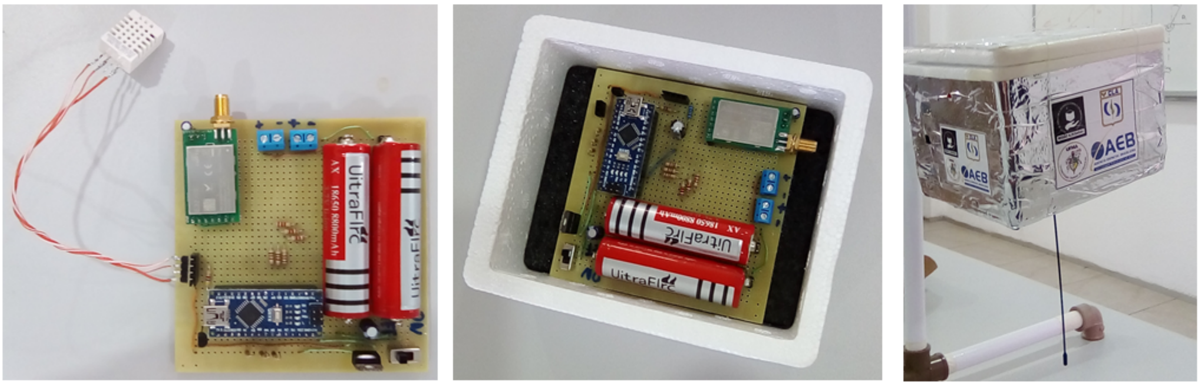

(a) (b) (c)

Figure 2: Embedded system of the first sonde: (b) System board. (b) Structure and system board. (c) Mounted sonde and coated with aluminum tape.

3.4.1. Embedded system board

In figure 2-(a) it's possible to see the embedded system board of the first sonde. All components were soldered onto an islanded phenolic board of size 10 cm x 10 cm. After assembling all the systems and packing them in the structure, the sonde was weighed using a digital scale, obtaining a mass of 285 g. In figure 2-(b) you can see the sonde installed in the structure and, in the background, the layer of material used as protection against shocks inside the sonde. Connected to the analog and digital ports of the Arduino NANO ATMega328P microcontroller board, the two sensors used in the experiment were connected: LM35 temperature sensor and DHT22 temperature and humidity sensor. The LoRa radio was connected to the Arduino NANO's digital communication ports, in order to enable the sending and receiving of data by the radio, as well as the configuration of transmission parameters during flight.

An RG58 coaxial cable was used to connect the LoRa radio to the antenna, located on the bottom of the sonde. The antenna used was a 3 dbi 433 MHz omnidirectional antenna with a 150 mm long SMA connector. The antenna was glued to the underside of the sonde, and secured with the adhesive tape used in the thermal protection of the sonde. The antenna cable passed through a hole drilled in the bottom of the structure, which was then filled with hot glue to prevent the temperature inside the sonde from getting too low. In the picture 2-(c) it's possible to see the mounted sonde, properly covered with Tectape aluminum tape for cooling. The tape served as a protective layer to prevent the low temperatures of the stratosphere from interfering with the batteries' operation.

Two 18650 Lithium rechargeable batteries connected in series were used to power the components on the board. Tests were made with the system transmitting the telemetry data and an average of 3 hours of battery charge duration was reached. An LM7805 voltage regulator was used to convert the voltage to 5V, in order to power the onboard components. A battery voltage sensor was developed by connecting the output of the batteries to one of the analog ports of the Arduino NANO. In this way, it was possible to send the voltage of the batteries within the telemetry data package and track the performance of the power system.

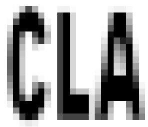

Figure 3: Image generated and saved in gray scale, 24 x 24 pixels, stored in firmware of first sonde microcontroller.

3.4.2. Data telemetry

To evaluate the transmission capacity of the LoRa radio in different scenarios of data transmission rates over the air, transmissions were performed at rates of 300 bps, 1200 bps, and 19200 bps. At transmission rates of 300 bps and 1200 bps, the following telemetry data were sent: sequence number, DHT temperature sensor, DHT humidity sensor, LM35 temperature, serial battery voltage. At the transmission rate of 19200 bps, a set of bytes representing a small image was transmitted, a test for the image transmission, to be performed in the second sonde. The image, generated from drawing software, and saved in PNG format, in gray scale and dimensions of 24 x 24 pixels can be seen in figure 3.

The image was converted into a sequence of bytes, where each byte represents the gray level of one pixel, and was stored as an array within the firmware source code written on the Arduino NANO board of the sonde's embedded system. The sonde's embedded software transmitted every 10 seconds a telemetry signal at 300 bps and then at 1200 bps. Every 30 seconds a signal containing the image recorded in the sonde's firmware was transmitted at 19200 bps, in blocks of 32 bytes.

3.5. Second sonde

The second sonde was launched on December 2, 2021, at the Meteorology Section of the Alcantara Launch Center (CLA), with the participation of five students and four professors, as well as some meteorology personnel. The launch took place at 10:15 am local time, after filling and tying the balloon to the parachute and sonde. From this moment on the team started the reception of the telemetry data and the tracking operation of the sonde. The weather balloon was the same one used to launch the first sonde.

3.5.1. Embedded system board

In figure 4 it is possible to see the schematic for connecting the components of the second sonde's embedded system. Three 18650 Lithium rechargeable batteries connected in parallel were used to power the components on the board. Tests were made with the system transmitting the telemetry data and an average time of 3 hours was reached for the battery charge duration. During the tests, data and image transmission times related to the power of the LoRa transmitter were evaluated, and battery consumption was observed. A BOOST DC converter based on the XL6009 component was used to raise the operating voltage to 5 V, and an LM1117 linear regulator to lower the operating voltage to 3.3 V.

After the assembly of all systems and packaging in the structure, the sonde was weighed using a digital scale, obtaining a mass of 485 g. The table 1 shows the list of all the components used to make the board.

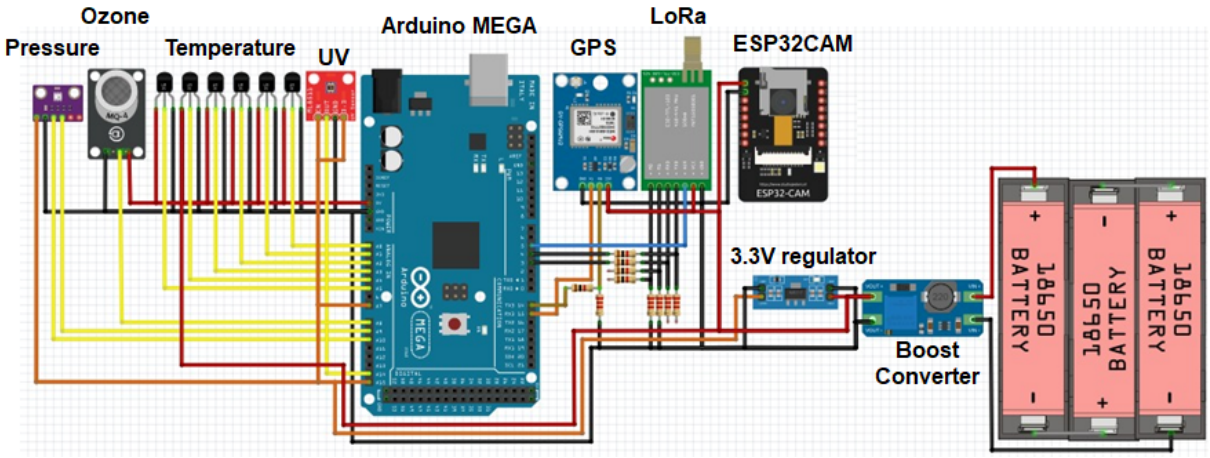

Figure 4: Assembled circuits for receiving data at different transmission rates.

Table 1: List of second sonde components.

ITEM	COMPONENTS	SPECIFICATIONS
EMBEDDED SYSTEMS	1 ARDUINO MEGA	Microcontroller: ATmega2560
	1 ESP32 CAM	ESP32 Camera OV2640- 2MP
	1 LORA	E32-433T30D Controller: SX1278 Max. Electric Power: 100mW Frequency: 433MHz
	6 TEMPERATURE SENSOR	Model: TMP36
	1 UV RAYS SENSOR	Model: ML8511
	1 PRESSURE SENSOR	Model: BMP280
	1 OZONE SENSOR	Model: MQ131
	GPS MODULE	Model: GY-GPS6MV1
	10 RESISTORS	10 kΩ, 20kΩ E 4.7 kΩ
POWER SYSTEM	STEP UP CONVERSOR (BOOST DC)	Model: XL6009
	2 RECHARBLE BATTERY	Model: 18650 Load voltage : 4.2 V Rated voltage : 3.7 V Batery: 2000mAh Material: Lithium
	1 TENSION REGULATOR	LM7805 AND LM1117 3.3V

3.5.2. Data telemetry

In the second experiment, transmissions were performed at rates of 300 bps and 9600 bps. The 300 bps rate was reserved for the telemetry data and the 9600 bps rate for transmitting the images captured by the camera used. The following telemetry data were sent: sequence number, 5 temperature sensors, ultraviolet, atmospheric pressure, ozone concentration, latitude and longitude, altitude, hour, minute, and second. The captured images were transmitted in 1600 x 1200 pixels resolution, JPEG compression, 8-bit color.

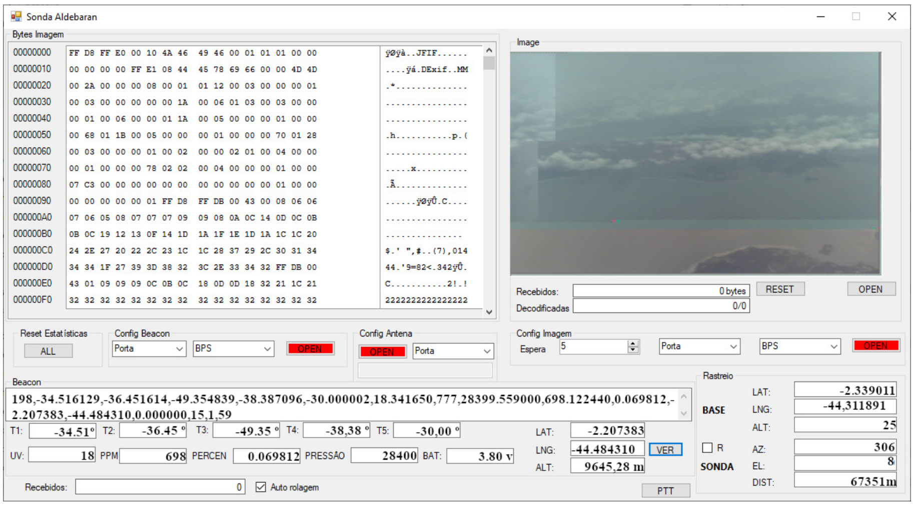

Figure 5: Software developed to display and save the telemetry data from the second sonde.

To assist in the data telemetry process, a visual application was developed in C# language, using Microsoft Visual Studio. This application connected to the serial ports of one of the computers used in the tracking station and received from the Arduino boards that were connected to the LoRa radios, the data transmitted by the sonde. In figure 5 it is possible to see the application screen when receiving the telemetry data and one of the transmitted images.

4. Results and Discussion

This section will present the results obtained from the launches of the two sondes and briefly analyze the use of the LoRa radio for the Aldebaran mission. As soon as the data was received, it was stored in ASCII text files in comma-separated values (CSV) format. The data could then be imported into Microsoft Excel for analysis.

In the first sonde, the GPS wasn't used and, for this reason, it was not possible to evaluate the trajectory. However, from the temperature and humidity data, it was possible to perform an analysis of the altitude reached by the sonde [8]. Comparing with the average vertical profile of the air pressure shown in the figure 6-(a), we realize that the vertical trajectory of the sonde, shown in the figure 6-(b), pIt has the same climb pattern. The first data was received at approximately 11:00 am and the last at 1:54 pm, so it is estimated that the flight time was 3 hours. Based on the figure 6-(b) It can be observed that the time of the balloon burst was approximately 12:58 pm local time.

The second sonde was equipped with a GPS. However, the GPS presented problems in providing altitude, due to this fact, it was necessary to calculate the altitude based on the atmospheric pressure provided by the sensor designed for this purpose. The data was exported in GPX format, compatible with Google Earth. The data were imported into Google Earth and it was possible to trace the 3D trajectory of the sonde. In this view, it is possible to see the variation in the sonde's altitude, as well as its direction.

Every 5 minutes, the sonde sent back images obtained from the onboard CAM. The image transmissions were made in blocks of 50 bytes, with a pause of 250 milliseconds

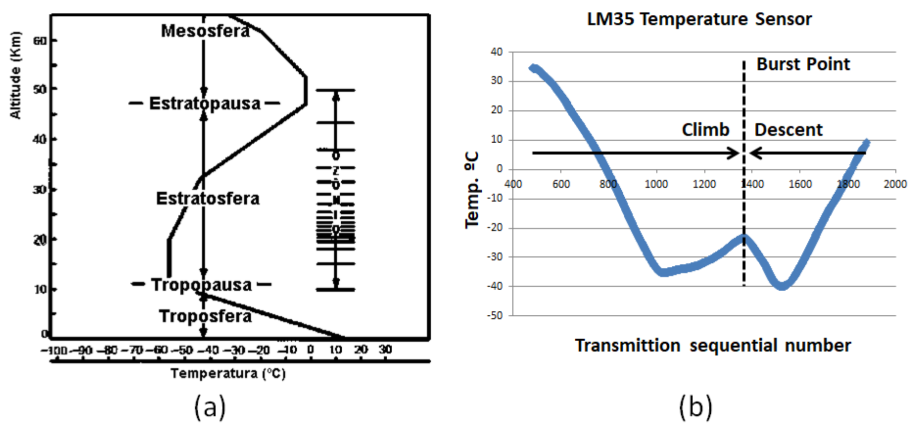

Figure 6: Average vertical profile of the air pressure [8]. Climb and Descent pattern of the first sonde.

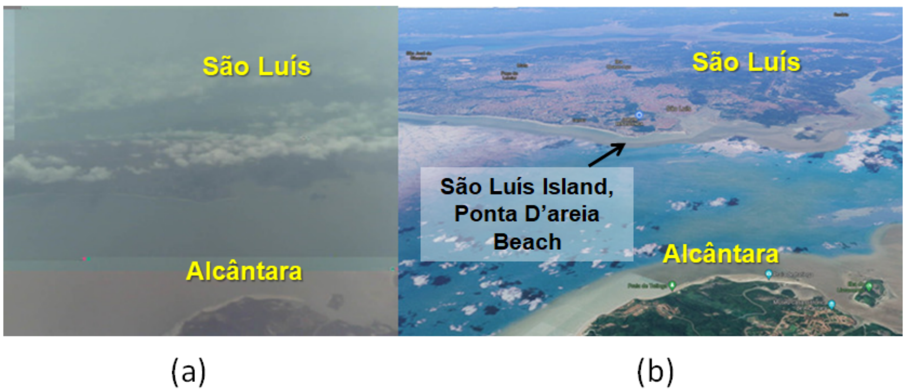

Figure 7: (a) Image transmitted from the second sonde. (b) Same image in the Google Earth.

between each transmission, so as not to drown the transmission of the LoRa radio, connected to the onboard Arduino MEGA. The transmission of a 1600 x 1200 pixels image took, on average, 2 minutes and 40 seconds. In the figure 7-(a) it is possible to see one of the photos received at the ground station. In the figure 7-(b) it is possible to see the same image, although in the Google Earth.

In the figure 8-(a) it is possible to see the trajectory of the sonde. The location and the distance to the place where the ground station was installed, as also the approximate location to the extreme points of the island of São Luís and the city of Alcantara, are framed in the image shown in figure 8-(b). The location was Latitude -2.224466 , Longitude -44.477798 and altitude 11352.33 km. The image was acquired and transmitted at approximately 11:52 am. The maximum altitude of second sonde was 15088,49 km.

5. Conclusion

The planning and implementation of a stratospheric sonde and its launching from a meteorological balloon make accessible, for students of Aerospace Engineering, a direct experience about sending artifacts into space. In this work, we present the construction process of two stratospheric sondes, designed to test radio frequency components based on LoRa technology, which will be used in the Aldebaran Mission.

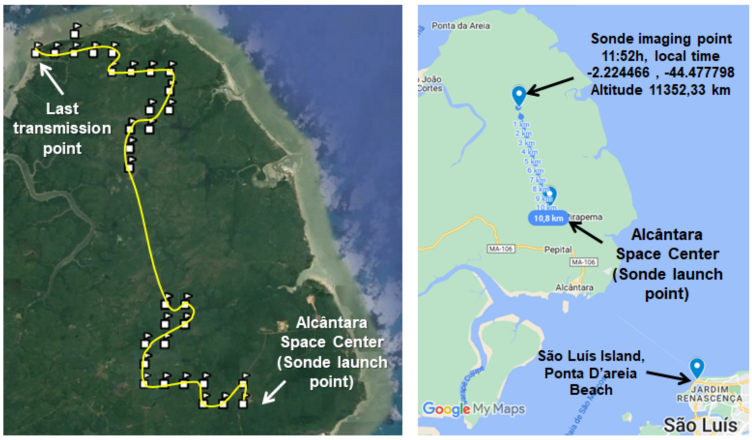

(a) (b)

Figure 8: (a) Sonde trajectory. (b) Location and altitude of the point where the image was taken and distance to the tracking ground station.

The sondes were developed by the students and teachers participating in the project and were launched from the Alcantara Space Center. The telemetry was performed using antennas and elaborated devices and, in this way, it was possible to perform flight trajectory analyses, as well as to receive data from the various onboard sensors. It was noticed that the technology proved adequate, both for the transmission of sensor data and images from the stratosphere. Thus, it is expected to initiate the field of Space Research and Engineering in Maranhão, motivating students to develop multidisciplinary activities and follow the development process of a space mission.

Acknowledgments

The autors thanks Brazilian Space Agency (AEB) and Alcântara Launch Center (CLA) for providing financial and logistic support that contributed to development of this work.

References

[1] N. Yajima, N. Izutsu, T. Imamura, T. Abe, Scientific Ballooning: Technology and Applications of Exploration Balloons Floating in the Stratosphere and the Atmospheres of Other Planets, Springer, 2009.

[2] A. A. Pulschen, G. G. de Araujo, A. C. S. R. de Carvalho, M. F. Cerini, L. de Mendonca Fonseca, D. G. F. Rodrigues, Survival of extremophilic yeasts in the stratospheric environment during balloon flights and in laboratory simulations, Applied and Environmental Microbiology 84 (2018).

[3] N. D. S. G. CONSORTIUM, The Near-Space Balloon Competition Handbook, NORTH DAKOTA SPACE GRANT CONSORTIUM, 2017.

[4] NASA, Scientific balloons overview, 2018.

[5] K. P. Queiroz, S. M. Dias, J. M. Duarte, M. M. Carvalho, Uma solução para o sistema brasileiro de coleta de dados ambientais baseada em nanossatélites, Applied and Environmental Microbiology 34 (2018).

[6] C.-J. Fong, M.-S. Chang, H. Chen, H.-C. Cheng, Y.-L. Kuo, C.-C. Liou, E. Yang, Personal satellite research and development for space experiment and application, in: Remote Sensing Satellite Technology Workshop 2014.

[7] W. Carlyle, Balloons offer near-space access for space biology researcher, 2020.

[8] J. O. BRIEN, Radiation beltss, Scientific American 208 (1963).

DESIGN AND ANALYSIS OF A COTS TT&C SUBSYSTEM FOR A CUBESAT IMAGING PAYLOAD MISSION

Ana Carolina L. Oliveira[(1)], **Carlos M. Zago**[(2)], **Diego W. B. Arruda**[(3)], **Gabriel A. Coelho**[(4)]

[(1)] *Universidade Federal de Minas Gerais (UFMG), +55 (71) 99934-4126, acloliveira2001@gmail.com*

[(2)] *Universidade Federal de Minas Gerais (UFMG), +55 (34) 9143-5788, czagofilho@gmail.com*

[(3)] *Universidade Federal de Minas Gerais (UFMG), +55 (24) 99878-5721, diego.wb.arruda@gmail.com*

[(4)] *Universidade Federal de Minas Gerais (UFMG), +55 (35) 9702-2210, gabbrielcoelho@gmail.com*

Keywords: *TT&C subsystem, CubeSat, Project design, Analysis, Low Price space mission*

The use of space as a scientific tool for applications such as data acquisition by remote sensing is extremely important for the advancement of knowledge. Since the beginning of space exploration, this perception of peaceful exploration and for the purpose of evolution have been of great value and driving force for the development of the area by scientists. However, only with the advancement in rocket projects, reducing the cost of deployment in orbit, and with the miniaturization of electronic components it was possible to democratize and allow more space objects to be built and launched. With the reduction in component sizes and costs involved, a new range of possibilities was born. If before large satellites were needed that performed various missions during their lifetime, today small satellites, with the size of shoeboxes, are used to perform very specific missions, for a determined time. These "small satellites" provided that new players arise in the market for space systems. With these objects, universities and their students can build their own projects, enabling prototypes of new sensors and components that should be tested in a space environment, fostering a new era in technology development with space applications and in other aspects of daily life. With the increase in the use of this category of satellites, an area that must be highlighted is that of communication systems, as it is one of the vital subsystems of any spacecraft. The communication system, many times called TT&C - Telemetry, Tracking and Command, is responsible for communication between the ground segments of the mission and the satellite. The incorrect functioning of this system can lead to the unusability of the spacecraft, making it impossible to receive commands sent by operators and to send telemetry and mission data. This paper aims to study and list proposals for architectures for developing a TT&C system. A comparative analysis between types of architecture and configurations (type of antenna, frequency, powers send and modulators) commonly used in small satellites and typical satellites is presented. In addition, a proposal for a TT&C architecture design project for an imaging mission on low orbit earth (LEO), considering requirements commonly found in data transfer missions for similar missions.

1. Introduction

Space exploration and the use of space technologies are of vital importance for the development and search for knowledge, being areas widely researched and with high investment. However, obtaining data from the space environment is only possible through the dialogue between space vehicles and ground stations. Thus, the presence of the Communication subsystem of an embedded system is vital, since this subsystem is the interface between the satellite and the ground segment, being responsible for tracking in orbit and for managing the communication between these segments. Its proper functioning becomes critical for the correct course of a remote mission because, although its incorrect functioning does not imply failures in the system itself, any failure in the TT&C prevents the generated and collected data from being transmitted to a database of operation. Thus, in aerospace systems, such as satellites, the communication failure may imply complete loss of the vehicle, since the correction of the problem may be impractical and/or impractical due to the environment in which the object is inserted and the difficult accessibility of space.

In this sense, it is essential to guarantee the reliability of this subsystem and to mitigate the occurrence of defects, and an adequate dimensioning. In the context of radio frequency communication systems design, we will be dealing, mainly, with two different types of defect: failure, which prevents something from occurring or working correctly, and imperfection or undesirable behaviors, when there is no failure. and that allows the transfer of data between the antennas to happen. However, because of imperfections, the received signal may be unreliable. In both cases, we consider that the communication link is not reliable and, to make it reliable, it is necessary to use information retrieval techniques.

Aiming at the ideal dimensioning, for analysis and specification of the subsystem, we can divide it into two distinct systems, an execution state management system, in which we can model the TT&C as a finite state machine, where each state is a different operating mode where operating modes define how the subsystem is currently performing. The other possible system is a communication link, or dynamic physical system. In addition, we must consider that the subsystem specifications must satisfy the restrictions imposed, such as geometry and operating frequency, as well as certain characteristics desired for the project, such as energy consumption, effective communication area and gain.

Thus, in the work developed, we sought to analyze essential aspects for the construction of the TT&C, evaluating the main causes of errors and methodologies for minimizing them, in addition to devising a proposal for a communication subsystem of a cubesat with a mission of low orbit imaging.

2. Literature Review

For Wiley J. Larson and James R. Wertz in Space Mission Analysis and Design [1], the TT&C subsystem comprises the communication of mission data, which is the payload data, and the housekeeping data, which is the state data of the satellite platform.

Furthermore, when talking about satellite communication links in Satellite Technology - An introduction, Andrew F. Inglis and Arch C. Luther define two types of links, the downlink, characterized by the transmission of signals by the satellite to the ground segment, and the uplink, characterized by transmission of signals from the ground segment to the satellite.

Beyond the payload and housekeeping data, which are necessary for the mission, other signals are sent by the orbiting satellite, called Beacon. It is used to track the spacecraft, playing an important role for the TT&C subsystem. This can be done by locating the direction of the emission source or by demodulating the Beacon signal with the location message.

Another important factor in the design of TT&C systems is the performance of electronic circuits. With the objective of minimizing the energy cost, actuation states are defined that are triggered under specific conditions or through the command of operators on the ground. These states are called [1] operational modes. Each mode represents an operational state in which the system acquires specific characteristics.

2.1. Restrictions

In the first analysis of telecommunication systems for cubesats, restrictions imposed on the project must be taken into account.

In general, CubeSats are a class of nanosats that have dimensions between 1U and 12U, where each 1U is equivalent to a 10x10x10 cm cube and has a mass of up to 2kg. Thus, they have restrictions due to their geometry.

In addition, most CubeSats are located in LEO (Low Earth Orbit), whose altitude varies between 100 km and 1000 km. In this band, there are limitations regarding the communication window with the ground station, and the distance of the communication link, implying in losses related to free space.

Another very important factor for choosing the communication system is the current legislation. Each country has its own telecommunication rules, in addition, any radio communication project for satellites is subject to international standards, such as those of the ITU.

2.2. Link Budget

The link budget is a tool with which the power gains and losses that affect a communication signal are taken into account, in order to determine the power needed for the signal to be received. With this, it is possible to guarantee that the information is received in an intelligible way with an adequate signal-to-noise ratio.

2.3. Noises

Noises are unwanted signals that are present in the transmission medium. The noise level determines the maximum sensitivity and reception range of a radio receiver.

In the presence of noise, if a radio transmission has an amplitude smaller than the amplitude of the noise, the noise will "muffle" the signal.

The noise level in a communication circuit is measured by the signal-to-noise ratio $\frac{S}{N}$. When this ratio is below one (0 dB), the noise is greater than the signal, requiring a special treatment to recover the information or preventing its transmission from taking place.

Among the many factors that can cause some type of noise, the main ones are: radiation from other emitters; bad weather such as fog, rain and storms; cosmic radiation, such as from the Sun; interference effects of waves reflected by the Earth, obstacles or layers of the atmosphere.

As most effects depend on complex systems, such as weather forecasting, modeling such noises can be complicated and even impractical. Commonly, statistical methods are used to determine possible noise values, considering the average of occurrence and the probability of reaching certain noise values [2].

2.4. Failure

A relevant factor for the dynamics of communication and very important for the transition between operating modes is failure. Failure can be the defect or lack of perfection in a given system. For cubesat projects, one of the goals of the design stage is to reduce or prevent these failures from occurring.

In the context of radio frequency communication, we will be dealing, mainly, with two different types of defect: failure, which prevents something from occurring or working correctly, and imperfection or undesirable behaviors, when there is no failure and which allows transfer of data between the antennas. However, because of imperfections, the received signal may be unreliable.

2.4.1. Failure Types

Failures can take many forms. Among them are the poor energy supply of the equipment, the operation outside the acceptable temperature range and the non-release of the antennas. Poor power supply is the fact of not reaching the minimum energy required for the subsystem to work, causing its shutdown, or exceeding the ideal voltage range, causing possible damage to the components and disturbing their perfect functioning. In the same way, temperature outside the acceptable range can damage the components.

Another important type of failure is not releasing the antennas. Although it does not necessarily completely inhibit communication, this failure can interfere and, depending on the severity, preventing correct communication, considering that the antenna may be obstructed from having an open field view with the communication link, but it can also damage devices that are sensitive to electromagnetic radiation that are on the satellite, since the signal transmission can be directed to the internal part or to the part that does not have adequate protection on the satellite.

In general, verifying the failure is not a complicated task, as it is possible to measure the behavior and state of the system and, with this information, verify that it is not working as expected. However, checking for damage due to the failure can be a more complex task.

During the system development, it is necessary to dimension the components with adequate redundancy to ensure that failures of any kind do not cause the mission to end prematurely.

2.4.2. Undesired Behaviour

Undesired behavior or system imperfections generally do not harm the system or prevent communication. However, they can lead to failures and generate high bits error rates - BER . The BER is an indicator of how many transmitted bits are unreliable or incorrect within a communication time interval and is an important way of evaluating the quality of the transmission link.

Among the scenarios in which they may imply undesirable behavior that the satellite may face, there are solar storms, storms or bad weather (rain), eclipse (satellite between the Sun and Earth), among other aspects related to the propagation path of the link.

During these moments, there is a probability of presenting a greater error of bits, since the solar radiation is emitted in the frequency used for the communication and the high amount of clouds make it difficult or prevent the transmission of signals. Therefore, it is desirable to avoid carrying out communication at these times.

Although all scenarios are easy to understand, there is little that can be done to avoid the occurrence of a bit error. As these types of events are relatively rare, in the case of eclipses and solar storms, the sending and receiving of signals is generally interrupted during the occurrence of these events. However, it is possible to model and consider the rain and the imprecise alignment of the Sun during the design phase, reducing the action of these factors through safer modulators, in terms of noise, and increasing the signal sending power.

2.5. Components

Generally, as many electronic systems as possible are used for cubesats compared to mechanical systems, due to their miniaturization. These electronic components are, for the most part, Systems on a single chip - SoC and made to work specifically for the proposed objective. For larger missions, with a greater financial budget, several systems are designed specifically for the mission, allowing even more optimization of geometric and energy resources.

In addition, the components used in cubesats projects, most of them are commercial off-the-shelf (COTS), must survive the space environment and be reliable, which makes the standardization of these components gaining strength in recent times.

2.5.1. Antennas

One of the most important components is the CubeSat antennas, which are the interface between the electrical currents, generated and received in the satellite's internal equipment, and the radio electromagnetic waves that propagate the information.

The main characteristics of choosing such equipment are the operating frequency, usable bandwidth, effective irradiation area and gain.

The antenna must, together with the other components, meet the needs identified by the link budget.

For various reasons, the CubeSat may not be able to get a proper annotation. In addition, the vehicle may also experience tumbling, or some form of loss of control. In general, the solution to this type of problem is the use of omnidirectional antennas.

2.5.2. Receiver and Transmitter

In wireless communication, the binary signal, used by OBDH and other subsystems, undergoes several transformations before being transmitted by the antennas.

The main transformations that occur between the binary signal, generated by the other subsystems and sent to the TT&C, and the transmission by the antenna are: signal modulation, signal amplification, signal filtering and, finally, the transmission of the signal through the antenna, on the downlink link. For the uplink link, the signal is received by the antenna, amplified, filtered, and then demodulated.

2.5.3. Modulator and Demodulator

Signal modulation is the process of varying characteristics of a periodic wave, called a carrier signal, through a signal with information to be transmitted, called a modulation signal. The result of this process is a modified carrier wave capable of carrying the data to be transmitted.

The carrier wave has its natural frequency equal to the desired frequency to be transmitted, which, depending on the modulation method, may vary with time.

The modulation method chosen is responsible for varying certain characteristics of the wave to print the information to be transmitted on it.

The main methods for digital modulation are ASK - Amplitude Shift Keying, FSK - Frequency Shift Keying, PSK - Phase Shift Keying and QAM - Quadrature Amplitude Modulation.

The demodulator, in turn, is responsible for converting the modified carrier signal received by the receiver back into the signal with the information, or modulation signal. In this process, due to possible obstacles and noise caused during the transmission, the demodulated signal may be different from the actual signal sent, causing transmission error and the appearance of bits failure.

It is important to note that the demodulator chosen must be of the same type as the modulator used.

2.5.4. Amplifier

A signal amplifier is a circuit that uses electrical energy to increase the amplitude of an input signal and emit this new version in its output terminals.

An ideal signal amplifier creates a perfect replica of the original signal, that has bigger amplitude but its identical in every other sense. In reality, a ideal amplifier isnt possible. The real behavior causes noises in the signal, what must be considered.

In transmitters, the amplifier is one of the main responsible for the power of the emitted signal. Therefore, the choice of this component is of paramount importance and must take into account the study of the link budget that was done.

In applications such as CubeSats, the amplifier ends up being an integrated circuit in the project of the entire transmitter, not being possible to build it externally.

However, in receivers, it is common to have an LNA (Low Noise Amplifier) placed before the demodulator, amplifying the signal received by the antenna.

2.5.5. Filter

Signal filters are devices or process that remove unwanted components of a signal. They also can filter the noise in the band of interest. Most of the time that means remove some frequencies or frequency bands.

To space applications, the filters are the band-pass type. Those filters allow the passage of a determined frequency range specific to the transmission without alterations, while all the other frequencies, that aren't useful to the communication, suffer attenuation.

3. Subsystem Specification

The subsystem specification must consider the mission criticality factor, and cannot suffer irrecoverable failures or failures that depend on human intervention, considering that ground commands may not be received. The engineering choices were such as to minimize the risk of failures that prevent communication with the CubeSat.

During the design stage, the legislation in force internationally must be taken into account, frequencies in the UHF and VHF range are usually adopted. An operating frequency of 451.87 MHz was chosen for uplink and for downlink was allocated to the frequency of 145.17 MHz.

3.1. Link Budget

The purpose of the link budget is to ensure that communication takes place at the lowest possible BER rate. Using the equation below, we can find the power range for the equipment to be able to successfully transmit data between the ground station and the satellite.

$$P_{Rx} = P_{Tx} + G_{Tx} - L_{Tx} - L_S - L_{Fs} + G_{Rx} - L_{Rx} \quad (1)$$

In this equation we have the received power (P_{Rx}) as the power at the input port of the receiver and its value must be greater than the sensitivity (smallest power that the equipment can receive without presenting large errors) of the chosen receiver .

The transmitted power P_{Tx} is the signal power at the transmitter output, related to the amplifier present in the transmission system and regulated by agencies related to telecommunications.

The gain of a transmit antenna G_{Tx} and the gain of a receive antenna G_{Rx} describe how well the antennas convert input power into radio waves directed in a specific direction.

The losses of the transmitter L_{Tx} and the losses of the receiver L_{Rx} are related to the cables, connections, duplexers and/or splitters used.

For most of the links studied, these values do not exceed 2 dB, thus, it becomes simpler and more usual to use them in the link budget.

The unmodeled losses existing in the transmission can arise from several factors and are included in the study of the link budget through the supplementary loss factor L_S.

Finally, the loss in free space L_{Fs} consisting of the power emitted in directions where there is no receiving antenna, according to IEEE Standard for Definitions of Terms for Antennas [3], and can be expressed through the equation:

$$L_{Fs} = \frac{P_{Tx}}{P_{Rx}} = \frac{(4\pi r)^2}{\lambda^2} \quad (2)$$

For this document, considering an imaging mission for a Brazilian cubesat, the supplementary loss used will be the losses due to atmosphere and rain, which are important models for the Brazilian territory that has considerable rainfall during the year.

Using TanSat mission data, a Chinese mission to study gases in the atmosphere [4], to simulate the system, it was defined that the TT&C system should reach a transmission rate of 10 kbit/s in uplink and 10 Mbit/s in downlink.

As already defined, the modulator used will be the BPSK which features a bitrate (bit/s) of $\frac{1}{2}$ of its bandwidth (Hz), and a transmission endowed with low BER [5].

In possession of this information, using Shannon Hartley's theorem, we can obtain the signal to noise ratio.

$$C = B\ log_2\ (1 + \frac{S}{N}) \quad (3)$$

Where C is Channel Capacity in bits/s, B is Channel Bandwidth (Hz), S is Received Signal Power (W), N is Noise Power (W).

Knowing the noise received by the antenna, it is possible to find the minimum received power necessary for the transmission.

Considering for a typical project that the ground antenna will be directed to the space, the main source of noise will be the Sun. For the CubeSat antenna, the main noise will be the reflection of the Sun's emissions by the atmosphere, the terrestrial albedo and the noise from the antennas of other communication links.

Free space losses are distance and frequency dependent. Modeling the critical scenario, the maximum distance must be used for calculation.

$$S = R_e[(\frac{r^2}{R_e^2} - cos^2(\delta))^{1/2} - sin(\delta)] \tag{4}$$

With R_e being the radius of the Earth, r the radius of the Earth plus the average altitude of the orbit, and δ the Angle of elevation.

For typical cubesat designs, some components are used quite frequently, and there are several manufacturers that produce COTS components. To simulate the tools presented and discussed, COTS components found in stores such as cubesatshop were chosen.

For the antenna on the cubesat, an antenna "ISIS Deployable antenna system" was chosen with an omnidirectional radiation pattern and a gain of 0dB. For the antenna of the ground station, the antenna "ISIS Full Ground Station Kit for VHF/UHF" was chosen with directional pattern of irradiation and gain of 12.3 in VHF and 15.5 in UHF, in dB.

For the transmission and reception circuit, the ISIS transceiver "UHF downlink/VHF uplink Full Duplex Transceiver" was chosen with a transmission power of 27 dBm, with BPSK and GMSK modulation, AX.25 protocol and sensitivity of -104 dBm for BER rate from 1E-5. Simulations will be carried out in order to verify the feasibility of using these components.

For additional losses, the propagation models developed in the work *Desenvolvimento de ferramenta computacional para análise da propagação por diferentes meios de transmissão de links de comunicação de nanosats*[6] will be used.

4. Results

Using the propagation model and simulating as a function of the parameters, the following attenuation curves were obtained.

Figure 1: Specific attenuation - Rainfall ITU-R Model

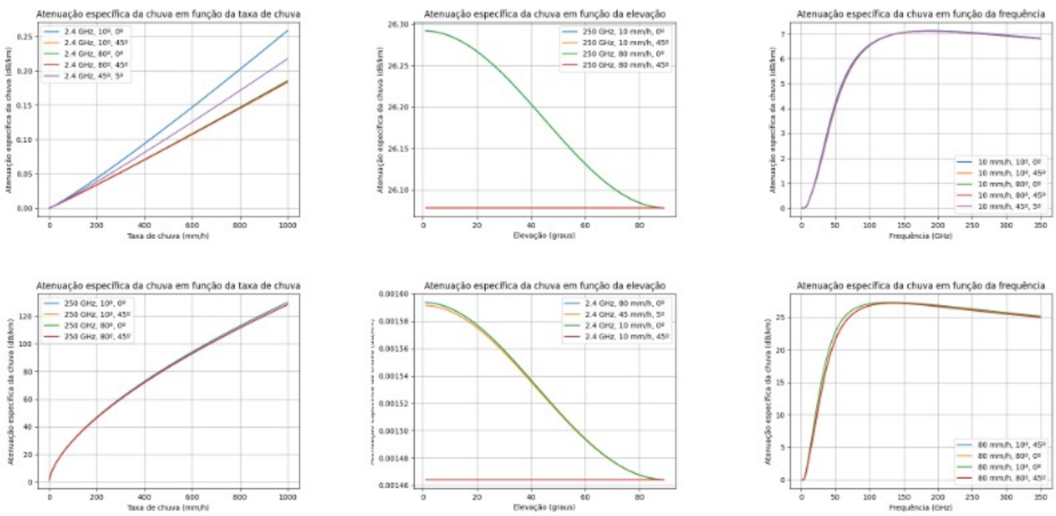

Figure 2: Specific attenuation - Atmospheric ITU-R model

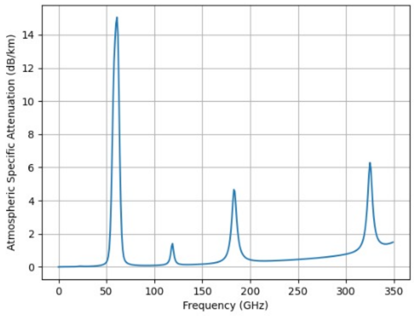

Furthermore, using the free path loss equation, simulating for different frequencies, the following total attenuation curve was found.

Figure 3: Attenuation - Free Space Path Loss

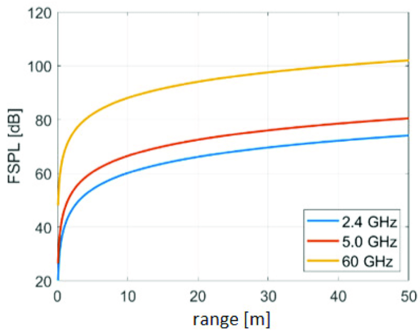

Using the link budget equation 1, for typical, maximum and minimum values of rainfall and atmosphere, that is, when the cubesat is passing through the horizon, we obtain the following results.

Table 1: Results for simulation

Model	Rainfall attenuation	atmospheric attenuation	FSPL	total
Minimum attenuation	0.001	0.28	87	89
Typical	0.004	0.56	94	97
Maximum attenuation	0.02	0.84	104	107

Rainfall rate of 1, 5 and 30 mm/hr was considered for the rainfall model, atmosphere range of 100, 200 and 300 km for the atmospheric model, and communication distance of 1000, 2500 and 7000 km was be consider. In addition to 500 MHz for the communication frequency.

5. Conclusion

In this work, the necessary requirements for the development of the communication subsystem were presented, as well as how to identify and use them. In addition, the TT&C sizing and simulation of a cubesat was carried out whose mission is to image using commercial components.

For components available off-the-shelf (COTS) and for the most extreme cases of interference, it was concluded that it is still possible to communicate with the cubesat, therefore, the proposed link is viable. However, for systems with a design frequency greater than 2.4GHz, the weather starts to be more prominent factors, according to the models in the figures 1 and 2, and should be better considered in stages of project.

In addition, other frequency-dependent models, which were not modeled, become important factors in the study of the link budget.

References

[1] W. Larson, J. Wertz, B. D'Souza, SMAD III: (Space Mission Analysis and Design, 3rd Edition) : Workbook, Space technology library, Microcosm Press, 2005.

[2] E. Notes, Radio signal path loss, Disponível em: ¡https://www.electronics-notes.com/articles/antennas-propagation/propagation-overview/radio-signal-path-loss.php¿ Acesso em: 20/10/2021, ????

[3] Ieee standard for definitions of terms for antennas, IEEE Std 145-2013 (Revision of IEEE Std 145-1993) (2014) 1–50.

[4] Tansat (chinese carbon dioxide observation satellite mission), Disponível em: ¡https://directory.eoportal.org/web/eoportal/satellite-missions/t/tansat¿ Acesso em: 27/10/2021, ????

[5] Lesson 21: Digital modulation, Disponível em: ¡https://www.usna.edu/ECE/ec312/Lessons/wireless/EC312_Lesson_21_Digital_Modulation_Course_Notes.pdf¿ Acesso em: 27/10/2021, ????

[6] D. W. B. Arruda, Desenvolvimento de ferramenta computacional para análise da propagação por diferentes meios de transmissão de links de comunicação de nanosats (2022).

9

Session 9 - Open Source Platforms

Open-Sourcing of CubeSat Bus for Capacity Building aimed to Acquire Original Space Development Capability

Tetsuhito Fuse[(1)], Mengu Cho[(2)]
[(1)] Kyushu Institute of Technology, 1-1 Sensui Tobata-ku Kitakyushu 804-8550 JAPAN, +81-93-884-3597, fuse.tetsuhito856@mail.kyutech.jp
[(2)] Kyushu Institute of Technology, 1-1 Sensui Tobata-ku Kitakyushu 804-8550 JAPAN, +81-93-884-3229, cho.mengu801@mail.kyutech.jp

***Keywords**: Nano satellite, Cubesat, Capacity building, BIRDS program, Open-source*

The BIRDS Program of Kyushu Institute of Technology (hereafter “Kyutech”) is a series of five projects. Each project involved 3 to 5 nations, and each took two years to implement. Ostensibly, the main purpose of BIRDS has been capacity building. However, another goal was to assist emerging nations put into space their very first satellite, and to encourage them to build their second satellite by themselves based on their experience of first satellite which from concept design to operation.

To promote worldwide capacity building activities, Kyutech has decided to provide the bus design on an "open source" basis. The rationale for this is that this bus has tremendous heritage in space.

Based on Kyutech's extensive experience of satellite building/operating, we believe this bus can be applied to a wide range of space exploration and commercial missions. This paper will mention how you can access this open-source BIRDS bus design and how you can acquire and develop your own space development knowledge and capability.

1. Introduction

While developed nations have forged ahead with space development, many emerging nations have yet to make their first step into space. Many are just observers on the side lines. To address this issue, Kyutech in 2015 conceived of the BIRDS Program. Kyutech realized that these nations are not moving forward because they do not have the requisite human resources. Using “launching the nation’s first satellite” as a point of inspiration and motivation, the BIRDS agenda is to help such nations move forward by training a cadre of engineers who master the skills needed to design, build, and test, that first satellite. It is presupposed that the engineers will return to their homelands and accomplish the following: (1) build the second satellite in the home country, and (2) train others in that process. If this process is repeated sufficiently, the nation gradually acquires the human resources for a sustainable space development program. Hence, the central goal is not the first satellite per se, but rather the central goal is a sustainable space program for the just-embarking country. The maiden satellite is a means to an end.

Each BIRDS project runs for two years because most participating students are masters-level graduate students; and at Kyutech the duration of the masters-level degree program is fixed at two years. During these two years, they design, build, test, and operate, a 1U CubeSat with minimal faculty supervision. Their satellites are launched before they graduate, and so they also experience the on-orbit operation of the satellites (which is a significant component of learning the entire satellite development process). The primary method for securing BIRDS stakeholders is to travel to each country which the author did. Through in-person negotiations, the BIRDS stakeholder is persuaded of the value of joining the project. The stakeholder agrees to pay satellite development cost to cover the hardware and launch costs of the satellite. In addition, the stakeholder provides the funds for 2 or 3 of its young citizens to: work on its first CubeSat project, and in parallel study towards a masters' degree or a Phd in the SEIC program of Kyutech.

This BIRDS BUS will not only support countries and universities that want to launch 1U CubeSat for their first satellite, but also help lower the threshold for various organizations to enter space. After the discussion, we decided to release BIRDS BUS Open-Sourcing information and focus on activities to encourage new stakeholders to enter the space sector.

2. BIRDS PROGRAM

The first satellite project, BIRDS-1 started in 2015. When BIRDS-1 started, there was no idea of doing a series of satellite projects. But, as BIRDS-2 started in 2016, the viewpoint as a continuous satellite program gradually emerged. Eventually, the BIRDS program delivered multiple CubeSats roughly every year since 2017. In total, the program generated 17 CubeSats and deployed from International Space Station (ISS) into space in five generations as following.
All the BIRDS projects and participants are shown in Table. 1.

Table 1: BIRDS Project with respective participants

Project	Launch date	Participating countries
BIRDS1	2017.7.7	Japan, Ghana, Mongolia, Nigeria, Bangladesh
BIRDS2	2018.8.10	Bhutan, Malaysia, Philippine
BIRDS3	2019.6.17	Japan, Nepal, Sri Lanka
BIRDS4	2021.3.14	Japan, Paraguay, Philippine
BIRDS5	Fall 2022	Japan, Zimbabwe, Uganda

The mission statement of BIRDS-1 was “By successfully building and operating the first national satellite, make the foremost step toward indigenous space program at each nation”. At this stage, we never imagined to do BIRDS-2 or later. Therefore, BIRDS-1 was considered as another satellite project, whose purpose was primarily education. Because the primary purpose is education, the most important constraint was to do the satellite project in two years including operation.

Since the emergence of small satellites, many non-space-faring countries tried to enter the space sector through small satellite development and operation. Various training programs via agencies, companies and universities in space faring countries existed before BIRDS program. They were often tied with sales of satellites (big or small). But many of them were not successful, especially if the training was done in agencies or companies. The reasons were mainly lack of hands-on experience and not covering the entire satellite system life cycle. Also, in many programs, there was a tragedy of trainees leaving the space organization after returning to their countries because the space program in the non-space-faring countries was not sustainable. The key for successful capacity building program are the following two points,

- Experience the complete cycle of designing, building, testing and operating

through hands-on
- Strategy for sustainability after the training

The short-term goal of the BIRDS-1 was to build and operate a satellite to give the students confidence that they can do it. But the long-term goal was that the students initiate their own space program in their home countries. Therefore, the full mission success criteria of BIRDS-1 was that the former students successfully build and operate the second satellite in their home countries. Therefore, the emphasis was placed on letting students learn the entire process of a satellite project from the beginning to the end. We let the students witness decision-making processes and then make decisions by themselves. By learning what are necessary to build and operate a satellite and what decision they have to make through their own experience, it becomes easy for them to initiate their own space program in home countries even if it starts from a CubeSat project. By starting their own small program by themselves, the program can be more sustainable by not heavily relying on big support from the government. We also asked the stakeholder of each country, mostly university, to make commitment of initiating space education/research program and hiring the BIRDS students as the initial core members.

In order to let the students experience the entire system lifecycle, we have to fit the project within the degree timeline, which is two years for the Master degree program. For Japanese students, we have three years as they usually spend three years in their laboratory, the senior year and two years in Master course. But we had to frame the timeline for foreign students. To fit into two years, we have selected 1U CubeSat and ISS deployment as the platform for this training. 1U CubeSat was chosen obviously as it was the simplest satellite. ISS deployment was chosen as there were routine flight opportunities once every three months in average.

The BIRDS program experiments the lean satellite approach. Lean satellites seek to deliver value to the customer (the end-user or the purchaser) or the stakeholder at minimum cost and in the shortest possible schedule by minimizing waste. We try to achieve the maximum reliability within the budget and schedule constraints. To do so, we evaluate, prioritize and mitigate risks properly to fit into the small budget and short schedule. When the students continue the space program in their home country, they have to adopt a lean approach anyway so that the program can run with a small team and at minimum cost.

In the BIRDS program, the overall satellite development activities are conducted within a radius of 30 m inside the campus. All the team members are placed in one room where they spend most of the time while they are in the campus. The clean room is located next to their room and the testing facility is located in the downstairs. The operation is done at the next building. To minimize the waste of waiting for reply, the students are encouraged not to use e-mail unless they need to broadcast to all the team members.

2.1 BIRDS workshops: promoting solidarity

Since 2016, the BIRDS Program has conducted an annual BIRDS International Workshop. The 2016 workshop was held in Kitakyushu City, Japan (Kyutech). The 2017 workshop was held in Ghana (ANU). The 2018 workshop was held in Mongolia (NUM). And the most recent one was held in Bangladesh (BRAC University); see Fig.

2. The workshops allow BIRDS stakeholders to engage face-to-face -- to enable networking. Such international gatherings are an important attribute of the BIRDS Program. Notes are exchanged between stakeholders of all BIRDS projects and future modes of collaboration are discussed in these informal settings. This personal networking by stakeholders is a significant way to promote sustainability of space development efforts across national borders. Going forward is less daunting when you are not walking alone.

Fig. 1 4BIW: 4th BIRDS International Workshop in Bangladesh

3. BIRDS HERITAGE and EXPANTION

Fig. 2 shows the evolution of BIRDS satellites. At each generation, we had to give changes to the satellite bus.

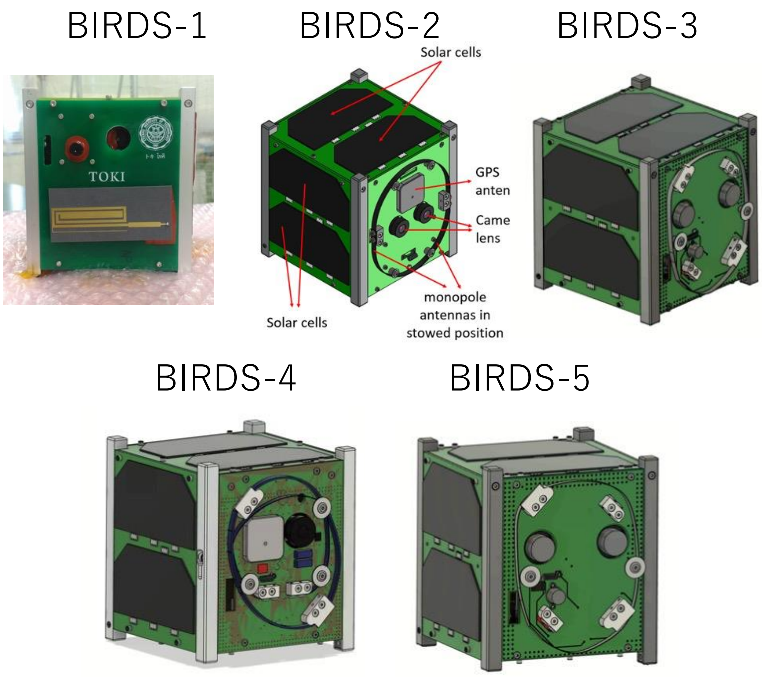

Figure 2: Evolution of BIRDS satellite

The satellite designs evolved constantly by reflecting the flight results and adapting the changes imposed by external causes. The design changes could be implemented rapidly as there were always overlaps of student generations. In 2018, when we started BIRDS-4, all the BIRDS-3 members were still at the school. We still had a majority of BIRDS-2 members and even three BIRDS-1 members. A group photo taken at the kick-off of BIRDS-4 is shown in Fig.3. In the figure, the three students in the top rows are students who worked on BIRDS-1. They were still at the schools as they moved to Ph.D. course after the Master-degree.

Since BIRDS-2, it became tradition that the students of the former generations tutor the new students in person. When there is a question in the satellite design, the student can go quickly to the senior students. By creating this system, the burden on the faculty members is relieved significantly, although relying too much on the intra-student tutoring led to the loss of the two BIRDS-4 satellites.

Knowledge transfer and maintenance is always an issue in university satellite programs. One obvious solution is to prepare documents. But it is very rare to find a student who like writing documents. It is good to have persons who experienced the satellite projects by themselves. In university satellite programs, students graduate. Therefore, the persons must be either faculty members or academic staffs. For the staffs, we have to consider how to secure the continuous funding for employment, the school regulation related to the term of employment, the academic carrier of the staffs, etc. For the faculty members, they have to commit themselves as a program director and spend a significant amount of time in each satellite project, which may affect the academic career of the faculty members especially if the person's rank is still at a junior level before obtaining tenuor.

In BIRDS program, we took a strategy of maintaining the knowledge and experience as "collective intelligence" among the students by overlapping several generations of satellite projects concurrently. The senior students teach the junior students the experience based on the operation results. This strategy requires the funding to support the multiple satellite projects. The principal faculty must work really hard to get the funding. Also, without supporting academic staffs, such post-doc or junior faculties, between the principal faculty and the students, the burden on the principal faculty is too heavy. The support by the junior staffs is critical. In turn, the principal faculty must think about the academic career of the junior staffs. Also, once the technology is fully matured after experiencing a number of orbital operations, an approach whereby the results of the projects are returned to society is desired by transferring the design and knowhow to enterprise, such as by making them available as opensource.

Figure 3: Group photo taken in Fall 2018.

4. BIRDS BUS Open-Sourcing Activity

Its variants are being used for other satellite projects, such as KITSUNE (6U CubeSat which was released from ISS in February 2022). Kyutech is also applying the BIRDS/KITSUNE bus to other 2U, 3U CubeSats with some modifications and also to science mission like lunar mission which is called LEOPARDO mission. The BIRDS bus is not only a good starting point for any emerging country who seeks to build satellites domestically without starting from scratch but also this asset has been expanded to simultaneously support the deployment of the second and third more advanced missions.

This asset will not only support countries and universities that want to launch 1U CubeSat for their first satellite, but also help lower the threshold for various organizations, including companies and institutions, to enter space and challenge further developmental missions. Therefore, we decided to release BIRDS BUS Open-Sourcing information and focus on activities to encourage new stakeholders to enter the space market.

The open-source project is currently carried out actively by involving not only BIRDS partners but those who were outside the BIRDS network. The idea of open-sourcing the BIRDS bus started in 2020. Using the idle time during the pandemic, we were having a monthly meeting with the former SEIC students. Many former students reported difficulty of promoting the domestic satellite projects in their countries. The full mission success criteria of BIRDS program is that the second satellites are built domestically by former BIRDS students. We found that the easiest solution for the second satellites was to duplicate or modify BIRDS satellites which they were very familiar with. But Kyutech is not a company and cannot maintain the satellite bus. Also, if a company commercializes the BIRDS bus, it will be expensive as the company needs to get a profit. The most affordable way is to let users work on the satellite by themselves. Also, we considered making others (non-BIRDS members) benefit from the initiative. Then the conclusion was to open-source all the technical information related to the BIRDS bus.

We have decided to put basically all the technical information related to the satellite design, which includes the following,

- Technical Drawing (i.e. CAD files)
- Source code (satellite and ground station)
- PCB design
- Assembly and testing procedure
- Parts list
- Test reports
- Interface Control Documents
- Textbook

As of June 2022, information about BIRDS-3 and 4 are available at GitHub[1]. By summer of 2022, information about BIRDS-5 will be posted at GitHub as well as the in-orbit results (temperatures, voltage, current, etc) of BIRDS-3 and 4. In an open-sourcing activity, it is important to define the licensing policy. In BIRDS bus open-source, we have decided to adapt so-called “MIT license”, which is the most flexible licensing option giving users wide freedom as long as they acknowledge the origin of the information ask the others to do so.

As of June 2022, there are five Japanese users who are using the BIRDS bus for their satellite projects. Internationally, there are four countries, all from the former BIRDS countries, using the BIRDS bus. This became possible because the BIRDS bus was designed so that it can serve as a CubeSat platform accommodating various mission payloads while having the minimum change in the satellite bus design. The information is open to anybody including non-BIRDS countries. All the information related to the open-source initiative is distributed at a portal site at [2].

5. Conclusions

Kyutech identified this global issue: Many emerging nations were sitting on the side lines as developed nations (space-faring nations) made progress in space development by leaps and bounds. The gap was large, and getting larger every year. Kyutech decided to mitigate this technological and industrial divergence between have and have-not members of the United Nations by suggesting to non-space-faring nations a means for getting started in space, thereby initiating a series of positive chain reactions benefitting such nations economically. Accordingly, the BIRDS concept was proposed to the nations shown in Table.1. Essentially, this novel approach served a dual function: (1) Spark national excitement and pride about space by orbiting their first satellite (creating their “Sputnik moment”), and (2) simultaneously training 2 or 3 elite engineers who master the entire satellite development process (so that they can design, build, test, and operate, the second satellite on home turf). In this paper, we covered some of the concrete results of BIRDS-3, BIRDS-4, and BIRDS-5, in these pioneering nations in table1. Thanks to the Internet and social media, public-activation results are often amplified as young people convey their newly-discovered excitement about space to their friends. National pride swells up when nations finally get into space. A national space agenda is born.

Putting one’s country’s first satellite into space is a tangible result for all to see. This accomplishment has captured the public’s imagination in all BIRDS nations. With the wind behind them in terms of public support, governments are then able to allocate more funds to space development. Moreover, high-profile space achievements encourage the best and the brightest of young people to pursue a career in space science and engineering. And with an expanding base of human resources with space skills, BIRDS nations can realistically begin to foster domestic space industries. These are needed for national economic growth and prosperity.

Kyutech is planning to further develop these BIRDS Program activities by open-sourcing BIRDS BUS to students who have returned to their home countries, as well as other players who are thinking of entering the space program, to use the accumulated legacy and encourage new activities. It also aims to apply BIRDS BUS to more advanced technology demonstrations and scientific missions beyond newcomers by using it on more players. This will also lead to more sustainable development mechanism of Kyutech's BIRDS BUS.

Acknowledgments

BIRDS program was supported financially by cooperative research contract with each BIRDS member. The authors thank all the stakeholders of BIRDS projects. The support was also given by the “Coordination Funds for Promoting Aerospace Utilization” from the Japanese Ministry of Education, Culture, Sports, Science and Technology (MEXT). Another support was given by JSPS Core-to-Core Program, B. Asia-Africa Science Platforms.

The authors express their gratitude towards all the parties and individuals who assisted the project, including the members of BIRDS-1, -2, -3, -4 and -5 teams, BIRDS ground station network, the amateur radio community, and JAXA.

References

[1] https://birdsopensource.github.io/.
[2] https://birds-project.com/open-source/

Development of a FlatSat Platform for GOLDS-UFSC and Future Missions

João C. E. Barcellos[a], **Anderson W. Spengler**[b], **Laio O. Seman**[c], **Eduardo A. Bezerra**[d]

[a]*Universidade Federal de Santa Catarina, Brazil, joao.claudio.barcellos@spacelab.ufsc.br*

[b]*Universidade Federal de Santa Catarina, Brazil, anderson.spengler@ufsc.br*

[c]*Universidade do Vale do Itajaí, Brazil, laio@univali.br*

[d]*Universidade Federal de Santa Catarina, Brazil, eduardo.bezerra@ufsc.br*

Keywords: *FlatSats, Embedded Systems, Small Satellites, CubeSats, V&V*

The number of small satellite missions is increasing, especially university-based missions. And a lot has been learned from them, and more robust and reliable V&V (Verification and Validation) campaigns were suggested and implemented. Furthermore, it is becoming clear that one of the practices that increase reliability is mounting a FlatSat during the V&V campaign. Then, knowing its importance to the reliability of missions involving small satellites, we proposed the development of a FlatSat platform for the GOLDS-UFSC and SpaceLab's future missions. For that matter, other student-led missions were analyzed, and their FlatSat platforms were evaluated. This evaluation led to the definition of the platform's design and main functionalities. For instance, the platform should incorporate a microcontroller, a MicroZed, to enable the HIL (Hardware-in-the-Loop) implementation and simulations. Moreover, the platform should have sensors to offer other ways to verify and validate the system. Additionally, it should be able to monitor the PC/104 bus, as well as inject faults into the bus. The verification and validation of the FlatSat platform are still in progress. However, the proposed platform offers exposure to the subsystems, is highly reusable, can interface with various equipment, and can be used to greatly improve the HIL. Then, taking into account all these features, it is going to aid the implementation of the V&V campaign. Early verifications with prototype versions of the subsystems are going to be possible. Moreover, it will reduce the time spent on the V&V, avoiding manual connections.

1. Introduction

FlatSats have been used for a long time, to evaluate the functionality of medium-sized and large satellites, like the Lunar Reconnaissance Orbiter [1], Hope [2] and a medium-sized satellite based on the Multi-Mission Platform (MMP) [3]. Although it is a common practice during the development of medium-sized and large satellites, its adoption is so useful that has been adapted for small satellites, too; this type of configuration increases the exposure of subsystems, enabling the probing of data and power buses, and components that would be inaccessible in the actual small satellite configuration, which is important during the development of the FSW (Flight Software) [4]. Furthermore, this configuration facilitates the detection of software and hardware faults during subsystems interface [5] and reduces the risks during the verification and validation of the system [2]. Additionally, it can be used in combination with the HIL (Hardware-in-the-Loop) technique, which is known for increasing the mission's reliability and reducing the time and cost of the development [6].

Then, knowing the importance of this structure, during the FloripaSat-1 and GOLDS-UFSC, two different FlatSat platforms were used. For the FloripaSat-1, the subsystems were interfaced using wire harnesses, over a workbench, as shown in Figure 1a. Alternatively, for the GOLDS-UFSC, a backplane was developed to interface the subsystems, as shown in Figure 2a. But both platforms presented some disadvantages and problems, which could be improved.

In fact, there are some FlatSat platforms used in other missions, like MOVE-II [7, 8, 9, 10], ISTSat-1 [11], BIRDS-3 [12], and projects, like VST104 [13, 14], that could be considered as starting points. For that matter, these platforms were compared and their features evaluated. Then, considering this evaluation, as well as the FlatSat platforms used in SpaceLab's past missions, another platform was developed. The new platform should be used extensively during the V&V campaign, facilitating the implementation of HIL and offering various ways to debug the system of the GOLDS-UFSC, Catarina Constellation, as well other future missions.

Consequently, a full description of the design and development of a FlatSat platform is presented in this paper. First, in Section 2, a small overview of the FlatSat platforms used in other missions and projects involving small satellites is going to be presented, identifying the most interesting and useful features. Subsequently, in Section 3, the previous FlatSat platforms are described, highlighting their problems and limitations. Finally, in Section 4, the proposed platform is displayed. Further information on the tests that could be conducted using the proposed FlatSat platform is going to be presented, too.

2. Platforms used in other missions

As mentioned, some FlatSat platforms used in other missions and projects involving small satellites were considered. To this matter, how the subsystems are interfaced, their structural and functional characteristics, and the type of tests conducted on them were analyzed, to propose our platform. These small satellite missions and projects are going to be presented below.

The MOVE-II mission, which is a follow-up of the first-MOVE mission, was conducted by students of the Technical University of Munich. During the V&V campaign, they used 2 FlatSat platforms, which could be attached. When combined, these platforms can support up to 8 subsystems. The connectors at their ends can be used to increase the size of the platform or to connect the Breakout Board, another board developed by them that connects all the power and data buses to a series of test points for monitoring purposes. They added $0\,\Omega$ resistors to the buses that can be replaced with different resistors, to simulate the behavior of a bus that has suffered from fretting corrosion. This PCB has four layers, the bottom and top ones were used for routing the PC/104 bus, and the inner ones were used as ground planes.

The ISTSat-1 mission is being developed at the University of Lisbon. To assemble the subsystems, they developed a FlatSat platform that can be divided into "modules", and each of them supports only one subsystem. This platform has connectors to interface with other equipment, like the EGSE, which, in this case, could simulate any subsystem.

Another interesting platform is used in the VST104, which is a project of Vision-Space Technologies, a company in Darmstadt. The proposed platform, known as Element Foxtrot, has 4 PC/104 connectors and can be extended using an FPC connector, allowing a simple way to connect multiple FlatSat platforms. There are USB-C and different connectors allowing the use of an external power supply. It supports voltages between 7 V and 14 V and currents up to 6 A. Furthermore, there are current sensors on it, to evaluate the power consumption of the system.

The last mission that is going to be presented is the BIRDS-3. They developed a platform that used a CPLD (Complex Programmable Logic Device), increasing its versatility. With this new approach, they made a highly reusable platform, and that has a flexible routing. However, this raises the potential of employing this approach to develop platforms with built-in microprocessors, for example. They could be used to act as sniffers or to facilitate the implementation of the HIL technique.

There are other interesting FlatSat platforms that were found, like those used in Aalto-1 [15], EIRSAT-1 [16, 17] and MIST [18, 19]. Some of these structural and functional characteristics were used to propose the new platform.

3. Previous platforms

The FlatSat platform used during the V&V of the FloripaSat-1 is shown in Figure 1. This type of platform can be mounted with cables, screws, double-sided tapes, and cable ties. Nevertheless, this does not mean, necessarily, that it is simple to mount or safe to use. For instance, it is impractical to use if the development team is inexperienced. As observed during the development of the FloripaSat-1 mission [20], some errors occurred because of the lack of experience of the team. Furthermore, there are some disadvantages of using this type of platform that should be considered. Connecting the subsystems with wire harnesses could be time-consuming because it is necessary to ensure that the wires and cables used are in good condition and that the interfacing is correct. In a catastrophic scenario, someone could accidentally short two buses together, leading to permanent damage to the hardware. Additionally, just a bad contact could take hours to diagnose in an assembled system.

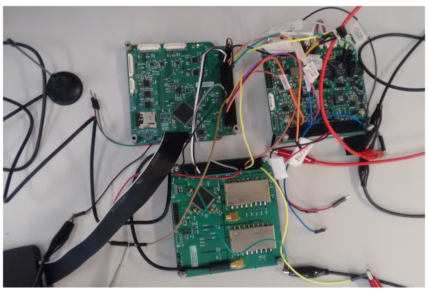

(a) Picture of the platform.

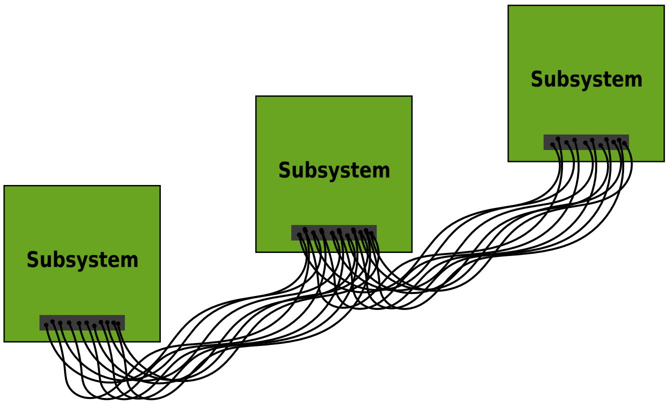

(b) Representation of the platform.

Figure 1: FlatSat platform used in FloripaSat-1.

For that matter, the platform shown in Figure 2 was developed. It should offer a faster, easier, and safer way to interface the subsystems, since it is similar to a PnP (Plug-and-Play) platform. Furthermore, other connectors are used to enable the interface of other equipment, like external power supplies, UART-USB converters, and antennas. Nevertheless, this platform still has disadvantages. First, the subsystems

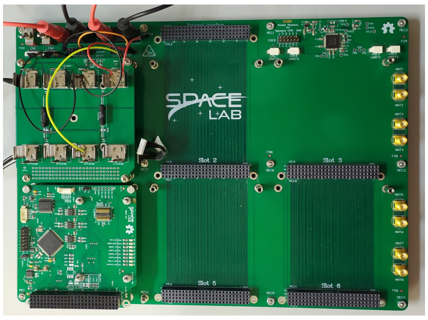

(a) Picture of the platform.

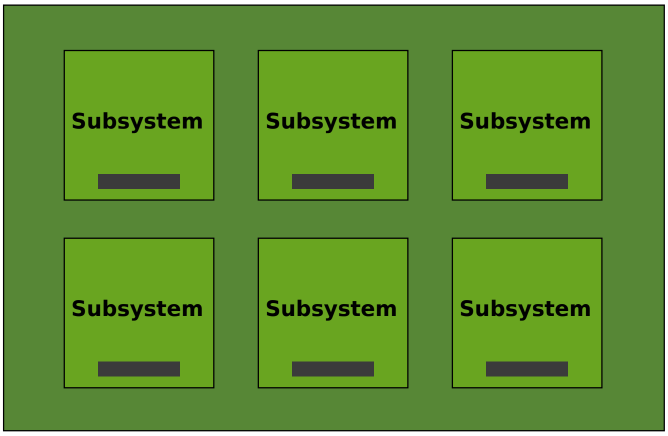

(b) Representation of the platform.

Figure 2: First FlatSat platform used in the GOLDS-UFSC.

are too close to each other, due to design errors, which makes it difficult to remove or connect them. In addition, the subsystems could have more exposure, since only the top surfaces are exposed.

4. Proposed platform

The proposed FlatSat platform, shown in Figure 3a, supports up to 6 subsystems or payloads, and offers ways to interface external equipment, like external power supplies, oscilloscopes, multimeters, and PCs. Its development was highly based on the platforms presented, aiming to improve SpaceLab's past platforms.

(a) Picture of the platform.

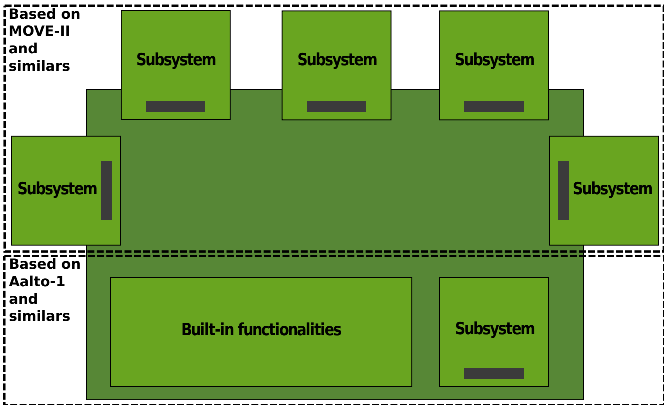

(b) Representation of the platform.

Figure 3: Proposed FlatSat platform.

In this sense, the hardware requirements were defined, which are listed in Table 1. It is noticeable that the platform used in the MOVE-II mission was particularly used as inspiration to develop the PCB itself. Moreover, its functionalities are inspired by BIRDS-3, VST104, Aalto-1, and other missions. More details are presented in the following subsections.

4.1. Platform's model

First, some aspects of the PCB are defined, like the number of layers, how the data and power buses are going to be routed, and even how the subsystems are connected

Table 1: Decision-making about platform's design and functionalities.

Development decisions	Guidance
Number of layers	Based on MOVE-II
Routing	Based on MOVE-II
Design of the platform	Based on MOVE-II, MIST, Aalto-1, EIRSAT-I and GOLDS-UFSC
Use of sensors	Based on VST104
Capacity of injecting faults in the PC/104 bus	Based on MOVE-II
Capacity of simulating other subsystems	Based on Aalto-1
Use of a soft-microcontroller	Based on BIRDS-3
Capacity of interfacing external equipment	Based on GOLDS-UFSC

to it, which are going to be described next.

4.1.1. Design of the PCB

The proposed platform merges the designs used in different missions, as shown in Figure 3b. The PCB is divided into 2 "sections". One of them is based on the design used in MOVE-II and MIST, as it permits the interface of many subsystems compactly. Furthermore, it offers greater exposure to them, because the bottom and top surfaces are exposed. The other one is based on the design used in the Aalto-1, EIRSAT-I, and even the platform that is being used in GOLDS-UFSC. The intention is to add more functionalities to the platform, and not just to interface the subsystems. In this sense, the platform can interface up to 6 subsystems, with great exposure, having built-in circuits that will be used for sensing, monitoring, and controlling the system during tests.

4.1.2. PC/104 bus routing and layers

A 4-layer PCB was developed, primarily because it would facilitate the process of routing the PC/104 bus and any additional circuitry. The bottom and top layers were used to route all the data buses, keeping all the horizontal traces in one layer, and all the vertical traces in another. This is a technique commonly known as Manhattan routing, which is useful to maintain all the routing organized. The two inner layers were used as ground and power planes.

4.2. Platform's functionalities

The next step was to define the functionalities that the platform should have. The block diagram of the platform is shown in Figure 4, which helps to present some of these functionalities.

4.2.1. Sensing power consumption and temperature

It was proposed the implementation of current and temperature sensors. The current sensors are employed to evaluate the power consumption of the system. For that

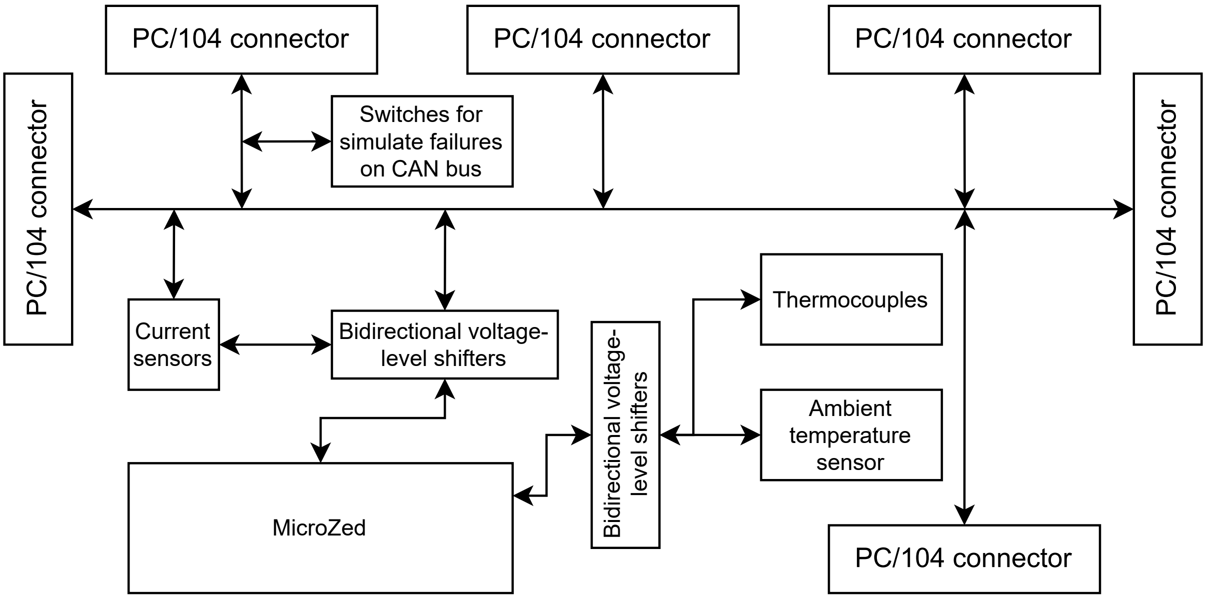

Figure 4: Block diagram of the proposed FlatSat platform.

matter, on each of the power buses, was added the INA219 [21]. This way, it is possible to measure the power consumption of each subsystem, individually, or the power consumption of the whole system.

Furthermore, two different temperature sensors were adopted, the TMP112 [22] and the LTC2983 [23]. The first one is used to measure the ambient temperature, which can be useful during those tests when the system is submitted to temperature changes. The second one makes use of thermocouples to measure the temperature of specific areas of the system, which could be useful for evaluating those components that are susceptible to overheating.

4.2.2. Injecting faults into the CAN bus

Unlike the FloripaSat-1 and GOLDS-UFSC missions, in which the communication between the subsystems is done using I^2C, SPI and UART, it is planned to use CAN in future missions. In this sense, it could be helpful if the FlatSat platform could be able to inject faults into the bus. Companies already offer boards that can simulate physical faults in the CAN bus [24]. Then, switches were employed to generate these faults.

4.2.3. Built-in microcontroller

Knowing the importance of implementing the HIL throughout the development and testing of the satellite, the platform should be capable of simulating the subsystems and/or sensors used in the satellite. Thus, it was necessary to use a microcontroller, which would be connected to the satellite's main bus, so that it could monitor and act on it.

However, as it is also intended to use this platform in future missions, it is necessary to implement a microcontroller capable of adapting to changes in the PC/104 bus. In this sense, a microcontroller in combination with a CPLD or a soft-microcontroller could be used. Considering that, in the past, the MicroZed [25] has already been used in some SpaceLab's projects, we chose to use it. MicroZed has programmable hardware, increasing its versatility.

The MicroZed is interfaced with the PC/104 bus using voltage translators, such as TXS0108E [26] and TXB0108 [27], isolating it from the subsystems connected to the FlatSat platform. Moreover, it permits powering the subsystems and the MicroZed with different voltages, if needed.

4.2.4. Interfacing external equipment

Considering the platform that is already being used during the development and testing of the GOLDS-UFSC, it was decided to maintain the existing interfaces. Thus, there are binding posts to enable the interface of power supplies, without needing to connect a battery to the EPS, or even without the need to use the EPS. The ability to interface with the PC, via UART, was maintained. The possibility of connecting equipment that uses the RS-485 protocol was added since this protocol could be used in the future.

4.3. Available procedures

Then, it is possible to briefly highlight how this platform can be used to evaluate the satellite's functioning, whether at the system or subsystem level. First, it can be noticed that the platform could be used to make long-term evaluations, which can be remotely monitored. This is already being implemented with the previous platform, presented in Figure 5, and has proven to be a useful practice.

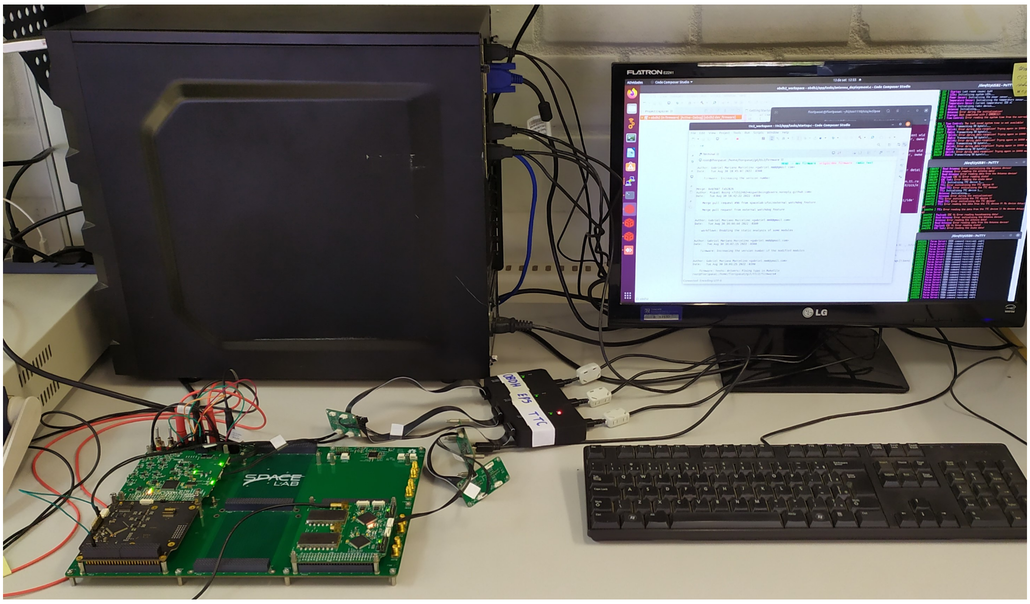

Figure 5: Long-term evaluations during the GOLDS-UFSC development.

Furthermore, considering that it has built-in sensors, it can be used during those procedures in which the system is submitted to some environmental conditions, in a thermal-vacuum chamber. For instance, the platform can measure the temperature that subsystems are being subjected to, serving as a reference. Then, this could be used to calibrate the subsystem's sensors or even as a parameter to control the temperature to which they are subjected. Another possibility is to monitor the behavior of specific components susceptible to overheating, such as the heaters attached to batteries, for example.

Considering that the platform has a built-in microcontroller, one or several orbit cycles can be simulated, as well as some specific mission scenarios. For instance,

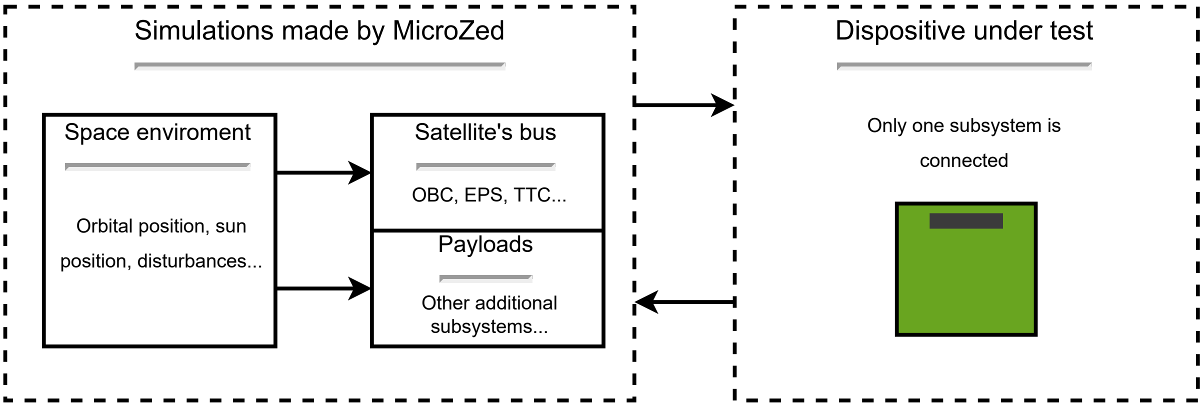

(a) Subsystem's functioning evaluation.

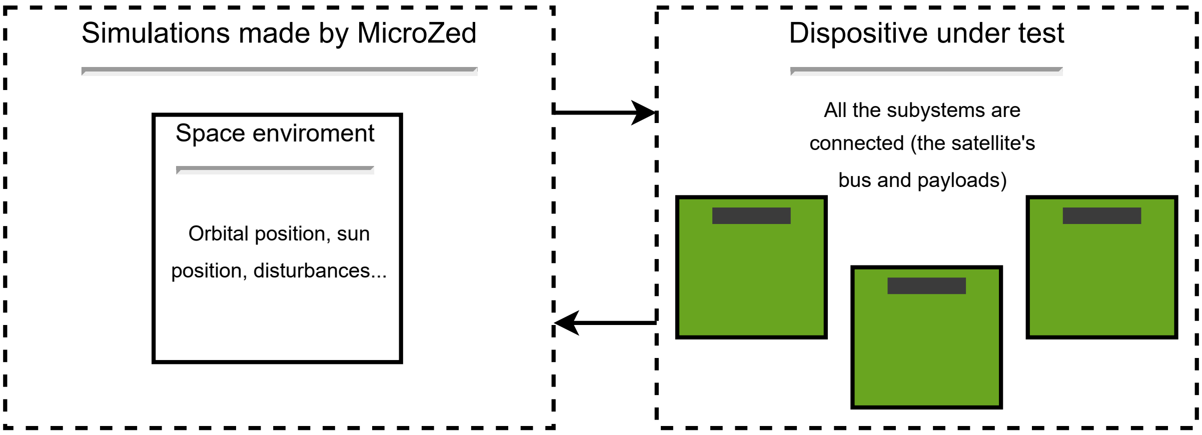

(b) System's functioning evaluation.

Figure 6: Simulating orbit cycles.

the simulation can be performed with just one subsystem connected to the platform, then the MicroZed would simulate the rest of the satellite, too. Therefore, it would be possible to evaluate its operation, individually, as represented in Figure 6a. But it would be possible to perform the simulation with the entire system, too, to evaluate the operation of the satellite, as represented in Figure 6b.

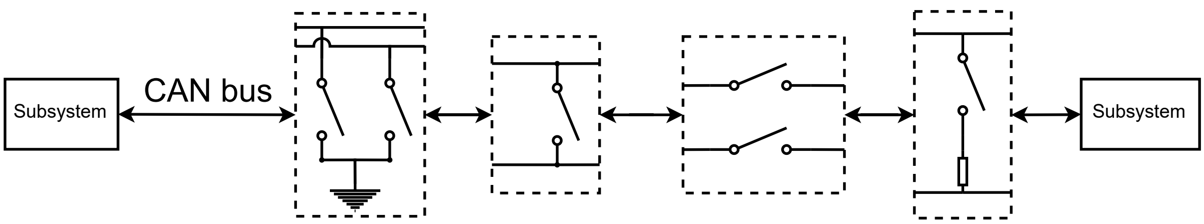

Figure 7: Fault-injection into the CAN bus.

Moreover, it allows simulating specific scenarios, like a communication failure between two subsystems, injecting corrupted or random data in the I^2C, UART, and SPI buses. Additionally, it can simulate physical failures in the CAN bus, as shown in Figure 7. It is possible to simulate a short circuit between CAN_L and CAN_H, a short circuit between CAN_L or CAN_H to GND, a rupture of CAN_L or CAN_H, and a loss of the termination resistor.

These are just some procedures that could be conducted on this platform, but it is clear that by using the built-in sensors and microcontroller, implementing the HIL can be greatly improved.

5. Conclusion

This paper presented the development of a FlatSat platform, which was based on platforms used in other student-led missions, as well as SpaceLab's past platforms. The proposed platform increases the exposure of subsystems, is capable of interfacing with various equipment, is able to monitor the PC/104 bus, as well as inject faults into it, and can be used to greatly improve the HIL, during the subsystem and system level tests. The platform was already manufactured, but not yet mounted, mostly because of the global electronic components shortage. Then, its verification and validation still need to be done.

Acknowledgments

The authors would like to acknowledge that this work was supported by CNPq/Brazil (National Council for Scientific and Technological Development - `http://www.cnpq.br`), and by AEB (Brazilian Space Agency - `http://www.aeb.gov.br`).

References

[1] J. Halverson, P. Calhoun, O. Hsu, J. Dongmo, R. Besser, B. Ellis, R. De Hart, Y. Tedla, S. Rosney, S. T. Snell, Testing of the Lunar Reconnaissance Orbiter Attitude Control System Re-Design Without a Gyro, in: Proceedings of the 42nd Annual AAS Guidance and Control Conference, Breckenridge, CO, USA.

[2] A. AlSuwaidi, Emirates Mars Mission Flight Simulator: FlatSat Overview, in: Proceedings of the IEEE Aerospace Conference, Big Sky, MT, USA, pp. 1–11.

[3] E. A. Bezerra, L. R. Azevedo, E. M. da Silva, Dependability Issues of INPE's ESA/CCSDS Telecommand/Telemetry Subsystem, in: Proceedings of the 5th Latin-American Symposium on Dependable Computing Workshops, São José dos Campos, SP, Brazil, pp. 58–63.

[4] S. A. Jacklin, Survey of Verification and Validation Techniques for Small Satellite Software Development, in: Proceedings of the Space Tech Expo Conference, Long Beach, CA, USA.

[5] H. Sukhwani, J. Alonso, K. S. Trivedi, I. Mcginnis, Software Reliability Analysis of NASA Space Flight Software: A Practical Experience, in: Proceedings of the IEEE International Conference on Software Quality, Reliability and Security, Vienna, Austria, pp. 386–397.

[6] S. Corpino, F. Stesina, Verification of a CubeSat via Hardware-In-The-Loop Simulation, IEEE Transactions on Aerospace and Electronic Systems 50 (2014) 2807–2818.

[7] M. Langer, Reliability Assessment and Reliability Prediction of CubeSats Through System Level Testing and Reliability Growth Modelling, Ph.d thesis, Technical University of Munich, Munich, BY, Germany, 2018.

[8] F. Schummer, Reliability Assessment of Small Spacecraft Before Launch, Master's thesis, Technical University of Munich, Munich, BY, Germany, 2017.

[9] J. Kiesbye, FlatSat, `https://github.com/JonisK/FlatSat`, 2019.

[10] J. Kiesbye, D. Messmann, M. Preisinger, G. Reina, D. Nagy, F. Schummer, M. Mostad, T. Kale, M. Langer, Hardware-In-The-Loop and Software-In-The-Loop Testing of the MOVE-II CubeSat, Aerospace 6 (2019).

[11] J. P. Monteiro, R. M. Rocha, A. Silva, R. Afonso, N. Ramos, Integration and Verification Approach Of ISTSat-1 CubeSat, Aerospace 6 (2019).

[12] T. Tumenjargal, S. Kim, H. Masui, M. Cho, CubeSat Bus Interface With Complex Programmable Logic Device, Acta Astronautica 160 (2019) 331–342.

[13] G. Filip, On-Board Computer for PC104 Format CubeSats, B.S. thesis, Czech Technical University in Prague, Prague, Bohemia, Czech Republic, 2021.

[14] G. Filip, VST104-Foxtrot, `https://github.com/visionspacetec/VST104-Foxtrot`, 2020.

[15] J. Praks, M. R. Mughal, R. Vainio, P. Janhunen, J. Envall, P. Oleynik, A. Näsilä, H. Leppinen, P. Niemelä, A. Slavinskis, et al., Aalto-1, Multi-Payload CubeSat: Design, Integration and Launch, Acta Astronautica 187 (2021) 370–383.

[16] S. Walsh, D. Murphy, M. Doyle, J. Reilly, J. Thompson, R. Dunwoody, J. Erkal, G. Finneran, G. Fontanesi, J. Mangan, F. Marshall, L. Salmon, D. de Faoite, L. Hanlon, A. Martin-Carrillo, D. McKeown, W. O'Connor, A. Uliyanov, R. Wall, S. McBreen, Development of the EIRSAT-1 CubeSat Through Functional Verification of the Engineering Qualification Model, Aerospace 8 (2021).

[17] M. Doyle, R. Dunwoody, G. Finneran, D. Murphy, J. Reilly, J. Thompson, S. Walsh, J. Erkal, G. Fontanesi, J. Mangan, F. Marshall, L. Salmon, L. Ha, A. Mills, D. Palma, D. de Faoite, D. Greene, A. Martin-Carrillo, S. McBreen, D. McKeown, W. O'Connor, K. Stanton, A. Ulyanov, R. Wall, L. Hanlon, Mission Testing for Improved Reliability of CubeSats, in: Proceedings of the International Conference on Space Optics, France, pp. 2699–2718.

[18] M. Gruber, Functional Testing of the MIST Satellite, Master's thesis, Royal Institute of Technology, Stockholm, Sweden, 2018.

[19] S. Barra, Functional Testing of the Electrical Power System of the MIST Satellite, Master's thesis, Royal Institute of Technology, Stockholm, Sweden, 2019.

[20] M. G. Mariano, F. E. Morsch, M. S. Vega, D. M. A. M. Pio, S. L. Oriel, S. L. Kessler, B. E. Augusto, Qualification and Validation Test Methodology of the Open-Source CubeSat FloripaSat-I, Journal of Systems Engineering and Electronics 31 (2020) 1230–1244.

[21] INA219, INA219 Zerø-Drift, Bidirectional Current/Power Monitor With I2C Interface (Rev. G), Texas Instruments, 2015. Available in: `https://www.ti.com/lit/ds/symlink/ina219.pdf`.

[22] TMP112, TMP112x High-Accuracy, Low-Power, Digital Temperature Sensors With SMBus and Two-Wire Serial Interface in SOT563 (Rev. I), Texas Instruments, 2018. Available in: `https://www.ti.com/lit/ds/symlink/tmp112.pdf`.

[23] LTC2983, Multi-Sensor High Accuracy Digital Temperature Measurement System (Rev. C), Analog Devices, 2014. Available in: `https://www.analog.com/media/en/technical-documentation/data-sheets/2983fc.pdf`.

[24] CAN Fault Board, Bus Fault Injection Board - Data Sheet, MACH SYSTEMS s.r.o., 2018. Available in: `https://www.machsystems.cz/wp-content/uploads/2018/01/Bus-Fault-Injection-Board-Data-Sheet.pdf`.

[25] MicroZed, MicroZed™ Evaluation Kit, Avnet, 2017. Available in: `https://www.avnet.com/wps/wcm/connect/onesite/99d164d2-3b62-4d24-a87f-9e7ede12347a/PB-AES-Z7MB-7Z010-G-V2.pdf`.

[26] TXS0108E, TXS0108E 8-Bit Bi-directional, Level-Shifting, Voltage Translator for Open-Drain and Push-Pull Applications (Rev. H), Texas Instruments, 2020. Available in: `https://www.ti.com/lit/ds/symlink/txs0108e.pdf`.

[27] TXB0108, TXB0108 8-Bit Bidirectional Voltage-Level Translator with Auto-Direction Sensing and ±15-kV ESD Protection (Rev. H), Texas Instruments, 2020. Available in: `https://www.ti.com/lit/ds/symlink/txb0108.pdf`.

10

Session 10 - Mission Applications III

UNLP's FIRST CUBESAT, USAT-I: GNSS-RO AND GNSS-R TECHNOLOGY DEMONSTRATOR

Sonia A. Botta[1,*], Frida A. Alfaro Rodríguez[1], Santiago Rodríguez[2], Elián Hanisch[2], Marcos D. Actis[1], David O. William Rogers[1], Simón Lombardozzo[2], Daniel Hamann[1], Guillermo Garaventta[1], Facundo Pasquevich[1], Gabriel Vega Leañez[2], Ernesto M. Lopez[2], Aldana Guilera[1], Adriana Barba[1], Santiago Ozafrain[2], Ezequiel Marranghelli[2], Mateo Salvo[1], Agustín Catellani[2]

[1] Centro Tecnológico Aeroespacial (CTA), Calle 116 between 47 and 48, La Plata, Argentina, phone: +54 (221) 423-6679
[2] UIDET Sistemas Electrónicos de Navegación y Telecomunicaciones (SENyT), Calle 116 and 48 (1900), La Plata, Argentina

[*] Corresponding author: sonia.botta@ing.unlp.edu.ar

***Keywords**: CubeSat, GNSS, university satellite.*

USAT-I is the first satellite under development in the National University of La Plata (UNLP, Argentina) University Satellite Program, which has planned a series of CubeSats. This satellite will be a 3U CubeSat, and its mission will be the technology demonstration of GNSS-RO and GNSS-R using an in-house-developed GNSS receiver. Most of the bus and payload is being developed by professionals or students at the UNLP Faculty of Engineering, making this project equally educational and technology-oriented. This paper presents USAT-I's mission and concept of operations, the overall satellite and mission architectures, the student involvement, the most recent developments, and some early lessons learned.

1. University Satellite Program and USAT-I

The University Satellite program was born from years of experience in the aerospace area at the Aerospace Technology Center (CTA) and other groups at the National University of La Plata (UNLP). It was created to bring together the trained human resources and the available infrastructure in a project of its own and to meet a growing demand in this area, partly evidenced by the creation of the Aerospace Engineering career in the Faculty of Engineering.

The program is proposed to consist of a series of satellites to generate a medium-term plan beyond the first system. Having more than one mission would allow it to take advantage of and consolidate the knowledge and developments achieved in previous systems. This series of satellites will be progressively more complex so that the developments achieved by each mission will make the next one possible. All components designed under this program will be designed with a compatibility mentality. This philosophy benefits the program, generating workflow and flight heritage, and potentially allows these technologies to be used on external missions.

In this context, USAT-I is the first project in this series and aims to design, manufacture, test and operate the first UNLP's satellite: a 3U CubeSat that will serve as a technology demonstrator, not only for the subsystems but also for a scientific payload (Figure 1).

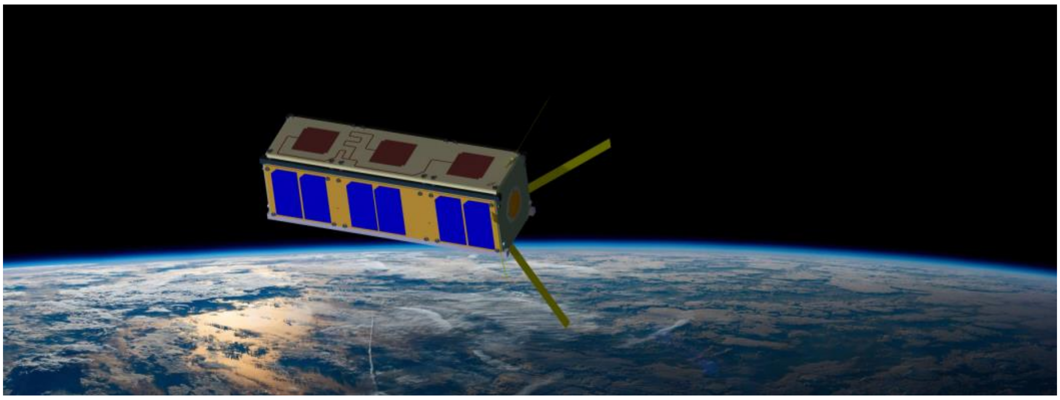

Figure 1: Render of the USAT-I satellite.

2. Mission and Concept of Operations

USAT-I's primary mission is the "Technology Demonstration of Scientific GNSS Techniques", specifically, GNSS radio-occultation and reflectometry. In addition to their use in navigation, Global Navigation Satellite System (GNSS) constellations can be leveraged for implementing scientific techniques. GNSS radio-occultation (GNSS-RO) is one of the most widely used methods for atmospheric measurements, both in the neutral region and in the ionosphere. On the other hand, GNSS reflectometry (GNSS-R) can be used to study certain characteristics of the Earth's surface, such as soil moisture, ocean surface winds, altimetry, and vegetation cover, among others. Although GNSS-RO has already been performed with CubeSats, GNSS-R, although theoretically feasible [1], has not yet been demonstrated. At least one CubeSat was launched with this objective (the 3Cat-2 [2]), although no results have been published.

2.1. Project and mission objectives

We have identified two groups of objectives: those related to the project and those related to the mission. This distinction is relevant for this first satellite since we seek to validate the design processes developed beyond the scientific and technology demonstration mission.

The objectives related to the project are:

1. To validate the systems engineering processes.
2. To validate the validation and verification processes.
3. To validate the design of the subsystems developed in-house by the UNLP.

The primary mission's objectives are:

1. To demonstrate the UNLP's GNSS system's performance for navigation and orbit determination.
2. To demonstrate the UNLP's GNSS system's performance for measurements using the GNSS-RO technique.

Additionally, we have identified the following objectives as secondary:

1. To demonstrate the UNLP's GNSS system's performance for measurements using the GNSS-R technique.
2. To obtain an approximation of the aerodynamic drag coefficient (C_D) to feedback the

perturbation models.

2.2. GNSS-RO and GNSS-R techniques

GNSS-RO

The GNSS radio-occultation technique indirectly measures the refraction of the signal emitted by GNSS satellites in the atmosphere. Depending on the receiver's position, it can be used to study characteristics of the upper layers of the atmosphere (e.g., ionosphere) or the lower layers (e.g., troposphere). GNSS-RO measurements are known as "events" and, for a CubeSat in LEO, typically last between 30 and 90 seconds, although they can have longer or shorter durations. These events are predicted using models of the GNSS constellations to be used. [3, 4]

The receiver must be able to acquire signals with low SNR (signal-to-noise ratio) since the GNSS-RO signals are highly degraded by the long path through the atmosphere. In the USAT-I mission, the satellite will acquire signals for 7 to 10 seconds that will be processed on-ground and offline for better use and learning of the information. The objective is to validate the receiver system for GNSS-RO type measurements.

GNSS-R

GNSS reflectometry is a technique that makes use of GNSS signals reflected from the Earth's surface. In this mode, the receiver and the transmitting GNSS satellite work as a bistatic radar. It is a relatively new type of GNSS science technique, which only began to be demonstrated on satellites a little over a decade ago. [5, 6]

GNSS-R signals also require that the receiver be carefully designed to work with poor SNR (Signal-to-Noise Ratio), given that the received signal intensity of the reflected waves is much lower than the direct waves. It must also be prepared to acquire the direct and reflected signals simultaneously and synchronously. In the case of the USAT-I mission, the data will also be processed on-ground with the objective of validating the receiver system for GNSS-R type measurements.

2.3. Success criteria

Table 1 lists the USAT-I mission success criteria. These criteria have been carefully developed for this first satellite, taking into consideration the mission objectives as well as the project ones.

2.4. Concept of Operations

Six general phases are distinguished for the operation of the CubeSat USAT-I, which create an overall ConOps for the satellite. From the description of these phases, sub-phases are developed, generating more specific concepts of operations for each one of them.

The overall ConOps starts with the pre-launch. Once all the requirements of this phase have been completed, the satellite is launched and placed in the desired orbit, entering the early orbit phase. During this phase, the satellite will deploy its UHF antennas and begin detumbling.

Table 1. USAT-I mission success levels and criteria.

Success level	Criteria
Minimum	• Establish a communications link with the satellite, obtaining sufficient housekeeping data to verify the health of the subsystems.
Marginal	• Obtain navigation data from the satellite, acquired through the GNSS receiver.
Functional	• Lifetime of 30 days. • Obtain a GNSS-RO-type measurement.
Ideal	• Lifetime of 90 days. • Obtain multiple GNSS-RO-type measurements. • Obtain a readable GNSS-R measurement.

Subsequently, the CubeSat will enter the commissioning phase. Once this phase is finished, the satellite is ready to operate correctly and carry out the corresponding tasks until the limit of its useful life, when it reaches the re-entry/end-of-life phase.

As USAT-I is a technology demonstration mission, the operations are expected to be flexible to allow for on-orbit testing. Therefore, although the GNSS-RO and GNSS-R operations have their general ConOps planned, the payload team will adapt them as needed.

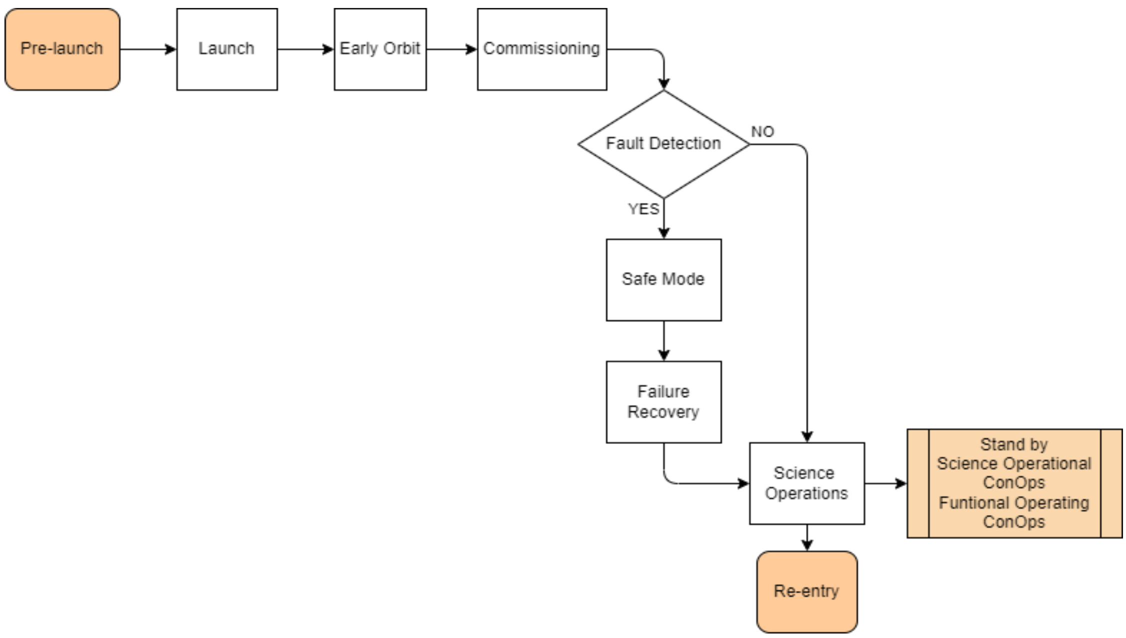

Figure 2. Overall Concept of Operations of Mission USAT-I

3. Mission architecture

To design the mission architecture, it is important to define a series of elements defined based on the requirements and objectives to be met for the USAT-I mission.

One of the mission requirements is to maintain as much flexibility as possible regarding the launch system and orbit. The flight segment will be launched as a secondary payload and is being designed to be compatible with most operative launchers.

Another critical point in the mission architecture is the ground segment. This segment will comprise the main station, located at the UNLP, and several auxiliary ground stations, to be determined according to availability. The operations will be managed by the project's own personnel.

From the considered elements, a diagram was made where the disposition of each one of the elements is exposed, considering the interaction with the mission concept. Figure 3 summarizes the different components of the mission architecture.

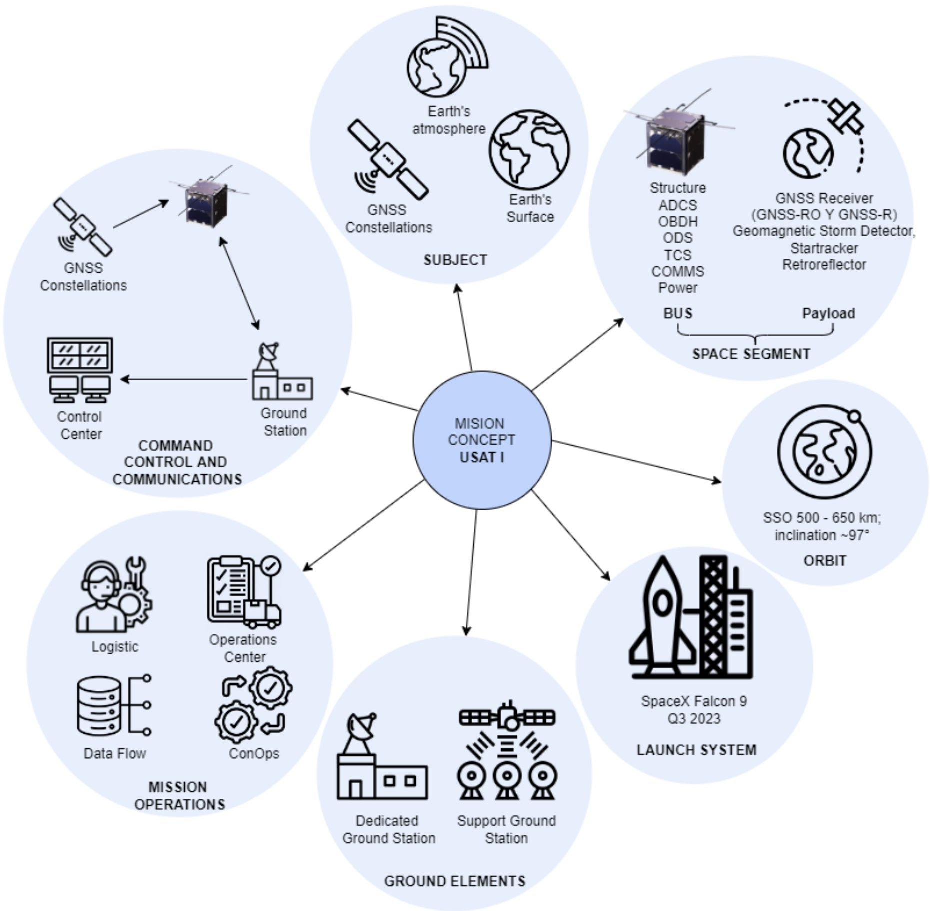

Figure 3: Mission architecture of USAT-I

4. Space segment

USAT-I follows the CubeSat standard [7], with a 3U configuration. Most physical requirements come from the CubeSat standard, such as mass, center of mass, dimensions, and protruding elements.

The other set of requirements comes from the mission and operational requirements. For example, the satellite shall be able to rotate from its nominal stable position (the Z axis aligned with nadir) to allow for the GNSS-R measurements (see Figure 8).

Figure 4 shows the most updated architecture for the space segment, while Figure 5 shows the configuration inside the satellite.

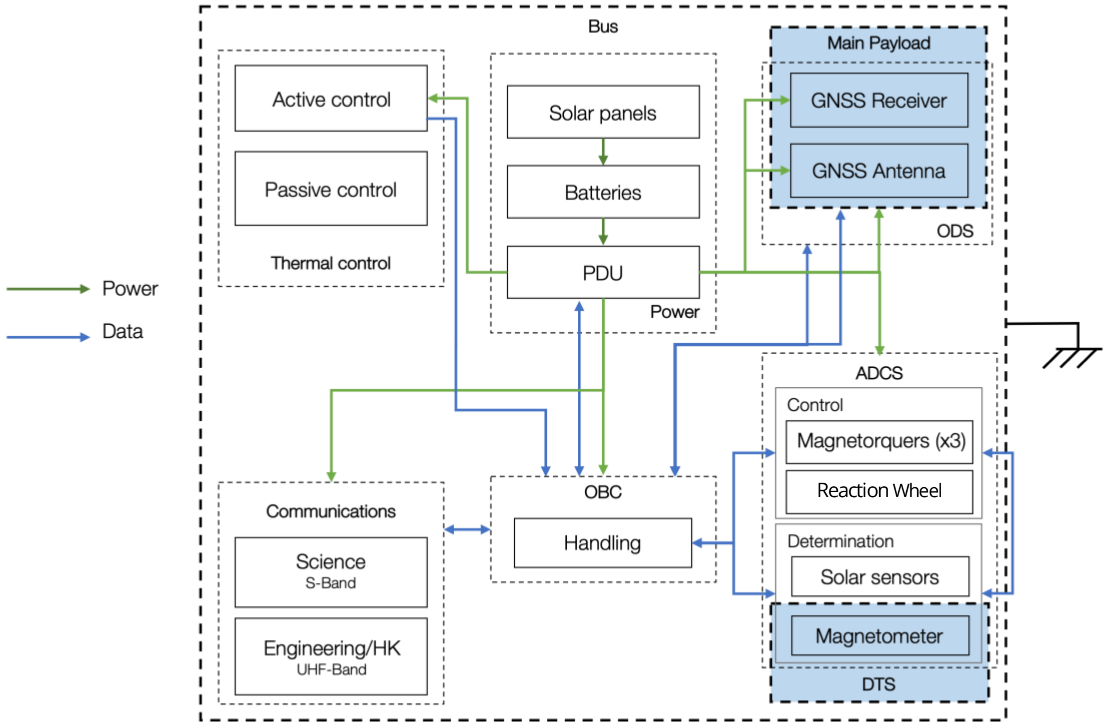

Figure 4: Space segment architecture.

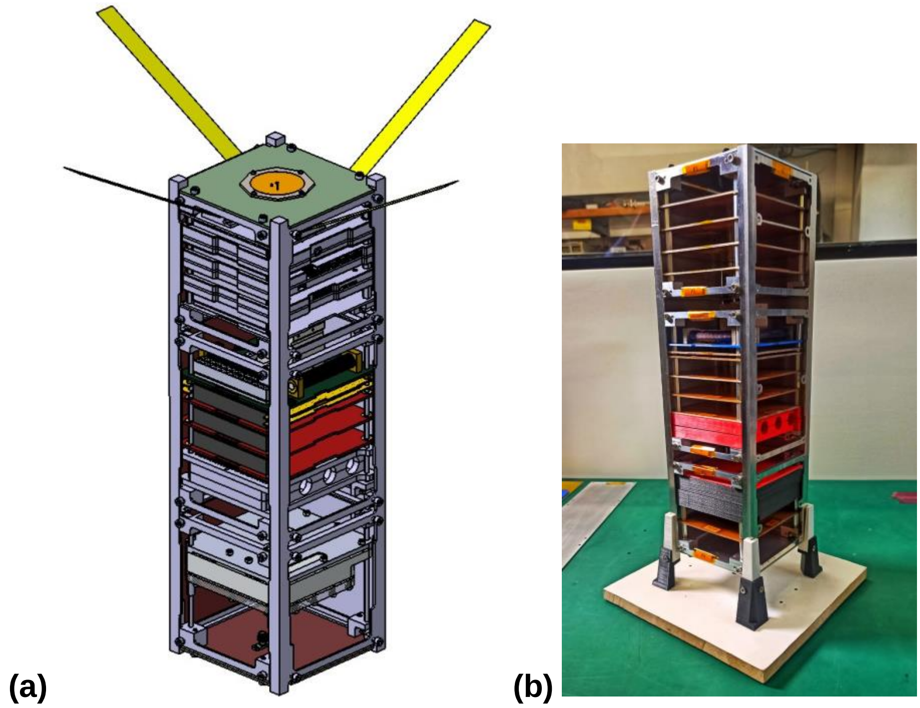

Figure 5: USAT-I internal configuration. (a) CAD model, (b) mockup, without shielding.

4.1. Bus design

The satellite bus has been mainly developed in-house, both by the Aerospace Technology Center (CTA) (structure, mechanisms, and power distribution system), and the Electronic Navigation and Telecommunications Systems Group (SENyT) (Communications, ADCS, ODS and OBC). The solar panels are manufactured by the

Argentine National Atomic Energy Commission (CNEA), with solar cells provided by the Argentine Space Agency (CONAE).

The components are majorly COTS, with the ADCS being the only subsystem with actuators specifically made for CubeSats.

4.1.1. Structure

The primary structure is made of aluminum 6061-T6. It consists of two lateral pieces connected by ribs. These lateral pieces form the rails required by the CubeSat standard and deployer. Internally, USAT-I is assembled using rods and stand-offs. Many of the PCBs have an aluminum shielding that, besides its main purpose of minimizing electromagnetic interference and radiation damage, gives internal rigidity.

4.1.2. Power generation, storage, and distribution

USAT-I's power source will be two solar panels with six 27%-efficiency GaAs solar cells. These panels are connected to an MPPT that controls the current to the batteries. The battery pack has four Lithium NCA 18650 batteries, with a total capacity of 47.4 Wh.

4.1.3. Communications

The communications subsystem works in two bands: UHF and S-Band. The UHF band acts as the robust link for uplink (1200 bps) and downlink (9600 bps), mostly for telemetry and command. The science data uses the S-Band downlink, with a data rate of 250 kbps. Therefore, the satellite has two communications antennas: a turnstile antenna for UHF and a patch antenna for S-Band.

4.1.4. Attitude Determination and Control

The attitude determination relies on six coarse solar sensors, one on each face of the CubeSat, and a magnetometer. These feed the attitude control system, consisting of the control electronics and actuators. USAT-I will have a 3-axis magnetorquer system, plus a reaction wheel for the turning maneuver required for the GNSS-R operations.

4.2. Payload design and operations

The payload will be the GNSS system (receiver + three antennas) developed by SENyT of the Faculty of Engineering of the UNLP. This receiver, pictured in Figure 6, is dual frequency (L1 and L2) and dual constellation (GPS and GLONASS). It consists of an assembly of two PCBs and is estimated to have a peak power of 2.5W.

The three GNSS patch antennas (Figure 7) complete the system, each with its specific function. For navigation, USAT-I has a 1U antenna, and for GNSS-RO and GNSS-R, it has two 3U antennas. All of them have been developed in-house and *ad hoc* for this mission. Figure 8 shows the operations of the 3U antennas working in the GNSS-RO and GNSS-R modes.

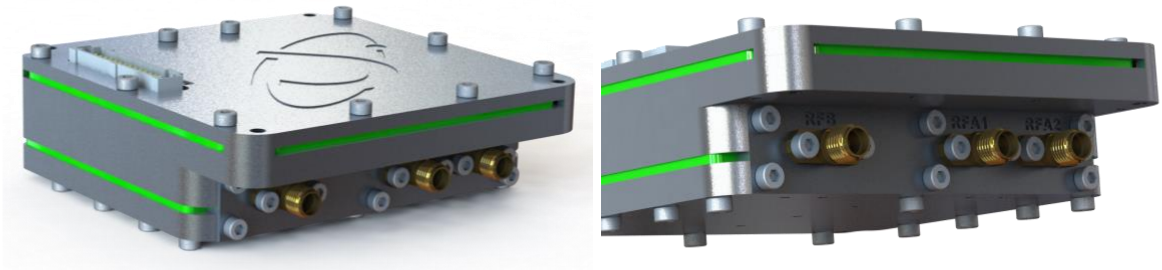

Figure 6. USAT-I's GNSS receiver, developed by SENyT at UNLP.

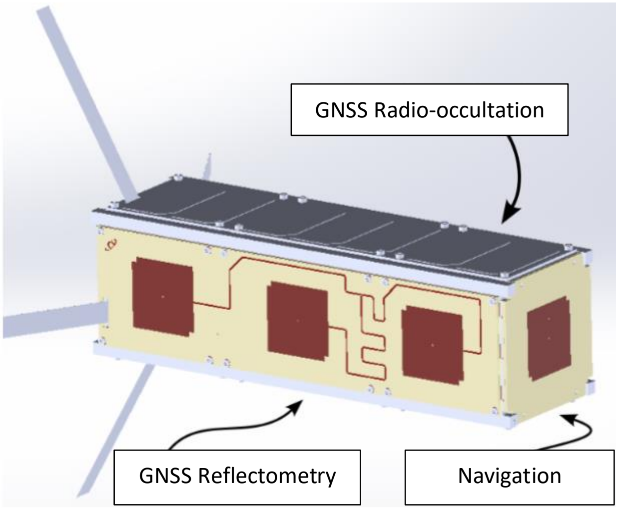

Figure 7. USAT-I's GNSS antennas for navigation, GNSS-RO and GNSS-R.

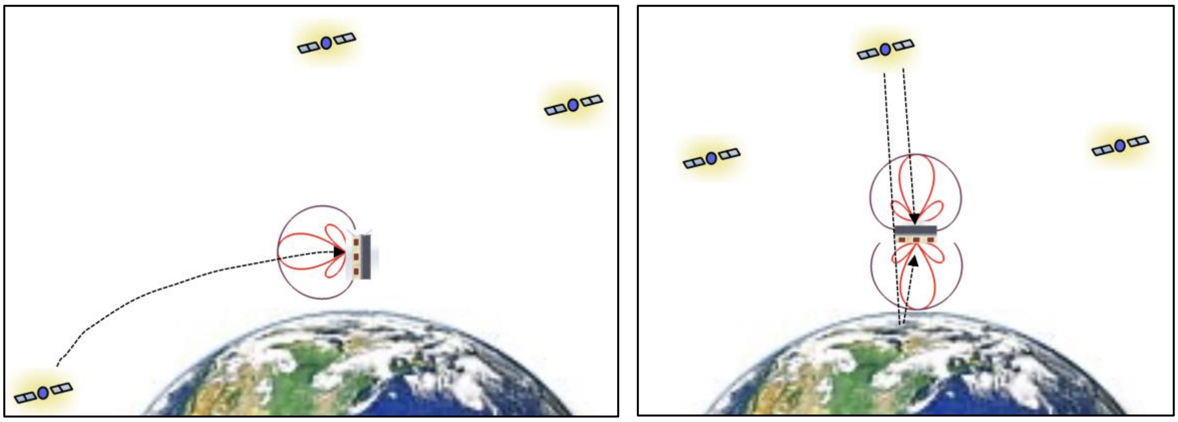

Figure 8. USAT-I's mode of operations and attitude for GNSS-RO (left) and GNSS-R (right).

5. Ground segment

As mentioned in the mission architecture, the ground segment is an essential element in the development of the University Satellite program. It consists of two parts: a dedicated ground station whose integration, operation and maintenance will be done at the UNLP. It will have UHF/VHF band emission and reception and S-band reception and will be located in the Department of Aeronautics of the Faculty of Engineering of the UNLP.

And another element consists of the support earth stations for which a feasibility study was carried out with five possible earth stations considering the exact location of the stations, the elevation angle, and the orbital characteristics of the satellite. In this analysis, we obtained the number of events, the duration, and the separation between contacts, discarding those contacts shorter than 30 seconds. We expect these results to guide our collaboration efforts with other universities and institutions.

6. Student involvement

As of September 2022, the project has awarded ten scholarships to undergraduate students. Seven students are currently working on different project areas, from systems engineering to payload design. Even though there are always professors and professionals supervising and managing, they have a degree of responsibility over the design decisions and criteria. They also teach and help other students when they begin working on the satellite. Therefore, not only do they learn technical skills but also soft skills, such as time and resources management, interpersonal relationships, criteria justification, and presentation skills, among others.

7. Programmatic and schedule

The project is currently finishing Phase C (Detailed design), having passed the Critical Design Review (CDR) in August 2022. The manufacturing process for flight hardware has already started, and assembly is expected to begin in December 2022. The next step will be subsystem verification testing before starting the final integration process around March 2023. The launch is planned for Q3 2023.

Figure 9 summarizes the schedule for the next milestone reviews.

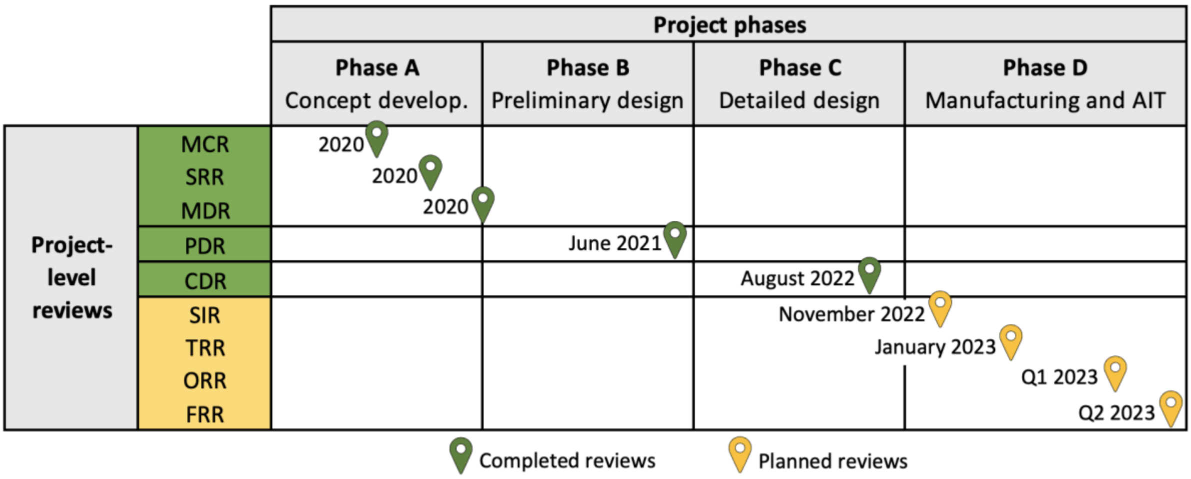

Figure 9. Planned review schedule for USAT-I.

8. Some early lessons learned

For a first-time satellite developer, everything is an opportunity to learn. The following points are an overview of some important lessons we had in the first two years of developing the USAT-I and we believe could help other first-timers.

- Keep track of every change, even the ones that could be considered "small". Even the most innocent change can bring up compatibility and interface problems if not communicated promptly.

- Document everything. More so with university satellite, where a large proportion of the team is students that eventually graduate. It is almost certain that someone will have to resume someone else's work at some point, and having a well-documented process can speed up the learning curve, avoid mistakes, and lower risks overall.
- In line with the previous point, overlap incoming and outgoing students whenever possible. Even a few days of interaction can be highly beneficial for keeping a continuous line of work.
- In countries with limited access to required COTS components, consider extra time for procurement. Most of the delays in the project were due to complications with getting the necessary parts.
- Integration can be as challenging as any other part of the project. Start thinking about it early on and be as hands-on as possible.
- Finally, software is as essential as hardware but usually more difficult to plan and time.

9. Summary and conclusions

This paper presented the mission concept and summary of the current development of the UNLP's USAT-I 3U CubeSat. This satellite will perform the technology demonstration of an in-house developed GNSS system for GNSS-RO and GNSS-R. It is expected to launch in Q3 2023. We also presented some early lessons learned regarding the management of the project, hoping to help other groups that are developing a satellite for the first time.

Acknowledgments

We want to thank CNEA and CONAE for their contribution to USAT-I, both in the solar panels and the reviews. We also thank the many collaborators who help us daily with this satellite. Their experience and knowledge are invaluable to us.

References

[1] D. Selva, D. Krejci, "A survey and assessment of the capabilities of Cubesats for Earth observation", Acta Astronautica 74 (2012) 50-68.
[2] H. Carreno-Luengo, A. Camps, P. Via et al., "^{3}CAT-2—an experimental nanosatellite for GNSS-R earth observation: Mission concept and analysis", IEEE Journal of Selected Topics in Applied Earth Observation and Remote Sensing 9(10) (2016) 4540-4551.
[3] A. Mannucci, C. Ao, W. Williamson, *GNSS Radio Occultation*, 2020.
[4] K. Cahoy, L. Dyrud, J. Fentzke et al., "Small and Low-Cost GNSS Radio Occultation Receivers", AGU Fall Meeting Abstracts (2011) SA24A-08.
[5] K. Yu, S. Han, J. Bu et al., "Spaceborne GNSS Reflectometry", Remote Sensing 14(7) (2020) 1605.
[6] A. Dielacher, H. Fragner, O. Koudelka, "PRETTY – passive GNSS-Reflectometry for CubeSats", e & i Elektrotechnik und Informationstechnik 139 (2022) 25-32.
[7] The CubeSat Program – Cal Poly SLO, *CubeSat Design Specification Rev. 14*, 2020.

BiomeSat: A Multi-Mission 6U Nanosat for Estimating Forests Health in Brazil

Walter A. dos Santos[1], Antonio C.O. Pereira Jr.[2], Lincoln Teixera[3], Bruno C. Junqueira[4], Marcus V. Cisotto[5], Antonio C. Julio Filho[6], Auro Tikami[7], Luiz A. R. Bueno[8], Lázaro A. P. Camargo[9] Ângelo J. A. Florentino[10], Antonio F. De Brito[11], Andrés F. P. Horna[12], Milton Kampel[13] and Manoel Cardoso[14]

National Institute for Space Research (INPE)
Av. dos Astronautas, 1758, Jd.da Granja, S. José dos Campos, Brazil
Phone: +55 12 3208 7377, Mail: (1)walter.abrahao, (2)acarlos.pereira, (3)lincoln.teixera, (4)bruno.junqueira, (5)marcus.cisotto, (6)cassiano.filho, (7)auro.tikami, (8)luiz.bueno, (9)lazaro.camargo, (10)angelo.florentino, (11)antonio.brito, (12)andres.horna , (13)milton.kampel, (14)manoel.cardoso [@inpe.br]

***Keywords**: Nanosatellites, Forests Monitoring, AIS, Environmental Data Collection, Space Weather.*

Forest conservation is very important in Brazil as they are home to a great variety of plant and animal species and they maintain high amount of water and carbon stocks and flows between the land surface and the atmosphere. Forests have a substantial impact on climate, biodiversity and the availability of natural resources. Due to the large Brazilian territorial extension, remote sensing is essential for monitoring the health those forests. This work presents the BiomeSat, a 6U nanosatellite proposal for providing information on forest conditions in Brazil, with a level of spatial and temporal detail useful for monitoring. The scientific and technological mission goals as well as high-level mission restrictions and requirements. The initial conception is planned to carry a set of payloads, namely: (1) a remote sensing camera for forest health monitoring which is the primary mission, (2) a data-environmental collecting transponder (EDC) which was developed by INPE´s Northeast site, (3) an AIS transponder for monitoring vessels in the Brazilian maritime authorities and, (4) a space-weather monitor (SEM) or tracking space environment mainly TID (Total Ionizing Dose) and SEE (Single Event Effects). The nanosatellite bus is envisaged to be a multi-mission platform for other future missions and serve as a complement to INPE´s larger remote sensing satellites like Amazonia and CBERs series. BiomeSat will also be a first prototype for a prospective constellation planned to be increase time revisiting and reach near real-time monitoring as well as enabling sensor fusion to existing larger remote sensing systems. Furthermore, this mission addresses 6/17 of the United Nations (UN) sustainable development goals (SDGs): 3 - Good Health and Well-being, 6 - Clean Water and Sanitation, 9 - Industry, Innovation and Infrastructure, 11 - Sustainable Cities and Communities, 13 - Climate Action and 15: Life on Land.

1. Introduction

Forest conservation in Brazil is important for several reasons. Forests are home to a high number of plant and animal species, and high values of water and carbon stocks and flows between the land surface and the atmosphere, thus having a substantial impact on climate, biodiversity and the availability of natural resources [1]. Due to the large territorial extension, remote sensing is essential for monitoring forests in Brazil.

Thus, to contribute to the forest observation programs in the country and agricultural monitoring, it is intended to generate information on the conditions of these areas using the collected data. Specifically, it is intended to collect data on the state of forests and agricultural crops using vegetation indices, which can aggregate the effect of various disturbances such as droughts, deforestation and fire, and present less complexity for data acquisition and calculation. The 6-U cubesat platform shown in Figure 1 will be planed be implemented around BiomeSat.

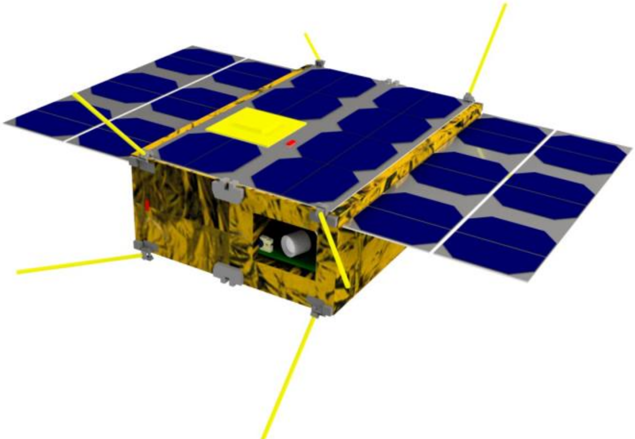

Figure 1: BiomeSat artistic view for forest health monitoring.

The BiomeSat main mission intends to continue monitoring environmental changes, deforestation and forest degradation but the imagery acquired will support applications in areas of vegetation, environment and education. Secondary mission's objectives will be performed by 3 other payloads: an environmental data collector transponder (EDC), an automatic identification system transponder (AIS) and a space-environmental monitor (SEM).

This paper is organized as follows: section 1 talks about the BiomeSat motivation; section 2 presents technological and scientific mission objectives; section 3 deals with technical planning of experiments and instruments; Section 4 refers to high level concerns for the project planning and management. Section 5 mentions about project and mission restrictions and initial requirements, finally Section 6 concludes this work.

2. BiomeSat Motivation

BiomeSat will contribute complementary to the existing bigger observation satellites available to INPE. The integration of several sensors allows reducing the influence of cloud cover in the interpretation process, as well as increasing the revisit rate to a few days. These features are extremely useful to forestry and agricultural applications.

2.1 INPE´s Legacy Missions

Brazil has technological and scientific experience in the construction and use of satellite data in the visible and infrared bands in these application areas. Annual rates of deforestation are produced based on data of 20-30 m of spatial resolution that are used as an indicator for the proposition of public policies.

INPE supports mainly the Brazilian Environmental Data Collection System (SBCDA). Currently, the SBCDA is a Brazilian satellite-based environmental monitoring system developed and operated by the Brazilian Institute for Space Research (INPE). Currently, SBCDA consists of 5 Low Earth Orbit (LEO) satellites (SCD-1, SCD-2, CBERS-4, CBERS-4A and Amazonia-1). Figure 2 shows a snapshot of INPE legacy missions covering earth observation as well as data collection missions among others satellite initiatives outside INPE.

Figure 2: INPE legacy missions on earth observation and data collection.

Data with spatial resolution of around 50-60 meters have been used in alerts for evidence of changes in forest cover in the national territory, as support for the inspection and control of deforestation and forest degradation by official institutional bodies.

2.2 BiomeSat Environmental Appeal

Climate changes are presently hitting hard the planet and BiomeSat pretty much will a key role into efforts to counterbalance the direct causes of these dreadful changes to Earth [2].

The 27th Conference of the Parties to the United Nations Framework Convention on Climate Change – COP27 [3], see Figure 3, is a follow-up to discussions on COP26 to act on a myriad of topics critical to dealing with climate emergency. Actions range from urgently reducing GHG (greenhouse gas emissions), structuring resilience, and adapting to the inevitable effects of climate change, to providing on the commitments to fund climate action in developing countries.

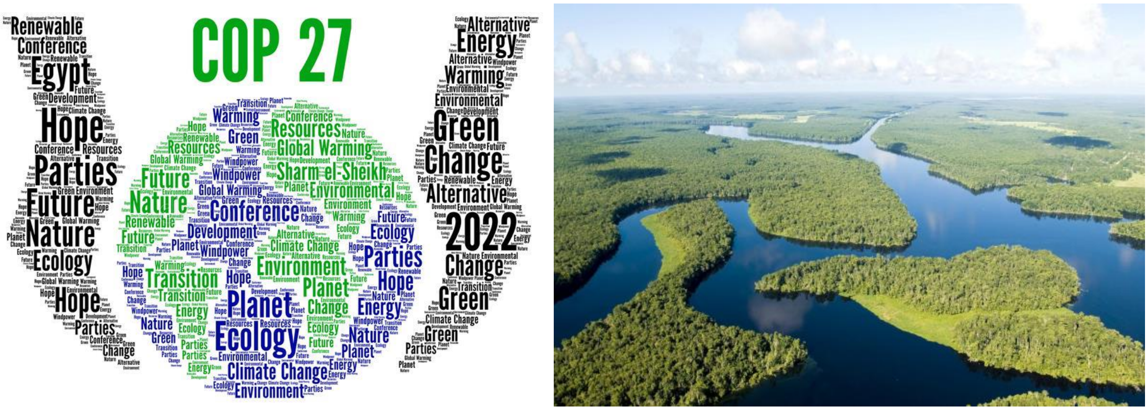

Figure 3: COP27 [4]: Climate chaos warnings amist the Amazon biome sanctuary.

Under the grounds of the Paris Agreement, COP27 is boosting renewed solidarity between countries in the middle of an increasing energy crisis, record GHG concentrations, as shown in Figure 4, and growing extreme weather events.

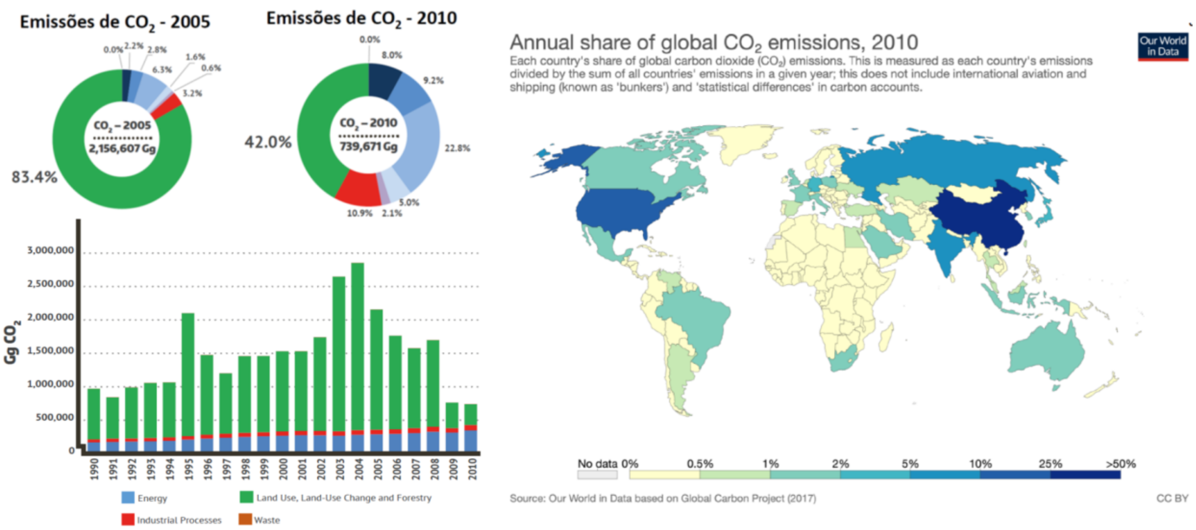

Figure 4: Dashboard of CO2 emissions [5]

In this context lies the main motivation for the BiomeSat project as the biome of Brazilian forests and, especially the sanctuary of the Amazon Forest, with its intricate advanced, and highly complex biological networks after millions of years of evolution. Forest conservation is very relevant to Brazil and world due to many facts some of them highlighted here: (1) Many plant and animal species live on them; (2) There is a high availability of natural resources and (3) Large stocks and surface-atmosphere flows of H_2O and C in a complex cycle that regulates life processes in the planet. Figure 5 devises the main links of this project to the UN sustainable goals.

Figure 5: BiomeSat main links to UN SDGs [6]

Therefore, Brazil has commitments to reduce GHG emissions and for that it will have to reduce deforestation and recovery of degraded areas as well as use of remote sensing technologies due to its large territorial extension which will drive BiomeSat mission definition next.

3. Mission Objectives

Based on the needs for the BiomeSat stated, we have split the mission goals into technological and scientific which are detailed hereafter. The choice of a 6U platform is a project decision since it will be realized a P-10 platform nanosatellite.

3.1 Scientific Mission Objectives

Using a 6U platform as a 1st constrain, the scientific is to continue the monitoring of environmental changes, deforestation and forest degradation, as well as support applications in the area of agriculture in order to obtain several benefits in different areas:

- Vegetation: monitoring of deforestation, degradation, and state of vigor of forests.
- Agriculture: estimate of planted area, vegetative vigor of crops, forecast of agricultural production, determination of areas of preservation of springs, forest reserves and agricultural areas, pointing out errors in fertilization, irrigation and soil preparation processes, regions with greater potential of production.
- Environment: assessment of the impact of fire, deforestation and drought on a given area, allowing a good rate of monitoring of environmental degradation, delimitation of continental water bodies, support for coastal management.
- Education: generation of material to support educational activities in geography, environmental sciences and other disciplines and generation of data and information for the development of scientific studies.

3.2 Technological Mission Objectives

The technological objectives are:

- Provide a 6U nanosatellite as a multi-mission platform for future other missions.

- Deliver payloads of interest to INPE´s Engineering:
    - EDC – Environmental data collection transponder developed by INPE-Natal with a high availability of natural resources;
    - Prospect a suitable thruster from the INPE´s Propulsion and Combustion group;
    - SMAE - Space Environment Monitoring System similar to one in CBERS satellites.
- Use nanosats as complements to large remote sensing satellites (AMZ/CBERs series) with lower manufacturing and launch costs.

4. Project Planning and Management

The concept of operations (CONOPs) diagram is shown in Figure 6 describes the target BiomeSat concept of operations where 4 payloads, namely: (1) a remote sensing camera for forest health monitoring which is the primary mission, (2) a data-environmental collecting transponder (EDC) which was developed by INPE´s North-east site, (3) an AIS transponder for monitoring vessels in the Brazilian maritime authorities and, (4) a space-weather monitor (SEM) or tracking space environment mainly TID (Total Ionizing Dose) and SEE (Single Event Effects).

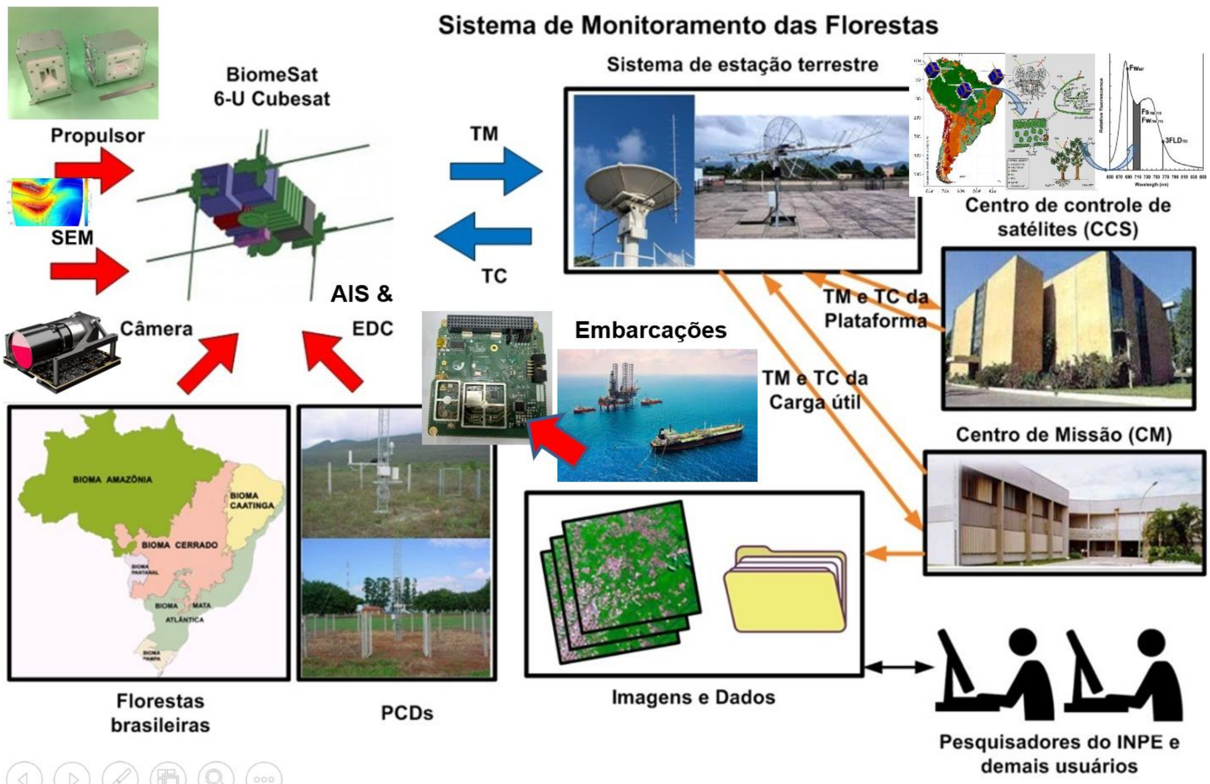

Figure 6: BiomeSat CONOPs – Concept of operations.

In order to commence the system technical planning, a desirable product is the map with estimates of photosynthesis activity [7] [8] where the target bands of interest for this phenomenon are defined helping the choice process for a suitable optical camera. Another point is estimating the orbital characterization in this case for a prospective 3U initially as shown in Figure 7.

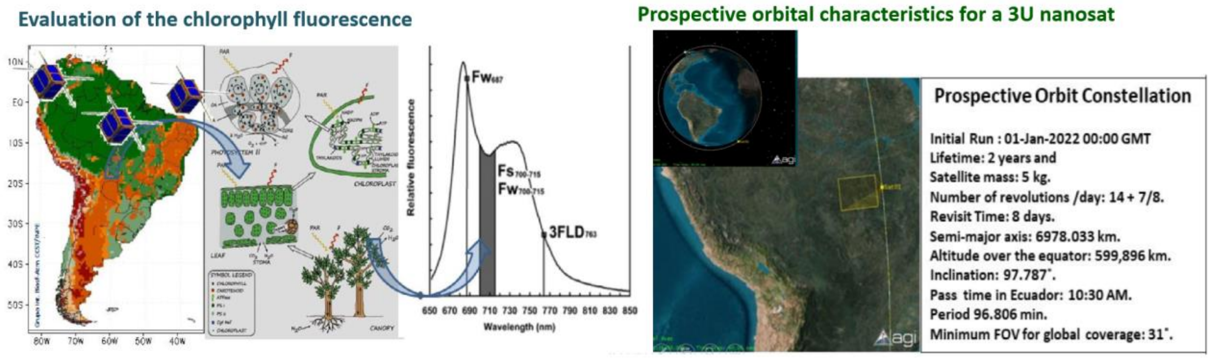

Figure 7: Photosynthesis activity estimates and early orbital characteristics 3U [7] [8] [9].

A preliminary constellation planning, see Figure 8 was performed and a sole BiomeSat can cover the Brazilian territory in 8 days in the orbit earlier mentioned, whereas 2 nanosats may drop this to 4 days.

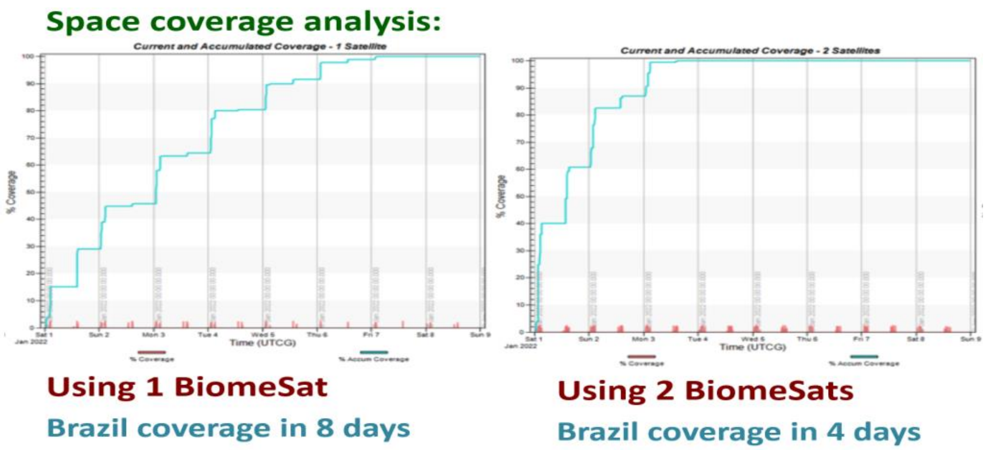

Figure 8: Preliminary land coverage for 1 and 2 BiomeSats constellation [10].

Currently, the following actions are being taken:

- Management plans still being performed
- Prospective selection of COTs equipment as pragmatic as possible
- Applications made for project financial support
- Identification of technological maturity level for equipment selection mainly for remote sensing imagers in the cubesats standard.

5. Initial Restrictions and Requirements

An early and initial mission analysis has come to the definition of some high-level requirements which were classified into operational, functional and programmatic categories:

- **Operational Requirements**: (1) Imaging only over the Brazilian territory and in sunlight; (2) Real-time image data transmission; (3) Data collection will be from

Brazilian PWDs only; (4) Continuous operation of the payload data collection and; (5) The nanosatellite must be discarded in EOL.

- **Functional Requirements**: (1) Pointing accuracy better than 1 degree; (2) Heliosynchronous orbit; (3) Revisit less than five days; (4) X-band or S-band data downgrade and; (5) The shelf life should be 24 months.
- **Programmatic Requirements**: (1) Development time between 01 to 02 years; (2) Structure will be acquired from companies specializing in CubeSats; (3) All subsystems will be acquired from specialized companies; (4) All embedded S/S software will be developed at INPE; (5) Use scalable platform for easy reuse in other 1U to 12U missions and; (6) It should be based on COTS components whenever possible.

Some restrictions were also defined such as: (1) The nanosatellite platform will be based on an architecture based on the CubeSat 6U standard and (2) The earth observation camera shall be COTS. As a result, Figure 9 shows the preliminary mechanical configuration drafted so far.

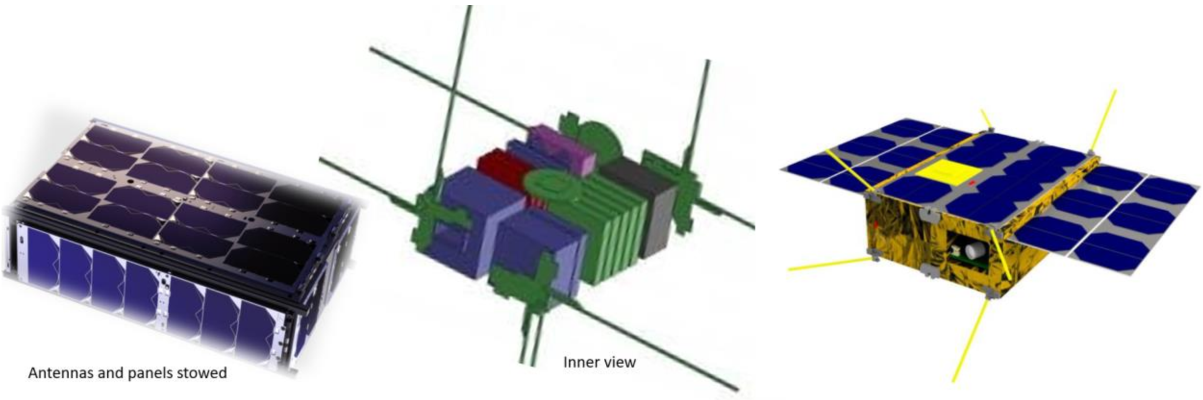

Figure 9: Preliminary mechanical configuration.

The initial conception is planned to carry a set of payloads, namely: (1) a remote sensing camera for forest health monitoring which is the primary mission, (2) a data-environmental collecting transponder (EDC) which was developed by INPE ´s North-east site, (3) an AIS transponder for monitoring vessels in the Brazilian maritime authorities and, (4) a space-weather monitor (SEM) or tracking space environment mainly TID (Total Ionizing Dose) and SEE (Single Event Effects).

The two transponders envisaged for BiomeSat are shown in Figure 10, one for environmental data collection and the other for AIS application which in our case is majorly for oil spillage tracking and vessel identification.

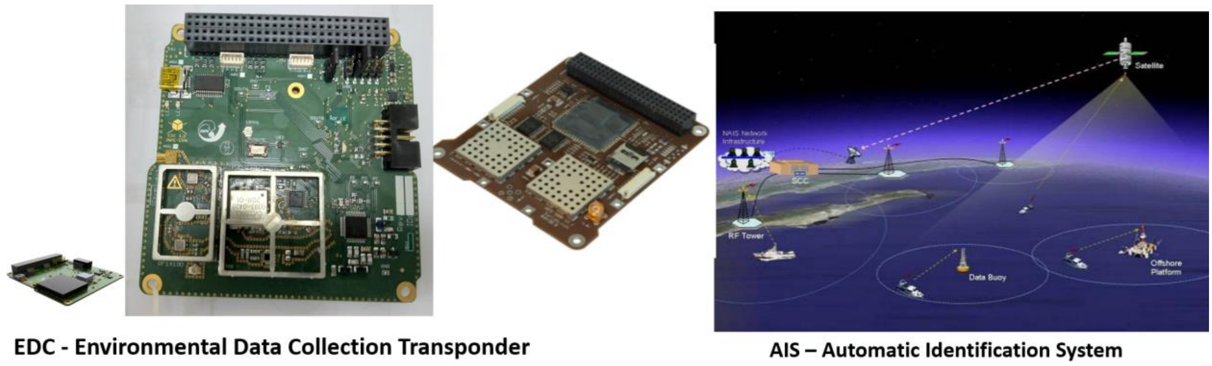

Figure 10: EDC and AIS transponder candidates as payloads.

The automatic identification system, or AIS plays many roles: (1) Transmits a ship's position so that other ships are aware of its position; (2) Large ships, including many commercial fishing vessels, to broadcast their position with AIS in order to avoid collisions and; (3) Oil-spillage surveillance and monitoring. This last one is the major motivation for using it at this nanosatellite.

The proposal for mapping forest conditions and agricultural monitoring considers the use of vegetation indices based on images collected in bands of electromagnetic waves corresponding to the visible and infrared spectrum, Figure 11 shows some preliminary requirements and a possible candidate optical camera. Some examples of these indices that use data in the red (R), green (G), blue (B) and near-infrared (NIR) ranges include, among others, the Visual Normalized Difference Vegetation Index (Visual NDVI), the Green Leaf Index (GLI), the Visual Atmospheric Resistance Index (VARI), as well as the Normalized Difference Vegetation Index (NDVI) and similar ones. These indices are related to chlorophyll content, differences between plants, exposed soil and non-vegetable material and are therefore appropriate for estimating vegetation conditions and agricultural crops.

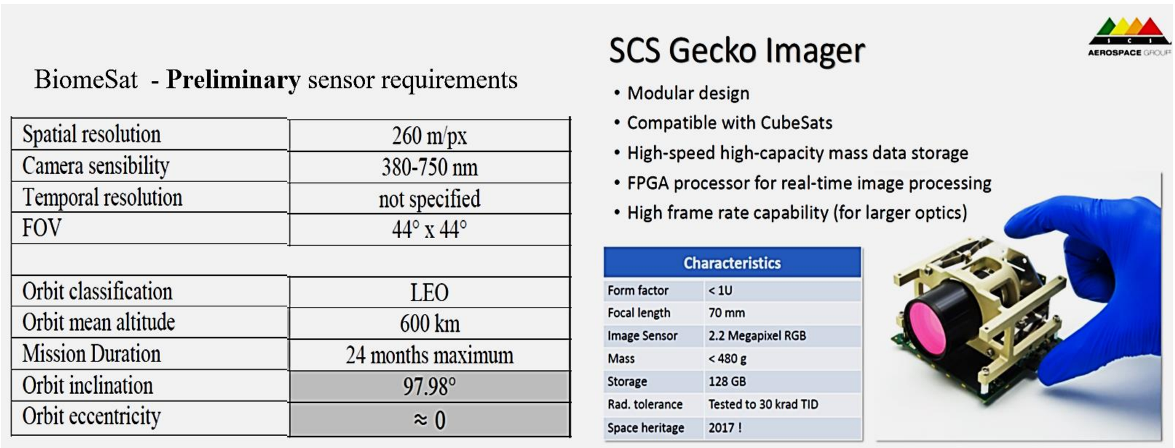
BiomeSat - **Preliminary** sensor requirements

Spatial resolution	260 m/px
Camera sensibility	380-750 nm
Temporal resolution	not specified
FOV	44° x 44°
Orbit classification	LEO
Orbit mean altitude	600 km
Mission Duration	24 months maximum
Orbit inclination	97.98°
Orbit eccentricity	≈ 0

Figure 11: Preliminary Optical requirements and a candidate camera.

Next steps in this research will be published after a report from a concurrent engineering session is concluded and is programmed to send out quite soon.

5. Conclusions

This paper presented a high-level view to the BiomeSat nanosatellite which is a 6-U cubesat that carries primary an optical camera as the main payload for monitoring forest conditions in Brazil and enabling a myriad of other remote sensing applications. As secondary payload we have three other payloads: (1) an EDC – Environmental data collection transponder developed by INPE-Natal with a high availability of natural resources. (2) An AIS transponder for vessel monitoring meanly those involved in oil-spillage events. and (3) SMAE - Space Environment Monitoring System similar to one in CBERS satellites. Prospection for an electrical Thruster from the INPE´s Propulsion and Combustion group is being investigated.

The project pursues an almost complete earth observation mission (without launch), involving not only the entire mission conceptualization, sensor and platform part, but also the commissioning, camera calibration & validation, control and reception, processing and dissemination of data.

BiomeSat may enable Brazil to support future satellite constellations with direct applications to environmental monitoring and territorial management, including continent and ocean. So far, platforms and sensors aim at high resolution constellation (10m) with daily revisits. Finally, this nanosat implementation will demand several engineering, computing and science challenges from INPE.

References

[1] Seppälä R., Buck A., Katila P. Adaptation of forests and people to climate change: a global assessment report, vol World Series Volume 22. Helsinki, IUFRO, 2009.

[2] BBC, *'Climate chaos' warning as UN summit begins*, available at https://www.bbc.com/news/science-environment-63517078 , 2022.

[3] United Nations, *COP 27 - Delivering for people and the planet*, available at https://www.un.org/en/climatechange/cop27, 2022.

[4] Clima & Sociedade, UN Climate Change Conference 2022 (COP 27) – iCS, available at https://climaesociedade.org/evento/un-climate-change-conference-2022-cop-27/ , 2022.

[5] MCTIC - 3rd National communication of Brazil to the UN framework on climate change, available at https://www.gov.br/mcti/pt-br/acompanhe-o-mcti/sirene/publicacoes/comunicacoes-nacionais-do-brasil-a-unfccc/arquivos/3mcti_volume_iii_ingles.pdf, 2022.

[6] Naccarato, K. - BiomeSAT Project-Monitoring forests health using nanosatellites technologies, Presentation at COPUOS 2019, available at https://www.unoosa.org/documents/pdf/copuos/stsc/2019/tech-34E.pdf , 2019.

[7] Greenbaum et al., The Earth Photosynthesis Imaging Constellation: Measuring Photosynthesis with a cubesat platform, IEEE Aerospace Conference. 2015.

[8] Porcar-Castell et al., Linking chlorophyll a fluorescence to photosynthesis for remote sensing applications: mechanisms and challenges, Journal of Experimental Botany, 2014.

[9] Dos Santos, W.A., *O Desenvolvimento de CubeSats no Brasil*, Presentation at SeCiAer - SeCiAer - Seminário de Serviços Científicos e Aeronáuticos, S.J. dos Campos, available at http://mtc-m21c.sid.inpe.br/ibi/8JMKD3MGP3W34R/3SFT53P?ibiurl.backgroundlanguage=pt-BR, 2018.

[10] Murcia J.O. et al., Preliminary analysis of a nanosat mission to integrate a lightning flashes detector with a biomass sensor in a CubeSat 3U configuration. 2nd International Academy of Astronautics Latin American Symposium on Small Satellites; Buenos Aires, Argentina. 2019.

The LECX experiment onboard the nanoMIRAX satellite

João Braga[(1)], **Otávio S. C. Durão**[(2)]
[(1)] INPE, Av. dos Astronautas 1758, S. J. Campos, SP, Brazil, +55-12-32087215, joao.braga@inpe.br
[(2)] CRON Sistemas e Tecnologias Ltda., Parque Tecnológico UNIVAP, Av. Shishimi Hifumi 2911 anexo 3, S. J. Campos, SP, Brasil, +55-12-997041361, otavio@cronsistec.com.br

Keywords: *cubesats, X rays, gamma-ray bursts, gravitational waves, detectors*

The nanosat/cubesat revolution has provided new opportunities to develop and launch small (~1000 cm^3), low-cost (~US$ 1M) experiments in space in very short timeframes (~2 years). We present here the development of an astronomical hard X-ray (30-200 keV) experiment, LECX ("Localizador de Explosões Cósmicas de Raios X"), which is the payload of the nanoMIRAX satellite. The mission is designed to detect and localize within a few degrees events like Gamma-Ray Bursts (GRB) and other cosmic explosive phenomena. The experiment uses 4 planar CdZnTe detectors ($10 \times 10 \times 2$ cm^3) and a passive shielding system (Pb-Sn-Cu) which determines a $53^\circ \times 53^\circ$(FWHM) field-of-view (FoV). The instrumental and aperture background spectra expected during operation in orbit, due the diffuse gamma-ray and particle fields, were calculated using the GEANT4 software package. The experiment sensitivity allows for detection of most known GBRs and the expected detection rate is of up to ~10 events per year in the experiment's FoV. An algorithm was developed to determine the incoming direction of the X rays during a cosmic burst that occurs in the FoV; the calculations are based on the registered detector counts and the attitude of the satellite. The satellite platform is a 2U CubeSat standardized bus with the LECX experiment, developed by INPE's astrophyscis Division, taking 1 "U" and the satellite service module, built by CRON Sistemas e Tecnologias, taking the other "U". This is the first CubeSat platform developed by the Brazilian private sector. We are currently building the flight model and hope to launch nanoMIRAX in 2023. In the current multimessenger era of astronomy, a constellation or swarm of small spacecraft such as nanoMIRAX can be a very cost-effective way to search for electromagnetic counterparts of gravitational wave events produced by the coalescence of compact objects.

1. Introduction

In order to develop competitive instruments to detect X- and gamma-rays from astrophysical sources, we are usually faced with several limitations which depend on available budget and resources. Non-focusing instruments such as coded-aperture telescopes (see 1 for a recent review) need both large detector areas to maximize source count rates and massive shielding systems to minimize background levels. With the current explosive growth of the nanosat phenomenon based especially on the so-called CubeSat platform, new opportunities for fast-development, low-cost small instruments have appeared.

In principle, X- and gamma-ray astrophysical instruments on such small satellites cannot compete with full-sized instruments operating on conventional large and complex satellite buses. Nevertheless, for very specific science goals, it is possible to design instruments compatible with cubesat buses that can meet the desired requirements. In this work we describe an instrument developed for a cubesat platform that is capable of not only to detect relatively strong cosmic explosions in the hard X-ray/low energy gamma-ray range but also to determine their position in the sky within a few degrees. The experiment, called “Localizador de Explosões Cósmicas de Raios X” (LECX), will be sensitive enough to detect and localize events like the well-known gamma-ray bursts (GRBs – see 2) in the 30–200 keV energy range. With its $53° \times 53°$ FWHM (“Full Width at Half Maximum”) FoV, it is estimated that LECX will detect up to$\sim$ 10 GRBs per year.

In the recently-inaugurated mutimessenger astrophysics era, it is of paramount importance that wide-field space instruments constantly patrol the sky in order to instantly detect electromagnetic (EM) counterparts of gravitational wave (GW) and/or neutrino cosmic bursting events. With the increased sensitivities of ground-based observatories of gravitational waves (e.g. LIGO/VIRGO) and neutrinos (e.g. IceCube), it is expected that the rate of such events will gradually increase over the years. X- and gamma-ray space experiments will then have higher probabilities of contributing to multimessenger detections of such phenomena.

The technology being developed for LECX builds upon what has been developed for the protoMIRAX project [3], a balloon experiment that represents a prototype of the MIRAX (*Monitor e Imageador de Raios X*, in Portuguese) space mission [4, 5].

LECX is in the flight model assembling phase and constitutes the payload of the nanoMIRAX satellite [6], which is based on a 2U-cubesat platform. nanoMIRAX is being developed by the Brazilian private company CRON Sistemas e Tecnologias Ltda. in partnership with INPE (National Institute for Space Research) and strong support from the Brazilian Space Agency (AEB).

2. The detector system and payload module

LECX employs four CdZnTe (CZT) planar detectors in a 2x2 configuration. Each detector is a 10mm x 10mm square with a thickness of 2mm, operating from 30 to 200 keV, described in detail in Braga et al. [3]. The lower limit is imposed by electronics noise and the higher limit is due to detector thickness. CZT room-temperature semiconductor detectors have been extensively used in astronomical X- and γ-ray space instruments due to their very high photoelectrical efficiency up to hundreds of keV and good energy resolution. They are also easy to handle and can be tiled to cover large surfaces. Pixelated CZT detectors can also be built for imaging instruments.

The separation between adjacent detector volumes in the LECX detector array is 3 mm due to the mechanical mounting and the presence of the detectors’ ceramic (alumina) substrates. The array is surrounded by a Pb (1.0mm), Sn (1.7mm) and Cu (0.3mm) graded shield box to minimize background and define the instrument FoV. The distance from the detector plane surface to the top of the shielding box is 20mm. In the upper part of the box there is an aperture of 23mm x 23mm that matches the detector plane area below (considering the gaps between the detectors). The area of the aperture is closed with a 0.4mm-thick carbon fibre plate to prevent the entrance of environment light, which induces noise in the detector electronics.

In Figure 1 we see a top view of the detector plane and the shielding walls surrounding the 4 detectors. The detector system is surrounded by a dielectric material (teflon) structure (also shown in the picture) that provides mechanical support and

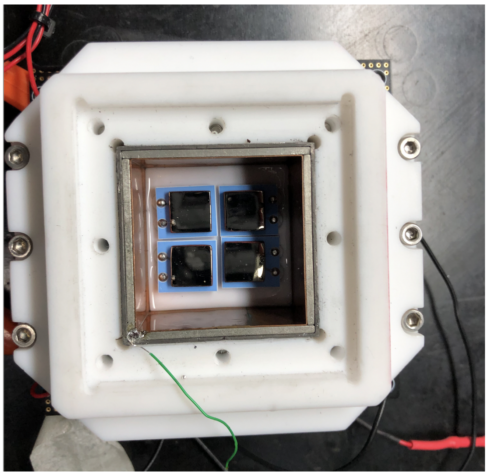

Figure 1: The 4 CZT detectors of LECX placed at the bottom of the shielding box, which is surrounded by the teflon support structure.

housing for batteries and electronic parts. Teflon is widely used in space application due to its suitable mechanical properties. The whole system is mounted on a standard 89mm×89mm cubesat printed-circuit board at the top of the satellite structure (the "top" direction hereafter refers to the instrument axis, i.e. the direction corresponding to the centre of its FoV). The front-end analog electronics for the detectors, which comprises four sets of charge pre-amplifiers and low-noise shaping amplifiers, is mounted on the opposite (bottom) side of the board. This PCB, as well as the other two board of the LECX payload, has multiple interconnected copper layers to provide electrical shielding. At the bottom part of the detector substrates lies the bottom part of the shielding box, so that the two electric leads (the one that polarizes the anode with the reverse bias and the one carrying the charge signal pulse from the cathode) perforate the shielding material, in teflon tubes, in order to reach the PCB underneath. The radiation shielding is also connected to the common ground to contribute to the electrical shielding.

Figure 2 shows two computer-generated pictures of the detector system mounted on a PCB.

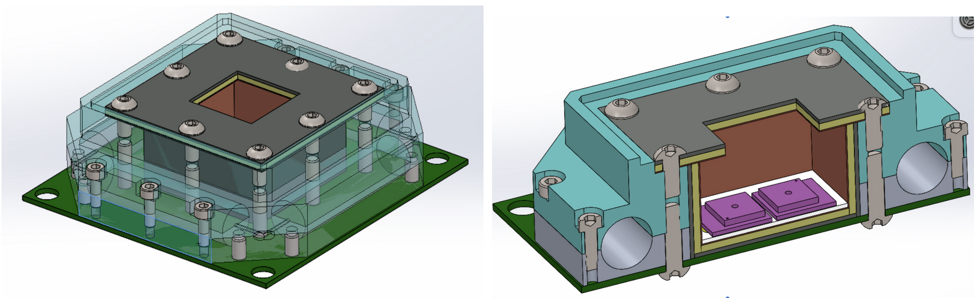

Figure 2: Computer model of the LECX detector system.

The performance of the detector plane has been demonstrated in the protoMIRAX experiment [3]. The reverse bias of -200 V was carefully chosen so as to minimize signal losses due to incomplete charge collection within the CZT material whilst keeping very low levels of dark current. The long-duration CR1216 Lithium Manganese Dioxide batteries used for the detector power supply are placed close to the detector plane and encapsulated in the teflon structure to avoid current leakage.

A second PCB, mounted underneath the detector board, houses the four Height-Time Converter (HTC) electronics, which linearly converts the heights of the pulses coming from the detectors to a digital high level signal. A third PCB, the experiment on-board-computer or digital board, houses the digital electronics, which is responsible for performing the following tasks: (a) receive signals from the 4 outputs of the TPCB; (b) measure the time duration of the correspondent high level signals and convert them into digital 8-bit words (this is proportional to the deposited energy of each event, divided in 256 channels), (c) flag the individual detector were the event occurred and convert it into a 2-bit word; (d) tag each event with the Universal Time from the satellite on-board computer (OBC), that uses a GPS receiver, with a resolution of 255μs; (e) build the event packages with time, detector ID and energy information (each event will generate a 24-bit word); (f) store data files and send copies to the spacecraft OBC for transmission to ground. The EOBC uses a commercial low power PIC24F32 microcontroller very suitable for this specific application. The power consumption of the LECX electronic system is less than 800 mW.

According to simulations of the radiation level to be measured in orbit the LECX payload will produce $\sim$ 100 bits/s in nominal operation, which will generate $\sim$540 kbits/orbit and $\sim$8.6 Mbits/day of data. Assuming at least one 10-minute ground station passage every orbit, this will require $\sim$900 bits/s telemetry capacity, well below the envisaged capabilities of the satellite.

The three PCBs of the nanoMIRAX payload, which comprise the LECX experiment, fill the first “U” of the satellite and constitute the payload module. The second “U”, the service module, mounted underneath the payload module, houses the subsystems of the satellite platform. Figure 3 shows a photo of the satellite being mounted in the lab, including both the payload module and the service module.

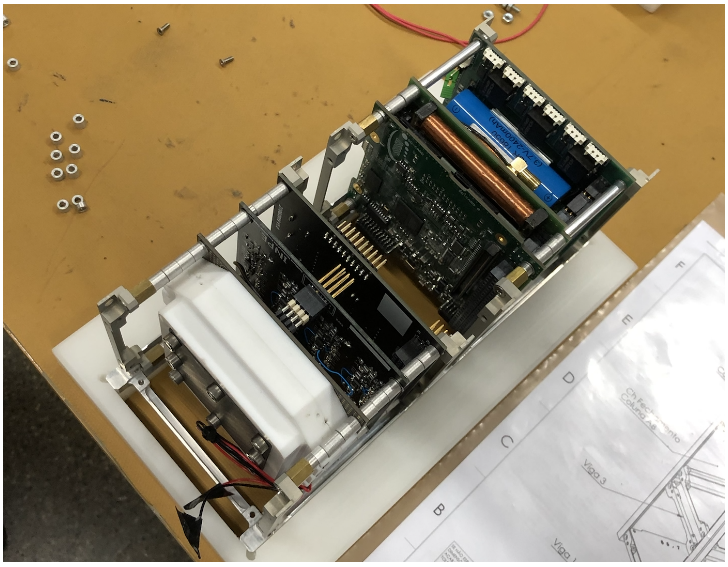

Figure 3: Photo of the nanoMIRAX satellite being mounted on the 2U cubesat structure in the lab.

3. Background and sensitivity

Estimation of the energy spectrum of the background signal and its spatial distribution over the detector plane is crucial for the design of hard X-ray and gamma-ray astronomy telescopes. In the case of an observation of a point source from an orbital space platform (i.e. a satellite), the background consists in the diffuse EM radiation coming through the telescope aperture, emission from other sources in the FOV, and the instrumental background, which arises from interaction of high-energy particles with the detectors and surrounding materials. Therefore, in order to foresee the performance of LECX in orbit and its sensitivity to cosmic explosions, we need to have a good estimate of the background radiation the detectors will measure. We have calculated this using the well-known GEANT4 package [7]. Details of our procedure to calculate the background of an instrument from angle-dependent spectra of photons and particles in space can be found in Castro et al. [8]. Considering a near-equatorial low-Earth orbit (LEO) and a mass model of the LECX experiment, we have obtained the main components of the expected background in orbit, outside the South Atlantic Geomagnetic Anomaly (SAGA). This is shown in Figure 4.

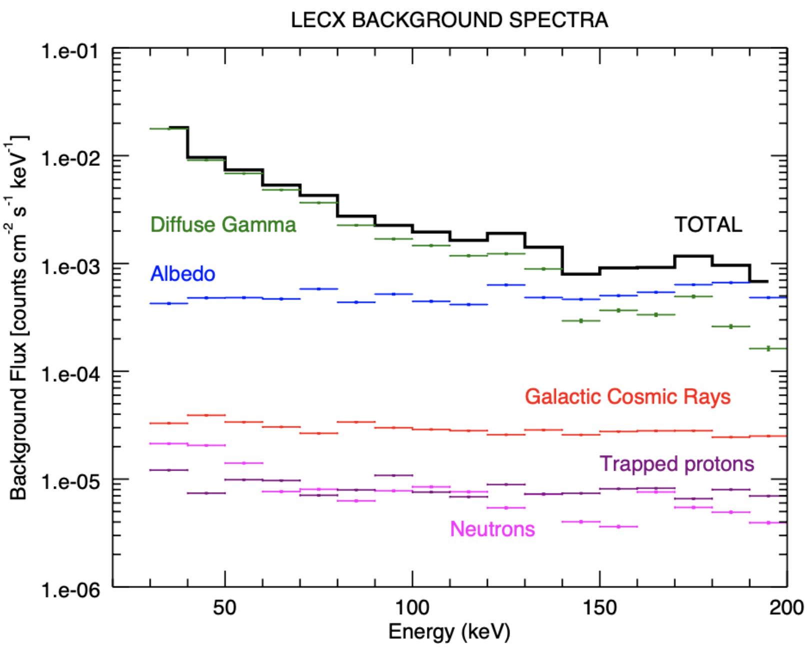

Figure 4: Simulated spectra of the main components of the LECX background in equatorial LEO, considering the 4 detectors as one unit and a spacecraft attitude in which the instrument's axis is pointed to the zenith.

We can see that the main contributions come from the diffuse electromagnetic flux entering the aperture (up to ~ 140 keV) and the albedo radiation coming from the Earth atmosphere (above ~ 150 keV). During the occurrence of a cosmic explosion event, it is reasonable to consider that the Compton-scattered events and fluorescence on the collimator walls will not add significantly to the background that will be present during the event, since the graded-shield walls were specifically designed to minimize these radiations with the help of GEANT4 simulations (see 8).

The sensitivity of LECX can be calculated considering that the number of counts in each detector, for a given integration time and a given energy bin, obey Poisson statistics. In the case of cosmic explosions observations, what will be measured are sudden increases in the total count rate that will last typically from a fraction of a second to tens of seconds during nominal operation. A trigger mechanism will detect these surges and automatically put the experiment in burst mode, which will end when the low count rates resume. During burst mode, the satellite service module will provide more frequent attitude information data. The electronics is designed so that all events will be time-tagged and stored onboard even if the count rate increases by a factor of ~ 100. All science and spacecraft data will be transmitted to the ground during the ground station passages.

Under nominal operations, the detector system will be measuring background radiation before and after the detected bursting events. We will select the best timescales to get good statistics for the background measurements. Since we may have significant background variations during one orbit, we also have to minimize this integration time to get more accurate values with respect to the background in effect during the occurrence of the event. During the event, we subtract the background counts from the total counts in each selected energy bin to obtain the source spectrum. It is easy to show that the minimum detectable flux, in photons cm^{-2}s^{-1}keV^{-1}, for each energy bin ΔE centred on energy E will be

$$F_{\min}(\Delta E) = \frac{N_\sigma}{\epsilon(E)} \sqrt{\frac{B(E)}{A_{\mathrm{det}}\Delta E}\left[\frac{1}{T_B} + \frac{1}{T_S}\right]} \tag{1}$$

where N_σ is the statistical significance (signal-to-noise ratio), $\epsilon(E)$ is the detector efficiency, $B(E)$ is the background in counts cm^{-2}s^{-1}keV^{-1}, A_{det} is the detector geometrical area in cm^2 (in this case 4 cm^2), ΔE the energy bin in keV, T_B the time spent measuring background and T_S in the time spent measuring source+background (both in seconds).

According to the expected count rates, ~5 minutes is a reasonable time to measure background before and after a triggered event, considering a $\sim$90-minute orbit. Using then 10 minutes for background integration, we have calculated the on-axis 3-σ sensitivity of LECX for 1, 10, 100 and 1000 seconds. The results are shown on Figure 5.

One can see that LECX is capable of detecting a wide range of typical GRB fluxes even with one-second integrations. For longer-duration GRBs, even somewhat weak events could be detected. The Crab spectrum [9] is shown in the figure just for comparison purposes, since the Crab it is a strong standard candle in these energies. LECX will not be able to detect the Crab since it would require pointing and very long stabilized observations, capabilities that the nanoMIRAX satellite will not have.

4. The localization algorithm

With the four CZT detectors placed inside the passive shielding box, the FoV of the detector system is a square region of the sky of $53^\circ \times 53^\circ$ FWHM ($\approx$ 7% of the sky) and $90^\circ \times 90^\circ$ FWZI ("Full Width at Zero Intensity"). In this section we describe the original algorithm we have devised to determine the celestial coordinates of strong cosmic explosions inside this FoV based on the intensities measured in each detector during the event.

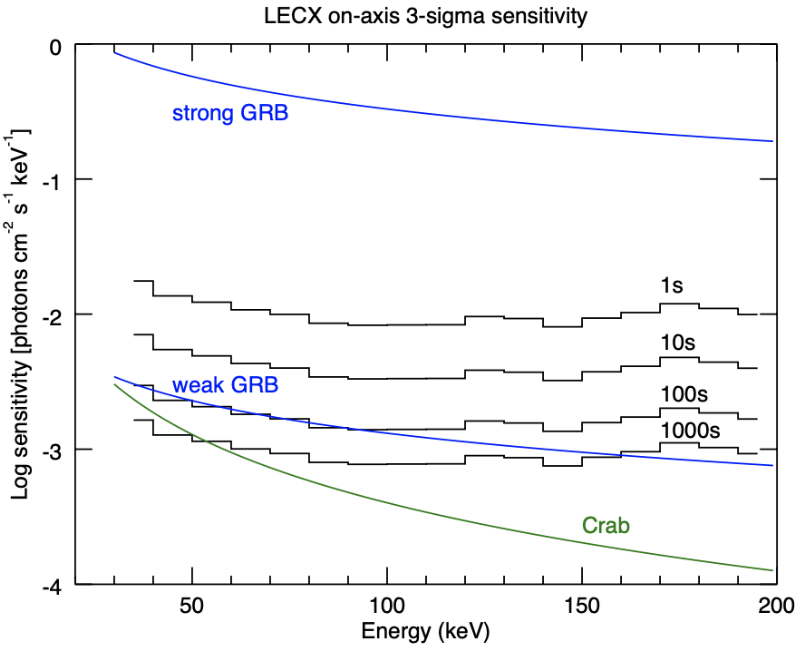

Figure 5: On-axis 3-σ sensitivity (minimum detectable flux) of LECX for different on-source integration times, considering 10 minutes for background integration. Strong and weak GRB spectra are shown in blue and the Crab spectra is shown in green for comparison.

In standard collimated high-energy detector systems, the fluxes of astrophysical sources are determined by subtracting a background level, measured separately, from the amount of radiation measured when the source is in the collimator FoV. For pixelated detector planes, one can use a coded mask in the aperture to obtain an image of the source field within the FoV (see, e.g. 1). In the LECX cubesat experiment described here, we have only 4 pixels (the four planar detectors) and a limited sensitivity due to the fact that the total area is only 4 cm^2. Since we are interested in detecting strong, short-duration point-source cosmic explosions one at a time, a coded mask placed in the experiment's aperture will not be adequate to use due to two main reasons: (a) the results to be obtained are not images of source fields, but only measured fluxes of short-duration ($\sim$seconds) point sources; and (b) the advantage of coded-mask systems in measuring source and background simultaneously are not important here, since we will have plenty of time to measure the background anyway, and in the same region of the sky.

During the detection of a radiation burst coming from a single direction (representing a cosmic explosion), the x and y extensions (with respect to the square shielding box and detector orientations) of the wall shadows on the detector plane is a function of the azimuth and zenith angles of the incoming photons. Since the number of source counts in each detector is proportional to the illuminated area, we can determine the source position in the sky by measuring the counts in each detector when the count rates suddenly increase during the occurrence of such an event in the FoV.

To explain the method, let us first define a coordinate system with axes x and y along the detector sides for a given detector plane orientation in which (looking from above the detector plane) "North" is to the upper direction (y axis) and "East" is to the right (x axis). The relevant units of distance are the detector side s (10mm in this case) and the height of the shielding walls above the detector surface, H (20mm). Starting from the upper left corner, let us call the detectors D_{11}, D_{12}, D_{21} and D_{22}, going clockwise.

If a cosmic explosion occurs in the FoV, let us define its direction by the “zenith angle” z with respect to the z axis, and the Azimuth angle A, defined in the $x - y$ plane, starting at the y axis (the “North” direction) and increasing clockwise. In this case, the x and y extensions of the shadows of the shielding walls over the detector plane will clearly be

$$L_x = H \tan z \cos A \quad ; \quad L_y = \tan z \sin A \tag{2}$$

Now, starting from the upper left corner, let us call the detector illuminated areas A_{11}, A_{12}, A_{22} and A_{21}, following the detector labels. If the explosive event happens in the ”SouthEast” quadrant, then

$$\begin{aligned} A_{11} &= s^2 \quad &; \quad A_{12} &= s(s - L_x) \\ A_{21} &= s(s - L_y) \quad &; \quad A_{22} &= (s - L_x)(s - L_y) \end{aligned} \tag{3}$$

since D_{11} will be fully illuminated, D_{12} and D_{21} will be shadowed by one wall each and D_{22} will have shadows from two walls.

In the general case, the algorithm first identifies the quadrant where the incoming direction lies by finding the detector with the most counts. Then it flags the other detectors in a decreasing order of counts. We then solve equations in the form of equations 3 (depending on the quadrant) for L_x and L_y, and finally use equations 2 to find A and z. The algorithm reproduces the incoming angles exactly when no statistical fluctuations are present.

For large zenith angles of incidence ($z > \arctan(s/H)$ in the orthogonal directions and up to $z > \arctan(\sqrt{2}s/H$ in the diagonal directions), the radiation coming from the source will miss one line of detectors entirely. In those cases, the algorithm can only determine ranges of A and z due to the lack of information from the four detector count numbers, which prevents us from calculating count ratios between detectors. Even in those cases, it is noteworthy that we can still get some localization despite using a very simple experimental setup. In particular, if the EM burst is coincident with a gravitational wave event, any independent localization may prove to be useful since the GW laser-interferometric detectors have poor localization capabilities. With the FoV of LECX, it is expected that the mission will detect up to ~ 10 cosmic explosions per year.

5. Simulation of cosmic explosions

In order to predict the performance of LECX for observations of GRBs and related phenomena, we have carried out a series of Monte Carlo simulations taking into account typical GRB spectra and the predicted LECX background. The details of these simulations can be found in [10].

GRBs are brief flashes of γ-rays with spectral energy distributions that peak around hundreds of keV and are expected to be detectable at a rate of ~ 1 event per day in the entire sky with the currently available instrumentation [11]. They represent the most energetic explosions in the Universe and can release up to 10^{54} ergs in a few seconds. GRBs follow a bimodal distribution in which most of the bursts last longer than ~ 2

seconds, clustering around tens of seconds, and about $1/3$ of them are shorter, clustering around 400 ms. The former are believed to be produced by the core collapse of massive, high-rotation stars, whereas the latter are best explained by the coalescence of neutron stars in a binary system. These short bursts are additionally interesting because they are expected to emit copious amounts of energy in the form of gravitational waves, as was dramatically demonstrated by the GW 170817 event (e.g. 12). As the current gravitational wave detectors (LIGO and VIRGO) are upgrading their sensitivities and new ones (KAGRA, LIGO-India) are about to start operating, it is expected that the rate of GW burst discoveries will significantly increase over the next years. It is extremely important that those detections are accompanied simultaneously by X- and γ-ray observations, since the GW instruments lack precise angular localization and the EM signals are complementary with respect to the characterization of the source. In a sense, we "see" the event through EM signals and "hear" it through the GW signal.

Short GRBs (SGRBs) usually have harder spectra and are less energetic than long GRBs [13]. However, the fluxes detected at Earth vary by several orders of magnitude depending on the GRB distance. The time-integrated fluxes (fluences) for all GRBs range approximately from 10^{-8} to 10^{-4} erg cm^{-2}. The observed photon spectra also show significant diversity and can usually be fit with the so-called Band model, a broken power-law with a smooth junction [14]. In any event, since we are interested in order-of-magnitude values for the simulations, we can approximately consider that a typical GRB photon spectrum measured at Earth is $F = AE^{-1}$, where A varies from 0.25 (weakest GRBs) to 200 (strongest GRBs), E is measured in keV and F is given in photons cm^{-2}s^{-1}keV^{-1}. This corresponds to a flat νF_ν spectrum. Figure 5 shows the limiting cases of these spectra.

In the simulations, we have considered the LECX instrument in a near-equatorial LEO and an incident flux coming from a GRB in a given direction. If on-axis, a very strong GRB would produce $\sim$1,900 counts in 1 s in the 30-200 keV energy range, whereas a very weak GRB would produce $\sim$2 counts. The background rate calculated using the GEANT4 simulations is $\sim$2.5 counts/s.

Using these numbers, we can simulate the signal-to-noise ratio (SNR) and the localization accuracy that we could achieve in a GRB detection with LECX. For the simulations reported here, we first calculate the illuminated areas on the four detectors, defined by the direction in the sky from which the photons are coming. In the real observations, this will depend not only on the azimuth and elevation with respect to the experiment reference frame but also on the satellite attitude given by the spacecraft's attitude control system. By combining the two coordinate systems, we then determine the celestial coordinates (e.g. right ascension and declination) of the event in the sky.

Once the illuminated areas are defined, we simulate random source counts at the level of the known sources in each detector using a Poisson distribution. These numbers scale with the illuminated fraction of the detector areas. The source counts are calculated convolving the source spectra with the response function of the instrument, which is given by the ratio of the effective area to the geometrical area of the detectors as a function of energy. In this case this will be essentially the photoelectric efficiency of the CZT detectors, since in these detectors the photoelectric effect is highly favoured with respect to Compton scatterings up to several hundred keV [15]. The background counts added to that are also Poissonian distributed and are given by the values provided by the GEANT4 simulations.

As a first example, we simulated a strong GRB occurring at $A = 20°$ and $z = 5°$.

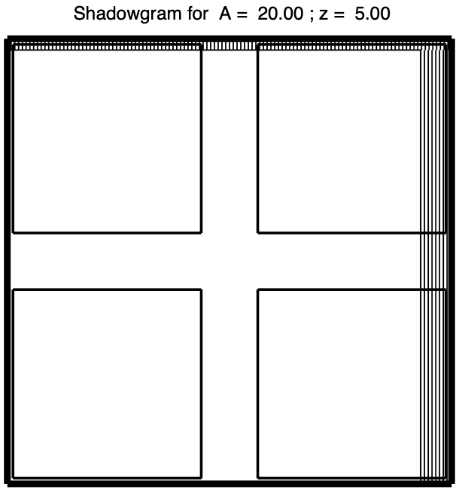

Figure 6: The detector shadow geometry for a strong GRB simulation. The simulated position in the sky is $A = 20^\circ$ and $z = 5^\circ$.

Figure 6 shows the shadow position at the detector plane. In this case we get a theoretical (Poissonian) SNR of ~37. After repeating the simulation 100 times to determine the dispersion on the parameters, we get $A = 8.94 \pm 24^\circ$ and $z = 6.13 \pm 2^\circ$. The values of the dispersions do not vary significantly for more than ~5 repetitions of the simulations, so these 1-σ dispersion values are very robust. The SNR of the detection is in close agreement with the Poissonian theoretical value. Figure 7 shows the 1-σ sky localization region for the GRB.

In a second example, we repeated the azimuth angle (20°) but simulated a burst coming at $z = 20^\circ$. The shadowgram is shown in Figure 8 and the localization box in 9.

It is noteworthy that, even though we get less counts due to the fact a larger area is shadowed (which is reflected by a smaller SNR of 19) , the algorithm gives a better determination of the localization of the source in the sky. This is due to the fact that the source is farther away from the instrument axis, which provides a higher contrast among the illuminated areas in the detectors.

A third example shows an explosion that happens outside the FWHM FoV, so that the wall shadows miss completely one line of detectors (see Figures 10 and 11). In this case the “zenith” angle is 40°.

Since two detectors do not register counts, the algorithm can only determine ranges of possible angles for the source position in the sky due to the lack of information from the four detector count numbers, which prevents us from calculating count ratios between detectors. Even in those cases, it is noteworthy that we can still get some localization despite using a very simple experimental setup.

Since the satellite attitude determination precision is of ~1° and we do not expect the spacecraft to rotate by more than 1° in 10 s, the conversion of instrument to sky coordinates will have an error of $\lesssim 1^\circ$, which will be a small fraction of the overall localization power for most detected GRBs.

These simulations demonstrate that LECX is able to detect cosmic explosions and determine their positions in the sky with enough accuracy to contribute to the search for EM counterparts of GW burst events detected by the new generation of GW laser-interferometric observatories.

Based on current estimates of GRB occurrence rates and LECX’s sensitivity, we

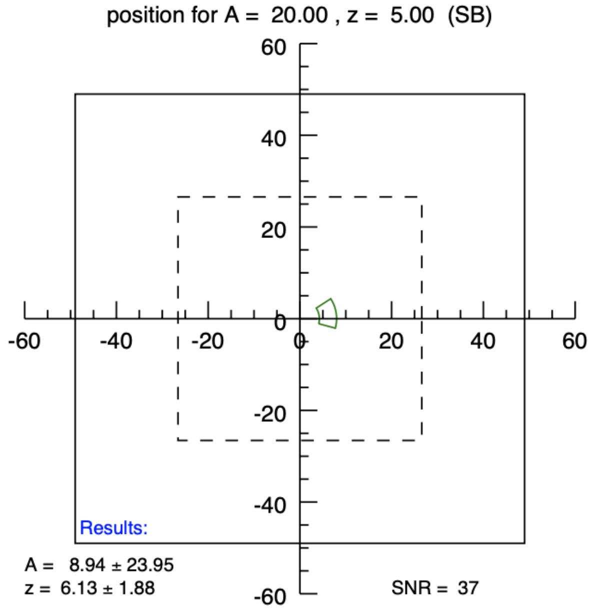

Figure 7: A simulated localization for a strong GRB. The green box gives the 1-sigma localization (in degrees) provided by the localization algorithm developed in this work. A and z are the polar angles (in degrees) in this plot, and the x and y coordinates are in degrees. The dashed square is the FWHM FoV (7% of the sky) and the solid square is the total FoV.

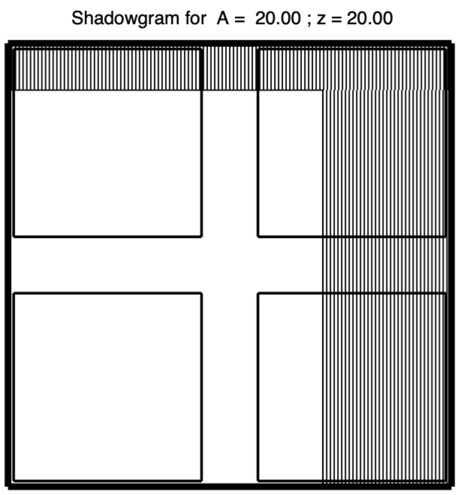

Figure 8: The detector shadow geometry for a strong GRB simulation. The simulated position in the sky is $A = 20^\circ$ and $z = 20^\circ$.

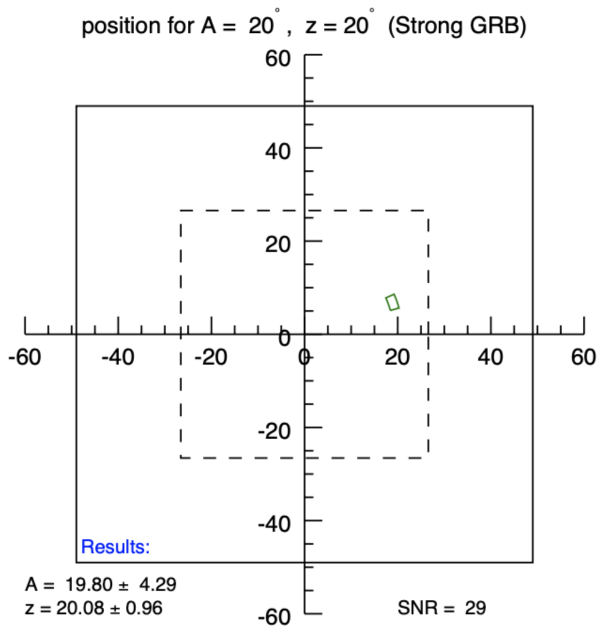

Figure 9: A simulated localization for a strong GRB. The green box gives the 1-sigma localization (in degrees) provided by the localization algorithm developed in this work. A and z are the polar angles (in degrees) in this plot, and the x and y coordinates are in degrees. The dashed square is the FWHM FoV (7% of the sky) and the solid square is the total FoV.

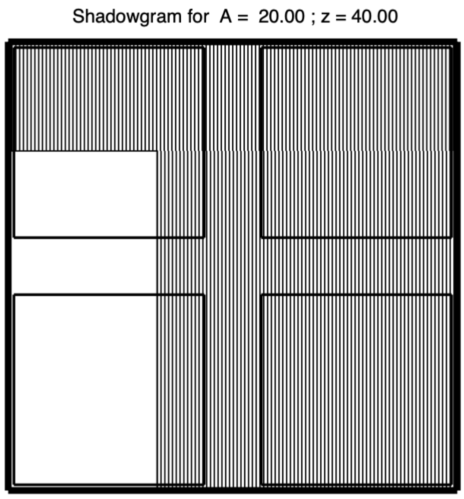

Figure 10: The detector shadow geometry for a strong GRB simulation. The simulated position in the sky is $A = 20°$ and $z = 40°$.

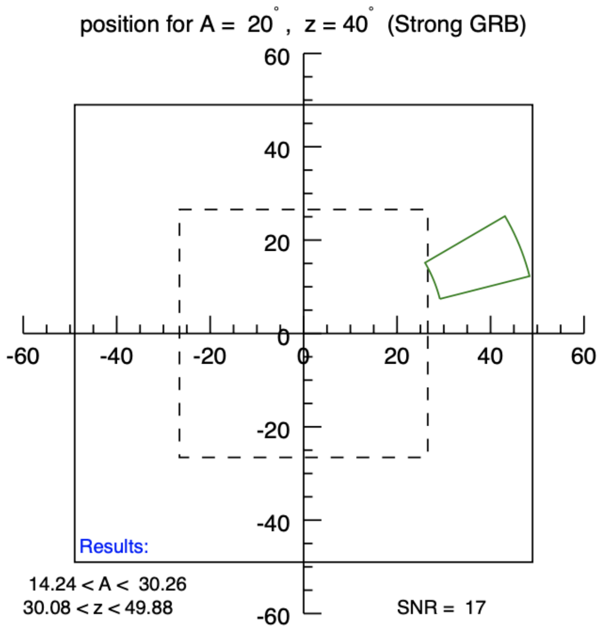

Figure 11: A simulated localization for a strong GRB. The green box gives the 1-sigma localization (in degrees) provided by the localization algorithm developed in this work. A and z are the polar angles (in degrees) in this plot, and the x and y coordinates are in degrees. The dashed square is the FWHM FoV (7% of the sky) and the solid square is the total FoV.

can estimate the rate at which we will be able to detect these events in our FOV. See [10] for details. Our best estimates is that, since our FWHM FOV covers 7% of the sky, this would allow us to detect $\sim$10 events per year or $\sim$1 event every 36 days.

It is important to stress that the GRB rate in the Universe is still subject to considerable debate, and the fact that the only localized neutron-star/neutron star coalescence event localized so far (GW170817 – 16) was also seen in gamma rays [17] seems to point towards more frequent multi-messenger observations of these events than previously thought.

6. Conclusion

LECX is a small high-energy astrophysics space experiment that is capable of contributing to the detection and localization of cosmic explosions that are characterized by intense emission of hard X-rays and low-energy γ-rays. The nanosat/cubesat revolution has opened new opportunities for the development of scientific space missions in the "smaller, faster and cheaper" paradigm. With creative ideas, it is possible to contribute to science with low budgets and limited resources. The experiment described here is an example of a cubesat mission that is capable of doing competitive and important science by detecting and localizing cosmic explosions in the gravitational wave era of astronomy. This is accomplished by a new algorithm that uses the shadowing of shielding walls over the detector plane to reconstruct the incoming directions of photons coming from a bright and short-lived cosmic point source.

Simulations described here show that LECX can detect most GRBs and locate them within a few degrees in the sky at a rate of $\sim$ 10 per year. With a constellation of satellites of this kind, it would be possible to increase this rate significantly and provide a low-cost, fast-development network of electromagnetic localizers of gravitational wave events that could complement the observations made by the ground-based gravitational wave observatories.

LECX is currently in the phase of assembling its flight model. We are analyzing launch opportunities and we expect to have the satellite launched by the end of 2023.

In Table 1 we present the baseline numbers of the LECX/nanoMIRAX mission.

Table 1: nanoMIRAX/LECX baseline parameters

LECX payload
Detector type: CdZnTe (CZT)
Dimensions: 10 mm $\times$ 10 mm $\times$ 2 mm (thickness)
Number of detectors: 4 (2×2)
Gap between detectors: 3 mm
Energy Range: $30 - 200$ keV
Geometrical area: 4 cm^2
Effective area: 3.9 cm^2@ 80 keV, 2.1 cm^2@ 150 keV
Energy resolution: 11% @ 60 keV
Time resolution: 255 μs
Expected nominal counting rate: 2.5 counts/s
(up to $\sim$100 counts/s in burst mode)
Shielding: Pb (external – 1.0 mm)
Sn (middle – 1.7 mm)
Cu (internal – 0.3 mm)
configuration: box around detectors with
23mm $\times$ 23mm aperture on top, 20mm height
Field of view: $53^\circ \times 53^\circ$ (FWHM); $90^\circ \times 90^\circ$ (FWZI)
Sensitivity: 10^{-2}photons cm^{-2}s^{-1}keV^{-1} for 1 s @ 100 keV
Cosmic Explosion (CE) Location Accuracy: a few degrees
(depending on position and intensity)
Expected CE detection rate: $\sim$10 per year
Science data creation rate: 100 bits/s
Payload mass: $\sim$600 g
nanoMIRAX satellite
Structure: 2U cubesat frame
Satellite dimensions: 20 cm $\times$ 10 cm $\times$ 10 cm
Total mass: $\sim$2.6 kg (including payload)
Power: 2.2 W total, 800 mW delivered to payload
Stabilization: $\lesssim 0\overset{\circ}{.}1$/s
Attitude knowledge: $\sim 1^\circ$
Communications: Telemetry (download): UHF, 482–486 MHz
Command upload: VHF, 130–160 MHz
Both at 1200–9600 bit/s
Orbit: TBD (possibly polar LEO)
Ground stations: 2 in Brazil (Santa Maria and Natal

Acknowledgments

We thank FAPESP and AEB for support.

References

[1] J. Braga, Coded Aperture Imaging in High-energy Astrophysics, Publications of the Astronomical Society of the Pacific: Invited Review Article 132 (2020) 012001.

[2] B. Zhang, The Physics of Gamma-Ray Bursts, Cambridge University Press, 2018.

[3] J. Braga, F. D'Amico, M. A. C. Avila, A. V. Penacchioni, J. Rodrigo Sacahui, V. A. de Santiago, F. Mattiello-Francisco, C. Strauss, M. A. A. Fialho, The protoMIRAX hard X-ray imaging balloon experiment, Astronomy and Astrophysics 580 (2015) A108.

[4] J. Braga, MIRAX Mission Overview and Status, in: F. D'Amico, J. Braga, R. E. Rothschild (Eds.), The Transient Milky Way: A Perspective for MIRAX, volume 840 of *American Institute of Physics Conference Series*, pp. 3–7.

[5] J. Braga, R. Rothschild, J. Heise, R. Staubert, R. Remillard, F. D'Amico, F. Jablonski, W. Heindl, J. Matteson, E. Kuulkers, J. Wilms, E. Kendziorra, MIRAX: a Brazilian X-ray astronomy satellite mission, Advances in Space Research 34 (2004) 2657–2661.

[6] O. S. C. Durão, J. Braga, V. R. Schad, M. B. Silva Neto, M. Esper, G. Rigobello, C. B. Ribeiro, CRON-1 – The First Brazilian Private Cubesat, Proceedings of the 2019 Small Satellite Conference (2019) 9.

[7] S. Agostinelli, J. Allison, K. Amako, J. Apostolakis, H. Araujo, P. Arce, M. Asai, D. Axen, S. Banerjee, G. Barrand, F. Behner, L. Bellagamba, J. Boudreau, L. Broglia, A. Brunengo, H. Burkhardt, S. Chauvie, J. Chuma, R. Chytracek, G. Cooperman, G. Cosmo, P. Degtyarenko, A. Dell'Acqua, G. Depaola, D. Dietrich, R. Enami, A. Feliciello, C. Ferguson, H. Fesefeldt, G. Folger, F. Foppiano, A. Forti, S. Garelli, S. Giani, R. Giannitrapani, D. Gibin, J. G. Cadenas, I. González, G. G. Abril, G. Greeniaus, W. Greiner, V. Grichine, A. Grossheim, S. Guatelli, P. Gumplinger, R. Hamatsu, K. Hashimoto, H. Hasui, A. Heikkinen, A. Howard, V. Ivanchenko, A. Johnson, F. Jones, J. Kallenbach, N. Kanaya, M. Kawabata, Y. Kawabata, M. Kawaguti, S. Kelner, P. Kent, A. Kimura, T. Kodama, R. Kokoulin, M. Kossov, H. Kurashige, E. Lamanna, T. Lampén, V. Lara, V. Lefebure, F. Lei, M. Liendl, W. Lockman, F. Longo, S. Magni, M. Maire, E. Medernach, K. Minamimoto, P. M. de Freitas, Y. Morita, K. Murakami, M. Nagamatu, R. Nartallo, P. Nieminen, T. Nishimura, K. Ohtsubo, M. Okamura, S. O'Neale, Y. Oohata, K. Paech, J. Perl, A. Pfeiffer, M. Pia, F. Ranjard, A. Rybin, S. Sadilov, E. D. Salvo, G. Santin, T. Sasaki, N. Savvas, Y. Sawada, S. Scherer, S. Sei, V. Sirotenko, D. Smith, N. Starkov, H. Stoecker, J. Sulkimo, M. Takahata, S. Tanaka, E. Tcherniaev, E. S. Tehrani, M. Tropeano, P. Truscott, H. Uno, L. Urban, P. Urban, M. Verderi, A. Walkden, W. Wander, H. Weber, J. Wellisch, T. Wenaus, D. Williams, D. Wright, T. Yamada, H. Yoshida, D. Zschiesche, Geant4 - a simulation toolkit, Nuclear Instruments and Methods in Physics Research Section A: Accelerators, Spectrometers, Detectors and Associated Equipment 506 (2003) 250 – 303.

[8] M. Castro, J. Braga, A. Penacchioni, F. D'Amico, R. Sacahui, Background and imaging simulations for the hard X-ray camera of the MIRAX mission, Monthly Notices of the Royal Astronomical Society 459 (2016) 3917–3928.

[9] P. Wallyn, J. C. Ling, W. A. Mahoney, W. A. Wheaton, P. Durouchoux, BATSE Search for the ~540 keV Feature in the Crab Spectrum Observed by Granat-SIGMA, The Astrophysical Journal 559 (2001) 342–345.

[10] J. Braga, O. S. C. Durão, M. Castro, F. D'Amico, P. E. Stecchini, S. Amirábile, F. Gonzalez Blanco, C. Strauss, W. Silva, V. R. Schad, L. A. Reitano, LECX: a cubesat experiment to detect and localize cosmic explosions in hard X-rays, Monthly Notices of the Royal Astronomical Society 493 (2020) 4852–4860.

[11] D. Williams, J. A. Clark, A. R. Williamson, I. S. Heng, Constraints on Short, Hard Gamma-Ray Burst Beaming Angles from Gravitational Wave Observations, The Astrophysical Journal Letters 858 (2018) 79.

[12] J. Granot, D. Guetta, R. Gill, Lessons from the Short GRB 170817A: The First Gravitational-wave Detection of a Binary Neutron Star Merger, The Astrophysical Journal Letters 850 (2017) L24.

[13] E. Berger, Short-Duration Gamma-Ray Bursts, Annual Review of Astronomy and Astrophysics 52 (2014) 43–105.

[14] D. Band, J. Matteson, L. Ford, B. Schaefer, D. Palmer, B. Teegarden, T. Cline, M. Briggs, W. Paciesas, G. Pendleton, G. Fishman, C. Kouveliotou, C. Meegan, R. Wilson, P. Lestrade, BATSE

Observations of Gamma-Ray Burst Spectra. I. Spectral Diversity, The Astrophysical Journal 413 (1993) 281.

[15] S. Del Sordo, L. Abbene, E. Caroli, A. M. Mancini, A. Zappettini, P. Ubertini, Progress in the Development of CdTe and CdZnTe Semiconductor Radiation Detectors for Astrophysical and Medical Applications, Sensors 9 (2009) 3491–3526.

[16] B. P. Abbott, R. Abbott, T. D. Abbott, F. Acernese, K. Ackley, C. Adams, T. Adams, P. Addesso, R. X. Adhikari, V. B. Adya, C. Affeldt, Multi-messenger Observations of a Binary Neutron Star Merger, The Astrophysical Journal Letters 848 (2017) L12.

[17] B. P. Abbott, R. Abbott, T. D. Abbott, F. Acernese, K. Ackley, C. Adams, T. Adams, P. Addesso, R. X. Adhikari, V. B. Adya, C. Affeldt, Gravitational Waves and Gamma-Rays from a Binary Neutron Star Merger: GW170817 and GRB 170817A, The Astrophysical Journal Letters 848 (2017) L13.

Payload-XL: A Case Study of Methodologies for Development and Documentation of Cubesat Subsystems Using ECSS Standards

Márcio Hermany Gomes de Oliveira(1), **Edilberto Costa Neto**(1), **Kleber Reis Gouveia Junior**(1), **Felipe Viel**(1),(2), **Miguel Boing**(1), **Gabriel Mariano Marcelino**(1), **André Martins Pio de Mattos**(1), **Laio Oriel Seman**(1),(2), **David Merodio Codinachs**(3), **Eduardo Augusto Bezerra**(1)

(1) Universidade Federal de Santa Catarina, Brazil
(2) University of Vale do Itajaí, Brazil
(3) European Space Agency (ESA), Netherlands

Keywords: *Space project management, Project Workflow, Cubesats, ECSS standards, AIV*

The Cubesat interest has significantly increased in the last decade due to their low cost, relatively fast development and potential for Earth Science and telecommunications. In order to demonstrate novel nanosatellite capabilities for the next generation of constellations, the GomSpace and European Space Agency (ESA) announced a payload collaboration opportunity as part of the GOMX-5 mission. It consists of a 12U Cubesat which is scheduled to be launched in the first half of 2022. One unit of the Cubesat (1U) is dedicated to the Advanced Payload Processors (APPs), developed by a consortium of several international institutions, which aims to demonstrate processing platforms based on state-of-the-art microcontrollers, processors, FPGAs and a GNSS Software Defined Radio (SDR). In order to ensure the safety of the mission, methodologies and concepts defined by the European Cooperation for Space Standardization (ECSS) were applied in this project. The standards are branched into 4 main disciplines: space project management; space product assurance; space engineering; and space sustainability. Each discipline is composed of several subdisciplines and norms. For instance, the standard ECSS-E-ST-10-02C, which establishes the requirements, processes and activities related to the verification of space systems to ensure compliance with restrict design requirements, and the standard ECSS-E-ST-10-03C, responsible for defining verification by testing of space segment elements and equipment on ground before launch. In order to fulfill these objectives, the Payload-XL and the APPs consortium follow these standards. A straightforward workflow for development, documentation, integration, verification and testing is proposed. Also, lessons learned and initial guidelines for academic projects are presented.

1. Introduction

The GOMX-5 mission was announced in December 2018 and is led by the Danish company GomSpace and the European Space Agency (ESA). The GOMX-5 consists

Email addresses: `marcio.hermany@posgrad.ufsc.br` (**Márcio Hermany Gomes de Oliveira**), `edilberto.costa.neto@posgrad.ufsc.br` (**Edilberto Costa Neto**), `eduardo.Augusto@ufsc.br` (**Eduardo Augusto Bezerra**)

of a 20kg class 12U nanosatellite whose main objective is to demonstrate the capabilities of the next generation constellation of nanosatellites operating in low earth orbit [1].

The satellite will be equipped with a series of payloads, divided according to their purposes into main and secondary ones. The payloads represent the primary objectives of the mission. The payloads will enable the establishment of a high-speed communication link for communication between the nanosatellites of the constellation, demonstrations of a miniaturized propulsion system for orbit transfer maneuvers, and the test of a high-precision GNSS receiver. In the case of secondary payloads, the objectives are established by each third-party company participating in the consortium following the requirements of ESA [1, 2].

A summary of the payloads that make up the mission and the responsible companies and respective countries of origin are shown in the table Table 1. As it is a European consortium, the standards required for the mission are established by ESA. Therefore, the European Cooperation for Space Standardization (ECSS) has been adopted.

Advanced Payload	Company	Country of Origin
High reflectarray antenna wins in X-band	Ticra	Denmark
X-band transmitter (coupled with antenna)	GomSpace	Denmark
Electric Propulsion	ThrustMe	France
ARGO 2.0 - Star Tracker Circuit	EICAS	Italy
PPP (Precise Point Positioning) GNSS Receiver	Syrlinks	France
G3PSTAR - High precision GNSS receiver	Deimos University of Padova	England Italy
APPs - Payload radhard processing with HW/SW GNSS	GMV CBK Cobham Gaisler AB SpaceLab - UFSC	Poland Poland Sweden Brazil
Theia EOI - Earth observational camera with radiometric calibration module Observatory	Tartu	Estonia
MIRAGE- Artificial Intelligence Technologies for use in space operations	AIKO Space	Italy
MIRAM (Miniaturized Radiation Monitor) - Miniaturized Radiation Monitor	Institute of Experimental and Applied Physics at Technical University of the Czech Republic	Czech Republic

Table 1: Characteristics of GOMX-5 mission payloads.

In this work, we present as the main contribution and objective the description of the processes of adaptation of the ECSS standards and their requirements to the secondary payload APPs project and development for the GOMX-5 mission.

2. Advanced Payload Processor – APP

The Advanced Processing Payload is a 1U processing platform composed of 5 combined subsystems developed by the consortium formed between Cobham Gaisler, GMV, Centrum Badań Kosmicznych (CBK), and SpaceLab-UFSC.

The objective of APPs in the GOMX-5 mission is the joint demonstration of different processing platforms based on microcontrollers, FPGA and Artificial Intelligence, and GNSS-SDR (Software Defined Radio) algorithms implemented in general purpose processors.

Rather than demonstrating these experiments individually, this combined investigation also allows for the observation of different technologies working together, increasing the added value of the payload.

Figure 1 presents the Computer Aided Design (CAD) model of the integrated APPs and their five subsystems. From top to bottom: GNSS-dig board and GNSS-front-end board (developed jointly by GMV and CBK), Payload XL (developed by SpaceLab-UFSC) and GR716 and GR740 boards (Developed by Gaisler) [2, 3]. The ECSS was chosen as the adopted standard in the elaboration, structuring, and verification of the APPs. This choice was made to be compatible with the specifications and requirements of the mission

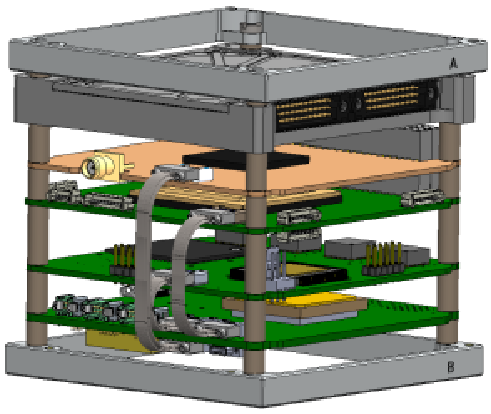

Figure 1: CAD model of advanced processor payload.

2.1. Payload-XL Subsystem

One of the experiments to be carried out by APPs in the Payload-XL subsystem is the in-place legitimation of the NG-Large electronic component, an FPGA tolerant to radiation effects, produced by the company NanoXplore.

The Payload-XL architecture focuses on the NG-Large FPGA, the central processing block. This FPGA implements several communication interfaces through GPIO, UART, I2C, CAN, SpaceWire and has access to Flash memories, RAM, temperature sensor, and voltage and current monitor at the system power input [3].

One of the tests to be carried out in orbit is reconfiguring the FPGA with a new bitstream sent via a ground station. For this, the Payload XL also has an MSP430 microcontroller that will assist in rewriting the FLASH memory of the FPGA. Figure 2 shows the block diagram of Payload XL.

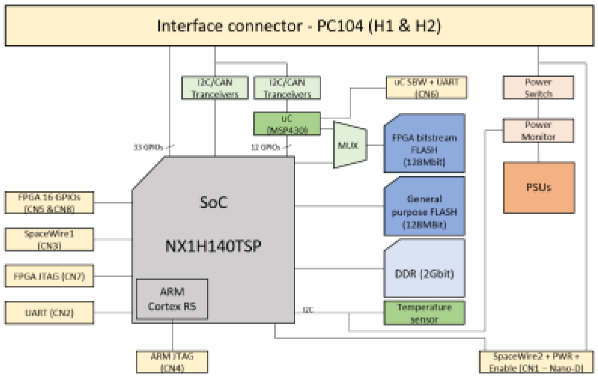

Figure 2: Block diagram of Payload-XL.

3. Tailoring Process

The following subsections describe the process of adapting the ECSS standards and their requirements to the needs of the APPs payload development project. The 7-step methodology recommended by ECSS in the document ECSS-S-ST-00-02 - Tailoring [4] was used as a reference for this step. The boundaries between each of the steps of the methodology were not clear enough in this project. Therefore, it was decided to raise the level of abstraction and divide the flow according to the group of activities (Preparation, Adaptation, Finalization) also presented in the document.

Another important source of reference for the adequacy of the standards seen below was the document “Tailored ECSS Engineering Standards for In-Orbit Demonstration Cubesat Projects” [5]. This document presents a guide showing which ECSS standards should be applied in the context of CubeSats missions and which parts should be adapted. This document is prepared by ESA and the European Space Research and Technology Center (ESTEC).

3.1. Preparation Activities

Despite the APPs being part of the GOMX-5 mission, all its development took place independently of the other segments of the system. From this point of view, the APPs platform can be considered as a CubeSat 1U project characterized by the following attributes:

- CubeSat Orbit Demo Mission.
- Acceptable high failure risk profile.
- Low level of complexity (compared to other ESA space projects).
- Low cost and short schedule.
- Limited redundancy.
- Limited fault tolerance.

- System-focused tests.
- Use of COTS in your development.
- Simple organizational level.

According to the Application of ESA approved standards (Application of ESA approved standards), projects with these similar characteristics are classified as "non-complex procurement activities, with simple industrial structures, conducted as contracts of lower cost and shorter duration ". This classification is due to low relative value, simpler project organization, short development timelines, and short-duration operations.

For activities of this type, most of the ESA-approved standards in the list may not be relevant, and only a few may be selected as applicable. In addition, the verification process should be adapted to reflect the reduced complexity of the project and the absence of one or more disciplines.

Thus, the design, development, and verification process in the APPs project does not follow the classic management, engineering, review, and quality assurance approach indicated by ECSS standards. A tailoring process is necessary to define which standards and requirements apply to the project.

3.2. Adaptation Activities

According to [5] the following ECSS standards listed in Table 2 have applicability for the context of CubeSats projects.

Due to the characteristics of the APPs platform, standards related to the system structure are not applicable since the structure provided by the company GomSpace, responsible for the mission, will be used. It is responsible for ensuring the points addressed in these standards.

Another criterion for refinement is that all communications with the APPS platform are determined in the Interface Control Document (ICD). Above the APPs subsystem level, all communications, including bi-directional communication between space and ground segments, are the responsibility of GomSpace. Therefore all communication-related standards are also not applicable in this project.

Standards related to non-existent components on the platform were also considered not applicable.

Finally, according to [5] for the design of CubeSats, the documentation resulting from the verification processes and their implementation can be condensed into a single Assembly, Integration, and Verification (AIV) document. The AIV is responsible for presenting the assembly and integration instructions of subsystems and the verification strategy to be followed during the project.

As a result of applying these criteria, we obtain Table 3 of standards applicable to the project.

3.2.1. ECSS-E-ST-10-03C Standard Requirements Selection - Tests

According to esa2016tailored recommends the list of tests presented in Table 4 for elements of the spatial segment for CubeSats.

From the tests of General type, the tests of optical alignment, polarity, and interface with the launcher are refined, as they do not apply to APPs. Performance testing

Norm	Title
ECSS-E-ST-10-02C	Verification
ECSS-E-ST-10-03C	Testing
ECSS-E-ST-10-04C	Space environment
ECSS-E-ST-20C	Electrical and electronic
ECSS-E-ST-20-08C	Photovoltaic assemblies and components
ECSS-E-ST-31C	Thermal control general requirement
ECSS-E-ST-32C	Structural general requirements
ECSS-E-ST-32-01C	Fracture control
ECSS-E-ST-32-02C	Structural design and verification of pressurized hardware
ECSS-E-ST-32-08C	Materials
ECSS-E-ST-33-01C	Mechanisms
ECSS-E-ST-35-01C	Liquid and electric propulsion for spacecraft
ECSS-E-ST-50C	Communications
ECSS-E-ST-50-05C	Radiofrequency and modulation
ECSS-E-ST-60-30C	Satellite attitude and orbit control system (AOCS) requirements

Table 2: Lists of ECSS standards applicable in CubeSats projects.

Norm	Title
ECSS-E-ST-10-03C	Testing
ECSS-E-ST-20C	Electrical and electronic

Table 3: List of ECSS standards applicable to the APPs project.

will only be performed at the subsystem level, and mission testing will be covered in functional testing.

For the mechanical tests, the measurement of physical properties will be done only considering the mass and dimensions of the system. The measurement of the center of gravity and the moment of inertia does not apply in this project because the APPs are an integral part of a larger system. The sinusoidal vibration test will cover static tests.

The heat balance test does not apply to the APPs situation and may be removed from the applicability list. Since there is no atmospheric entry for the APPs and the mission is unmanned, the specific tests may also be removed.

After refinement, the list of tests presented in Table 5 applicable for the APPs project context is obtained.

The ECSS-E-ST-10-03C [6] standard provides test levels and durations, tolerances, and accuracies. In addition, conditions listed in [7] were used during the vibration tests,

Type	Test
General	Optical Alignment Functional (FFT/RFT) Performance (PT) Mission (MT) Polarity Launcher interface
Mechanical	Physical properties Static Random vibration Sinusoidal vibration
Thermals	Thermal vacuum Thermal balance
Electric/RF	EMC Electromagnetic self-compatibility
Specific	Aero-thermal Micro-vibration emission

Table 4: List of tests applicable for space segment elements in cubeSats.

Type	Test
General	Functional (FFT/RFT)
Mechanical	Physical properties Random vibration Sinusoidal vibration
Thermal	Thermal vacuum

Table 5: List of tests applicable for the APPs project.

and the mission organizer defines the Vacuum Thermal test specifications.

3.2.2. ECSS-E-ST-20C Standard Requirements Selection - Electrical and Electronics

The ECSS-E-ST-20C - Electrical and electronic [8] standard defines the specific requirements for electrical subsystems and payloads, arising from the system engineering requirements established in ECSS-E-ST-10 - System engineering general requirements [9]. A pre-tailoring matrix according to the project and its characteristics is presented in Section 8 of the standard to facilitate the adaptation process.

Using this matrix and applying the appropriate refinements to the APPs project, it is observed that the applicability of the ECSS-E-ST-20C standard for the project is partial. Only clause 5.9 a) "Design of electronic subsystems and payloads shall be in accordance with ECSS-Q-ST-40" shall be considered.

3.3. Finalization Activities

Finalization activities include adding mission-specific requirements, checking the consistency of applicable requirements, and documenting them. When verifying the consistency of the applicable requirements selected in the previous activity, it was noted that the ECSS-Q-ST-40 - Safety [10] standard does not fit with functions performed by APPs since the APPs payload does not perform mission-critical functions.

This standard and ECSS-E-ST-20C can be refined and considered not applicable for this situation. Verifying the subsystem following the AIV plan is considered a sufficient safety measure.

4. Phases

During the execution of the project, it was necessary to adapt to the management methods. After studying the ECSS-M-ST-10C standard - Project planning and Implementation [11], considering the greater simplicity and singularities of the advanced payload APPs project, and taking as a reference the tailoring processes carried out by [3, 12, 13, 14] the most relevant documents for each phase were selected as deliverables and four design reviews that mark key points in the development, they are: Preliminary Requirements Review - PRR, Preliminary Design Review - PDR; Critical Design Review - CDR; Acceptance Review - AR. Additional design reviews may be required after AR. However, these depend on the interaction with the mission organization, being outside the scope of this work.

The customized life cycle for the APP project was divided into 6 phases: Initial Planning, Definition, Design and Verification, Testing and Implementation, Operation, and Completion. The life cycle, including activities and formal reviews, is shown in Figure 3.

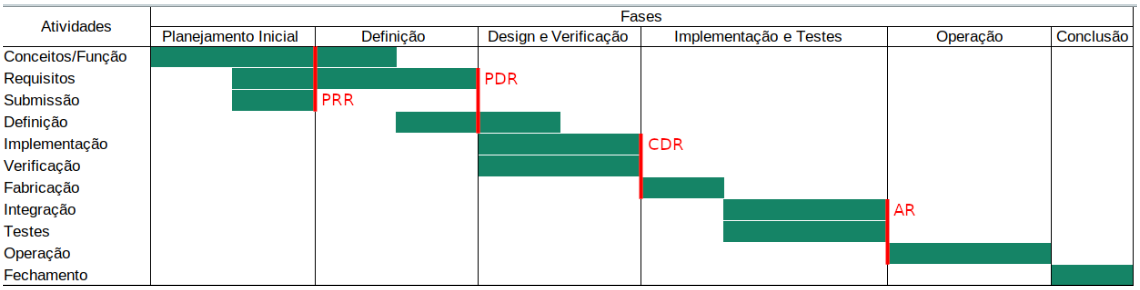

Figure 3: Customized life cycle for the APP project.

4.1. Initial planning phase

The initial planning phase takes into account the technical and programmatic constraints of the GOMX-5 mission and the fulfillment of the mission statement and has as main objectives:

- The elaboration of the preliminary functional and technical requirements of the APPs platform and of each of the subsystems that comprise it.
- Identification of the concepts and functions to be performed by the APPS platform at the system level and individually by each of its subsystems.
- Preparation of the preliminary proposal for integration between the subsystems.
- Preparation of the preliminary proposal for testing the integrated system.
- Submission of the proposal (and all related legal parts) to the mission organizer (GomSpace).

The Preliminary Requirements Review (PRR) is the first project review foreseen in the APPs development lifecycle. It determines the end of the Initial Planning phase and the fulfillment of the objectives established for this phase.

4.2. Definition Phase

The Definition phase has as main objectives:

- Conclusion of the preliminary functional and technical requirements of the APPs platform and of each of the subsystems that comprise it;
- Conclusion of the concepts and functions to be performed by the APPS platform at the system level and individually by each of its subsystems.
- Preliminary design of the subsystems architecture and integration proposal.
- Preliminary design of the environmental testing proposal.
- Preparation of the preliminary system AIV document.

The Preliminary Design Review (PDR) marks the closing of the design phase of the project. It verifies that the main objectives established for the definition phase have been completed.

4.3. Design and Verification Phase

The Design and Testing phase comprises the activities of:

- Final design of the architecture of the subsystems.
- Update of the proposal for environmental tests of the integrated system.
- Finalization of the integration solution between the subsystems.
- Independent implementation, verification and validation of each subsystem.
- Manufacturing of subsystems.

The Critical Design Review (CDR) marks the close of the design and verification phase of the project and verifies that the project is fit for the next phase.

4.4. Integration and Testing Phase

As the name suggests, this phase is intended for integrating the subsystems that make up the APP and the execution of environmental tests on the integrated platform. In order to determine the closure of the Integration and Tests stage, Acceptance Review (AR) is performed.

4.5. Operation and Conclusion

The Operation Phase comprises all launch, commissioning, and operations of the in-orbit system and subsystems. Finally, the Completion Phase comprises all mission completion activities and the CubeSat removal protocol from orbit by the mission organizer following European and international regulations.

5. Conclusion

A process suggestion was presented in this paper, based on the experience of the team in the GOMX-5 project, applied to ECSS standards. The Tailoring made it possible for the consortium companies to better adapt to the needs of the main satellite. This adoption has required the elaboration, structuring, and execution of the payload integration processes, inspection and verification of the subsystems, and, consequently, the tests of the APPs. As a final result, a very structured project was obtained with predictability and guarantees for the operation of the APPs. We observe that the adaptation process is not easy, and sometimes there is a lack of information to adjust and adapt to the established norms. For this, the step-by-step developed during the paper can be used as a reference for deployments for future payloads that use ECSS standards. For future works, it is recommended to extrapolate this work for the digitization and automation of some steps for structuring a new project. So that more projects can follow the recommended standards with quality and guarantee in the formalization of documents for systems engineers.

Acknowledgments

The authors would like to thank the funding from Conselho Nacional de Desenvolvimento Científico e Tecnologico (CNPq) - Process 140368/2021-3 and Fundação Stremmer para Pesquisa, Desenvolvimento e Inovação (FEESC) - Process 23080.033 828/2021-30.

References

[1] GOMSPACE, ESA and GomSpace sign contract for continuation of the GOMX-5 mission, 2020.
[2] R. Weigand, GOMX5 Advanced Payload including new European space components, 2021.
[3] K. R. G. Júnior, Fluxo de apoio à concepção de hardware para o segmento espacial visando melhoria de confiabilidade de missões cubesat., Master's thesis, Universidade Federal de Santa Catarina, 2021.
[4] ESA Requirements and Standards Office, ECSS-S-ST-00-02C Draft1 - Tailoring (15 June 2020).
[5] ESA, Tailored ECSS engineering standards for in-orbit demonstration cubesat projects, ESA, ESTEC: Noordwijk, The Netherlands (2016).
[6] ESA Requirements and Standards Office, ECSS-E-ST-10-03C - Testing (1 June 2012).
[7] ESA, Launch Environment Loads Guidelines for ESA IOD CubeSat Missions, ESA-TECSP-TN-014252. [S.l.] (2019).
[8] ESA Requirements and Standards Office, ECSS-E-ST-20C Rev.1 – Electrical and electronic (15 October 2019).
[9] ESA Requirements and Standards Office, ECSS-E-ST-10C Rev.1 – System engineering general requirements (15 February 2017).
[10] ESA Requirements and Standards Office, ECSS-Q-ST-40C Rev.1 – Safety (15 February 2017).
[11] ESA Requirements and Standards Office, ECSS-M-ST-10C Rev.1 – Project planning and implementation (6 March 2009).
[12] A. P. L. Sha Luo, Eng Keng Soh, Supervising multidisciplinary final-year engineering students to develop cubesats with an innovative project management method, 2018 IEEE Frontiers in Education Conference (FIE) [S.l.: s.n.] (2018) 1–4.
[13] G. M. Marcelino, et al., A critical embedded system challenge: The floripasat-1 mission, IEEE Latin America Trans. 18 (2020) 249–256.
[14] C. Cappelletti, S. Battistini, B. Malphrus, CubeSat Handbook: From Mission Design to Operations, Elsevier Science, 2020.

11

Session 11 - Space Debris

SPACE DEBRIS: IMPACTS GENERATED BY THE DISPOSAL OF CUBESATS

Fernanda Diógenes Gomes Vieira(1), Carlos Eduardo Valle Rosa(2)
(1) Universidade da Força Aérea, fediogeness@gmail.com
(2) Universidade da Força Aérea, eduvalle80@hotmail.com

***Keywords**: CubeSats, Space Debris, Space Sustainability.*

Artificial space debris has the potential to interfere with the sustainability of space activities in the low-Earth orbit (LEO). In general, this problem derives from causes associated with conventional, medium and small satellites. The exponential expansion of the number of CubeSats operating in this orbit has brought to the international debate the possibility of increasing the volume of space debris generated after the end of the useful life of this type of small satellite. The article analyzes mitigating measures for the issue of space debris resulting from the proliferation of CubeSats in LEO. Furthermore, this susceptibility to environmental impact in the low-Earth orbit caused by defunct CubeSats tends to generate conflicting situations in the field of space law and international relations. The article concludes that the need for sustainable practices regarding the disposal of this type of small satellite can reduce geopolitical tensions associated with the rational use of outer space.

1. Introduction

The aerospace technological race that started in the 1950s with the launching of the artificial satellite Sputnik 1, on October 4th, 1957, by the Soviets and was boosted by the other states' space programs, made it possible for our society to go beyond the atmospheric frontier and start exploring the space environment, which seemed to transform science fiction into real facts.

Despite the great scientific-technological gain for mankind, the exploration and use of this natural resource did not have as one of its purposes the balance between socioeconomic development and environmental sustainability, resulting in the emergence of a serious problem known as space debris, also known as orbital debris or space junk.

With the insertion of new players in the space market, there has been a significant increase in the launching of constellations of small satellites into terrestrial orbits with the intention of providing the most diverse satellite services on behalf of society, becoming viable due to the low cost that the CubeSat model provides, and the free access to space established by the 1967 Outer Space Treaty.

Thus, the large volume of space debris generated after the end of the useful life of these small satellites is a matter of concern for the international community. Seeking to contribute to this discussion, this paper analyzes mitigating measures for the potential risk to the space environment that CubeSats debris present in Earth orbits, especially in low Earth orbit (LEO), may cause.

In relation to the methodological aspects, the study comprised a theoretical discussion through bibliographical and documentary research about the amount of CubeSats launched into space and the impacts generated by CubeSats with no useful life in the environmental, political and economic spheres. A counterpoint is established to the existing space debris mitigation measures addressed in the research.

The hypothesis presented is that the need for sustainable practices regarding the disposal of this type of small satellite can reduce the geopolitical tensions associated with the rational use of outer space.

2. CubeSats

The scientific community has created specific standards for nanosatellites, which allow for their construction and application in the space environment, in order to provide the most diverse services to humanity, such as defense, remote sensing, communication, science, technology, and education. In view of these facilities, the space activities performed with nanosatellites have led to a significant increase in the launching of these space objects in recent years.

In 1999, a prototype small satellite was proposed, called CubeSat, fruit of studies conducted by professors Jordi Puig-Suari, San Luis Bispo, and Bob Twiggs, who are representatives of California Polytechnic and Stanford university's respectively [2]. CubeSats are characterized by being nanosatellites or picosatellites due to their mass ranging from 0.1kg to 10kg, being launched usually in low Earth orbit (LEO) [10]. They enable the capture of space resources in order to assist in the development of scientific research, becoming the most populated types of satellites in space today [11].

According to the document containing their specifications called CubeSat Design Specification (CSD), these small satellites have the standard dimensions 10x10x11cm, have mass up to 1.33kg, which is equivalent to 1U (one unit), and can vary their sizes from 0.25U to 27U [8] and are made up of the components known as Commercial off-the-shelf (COTS), as can be seen in Figure 1 below:

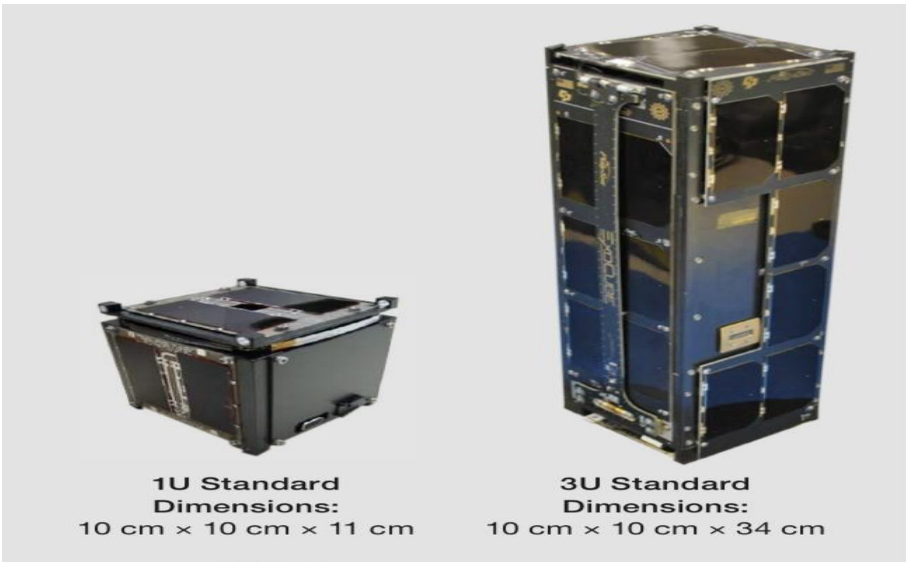

Figure 1: CubeSats formats.

With this format, it makes it possible to launch multiple CubeSats in a structure called a dispenser, which serves as a means of connection between the CubeSat and the launch vehicle. This dispenser attaches the small satellite to the launch vehicle, safeguarding it throughout its trajectory and, at the programmed moment, expels it into Earth orbit. It should be noted that the first dispenser used was the Poly-Picosatellite Orbital Deployer (P-POD) designed by California Polytechnic State University (CalPoly). Today, different models of dispensers can be found on the market to accommodate CubeSats in order to further facilitate their launches.

Accordingly, CubeSats can be sent on the most diverse missions, such as a mission to supply the International Space Station or the Artemis I mission, and inserted in the varied types of launch vehicles, such as Super Strypi, Minotaur I, Minotaur IV, Long March, Delta I, Antares, Falcon 9, among others [11]. In this sense, figure 2 below shows the quantity of the most used vehicle types in payload launches during the period from 1998 to 2027.

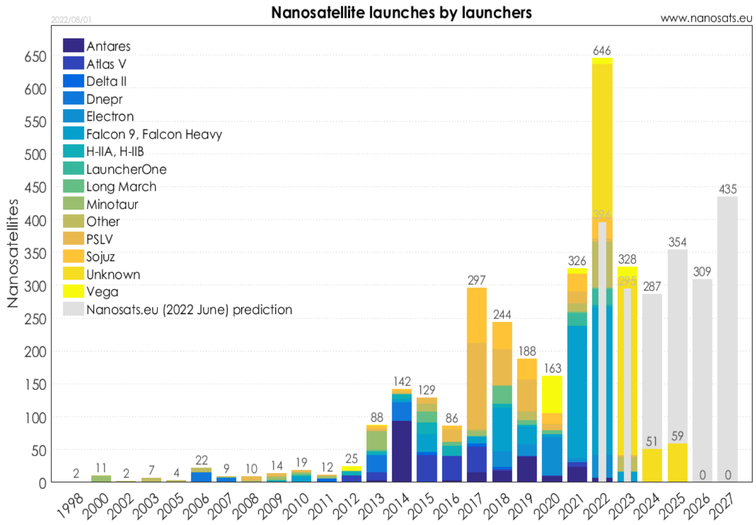

Figure 2: Most commonly used CubeSats launch vehicles.

Despite the misgivings surrounding the CubeSat methodology in the scientific community, there has been an exponential growth in the success rate of missions during the years between 1998 and 2022. Regarding the number of CubeSats launched into Earth orbits, the first CubeSat launch occurred in 2003, but the official milestone is considered to be 2005.

In the period from the years 2005 to 2012, a total of 115 CubeSats were put into orbit. In the years 2013 to 2015, 359 CubeSats were launched. In 2017, there were about 297 launches of this small satellite, and in 2018, the numbers dropped to 244 launches. It is estimated that in 2021, 326 CubeSats were launched and in 2022, it had a total of 646 launches, as shown in the figure 3 below [5].

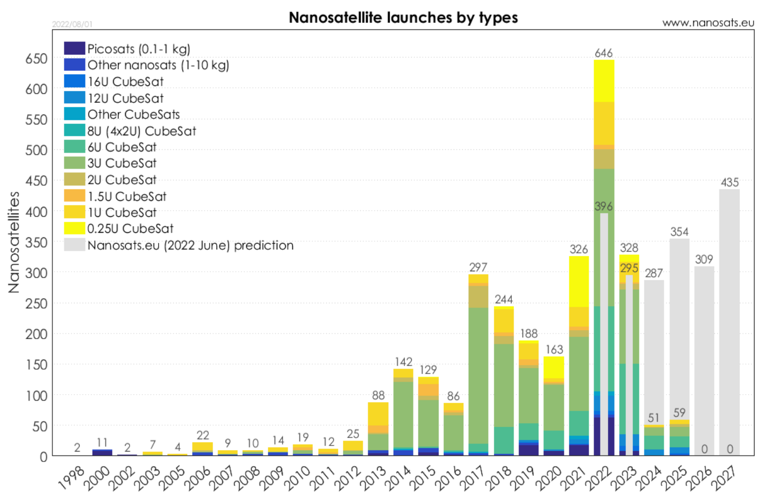

Figure 3: CubeSats launches.

With regard to the launching countries, it has that, of the total of 2.068 objects launched between the years 2005 to 2022, the United States of America (USA) is the state that has made the most nanosatellites launches with about 1.375 (one thousand three hundred and seventy-five). In second place is China with about 80 (eighty) small satellites launched, and in third place is Japan with 64 (sixty-four) objects launched, according to the figure 4 below [6].

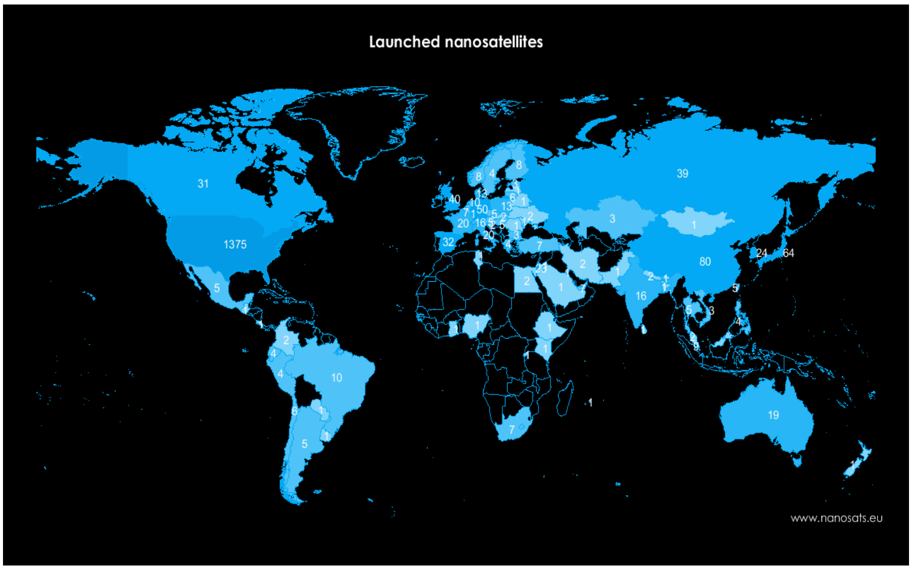

Figure 4: CubeSats launches by countries.

Thus, of those objects launched into space, only 1192 are operational. According to the Satellite Industry Association (SIA) 2021 report, the revenue generated by the satellite industry was around $271 billion in 2020, among this amount, $117.8 billion is from satellite services, $135.3 billion is from ground equipment, $12.2 billion is from satellite manufacturing, and $5.3 billion is from launch [13]. This highlights the importance of satellites for the socio-economic development of a country.

4. CubeSat debris impacts on space

The space environment is affected by several natural phenomena, such as electromagnetic radiation, dense plasma flows, reactive species, and variable neutral gas densities [1]. In addition to these disturbances, there are others that CubeSats are likely to face in space, such as atmospheric drag, solar winds, sudden temperature changes, solar flares, and space debris.

Space debris, also referred to as orbital debris or space junk, is divided into two categories: man-made and natural. They are composed of so-called artificial orbital debris and natural meteoroids. However, the present study is based on artificial space debris, which are man-made objects, including their fragments and parts, although they remain located in Earth orbits, mainly in Low Earth Orbit (LEO) and Geostationary Orbit (GEO), but no longer perform any useful function [14].

When referring to the average lifetime of the CubeSat in Earth orbit, it is around 8 (eight) months, varying in days or even 5 (five) years [4]. However, due to technological advances, this lifetime of the CubeSat will be improved in order to optimize its operation in space. Nevertheless, the CubeSat is considered by the space community to be "debris sat" [7], given that their lifetime is short, they are small and depend on atmospheric drag to perform their reentry within the timeframe established by the 25-year rule contained in ISO Standard 24113 of 2011.

According to current data from the European Space Agency (ESA), there are 31,690 pieces of space debris that are being tracked and catalogued by the space surveillance network, as well as there are 36,500 space objects larger than 10cm, 1 million pieces between 1cm to 10cm, and 130 million debris between 1mm to 1cm [15]. Currently, there are 243 non-operational trackable small satellites in the Earth orbits.

The outer environment is considered an extension of the Earth's environment, which is why it must be protected given its functionality that is necessary for humanity. Thus, the impacts generated by space debris can be pointed out from the following perspectives: a) environmental; b) political; and c) economic.

As for environmental impacts, Borges [3] states that "any human activity is subject to produce impacts on the environment, whether beneficial or harmful. Environmental impacts are understood as the interventions that modify physical, chemical or biological characteristics of the environment, thus the presence of debris sats, which are man-made and placed in terrestrial orbits, would already configure changes in the local environment due to the pollution caused there, which would undermine the sustainability of space.

It should also be noted that the quantity of these space objects can increase significantly due to the Kessler Syndrome, a theory created by the American astrophysicist Donald J. Kessler in 1978. These are fragmentation events of space objects due to collisions between them that are fed back by gravity, especially in LEO, resulting in the so-called "domino effect". In this understanding, figure 3 below brings the study done by NASA in 2018, pointing out the increased risk of collisions of these space objects by not executing the techniques about the mitigation of space debris, as can be seen by the red bars of the graph.

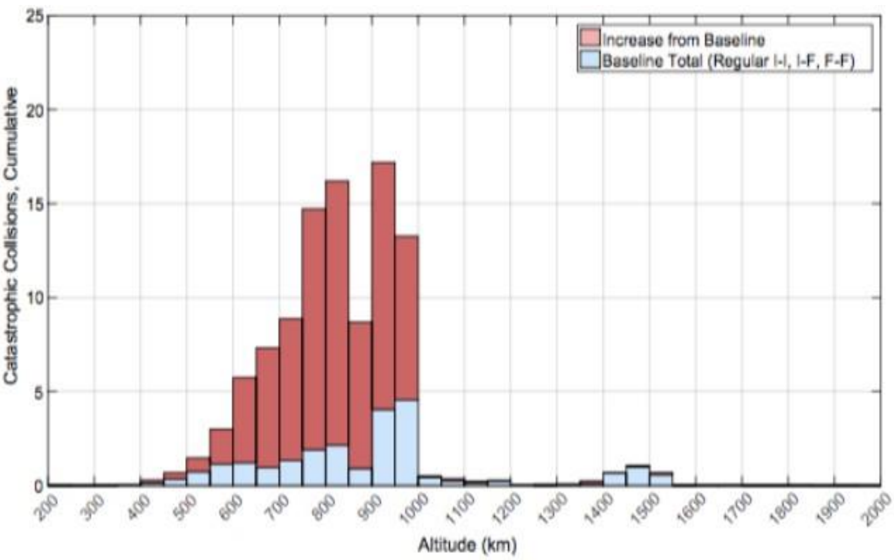

Figure 3: Risk of space debris collisions.

In relation to political impacts, there is the non-attainment of long-term sustainable development goals established by the United Nations (UN) through 2030 Agenda and incorporated in the Space2030 Agenda by COPUOS, which would cause significant tension among member states, resulting in the shaking of international relations concerning cooperation for the preservation of the space environment and, consequently, for the operational safety of space activities.

There is the possibility of a violation of Article 9 of the 1967 Outer Space Treaty, which extends to the signatory states the responsibility to "exploit [space] in such a way as to avoid the harmful effects of its contamination" [16].

It is also noteworthy that, according to Article 1 of the Outer Space Treaty, the space environment is a common good, not subject to national appropriation by any state and all must ensure the right to a healthy environment for present and future generations.

As far as economic impacts are concerned, there is the viability of space activities, i.e., it can jeopardize the launching of satellites that are vital to our subsistence. And even the collision of space debris with existing debris can cause gigantic economic losses, culminating in the paralysis of daily activities on Earth.

4. Space debris mitigation measures

Among the 5 (five) basic documents of International Space Law, the Treaty on Principles Governing the Activities of States in the Exploration and Use of Outer Space, Including the Moon and Other Celestial Bodies, or simply the Outer Space Treaty, is the main regulatory document in existence, which has been in effect since October 10, 1967, and determines the legal regime of outer space and celestial bodies.

In addition to the Outer Space Treaty, there are also non-binding space debris mitigation guidelines that have been developed by international organizations, such as COPUOS and IADC. These guidelines bring together best practices aimed at the sustainability of the space environment. They serve as guides for states' space activities and even as an incentive for states to draft their own national legislation aimed at the long-term sustainable development of space.

There is the 25-year rule, which is understood to be a rule that after the end of a space object's mission, it must be positioned by its operators in orbits that will allow them to make a natural re-entry into the Earth's atmosphere within a period of 25 years. This time limit has been set by the IADC so that these inactive space objects will be actively retired by their owners after their missions are completed, since in orbits of certain altitudes they can last for eternity.

In an attempt to solve or reduce the problem of space debris in Earth orbits by means of active removal, some equipment for the collection and disposal of such debris has been created to contribute to the safety of space missions and to maintain and preserve the environment, among which are CleanSpace One, aerogel, foam, electrodynamic rope, lasers, solar sail, robotic arms, nets, RemoveDEBRIS, anti-satellite weapons, and ELSA-d.

Despite the equipment and normative devices presented that are aimed at mitigating space debris, there is a noticeable growth in the population of small satellite debris in Earth orbits proportionally to the increase in the launching of these objects into outer space, so that it is necessary to look for new alternatives or improve those that already exist to eliminate the space debris problem.

5. Conclusions

Given the above, it can be seen that the low operational cost of CubeSats and the freedom of access to space, with no established limit on the launching of these space objects per country, contributes to the increase of their population in terrestrial orbits, which ends up increasing the number of space debris in the local environment potentiated by Kessler's syndrome.

The 1967 Outer Space Treaty does not expressly address the space debris issue in its content, due to the historical moment of that time, relative to a war context and there was no way to predict the proportions that space debris would take to the space environment.

To fill the gap left by the treaty, international organizations, IADC and COPUOS, have formulated space debris mitigation guidelines for States to follow and even draft their national legislation to reduce space pollution. However, few countries have their own standards for this and the guidelines of these organizations are not binding, i.e., a state can accept them or not.

The 25-year rule is a viable alternative, but this recommendation was established at a time when the traffic flow of space objects was not as intense as it is today, which is why this time frame should be reviewed to better suit the environmental demands of space, since CubeSats do not have a longer lifetime.

As for the active debris removal equipment, it is expensive for the States, which ends up being an obstacle for its use.

It should be noted that the occupation of these limited spaces, especially low Earth orbits and geostationary orbits, is a reason for geopolitical disputes between states, given how precious it is to a country's sovereignty, security, and national defense. Therefore, the need for more truly enforceable sustainable practices regarding the disposal of small satellites can reduce the geopolitical tensions associated with the rational use of outer space.

Acknowledgments

We are grateful to the Universidade da Força Aérea (UNIFA) for providing all the academic supported.

References

[1] Anderson, B., Mitchell, D, the space environment, in: Pisacane, Vincent L., fundamentals of space systems. New york: oxford university press, 2005.
[2] Alves, Alex c. R., Dias, Samaherni M., Queiroz, Kurios I. P. M, desenvolvimento de um sistema para controle de bordo de nanossatélite, in: simpósio brasileiro de automação inteligente, xiv, 2019, ouro preto, anais eletrônicos. Campinas: galoá, 2019, p. 2821-2826.
[3] Borges, Leonardo Estrela, os impactos do terrorismo no meio ambiente, in: Brant, Leonardo Nemer caldeira (coord.), terrorismo e direito: os impactos do terrorismo na comunidade internacional e no brasil: perspectivas político-jurídicas. Rio de janeiro: forense: 2003. P. 379-509.
[4] Bouwmeester, J.; Guo, J. Survey of worldwide pico- and nanosatellite missions, distributions and subsystem technology. Acta astronautica, v. 67, n. 7-8, p. 854-862, 2010.
[5] Kulu, Erik. Launches by types. Nanosats database, figures, 08 aug. 2022. Available on: https://www.nanosats.eu. Access on: 02 aug. 2022.
[6] Kulu, Erik. World Map. Nanosats database, figures, 08 aug. 2022. Available on: https://www.nanosats.eu. Access on: 02 aug. 2022.
[7] Gruss, Mike. Are cubesats a nuisance to space situational awareness efforts?. Space news, 23 set. 2016. Available on: https://spacenews.com/are-cubesats-a-nuisance-to-space-situational-awareness-efforts/. Access on: 02 aug. 2022.
[8] Kulu, Erik. What is a cubesat & other picosatellites?. Nanosatellite cubesat database, cubesat, 2022. Available on: http://www.nanosats.eu/cubesat.html. Access on: 28 july 2022.
[9] Kulu, Erik. Launches by launchers. Nanosats database, figures, 08 aug. 2022. Available on: https://www.nanosats.eu. Access on: 02 aug. 2022.
[10] Mabrouk, Elizabeth. What are smallsats and cubesats?. Nasa, science instruments, 26 fev. 2015.

Available on: https://www.nasa.gov/content/what-are-smallsats-and-cubesats. Access on 02 aug. 2022.

[11] Nasa Cubesat launch initiative. Cubesat 101: basic concepts and processes for first-time cubesat developers. California: california polytechnic state university, 2017. Available on: https://www.nasa.gov/sites/default/files/atoms/files/nasa_csli_cubesat_101_508.pdf. Access on 28 july 2022.

[12] Nasa. Cubesat study project review. In: orbital debris quarterly news, v.22, n.1, feb. 2018, p.6-8. Available on: https://orbitaldebris.jsc.nasa.gov/quarterly-news/pdfs/odqnv22i1.pdf. Access on 02 aug. 2022.

[13] Satellite Industry Association, State of the Satellite Industry Report, Sia.org, News & Resources, jun. 2020. Available on: https://sia.org/news-resources/state-of-the-satellite-industry-report/. Access on 24 jun. 2022.

[14] Scientific and Technical Subcommittee of the Uncopuos. Technical report on space debris. 1st edition. New york: united nations publication, 1999. Available on: Https://www.orbitaldebris.jsc.nasa.gov/library/un_report_on_space_debris99.pdf. Ace Access on 02 aug. 2022.

[15] Esa. Space debris by the numbers. Esa, space safaty, 11 jul. 2022. Available on: https://www.esa.int/space_safety/space_debris/space_debris_by_the_numbers. Access on 02 aug. 2022.

[16] United Nations Office for Outer Space Affairs. International space law: united nations instruments. New york: united nations office, 2017.

12

Session 12 - Constellations and Formation Flights

MOSCOW UNIVERSITY CONSTELLATION OF NANO-SATELLITES FOR SPACE WEATHER AND TLE MONITORING

Sergey S. Svertilov(1), Vitaly V. Bogomolov(2), Yurii K. Zaiko(3), Ivan A. Zolotarev(4), Anatoly F. Iyudin(5), Vladimir V. Kalegaev(6), Pavel A. Klimov(7), Vladislav I. Osedlo(8), Oleg Yu. Peretyat'ko(9), Vasilii L. Petrov(10)

(1) M.V. Lomonosov Moscow State University, 1(2), Leninskie gory, GSP-1, Moscow 119991, Russian Federation, +7495-939-51-60, sis@coronas.ru

(2) M.V. Lomonosov Moscow State University, 1(2), Leninskie gory, GSP-1, Moscow 119991, Russian Federation, +7916-726-82-32, bogovit@rambler.ru

(3) M.V. Lomonosov Moscow State University, 1(2), Leninskie gory, GSP-1, Moscow 119991, Russian Federation, +7903-795-98-64, zaikoiurii@yandex.ru

(4) M.V. Lomonosov Moscow State University, 1(2), Leninskie gory, GSP-1, Moscow 119991, Russian Federation, +7968-930-15-45, brilkov@yandex.ru

(5) M.V. Lomonosov Moscow State University, 1(2), Leninskie gory, GSP-1, Moscow 119991, Russian Federation, +7968-910-96-93, aiyudin@srd.sinp.msu.ru

(6) M.V. Lomonosov Moscow State University, 1(2), Leninskie gory, GSP-1, Moscow 119991, Russian Federation, +7905-701-44-93, klg@dec1.sinp.msu.ru

(7) M.V. Lomonosov Moscow State University, 1(2), Leninskie gory, GSP-1, Moscow 119991, Russian Federation, +7921-439-21-87, pavel.klimov@gmail.com

(8) M.V. Lomonosov Moscow State University, 1(2), Leninskie gory, GSP-1, Moscow 119991, Russian Federation, +7925-504-51-74, osedlo@mail.ru

(9) M.V. Lomonosov Moscow State University, 1(2), Leninskie gory, GSP-1, Moscow 119991, Russian Federation, +7916-126-10-43, pouoleg@mail.ru

(10) M.V. Lomonosov Moscow State University, 1(2), Leninskie gory, GSP-1, Moscow 119991, Russian Federation, +7926-238-30-51, vas@srd.sinp.msu.ru

Keywords: *constellation, nano-satellites, space, weather, TLE, monitoring*

In frame of the space program of Moscow University, the Universat-SOKRAT project is developing now. The aim of this project is elaboration of a spacecraft constellation for real-time monitoring of space hazards including radiation and transient luminous events (TLE) in the Earth atmosphere. During the first stage of the project implementation, 8 spacecraft of the CubeSat type were launched. To date, there are 5 such spacecraft operating in near-earth orbit, which regularly transmit scientific and telemetric data. These are the Amursat and VDNKh-80 satellites of the 3U format, which were launched into orbit on July 5, 2019 as a by-pass mission from the Vostochny cosmodrome, as well as 6U format DEKART and Norby cubesats (together with the Novosibirsk State University), cubsat Yarilo-2 of 1.5U format (together with the N.E.Bauman Moscow State Technical University), launched as a by-pass mission from the Plesetsk cosmodrome on September 28, 2020. These satellites operate on polar orbits with an altitude of about 550 km and an inclination of about 98^{o}. They are equipped with the same type of instruments of the DeKoR type for space radiation monitoring, two (VDNKh-80 and DEKART) are also equipped with the AURA instruments for detecting of the ultraviolet radiation (UV) from the Earth's atmosphere. These instruments can be used also for TLE observations. Thus, for the first time, a unique multi-satellite constellation has been realized, which makes it possible to simultaneously measure the fluxes of particles and quanta using the same type of instruments at different points in the near-Earth space. Such measurements provide unique information on the dynamics of sub-relativistic electron fluxes in near-Earth space. In addition to the applied aspects related to the task of space weather monitoring, such measurements will provide important data necessary for understanding the mechanisms of acceleration and loss of trapped and quasi-trapped electrons. Simultaneous observations of radiation fluxes and UV emission from the upper Atmosphere give a good opportunity to study mutual influence of electron precipitation and energetic processes in the upper Atmosphere.

1. Introduction

The main components of space radiation in near-Earth orbits are protons and heavy charged particles of galactic and solar cosmic rays, as well as electrons and protons of the Earth's radiation belts (ERBs). A certain contribution to the background fluxes detected on board spacecraft can be made by neutral radiation, i.e. gamma quanta and neutrons from the Earth's atmosphere (the so-called albedo) and generated in the matter of the spacecraft (local and induced radiation). Variations of fluxes of ERB as well as quasi-captured and precipitating electrons and protons together with short-term solar cosmic ray (SCR) flux increasing are the main factors of so-called space weather. Thus, space weather effects are based on various manifestations of solar and geomagnetic activity.

Space weather effect monitoring is necessary for prediction of particle and quantum fluxes in the near-Earth space. Typically charge particle flux prognosis is based on the use of models that give distributions of radiation fluxes mainly in the areas of trapped radiation. Such models that exist today are quasi-static, so they give an average picture, while in reality, even in geomagnetically quiet conditions, the trapped particles fluxes can experience very significant medium- and long-term variations. A separate problem is the need to take into account short-term variations. Thus, the need of particle and quantum flux operative real time monitoring is very relevant.

Another potential source of radiation in near-Earth space can be transient atmospheric phenomena. During the energetic processes in the middle and upper layers of the Atmosphere, electrons can be accelerated effectively, and then they can penetrate into the magnetosphere (the so-called TEB, i.e. Terrestrial Electron Beam), also they can produce burst of energetic gamma quanta (TGF - Terrestrial Gamma-ray Flash). Therefore, monitoring measurements of transient atmospheric radiation in the visible and near UV ranges, simultaneously with the detection of the charged component and gamma rays, can be an additional source of information about the processes occurring both in the atmosphere and in near-Earth space.

Monitoring of space radiation and optical phenomena in the atmosphere, taking into account the limitations noted above, has been carried out on various spacecraft over the past decades. In recent years, Moscow University has been implementing its own space program, which involves research on particle flux dynamics and high-energy photons in near-Earth space. In this regard, the successful launch of such satellites as Universitetsky-Tatiana [1], Universitetsky-Tatyana-2 [1], Vernov [2], Lomonosov [3] should be noted. The next step in this direction may be connected with new space project of Lomonosov Moscow State University (MSU), so-called, Universat-SOKRAT [4]. During the implementation of this project, it is planned to create a spacecraft system that allows, in a mode close to real time, to determine the levels of ionizing radiation not only in the areas of the spacecraft (SC) orbits, but also to determine the radiation environment in a significant part of the radiation belts, up to the orbits of global navigation satellite systems (GNSS) or geostationary orbits (GSO).

2. Nano-satellite Constellation Concept

The main difference between this project and the currently existing meteorological and geophysical missions intended for control of the radiation environment in the near-Earth space is to determine the radiation loads and alert about dangerous situations in the mode time close to real time. This implies detection of energetic particle flux variations with times typical for geomagnetic disturbances, i.e. from tens of minutes and hours to several days or even weeks. As follows from observations, during the main phase of a magnetic storm or sub-storm the radiation fluxes in the areas near the ERB outer edge, which corresponds to the GNSS and GSO orbits, can change on such time scales. In this case, radiation doses, the probability of internal and external electrization of the satellite, etc. can change significantly (see, for example, [5]). It should be noted that variations of radiation fluxes will be different at lower and higher orbits. For example, at lower orbits, changes in radiation conditions occur more slowly and with a delay relative to the onset of a geomagnetic disturbance than in higher orbits. As noted above, this task meaning the determinations of the radiation loads at different spacecraft orbits during time intervals comparable to the typical times of radiation flux variations in near-Earth space is the main for this project, and this is its difference from existing and planned space missions, which allow, really, identify only local changes of radiation fluxes and are not able to estimate from these data the radiation levels affecting other spacecraft, on which radiation monitoring instruments are not installed.

At present, measurements of energetic charged particle fluxes are carried out by a number of spacecraft. It should be noted the system of geophysical observations of the American agency NOAA, which has been operating since the 1970s, which uses satellites of the POES series on low polar orbits and GOES on geostationary orbit (simultaneously ≥ 2 satellites at each orbit). In 2012, two NASA spacecraft Van Allen Probes were launched into a highly elliptical near-equatorial orbit to study the structure and parameters of the radiation belts. Russian instruments for measuring of energetic charged particle fluxes, which were elaborated by SINP MSU, operates on Russian meteorological satellites, such as Meteor-M (low orbit), Arktika (high apogee orbit) and Elektro-L (geostationary orbit) series. There are also a number of satellites, including small spacecraft that carry out such measurements. But almost all these spacecraft measure the fluxes of energetic charged particles only in a limited region of space and in the limited range of pitch angles (the angle between the vectors of particle velocity and magnetic field induction).

The Van Allen Probes [6] satellites, which are closest to our project in terms of the concept of measurements, do not have the tasks of operational radiation monitoring in the near-Earth space and operate only for scientific purposes.

Currently, the European Space Agency is developing the D3S (Distributed Space weather Sensor System) project [7], which mean creation of constellation of small satellites for monitoring of energetic charged particle fluxes in the region from low to geostationary orbits and auroras. But this project is currently in the "zero" phase; the scientific and technical concept of measurements and ground data processing are not clear.

Another number of problems that can be solved with the use of a multi-satellite constellation for radiation monitoring are related to the study of short-term variations of energetic charged particle fluxes, including precipitation. It means:

1) sequential passage of the same area by closely spaced satellites will allow the most reliable separation of spatial and temporal effects;

2) simultaneous measurements at different L-shells are necessary to restore the dynamic picture of the distribution of trapped particle fluxes in a wide range of orbits, which, in particular, will make it possible to observe the shift of the maxima of the radiation belts during geomagnetic disturbances;

3) simultaneous measurements at the same height with the same type of instruments located on several satellites, shifted in longitude relative to each other, will allow us to estimate the influence of the local time factor on of particle flux dynamics.

The first stage of Universat-SOKRAT project realization implies the launch of number of nano-satellites of cubesat type on near-Earh orbits. In 2018-20 8 satellites were launched [8]. Once more 3 satellites with Moscow University instruments were launched on August 9, 2022.

Among those satellites, which were launched before 2022 year, 4 ones are operating currently and regularly transmit scientific and telemetric data. There are the Amursat and VDNH-80 satellites of the 3U format, which were launched into orbit on July 5, 2019, as well as the 6U cubesats DEKART and Norby (together with the Novosibirsk State University) launched on September 28, 2020. These satellites operate in polar orbits with an altitude of about 550 km and an inclination of about 98^o. They are equipped with the same type of instruments (DeCoR-1) for monitoring space radiation, two spacecraft (VDNKh-80 and DEKART) are also equipped with instruments (AURA type) for observations of upper Atmosphere in visible and ultraviolet bands. Three 3U cubesats launched in 2022 (Monitor, SkolTech-1B, SkolTech-2B) on the same orbit, there are equipped by new types of instruments also intended for space radiation monitoring (DeCoR-2 and KODIZ). In the nearest the MSU satellite constellations should be added by about 10 cubesats more.

The DeCoR-1 instrument is designed to study the time variations of electron and gamma quantum fluxes [8]. The instrument detecting element is a phoswich, i.e. combination of a 3 mm thick plastic scintillator and a 10 mm thick CsI(Tl) crystal, viewed by two photomultipliers. It has an effective area of about 18 cm^2 and an energy release range from 50 keV to 2 MeV. The main advantage of this instrument is very high time resolution. It can operate in so- called event by event mode, in which for any detected particle and quantum energy release in both scintillators and time of detections are stored. Thus, in this case time resolution is limited only by detector dead time (about 10 mcs) that allows studying very fast variations of detected fluxes. Three such instruments with mutually normal axes are installed on DEKART satellite, due to this the angular distributions of electron fluxes can be also estimated.

The DeCoR-2 instrument in comparison with DeCoR-1 one has a larger effective area (about 65 cm^2). It improves sensitivity and allows detection of gamma-ray bursts of different nature (astrophysical, solar and terrestrial). Four pad detectors are used in this instrument. Each of them is 40x40 mm phoswich pad consisted from 3 mm layer of plastic scintillator and 9 mm layer of CsI(Tl) crystal both viewed by the same photo-receivers. In the instruments on-board SkolTech satellites vacuum photomultiplier tubes (PMTs) are used for viewing scintillators, one PMT for each pad, i.e 4 PMTs in the instrument. In future modifications assembly of silicon photomultipliers (SiPMs) should be used. Combination of plastic scintillator and CsI(Tl) crystal makes it possible to separately detect gamma quanta and electrons in the energy release range from 20 keV to 1 MeV, which is important when conducting an experiment in a polar orbit. The instrument data is recorded both in the form of monitoring (count rate in several channels) and in the form of a detailed event-by-event record. The processor, which is part of the complex, serves to select the most important data sections for transmission to Earth in the primary form. The daily amount of scientific data is ~100 MB.

One of the payloads for small spacecraft is the AURA series of instruments, which are four-channel photometers based on silicon photomultipliers for Atmosphere glow observations in near UV (300-400 nm). The use of silicon photomultipliers is due to their advantages over traditional vacuum PMTs: small dimensions and weight, as well as low supply voltage. The first of these instruments was launched in 2019 aboard the VDNKh-80 satellite [9]. The second version of the AURA-2 detector has a higher time resolution (1 ms) and an increased field of view (up to 90^o). This instrument has been operating on the DEKART satellite since September 2020. The detector's photodetector is a matrix of 64 SiPMTs (pixel size 3×3 mm) with fast readout electronics providing time resolution up to 1 mcs. The optical system is a compact Fresnel lens with a diameter of 9 cm, which provides focusing of radiation on the photodetector and high sensitivity of the device.

The KODIZ instrument is combination of different detectors intended for monitoring of high energy particle fluxes, galactic and solar cosmic rays mainly. It consists from Cherenkov radiation detector, which is a plexiglass cylinder with a diameter of 38 mm and a height of 20 mm, viewed by a photomultiplier. The instrument also includes two silicon semiconductor detectors for dosimetry of charged particles with a thickness of 0.3 mm and an area of about 1 cm^2 behind an aluminum shielding thickness of 0.5 and 5.0 g/cm^2. The instrument provides detection of fluxes of protons and nuclei with Z>1 with an energy of more than 30 - 50 MeV/nucleon in the range from 10 to 10^4 particles/cm^2 s, fluxes of protons and nuclei with Z>1 with an energy of more than 330 MeV/nucleon in the range of 10 up to 10^3 particles/cm^2 s, thermal and epithermal neutron fluxes in the range from 10 to 10^3 neutrons/cm2 s, absorbed dose rate of charged particles of space radiation in the range from 10^{-8} to 10^{-5} Gray.

In the next sections we present the examples of observations of space weather effects as well as TLEs with the instruments on-board MSU constellation satellites.

3. The space weather effects observed with MSU satellites

Several space weather effects were observed with DeCoR-1 instrument on-board Norbi satellite. As an example, electron precipitation in polar cap observed on September 28, 2021 is illustrated by curves in Figure 1. There are presented time dependences of electron abd gamma quantum counts as well as L values along the satellite orbit. Two quite visible peaks in electron counts are corresponing to the crossing of outer ERB. In the interval between them satellite as in polar cap. The peak of smaller intensity at about 04:48 UT should be noted. Possibly it may be caused by precipitation of electrons from magnetosphere tail.

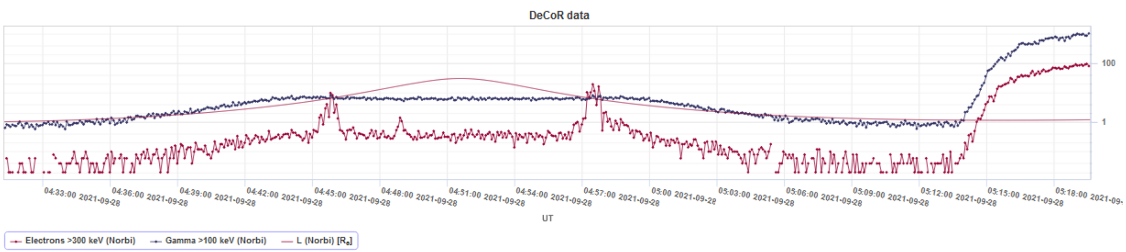

Figure 1: Time dependences of electron (red), gamma quantum (blue) counts and L values (magenta) on September 28, 2021 from DeCoR-1 Norbi satellite data.

The other example of space weather effect observed by DeCoR-1 instrument on-board Norbi satellite is observation of polar cap filling by solar particles due to solar flares occurred on October 28, 2021. The corresponding time dependencies of electron counts are presented in Figure 2. There we can see the typical picture in quiet time (see top panel) on October 25, 2021, the intense peaks corresponding to the satellite crossing of outer ERB are quite visible. Then, after solar particles filled the polar cap on October 28, 2021, the outer ERB peaks are disappeared because intensity of solar particles in polar cap is higher (see middle panel). After several days particle intensity in polar cap began to restore, as it could be seen from bottom panel of Figure 2 presented observations on November 3, 2021.

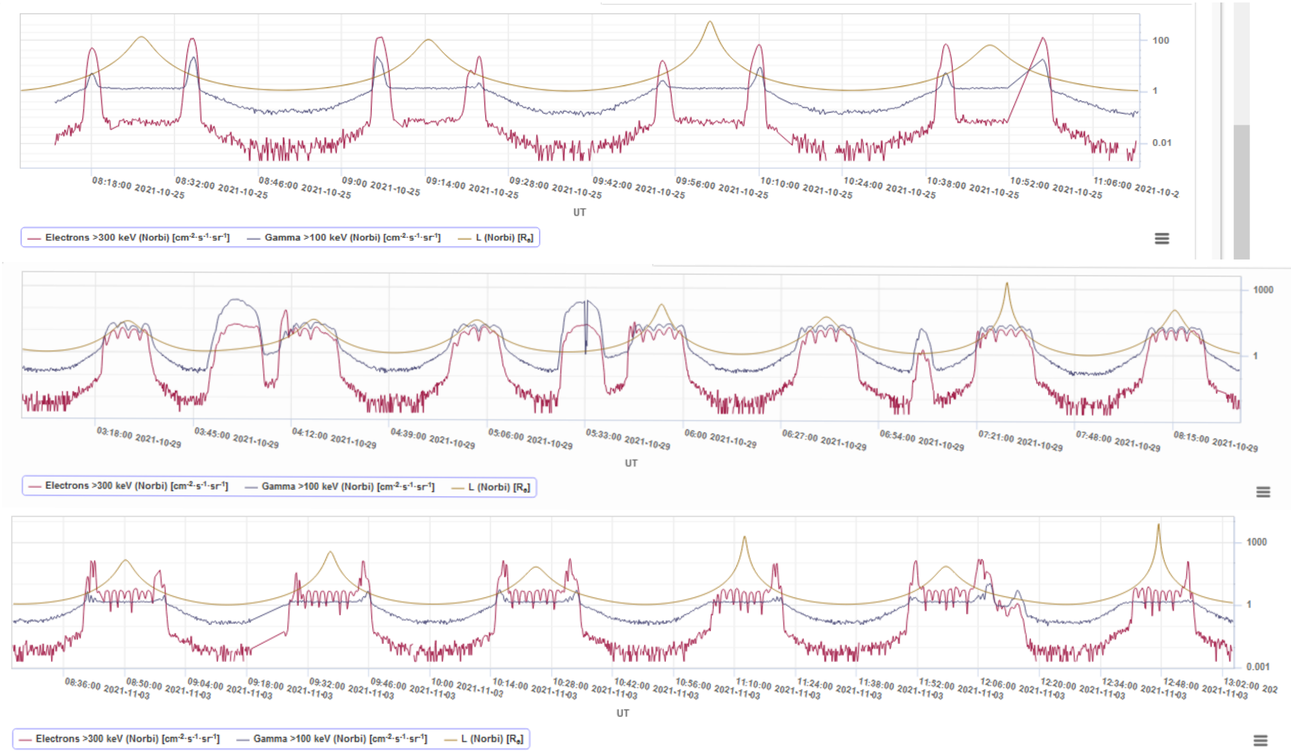

Figure 2: Time dependences of electron (red), gamma quantum (blue) counts and L values (magenta) on October 25, 2021 (top panel), October 28, 2021 (top panel), October 25, 2021 (top panel), November 3, 2021 from DeCoR-1 Norbi satellite data.

Among different phenomena in near-Earth space, electron flux dynamics at low dift shells (near the geomagnetic equator) is of special interest. Presence of sub-relativistic electrons at drift shells with L < 1.2 is very interesting phenomenon, because theoretically the stable electron fluxes should not exist at such L-shells due to mortality in the SAA during less than one drift period. Nevertheless there are observed by various space experiments at different phases of solar cycle regardless of geo-magnetic activity level [10].

Electron fluxes near the geo-magnetic equator were also observed with DeCoR-1 instrument on board cubesat satellites. The example of monitor time dependences (with 1 s time resolution) of counting rate in plastic scintillator (mainly electrons with energies >300 keV), CsI(Tl) (mainly gamma quanta with energies >100 keV) and total from DeCoR-1 instrument during one orbit of AmurSat cubesat in 2019, August 30 is presented in Figure 3. There are clearly seen in the figure the maxima at the moments when the satellite was in the outer radiation belt of the Earth.

During the flight near the equator (10:55 - 11:10 UTC), a smooth increase in electron fluxes is seen, while the counting rate of background gamma quanta remains unchanged.

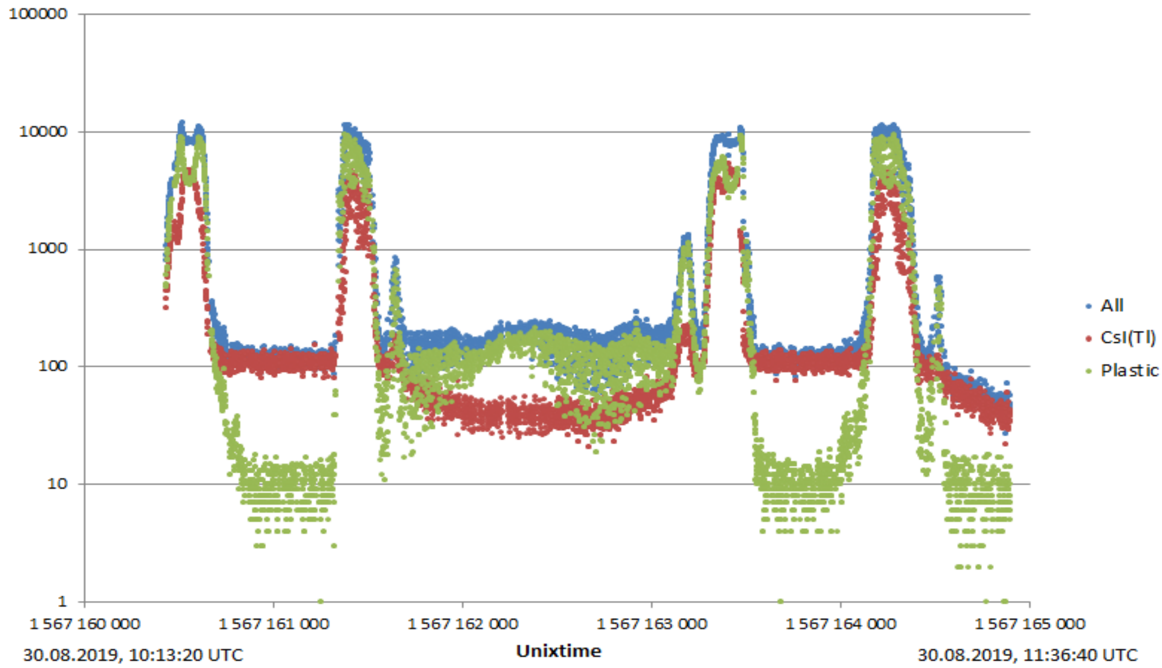

Figure 3: Monitoring counting measured 30.08.2019 during one orbit in plastic scintillator (green points), CsI(Tl) (red points) and total (blue points).

The similar picture was obtained from observations with DeCoR-1 instrument onboard DEKART cubesat. The corresponding count rate time dependences (electrons with energies >300 keV, gammas with energies >100 keV and total) are presented in Figure 4. Significant maximum in electron counting rates is observed near the geomagnetic equator (~11:50 UTC).

As it could be seen from presented above figures, the near-equatorial electrons observed at the same region in epochs separated in time by about 2 years. It indicates that this is quite stable phenomenon. Since electron fluxes on drift shells $L < 1.2$ must be destroyed by SAA as a result of drift, there should be a constantly existing mechanism for replenishment of stable electron fluxes near the geomagnetic equator. The classical mechanism of precipitation from the radiation belts through pitch-angle diffusion can hardly explain this phenomenon, since it does not provide transfer across the magnetic field lines and, accordingly, the movement of particles between drift shells. The shells $L < 1.2$ correspond to the heights of the magnetic field line tops below the internal radiation belt. Very strong magnetic field disturbances are necessary to ensure the transport of particles across field lines in the inner magnetosphere. However, electron fluxes with $L < 1.2$ are observed at various levels of geomagnetic activity. Therefore, the mechanism of these fluxes filling from below, i.e. from Atmosphere, seems more probable. In particular, high-altitude electromagnetic discharges, in which electrons can be accelerated to relativistic energies and exit into the near-Earth space along the magnetic field lines, can be a source of near-equatorial electrons. In this regard, it should be noted that equatorial electron fluxes are observed just above the regions in which high-altitude discharges occur quite often.

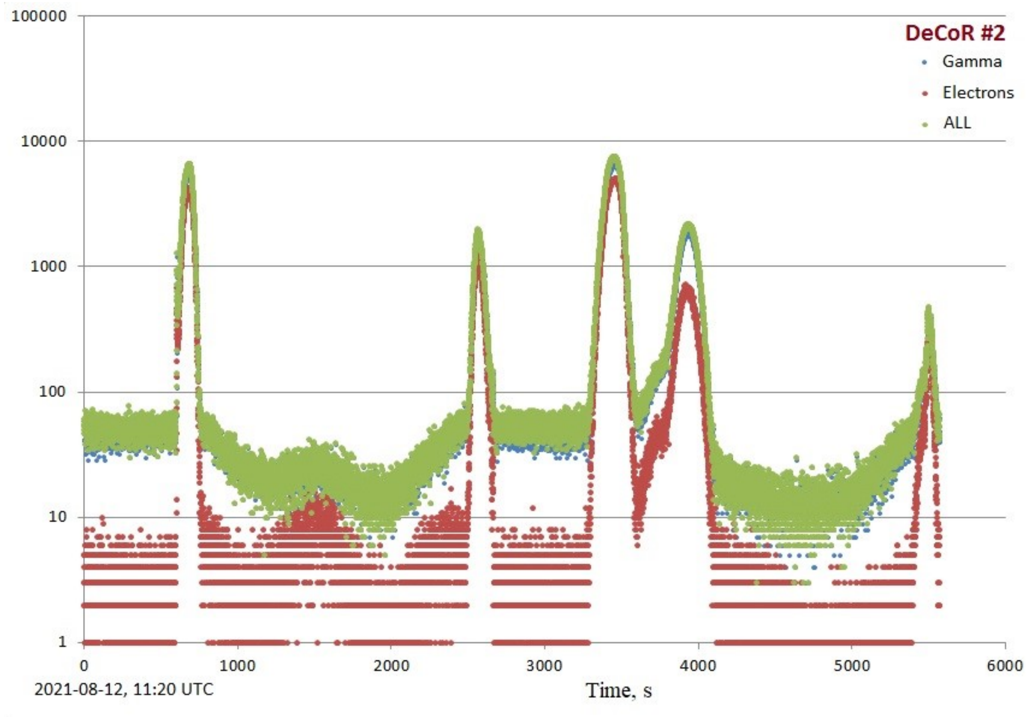

Figure 4: Monitoring counting measured 12.08.2021 during DECART satellite one orbit in plastic scintillator (red points), CsI(TI) (blue points) and total (green points).

4. Observations of TLE on MSU cubesats

The first experience of Atmosphere UV glow observations was obtained with AURA instrument on-board VDNKh-80 satellite. It carried out a series of successful measurements, demonstrating its reliability and performance under conditions of highly variable atmospheric glow intensity due to a special SiPMT sensitivity control system. In the absence of a stable orientation of the spacecraft, the detector detected both the weak glow of the night atmosphere and direct sunlight.

The next step for more detailed Atmosphere observations in UV was made with the use of AURA-2 instrument on-board DEKART satellite. The AURA-2 instrument has sufficiently higher time resolution. The measurements take place at a frequency of 100 Hz (time resolution 10 ms). At the same time, the voltage on the SiPMT is measured (the voltage values are stable) and the temperature, which drops slightly as the spacecraft moves on the shadow side. When the AURA-2 instrument launcher is switched on the night side of the satellite orbit, all instrument subsystems are switched on normally. AURA-2 instrument measures atmospheric UV radiation with all four silicon photomultiplier tubes (SPMs) directed to different areas of space.

Thus AURA-2 instrument is able not only to detect the slow varying Atmosphere glow, but short-time increases of UV intensity, i.e. UV flashes also. The example of such observations is presented in Figure 5.

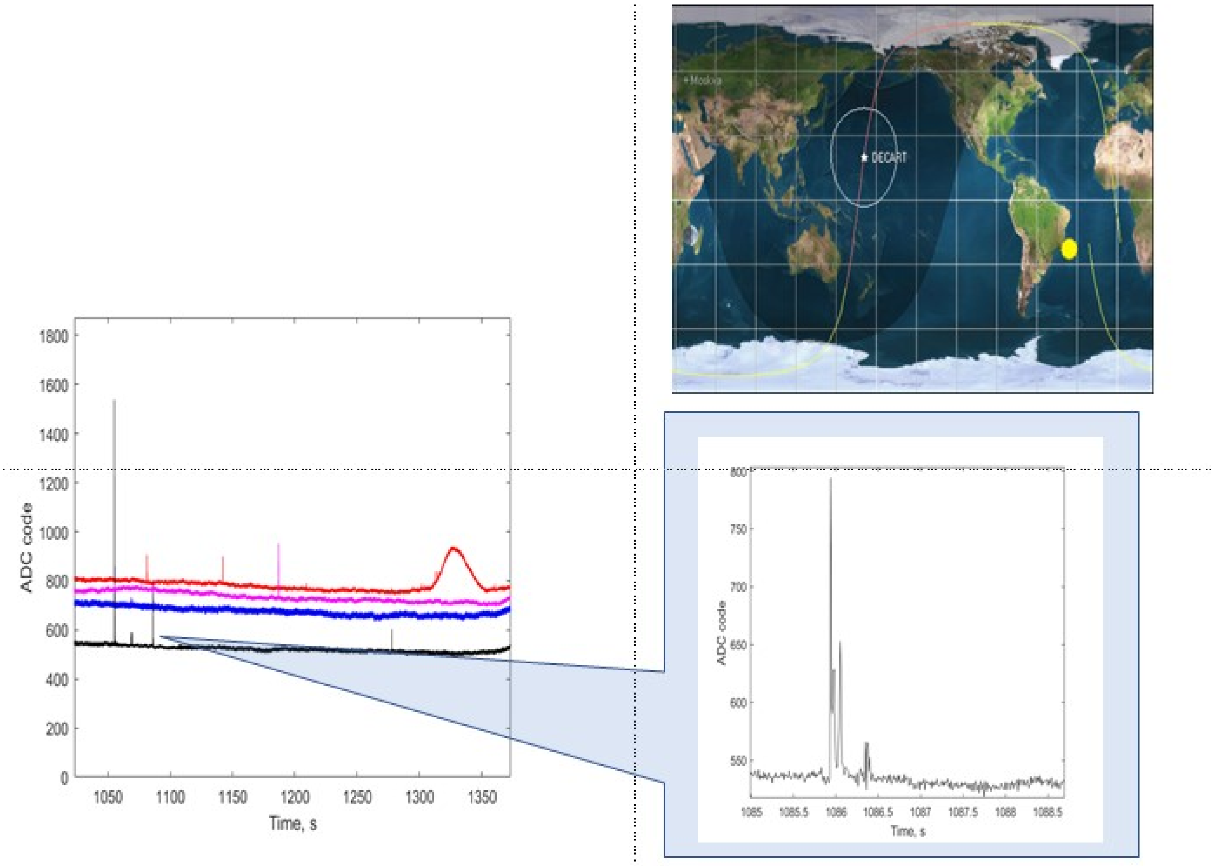

Figure 5: Example of detection of UV flash series with the use of AURA-2 instrument on-board DEKART satellite. The right top panel presents the map with marked observation area, the left bottom panel presents the waveform of detected UV intensity and right bottom panel presents it more detailed scan.

On this Figure we can see the series of UV flashes connected with thunderstorm activity in the western area of Pacific. Such UV flashes were discovered in experiments during Tatiana-Universitetskii mission and then studied in details during Tatiana-2, Vernov and Lomonosov missions [1-3].

5. Conclusions

Thus, for the first time, a unique multi-satellite constellation has been implemented, which makes it possible to carry out simultaneous measurements of particle and quantum fluxes, as well as TLEs using the same type of instruments at different points in the near-Earth space. Such measurements provide unique information about the dynamics of sub-relativistic electron fluxes. As examples, we considered the precipitation of electrons in the polar cap in October 2021, the increase in fluxes of energetic particles in the polar cap in late October - early November 2021 due to the arrival of solar cosmic rays, as well as the detection of sub-relativistic electrons near the geomagnetic equator. It should also be noted that with the use of the AURA-2 instrument installed on the DEKART satellite, for the first time using matrices of silicon photodetectors, photometry of the UV glow of the Earth's atmosphere at various geographical latitudes was carried out, a series of powerful and short (10-100 ms) UV flashes were detected .

The results of the first stage of the implementation of the Universat-SOCRAT project have shown that the constellation of small spacecraft is an effective system that makes it possible to obtain a current picture and a predictive estimate of radiation conditions in a large area of near-Earth space. In the future, it is planned to build up the constellation of MSU nano-satellites by launching new spacecraft of the cubesat format, which will expand its capabilities for operational monitoring of space cosmic radiation, as well as for TLE observations.

References

[1] V.A. Sadovnichy, M.I. Panasyuk, S.Y. Bobrovnikov, et al. First results of investigating the space environment onboard the Universitetsky-Tat'yana satellite, Cosmic Research. V.45 (2007), pp. 273–286.

[2] M.I.Panasyuk, S.I.Svertilov, V.V.Bogomolov, et al. RELEC mission: Relativistic electron precipitation and TLE study on-board small spacecraft. Advances in Space Research. V.57 (2016), pp. 835–849.

[3] V.A. Sadovnichii, M.I.Panasyuk, A.M.Amelyushkin, et al. "Lomonosov" Satellite—Space Observatory to Study Extreme Phenomena in Space. Space Science Reviews, V.212 (2017), pp. 1705-1738.

[4] M.I. Panasyuk, P.A. Klimov, S.I. Svertilov, et al. Universat-SOCRAT multi-satellite project to study TLEs and TGFs. Progress in Earth and Planetary Science. V.6 (2019), pp.35-54.

[5] M.I.Panasyuk, V.V. Kalegaev, I.N. Myagkova, et. al. Radiation environment at the end of active functioning of "Vernov" satellite. Cosmic Research. V.55 (2017), pp. 464 – 468.

[6] N. Fox and J.L. Burch. The Van Allen Probes Mission, Springer, 2014.

[7] S. Kraft, A. Lupi, J.-P. Luntama J.-P. ESA's Distributed Space Weather Sensor System (D3S) utilizing hosted payloads for operational space weather monitoring, in Proceedings of the 67th International Astronautical Congress, Guadalajara, Mexico. 26–30 September. 2016, p. IAC-16,D1,7,1,x35329.

[8] V.V.Bogomolov, A.V.Bogomolov, Yu.N. Dement'ev, et al. A First Experience of Space Radiation Monitoring in the Multi-Satellite Experiment of Moscow University in the Framework of the Universat-SOCRAT Project. Moscow University Physics Bulletin. V.73 (2020), pp.676–683.

[9] D.V. Chernov, E.V. Glinkin, P.A. Klimov, and A.S. Murashov. First results of UV radiation measurements made by AURA detector onboard VDNH-80 cubesat. Advances in the Astronautical sciences. V.173 (2020), pp.519-527.

[10] V.L. Petrov, A.V.Bogomolov, V.V.Bogomolov, et. al. Spatial and Temporal Characteristics of Subrelativistic Electron Fluxes in the Near-Earth Space from the Vernov Satellite Data. Geomagnetism and Aeronomy. V.60 (2020), pp.151-161.

ORBIT DESIGN ANALYSIS FOR A NANOSATELLITE CONSTELLATION: A CATARINA CONSTELLATION'S CASE STUDY

Rodrigo da S. Cardozo(1), **Nicole K. Borges**(2), **Damylle C. X. Donati**(3), **Talita S. Possamai**(4)

(1) *Centro Tecnológico de Joinville, Universidade Federal de Santa Catarina; rodrigodasilvacardozo@gmail.com*

(2) *Universidade do Vale do Paraíba, nicole.k.borges*

(3) *Centro Tecnológico de Joinville, Universidade Federal de Santa Catarina; damylle.xavier@t2f.ufsc.br*

(4) *Centro Tecnológico de Joinville, Universidade Federal de Santa Catarina; talita.possamai@ufsc.br*

Keywords: *Orbit Design, Catarina Constellation, Nanosatellite Constellation, Cubesats.*

In order to ensure communication between the satellites of Catarina Constellation and both its designated earth station and its data collection platforms (PCDs), a detailed orbit study was developed. Derived from the functional architecture resulting from the mission design, a constellation modeling was developed with the aid of the General Mission Analysis Tool (GMAT) and Systems Tool Kit (STK) to verify how the variation of a series of crucial factors for the development of the mission would influence both its effectiveness and efficiency. Orbital parameters, number and configuration of satellites were some of the variables studied. The analysis supported the choice of one cubesat of 2U or 3U configuration. Initial results indicated that the threshold altitude for decaying in 25 years for a 2U is about 740 km while for a 3U is 680 km. A 20º inclination orbit was found as the best inclination for communication with both ground segments located in Natal-RN and Florianólis-SC (Brazil) although not a common launch inclination for cubesats.

1. Introduction

A several number of disasters have occurred over the last few decades. Data from CRED (Centre for Research on the Epidemiology of Disaster) estimate a significant increase from the occurrence of disasters since the 1970s. Marcelino E. V. et al [1] studied the frequency of disasters in the state of Santa Catarina . The authors analyzed 3,373 natural disasters (between 1980 - 2003), of which 2,881 (about 85%) were associated with severe atmospheric instabilities. Santilli et al [2] analyzed the use of constellations of cubesats for monitoring disasters on the Amazon region indicating it as a possibility with the advances of cubesat technologies. Marinan A. D. [3] provide an analysis of how to evolve from a single Earth observing CubeSat to an effective CubeSat constellation and consider the practical challenge of launching a constellation of cubesats. One of its mains suggestions it to design the space system considering the worst orbital scenario for the constellation.

The Catarina Consortium, analyzed in this work, was created as a constellation of nanosatellites to monitor climate changes and meet the demands of interested customers, using ground and space segments. Divided into fleets, the purpose of fleet

A of Catarina Constellation is technological validation of communication between data collection points (PCD), cubesats and the Natal Multi Mission Station (EMMN).

Figure 1 presents historical data from 2U and 3U Cubesat launches, where the first number in each label represents the launch orbit, the second number represents the altitude in km and the third number represents the quantity of Cubesats in that label. It is possible to identify the inclination and altitude of 51.6º and around 97º as common launches in the last 10 years and altitudes of 400 km (for the 51.6º inclination - launches from the ISS) and between 485 and 700 km for the 97º.

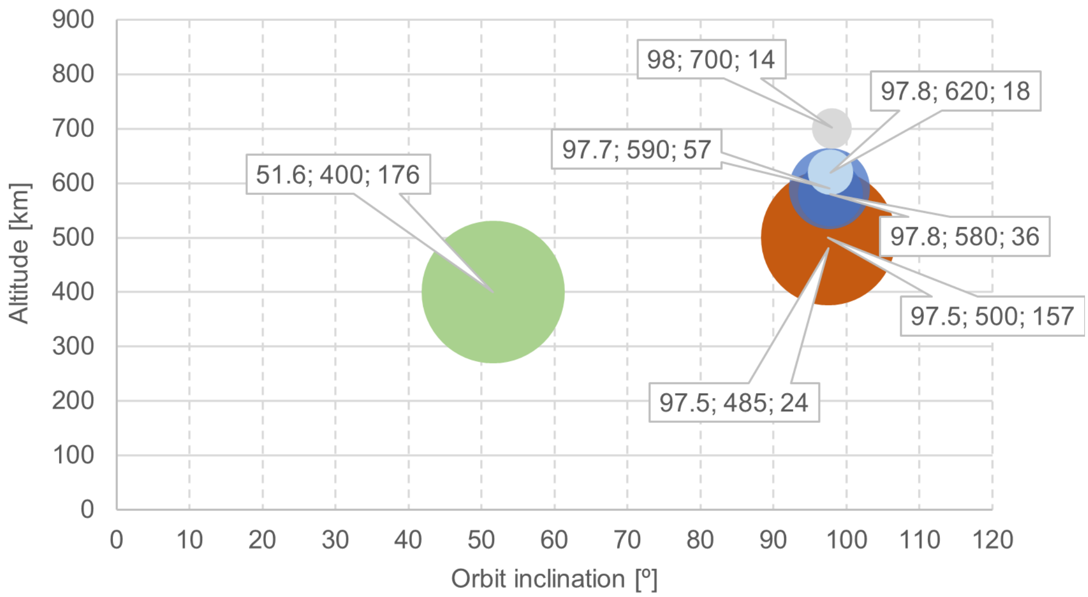

Figure 1: Frequency and inclination of 2U and 3U Cubesats launchs from 2010 to 2019. Adapted from [4].

Based on different models and dates, the worst case scenario for the orbit behavior of a Cubesat can be estimated. However since some variables carry a lot of uncertainties due to perturbations like Earth's gravity, third-bodies gravitational attractions, atmospheric drag and solar radiation pressure estimations of decay and attitude may not be accurate. That can be seen by the results of Thaheer et al [5] where his estimation of a 1U Cubesat decay did not match historical data from real decaying of similar Cubesats indicating two times more time in orbit for the model estimation than that of real 1U Cubesats launched from the same altitude.

Communication time between data collection points and data distribution is very important to anticipate weather phenomena. In this way, several orbital analyzes were carried out to map which orbits have the greatest potential to meet the following requirements: longer time to re-entry, longer antenna sighting time, shorter time to the next revisit and higher daily visit frequency. In this work orbit analyzes were performed using the GMAT program and the System Tool Kit (STK) program. The orbits chosen were based on higher launch frequencies for nanosats and ranged between 20° and 98° with altitudes between 400km - 700km.

The main objective of this work is to present a preliminary investigation of orbits decay time, frequency of contact between ground targets, communication time and time until the next visit for one cubesat alone. The simulations took into account 2U and 3U size cubesats.

2. Methodology

The analysis was performed for 3 different altitudes and 3 different inclination, totaling 9 cases. The input data are indicated in table 1. As shown, the 6 classical orbital parameters were entered in that order but only the inclination and the altitude is considered not zero. Only circular orbits were considered, and for each altitude, 3 inclinations. With these data, it is possible to propagate the orbits using the existing model in the GMAT (the model used gravity were JGM-2), reducing to only the most prominent perturbations in LEO (Low Earth Orbit), which are the drag of the atmosphere and the effect of the Earth's flattening [6]. Disturbances such as solar radiation pressure and the effect of gravity from other bodies, were disregarded. All simulations were performed with an initial date of July first, 2023, a possible date to launch the nanosats.

Orbital Parameters						
Cases	a	e	Ω	i	ω	θ
Case 1	400 Km	0	0	20°	0	0
Case 2	400 Km	0	0	51°	0	0
Case 3	400 Km	0	0	97°	0	0
Case 4	600 Km	0	0	20°	0	0
Case 5	600 km	0	0	51°	0	0
Case 6	600 km	0	0	97°	0	0
Case 7	700 km	0	0	20°	0	0
Case 8	700 km	0	0	51°	0	0
Case 9	700 km	0	0	97°	0	0

Table 1: Orbital Parameters for Differents analisys

3. Results

The results can be divided into 3 categories: 1 - Lifetime, 2 - Visit time and 3 - Time until revisit and daily number of visits. For each case, a PCD station in Florianópolis and a ground station in Natal were used as ground segments targets of Fleet A. The PCD in FLorianopolis-SC is from where the data is collected by the space system and the ground station in Natal-RN is where the data is delivered by the space system.

3.1. Life Time

The lifetime takes into account the drag suffered by the body. Although the density is extremely small, the speed at which the body moves is large enough for this effect to be noticed. Fig. 2 shows the decay curve for a 2U cubesat with an initial altitude of 540 km. The reference area is obtained from the equation [7]:

$$A_{ref} = \frac{1}{4}\sum_{k=1}^{n} A_k \tag{1}$$

Where A_k is the area of each outer face of the cubesat. The drag coefficient is constant and equal to 2.2. The density varies as the altitude of the cubesat decreases. The model for the atmospheric drag was the MISISE90 which is already inserted in the GMAT.

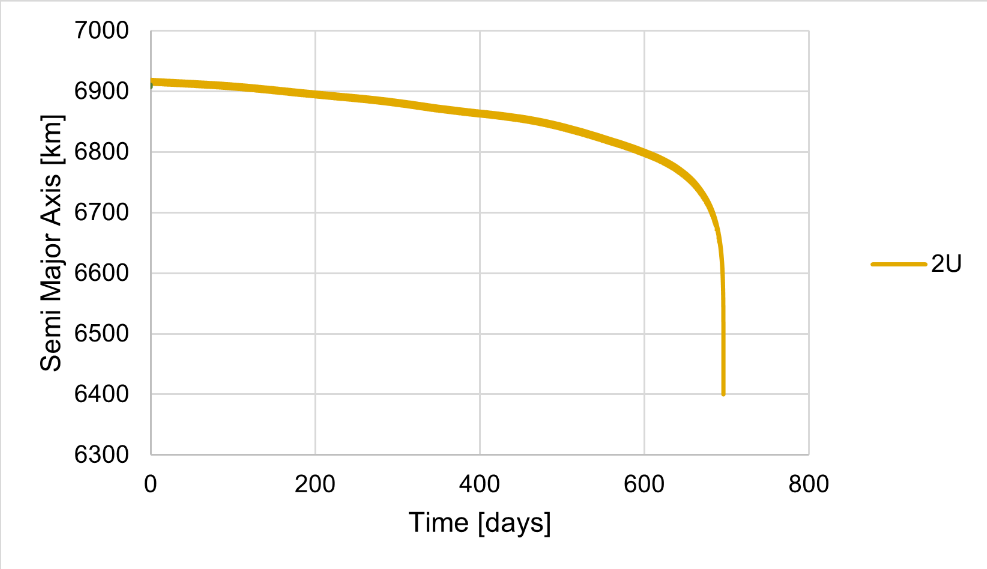

Figure 2: Life Time for a 540 km altitude

The European standard [8] establishes that objects in LEO (below 2000 km) must re-enter within 25 years. Thus, as the nanosats have different masses, it is interesting to determine what is the altitude limit at which they can be launched into orbit to comply with this limitation. Fig. 3 shows the trend curves for a 3U cubesat (4 kg) and a 2U cubesat (2.6 kg). Orbit inclination was considered as 98º for all cases. Variations in orbit inclination were found to affect the results estimated herein below 20 percent and were not further investigated. It is noticed that the nanosat with greater mass tends to stay in orbit longer, since it has more energy. Thus, the maximum altitude is approximately 680 km for the 3U nanosat and 740 km for the 2U nanosat. Notice that the trend is exponential, and behaves with the inverse of the atmospheric density variation. It is interesting to highlight that the decay time depends from different factors like total mass and projected area of the space system, not analyzed herein. Just for comparison, for the 2U configuration presented in this work a mass of 2.6 kg was considered for the space system, indicating a decay time of 132 days for an altitude of 400 km. For identical conditions but with a mass of 2 kg the decay time was estimated in 107 days for the same altitude.

The work of Piñeros, J. O. M. et al [9] indicated similar time of decay for a 1U Cubesat at 400 km altitude and identical drag coefficient. Considering the higher mass of a 2U Cubesat, the results presented here may be underestimated. Another indication of this is the historical data [4] that shows that the average life in orbit of 2U Cubesats launched at 400 km and 51.6º is approximately 1 year.

3.2. Number of Occurrence

Figure 4 plots the occurrence of each contact point for the altitudes of 500 km and 600 km for the three inclinations analyzed versus the duration of the contact point. On

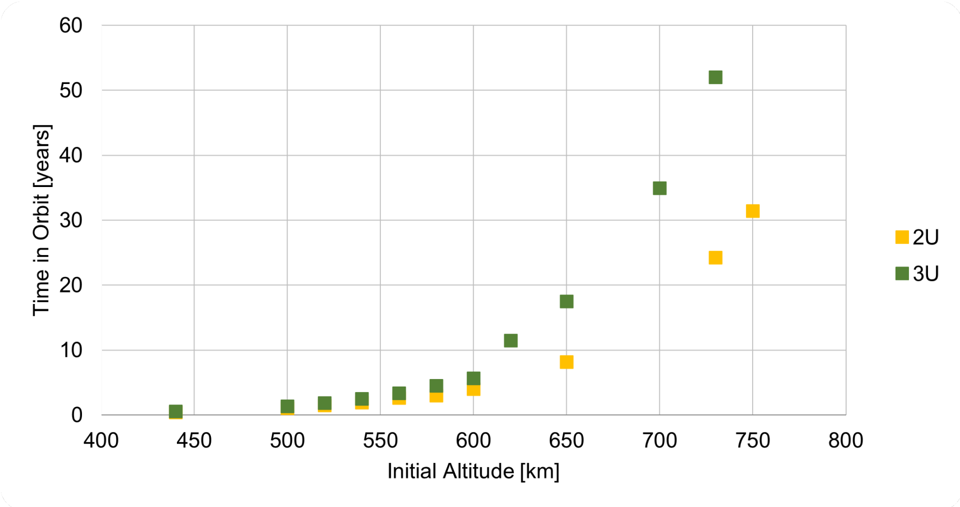

Figure 3: **Life Time for a 2U and 3U per Initial Altitude**

the top-left plot we can see the duration and the total number of the contact points for 500 km for each inclination between PCD and space system (SS). For example, for the inclination of 20°, a total of approximately 1440 contact points were estimated through the period of 02/06/2023 to 30/05/2024. From this 1440 contacts only 12 contact had a duration under 50 seconds. Most contact for all inclinations and altitudes analyzed are concentrated above 200 seconds. The angle considered for contact between ground segment and space segment was 10º for all analysis and no orbit decay was considered. For more accurate results the orbit decay estimated should be taken into account.

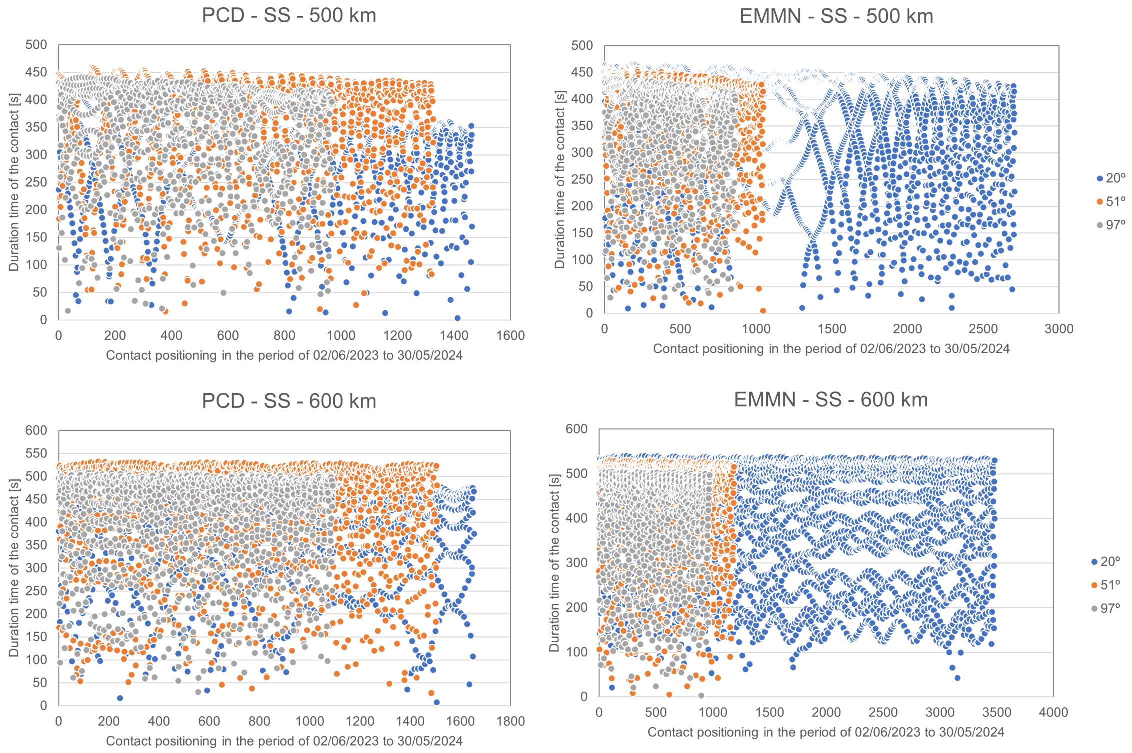

Figure 4: Communication time during 02/06/2023 to 30/05/2024 for altitudes of 500km (left) and 600km (right)

The orbit inclination of 20º showed a good orbit for communication with both ground segments, in Santa Catarina and Natal as can be seen by the higher frequency of points of contact between space system and both ground systems. However, as shown in Figure 1, this is not a common launch orbit for Cubesats historically. Also, as expected, for higher altitudes (600 km) a higher number of contact points was estimated.

3.2.1. Number of communication per day: SS - PCD

The number of times one of the space systems has contact with the PCD at Santa Catarina is indicated below for the orbit inclination of 20°, 51° and 97°, for the altitude of 500 km and 600 km over one year. The data is presented in different graphs for the minimum number of contacts per day on the month, average number of contacts per day in the month and maximum number of contacts per day in the month.

As can be noted, the minimum number of contact per day for all configurations is 1. As an example, for the altitude of 500 km and inclination of 97°, in May 2024 at least one day will have only one contact point between PCD and space system. For the same inclinations all other months will have at least 2 contacts per day. The average contacts number is between 2 to 3 (for 97°), 3 to 4 (for 51°) and 3 to 4 (for 20°). Figure 5 shows the communication time for Space system (SS) to PCD. The data for 400 km of altitude were not considered because the life time was below the project original threshold for minimum space system operational life.

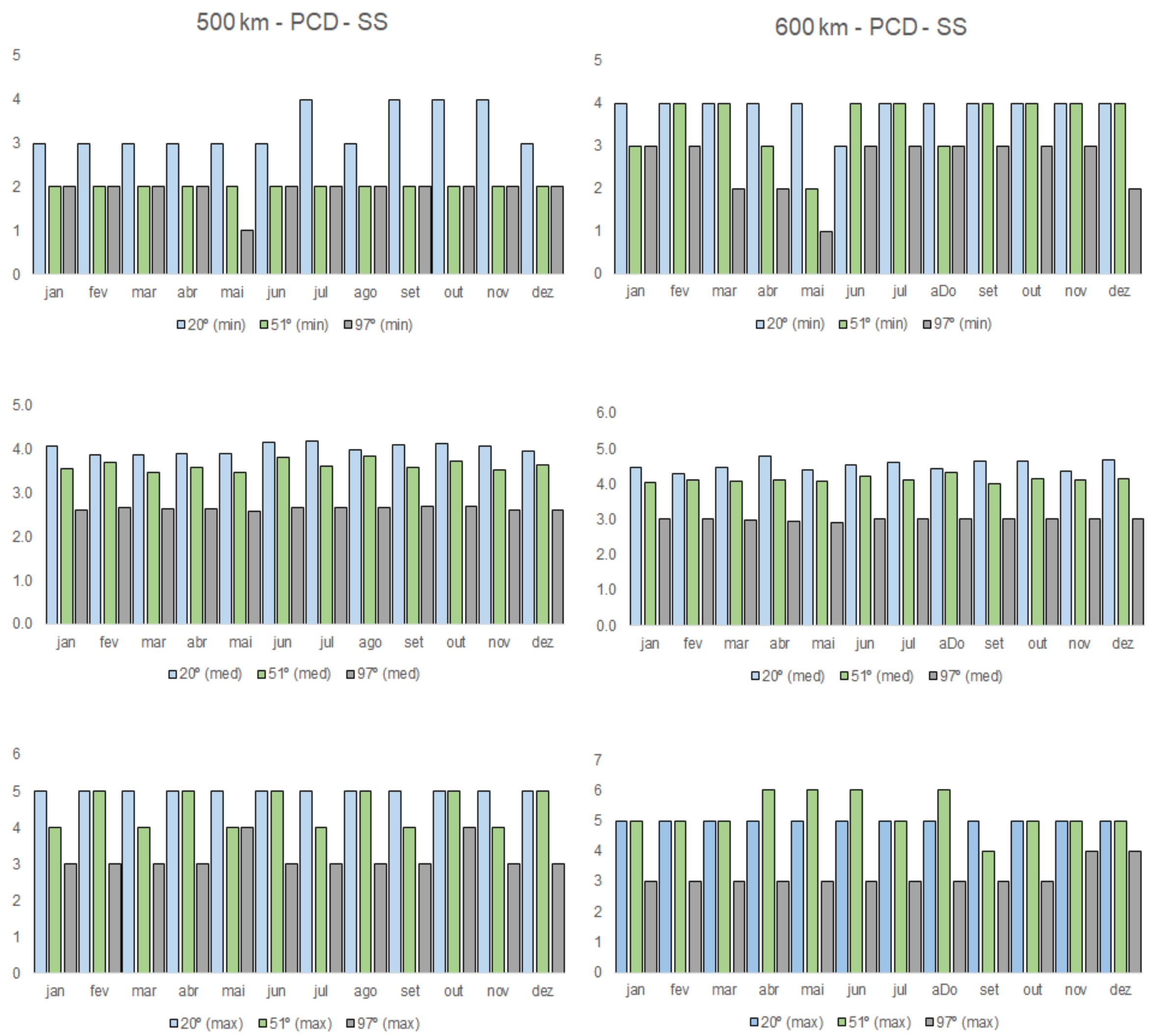

Figure 5: PCD-SS communication number of times per day per month during 01/06/2023 to 31/05/2024 for altitudes of 500km (left) and 600km (right). From top to bottom: Minimum number, average number and maximum number.

3.2.2. Number of communication per day: SS - EMMN

The same analysis is presented below for contact point between space system and the ground station in Natal. Here we can see that the inclination of 20° has a much higher number of contact points per day than the other inclinations. However the minimum contact number for all inclinations and altitudes considered herein is still 1, at least one day in May 2024 and June 2023.

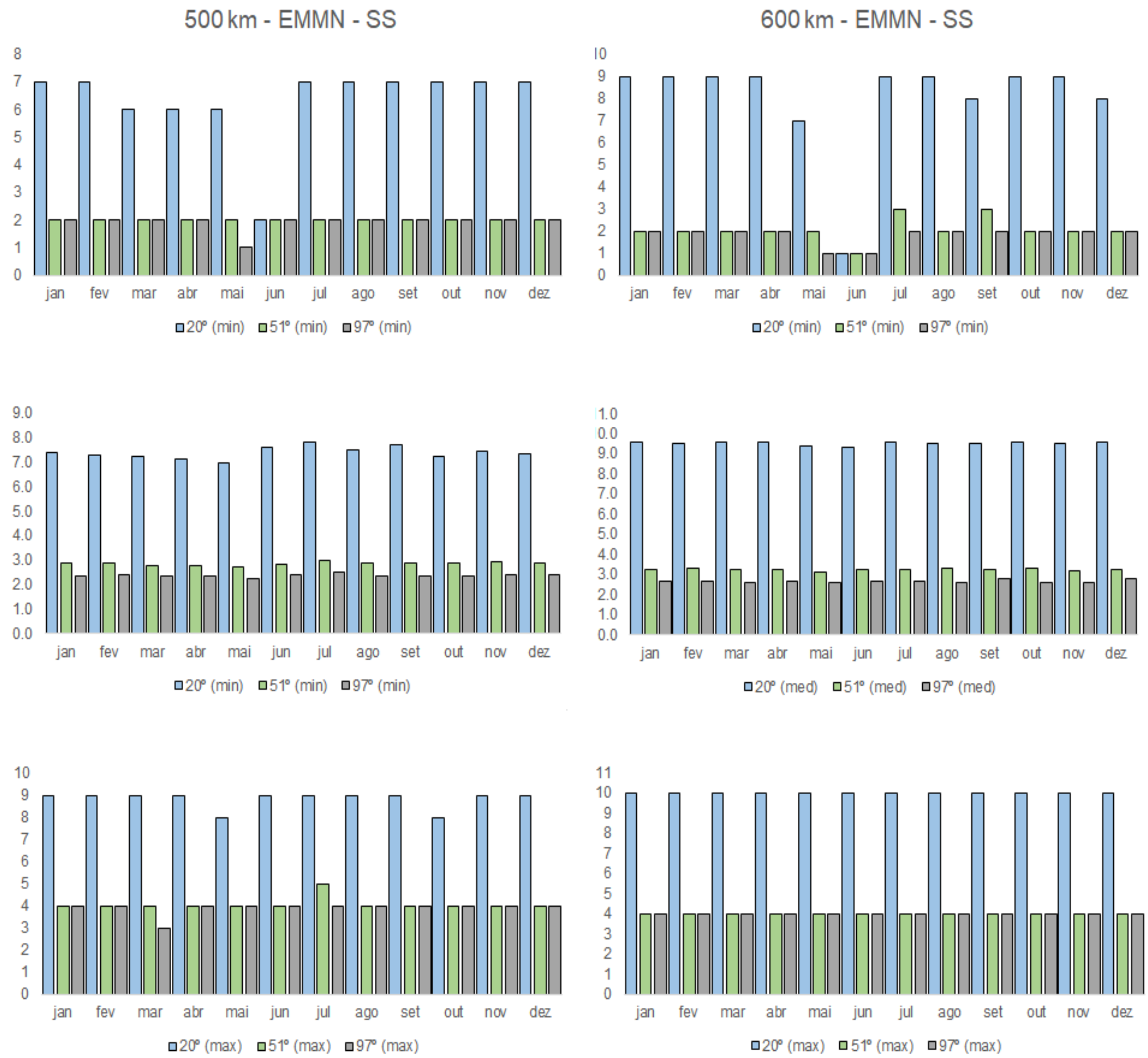

Figure 6: EMMN-SS communication number of times per day per month during 01/06/2023 to 31/05/2024 for altitudes of 500km (left) and 600km (right). From top to bottom: Minimum number, average number and maximum number.

4. Conclusion

Analyzing all the parameters obtained for the preliminary orbital analysis, it is possible to conclude that the preliminary most suitable scenario based on the parameters of average communication duration time per visit, average revisit time and average number of visits are those up to 600 km of altitude, with smaller orbit inclination. They have the longest communication period, the shortest revisit times, and the highest numbers of daily visits to them. Lower orbits have the disadvantage of re-entering very quickly, which leads to an increase in the replacement cost of nanosats. It's important to take account the budget for the launches.

Another interesting point is that the results presented here for the decay time showed lower time in orbit than average historical data [4] indicating that the model applied may be underestimating this result and should be further investigated. Also, results for the frequency of contact points between space segment and ground segments do not take into account the decaying of the space system and may be overestimated.

Acknowledgments

We thank the Brazilian Space Agency for their support of the project and guidance for this work.

We thank the Santa Catarina Parliamentary Bench for the financial support for the development of Catarina Constellation.

References

[1] Marcelino E. V. Nunes L. H. Kobiyama M., NATURAL DISASTERS RISK MAPPING OF SANTA CATARINA STATE, CAMINHOS DE GEOGRAFIA 8 (2006) 72–84.
[2] Santilli, G. Vendittozzi, C. Cappelletti, C. Battistini, S. Gessini, P., CubeSat constellations for disaster management in remote areas, Acta Astronautica 145 (2018) 11–17.
[3] Marinan A. D., From CubeSats to Constellations: Systems Design and Performance Analysis, Master's thesis, University of Michigan, 2013.
[4] Kulu, E., Nanosats Database, 2014 - 2022.
[5] Thaheer, M. Shaqeer, A. Norilmi I., Orbit design and lifetime analysis of mysat: A 1u cubesat for electron-density measurement.
[6] H. D. Curtis, Orbital Mechanics for Engineering Students, Elsevier, 2005.
[7] NASA-STD-8719.14A - Process for Limiting Orbital Debris, NASA, 300 E. Street SW, Suite 5R30 Washington, DC 20546, 2011.
[8] ISO 24113:2019 - Space debris mitigation requirements, International Organization for Standardization, CP 401 - 1214 Vernier, Geneva, Switzerland, 2019.
[9] Piñeros, J. O. M. Santos, W. A. Prado, A. F. B. A, Analysis of the orbit lifetime of CubeSats in low Earth orbits including periodic variation in drag due to attitude motion, Advances In Space Research 67 (2021) 902–918.

EDUCATIONAL AND SCIENTIFIC PROJECT MONITOR BASED ON CUBESAT CONSTELLATION

Vladislav I. Osedlo[(1)], Georgy I. Antonyuk[(2)], Victor V. Bengin[(3)], Vitaly V. Bogomolov[(4)], Ivan A. Zolotarev[(5)], Vladimir V. Kalegaev[(6)], Oleg Yu. Nechaev[(7)], Vladimir V. Radchenko[(8)], Sergey S. Svertilov[(9)]

[(1)] M.V. Lomonosov Moscow State University, 1(2), Leninskie gory, GSP-1, Moscow 119991, Russian Federation, +7925-504-51-74, osedlo@mail.ru

[(2)] M.V. Lomonosov Moscow State University, 1(2), Leninskie gory, GSP-1, Moscow 119991, Russian Federation, +7968-737-06-45, antonjuk.gi15@physoics.msu.ru,

[(3)] M.V. Lomonosov Moscow State University, 1(2), Leninskie gory, GSP-1, Moscow 119991, Russian Federation, +7926-311-10-54, v_benghin@mail.ru

[(4)] M.V. Lomonosov Moscow State University, 1(2), Leninskie gory, GSP-1, Moscow 119991, Russian Federation, +7916-726-82-32, bogovit@rambler.ru

[(5)] M.V. Lomonosov Moscow State University, 1(2), Leninskie gory, GSP-1, Moscow 119991, Russian Federation, +7968-930-15-45, brilkov@yandex.ru

[(6)] M.V. Lomonosov Moscow State University, 1(2), Leninskie gory, GSP-1, Moscow 119991, Russian Federation, +7905-701-44-93, klg@dec1.sinp.msu.ru

[(7)] M.V. Lomonosov Moscow State University, 1(2), Leninskie gory, GSP-1, Moscow 119991, Russian Federation, +7916-916-06-35

[(8)] M.V. Lomonosov Moscow State University, 1(2), Leninskie gory, GSP-1, Moscow 119991, Russian Federation, +7903-251-94-09, vrad1950@yandex.ru

[(9)] M.V. Lomonosov Moscow State University, 1(2), Leninskie gory, GSP-1, Moscow 119991, Russian Federation, +749593951-60, sis@coronas.ru

***Keywords**: education, scientific, nano-satellites, cubesat, constellation*

The aim of the scientific and educational project Monitor is realization of a space experiment on two satellites of cubesat 3U type for monitoring radiation in order to predict space weather and involving schoolchildren in space research by participating in the processing and analysis of measurement data. During the implementation of the project, two instruments are to be elaborated, i.e. the DeCoR-2 space radiation detector and the KODIZ combined space radiation detector. It is planned to install these instruments on two spacecraft of the 3U cubesat type, i.e. DeCor-2 on one of these satellites, KODIZ on the other. DeKor-2 and KODIZ instruments complement each other, since the DeKor-2 instrument monitors the electron and gamma quantum fluxes in the energy range 0.05-2.0 MeV, and the KODIZ instrument monitors the fluxes of protons and nuclei with Z> 1with energies more than 30-50 MeV/nucleon. Thus, being installed on spacecraft launched during one by-pass launch, they will provide monitor measurements of various components of space radiation in similar orbits. The most important task of the project is the educational component. It is assumed that schoolchildren will be involved in the elaboration and manufacturing of electronic components of the instruments, its ground experimental testing. During the experiment, it is planned to use data receiving stations deployed on the basis of schools. Schoolchildren will have to participate in the replenishment of databases used for space weather forecasting, processing and analysis of data obtained during the implementation of the space experiment. The results of the space experiment will be used in the educational process as material for lectures and seminars, as well as in a workshop on processing and analyzing data from space experiments.

1.Introduction

The Monitor project is aimed on developing a system for multi-satellite monitoring of the radiation environment of near-Earth outer space. Within the framework of the project, a number of nano-satellites are prepared to be launched on polar orbits. They should be used for measuring of ionizing radiation fluxes. The other direction of cubesat satellite using is study of so called transient electromagnetic phenomena such as cosmic gamma ray bursts, hard X ray and gamma ray emission of solar flares and gamma ray and optical flashes from the Earth atmosphere, so called Terrestrial Gamma-Ray Flashes (TGF) and Transient Lightning Phenomena (TLE). In other words this project is directed on study and monitoring of potentially dangerous phenomena in the near-Earth space and upper Atmosphere. The scientific and applied goal of the Monitor project is creation und using of nano-satellite constellation for location of hazards, which may be crucial for space missions (see Figure 1).

At the first stage of the project, it is planned to set up a space experiment on monitoring radiation and electromagnetic transients on a few cubesat satellites in order to conduct scientific research in the field of space weather, as well as to involve schoolchildren in space research by participating in the reception, processing and analysis of measurement data.

The project is also expected to create a network of ground receiving stations located at different longitudes. This will significantly increase the volume of data received from satellites, as well as improve the efficiency of monitoring measurements. It is also planned to involve schoolchildren in the work of this ground-based network of stations. It is supposed that schoolchildren will take part in the reception and processing of satellite data.

2. Monitor Constellation Concept

Thus, the concept of the Monitor project is to create a system for operational monitoring and forecasting of the radiation fluxes in the near-Earth space based on a constellation of cubesat nanosatellites and a system of ground receiving stations. At the same time, the most important component of the project is the educational part, which assumes the direct involvement of students in space research, primarily in their participation in the processing and analysis of satellite data.

During realization of Monitor project several tasks should be solved, among them:

- expanding the constellation of nanosatellites with the possibility of promptly dumping of scientific data on a distributed system of ground stations based on educational institutions,
- expansion of the orbital instrument base,

- involvement of schoolchildren and students in space activities through the involvement in the analysis of data from spacecraft constellation.

The satellites of the Monitor constellation should carry two complementary instruments of a new generation for studying near-Earth radiation as a payload. These are the DeCoR-2 space radiation detector, which monitors electron and gamma-ray fluxes in the energy range of 0.05-2.0 MeV, and the combined cosmic radiation detector KODIZ, which monitors proton and nuclear fluxes with Z>1 with energies over 30-50 MeV/nucleon. It is planned to install these instruments on two 3U cubesat spacecraft, each onto own satellite. The DeCoR-2 also can be used for observations of transient electromagnetic phenomena in hard X rays and gammas.

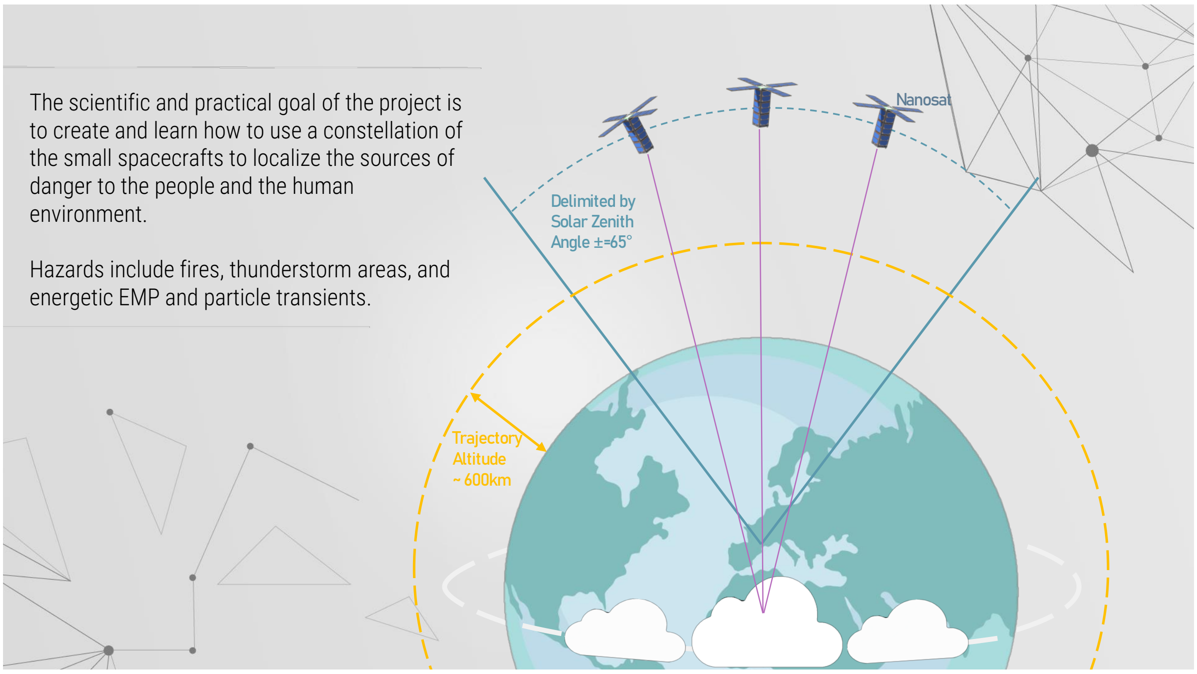

Figure 1: Experiment scheme

The DeCoR-2 instrument is an updated version of the DeCoR-1 instrument, successfully operating on nanosatellites SiriusSat, AmurSat, VDNKh-80, Norbi, DEKART, etc. [1 - 3]. It has an effective area increased to 65 cm^2, which will make it possible to study not only captured and precipitating electrons, but also gamma-ray bursts of various nature. A composite scintillation detector consisting of a 3 mm plastic scintillator and 9 mm CsI(Tl) scanned by vacuum photomultipliers or by an assembly of silicon photomultipliers (SiPM) makes it possible to separately detect gamma quanta and electrons, which is very important for identifying the types of increases in an experiment in polar orbit. Sufficiently large area of the detector contributes not only to improving the sensitivity of the instrument, but also to increasing its temporal resolution, which is determined primarily by the statistics of detected events. Data will be accumulated both in the form of monitoring (count rate in several channels) and in the form of a detailed event-by-event record. The DeCoR-2 device includes an additional calculator that will be used to select the most interesting data sections in order to transmit them to Earth in their primary form.

The KODIZ instrument is intended primarily for the detection and study of solar cosmic ray particle fluxes, which can create an additional radiation load on board spacecraft and aircraft flying in the polar regions. The KODIZ instrument includes detectors of several types, i.e. a Cherenkov particle detector with a plexiglas radiator with an area of ~11 cm^2, two neutron detectors with lithium glasses, and a semiconductor telescope made of two 300 μm silicon layers. The instrument will detect the fluxes of protons and nuclei with Z>1 with an energy of more than 30 - 50 MeV/nucleon in the range from 10^1 to 10^4 particles/cm^2 s, the fluxes of protons and nuclei with Z>1 with an energy of more than 330 MeV/nucleon in the range of 10^1 up to 10^3 particles/cm^2 s, thermal and epithermal neutron flux in the range from 10^1 to 10^3 neutrons/cm^2 s. Based on the readings of the instrument's detectors, the absorbed dose rate of charged particles of cosmic radiation will be determined in the range from 10^{-8} to 10^{-5} Gray/s.

3. System of satellite data receivers

As part of the Monitor project, it is planned to deploy a network of receiving stations, which should be located at different longitudes, corresponding to the distance of time zones by about 2 hours from each other, throughout Russia, from the Kaliningrad region to Kamchatka is presented in Figure 2. These stations should be based in educational institutions and ensure prompt reception of data from satellites flying over them. In addition, the satellites of the constellation will be controlled through these stations from a unit control center based at the SINP MSU.

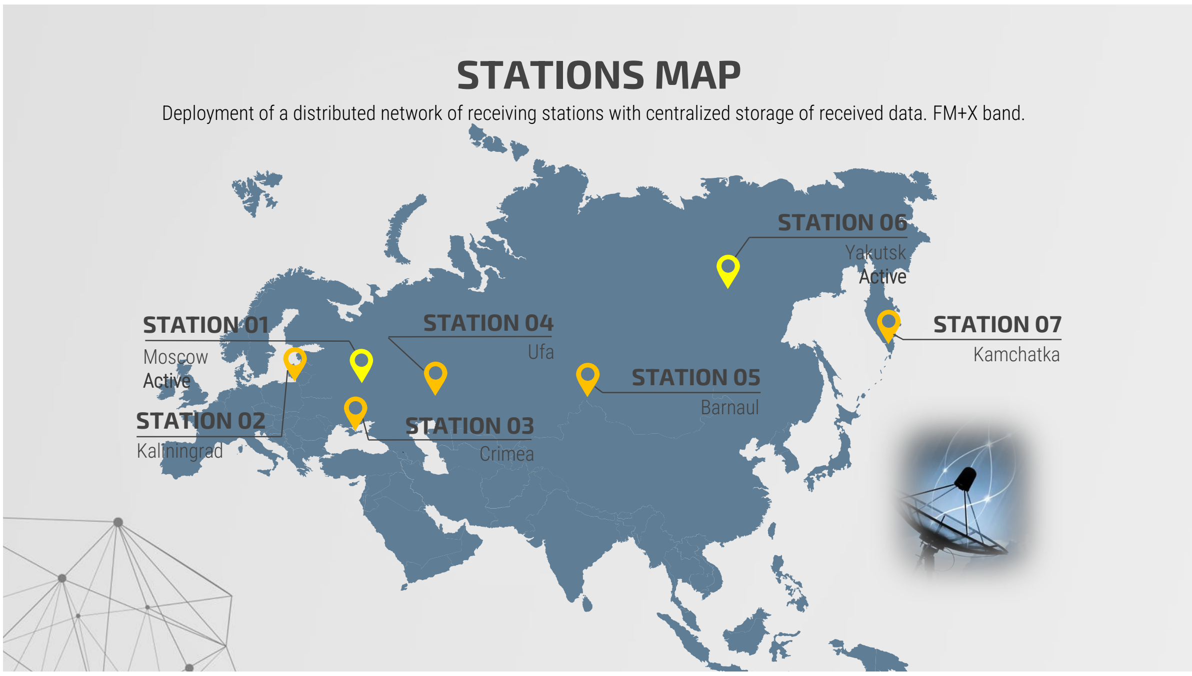

Figure 2: Locations of receiving stations.

As a working option that implements the above tasks, it can be considered a two-way dual-band space communication station based on a receiver with a parabolic antenna with a feed on the X band (optionally S or L band) in combination with a VHF receiver-transmitter for receiving telemetry and sending commands.

The scheme of interaction between the space and ground segments is shown in Figure 3.

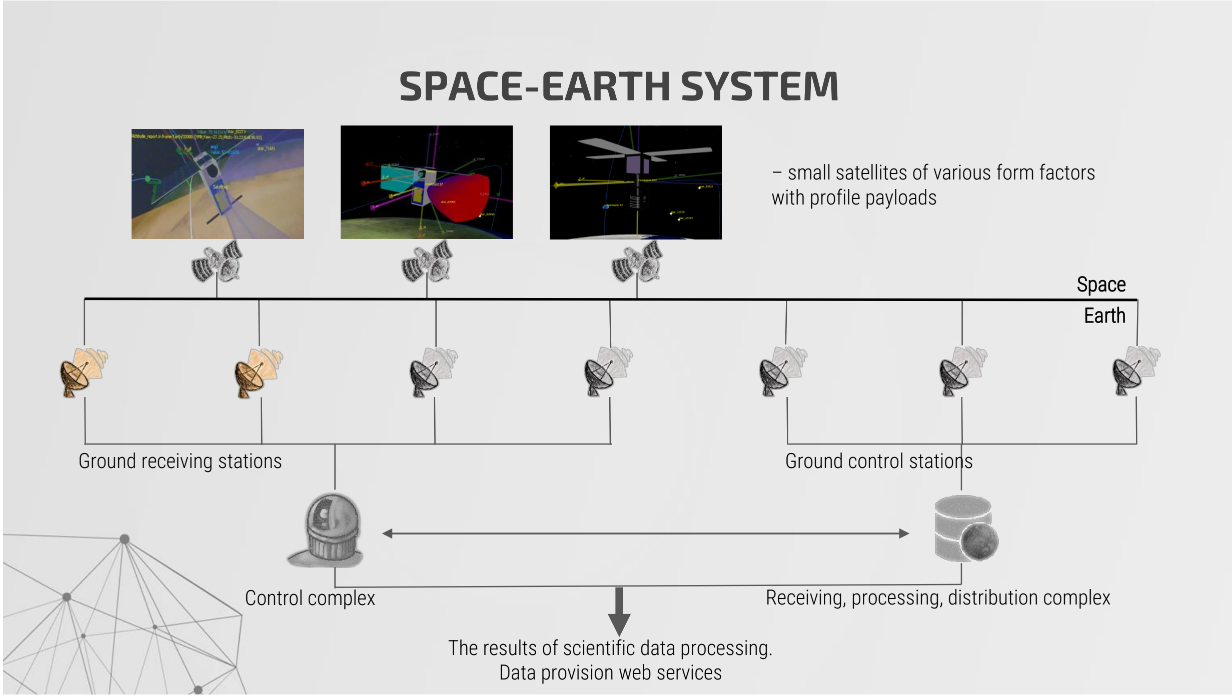

Figure 3: Space and ground segments.

4. Educational component of Monitor project

The most important goal of the project is the educational component [4], see Figure 4. The educational component of the project is aimed at involving schoolchildren and students in space research. In particular, it is planned to create a network of receiving stations based in schools and other educational institutions. Schoolchildren and students are expected to participate in the preparation and conduct of space experiments, the reception and processing of scientific and telemetric information obtained using antennas installed directly on the territory of the schools participating in the project.

As part of this work, schoolchildren will be involved in the creation of electronic components of instruments, in particular, in their ground-based experimental testing, in obtaining and systematizing calibration data. During the implementation of the experiment itself, it is planned to use data receiving stations deployed on the basis of schools from various Russian cities. Schoolchildren will have to participate in updating the databases used for space weather forecasting, processing and analyzing data obtained during the implementation of the space experiment. To this end, workplaces will be created in a number of schools, where online access to the most up-to-date data coming from satellites to the servers of the SINP MSU space monitoring department will be organized. Employees of SINP MSU and the Department of Space Physics of the MSU Faculty of Physics will provide the necessary support to young project participants in the form of master classes and consultations, as well as train teachers who organize work in specific schools.

The results of the space experiment will be used in the educational process of students as material for lectures and seminars, as well as in a workshop on processing and analyzing data from space experiments. For many years, such a workshop has been held by the Department of Space Physics of the Faculty of Physics of Moscow State University for students of 3-4 courses. In 2020-2021, the data from the Universitetsky-Tatiana satellite, traditionally used in student workshops, was supplemented with data from décor-1 instruments that measure radiation at the AmurSat, VDNKh-80, Norbi and DEKART cubesats.

Figure 4: A team of schoolchildren led by scientists from Moscow University at the Sirius Center designed and implemented CubeSat.

Separately, it should be noted the participation of students in the preparation of the space experiments described above, in particular, the work of future bachelors and masters of the Faculty of Physics of Moscow State University, related to setting up and programming the components of the KODIZ device, with the optimization of algorithms for detecting gamma-ray bursts against the background of variations in electron flows in the DeCoR-2 device , with detector calibration.

5. Conclusions

Thus, the following tasks will be solved during the Monitor project:

- the spatial-temporal parameters of the energetic charged particle flux distributions in various regions of the near-Earth space are determined;
- the mechanisms of fast variations of high-energy electron fluxes in the outer radiation belt of the Earth were determined;
- monitoring of galactic and solar cosmic ray proton fluxes was carried out to build a dynamic space weather model;
- interactive programs for teaching schoolchildren and other categories of students how to process and analyze data from space experiments have been created.

References

[1] V.V.Bogomolov, A.V.Bogomolov, Yu.N. Dement'ev, et al. A Scientific and Educational Space Experiment on the SiriusSat-1,2 Satellites. Moscow University Physics Bulletin. V.73 (2020), pp.666–675.

[2] V.V.Bogomolov, A.V.Bogomolov, Yu.N. Dement'ev, et al. A First Experience of Space Radiation Monitoring in the Multi-Satellite Experiment of Moscow University in the Framework of the Universat-SOCRAT Project. Moscow University Physics Bulletin. V.73 (2020), pp.676–683.

[3] M.I. Panasyuk, P.A. Klimov, S.I. Svertilov, et al. Universat-SOCRAT multi-satellite project to study TLEs and TGFs. Progress in Earth and Planetary Science. V.6 (2019), pp.35-54.

[4] V.V.Bogomolov, G.I. Antonyuk, V.V. Bengin, et al. Scientific and Educational Project Monitor Based on Satellites in Cubesat Format, in Proceedings of the 1-st International Conference on Space Education "Road to Space", Moscow, Russia, October 5-8, 2021, pp. 53-54.

Introducing SARA Constellation: Satellite for Agriculture and Remote Areas®

Felipe de S. N. Coelho[(1)], **Luis M. C. Acosta**[(2)]
[(1)] *Acosta Aerospace, São José dos Campos, +55 12 3947-5843,*
felipe.coelho@acosta-aerospace.com
[(2)] *Acosta Aerospace, São José dos Campos, +55 12 3947-5843,*
luis@acosta-aerospace.com

Keywords: *Nanosatellite, Constellation, IoT/M2M, Remote Areas, Orbit design*

This paper introduces the SARA Constellation for data telecommunication in remote areas. We investigate the performance of a 5-nanosatellite based LEO constellation considering different designs and different locations in South America. In order assess the performance of several constellation designs, we consider a scenario with four target locations, and discuss four figures of merit such as *satellite availability, satellite time-in-view, coverage gap,* and *timing consistency.* Simulation results indicate enough coverage performance to meet our basic mission goals. We also provide a brief description of the overall mission requirements and the system architecture.

1. Introduction

Internet connectivity is considered a basic infrastructure in urban centers but is not the case in most remote and rural areas. In *Mato Grosso,* Brazil's largest soybean, cotton, and corn producer, internet connectivity is available in 86% of farms, but signal coverage runs in only 3% of production fields. A similar lack of connectivity is found in other remote areas such as borders, mining sites, and over oceans and large forests. With the advancement of space qualified *components-off-the-shelf (COTS)*, and IoT-oriented technology for CubeSats, we have seen the development and deployment of nanosatellite-based LEO constellations for IoT service [1, 2].

In this paper, we introduce the SARA Constellation to provide IoT/M2M data telecommunication in remote areas. Our work presents preliminary trade-off results of SARA's R&D and the its conceptual design phase. In the sequel, we give attention to the constellation design and analysis. We investigate constellation design candidates in order to fulfill our most basic mission premise, that is: *A constellation of nanosatellites to provide IoT telecommunication service to remote areas. The initial constellation shall consist of 5 satellites of the type 6U CubeSat operating in LEO. The constellation shall provide coverage primarily over the Brazilian territory, and the South American territory. The coverage shall also (i.) provide at least two accesses per day for all locations; and (ii.) be uniform.* At the end, we describe our system architecture, providing description of mission requirements, payload and bus.

2. Constellation Design and Analysis

2.1. Orbit design

Let us begin by defining the *Walker Delta Pattern* (WDP) as the design framework. Among other frameworks, the WDP is of particular interest due to its symmetry, uniform distribution, and low complexity characteristics [3]. The WDP framework is essentially

Table 1: Design variables and constraints for SARA constellation.

Variable	Concerns	Evaluation Criteria	Design Constraints	
N# of satellite, N	-Mission costs; and -Coverage capacity.	Minimize with respect to mission requirements.	5 satellites	
N# of planes, P	-Coverage enhancement; -Degradation; and -Mission costs.	Minimize with respect to mission requirements.	1 plane	5 planes
Configuration	-Coverage uniformity.	Select for best coverage and mission objectives.	WDP defined by N and P and orbit parameters $\{h, i, e\}$.	
Plane spacing, $\delta\Omega$	-Coverage uniformity.	Choose to best meet the mission requirements.	$\delta\Omega = 0^o$	$\delta\Omega = 72^o$
Sat. phasing, $\delta\phi$	-Coverage uniformity.	Choose to best meet the mission requirements.	$\delta\phi = 72^o$	$\delta\phi = \{0, 72\}^o$
Eccentricity, e	-Mission complexity.	Choose to best meet the mission requirements.	$e = 0.001$	
Altitude, h	-Coverage quality; -Time in view; -Link budget; and -Launch costs.	*Performance vs. Costs.*	$h = \{500, 600, 700\}$ km	
Inclination, i	-Coverage quality; -Launch costs.	*Performance vs. Latitude* *Performance vs. Costs*	$50^o \leq i \leq 100^o$	

characterized by three integer parameters: *(i.)* a total number of N satellites evenly distributed over *(ii.)* a number of P orbital planes evenly spaced along the equatorial plane, and *(iii.)* a phasing parameter, $\delta\phi$, between satellites of adjacent planes. Provided that our mission is restricted to 5 satellites in its initial fleet, we thus have two possible configuration based on WDP: *(i.)* a constellation of 5 satellites evenly distributed over 1 orbital plane; or *(ii.)* a constellation with 5 evenly spaced orbital planes with one satellite per plane. We shall see that either configuration presents advantages and disadvantages, but can be complementary to each other, nonetheless.

Other parameters of particular impact in a constellation performance are the altitude, inclination and eccentricity. Table 1 summarizes the most relevant design variables, along with evaluation criteria and constraints in our work. Given our mission objectives, circular orbits are preferred due to coverage and service uniformity. We assumed a rather practical figure eccentricity $e = 0.001$, as can be observed for operational LEO satellites with similar purposes. As for the altitude and inclination, the choice of these parameters must follow a trade-off of performance and mission budget, such as coverage quality and time in view against costs and different latitudes [4, 5]. Here, we assess the orbital parameters variation under J_2 perturbation due to the earth oblateness. From the *method of averaging* [6] we find that h, i and e, in average, are not affected, *i.e.*, $\Delta h = \Delta i = \Delta e = 0$, but such parameters have impact in the averaged variation of both the right ascension of the ascending node, Ω, and the argument of periapsis, ω. That is:

$$\Delta\Omega = -\left[\frac{3}{2}\frac{nJ_2R_\oplus^2}{a^2(1-e^2)^2}\right]\cos i \tag{1}$$

$$\Delta\omega = -\left[\frac{3}{2}\frac{nJ_2R_\oplus^2}{a^2(1-e^2)^2}\right]\left(\frac{5}{2}\sin^2 i - 2\right) \tag{2}$$

where: n is the mean motion; $R_\oplus \approx 6378.16$ km is the Earth mean equatorial radius; $a = r_p/(1-e)$ is the semimajor axis as function of the perigee radius, which we assume $r_p \equiv R_\oplus + h$, with h as our design altitude; and $\Delta * \equiv \frac{\bar{d*}}{dt}$ corresponds to the averaged variation.

Figures 1-(A,B) show the variation of Ω and ω, respectively, given $e = 0.001$ and varying values for altitude, $500km \leq h \leq 700km$, and inclination $0^o \leq i \leq 100^o$. It can be observed that $\Delta\Omega \to 0$ for highly inclined orbits as $i \to 90^o$, which tends to be favourable to coverage timing consistency. That is, the smaller the $\Delta\Omega$, the more timely consistent will be a satellite pass over a particular location. Ideally, $\Delta\Omega = 0$ for $i = 90^o$, yet this inclination is not recommended considering the scalability of the constellation as the probability of self-induced collisions over the poles may increase with the growth of the constellation. From eq. (1), by setting $\Delta\Omega = 1^o$/day, one can derive a family of *Sun-Synchronous Orbits (SSO)* with inclination ranging from 97^o to 98^o as function of altitudes from 500 km to 700 km. From eq. (2) when $\Delta\omega = 0$, one can derive the *Frozen Orbits (FRO)* defined by the critical inclination $i = \arcsin\sqrt{4/5} \approx 63.43^o$ for all values of altitude. We have also considered in our analyses inclined orbits with $i = 50^o$, in this paper labelled as *i50* orbits, as it can also meet the coverage requirements over the Brazilian and South American territory. Table 2 provides information of the orbit designs considered in our work.

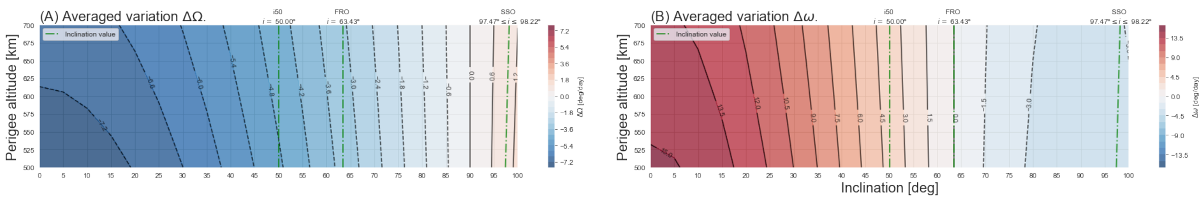

Figure 1: Averaged variations $\Delta\Omega$ and $\Delta\omega$ due to the earth's oblateness.

Table 2: Variation of parameters for inclined, frozen and sun-synchronous orbits.

Circular Orbit ($e = 0.001$)		**Inclined Orbit**	**Frozen Orbit**	**SSO**	
$h = 500.0$	km	$i = 50.0$	$i = 63.43$	$i = 97.43$	deg
$T = 94.76$	min	$\Delta\Omega = -4.90$	$\Delta\Omega = -3.41$	$\Delta\Omega = 0.99$	deg/day
$n = 15.20$	rev/day	$\Delta\omega = 4.06$	$\Delta\omega = 0.00$	$\Delta\omega = -3.49$	deg/day
$h = 600.0$	km	$i = 50.0$	$i = 63.43$	$i = 97.79$	deg
$T = 96.69$	min	$\Delta\Omega = -4.66$	$\Delta\Omega = -3.24$	$\Delta\Omega = 0.99$	deg/day
$n = 14.89$	rev/day	$\Delta\omega = 3.86$	$\Delta\omega = 0.00$	$\Delta\omega = -3.30$	deg/day
$h = 700.0$	km	$i = 50.0$	$i = 63.43$	$i = 98.19$	deg
$T = 98.77$	min	$\Delta\Omega = -4.43$	$\Delta\Omega = -3.08$	$\Delta\Omega = 0.99$	deg/day
$n = 14.58$	rev/day	$\Delta\omega = 3.68$	$\Delta\omega = 0.00$	$\Delta\omega = -3.11$	deg/day

Having the orbit types *i50, FRO,* and *SSO* as reference, we have iterated the altitude taking into account $\Delta\Omega$ and the rotation of the Earth to obtain repeating track orbits for a reference mean motion value. Figure 2 shows the mean motion for a range of altitudes for *i50, FRO,* and *SSO* designs and the intersection where $n = 15\,rev/day$, that is: $h \approx 609.0\,km$ for *i50* orbits; $h \approx 590.0\,km$ for *FRO* orbits; $h \approx 535.0\,km$ for *SSO* orbits, with $i \approx 97.56^o$. Therefore, considering the design variables in Table 1 and having defined the orbit parameters, Figure 3 shows our constellation design candidates breakdown for SARA Constellation.

2.2. Coverage assessment

Following analytic approximations in [4], one can assess the coverage percentage against latitude for a range of inclination values. For the proposed mission, we assume that the contact between target and satellite is established at a minimum elevation angle $\varepsilon_{min} \equiv 15^o$. Assuming altitude $h \equiv 500.0\,km$, the maximum *earth central angle*,

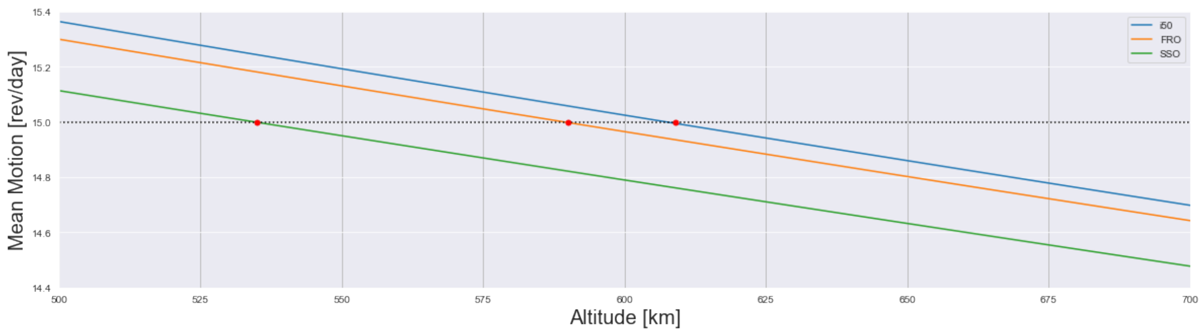

Figure 2: Mean motion against altitude for *i50, FRO,* and *SSO* designs.

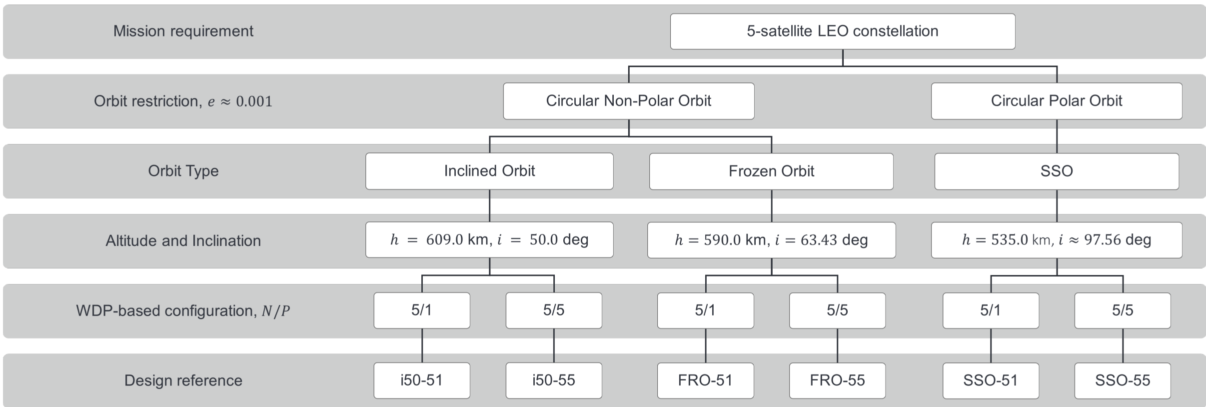

Figure 3: Constellation design breakdown.

λ_{max}, and the maximum range, d_{max}, are:

$$\lambda_{max} = 90^o - \varepsilon_{min} - \eta_{max} \approx 11.4^o \tag{3}$$

$$d_{max} = R_\oplus \frac{\sin \lambda_{max}}{\sin \eta_{max}} \approx 1407.52\ km \tag{4}$$

$$\text{with } \sin \eta_{max} = \sin \left(\frac{R_\oplus}{R_\oplus + h} \right) \cos \varepsilon_{min} \tag{5}$$

where η is referred to as the *nadir angle* between the satellite nadir and the line-of-view to target. Eqs. (3)-(4) estimate that a satellite will be in range of contact at a maximum distance of $1518.37\ km$ to a target within the *swath width* of $2\lambda_{max}$.

Figure 4 shows the *coverage percentage (PC%)* for a series of inclination values against latitude [4]. Our goal is to assess the coverage performance for the *i50, FRO,* and *SSO* designs represented by the dash-dotted line according to the orbit inclination. Observed advantages and disadvantages are:

1. the coverage requirement over the Brazilian and South American territory is met as both *i50, FRO,* and *SSO* designs lie within the region constrained by the dotted and dashed horizontal lines with $CP\% > 0$;
2. non-polar, inclined orbits, such as *i50* and *FRO,* designs provide more $CP\%$ compared to the *SSO* orbits, yet coverage degrades at very high latitudes;
3. polar orbits, such as *SSO* design, can provide global coverage, yet coverage degrades at low latitudes.

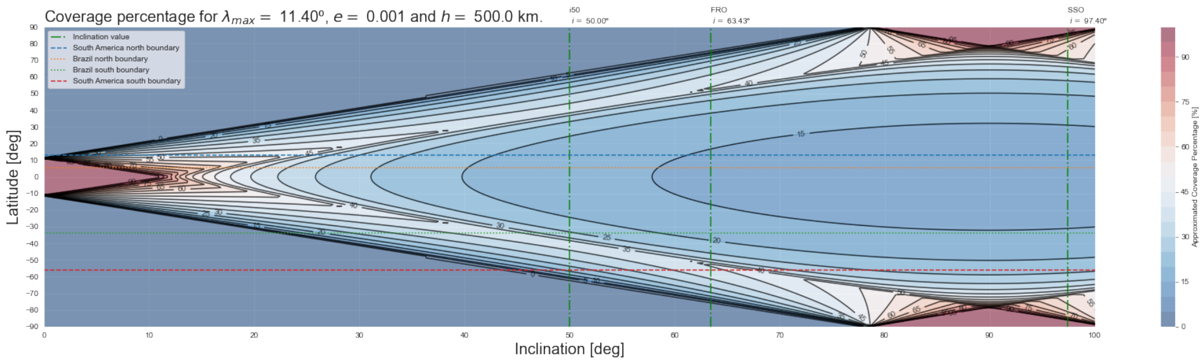

Figure 4: Approximated coverage percentage for a range of inclination values.

Next, we present simulation results for several constellation designs.

2.3. Simulations Results

In this section, we discuss the simulation results for different constellation designs (*cf.* Figure 3) and scenarios considering some locations of interest across the South American territory, as given in Table 3 and Figure 5. Simulations were all run using STK® for a time span from *01 January 2022 01:00:00.0 UTCG* to *30 April 2022 23:59:59.0 UTCG*. Next, we compare the performance of our constellation designs in terms of four figures of merit: *(i.) satellite availability, (ii.) satellite time-in-view, (iii.) coverage gap,* and *(iv.) timing consistency.*

Table 3: Examples of reference locations.

Location	Country	Latitude	Longitude
Location 1	Brazil	06.041 S	50.177 W
Location 2	Peru	10.215 S	76.379 W
Location 3	Brazil (off-shore)	21.238 S	39.963 W
Location 4	Argentina	48.383 S	68.264 W

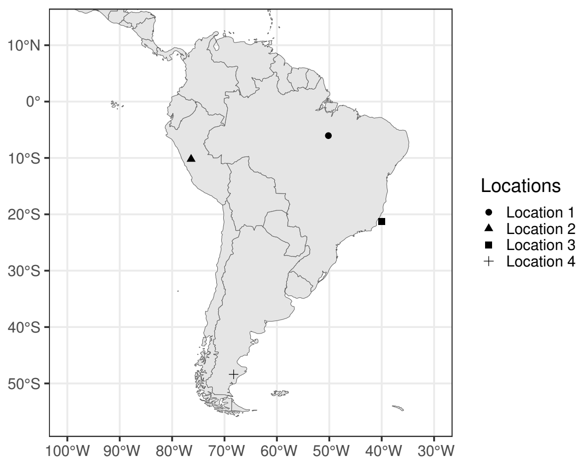

Figure 5: South America view and reference locations.

2.3.1. Satellite availability assessment

We begin by assessing the satellites daily availability, *i.e.*, the number of contacts over a target location. Figure 6 shows the averaged contact count per week day for each SARA (*i.e.*, *SARA-01, 02, ..., 05*) over the target locations (by rows) for each constellation design (by columns). We can observe that all SARAs accomplished a contact pass, in average, more than twice a day for all designs. Also, we can see that all designs accounts more contact passes at very high latitudes, such as location 4, and low-inclination designs, such as *i50* and *FRO,* are more likely to account more contacts than polar-orbit-based designs, as *SSO,* for most scenarios.

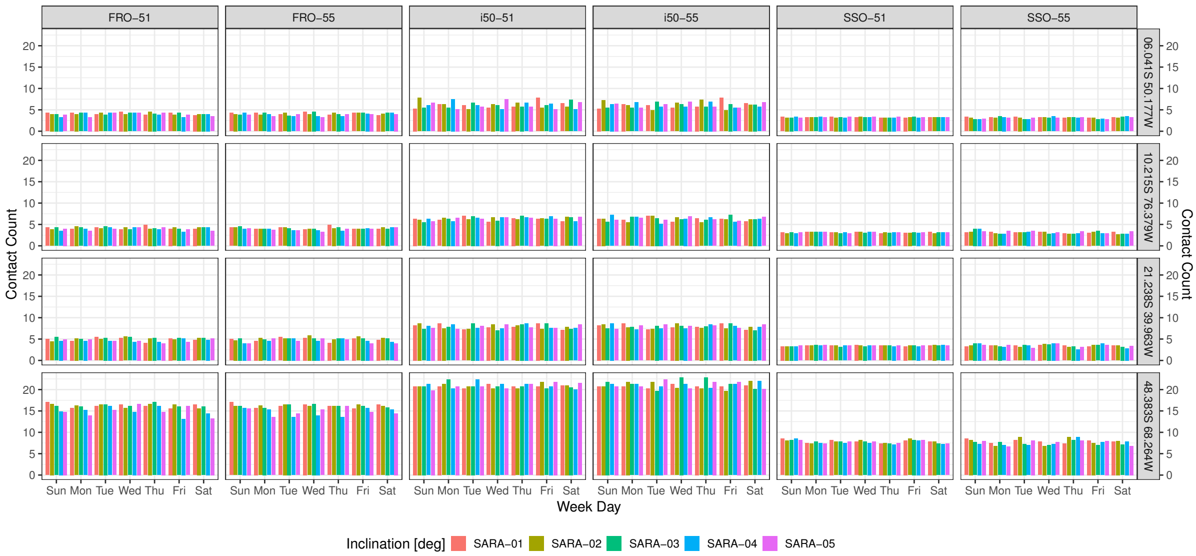

Figure 6: Overall number of contact passes breakdown.

2.3.2. Satellite time-in-view and coverage gap assessment

Time-in-view refers to the time within which a target on the ground is seen by a satellite above the minimum elevation angle, *i.e.*, $\varepsilon_{sat} > \varepsilon_{min}$. Whenever the satellite is out of range, the time to next contact is accounted as a gap coverage. Figures 7 and 8 compare *time-in-view* and *coverage gap* duration for all constellation designs over our target locations (*cf.* Table 3). Figure 7 shows that all proposed designs provided a mean time-in-view above 4 minutes. According to our designs (*cf.* Figure 3), those of higher altitudes provide longer time-in-view exposures. As for coverage gaps, in Figure 8, we can compare coverage performance and degradation. As discussed in Section §2.2, coverage degrades for higher inclination over lower latitudes.

2.3.3. Timing consistency assessment

Timing consistency here refers to the regular availability of the satellites every day. Taking the time-in-view peak hour as reference, *i.e.*, when the satellite is at the minimum distance from the target location, Figure 9 shows the time of contact for each SARA over *Location 1* (*cf.* Table 3), for each design inclination and configuration. In contrast to the results for the previous figures of merit, here we can note that SSO-based constellations are more consistent compared to the other designs. Because of greater $\Delta\Omega$ induced by lower inclinations, satellites will be in view in different times each day. Especially for the 5/1 configuration, this can pose disadvantages to time-sensitive service. Another aspect to note is the impact of the configuration. While the 5/5-based constellations feature better distribution during the day, the 5/1-based constellations rather concentrates contacts during short time windows of the day. The

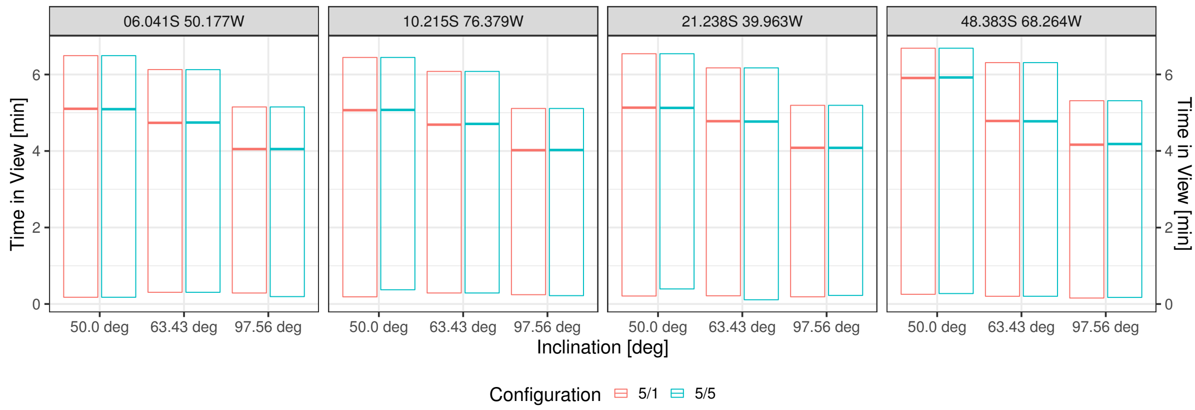

Figure 7: Overall comparison of time-in-view over locations.

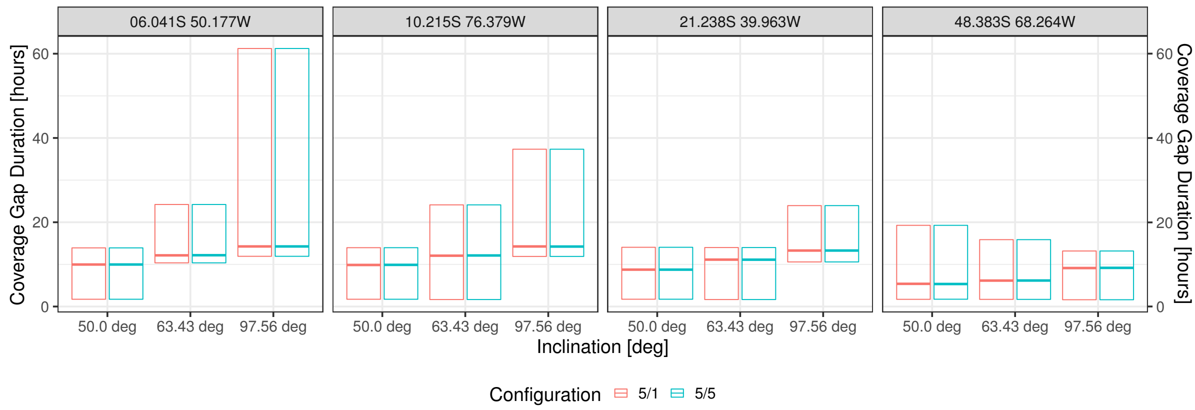

Figure 8: Overall comparison of coverage gap duration over locations.

latter, however, especially for the *SSO* design, may grant robustness to the service provided. That is, in case of a satellite loss, service can still be provided by the other satellites. Also, when considering the scalability of the constellation, we identify that those uncovered time windows could be mitigated as more fleet of satellites are being added to the constellation in complementary orbital planes.

3. System Architecture for SARA

The proposed SARA Constellation is made up of five nanosatellites dedicated to providing IoT/M2M connectivity for agriculture operations and remote area monitoring. Essentially, the constellation will receive telemetry from M2M terrestrial networks, delivering it to the end-users via the internet, enabling continuous monitoring and rapid response in critical scenarios. The individual satellites and the constellation architecture are under development following the requirements shown in Table 4.

3.1. Satellite payload

Our system design considers a multifunctional constellation for data telecommuncations. That is, in order to leverage the full potential of a LEO constellation, SARA integrates multiple payloads as described in Table 5.

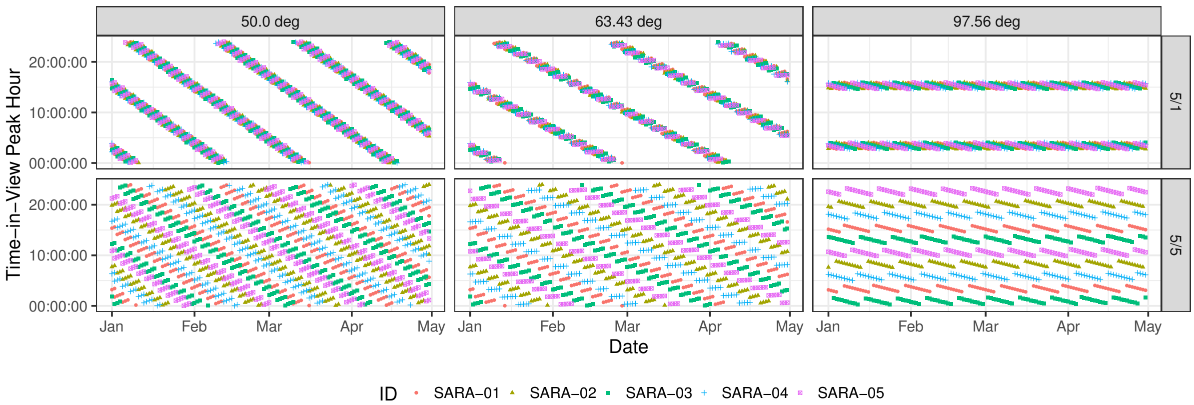

Figure 9: Daily time-in-View peak hour over Location 1.

Table 4: Top-level mission requirements for SARA Constellation.

Functional	Performance	A fleet of 5 nanosatellites of type 6U; Capacity of multi-access for IoT devices.
	Coverage	Daily access windows; Brazilian and South American territory.
	Responsivity	*Store & Dump.*
	Payload	IoT and vehicle monitoring.
Operational	Life time	<5 years per satellite.
	Availability	Minimum of two accesses daily for all location.
	Survivability	LEO qualified; Collision-free; Corrective maneuvering.
	Payload data transmission	Transmission to ground stations.
	Throughput	Packages of up to 1 MB
	Targets	IoT/M2M devices, data collection platforms, transponders.

3.2. Satellite bus

The SARA Constellation service module is COTS-based, designed to accommodate a state-of-the-art ADCS, a high-capacity AI-enabled internal storage system, a high-performance OBDH, and a micro propulsion system to enable small orbit corrections and deorbiting at the end of life. Table 6 describes the overview of the expected bus for SARA.

4. Conclusion

We have introduced the SARA Constellation under development to provide data telecommunication service in remote areas, focusing on the Brazilian and South American territory. Our proposed constellation considers an initial fleet of 5 nanosatellites 6U standard. We have investigated several constellation designs assuming the Walker Delta Pattern framework, a range of altitudes and inclinations. Coverage performance of the proposed designs over four target locations across the South American territory are then compared in terms of different figures of merit. In some aspects, such as satellite availability and gap coverage, non-polar-orbit-based designs presented better performance than the polar-orbit-based designs. However, for daily timing consistency, polar-orbit-based designs presented better performance. As for the system architecture for SARA Constellation, we have presented a description of the satellites characteristics.

Table 5: Payload for SARA Constellation.

Service	RF band	Performance
IoT/M2M	Tx/Rx: S band	1.0–100.0 Mbps
	Tx: X band (TBD)	100.0–200.0 Mbps
Vehicle Monitoring	Rx: UHF band	9.6–38.4 kbps

Table 6: Bus description for SARA Constellation.

Subsystems		Specifications
ADCS		
	Objective:	Active 3-axis stabilization and control.
	Attitude control:	3-axis reaction wheels and 3-axis magnetorquers suite;
	Attitude determination:	3-axis Gyroscope, Star-tracker, Sun sensors, Magnetometers suite.
Propulsion		Low-thrust propulsion for small orbit corrections and end-of-life deorbiting.
OBDH		High performance onboard computer and massive data storage.
TMTC		
	Modules:	UHF-band primary comms. and S-band secondary comms.
	Antenas:	Deployable UHF antennas and S-band patch antennas.
Structure		6U standard equipped with deployable solar panels.
Thermal control		Passive control.
		EPS-integrated active monitoring and control.
Power		
	Primary:	Deployable solar panels;
		Minimum of 10 W.
	Secondary:	Li-ion batteries;
		Minimum capacity: 1 Ah.
	PCDU:	Regulated/non-regulated bus;
		MPPT control;
		Parallel recharge;

Acknowledgments

This work is partially supported by FAPESP grant no. 2020/05196-4, and CNPq grant no. 424198/2021-5.

References

[1] Z. Yoon, W. Frese, K. Briess, Design and implementation of a narrow-band intersatellite network with limited onboard resources for IoT, Sensors 19 (2019) 4212.
[2] Z. Qu, G. Zhang, H. Cao, J. Xie, LEO satellite constellation for internet of things, IEEE Access 5 (2017) 18391–18401.
[3] J. J. Davis, D. Mortari, Reducing walker, flower, and streets-of-coverage constellations to a single constellation design framework, Advances in the Astronautical Sciences (2012).
[4] J. R. Wertz, W. J. Larson (Eds.), Space Mission Analysis and Design, Microcosmo Press & Kluwer Acaemic Publishers, 3rd edition, 1999.
[5] S. Huang, C. Colombo, F. Bernelli-Zazzera, Multi-criteria design of continuous global coverage walker and street-of-coverage constellations through property assessment, Acta Astronautica 188 (2021) 151–170.
[6] H. D. Curtis, Orbital Mechanics for Engineering Students, Butterworth-Heinemann, Oxford, 3rd edition, 2014.

13

Session 13 - Technology Development for Space

Design and implementation of DC-DC converters for CubeSat in Simulink

Germain Rosadio Vega[a], **Kiara Rodriguez Bautista**[b], **Sheyla Claribel Lozano Burga**[c], **Abad Antialon John Haile**[d], **Omar Enrique Blas Morales**[e]

[a]*National University of Engineering, 15307, +51997813640, grosadiov@uni.pe*
[b]*National University of Engineering, 15018, +51924986997, krodriguezb@uni.pe*
[c]*National University of Engineering, 15018, +51999220421, slozanob@uni.pe*
[d]*National University of Engineering, 15082, +51931274097, john.abad.a@uni.pe*
[e]*National University of Engineering, 15333, +51927966284, oblasm@uni.pe*

Keywords: *CubeSat, EPS, DC-DC Converter, Parameterization*

The present work focuses on the design and simulation of the DC-DC converters used in an Electric Power System (EPS) of a CubeSat through Simulink. The design begins with the sizing of the converter with a set of equations that determine thresholds for the passive components, and whose optimization is studied quantitatively by parameterizing the capacitance and inductance based on the thresholds. The design and parameterization are simulated in LTspice where it is shown that capacitance has an inverse influence on the ripple level, while it slightly increases the efficiency value and has no effect on the overshoot, while inductance increases the efficiency and decreases the overshoot, but does not affect the ripple level. The choice of capacitance and inductance based on the analysis of the characteristic parameters allows an optimization of the boost converter in terms of the ripple level and overshoot of the resulting voltage, and of the working efficiency. We can also get the efficiency curve by parameterizing R and implement it in the DC-DC Converter block in Simulink with an EPS model.

1. Introduction

A CubeSat is a satellite whose manufacturing standard is 1U, which represents a cube with an edge of 10 cm and a mass of up to 1.33 kilograms [1]. Its conceptual development began for the first time in 1999 and was developed for experimental and educational purposes for the university community [2]. The main advantages of a CubeSat are its rapid development, lower manufacturing cost and positioning in orbit. In addition, depending on the start-up period of the project, the needs may vary and this type of satellites are flexible to technology upgrades.

Due to the small size of this satellite, one of the main challenges in its manufacture lies in energy self-sufficiency, that is, having the capacity to generate, store and distribute the electrical energy needed by its components. To meet this objective, it is necessary to design an Electrical Power System (EPS) that can perform all the above mentioned functions; a common EPS is composed of the following subsystems: photovoltaic cells, rechargeable batteries, and a Power Distribution and Conditioning Unit

(PCDU). The photovoltaic cells have the function of supplying electrical energy to the satellite during its orbit when there is incidence of sunlight to charge the battery and keep the other modules operational, they are the main source of energy used in the CubeSat missions [3]. Batteries are intended to store excess energy from the cells and use it when the energy required exceeds the energy they supply, they are considered secondary energy sources and are classified into primary (non-rechargeable) and secondary (rechargeable) batteries. Finally, the PCDU ensures a proper and reliable electrical connection between the power sources and the other modules of the satellite, consisting of a microcontroller, DC-DC converters, a power protection system, sensors, etc.

For proper operation, the EPS of a CubeSat must power an On-board computer, an Automated data control system intended to control the satellite's orientation with respect to the earth, communication receiver and transmitter and payloads as needed.

2. EPS Considerations

2.1. Orbit considered

The importance of taking into account the characteristics of the CubeSat orbit lies in the fact that it mainly influences the irradiation to which the nanosatellite faces will be exposed as well as the external temperature variations it will experience during its orbit; these two aspects affect the performance of the photovoltaic cells and must therefore be considered.

The CubeSat orbit characteristics are considered based on the available data from the MySat-1 nano-satellite project developed by Khalifa University [4, 5, 6], these are summarized in Table 1, while the type of CubeSat motion and orientation is considered according to the nadir pointing scenario [7], which is depicted in Figure 1.

Table 1: MySat-1 orbit characteristics [6]

Parameter	Value
Altitude	450 km
Orbital period (P)	96 min
Illumination time in 1P	60.02 min
Time of darkness in 1P	35.98 min
Start of illumination	727 s
Inclination	51.6°

2.2. CubeSat module power consumption

The CubeSat studied includes the following modules: On-Board Computer (OBC), EPS, Communication Receiver (COM-RX), Communication Transmitter (COM-TX), Attitude Determination and Control System (ADCS), and Payloads. Each of these systems has a certain power consumption and minimum operating voltage in a normal mode and safe mode, these are presented in Table. 2. Here it is visualized that in normal mode all modules will be operating regularly, while in safe mode the ADCS and Payload are turned off and the COM-TX module is on for less time, i.e., the satellite transmission time decreases.

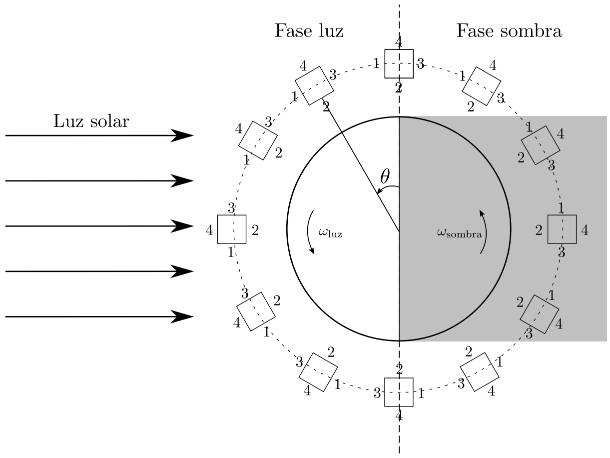

Figure 1: CubeSat path during orbit.

Table 2: CubeSat Power Consumption in normal and safe mode

Module	Power (mW)	Voltage (V)	$t_{ON,normal}$	$t_{ON,safe}$
OBC	400	3.3	1	1
EPS	160	3.3	1	1
COM-RX	480	7.4	1	1
COM-TX	4000	7.4	0.176	0.0667
Camera-Idle	500	5	0.052	—
Camera-Active	1000	5	0.0104	—
ADCS-idle	175	5	0.825	—
ADCS-Active	1200	5	0.176	—

t_{ON}: On-time normalized to orbital period (96 min).

In order to build a power consumption profile of the systems it is also necessary to know their operating modes, such as the instants in which they are activated, and the duration of operation, with this it is possible to build a consumption profile of each system for 1P. The operating time of the systems studied are also presented in Table 2 where the time is normalized with respect to the duration of 1P, and the starting instants are described below:

- The OBC, EPS and COM-RX systems are kept ON during the entire orbit period.
- The Payload system, which is a camera, starts in the OFF state and turns on in idle mode 5 min before the onset of the light phase, where it switches to active mode taking images during 1 min.
- The COM-TX system is turned on right after the Payload finishes operating to transmit its data to an earth station during 16.9 min.
- The ADCS system starts in idle state and at the beginning of the light phase changes to the active state but not in a continuous way, but in the form of pulses, this because it must control the orientation continuously during the light phase if you want a face is fixed to the ground, the total active time is 16.9 min.

The modes of operation of the systems just described result in a total consumed power as in Figure 2, where the gray region represents that the CubeSat is in shadow phase, and in the yellow region in light phase, in addition the total power consumption in normal and safety consumption mode during 1P is presented.

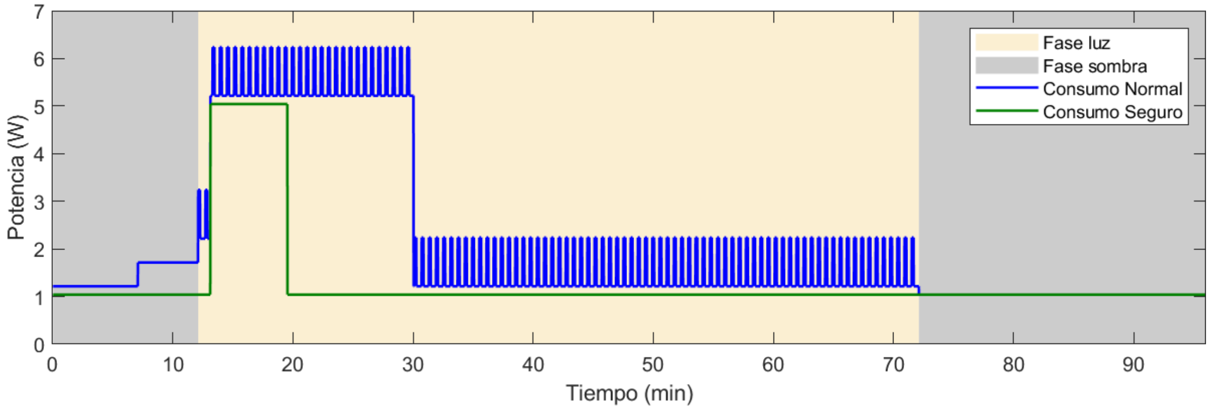

Figure 2: Total power consumption of the loads. In normal mode: P_{min}=1.04 W, P_{max}=6.24 W. In safe mode: P_{min}=1.04 W, P_{max}=5.04 W

3. PCDU Simulink model

The PCDU design is the most customized of the other EPS subsystems since the elements it implements will depend greatly on the mission and requirements, in the work done the PCDU (Figure 3) consists of three DC-DC converters that will adapt the voltage resulting from the cell-battery array to that required by the modules according to the Table 2. It also incorporates a block that will act as a microcontroller evaluating multiple processes during the simulation, this is mainly done by a state diagram.

It is possible to design and simulate a converter such as the boost in Figure 3b in Simulink; however it becomes infeasible to implement in other designs that require very large simulation time because the operating frequency is on the order of kHz (10 kHz [4]). However, Simspace has the block presented in Figure **??** that simulates a DC-DC converter that can be controlled by a voltage signal that will indicate the desired voltage at the output, 5.0 V in the Figure 3b, this block also allows to characterize it with an efficiency curve of a converter, like the one shown in Figure 3c.

The MICRO block contains the state diagram shown in Figure 3d, which has 5 modes of operation of the satellite:

Safety: Safety mode, aims to prevent the battery from being fully discharged. Sending safety mode signal for OBC when SOC decreases from 40%, commanding to start safety consumption.

Batery_dch: Battery discharge mode occurs when the power consumed by the satellite is greater than the power supplied by the cell array, thus the batteries assist the cells in supplying power to the satellite.

Normal_Eclipse: Nominal mode of operation of the EPS when it is in eclipse, where the batteries discharge to supply the satellite's power demand.

Normal_Sol: Nominal mode of operation of the EPS when it is being illuminated by the Sun, where the batteries are recharged and the solar panels supply power to the satellite.

Batery_full: Full battery charge mode occurs when the satellite is being illuminated by the Sun, the battery is at maximum charge (100%) and the cells are supplying power to the satellite.

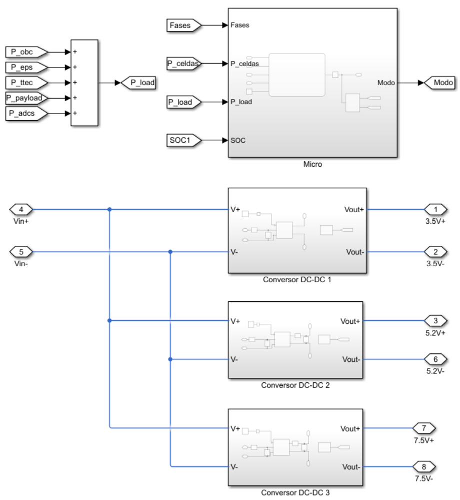

(a) Components of the PCDU.

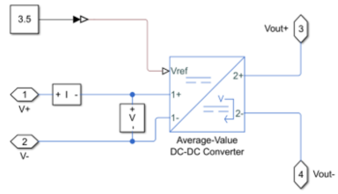

(b) DC-DC converter block

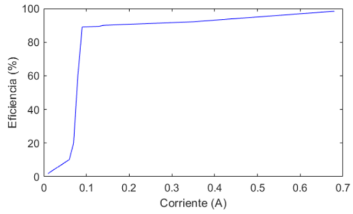

(c) Converter Default Efficiency Curve.

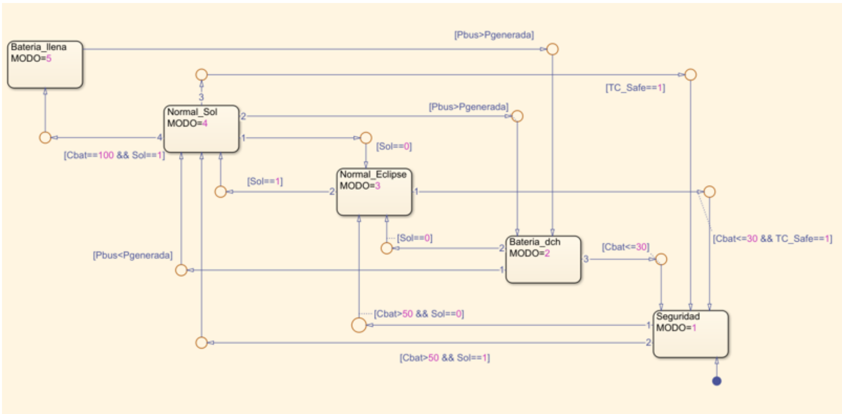

(d) State diagram implemented as microcontroller.

Figure 3: Simulink design of the PCDU implemented in the EPS model.

4. DC-DC Converter design in LTspice

In this section we will describe the design of the DC-DC converters that will adapt the voltage delivered by the batteries to the modules according to the voltage level required by Table 2. These modules will behave as loads with a resistance and current consumption defined from their consumed power and operating voltage, relationship given by

$$R = \frac{V^2}{P} \qquad\qquad I = \frac{P}{V}$$

Table 3: Electrical parameters of the modules

		Active			Idle		
Module	V (V)	P (W)	I (A)	R (Ω)	P (W)	I (A)	R (Ω)
OBC	3.5	0.4	0.1143	30.63			
Payload	5	1.0	0.2000	25.00	0.500	0.1000	50.00
ADCS	5	1.2	0.2400	20.83	0.175	0.0350	142.86
TTEC	7.4	4.0	0.5405	13.69	0.480	0.0649	114.08

4.1. Boost Converter Sizing

The sizing of the converter consists of determining the parameters (duty cycle and switching frequency) and passive components (capacitor, inductor and resistor) that will produce the desired voltage level and good performance. As the resistor is the load of the module, it is not taken into account in the sizing, but the capacitance and inductor are.

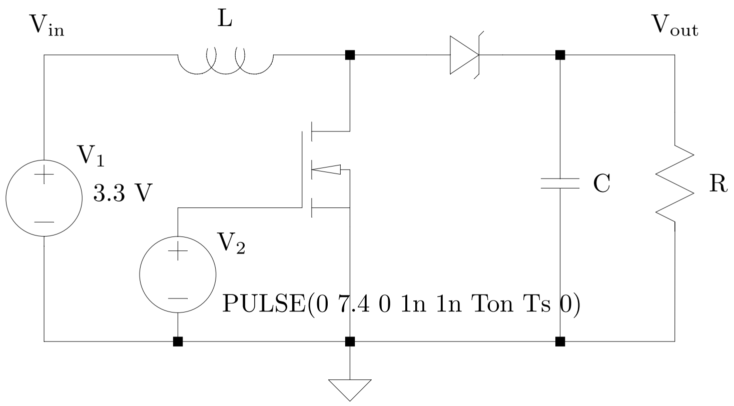

Figure 4: Boost Converter design.

4.1.1. Inductor sizing

Knowing the parameters of the converter, it is possible to determine the optimal and ideal value of L for the converter to work above the continuous and discontinuous driving limit, by means of the Equation (1).

$$L_{min} = \frac{D \cdot R \cdot (1-D)^2}{2 \cdot f_s} \tag{1}$$

4.1.2. Capacitor sizing

In consequence to the output voltage power variations of the boost converter, a design criterion is used, which mentions that only a ripple voltage of up to 2% of the nominal output voltage should be allowed. Equation (2) represents a linear approximation of discharge of the output capacitor with a resistive load of R value, during the state in which the switch is in working position.

$$C_{min} = \frac{100 \cdot D \cdot T_s}{R} \tag{2}$$

Then with Equations (1) and (2) it is possible to calculate the minimum capacitance and inductance in the Boost converter design if used with the equivalent resistances of the modules given in the Table 3, this result together with the required duty cycle, and other parameters, are summarized in the following Table.

Table 4: Boost converter design parameters

	Vd (V)	Vo (V)	R (Ω)	D (%)	Ton (μs)	Cmin (μF)	Lmin (μH)
1	3.3	3.3	30.625	19.86	1.986	6.619	19.131
2	3.3	5.0	25.00	43.90	4.39	17.560	17.270
3	3.3	7.4	13.69	62.09	6.209	45.358	6.107

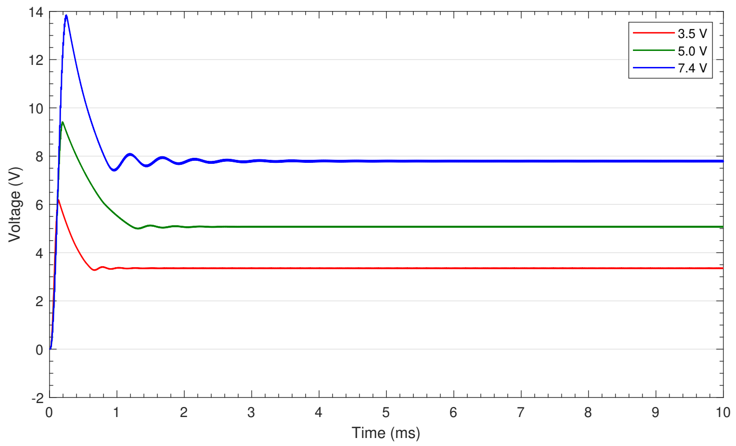

Figure 5: Voltage converters for 3 voltage levels.

Table 5: Theoretical design characteristic parameters

	V_{avg}	T_r (μs)	OS (%)	T_s (ms)	r (%)	Eff (%)
1	3.352	41.00	84.67	0.63	0.41	74.92
2	5.072	61.40	85.64	1.10	0.47	81.97
3	7.796	81.13	77.65	1.62	0.86	89.95

4.2. Optimization by parameterization

The Equations (1) and (2) give us a whole set of values that, applied on pasive components, give us the desired voltage, but we can also optimize the voltage signal in terms of ripple, settling time, overshoot, and others. An optimization method has been proposed by [8, 9] where a variation of the RCL components of the converter circuit is performed in order to find the optimum values in the design. The effect of these components on the converter's performance, in terms of the voltage, can be seen in what we will call characteristic parameters, which include: rise time (Tr), overshoot percent (OS), settling time (Ts), ripple percent (r), and conversion efficiency (η). The effect of RCL values will affect one or more of these characteristic parameters, which will be analyzed to find the appropriate values for our EPS.

As a representative example, the parameterization of the Boost 3.3V to 5.5V converter corresponding to the Payload module is shown, starting from the design proposed in the previous section with the formulas used. In the parameterization of C and L values are swept around those chosen and greater than their minimum values obtained, C values are used between 20 µF to 110 µF with a step of 10 µF and L values between 20 µF to 200 µF with a step of 10 µF. The resulting simulation will then give us the voltage V_{out} maintained by the converter for each case of C and L respectively, these are shown in the Figure 6b. Here it can be noted the dependence of some characteristic parameters on C or L, these can be deduced quantitatively if we extract the characteristic parameters from the voltage curves shown. In this case since the settling time and rise time are in the order of ms and µs, these parameters can be ignored. The parameters that are important in this analysis are overshoot, ripple, and efficiency; in varying C, no change in overshoot is observed, while increasing C there is a slight increase in efficiency and a better ripple is obtained (ripple decreases). Increasing L also shows a slight decrease in overshoot and an increase in efficiency while the ripple remains unchanged. From this we can deduce that overshoot depends only inversely on L, while ripple depends only inversely on C, and efficiency depends directly on both variables, with L being the most prominent.

It is clear that a high value of capacitance C generates a better response of the converter voltage, so a capacitor of 120 µF is chosen, a value that maximizes efficiency and minimizes ripple. As for the inductor, the efficiency remains almost constant from 120 while the overshoot decreases as L increases, an inductor of 150 can be chosen.

The same process can be performed to the Boost converters corresponding to the OBC and TTEC module, where the parameterization values will depend on the one obtained in the sizing. The values chosen for the final design are a capacitance of 120 µF for the three designs, while an inductance of 200 µH, 150 µH and 10 µH is obtained for the converters 3.5 V, 5.0 V and 7.4 V respectively. With the components selected the characteristic parameters of the new design take the values presented in the Table 6.

Table 6: Characteristic parameters of the final design

	V_{avg}	T_r (µs)	OS (%)	T_s (ms)	r (%)	Eff (%)
1	3.366	206.28	85.49	3.14	0.06	78.80
2	5.087	257.21	83.41	4.44	0.40	85.70
3	7.798	99.62	77.10	1.67	0.38	94.99

The main highlight of these results is the increase in efficiency achieved with the new parameters, reaching an increase between 4% and 5% of the values previously presented in the Table 5. It is also worth mentioning the change in the characteristic parameters, the most notorious is the increase in the rise and settling times, since those obtained are approximately 4 times larger; however, as mentioned, these are not relevant in the performance as long as they are maintained in an almost instantaneous time magnitude. As for the overshoot, no significant changes are obtained with the new parameters, while the ripple level is further decreased, which reproduces a finer voltage output.

It is also possible to perform a parameterization of R whose effects are mainly manifested in the ripple and overshoot [8], but in this case such a process would be

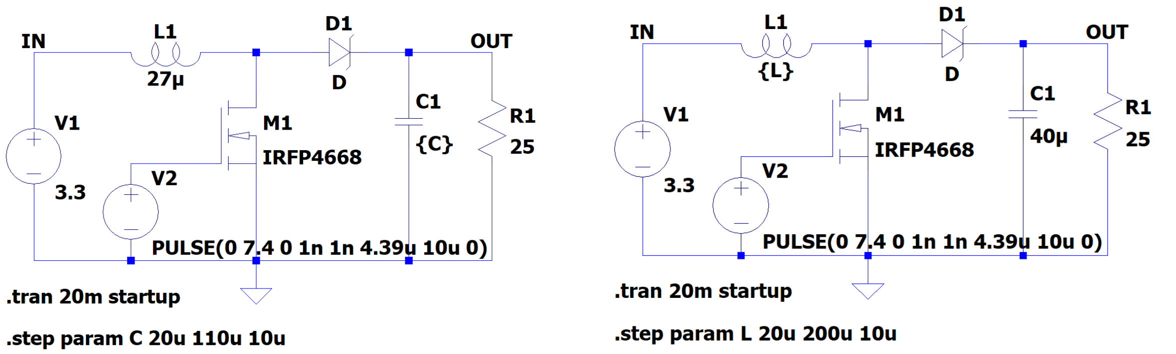

(a) LTspice designs for C and L parameterization.

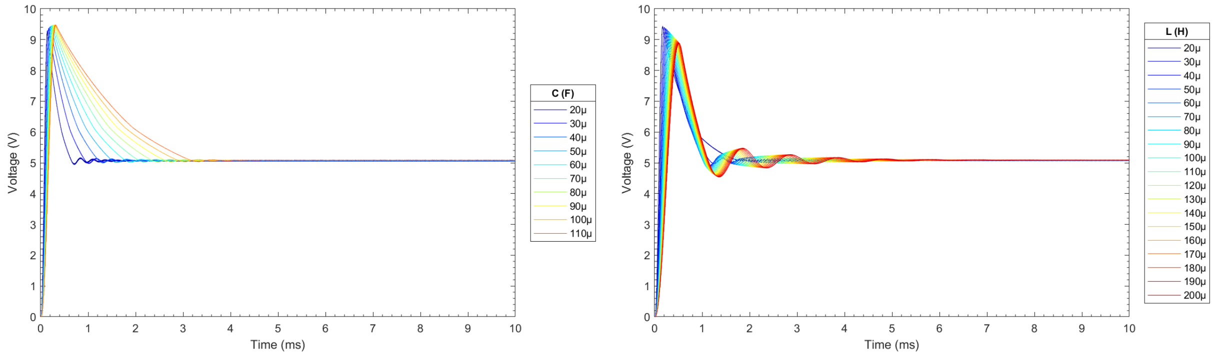

(b) C and L parameterization response voltages.

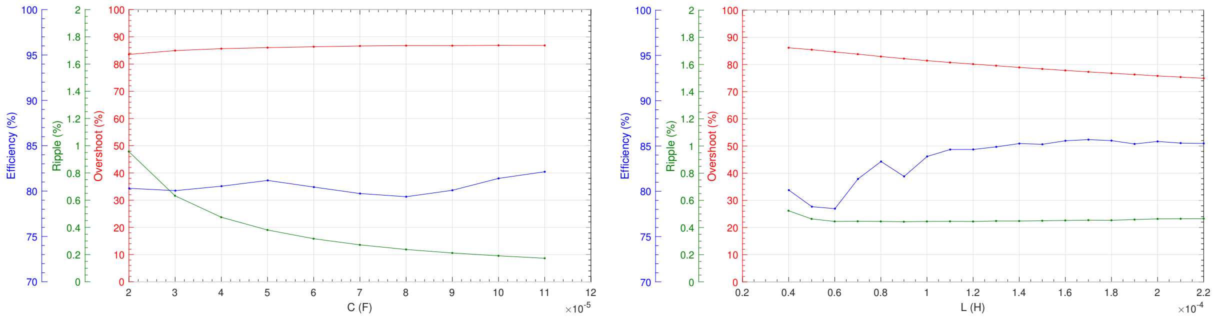

(c) Characteristic parameters of the parameterization of C and L.

Figure 6: Parameterization of capacitance C and inductance L in the Boost converter $3.3\,\mathrm{V}$ **to** $5.0\,\mathrm{V}$**.**

unnecessary in terms of converter design since the resistance is defined by the load according to the values presented in Table 3. However, the parameterization of R must be done to know the efficiency values at certain current consumptions, i.e., to obtain the efficiency curve of the DC-DC converter. For this purpose, the efficiency of the converter could be probed for a wide range of R values, but performing such a task in LTspice would be computationally expensive and perhaps unnecessary, so instead only the values of R that the model will require can be probed, such as the values presented in the Table 3.

5. EPS simulation results

Here we present the results related to the DC-DC converters designed in an EPS model in Simulink whose PCDU design is the one described in Figure 3, which includes

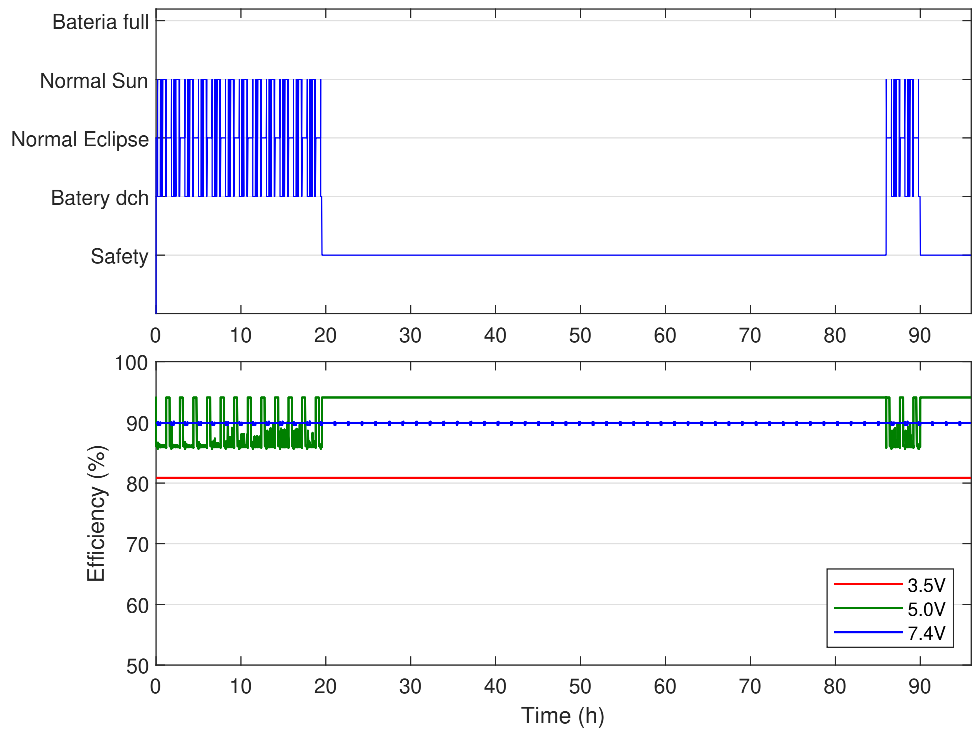

Figure 7: DC-DC converters efficiency during the simulation for 60P.

three Boost converters 3.3 V to 3.5 V, 5.0 V and 7.4 V which were characterized with the efficiency curve obtained from the parameterization in R, and with the 5 operational modes which indicate the state in which the EPS is operating. The output of the state diagram shows the transition between these modes, but the relevant ones for the converters are the safe mode and normal mode (any other mode) because when the safe mode is activated (SOC less than 40%) the Payload, the ADCS, and the usage time of the COM-TX module is reduced, this causes a lower power consumption and therefore another working point in the efficiency curve of the converter, when the safe mode is deactivated (SOC returns to 50%), it returns to the normal power consumption.

The Figure 7 shows the transition between the EPS operational modes and the efficiency values reached by each of the DC-DC converters. In the first 20 h it is observed that the modes oscillate in three types that present a normal power consumption, and after this time the safe mode is activated until almost 85 h of simulation. In all the time lapse we notice that the 3.5 V converter does not present any alteration because the OBC module works continuously regardless of the operating mode that is activated. On the other hand, in the first time lapse we observe fluctuations in the efficiency of the 5.0 V converter, this because the ADCS are maintained in a periodic operation as indicated in the Figure 2, while in the safe mode time lapse, where their corresponding modules (ADCS and Payload) are turned off, a uniform behavior is evidenced because the implemented efficiency curve does not consider the null consumptions (since it would imply an infinite resistance). Finally, it is observed that the 7.4 V converter presents an almost uniform efficiency, with periodic unevenness corresponding to the operation of the COM-TX module.

6. Conclusions

The proposed methodology for the design of a Boost converter starts from the sizing of its components C and L with Equations (1) y (2). From the resulting simulation in LTspice, the voltage maintained by the converter can be obtained as shown in the Figure 5, from which the characteristic parameters of this signal, such as overshoot, time constants, ripple, and efficiency, can be extracted. If required, it is possible to optimize the design by parameterizing C and L where its effect on the output voltage signal will be observed. By extracting the characteristic parameters of the voltage signals obtained from the parameterization we will have a quantitative result of this dependence, which is used to probe the values of C and L that make the converter response optimal, such as efficiency. If the values of C and L are properly chosen, we will obtain an optimal design of the converter, which will take advantage of the energy supplied by the EPS, improving its efficiency as presented in Table 6.

In addition, a parameterization is performed in R which is used only to get the efficiency curve as a function of the output current and which is implemented in the DC-DC converter blocks of Simulink. This last step is the most important since it allows to transfer the behavior of the converter designed in LTspice to the EPS model in Simulink by means of the efficiency curve.

The parameterization process can also be employed if it is desired to decrease other parameters such as overshoot or even the time constants if they are taken into account in the analysis. In addition, the implementation of the efficiency curve in Simulink allows performing the simulation of the DC-DC converter for very large time periods, which would be unfeasible if the design is based on a switching frequency (originated by the MOSFET) due to the large difference in time scales.

References

[1] S. W. J. Puig-Suari, R. Coelho, The cubesat design specification rev. 12, CubeSat program, Cal. Poly SLO (2009).

[2] N. C. L. Initiative., Basic concepts and processes for first-time cubesat developers, https://www.nasa.gov/sites/default/files/atoms/files/nasa csli cubesat 101 508.pdf (2017).

[3] B. Yost, S. Weston, G. Benavides, F. Krage, J. Hines, S. Mauro, S. Etchey, K. O'Neill, B. Braun, State-of-the-art small spacecraft technology (2021).

[4] S. Acharya, F. Alshehhi, A. Tsoupos, O. Khan, M. Elmoursi, V. Khadkikar, H. Zeineldin, M. A. Hosani, Modeling and design of electrical power subsystem for cubesats, IEEE, 2019, pp. 1–6.

[5] A. Edpuganti, V. Khadkikar, M. S. Elmoursi, H. Zeineldin, M. A. Hosani, A novel eps architecture for 1u/2u cubesats with enhanced fault-tolerant capability, IEEE, 2020, pp. 1–6.

[6] A. Edpuganti, V. Khadkikar, H. Zeineldin, M. S. E. Moursi, M. A. Hosani, Comparison of peak power tracking based electric power system architectures for cubesats, IEEE Transactions on Industry Applications 57 (2021) 2758–2768.

[7] S. Sanchez-Sanjuan, J. Gonzalez-Llorente, R. Hurtado-Velasco, Comparison of the incident solar energy and battery storage in a 3u cubesat satellite for different orientation scenarios, Journal of Aerospace Technology and Management 8 (2016) 91–102.

[8] D. Naveda-Castillo, L. Adanaque-Infante, Characterization of dc converters for energy power systems on cubesats, in: 2020 IEEE XXVII International Conference on Electronics, Electrical Engineering and Computing (INTERCON), IEEE, pp. 1–4.

[9] J. D. G. Llorente, R. H. Velasco, S. A. S. Sanjuán, D. O. R. Duarte, A. J. R. Vecino, Obtención de energía solar y uso eficiente en la orientación de pequeños satélites, Fondo de publicaciones Universidad Sergio Arboleda, 2016.

METHODOLOGY FOR DEVELOPING TT&C SUBSYSTEMS IN ACADEMIC CUBESATS

Daniel Curcio Lott Guimarães[(1)], **Ricardo Adriano**[(2)], **Maria Cecilia Pereira**[(3)]
[(1)] *DEMEC/UFMG, dlott@ufmg.br*
[(2)] *DEE/UFMG, rluiz@ufmg.br*
[(3)] *DEMEC/UFMG, cecilia@demec.ufmg.br*

Keywords: *TT&C, Power, Communication, Antennas, Telemetry*

PdQSat is the first academic satellite to be designed and built by the Federal University of Minas Gerais (UFMG). The design of the Telemetry, Tracking and Control (TT&C) subsystem is seen as a critical one, both under technical and educational points of view. The first because, on unmanned missions, a failure in this subsystem is catastrophic, and results in a premature end to the mission. The second because it simultaneously requires concepts from Aerospace, Electrical and Systems Engineering, which an engineering student from any of these specializations may not fully grasp.

In this context, this work aims not only to provide a set of low-level necessities (which are later formalized as requirements) that likely guarantee proper operation and integration of the TT&C subsystem, but also to document the methodology used to obtain these necessities and to present the basic concepts (and technical references) that govern the physics behind such a critical subsystem, so that students with different backgrounds can understand and design robust implementations of TT&C subsystems on an academic level.

This work mainly addresses the minimum power and transmission speed needed to completely transmit a payload during a communication window, exploring the impact that parameters from the selected hardware, satellite orbit, and attitude control can have on them. Later, simulations with typical CubeSat orbits (ISS and Sun-synchronous), and a sensibility analysis regarding alignment and tracking errors are performed before presenting a final set of necessities that encompasses all the discussed topics.

1. Introduction

The Federal University of Minas Gerais (UFMG) has a history of designing and building aircraft, but is only now starting to design its first spacecraft, the PdQSat. Being its first CubeSat, the university has not only to design each and every subsystem for the first time, but also to document the acquired know-how so that its future students can continue to develop CubeSats.

On an unmanned mission, the Telemetry, Tracking and Control (TT&C) subsystem is seen as critical, given that its failure inhibits the ability to send commands and retrieve telemetry and payload data, which results in a premature end to the mission. From an educational standpoint it is also a difficult subsystem to design. The main concepts needed to understand its operation are from Electrical Engineering, but its design is still heavily dictated by the challenges and particularities of space, which means that students from both Electrical and Aerospace backgrounds may not fully grasp the concepts needed without a dedicated resource to guide them.

Therefore, this work's objectives are to present the basic concepts and technical references needed to understand this subsystem, so that engineering students, regardless of background, can effectively discuss and design it; to obtain a set of necessities for proper operation and integration of the subsystem that will be used in PdQSat's Model-based Systems Engineering approach; and to document the methodology and tools used to obtain these necessities, so that future projects can benefit from them.

2. Theoretical approach

The theoretical approach is mainly based on Balanis [1], NASA [2], Beech et al. [3] and Zielinski [4] for the telecommunications definitions, and on Kuga et al. [5], Curtis [6] and Chobotov [7] for the orbital mechanics definitions.

2.1. Friis transmission equation

The Friis transmission equation provides the power ratio between two antennas in free space:

$$\frac{P_r}{P_t} = e_{cd,t} e_{cd,r} \left(\frac{\lambda}{4\pi r}\right)^2 D_t(\theta_t, \phi_t) D_r(\theta_r, \phi_r) \tag{1}$$

Where P is power, e_{cd} is the radiation efficiency, λ is the wavelength, r is the distance between antennas, D is the directivity, ϕ and θ are the polar and azimuthal view angles, and $\square_t$ and $\square_r$ denote coefficients from the transmitting and receiving antennas.

Equation 1 assumes antennas with matching impedance and polarizations in free space, with coefficients expressed in their dimensionless forms. A budget link equation can be obtained by converting the equation to Decibel, then isolating the received power:

$$P_{r,dB} = P_{t,dB} + G_{t,dB}(\theta_t, \phi_t) + G_{r,dB}(\theta_r, \phi_r) + 20 \log_{10} \left(\frac{\lambda}{4\pi r}\right) \tag{2}$$

Where G is the gain, which is the same as $e_{cd} \cdot D(\theta, \phi)$, and $\square_{dB}$ denote that a coefficient is expressed in Decibel. Equation 2 can be generically interpreted as:

$$P_{r,dB} = P_{t,dB} + Gains_{dB} - Losses_{dB} \tag{3}$$

All parameters from equations 1 and 2 are dependent on the system's selected components, with the exception of r, which is dependent on the space segment's trajectory.

2.2. Keplerian orbits

Given the typical missions of CubeSats, only closed orbits were considered, which, for the two-body problem, has an analytical solution given by:

$$\vec{r}_{pf} = a \cdot \begin{bmatrix} \cos(u) - e \\ \sin(u)\sqrt{1 - e^2} \\ 0 \end{bmatrix} \tag{4}$$

$$\sqrt{\frac{\mu}{a^3}}(t - t_0) = u - e \sin(u) \tag{5}$$

Where a is the orbit's semi-major axis, u is the eccentric anomaly, e is the eccentricity, μ is the standard gravitational parameter, t is time, and t_0 is the reference time at which u is 0°. Equation 4 provides the position in the perifocal coordinate system ($\vec{r}_{pf}$), which is then rotated to the inertial geocentric coordinate system ($\vec{r}$):

$$\vec{r}_{pf} = \begin{bmatrix} \cos(\Omega) & \sin(\Omega) & 0 \\ -\sin(\Omega) & \cos(\Omega) & 0 \\ 0 & 0 & 1 \end{bmatrix} \begin{bmatrix} 1 & 0 & 0 \\ 0 & \cos(i) & \sin(i) \\ 0 & -\sin(i) & \cos(i) \end{bmatrix} \begin{bmatrix} \cos(\omega) & \sin(\omega) & 0 \\ -\sin(\omega) & \cos(\omega) & 0 \\ 0 & 0 & 1 \end{bmatrix} \vec{r} \tag{6}$$

Where Ω is the orbit's longitude of the ascending node, i is the orbit's inclination, and ω is the orbit's argument of perigee.

3. Methodology

Since, at this stage of development, there are no system-level requirements to be flowed down, instead, the first step is to outline the system's problem statement:

> *The TT&C system shall be capable of transmitting the payload data to the ground segment for each communication window.*

Using the theoretical approach described in section 2, the problem statement is derived into high-level functional necessities:

1. The system shall transmit[1] the data with sufficient power to overcome the path losses to the ground segment;
2. The system shall transmit the data with sufficient speed to complete the transmission in a single communication window.

For each high-level necessity, an analytical formula or numerical method that represents its underlying physical phenomena is obtained. These are then used to flow the necessities down into low-level necessities that rationally prove the conformity of their higher-level pairs. Later, the low-level necessities are used to elaborate a candidate solution, which is formalized in terms of requirements.

4. Results

4.1. Values selected for simulation

Although the formulas and methods obtained in this section are generic, it is not possible plot them along every possible axis, therefore reasonable values were selected for the simulations based on state of the art hardware from NASA [2], NASA [8] and ISIS [9]. Table 1 presents these values.

The receiving antenna is based on ISIS [10], with a single $cos^n(\theta)$ lobe:

$$G_{r,dB}(\theta, \phi) = 15 + 10\log_{10}\left(\cos(\theta)^{\frac{\sqrt{1000}}{2}-1}\right) \tag{7}$$

The transmitting antenna is based on ISIS [11], with isotropic, bidirectional and cardioid components:

$$G_{t,dB}(\theta, \phi) = 5 + 10\log_{10}\left(0.0317 + 0.0727\cos(\theta)^6 + 0.8956\cos(\theta/2)^{8.9238}\right) \tag{8}$$

[1]The communication is bidirectional, and while the system shall also receive the data with sufficient power, the down-link is the critical condition since the space segment has power limitations.

Table 1: Selected values for simulation.

Power	Sensibility	Bit rate	Frequency	Gain	VSWR
30 dBm	−120 dBm	2400 bps	437 MHz	Equations 7 and 8	1.20 : 1

4.2. Geometrical parameters

Figure 1 presents the geometry of a typical communication operation between the ground and space segments, where R_e is the Earth's radius, r is the space segment's distance in the inertial geocentric coordinate system, and h is the space segment's elevation in the topocentric coordinate system, from which the space segment's distance in the topocentric coordinate system r_{tc} (link distance), the angle between ground and space segments in the inertial geocentric coordinate system ϕ_{gc}, and the angle between the space segment's nadir and the ground segment in the body-fixed coordinate system ϕ_{bf} (view angle of the transmitting antenna) can be calculated through equations 9, 10 and 11.

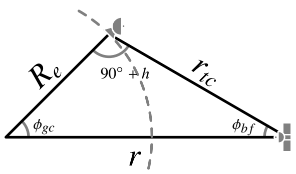

Figure 1: Geometry of a communication operation.

$$r_{tc}(r,h) = -R_e \sin(h) + \sqrt{r^2 - R_e^2 \cos^2(h)} \tag{9}$$

$$\phi_{gc}(r,h) = \cos^{-1}\left(\frac{R_e^2 + r^2 - r_{tc}(r,h)^2}{2R_e r}\right) \tag{10}$$

$$\phi_{bf}(r,h) = 90° - \phi_{gc}(r,h) - h \tag{11}$$

4.3. Minimum transmission power

From equation 2, using equation 9 to obtain the link distance, the minimum transmission power can be calculated to match the receiver sensibility. Figure 2 presents the transmission power envelope, with the solid line being the best case scenario with minimal distance ($h = 90°$), perfectly aligned antennas, and matching impedance and polarization, and the hatched area being the increase in power needed for the worst case scenario[2], with maximum distance, corresponding gain reduction from the view angle given by equation 11, as well as mismatching impedance.

4.4. Communication window

The communication window duration is obtained by simulating the orbit of the space segment, and the movement of the ground segment around the globe, then, for each instant, checking if the ground segment has line of sight of the space segment.

4.4.1. Circular equatorial orbits

For circular equatorial orbits, every communication window is identical, as the angular speeds of the ground and space segments are constant and aligned, which yields an analytical solution:

[2] Ignoring atmospheric losses and alignment errors.

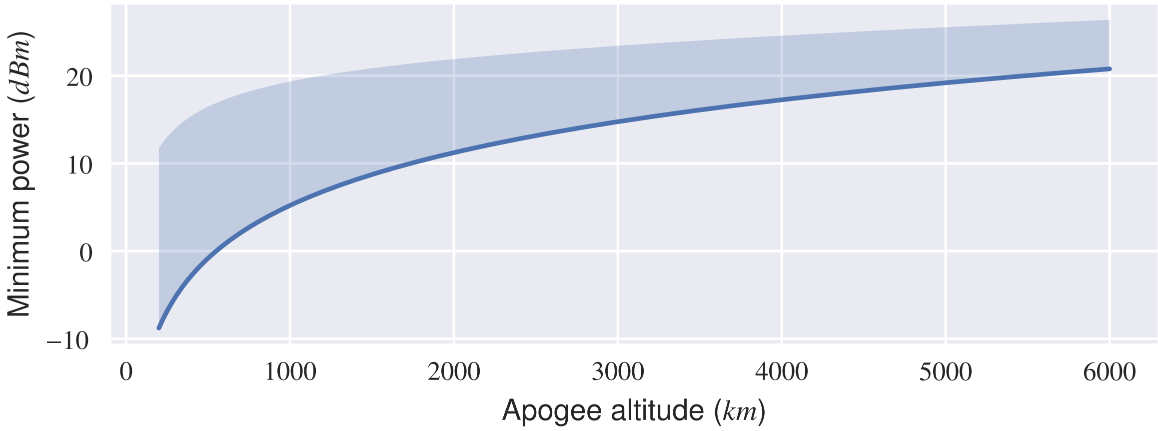

Figure 2: Minimum transmission power in terms of orbit's apogee.

$$\Delta t = 2 \cdot \frac{\phi_{gc}(|\vec{r}|, h)}{\left| \sqrt{\frac{\mu}{a^3}} - \frac{2\pi}{T_e} \right|} \tag{12}$$

Where Δt is the duration of the communication window, and T_e is the duration of a sidereal day.

4.4.2. Influence of orbital parameters

For more complex orbits, the duration of the communication window is not constant. In inclined orbits the maximum window duration occurs when the space segments passes through the ground segment's zenith, while for eccentric orbits the ground segment's zenith must also align with the orbit's apogee.

Relative to a circular equatorial orbit of the same semi-major axis, an inclined orbit presents shorter communication windows, while an eccentric orbit presents longer windows near the apogee and shorter windows near the perigee. For both types of orbit the absolute difference increases with the orbit's semi-major axis, as well as with inclination or eccentricity.

The first column of figure 3 presents the influence of the eccentricity, the solid line is the unperturbed orbit, the hatched area is the envelope for a maximum eccentricity of 0.05, and the dashed line is the semi-major axis used to plot the second graph, which shows the effect of eccentricity at a fixed semi-major axis. The second column presents the same information, but considering the orbit's inclination.

Since the duration of the communication window is not constant for these types of orbits, a statistical analysis is necessary. This is performed by simulating a representative amount of orbits and measuring the communication window durations and the intervals between consecutive windows, then plotting their distributions to determine the worst-case communication window based the desired coverage. For quasi-circular orbits, it is also reasonable to use the distribution of chords in a circle as a first approximation of the probability density function:

$$f(\Delta t) = \frac{\Delta t}{\Delta t_{max}^2 \sqrt{1 - \left(\frac{\Delta t}{\Delta t_{max}}\right)^2}} \tag{13}$$

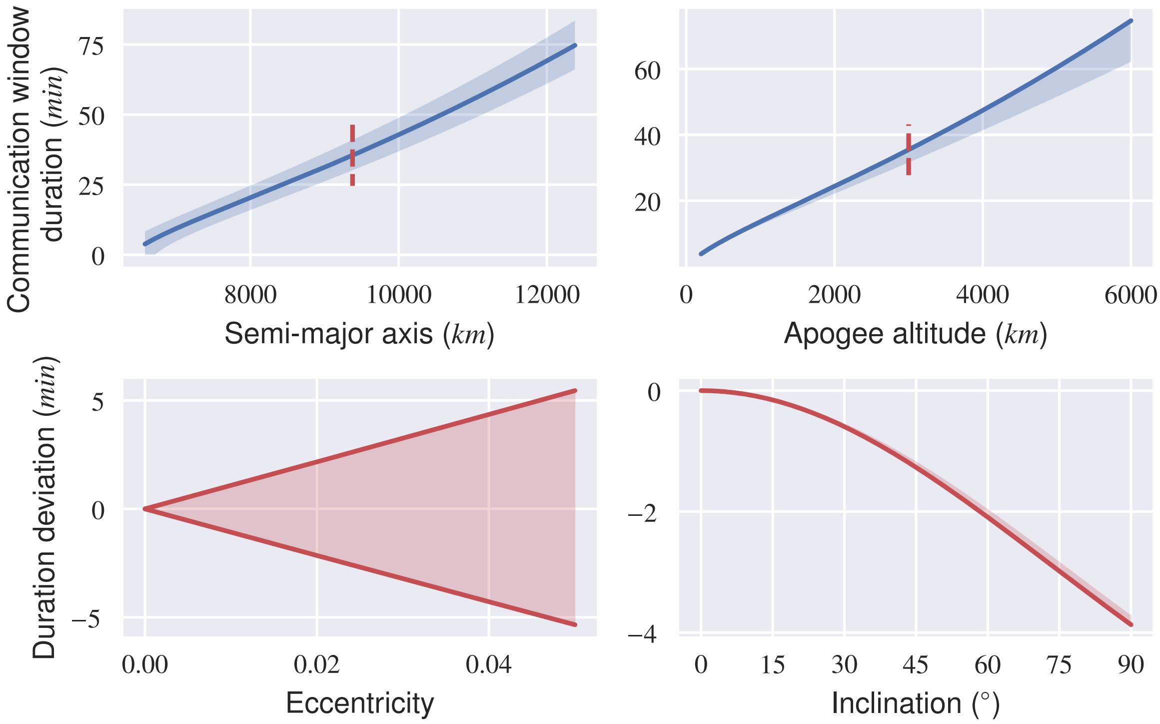

Figure 3: **Communication window duration for inclined and eccentric orbits.**

Figure 4 presents a histogram with the duration of communication windows obtained by simulating 2 years of ISS' orbit. In it the distribution of equation 13 is also displayed.

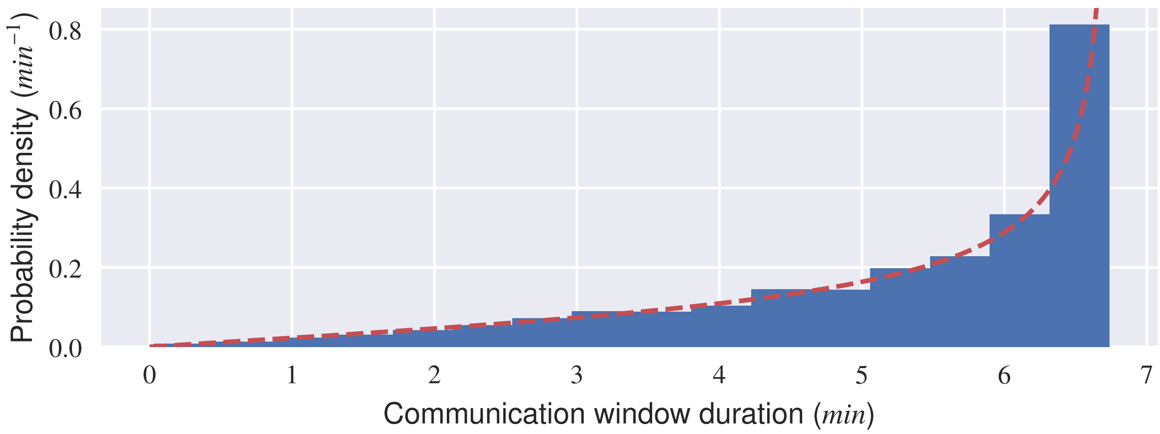

Figure 4: **Typical communication window duration distribution.**

4.5. Effective bit rate

A transceiver's bit rate refers only the physical layer, which means that overheads from the chosen data link protocol (and further layers if applicable) must be considered before calculating the amount of data that can be transmitted per communication window. Using Zielinski [4]'s analytical model of the AX-25 protocol on half-duplex transceivers considering 7 consecutive 256 Byte frames, which is the maximum for both parameters, the total time of each transmission is:

$$\Delta t = \frac{256}{p+1}\frac{T_{102}}{2} + 2T_{103} + 7 \cdot \frac{63}{62} \cdot \frac{8 \cdot (20+256)}{bitrate} + T_2 + \frac{63}{62} \cdot \frac{8 \cdot 20}{bitrate} \tag{14}$$

Where T_{102}, T_{103}, T_2, and p are parameters from the transceiver's implementation of the AX-25 protocol. This means that a 2400 bps transceiver with typical parameters ($T_{102} = 100$ ms, $T_{103} = 300$ ms, $T_2 = 50$ ms, and $p = 63$) can transmit 1792 Bytes of payload data every 7.5 s, for an effective bit rate of 1921 bps.

4.6. Simulations using relevant orbits

Figure 5 presents simulated maximum and minimum communication windows for the ISS' orbit and a 15-revolution per sidereal day sun-synchronous orbit, with UFMG's campus as the ground station for both. The simulation did not limit tracking speed or azimuth movement, but limited elevation movement between 0° and 90°, which causes the discontinuity observed on the maximum communication window.

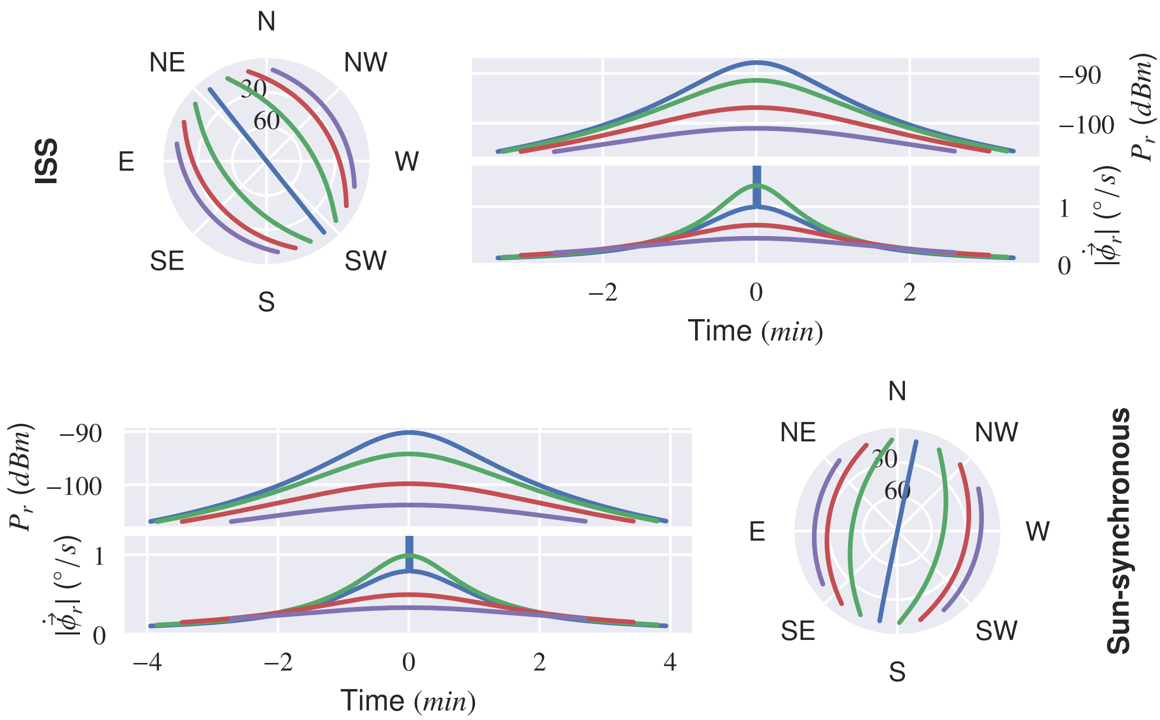

Figure 5: Communication window simulations using relevant orbits.

4.7. Sensibility analysis

The previous sections assume that the alignment and tracking is perfect, which is not the case for real systems. To guarantee the robustness of the TT&C system, it is necessary to evaluate its sensibility to errors.

4.7.1. Alignment errors

Figure 6 presents the variation in antenna gain in terms of alignment error. For the receiving antenna in the ground segment, the reference is the space segment's direction, and the reference view angle is always $0°$. As for the transmitting antenna, the reference is the nadir, and the reference view angle can vary between $0°$ and $90°$. The solid line represents the gain variation considering the maximum gain as reference, with the hatched area considering all remaining directions.

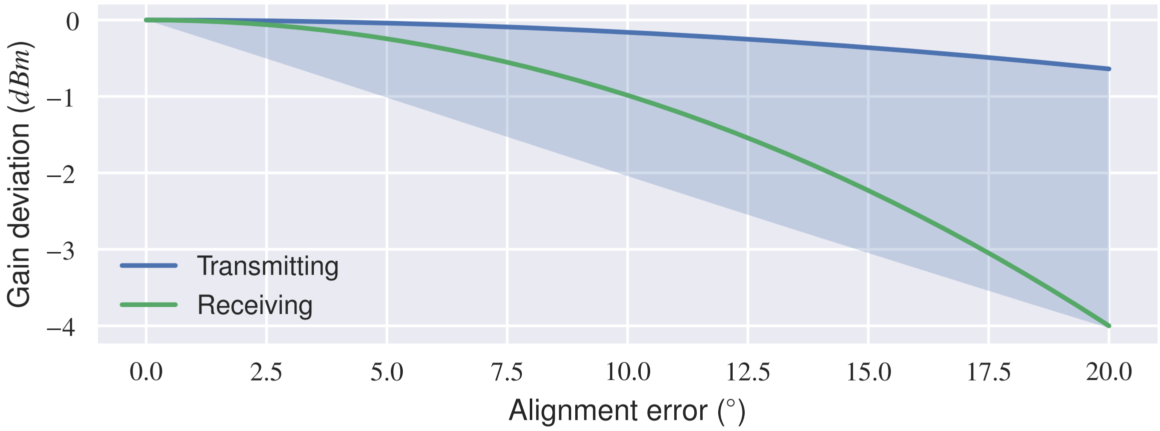

Figure 6: Gain variation in terms of alignment error.

4.7.2. Tracking errors

An alignment error can be introduced if the space segment moves faster than the ground segment can track it. This is especially relevant for passes near the zenith, where discontinuities in terms of azimuth can occur. Figure 7 explores this possibility by limiting the tracking speed of each axis to $6\,°/\mathrm{s}$, using ISS' maximum communication window (from figure 5) as reference. Note that the resulting alignment error is small, and occurs in the region of maximum received power.

4.8. Low-level necessities

Finally, the low-level necessities can be written in terms of the analytical formulas and numerical methods obtained in the previous sections:

1. The TT&C system shall transmit the data with power above margin considering the minimum power calculated for the orbit's apogee (section 4.3);
2. The TT&C system shall transmit the data with effective bit rate (section 4.5) above margin considering the minimum effective bit rate calculated for the worst-case communication window (section 4.4);
3. The GNC system shall keep the space segment's antennas aligned, within margin, towards the nadir (assumption of sections 4.3 and 4.7.1);
4. The GNC system shall operate with sufficient precision so that the power loss due to alignment error is within margin (section 4.7.1);
5. The ground segment shall track the space segment with sufficient precision so that the power loss due to alignment and tracking errors are within margin (sections 4.7.1 and 4.7.2);

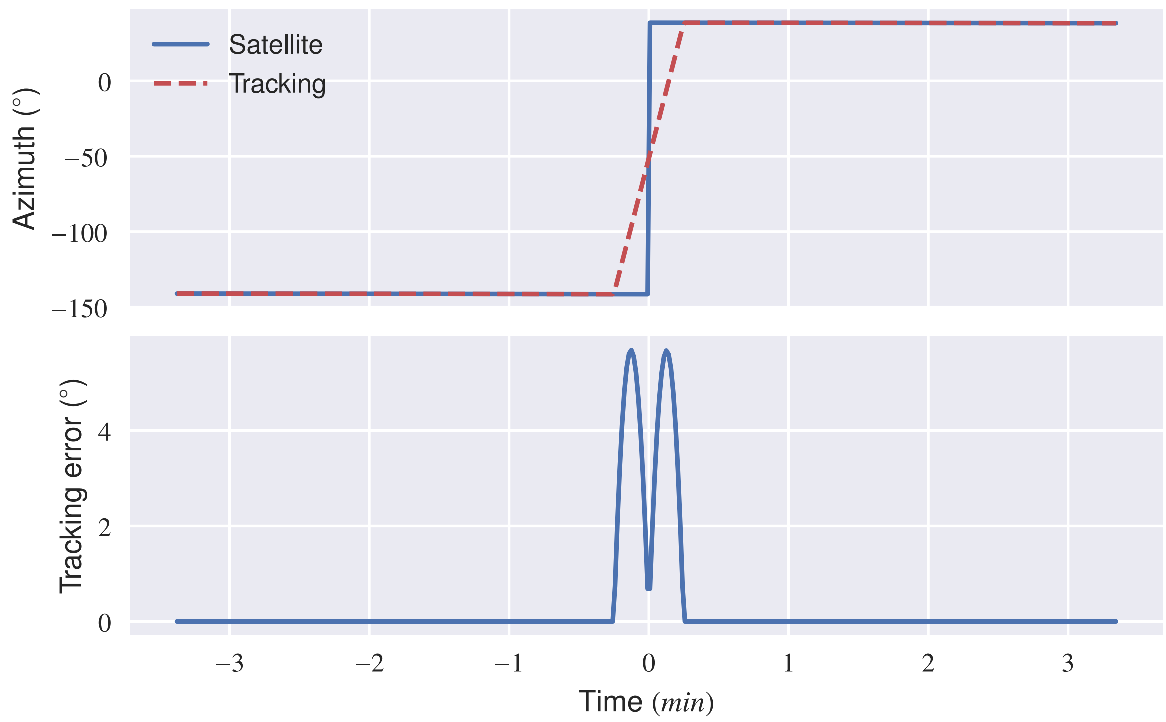

Figure 7: Tracking error due to azimuth discontinuity.

Note that these low-level necessities correspond to the minimum values for a physically feasible transmission. It is up to the project's designers to define the margins above which to operate. Lastly, these necessities do not include decisions due to the mission's architecture, such as weight and power budgets, or operating temperature targets.

5. Conclusion

As stated in the introduction, this work aimed to document the process by which the high and low-level necessities were obtained to start the development of PdQSat, so that students with Aerospace, Electrical, or Systems Engineering backgrounds could understand and implement CubeSat TT&C subsystems at an academic level.

First, basic concepts of telecommunications and orbital mechanics were presented before outlining the TT&C's problem statement, from which a set of high-level necessities was derived. Then, a number of analytical formulas and numerical methods were obtained to rationally represent the high-level necessities underlying physical phenomena, which are finally condensed into low-level necessities.

For future works, the same methodology used to design the space segment's TT&C subsystem can be applied to design its ground station, potentially from scratch (without the need of COTS components). Another possibility is to integrate the model (available on `github.com/bss-aero/cubesat-ttc-utils`) with other models being developed for PdQSat for a complete simulation of the CubeSat's systems.

Finally, it is also possible to improve upon the model by considering the effect of the atmosphere, weather, thermal noise, and other electromagnetic interferences to increase its accuracy, or to consider orbital perturbations to assess the expected changes to the system's performance throughout the mission's expected duration.

References

[1] C. A. Balanis, Antenna theory: analysis and design, John Wiley & Sons, Hoboken, New Jersey, 4 edition, 2016.
[2] NASA, State of the art of small spacecraft technology, 2020.
[3] W. A. Beech, D. E. Nielsen, J. T. Noo, AX.25 link access protocol for amateur packet radio, Tucson Amateur Packet Radio Corporation (1998).
[4] B. M. Zielinski, Effective transmission speed in AX.25 protocol, in: IEEE EUROCON 2009, pp. 1763–1768.
[5] H. K. Kuga, R. R. Kondapalli, V. Carrara, Introdução à mecânica orbital, INPE, Sao José dos Campos, 2 edition, 2012.
[6] H. Curtis, Orbital mechanics for engineering students, Butterworth-Heinemann, Oxford, 2005.
[7] V. A. Chobotov, Orbital mechanics, AIAA, Reston, Virginia, 3 edition, 2002.
[8] NASA, Smallsat parts on orbit now, 2021.
[9] ISIS, Cubesatshop.com, 2021.
[10] ISIS, VHF/UHF Ground Station Kit Data Sheet, ISIS, 2019.
[11] ISIS, Antenna Systems, ISIS, 2016.

NumPPTG: a Pulsed Plasma Thruster Simulation Tool

Fernando B. V. Mendes(1), **Paolo Gessini**(2)
(1) *University of Brasilia, fernandobvm@gmail.com*
(2) *University of Brasilia, paolo.gessini@aerospace.unb.br*

Keywords: *Numerical Simulation, Pulsed Plasma Thruster, Electromechanical Model, Matlab, Electric Propulsion*

The present work aims to create a numerical-computational tool to assist the development of Pulsed Plasma Thrusters at the Space Systems Laboratory of the University of Brasília - UnB. Such tool is developed combining numerical models already established in order to obtain results consistent with those obtained experimentally. For the development of the tool, two similar numerical models were used, since one of them is an improved version of the other, which constitute simplified models of the operation of a Pulsed Plasma Thruster. In order to evaluate the performance of the tool, in terms of the results obtained, two different thrusters were used: a coxial one and a parallel-plate one. The results obtained were satisfactory because, when compared to experimental data, the error was around 10% for parallel plate geometry and around 30% for coaxial geometry even using a simplified numerical model.

1. Introduction

Electric thrusters are widely used because of their highly efficient utilization of propellant mass [1], that is, their high specific impulse when compared to values obtained using chemical propulsion, with its intrinsical physical limits [2]. Therefore, using electric thrusters is expected to yield higher values of payload mass fraction than using chemical thrusters, for the same mission.

The various types of electric thrusters differ in size, power, propellants utilized, physical phenomena involved and are used in different types of space missions. An overview of the most commonly used electric thrusters, with the relation between specific impulse and required power, can be seen in Figure 1 [3].

Pulsed Plasma Thrusters (PPT) are an excellent option when an intermediary specific impulse is needed and not much power is available, as can be seen in Figure 1 [3]. During past years, PPTs became widely used on CubeSats and PocketQubes as a result of their miniaturization capabilities, demonstrated in literature [4].

As PPTs have been widely studied and tested in past 50 years [5] and are low complexity thrusters, they became the best choice for propulsive systems development to satellites focused on academic studies. This type of thruster uses pulsed high voltage electric discharges to ablate, ionize and accelerate propellant [5].

Although some Side-fed PPTs have been studied to be used on CubeSat missions [6, 7], the most used geometries are Breech-fed and Coaxial, both presented in Figure 2, because these configurations deal better with dimensions limitations commonly faced on Cubesat missions. The Breech-fed configuration consists of two parallel plates (electrodes), the propellant, and a spring used to maintain the propellant surface near the discharge. On the other hand, the Coaxial configuration is made of two concentric cylindrical electrodes and the cylindrical propellant.

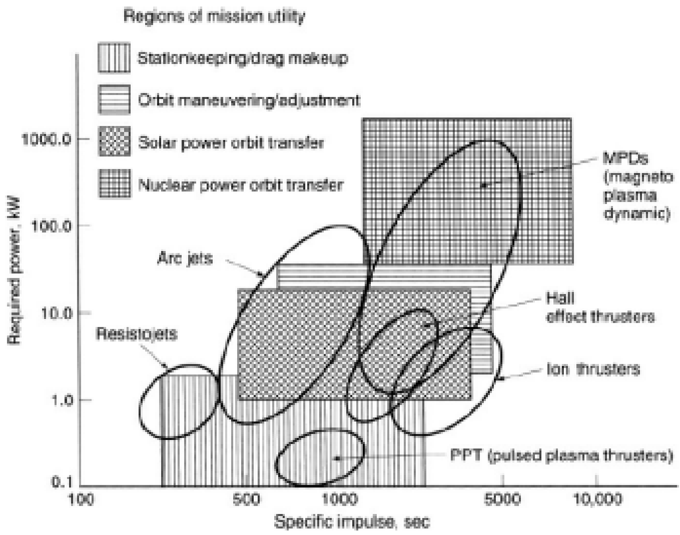

Figure 1: Overview of different eletric thrusters and their applications. Adapted from [3].

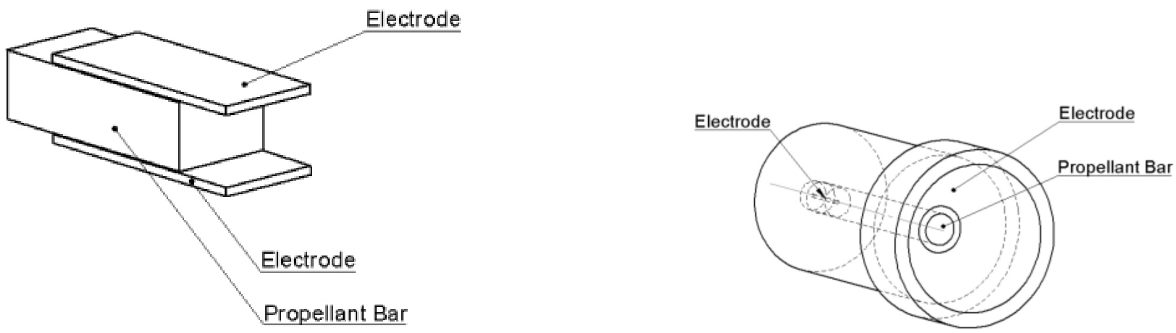

Figure 2: (a) Breech-fed geometry; (b) Coaxial geometry. Adapted from [8]

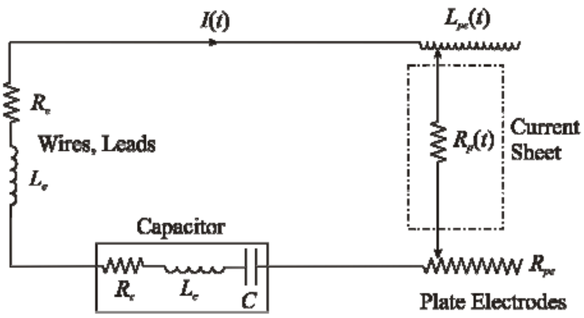

Figure 3: Electrical circuit described in the electromechanical model. Adapted from [9]

Computational simulations are becoming more popular in aerospace applications because they can increase the speed of technology development and decrease the costs related to test and prototype production. Thereby, a huge number of aerospace companies already have engineers focused on the development and improvement of simulation techniques and codes. This tool is being used in additive manufacturing, aircraft drag reduction, internal ballistics of rocket motors, and the improvement of aircraft flight computers.

Using this tool in the context of PPT turns into a way to improve the development process and speed up the framing of new designs. Although PPTs have been widely studied in the past 50 years, the physics involved is not fully understood. So, this fact contributes a lot to making the development process of new designs quite slow due to the need of many experiments.

Therefore, by using numerical techniques and simplified models of thruster behavior it is possible to obtain an estimate of thrusters' performance parameters more quickly and cheaply, considering that no experimental evaluation is needed. Then, the main goal of this work is to develop a computational tool using Matlab App Design to assist the development of new PPTs in the Space Systems Laboratory at the University of Brasilia (UnB).

2. Methodology

In this section the two electromechanical models used in the computational tool and the use of Matlab to develop the tool will be discussed.

2.1. Electromechanical Model

The PPT's electromechanical model consists of the set of equations capable of describing the behavior of the thruster during its operation. The plasma flow inside the PPT is governed by a set of magnetohydrodynamics equations [9]. Thus, the concept behind the electromechanical model is to consider the thruster as an electromechanical device (electrical circuit) interacting with a dinamic system [9].

The electrical circuit that is the base of the model, considering that current and voltage curves are strongly correlated to thruster performance parameters, is shown in Figure 3. In this context, the inductance variables L_c, L_{pe} and L_e are due to, respectively, the capacitor, the thruster geometry and the electric cables. Similarly, the resistive terms R_c, R_e, R_{pe} and R_p are assignable to the capacitor, the cables, the electrode geometry and the plasma sheet.

Accordingly, the set of equations used is dependent on the thruster geometry because of the impact of thruster self-inductance on the electromagnetic field generated during operation. On account of that fact, the set of equations will be presented for the most used thruster geometries: Breech-fed parallel plate and Coaxial.

2.1.1. Parallel Plate PPT Equations

The schematics of the parallel plate thruster model is shown in Figure 4. Therefore, in [10] the authors show that by using Kirchoff's and Ampere's laws to calculate the induced electromagnetic field inside the thruster it is possible to obtain the set of equations described by Eqs. 1 to 4. Considering that the study is based on Slug dynamic model the α value becomes zero in Eq. 3, then, as a result of this fact, the ablated mass will be constant.

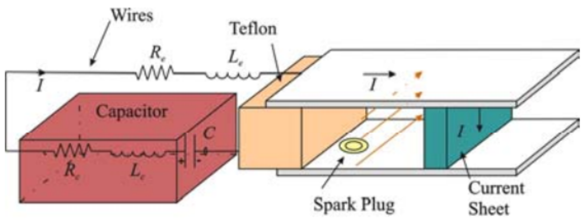

Figure 4: Parallel plate PPT schematics. Adapted from [10]

$$V_0 - \frac{1}{C}\int_0^t I(t)dt = I(t)\left(R_c + R_e + R_{pe} + R_p\right) + \left[L_c + L_e + \mu_0\frac{h}{w}x_s(t) + \mu_0\frac{\delta}{2}\frac{h}{w}\right]\dot{I}(t) + \mu_0\frac{h}{w}\dot{x}_s(t)I(t) \tag{1}$$

$$\frac{d}{dt}\left[m\dot{x}_s(t)\right] = \frac{1}{2}\mu_0\frac{h}{w}[I(t)]^2 \tag{2}$$

$$m(t) = m_0 + m_t\left[1 - \left[1 - \frac{x_s(t)}{l}\right]^{\frac{1}{1-\alpha}}\right] \tag{3}$$

$$R_p = 8.08\frac{h}{T_e^{\frac{3}{4}}w}\sqrt{\frac{\mu_0 \ln\left[1.24\times10^7\left(\frac{T_e^3}{n_e}\right)^{\frac{1}{2}}\right]}{\tau}} \tag{4}$$

$$x_s(0) = 0, \dot{x}_s(0) = 0, \int_0^{t=0} I(t)dt = 0, I(0) = 0 \tag{5}$$

Solving the system of differential equations for the current function $I(t)$ and plasma sheet position x_s the system behavior is obtained. Then, to numerically solve the system it is necessary to define the initial values according to the physical phenomenon seen in the thruster. So, Eq. 5 presents the initial values used by the tool to solve the problem for parallel plate geometry.

2.1.2. Coaxial PPT Equations

The equations for coaxial geometry are similar to the ones presented previously for parallel plate geometry, knowing that the difference lies in the geometry self inductance term. So, Eqs. 6 to 9 describe the set of differential equations used to calculate the behavior of the thruster during operation and Eq. 10 describes the initial values used to solve the system numerically. Then, the same technique used before can be applied to solve this system of equations.

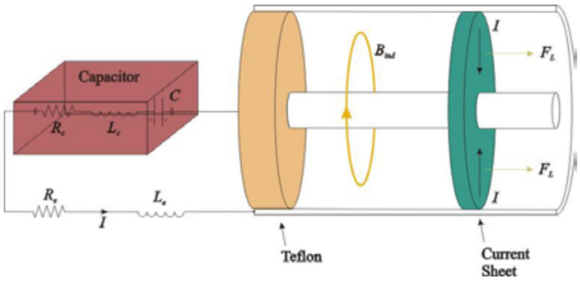

Figure 5: Coaxial PPT schematics. Adapted from [10]

$$V_0 - \frac{1}{C}\int_0^t I(t)dt = I(t)\left\{R_c + R_e + R_{pe} + R_p\right\} + \left[L_c + L_e + \frac{\mu_0}{4\pi}\ln\left(\frac{r_o}{r_i}\right)x_s(t) + \mu_0\frac{\delta}{4\pi}\ln\left(\frac{r_o}{r_i}\right)\right]\dot{I}(t) + \frac{\mu_0}{4\pi}\ln\left(\frac{r_o}{r_i}\right)\dot{x}_s(t)I(t) \tag{6}$$

$$\frac{d}{dt}\left[m(t)\dot{x}_s(t)\right] = \frac{1}{4\pi}\mu_0\ln\left(\frac{r_0}{r_i}\right)[I(t)]^2 \tag{7}$$

$$m(t) = m_0 + m_t\left[1 - \left[1 - \frac{x_s(t)}{l}\right]^{\frac{1}{1-\alpha}}\right] \tag{8}$$

$$R_p = 2.57\frac{r_o - r_i}{T_e^{\frac{3}{4}}(r_o + r_i)}\sqrt{\frac{\mu_0\ln\left[1.24\times10^7\left(\frac{T_e^3}{n_e}\right)^{\frac{1}{2}}\right]}{\tau}} \tag{9}$$

$$x_s(0) = 0, \dot{x}_s(0) = 0, \int_0^{t=0} I(t)dt = 0, I(0) = 0 \tag{10}$$

2.2. Modified Electromechanical Model

The first model described is based on the fact that the ejected mass by pulse is constant during the entire thruster operation. Nonetheless, this assumption is not realistic and results can not fully describe thruster behavior during experimental analysis. So, in [11] the authors discuss about adding an extra equation to the previous model to consider the variation on ablated mass. Thus, the equation derived from Newton's second law must be modified to consider a time derivative of the ablated mass term, as shown in Eq. 11.

Considering that the force acting on the plasma sheet is a sum of Lorentz force $F_L(t)$ and the gas-dynamic force $F_g(t)$ [11], we have

$$\frac{d}{dt}\left[m(t)\dot{x}_s(t)\right] = m(t)\ddot{x}_s(t) + \dot{m}(t)\dot{x}_s(t) = F_L(t) + F_g(t), \tag{11}$$

where $\dot{x}_s(t)$ e $\ddot{x}_s(t)$ are, respectively, the velocity and the acceleration of the plasma sheet. Furthermore, the equation that describes the ablated mass time derivative is derived from an analytical *quasi-steady* idealized model. According to the authors in [11] this analytical model is based on the assumption that in PPTs typical conditions there is a magnetosonic point in the flow along the discharge channel. Then, this point is used to relate the plasma exhaust velocity to Alven's critical velocity and, thence, estimate mass ablation on the propellant surface. The Eqs. 12 and 13 are used to consider the ablated mass variation during thruster operation.

$$m(t) = \frac{\mu_0 h}{4.404 w V_{critic}} \int_0^t I^2(t)dt \tag{12}$$

$$\dot{m}(t) = \frac{I^2(t)\mu_0 h}{4.404 w V_{critic}} \tag{13}$$

So, to finish the set of equations, the gas-dynamic force $F_g(t)$ must be calculated, according to authors in [12], using the following equation

$$F_g(t) = \dot{m}(t)\sqrt{\gamma R T_e} C_f / C_m, \tag{14}$$

where γ, T_e, and R are, respectively, the specific heat ratio, plasma electrons temperature, and gas constant. The coefficients are given by

$$C_f = \gamma\left(\frac{2}{\gamma+1}\right)^{\frac{\gamma}{\gamma-1}} + \left(1+\frac{\gamma-1}{2}\right)^{-\frac{\gamma}{\gamma-1}}, C_m = \gamma\left(\frac{2}{\gamma+1}\right)^{\frac{\gamma+1}{2(\gamma-1)}}, \tag{15}$$

The set of equations that describe the modified electromechanical model is composed by Eqs. 1, 11, 12, 13 and 4.

2.3. Matlab

The NumPPTG software was developed using commercial software Matlab and its tool named App Designer where is possible to create a graphical interface that runs a Matlab code. The biggest advantage of this approach is that it is not necessary to have a Matlab installation to run NumPPTG.

In this context, the Matlab function *ode45* is used to solve numerically the set of equations described on both models that were studied in this paper. So, the graphical interface receives the input values and then, after executing the Matlab code, displays the voltage curve, current curve, energy curves, and thruster performance parameters.

3. Results and Discussion

To evaluate the performance of NumPPTG, two experimentally tested PPTs available in the literature were used, one of parallel plate geometry and the other of coaxial geometry. Thus, the voltage curve and the values of exhaust velocity, specific impulse, and impulse per pulse obtained experimentally were compared to the results obtained by the software. In addition, it was evaluated whether the modified electromechanical model is able to obtain better results than the default version. Therefore, firstly the results for the parallel plate thruster will be presented, and then the results for the coaxial geometry thruster.

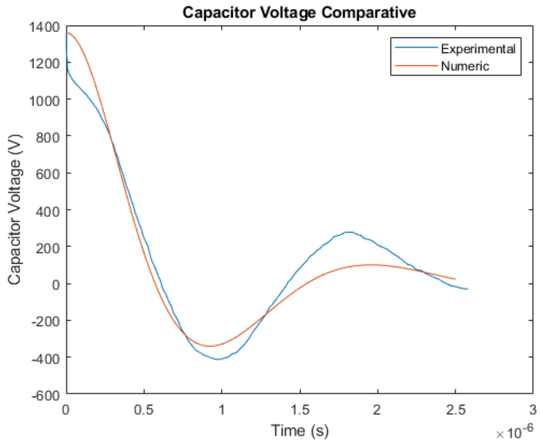

Figure 6: Comparison between numerical and experimental curves of capacitor voltage.

Table 1: Overview of parallel plate thruster performance parameters obtained using NumPPTG and on experimental analysis.

Parameters	Experimental	Numeric	Error (%)
Exhaust Velocity (m/s)	3000	3240.41	8.01
Specific Impulse (s)	312	330.32	5.87
I_{bit} (μN-m)	32	32.50	1.56

3.1. Parallel Plate PPT

A comparison between the numerical and experimental capacitor's voltage curve is shown in Fig. 6. Then is noted that the curves have the same trend, but the values differ a bit because of the assumptions made in model equations. This difference may be explained by simplifications adopted about the plasma generated inside the PPT, mainly due to considering the plasma resistance constant during the thruster pulse.

The comparison between the NumPPTG output parameters and the experimental values presented by the authors in [13] is shown in Table 1. Thus, it is concluded that, although the curves presented above do not perfectly describe the behavior of the thruster during the pulse, the final values, calculated by the tool, are satisfactory, because even with several simplifications made, the largest numerical error on output parameters was 8%.

The results from the use of the modified electromechanical model to simulate the operation of the PPT of the LES 6 are shown in Fig. 7 and Table 2. Thus, it is noted that, even with one more equation, the results are very close to those presented pre-

Table 2: Overview of parallel plate thruster performance parameters obtained using NumPPTG and on experimental analysis for modified electromechanical model.

Parameters	Experimental	Numeric	Error (%)
Exhaust Velocity (m/s)	3000	3077.18	2.57
Specific Impulse (s)	312	313.68	0.54
I_{bit} (μN-m)	32	32.54	1.69

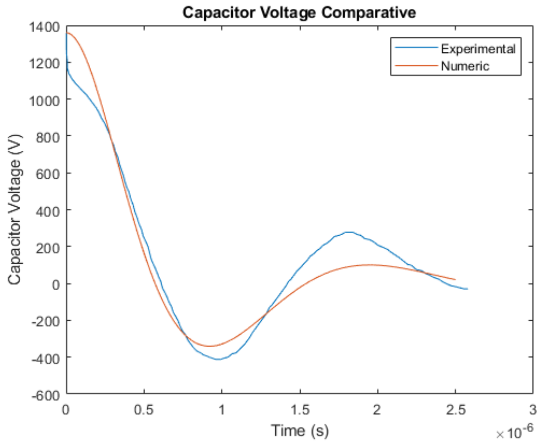

Figure 7: Comparison between numerical and experimental curves of capacitor voltage for the modified electromechanical model.

viously in the default electromechanical model. Therefore, it is concluded that the inclusion of the equation that deals with the mass ablation rate have little influence on the general behavior of the results.

As a result, the mass equation, although not added to solve it, was not able to better describe the behavior of the voltage at the capacitor, and, therefore, all the problems discussed above remain present in this model. However, from the point of view of the output values illustrated in Tab. 2, this numerical model was able to obtain results closer to the experimental values and, consequently, reduce the error associated with the values of gas exhaust velocity, the thruster specific impulse and the I_{bit}.

Therefore, in the context of the final simulation results, the modified electromechanical model performed better than the default electromechanical model, since the highest numerical error obtained was about 2.57%.

3.2. Coaxial PPT

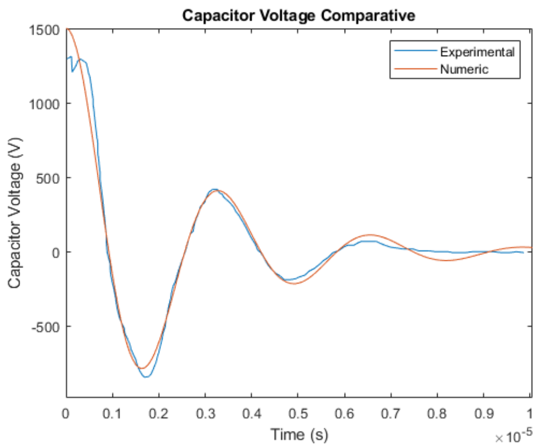

Figure 8: Comparison between coaxial numerical and experimental curves of capacitor voltage for electromechanical model.

Analyzing the results obtained using the default electromechanical model for Coaxial PPT is noted that the behavior is very similar to the results for Parallel Plate PPT.

The numeric curve can not fully describe the reality, but it is a very good preliminary result to be used during thruster development, as can be seen in Fig. 8.

Table 3: Overview of coaxial thruster performance parameter obtained using NumPPTG and on experimental analysis.

Parameters	Experimental	Numeric	Error (%)
I_{bit} (μN-m)	22.50	28.85	28.2

Then, the results obtained from NumPPTG and experiments presented by authors in [14] are compared are shown in Table 3. The authors also used the same electromechanical model to estimate the thruster parameters numerically and got values similar to NumPPTG results.

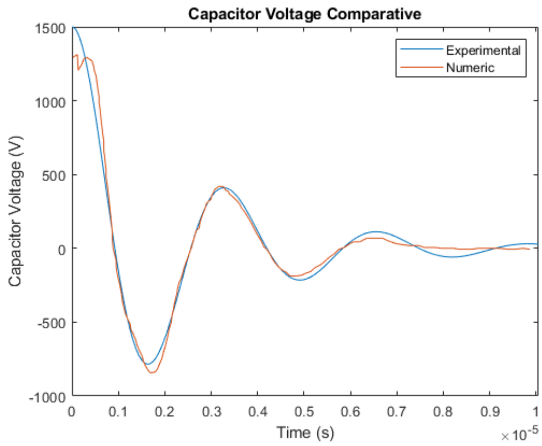

Figure 9: Comparison between coaxial numerical and experimental curves of capacitor voltage for modified electromechanical model.

Finally, the modified electromechanical model was used in an attempt to obtain better estimates of the thruster performance, however, as shown in Fig 9 and the data in Table 4, the model was not able to capture the phenomena with greater fidelity. Therefore, as seen for parallel plate geometry, the simplifications made about plasma dynamics were relevant to the final result obtained.

Table 4: Overview of coaxial thruster performance parameter obtained using NumPPTG and on experimental analysis for modified electromechanical model.

Parameters	Experimental	Numeric	Error (%)
I_{bit} (μN-m)	22.50	28.80	28.0

4. Conclusion

The main goal of this work was the development of a numerical tool capable of simulating the behavior of a PPT during its operation and, consequently, obtaining an estimate of important output parameters such as the exhaust velocity of the gases, the specific impulse, the thrust and the impulse generated by pulse.

The numerical approach used in the present work proved to be satisfactory to achieve the previously established objectives. However, the curves obtained numerically were not able to fully describe the phenomena present in the experimental curves, so in some cases the tool overestimated values and in others it underestimated them.

Although the curves obtained did not fully present the expected behavior, as it is a simple and quick model to calculate, the tool is able to contribute to the development of new thrusters geometries. This is due to the fact that the use of NumPPTG is capable of supplying the need to carry out preliminary experiments in the development of the thruster geometry. But the software is limitated by the neglection of plasma dynamics inside the thruster and propellant ablation, facts that have a huge impact in thruster final behavior.

Finally, it is concluded that this work achieved the objectives and expected results in such a way that it is possible to obtain a preliminary PPT design taking important physical phenomena into consideration very quickly, as the code does not require great computational power to be executed, with results similar to what would be obtained during experiments. Then, the future steps are to improve the graphical interface, add a propellant ablation model and a plasma dynamics behavior model.

References

[1] R. G. Jahn, Physics of electric propulsion, Courier Corporation, 2006.

[2] M. J. Turner, Rocket and spacecraft propulsion: principles, practice and new developments, Springer Science & Business Media, 2008.

[3] G. P. Sutton, O. Biblarz, Rocket propulsion elements, John Wiley & Sons, 2016.

[4] D. Krejci, B. Seifert, C. Scharlemann, Endurance testing of a pulsed plasma thruster for nanosatellites, Acta Astronautica 91 (2013) 187–193.

[5] R. Burton, P. Turchi, Pulsed plasma thruster, Journal of Propulsion and Power 14 (1998) 716–735.

[6] S. Ciaralli, M. Coletti, S. Gabriel, Performance and lifetime testing of a pulsed plasma thruster for cubesat applications, Aerospace Science and Technology 47 (2015) 291–298.

[7] M. Coletti, F. Guarducci, S. Gabriel, A micro ppt for cubesat application: Design and preliminary experimental results, Acta Astronautica 69 (2011) 200–208.

[8] P. Gessini, L. T. Habl, M. N. Barcelos Jr, J. L. Ferreira, R. I. Marques, M. Coletti, Low power ablative pulsed plasma thrusters, in: Proc. of the 33rd Int. Electric Propulsion Conf.(Washington, DC), pp. 2013–344.

[9] D. Laperriere, N. Gatsonis, M. Demetriou, Electromechanical modeling of applied field micro pulsed plasma thrusters, in: 41st AIAA/ASME/SAE/ASEE Joint Propulsion Conference & Exhibit, p. 4077.

[10] D. D. Laperriere, Electromechanical modeling and open-loop control of parallel-plate pulsed plasma microthrusters with applied magnetic fields, Ph.D. thesis, Worcester Polytechnic Institute, 2005.

[11] L. Yang, X.-y. Liu, Z.-w. Wu, N.-f. Wang, Analysis of teflon pulsed plasma thrusters using a modified slug parallel plate model, in: 47th AIAA/ASME/SAE/ASEE Joint Propulsion Conference & Exhibit, p. 6077.

[12] E. Henrikson, P. Mikellides, Experimental assessment of a benchmark ablation-fed pulsed plasma thruster, in: 43rd AIAA/ASME/SAE/ASEE Joint Propulsion Conference & Exhibit, p. 5221.

[13] R. Vondra, K. Thomassen, A. Solbes, A pulsed electric thruster for satellite control, Proceedings of the IEEE 59 (1971) 271–277.

[14] H. Li, Z. Wu, G. Sun, K. Zhu, T. Huang, X. Liu, W. Y. L. Ling, N. Wang, A model for macro-performances applied to low power coaxial pulsed plasma thrusters, Acta Astronautica 170 (2020) 154–162.

14

Session 14 - Thermal Simulation

Thermal simulation of the CubeSat Catarina-A1

Caique S. M. Gomes[a], **Edemar M. Filho**[b], **Laio O. Seman**[c], **Eduardo A. Bezerra**[d], **Talita S. Possmai**[e]

[a]*Federal University of Santa Catarina, R. Eng. Agronômico Andrei Cristian Ferreira, s/n - Trindade, Florianópolis - SC, 88040-900, Brazil, kiqsmg@gmail.com*

[b]*São Paulo State University, Av. Profª Isette Corrêa Fontão, 505, Jardim das Flores, São João da Boa Vista - SP, 13876-750, Brazil, edemar.filho@unesp.br*

[c]*University of Vale do Itajai, R. Uruguai, 458 - Centro, Itajaí - SC, 88302-901, laio@univali.br*

[d]*Federal University of Santa Catarina, R. Eng. Agronômico Andrei Cristian Ferreira, s/n - Trindade, Florianópolis - SC, 88040-900, eduardo.bezerra@ufsc.br*

[e]*Federal University of Santa Catarina, R. Dona Francisca, 8300 - Bloco U - Zona Industrial Norte, Joinville - SC, 89219-600, talita.possamai@ufsc.br*

Keywords: *thermal simulation, temperature, nanosatellite, heat transfer, heat pipe*

In every satellite project, the engineers must know the spacecraft's environment in orbit and propose adequate solutions to support the conditions of outer space. This study is related to thermal simulations of the space segment of mission Catarina-A1, a CubeSat 2U under development by the Federal University of Santa Catarina (UFSC) to monitor large areas of Brazil through Data Collection Platforms (PCDs) in the context of the Catarina Constellation. Thermal assessment of its operation in orbit is essential to assure that the temperature levels of its main parts do not extrapolate the recommended values, reducing the risks of failures by inappropriate hot or cold conditions. Therefore, this work aims to solve the energy equation over Catarina-A1 to obtain the temperature field of its main parts in relevant orbital scenarios. This information will support the thermal control's development of the Catarina-A1 and assist in the thermal tests conducted before the launch. The software Ansys CFS is used to perform transient and three-dimensional simulations of Catarina-A1 for typical orbits and attitudes of CubeSats in Low Earth Orbit (LEO). The simulations include a launch scenario from the International Space Station (ISS) at 430 km and a Sun-Synchronous Orbit (SSO) at 620 km. Along with the operation in orbit, the CubeSat will face different eclipse durations, so each launch scenario is tested in the worst hot and cold conditions. The hottest case is experienced by the orbit with less eclipse, while the coldest results from the orbit whose eclipse is the longest. The boundary conditions on the external surfaces of the CubeSat include heat flux from the sun, emission by the earth, the reflection of solar rays at the earth's surface (albedo), and emission of radiation by the satellite to outer space. Internally, the surfaces are adiabatic. Heat pipes connecting opposite sides are inserted in the simulation to verify their potential to reduce the temperature of solar panels and significantly impact the temperature fields.

1. Introduction

The constellation Catarina is a project under the supervision of the Brazilian Space Agency, and executed at UFSC (Universidade Federal de Santa Catarina) and ISI SENAI (Sistema de Inovação do Serviço Nacional de Aprendizagem Industrial). It is expected that his project will result in twelve nanosatellites, all of them based on the CubeSat standard. The project has started in 2022, and has already passed through the Mission Design Review (MDR) and System Requirements Review (SRR).

Thermal control is one of the subsystems found in most of the typical satellites, including the nanosatellites [1, 2]. Each component of the space segment has a range of appropriate temperature for its operation, and levels beyond it must be avoided to reduce failures [3]. Therefore, the main role of the thermal control is directly related to the temperature control. One further benefit that can be achieved by proper thermal management regards the power generation by photovoltaic cells. In fact, photovoltaic cells use only a fraction of the incident solar radiation spectrum to generate electrical energy, close to ultraviolet and visible light, with the infrared wavelength being harmful to their operation. This occurs because the infrared portion is absorbed by the surface, but promotes the heating of the cells, which causes a reduction in the energy conversion efficiency. Decreases around 0.5% in the electrical efficiency of conversion are reported in the literature for every 1°C increase in temperature [4], and currently the efficiency of conversion of traditional photovoltaic cells for spatial applications are around 30% [5].

This paper regards the thermal simulation of the Catarina-1A, a CubeSat 2U with launch expected for 2023. Its orbit is not yet defined, therefore the simulations are conducted for two orbit configurations that are the most commons: launch from the International Space Station (ISS) and Sun-Synchronous Orbit (SSO) [6]. The analysis focus on the extreme maximum and minimum thermal radiation over the nanosatellite, which results in the worst hot and cold conditions scenarios.

2. Bibliography Review

Thermal simulation for CubeSats requires knowledge over several fields, principally thermodynamic properties of materials, spatial environment, radiative heat transfer and electric power management. In fact, temperature on satellites is impacted by more than 20 parameters, divided into 3 main groups [7]:

- Environment: radiation, orbital parameters, sun's position, satellite's attitude;
- Configuration: Size, geometrical format, thermal control solutions;
- Material properties: surface, absorptivity, emissivity, thermal conductivity, heat capacity.

The great majority of CubeSats are in Low Earth Orbit (LEO), below 600 km [6], where the sun is the main thermal source, therefore the period of the orbit with sunlight and the CubeSat's projection, given by the attitude, are essential to estimate the thermal radiation achieving it, which also includes the thermal radiation called albedo and infrared from the earth [8]. These heat fluxes are boundary conditions for the thermal simulations, whose are usually concerned about the worst hot and cold scenarios [9, 10, 11].

The primary role of thermal control is to maintain all the sub-systems of the satellite within an appropriate range of temperature, which is executed through two possibilities: passive and active thermal control. Examples of passive thermal control for satellites include Multi-Layer Insulation (MLI), paints, coats, thermal strap, heat pipes, deployable radiators, and storage energy units based on phase change material. In contrast, electrical heaters, heat pumps, refrigerators, and thermoelectric coolers are active controls. The difference between the categories is the necessity of electrical power for the operation [7].

The heat transfer in the CubeSat only occurs by conduction and radiation process. A simple device used in traditional satellites to improve the heat transfer across its parts is the Heat Pipe (HP), which can be regarded as a material having a thermal conductivity much more significant than any known metal [12]. The development of HP is intrinsically related for usage in satellite, for this reason there are several spacecrafts with successful thermal management assisted by HP and many studies about tests and models for satellite applications, including theoretical models, experimental tests in laboratory, in vacuum chambers, in sounding rockets and on board of satellites [13, 14, 15, 16].

3. Methodology

3.1. Numerical model

To find the transient temperature fields of the satellite the equation of conservation of energy will be solved, as shown in Equation 1:

$$\rho c \frac{\partial T}{\partial t} - k\nabla.(\nabla T) - S = 0 \tag{1}$$

where ρ is the density [kg/m^3], c is the heat capacity [J/kgK], T is the temperature [K], t is the time [s], k is the thermal conduction coefficient [W/mK] and S is the source term [W/m^3].

The simulations are based on the Finite Volume Method (FVM), and the boundary conditions include the external heat transfer by radiation and internal heat generation, as explained in the next section.

3.2. Boundary conditions

The external incoming heat are radiation (Q_r) on each external side w of the CubeSat, as shown in Equation (2) [11]:

$$Q_{r_w} = Q_{\mathrm{sun}_w} + Q_{\mathrm{alb}_w} + Q_{e_w} - Q_{\mathrm{out}_w} \tag{2}$$

Solar radiation (Q_{sun_w}) is the main thermal source, given by the following expression:

$$Q_{\mathrm{sun}_w} = Q_s'' A_w F_{w\to\mathrm{sun}} \psi \tag{3}$$

where Q_s''=1367 W/m^2 is the solar heat flux, A_w is the surface's area of side w, $F_{w\to\mathrm{sun}}$ is the view factor of surface w towards the sun, and ψ is a variable to express the shadow of the Earth.

Another thermal source for the CubeSat is called albedo (Q_{alb_w}), which is the solar radiation reflected by the Earth's surface, given by:

$$Q_{\mathrm{alb}_w} = Q_s'' A_w F_{w\to\mathrm{e}} \cos(\theta)\, b \tag{4}$$

where $F_{k\to\mathrm{e}}$ is the view factor of surface w towards the Earth, θ is the angle between a solar ray crossing the center of the Earth and the a vector position of the CubeSat.

The parameter b is the reflexive index of solar radiation by the Earth's surface, here a constant value of 0.3 [17, 18].

The last external thermal source in the CubeSat is the infrared radiation emitted from the Earth. An average and constant value for its heat flux is $Q_e^{''}$=237 W/m^2 [7, 19], and the total heat source is:

$$Q_{e_w} = Q_e^{''} A_w F_{w \to e} \tag{5}$$

Simultaneously to these previous incoming heat sources, the CubeSat transfer its energy to the space through radiation emission, as follows [20]:

$$Q_{\text{out}_w} = \varepsilon_w \sigma A_w \left(T_w^4 - T_\infty^4\right) \tag{6}$$

where ε_w is the emissivity, σ is the Stefan-Boltzmann constant, T_w is the temperature of CubeSat's surface, and T_∞ is the outer space temperature (2.7 K).

The CubeSat can also have internal heat generation as consequence from the operation of its electronic components, or then by active heaters dedicated to control the temperature, for example at the batteries.

3.3. The domain

The geometry of the CubeSat Catarina-A1 is in Figure 1. This is a CubeSat 2U, with solar panels covering all the external surfaces, a structure made of aluminium, two payloads, one TT&C, one OBDH, one EPS, four batteries, and a passive attitude control. Behind the solar panels there are aluminium shields (3 mm of width) to protect the electronic components from the radiation of outer space. The thermal control has two main parts: heaters and heat pipes. To avoid low temperatures at the batteries, heaters are placed over them and its control is the type on/off. The heat pipes connect opposite sides +Y and -Y of the satellite to reduce the temperature of the solar panel that is exposed to the sun. This configuration is an experiment dedicated to increase the energy generation of the photovoltaic cells, as this process is more efficient at low temperatures [21]. Opposite solar cells can not face the sun at the same time, therefore the side exposed to it is generating energy but simultaneously becomes hotter, while the other side is only emitting thermal radiation to the cold space environment and does not produce any power.

The thermal model of Catarina-A1 is a simplified geometry from previous detailed illustration, shown in Figure 2. The components in the Printed Circuit Boards (PCBs) are no included, only the main board.

The material and surface properties of the CubeSat are summarized in Table 1:

Table 1: Thermal and surface properties of main parts.

	Thermal property			Surface property	
Part	ρ [kg/m^3]	c [J/kg.K]	k [W/m.K]	ε [-]	α [-]
Solar panel	1840	800	1.03	0.60	0.68
Structure	2810	936	130	0.08	0.37
PCB	1840	800	0.25	0.22	0.85
Battery	2122	933	12.5	0.7	-

The heat pipe will be simulated as a pure solid domain, with a high thermal conductivity of 10.000 W/mK to simulate its great capacity to transfer heat during its operation

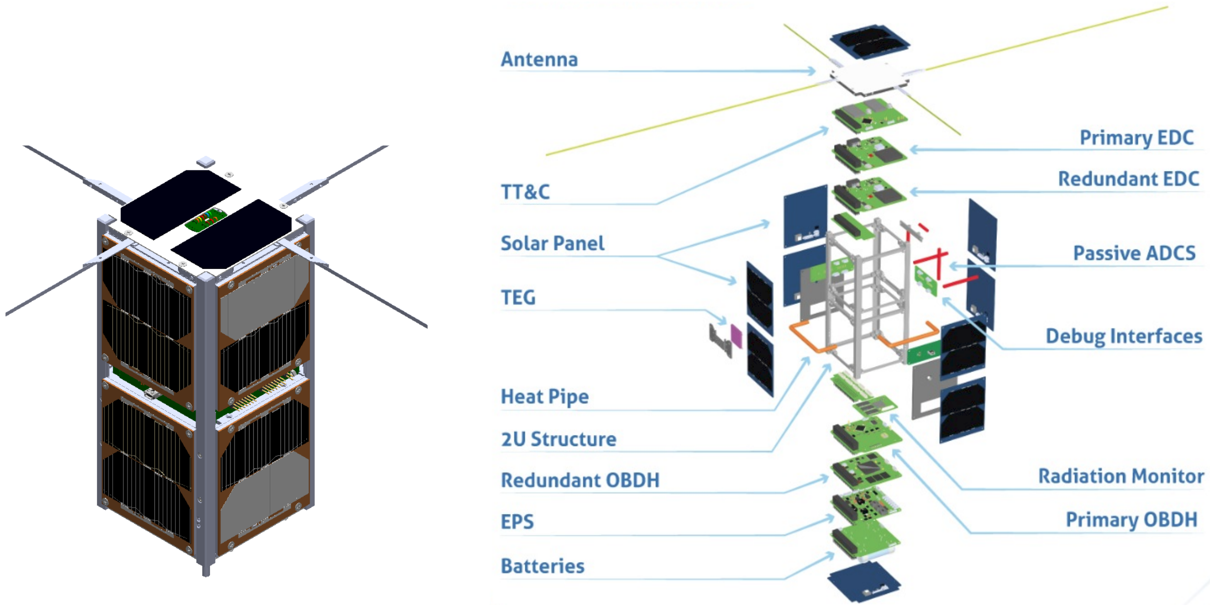

(a) Virtual flight model. (b) Exploded view.

Figure 1: The CubeSat Catarina-1.

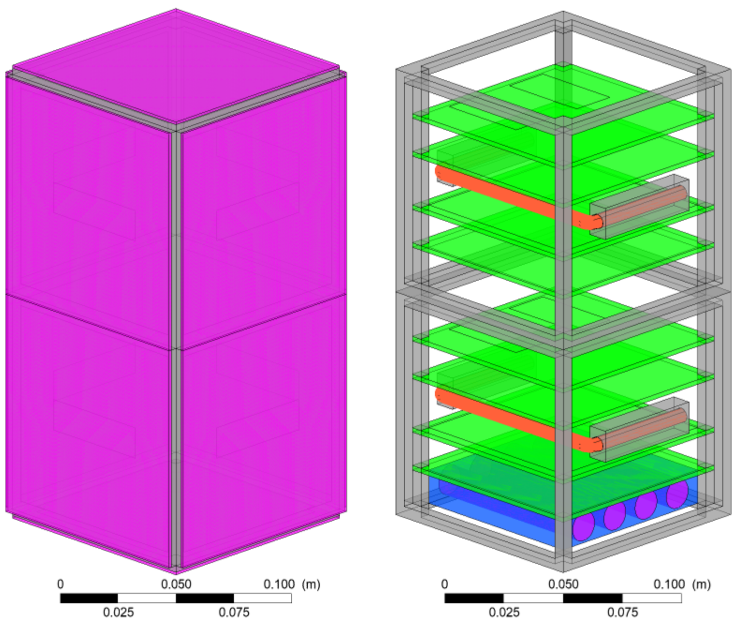

(a) With solar panels and shields. (b) Without solar panels and shields.

Figure 2: The thermal model.

3.4. *Study cases*

The following scenarios of circular orbits will be tested:

- ISS: inclination of 51.5°, altitude of 430 km, with maximum eclipse and without eclipse, and attitude aligned to the Earth's magnetic field;
- SSO1: inclination of 97.5°, altitude of 620 km, with maximum eclipse and without eclipse, and attitude aligned to the Earth's magnetic field;

- SSO2: inclination of 97.5°, altitude of 620 km, with maximum eclipse, and three surfaces simultaneously and equally exposed to the sun.

Initially are presented the results without the presence of heat pipes, and later their integration between Y solar panels are considered.

4. Results

The first result in Figure 3 shows the temperature at external the center of each solar panels along the orbit for the ISS scenario, with and without eclipse. The solid and dashed lines refer to the first and second level of the CubeSat, respectively. For the condition of maximum eclipse, the maximum and minimum temperatures are around 308 K and 242 K, respectively. In this case, when the satellite enters the Earth's shadow, all the temperatures fall down and reach minimum around that instant. For the condition without eclipse, the thermal variation occurs exclusively by the rotation of the satellite around its axis, which keeps side +X and -X without any exposition to the sun. In this scenario the satellite becomes hotter, reaching a maximum around of 320 K, but the minimum is lower, around 222 K. In both conditions of eclipse, the temperature levels of first and second levels are essentially the same for a given side.

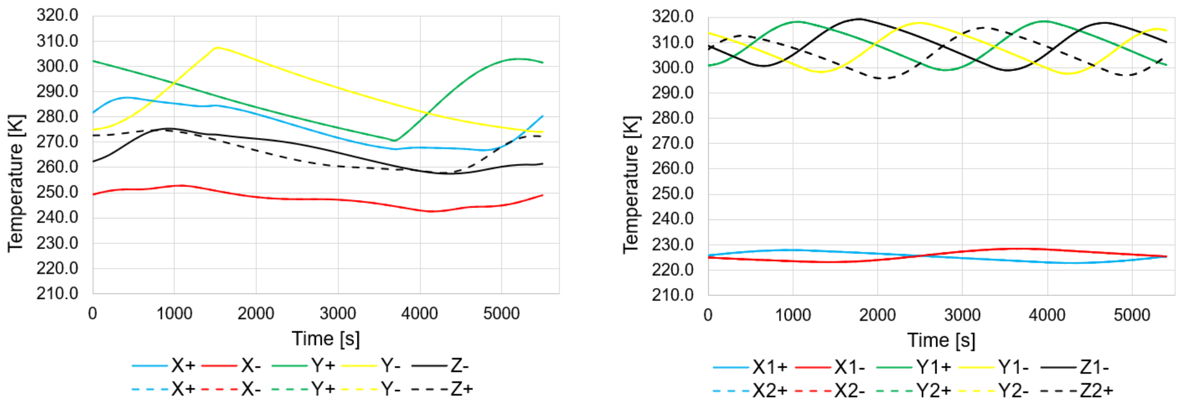

(a) With eclipse.

(b) Without eclipse.

Figure 3: Temperatures at the center of solar panels for orbit ISS, without heat pipe. Solid lines are for the first level and dashed lines are for the second level.

Result in Figure 4 shows the temperature at the external center of each solar panels along the orbit, considering the SSO1 scenario. The temperature field is slightly different from the previous case because the heat fluxes (boundary conditions) are not exactly the same, resulting in extreme values of 305 K and 240 K for the condition with eclipse. When there is no eclipse, the temperatures are generally higher because the exposition to the sun exist for the entire orbit, with maximum of 318 K and minimum of 220 K. As before, not all sides faces the sun and for this reason they are colder.

Figure 5 is the final scenario SSO2, where the CubeSat always keeps the same three faces simultaneously and equally exposed to the sun. In this condition, the sides towards the sun are hotter than previous cases, reaching the maximum of 329 K, while the opposite sides are very cold because the solar radiation is absent for them. The minimum here is around 220 K, and a significant thermal gradient is observed for this specific condition of attitude. The sides with constant exposition to the sun,

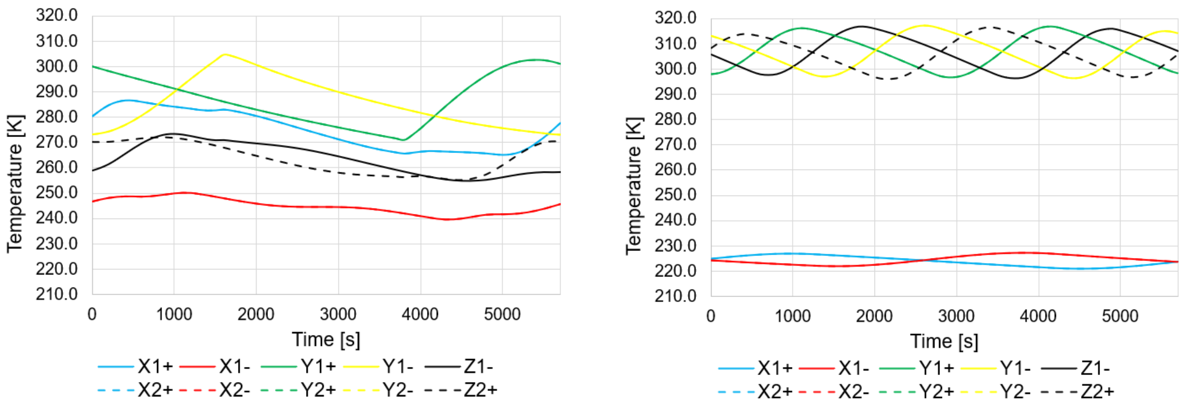

(a) With eclipse. (b) Without eclipse.

Figure 4: Temperatures at the center of solar panels for orbit SSO1. Solid lines are for the first level and dashed lines are for the second level.

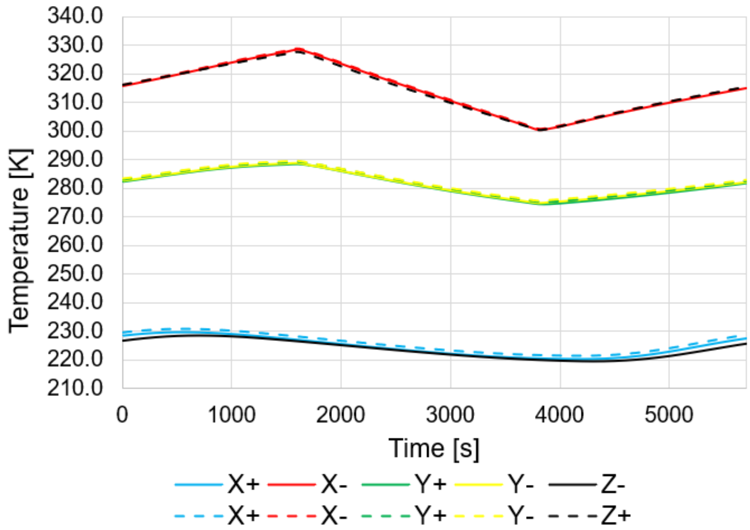

Figure 5: Temperatures at the center of solar panels for orbit SSO2. Solid lines are for the first level and dashed lines are for the second level.

consequently the hottest, would be generating power and therefore this process would not be the most efficient.

To illustrate the potential and benefits for heat pipes in CubeSat missions, the following figures focus only in the temperature of Y sides. The results from the configuration without heat pipes are given by solid lines, while the dashed lines are valid for the condition with heat pipe. All the cases show that smaller thermal gradients are achieved when the heat pipe is considered. As expected, the first and second cases are similar, as already seen in previous results. The condition with only three sides equally and continuously exposed to the sun shows a significant improvement in the performance, reducing the temperature at the hottest side by around 40 K, while increases the cold side by 60 K.

5. Conclusions

Thermal simulations of the CubeSat Catarina-A1 were performed to investigate the temperature fields under two typical cases of orbit scenarios. Two different config-

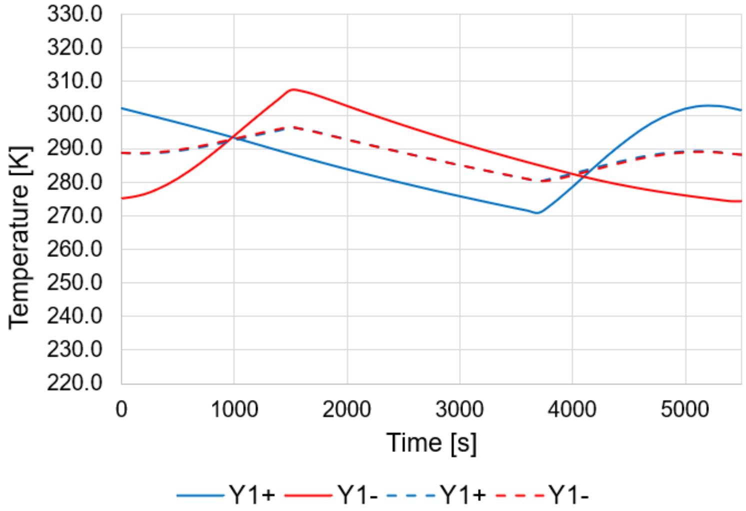

(a) Orbit ISS.

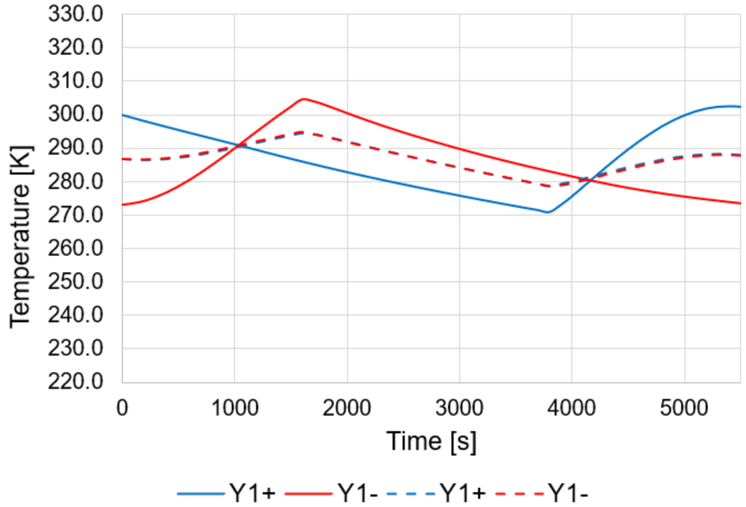

(b) Orbit SSO1.

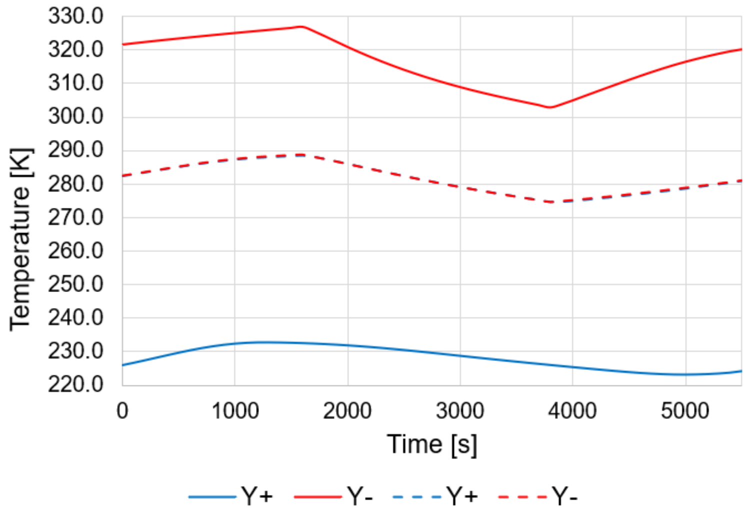

(c) Orbit SSO2.

Figure 6: Temperatures at the center of solar panels Y+ and Y-. Solid lines are valid for cases without heat pipe, and dashed lines with heat pipe.

uration of attitude were also tested, revealing the impact of these parameter in the outcomes.

The introduction of heat pipes among solar panels played a major role in the thermal scenarios and showed it has a significant potential to reduce thermal gradients. All tested scenarios were impacted by the heat pipes, however the case with three sides exposed to the sun was the most meaningful one, which illustrates that a thermal management based on heat pipes has the capacity to improve the efficiency of power generation through photovoltaic cells.

Acknowledgments

We would like to thank the support from the Brazilian Space Agency and from the Catarina Constellation.

References

[1] P. Fortescue, J. Stark, G. Swinerd, Spacecraft Systems Engineering, Wiley, 2003.
[2] C. Cappelletti, S. Battistini, B. Malphrus, CubeSat Handbook: From Mission Design to Operations, Academic Press, 2020.
[3] V. Knap, L. K. Vestergaard, D.-I. Stroe, A review of battery technology in cubesats and small satellite solutions, Energies 13 (2020).
[4] F. Karimi, H. Xu, Z. Wang, J. Chen, M. Yang, Experimental study of a concentrated pv/t system using linear fresnel lens, Energy 123 (2017) 402–412.
[5] N. R. E. L. (NREL), Best research-cell efficiency chart, 2022.
[6] E. Kulu, Nanosats database, 2022.
[7] D. Gilmore, M. Donabedian, Spacecraft Thermal Control Handbook: Fundamental technologies, Spacecraft Thermal Control Handbook, Aerospace Press, 2002.
[8] E. M. Filho, L. O. Seman, C. A. Rigo, V. d. P. Nicolau, R. G. Ovejero, V. R. Q. Leithardt, Irradiation flux modelling for thermal–electrical simulation of cubesats: Orbit, attitude and radiation integration, Energies 13 (2020).
[9] R. Kovács, V. Józsa, Thermal analysis of the smog-1 pocketqube satellite, Applied Thermal Engineering 139 (2018) 506–513.
[10] S. Corpino, M. Caldera, F. Nichele, M. Masoero, N. Viola, Thermal design and analysis of a nanosatellite in low earth orbit, Acta Astronautica 115 (2015) 247–261.
[11] E. Morsch Filho, L. O. Seman, V. de Paulo Nicolau, Simulation of a cubesat with internal heat transfer using finite volume method, Applied Thermal Engineering 193 (2021) 117039.
[12] G. Peterson, An introduction to heat pipes: modeling, testing, and applications, Wiley series in thermal management of microelectronic & electronic systems, Wiley, 1994.
[13] H.-U. Oh, S. Shin, C.-W. Baek, Thermal control of spaceborne image sensor using heat pipe cooling system, Aerospace Science and Technology 29 (2013) 394 – 402.
[14] K. Paiva, M. Mantelli, L. Slongo, Experimental testing of mini heat pipes under microgravity conditions aboard a suborbital rocket, Aerospace Science and Technology 45 (2015) 367 – 375.
[15] P. Mashaei, M. Shahryari, Effect of nanofluid on thermal performance of heat pipe with two evaporators; application to satellite equipment cooling, Acta Astronautica 111 (2015) 345 – 355.
[16] H. Brouwer, Z. de Groot, J. Guo, H. J. van Gerner, Solving the thermal challenge in power-dense cubesats with water heat pipes, in: Proceedings of the Small Satellite Conference.
[17] B. Anderson, C. Justus, G. Batts, Guidelines for the selection of near-earth thermal environment parameters for spacecraft design, 2001. NASA/TM-2001-211221.
[18] E. . Requirements, Standards Division, ECSS-E-ST-10-04C Space environment, 2/E, ECSS, 2008.
[19] R. Lyle, J. Leach, L. Shubin, Earth albedo and emitted radiation, Technical Report NASA-SP-8067, NASA, 1971.
[20] T. Bergman, F. Incropera, D. DeWitt, A. Lavine, Fundamentals of Heat and Mass Transfer, Wiley, 2011.
[21] S. Dubey, J. N. Sarvaiya, B. Seshadri, Temperature dependent photovoltaic (pv) efficiency and its effect on pv production in the world – a review, Energy Procedia 33 (2013) 311–321. PV Asia Pacific Conference 2012.

THERMAL SIMULATION OF A HIGH ALTITUDE BALLOON

João G. B. Marques[a], **João L. C. Santos**[b], **Lucas S. Azulay**[c], **Carlos A. R. B. Junior**[d], **Edemar M. Filho***[e], **José R. B. P. Junior**[f], **Luis C. O. Silva**[g]
[a]*Federal University of Maranhão, Av. dos Portugueses, 1966 - Vila Bacanga, São Luís - MA, 65080-805, Brazil, jgb.marques@discente.ufma.br*
[b]*Federal University of Maranhão, Av. dos Portugueses, 1966 - Vila Bacanga, São Luís - MA, 65080-805, Brazil, joao.lcs@discente.ufma.br*
[c]*Federal University of Maranhão, Av. dos Portugueses, 1966 - Vila Bacanga, São Luís - MA, 65080-805, Brazil, lucas.azulay@discente.ufma.br*
[d]*Federal University of Maranhão, Av. dos Portugueses, 1966 - Vila Bacanga, São Luís - MA, 65080-805, Brazil, carlos.brito@ufma.br*
[e]*Federal University of Maranhão, Av. dos Portugueses, 1966 - Vila Bacanga, São Luís - MA, 65080-805, Brazil, edemar.filho@ufma.br*
[f]*Federal University of Maranhão, Av. dos Portugueses, 1966 - Vila Bacanga, São Luís - MA, 65080-805, Brazil, jrbp.junior@ufma.br*
[g]*Federal University of Maranhão, Av. dos Portugueses, 1966 - Vila Bacanga, São Luís - MA, 65080-805, Brazil, claudio.luis@ufma.br*

Keywords: *thermal simulation, weather balloon, temperature*

The proper operation of payloads onboard balloons located at high altitudes and large distances is a valuable tool to prove the feasibility and increase the Technology Readiness Level (TRL) of diverse equipment, such as CubeSats. Typical high-altitude balloon experiments use a container to allocate the payload and the entire electronic system of the project inside it. These temperature-sensitive electronic components may fail if temperature levels exceed the manufacturer's recommended values. The CubeSat 1U called Aldebaran, under development at Federal University of Maranhão (UFMA), tested some of its subsystems onboard high-altitude balloons. In one of the tests, a LoRa (Long Range) transceiver sent the telemetry of sensor readings and a small picture to the ground station based. The conditions at high altitudes create a relevant environment of low temperature and pressure, difficult to reproduce in a laboratory, which the electronic components must support. This study focuses on the thermal simulation of a typical container used in high-altitude balloon projects. At high altitudes, the heat transfer occurs by radiation and convection, where the first is mainly responsible for warming the surfaces of the body. In contrast, the heat transfer by convection removes heat from the object because the freestream air becomes very cold at high altitudes. In this work, a nodal model solves the heat transfer for the steady-state condition, where one node is attributed for each side of a rectangular box made of an insulation material. A second simulation performed in the commercial software Ansys CFX solves the temperature field for a transient and three-dimensional domain. The boundary conditions are heat fluxes from the sun (direct, reflected, and diffuse) and the earth, evaluated from the ground level until 33 kilometers of altitude. Although each side has a different angle towards the sun and the earth, the temperature fields present a narrow temperature gradient due to the low value of the thermal conductivity coefficient. The simulations performed in this work agree with experimental results found in the literature, where low values as -50 ℃ are observed around 11 kilometers of altitude, at the beginning of the stratosphere. The results indicate that integrating an active thermal control should avoid failures in the electronic components by excessive low temperatures.

1. Introduction

High altitude balloon missions play an essential role in studies and technologies regarding atmospheric experiments, long-distance communications, aerial photography, internet signal transmission, radio amateur, and many others [1, 2]. It is also noted that balloons are a low-cost option for carrying payloads and enable the development of technologies for future space missions [3]. The basic configuration of a typical high-altitude balloon mission is composed of payload, balloon, gas, parachute, and rope, while the flight is divided as the ascent, fluctuation, descent, and payload recovery [4].

An essential feature of high-altitude balloon missions is the possibility of recovery of the payload after the flight, allowing significant amount of information about the instrument after its operation [5]. More than 2,000 stratospheric balloons have already been released on four continents, covering diverse scientific purposes in almost the entire atmosphere [6]. UFMA (Universidade Federal do Maranhão) has also contributed to this scenario, with two balloons equipped with stratospheric probes, launched by the Laboratory of Electronics and Spaced Systems (LABESEE) in partnership with the Alcantara Launch Center (CLA). At those times, balloons were developed to involve UFMA engineering students in a real engineering problem, as well as to serve as a preliminary testing platform for the Aldebaran-I mission, which could become the first CubeSat-type satellite developed in the northeastern region of Brazil.

Although the environmental conditions of the payload at high altitude ($\approx$35 km) are not the same as actual space missions ($\geq$400 km), heat transfer at high altitude or in space can lead to similar minimum temperature values. Thus, the conditions obtained at high altitudes make up an appropriate environment which is difficult to reproduce in the laboratory, therefore helpful for testing different systems and to increase the level of maturity of the technology.

It is essential to know the conditions under which any technology will be exposed throughout its lifecycle in order to minimize the occurrence of failures in its operation. Between the moment the balloon leaves the ground and the moment it reaches its maximum altitude, it will face a significant variation in the density, pressure, and temperature of the atmosphere [6]. At low altitudes, when the atmosphere is not yet very rarefied, convection with ambient air is one of the primary heat exchange modes of the payload. At higher altitudes, convection is still present, but it occurs with air at much lower temperatures, reaching up to -70°C [5]. This highlights the importance of the study of heat transfer in the ascent phase of the balloon for its proper design.

Thus, the purpose of this article is to obtain the temperature in the payload of a high-altitude balloon during the ascent phase. When analyzing the results obtained by the developed models, it is noticeable how they approach the atmospheric temperature and that the nodal model presents almost the same response as the three-dimensional one, making it sufficient for an analysis of the thermal behavior for the proposed conditions, and evidencing that the three-dimensional effect is not significant for the assumed conditions and hypotheses.

2. Bibliography review

This work focuses on the thermal analysis of the payload compartment, so the following studies are discussed to present an overview of the subject.

In the article of González-Bárcena et al. [6], the focus of the study was to carry out an in-depth determination of the thermal environmental conditions during the ascent phase (≈40 km) of the payload through a statistical treatment of the actual data obtained from different sources, including atmospheric surveys, radar, and satellite. Conducted at the center of the Swedish Space Corporation, which is one of the main launch sites for stratospheric balloons in Europe, the study highlights the thermal influence of the strong winds found in the tropopause, the environment conditions, and the quantification of convective and radioactive loads obtained during the ascent phase. The work presents models for the radiation involved in a typical balloon launch to the stratosphere, which is the direct solar radiation, reflected radiation (albedo), radiation emitted by the earth, radiation from the sky, and that emitted by the body itself, as illustrated in Figure 1. In the results, the authors evaluate the influence of different properties involved in radiation, such as the emissivity and absorption of the surface, as well as the Solar Zenith Angle (SZA).

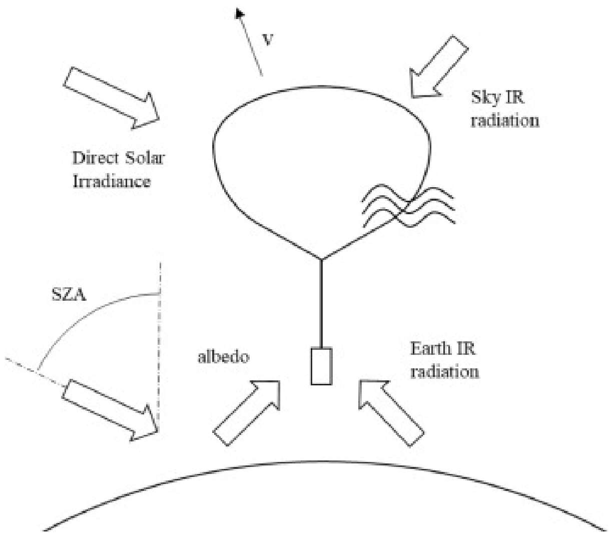

Figure 1: Scheme of radiation flows over an atmospheric balloon.
Source: González-Bárcena et al. [6].

The work of Pérez-Grande et al. [5] present an approach to the thermal behavior of the payload during the ascent phase to the altitude of approximately 40 km. To carry out the analysis, it was assumed the existence of convective, radiative and conductive thermal radiation, the first two dependent of altitude. The authors developed two non-linear models and used Runge-Kutta's numerical method to find the temperature. In one of the models, the authors considered a single point (node) for the entire simulation, representative of the box only. In the other model, an additional point was inserted to represent the electronic equipment inside the box.

In González-Llana et al. [7], the authors focus only on the cruise phase of the balloon, which is when the balloon reaches a fluctuating altitude, at 37.5 km. Much of the effort in the article is to obtain more accurate values of albedo and infrared radiation from the land of the area where the balloon passes. The authors also discuss the relationship between absorption and material emissivity of the payload for temperature variation, while using a formulation for the boundary conditions similar to the seen in the work of González-Bárcena et al. [6]. Finally, they establish values of albedo coefficient and infrared radiation from earth to reach extreme temperatures for specific values of this ratio.

In the work of Xiong et al. [8], the authors developed an analytical model for determining the temperature of a balloon in the high-altitude fluctuation phase. Simplified heat transfer models by radiation and convection have been developed to estimate the absorption and emission of a balloon film and the lifting gas. The model is still used to calculate the temperature during daytime and night periods and reaches good agreement when compared with experimental data of a balloon at 24 km of altitude.

Finally, in Dai et al. [9], transient dynamic and thermal models are established to numerically study high-altitude balloons in the rise and fluctuation phase. A model was developed and simulated in FORTRAN, where the influence on the thermal behavior of the radiation of the balloon film and the clouds were discussed in detail. In the end, the accuracy of the models was verified by comparison with the data of a balloon launch performed by NASA, which reached a constant altitude of 30.5 km in the fluctuation phase.

Due to the above revision, this work is predominantly based on references from Pérez-Grande et al. [5] ,Xiong et al. [8], and Dai et al. [9].

3. Methodology

The purpose of this study is the thermal analysis of a stratospheric balloon mission in a scenario where the altitude varies between 0 km and 33 km, focusing on the payload simulation during the flight ascent phase. To do this, the problem will be solved by two distinct models, the simplified nodal numeric model, solved in MATLAB software, and the three-dimensional numeric model, solved in Ansys CFX Student commercial software. This session will define the domain of the problem, the energy balance, and its boundary conditions.

3.1. Problem Domain

The thermal simulation will be performed only on the payload compartment of a typical mission involving a high-altitude balloon, more specifically on the one used in the launches made by UFMA in the CLA, according to Figure 2a. The load itself is a box made of expanded polystyrene (EPS) and has a rectangular geometry. However, in the analysis, for better understanding and to facilitate the calculations, it will be considered as being cubic, having six faces whose outer edge is 11.5 cm each, and the thickness of the wall is 1.1 cm. Each side of the box is identified by the reference system positioned in its center, according to Figure 2b.

In addition, during the simulation of both models used, it will be adopted that this box will be subjected to atmospheric pressure, atmospheric temperature and atmospheric density by the functions established by the standard model of the US atmosphere, which was also used in the articles [9] and [8].

3.2. Energy balance

To achieve the objective of this article, thus finding the temperature, it is necessary to solve the equation of energy conservation over the control volume (domain of the

(a) Payload launched by UFMA.

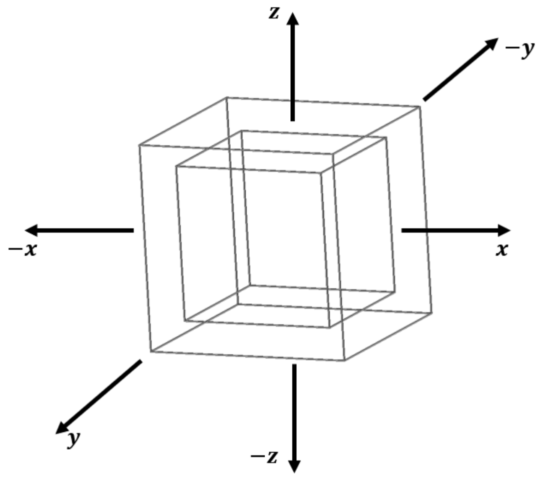

(b) Problem Domain.

Figure 2: The geometry.

problem), which is the box described in the previous section. The energy balance is known to be [10]:

$$E_{in} - E_{out} + E_g = E_{acu} \tag{1}$$

Where E_{in} is the energy's rate that enters the control volume, E_{out} is the energy's rate that goes out of the control volume, E_g is the energy's rate generated in the control volume, and E_{acu} is the accumulated energy's rate.

The external heat sources and sinks applied in the study are summarized by the direct solar radiation, diffuse solar radiation, reflected solar radiation, and emission of infrared radiation. The dissipated power (due to the thermal dissipation of the electronic components of the experiment) also provides heat to the box, increasing its temperature. On the other hand, the box transfer heat by convection with air (if the air temperature is below the box temperature) and by the emission of infrared radiation, reducing the temperature of the object. These parameters are equivalent to the boundary conditions of the problem and will be described more deeply throughout this section.

By replacing the heat sources and sinks acting on the box in previous equation, the energy balance equation becomes:

$$Q_{di} + Q_{si} + Q_{ri} + Q_{irei} + Q_{cei} + P_{dis} + Q_k = m_c \frac{dT}{dt} \tag{2}$$

Where Q_{di} is the direct solar radiation absorbed, Q_{si} is the absorbed diffuse solar radiation, Q_{ri} is the reflected solar radiation (albedo) by the earth and absorbed in the box, Q_{irei} is the external infrared radiation (balance between absorbed and emitted), Q_{cei} is the heat exchange by convection, P_{dis} is the internal power dissipation, Q_k is the heat exchange by conduction, m is mass, c is the specific heat, T is temperature, and t is time.

Assuming steady-state, the energy balance can be rewrite as follows:

$$Q_{di} + Q_{si} + Q_{ri} + Q_{irei} + Q_{cei} + P_{dis} + Q_k = 0 \tag{3}$$

3.3. Boundary conditions

To formulate the boundary conditions, the following hypotheses are assumed: the box is not rotating, balloon shading is ignored, and thermal interactions between balloon and box are ignored. The simulations are run for steady-state condition, and the internal heat dissipation (P_{dis}) will be assumed to be a hypothetical value of 0.1 W.

Having already been quoted quickly in the course of this section, the boundary conditions are the following functions:

Table 1: Boundary conditions

Heat source/sink	Function
Direct Solar Radiation	$Q_{di} = \alpha A_{fi} I_d \cos(\theta) f_s$
Diffuse Solar Radiation	$Q_{si} = \alpha A_{fi} I_s [0,5 - 0,5\cos(\phi)]$
Reflected Solar Radiation	$Q_{ri} = \alpha A_{fi} I_r [0,5 + 0,5\cos(\phi)]$
Infrared Radiation	$Q_{irei} = \varepsilon A_{fi} \sigma \left[F(T_e^4 - T_{ci}^4) + (1-F)(T_{ceu}^4 - T_{ci}^4)\right]$
Convection	$Q_{cei} = h_c A_{fi}(T_a - T_{ci})$

In these functions, α is the solar absorptivity, A_{fi} is the surface's area of side i from the box, θ is the angle between the normal surface and the solar irradiation, f_s is the factor that checks if the side i is facing the sun. Remember that the box has six surfaces, so $i = 1,...,6$. The parameter ϕ is the angle between the normal and a vertical vector, set to the side, top and bottom faces as $\pi/2$, 0 and π, respectively. The term ε is the emissivity of the box surface, σ is the Stefan-Boltzmann constant, F is the form factor from the surface i to the earth, T_e is the ground temperature in Kelvin, T_{ceu} is the equivalent temperature of the sky, T_{ci} is the surface temperature i of the box, and the h_c is the heat transfer coefficient. Finally, the I_d, I_s, and I_r are the intensities of direct solar radiation, diffuse solar radiation, and reflected solar radiation, respectively.

3.4. Simplified nodal model

In order to solve Equation 3, thus discovering the temperature on each side of the box, the simplified nodal model considers each surface to be single points, totaling 6 points. For this, thermal exchanges by conduction between the faces will be ignored.

From this, the Equation 3 will is rewritten to meet this condition, becoming:

$$Q_{di} + Q_{si} + Q_{ri} + Q_{irei} + Q_{cei} + P_{dis} = 0 \tag{4}$$

The simplified nodal model uses Equation 4 to find the payload temperature by applying the Newton-Raphson iterative method.

3.5. Three-dimensional numeric model

In order to carry out evaluations of the three-dimensional temperature field of the box, simulations were performed in the commercial software Ansys CFX Student, which is based on the Finite Volume Method (FVM).

The main advantage of the FVM over the nodal model is the conservative nature of the integral solution since the flow entering a given volume is identical to that leaving the adjacent volume [11]. In this method, the domain is discretized into a finite number of volumes adjacent to each other (forming a mesh) where the conservative equations are solved, resulting in solutions that make up a three-dimensional model. In doing so, the numerical solution maintains the conservative principle of the physical phenomenon [12].

This method will be used to solve the Equation 2, where the heat transfer coefficient by conduction is assumed to be 0.1 W/mK, because the box is made of expanded polystyrene (EPS), which is a thermal insulation material with poor thermal conductivity.

4. Results

This section presents and discusses the results obtained by the simplified nodal model solved in MATLAB and the results achieved by the simulated three-dimensional model in Ansys CFX Student.

4.1. Simplified nodal model

Figure 3 is the total incoming radiation in each face of the box, for diverse altitudes. The -Z face had the highest growth and the highest absolute value due to its projection towards the earth. The Y-face received the most heat from the side faces, as it was designed to be more exposed to the sun. The faces -X and -Y are overlapped in the graph and were the ones that received minimum heat by radiation, as they did not come into contact with the Sunlight.

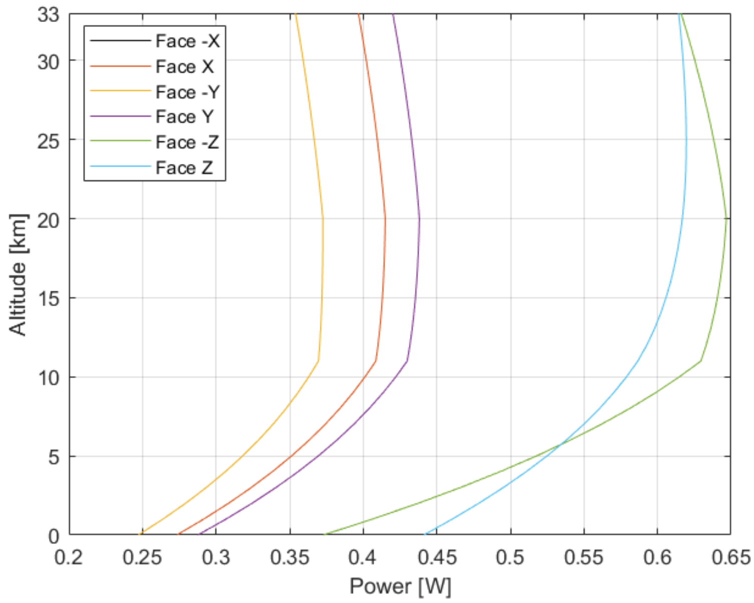

Figure 3: Total incoming radiation on surfaces according to altitude.

In Figure 4, temperatures on each face are plotted. It is noticed that up to the altitude of 11 km, the temperatures remained practically the same and constantly reduced from the initial temperature of 287 K, at ground level. After that, they begin to heat at different rates, especially after 20 km. The Z-face and the -Z-face overlap on the graph and are the ones that warmed the most, as expected by radiation analysis. From the side faces, the X and Y faces were the others that warmed the most because they were exposed to direct solar radiation.

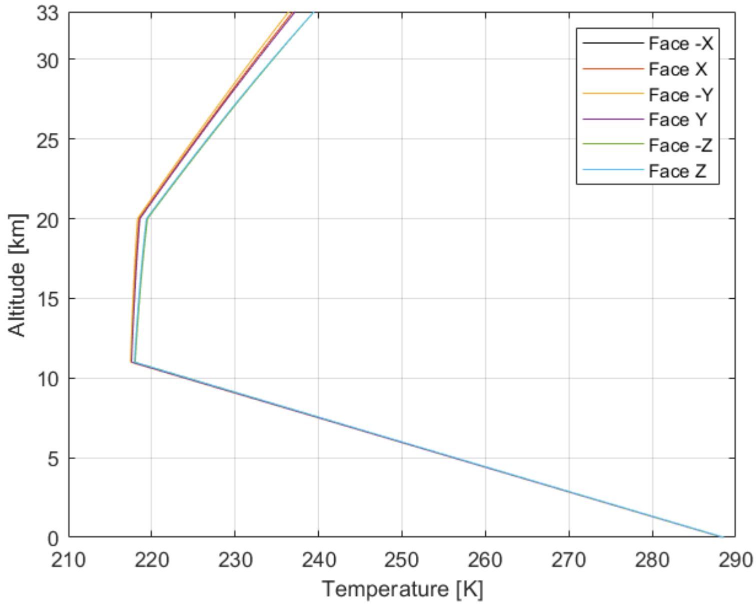

Figure 4: Temperature on surfaces according to altitude.

4.2. Three-dimensional model

To analyze the results of the three-dimensional model solved in the software Ansys CFX Student, four altitudes were chosen 0 km, 11 km, 20 km, and 33 km. On all cases, there is a low-temperature gradient, as illustrated in Figure 5, for the altitude of 33 km.

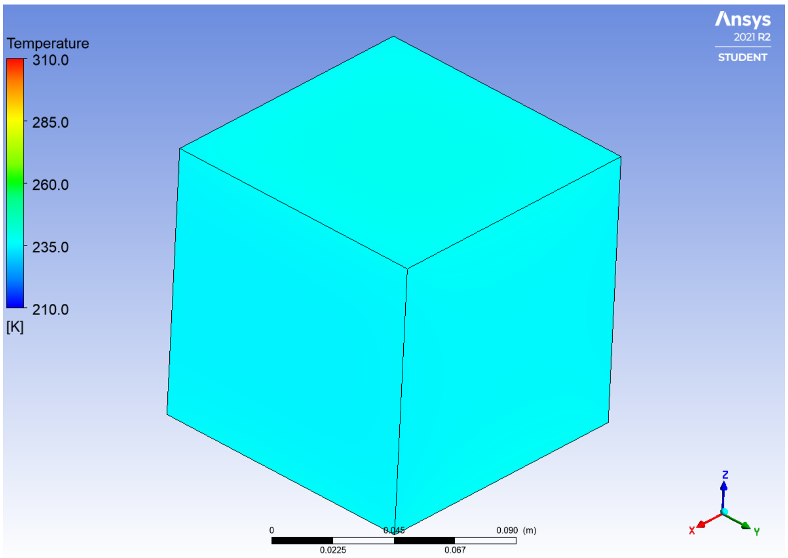

Figure 5: Temperature field for the three-dimensional numerical model, at 33 km.

4.3. Comparisons between the models

In Figure 6 are plotted the temperature values observed in each model, as well as the atmosphere temperature model. It is noticed that the temperatures of the simplified nodal model and the three-dimensional have very close values, with the most significant difference being 1.3 K at an altitude of 33 km. It is also observed that in the two models, the temperatures were higher than the atmospheric, which was expected due to the heating of the faces by radiation. Finally, the simplified nodal model can capture the overall results seen in the more complex three-dimensional model with reasonable accuracy.

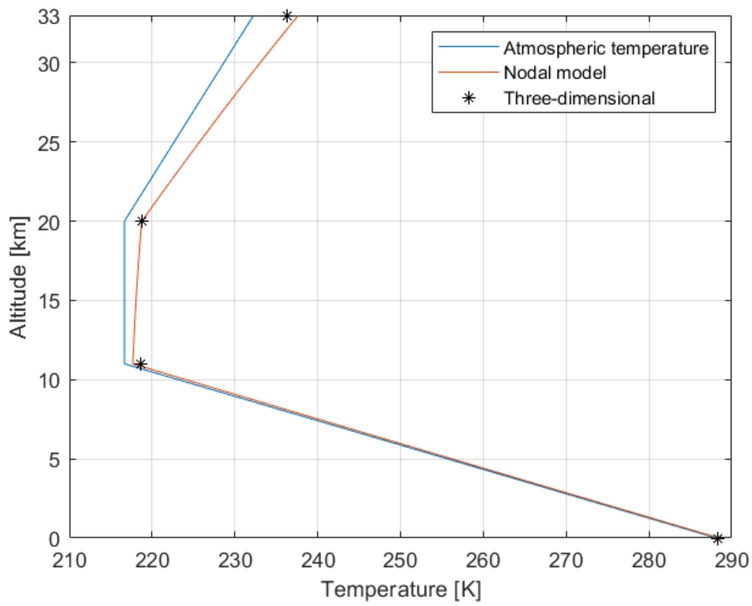

Figure 6: Temperature obtained in each model, along with the atmospheric temperature model.

5. Conclusions

Analyzing the results obtained by the developed models, it is noticeable how they both approach the atmospheric temperature, and that the nodal model presents virtually the same response as the three-dimensional one. Therefore, it is reasonable its adoption for thermal analysis of the container lifted by weather balloons. Future works regarding the effect of internal heat dissipation by active heaters should be investigated for thermal control of the payload, as well as for the power budget associated to it.

References

[1] S. Levy, How google will use high-flying balloons to deliver internet to the hinterlands, 2013. Accessed on: December 14th, 2021.

[2] ARRL, Balloons carrying amateur radio payloads still circling earth, 2014. Accessed on: December 12th, 2021.

[3] F. Lefevre, History and perspectives of scientific ballooning, volume 471, 2001.

[4] S. L. Larson, J. C. Armstrong, W. A. Hiscock, The first frontier: High altitude ballooning as a platform for student research experiences in science and engineering, American Journal of Physics 77 (2009) 489–497.

[5] I. Pérez-Grande, A. Sanz-Andrés, N. Bezdenejnykh, P. Barthol, Transient thermal analysis during the ascent phase of a balloon-borne payload. comparison with sunrise test flight measurements, Applied Thermal Engineering 29 (2009) 1507–1513.

[6] D. González-Bárcena, A. Fernández-Soler, I. Pérez-Grande, Ángel Sanz-Andrés, Real data-based thermal environment definition for the ascent phase of polar-summer long duration balloon missions from esrange (sweden), Acta Astronautica 170 (2020) 235–250.

[7] A. González-Llana, D. González-Bárcena, I. Pérez-Grande, Ángel Sanz-Andrés, Selection of extreme environmental conditions, albedo coefficient and earth infrared radiation, for polar summer long duration balloon missions, Acta Astronautica 148 (2018) 276–284.

[8] J. Xiong, J. Bai, L. Chen, Simplified analytical model for predicting the temperature of balloon on high-altitude, International Journal of Thermal Sciences 76 (2014) 82–89.

[9] Q. Dai, X. Fang, X. Li, L. Tian, Performance simulation of high altitude scientific balloons, Advances in Space Research 49 (2012) 1045–1052.

[10] T. Bergman, F. Incropera, D. DeWitt, A. Lavine, Fundamentals of Heat and Mass Transfer, Wiley, 2011.

[11] F. Moukalled, L. Mangani, M. Darwish, The Finite Volume Method in Computational Fluid Dynamics: An Advanced Introduction with OpenFOAM® and Matlab, Fluid Mechanics and Its Applications, Springer International Publishing, 2015.

[12] E. M. Filho, A Coupled Irradiance - Thermal 3D Numerical Framework for Simulation of CubeSats, Ph.D. thesis, Universidade Federal de Santa Catarina, Joinville, SC, 2021.

15

Session 15 - On-Board Computer and EPS

Simulation of CubeSat on-board computer system operating modes using MATLAB

Jesus Tapia[(1)], **Jhasmin Huillca**[(2)], **Omar Blas**[(3)], **Haile Abad**[(4)]
[(1)] *Universidad Nacional de Ingeniería, +51 976485545, jtapiag@uni.pe*
[(2)] *Universidad Nacional de Ingeniería, +51 932698715, jhuillcaa@uni.pe*
[(3)] *Universidad Nacional de Ingeniería, +51 989546590, oblasm@uni.pe*
[(4)] *Universidad Nacional de Ingeniería, +51 931 274 097, john.abad.a@uni.pe*

Keywords: *On-Board Computer, CubeSat, MATLAB, StateFlow.*

A fundamental part of a nanosatellite is its control subsystem and on-board computer (OBC) whose functions are to receive and transmit commands, provide data storage, execute the commands and ensure the good state of the nanosatellite. It is therefore important to perform as many tests and simulations as possible, in that sense a simulation of the different operating modes of a Cubesat during a period of 24 hours using state machines in Stateflow has been developed. For this purpose, data from the CubeDesign 2021 competition (organized by the National Institute for Space Research of Brazil-INPE) have been used, and the robustness of our system has been achieved by considering the largest number of possible scenarios, since a failure would be fatal for the mission. All this work is framed in the development of a future nanosatellite that aims to follow in the footsteps of CHASQUI I (CubeSat created in the facilities of the National University of Engineering and launched into space in 2014). The MATLAB simulation platform and its control logic tool StateFlow have been used for this work.

1. Introduction

At present, the development of Cubesat nanosatellites is in a continuous evolution, its fundamental structure is 1U (standard dimension of 10x10x10cm) with a mass ranging from 1 to 1.33 kg. In the academic and research fields, its study has increased in recent years, proving to be an important tool for the introduction of aerospace technology. In this context, the National Institute for Space Research of Brazil (INPE) organized the Virtual CubeDesign 2021 competition, whose objective was that the teams were able to develop modeling and simulation activities of space systems, fundamental for the analysis of a space mission.

For the development of the challenge, the Simulink/Stateflow tool was used to model and simulate the behavior of the OBC, the input data for this challenge were provided by the organizing committee, three important factors were considered when modelling the simulation, which were the simulation step, the total simulation time and the mode of operation.

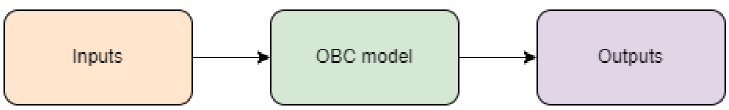

Figure 1: System overview.

Figure 1 shows a summary of the work performed, being the inputs the data provided by the organizer (battery status, latitude, longitude, etc) and requiring the output in the form of graphs and tables (battery voltage, visibility, operating modes achieved, etc). Among the main limitations of the work are that the simulation will be carried out at subsystem level and does not consider all aspects at component level, also the challenge considers hypothetical situations. Therefore, in a real mission, it is necessary to adapt some approaches so that the model and, consequently, the simulation result is faithful to the mission requirement [1].

To better understand the challenge and the information management subsystem, it is necessary to mention some important concepts.

- **State machines** They are a method that allows us to model a wide variety of systems whose outputs depend on the history of inputs and not only on their current value, in addition, certain Boolean conditions must be met to pass from one state to another (see figure 2).

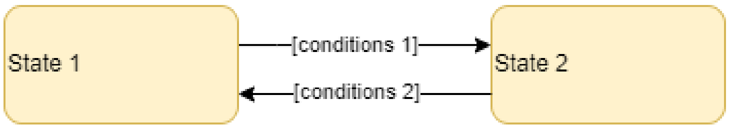

Figure 2: Two-state system.

- **On-Board Computer.** The on-board computer, commonly known by the acronym OBC (On Board Computer), is the brain of the satellite or spacecraft. It determines the satellite's mode of operation, communicates with each of the subsystems and is responsible for transferring information. Another of its functions is the response to the telecommands sent from the ground station, as well as the supervision of space missions, etc. It also includes autonomous failure management functionalities to ensure that the spacecraft can automatically recover from major anomalies and enter a safe state without the interaction of ground operators, in case of an emergency. Figure 3 shows the general scheme adopted for the operation of Cubesat.

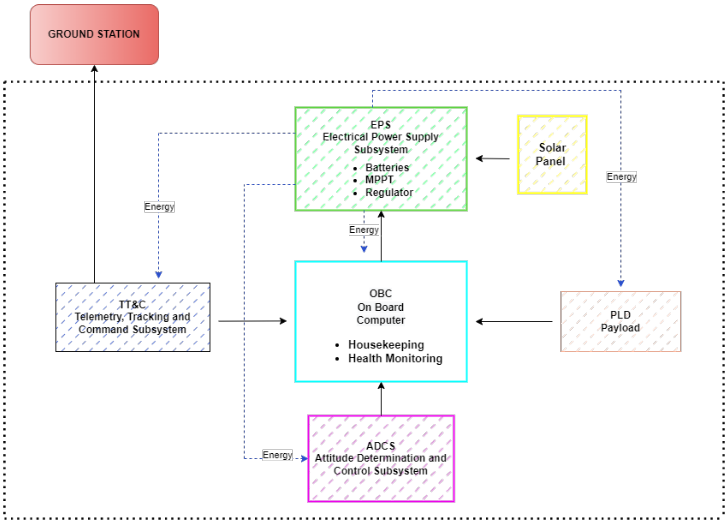

Figure 3: Schematic diagram of Cubesat operation.

In the work of Osman and Mohamed [2] performed a simulation of the OBC system and modes of operation in Proteus, they considered that this system had only two modes of operation (normal and interrupt), on the other hand, Rutwik Jain et al. [3] defined 12 operational modes for the satellite with a hyperspectral camera as payload. In our work we have considered six operational modes and we will treat both the satellite and the OBC system operational modes indistinctly.

2. PROCEDURE

2.1. Modes of operation

The OBC operates in different modes of operation that determine the tasks that it must perform at any given time. According to the regulations provided by the INPE, the following modes of operation that can be achieved by the CUBESAT during the mission must be considered.

Off, is the state where the OBC is completely switched off, this state is also reached due to the lack of power supply from the EPS or by Hard Reset remote control. When designing Stateflow, we chose to define this state as a default state, and it can also be reached from any other operating mode.

Boot, is the start state of the OBC software, this state is reached after the power supply that the OBC receives from the EPS, this power supply must exceed a certain threshold voltage (system minimum). We have as an output condition that this state must occur immediately after the identification of the deployed state.

Deployment, in this state the antennas are deployed, the exit from this mode of operation occurs after 10 unsuccessful attempts.

Safe is the operational satellite state and is reached in three situations: when a failure occurs in the nominal and transmitting state, after completion of the deployment state and by telecommand. It can only be exited by means of a valid telecommand.

Nominal, the main operating state that can only be switched to the safe state in the event of a system failure.

Transmitting is the transmission of information obtained by sensors or cameras. It is reached when the ground station is visible or, failing that, by telecommand. Visibility shall be defined by the range of the earth station by taking the longitude and latitude data; if it is not within the range, it shall be set to the nominal state.

In order to plot the states reached, the notation in Table 1 will be considered.

Table 1: Operational modes.

#	Modo de Operación
0	Off
1	Boot
2	Deployment
3	Safe
4	Nominal
5	Transmitting

2.2. Telecommands

Within the behavioral system of the OBC, received telecommands have higher priority and will change the operating mode of the system regardless of autonomous operation.

The telecommands defined in the work for the simulation are: ”hard reset”, ”soft reset”, ”nominal”, ”safe” and ”transmitting”. The ”hard reset” turns off the OBC system, while the ”soft reset” only represents a software startup. On the other hand, the ”nominal”, ”safe” and ”transmitting” telecommands set the operating mode to the state of the same name.

In the challenge we have considered it appropriate to facilitate the work by defining the telecommands as integers as shown in Table 2, in a real situation it would be implemented as an interrupt in which we would need to define priorities.

We have defined the telecommands in the MATLAB Workspace as a timeseries object so that a continuous reading of -1 indicates that no information is being received from the ground station, while a value from 0 to 4 allows us to enter a specific operation mode for the CubeSat.

3. Result

In the figure 4 we observe the general architecture, the telecommand and visibility variables use the latitude and longitude information to indicate if it is possible to send data to the ground station. The parameter that defines the transition from ”Off” to ”Boot” mode is the battery voltage, using as reference [4] we define that $V_{battery} > 3.3V$

Table 2: List of telecommands used.

Telecomando	Operation Mode
-1	No actions
0	Hard Reset
1	Soft Reset
2	Nominal
3	Safe
4	Transmitting

must be satisfied for the transition to occur. In the ”Boot” mode, the processor initialization must be performed in order to start the Real Time Operative System (RTOS) and the software layer [5]. Once the antenna is deployed, the transition to the ”Safe” state takes place.

In the ”Safe” state, the attitude stabilization and energy generation will take place by means of the orientation of the solar panels. The change to another state is only done by remote control. In the figure 5 we see the design in StateFlow, the data processing and the graphs are obtained in a Matlab script (.m file). For the simulation in Simulink, steps of 5 seconds have been considered, being the total time of one day (86400 s).

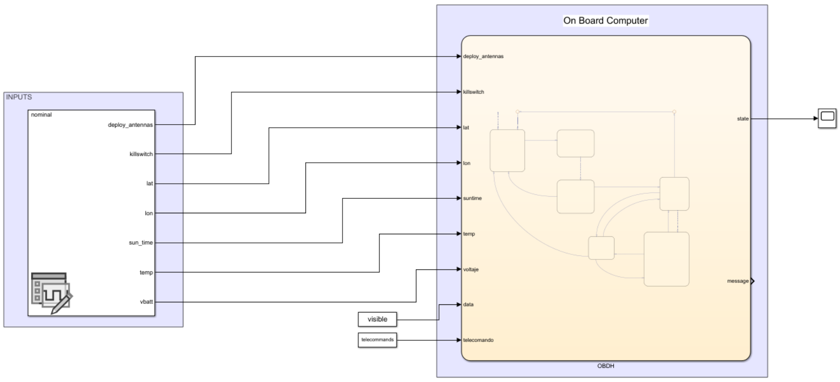

Figure 4: **General view in Simulink.**

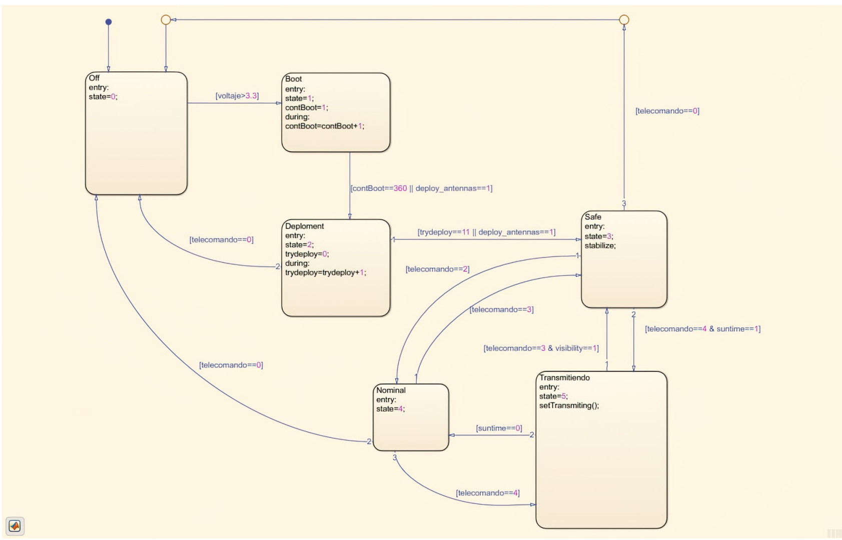

Figure 5: **Model in Stateflow.**

In the figure 6 we observe the battery voltage throughout the day, we notice that there are small variations (the maximum value is 8.5V and the minimum is 8.0795V) this is due to the pointing of the nanosatellite.For the power supply of the different subsystems a buck converter would have to be used since the operating voltages vary depending on the selected components and the payload, for example, in the case of the CubeSat OUFTI-1 they considered buses of 3.3V, 5V and 7.7V for the OBC1, OBC2 and communications subsystems respectively [6].

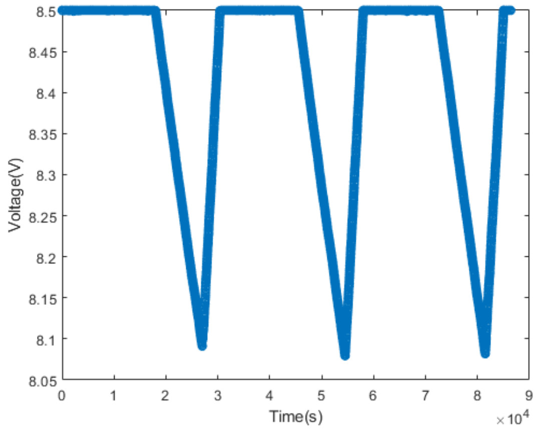

Figure 6: Battery voltage throughout the mission.

Using the data from the table 3 we can calculate the visibility time of the ground station, in the figure 7 we can see the trajectory of the nanosatellite and the position of the station (it has been considered that it is located in the facilities of the National University of Engineering). The figure 8 shows the interval in which the satellite can send data to the ground.

Table 3: Characteristics of the orbit.

Parameter	Value
Altitude	350km
Inclination	$97.55756°$
Semi-major axis	6927 km
eccentricity	2.06×10^{-3}

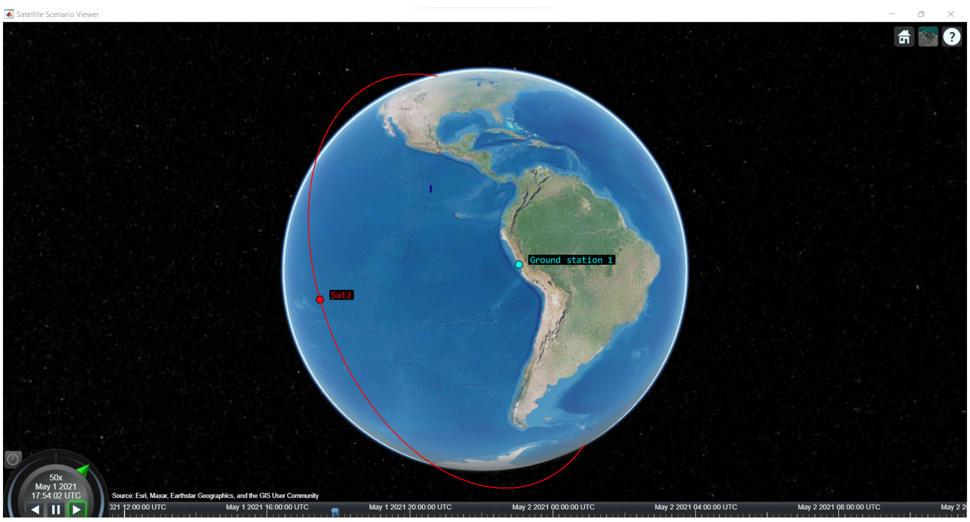

Figure 7: Trajectory of the nanosatellite.

Source	Target	IntervalNumber	StartTime	EndTime	Duration
"Sat2"	"Ground station 1"	1	01-May-2021 13:08:00	01-May-2021 13:11:00	180
"Sat2"	"Ground station 1"	2	01-May-2021 14:38:00	01-May-2021 14:49:00	660
"Sat2"	"Ground station 1"	3	02-May-2021 01:09:00	02-May-2021 01:17:00	480
"Sat2"	"Ground station 1"	4	02-May-2021 02:42:00	02-May-2021 02:53:00	660

Figure 8: **Visibility of the ground station.**

Finally, figure 9 shows the states reached during the mission in one day.

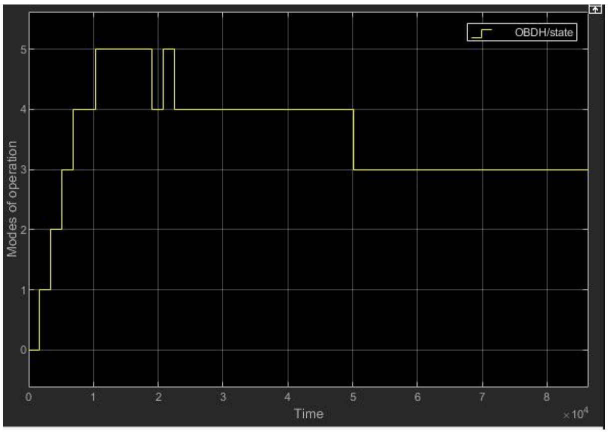

Figure 9: **Operating modes achieved during the simulation according to the table 1.**

4. Conclusion

The behavior of the on-board computer was modeled and simulated over a 24-hour period using state machines, also the visibility times of the ground station and the CubeSat trajectory were successfully calculated and plotted.

The development of the OBC CubeDesign challenge was essential for the members of the CHASQUI II group (Cubesat under development at the National University of Engineering facilities) to be able to understand the functioning and operation modes of the on-board computer.

As future research, it is proposed to extend the present work to include the simulation using Proteus, where the programming of the microcontroller and the reception of data from the rest of the subsystems would be more realistic.

References

[1] I. N. de Pesquisas Espaciais, Cubesat virtual 2021, `http://www.inpe.br/cubedesign/2021/es/CubeSat/reglamento.php`, 2021.

[2] D. A. M. Osman, S. W. A. Mohamed, Hardware and software design of onboard computer of ISRASAT1 CubeSat, in: 2017 International Conference on Communication, Control, Computing and Electronics Engineering (ICCCCEE), IEEE, 2017.

[3] R. Jain, S. Sharma, K. Aggarwal, T. Goyal, A. Sundhar, U. Anand, N. Sahu, J. Parikh, Modes of operation for a 3u cubesat with hyperspectral imaging payload.

[4] ISIS, Isis on board computer, `https://www.isispace.nl/wp-content/uploads/2016/02/IOBC-Brochure-web-compressed.pdf`, 2016.

[5] J. Eickhoff, Onboard Software Static Architecture, Springer Berlin Heidelberg, Berlin, Heidelberg, pp. 87–118.
[6] P. THIRION, Design and Implementation of On-board Electrical Power Supply of Student Nanosatellite OUFTI-1 of University of Liège, Master's thesis, Applied Science Faculty, 2008.

Onboard Computer for a LEO CubeSat Nanosatellite

Camila Barbosa(1), **Samaherni Dias**(1), **Kurios Queiroz**(1), **Alex Alves**(1)
(1) *Federal University of Rio Grande do Norte, UFRN, camila.barbosa.095@ufrn.edu.br*

Keywords: *OBC, Nanossatellite, CubeSat, PCB, FreeRTOS.*

Traditionally, the aerospace industry has been associated with large, sophisticated, and expensive devices, and it has been historically financed by governmental agencies. The space missions based on satellites were no exception to the rule. In recent decades, CubeSat nanosatellites have made it possible for universities and small companies to study these technologies and go to space. In this context, the National Institute of Spatial Research (INPE) proposed the CONASAT project, which has as its goal to update the Brazilian Environmental Data Collection System (BDCS), replacing the old satellites with a new CubeSat constellation. The BDCS, beyond satellites, is also composed of ground stations and Data Collection Platforms (DCPs) spread across the Brazilian territory. The INPE chose a 1U size CubeSat equipped with their Environmental Data Collector (EDC) as payload to collect DCPs data and send it to the ground stations. This work presents the design of an onboard computer (OBC), made of components off-the-shelf (COTS), for low-orbit CubeSat satellites. Aiming to obtain the requisites for digital systems in low-orbit, it proposes the electronic schematic and the printed circuit board (PCB) of an onboard computer compatible with the architecture of the first satellite in the BDCS constellation, the CONASAT-01, as well as the software and operating system required for the mission. The CONASAT-01 is a 1U size CubeSat with four subsystems: Electrical Power Subsystem (EPS), UHF communication subsystem, Attitude Determination and Control Subsystem (ADCS), and On-Board Computer (OBC). A third company developed the CONASAT-01's hardware, and the proposed OBC must be compatible with all CONASAT-01 subsystems. The developed board embeds FreeRTOS on an STM32 microcontroller to manage and execute the missions' tasks, such as housekeeping, supervising telecommand & telemetry, and sending and receiving data from ground stations. All the communications drivers were also developed. The nationalization of the OBC compatible with the scheduled mission and with the global market is one of the main contributions of this project: it strengthens Brazilian satellite research as it helps to develop the next CONASAT CubeSats.

1. Introduction

Since the Soviet Union launched Sputnik I, the first artificial satellite, in 1957, over 9000 satellites have been launched by more than 40 countries. Nowadays, there are about 3300 operating [1].

In 1985, Brazil had its first launched satellite, the Brasilsat A1, built by a Canadian manufacturer and a crucial piece for the national telecommunications sector in the '80s. Over the years, the country launched more satellites, among these, the Data Collector Satellites (DCSs), the DCS 1 and 2, built by the National Institute of Space Research (INPE). Operating with the Data Collector Platforms (PCDs), which are dispersed countrywide, they aim to provide daily environmental data from all regions in Brazil [2, 3].

Traditionally, the aerospace industry requires a large engineering team, which, historically, is financed by governmental agencies [4]. In the last decade, however, advances in miniaturizing technologies allowed the development of smaller spaceships with Commercial off-the-shelf (COTS) components, which are compact, low-cost, and have low power consumption [5, 6].

Nanosatellites became an accessible opportunity to go to space and study aerospace technologies. Proposed in 1999 by Jordi Puig-Suari, from California Polytechnic State University and Robert Twiggs from Stanford University, the CubeSat pattern allows researchers to participate in an entire space project: project, manufacture, testing, launch, and operation of a satellite [7].

A CubeSat is based on a standardized unit of mass and volume. The basic CubeSat unit (1U) measures 10x10x10 centimeters and has a maximum mass of 1,33 kilogram. These units may be combined (2U, 3U, 6U, 12U, etc) for bigger satellites [8]. These settings are illustrated in Figure 1.

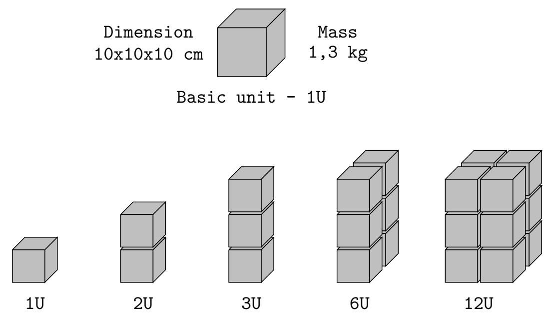

Figure 1: CubeSat settings based on the basic unit U [9]

Due to the dimensions, cost, and development time considerably decreased in comparison to traditional satellites [6], the CubeSat pattern has become very popular, not only in university groups, but for researchers, space agencies, governments, and companies as well.

CubeSat Nanosatellites are commonly organized in stacked modules (See Figure 2). Each module represents a satellite subsystem:

- Electrical Power System (EPS);
- Attitude Determination and Control System (ADCS);
- Telemetry, Tracking & Command (TT&C);
- Onboard Computer (OBC);
- Payload;

Every subsystem plays an important part in the nanosatellite operation. This work highlights the onboard computer, which is the subsystem responsible for the processing of the internal satellite's data. The OBC provides a platform for data management among all the nanosatellite subsystems [10].

Currently, the price of an OBC from manufacturers such as ISIS, EnduroSat, and GomSpace varies between 3500 and 9000 USD dollars [11, 12, 13]. Although this is

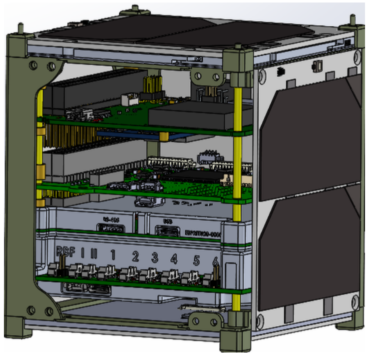

Figure 2: 1U CubeSat's stacked modules

about 1000 times cheaper than conventional satellites, it is still a high cost for national academic studies.

Thus, this work proposes an onboard computer for a low earth orbit (LEO) CubeSat nanosatellite. Aiming to meet all the digital systems requirements in LEO (reliability, robustness to the space environment, power efficiency, redundancy), the electronic project, and the printed circuit board (PCB) of a CONASAT-01 compatible OBC are presented here.

This work is structured as follows: section 2 presents the related works as well as the theoretical background used in these papers. Section 3 presents the CONASAT-01 CubeSat. The proposed method is given in section 4, and in section 5, we make our final remarks.

2. CubeSats, OBC, and the Low-Earth Orbit Environment

In the last decades, the participation of small satellites in space missions increased considerably. And the CubeSat designer specifications are one of the leading factors that determined this [14].

Proposed in 1999 by university professors, the CubeSat designer specifications were designed aiming at cost and development time reduction. Thus, allowing academics and small companies to have access to this technology [7].

About 1474 nanosatellites were launched until January 2021, and 1357 of these are CubeSats [15], most of them in the last eight years.

As mentioned, nanosatellites are composed of different subsystems, each one performing a specific task. The onboard computer is the system responsible for data management of the satellite, the communication between the subsystems, and processing the data transmitted to the satellite [10, 16].

According to [17], the main elements of an OBC are processor units, memory, data buses, power supply, clock, and additional peripherals.

The processor unit affects the OBC project as well as the entire satellite design. CubeSats have distinct processing units, for example, FPGAs, one or multiple microcontrollers [18, 19, 10], MPSoC [14], and even open-source platforms such as Arduino, Raspberry Pi, and BeagleBone [5, 20].

A common option for the development of a CubeSat OBC is the acquisition of a market solution. Today, subsystems may be commercialized individually or joined in a complete platform. These products usually have a robust hardware architecture, flight heritage and allow software customization [21]. Among others, there are the iOBC from ISIS [11], the OBC from EnduroSat [12], and the NanoMind A3200 from GomSpace [13].

When developing an OBC, mostly while selecting the components, it must be taken into consideration some attributes:

- The low-power consumption;
- The temperature range in LEO;
- The radiation in LEO;

The last two refer to the effects of the space environment on electronic components. From radiation, the most common effects are the Total Ionizing Dose (TID) [10] and Single Event Effect (SEE) [14, 10].

Some fault-tolerant techniques are used to mitigate these effects. Considering budget and dimensions limitations, protections against radiation are not usual in CubeSats. Radiation-resistant processor units, for instance, cost about 1000 times more than an ARM-based one. In consequence, OBC projects usually adopt countermeasures. Among the ones implemented in hardware are cold and hot redundancy, triple modular redundancy (TMR), error detection and correction (EDAC), and memory cleaning [22, 10, 23].

Beyond this, the OBCs need a real-time computational answer with priority levels. Then, it is common for CubeSats to use RTOS (Real-time operational system) on OBC. One of the tasks that require an RTOS in an OBC is the ADCS. Considering RTOS, we can highlight the FreeRTOS, developed by source code license [24], which shows high portability (configured for 35 microcontrollers). The FreeRTOS was used in several CubeSat missions [25, 26, 27] and is supported by the majority of COTS's processors' suppliers.

3. The CONASAT-01

The Brazilian Data Collect System (SBCD) is a system that collects several environmental information from PCDs spread across all Brazilian territories. The SBCD is composed of PCDs, satellites in earth orbit, ground stations, and mission control. The PCDs are embedded systems with environmental sensors that collect data such as temperature and humidity and send them to satellites, which resends these data to ground stations in specific places in Brazil. Finally, the ground stations are responsible for jointing all received information and sending them to mission control. [3, 28]

The SBCD has three satellites they are SCD-1, SCD-2, and CBERS 4A. The two first are out of lifetime and can stop to operate at whatever moment. In this context, INPE introduced the CONASAT project, which proposes the launch of a constellation of environmental nanosatellites. Within this scenario, the constellation would be able to join the SBCD, to receive, manipulate and transmit the data sent by the PCDs [3].

For the first mission, the INPE is developing just OBC's onboard software for the first satellite of the constellation, the CONASAT-01, a 1U CubeSat from the Bulgarian company EnduroSat (see Figure 3) equipped with the modules: EPS, TT&C, and the onboard computer.

The CONASAT-01 is being developed to have as payload the Environmental Data Collector (EDC). This subsystem will be responsible for receiving data from PCDs

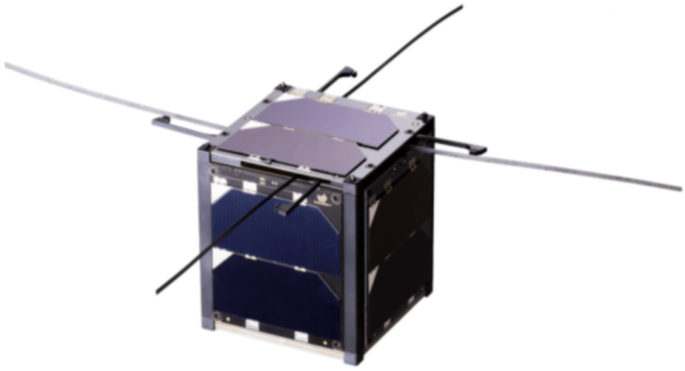

Figure 3: EnduroSat's 1U cubesat.

spread through Brazilian territory. Afterward, the data must be transmitted by telemetry to earth stations [29].

The ADCS of CONASAT-01 is within the OBC. The subsystem consists of a set of sensors such as magnetometers, accelerometers, solar and temperature sensors. These help determine the satellite orientation, and also control magnetorquers. The satellite power comes from solar panels positioned in the CubeSat's faces. The CONASAT-01 in its test bench is presented in Figure 4.

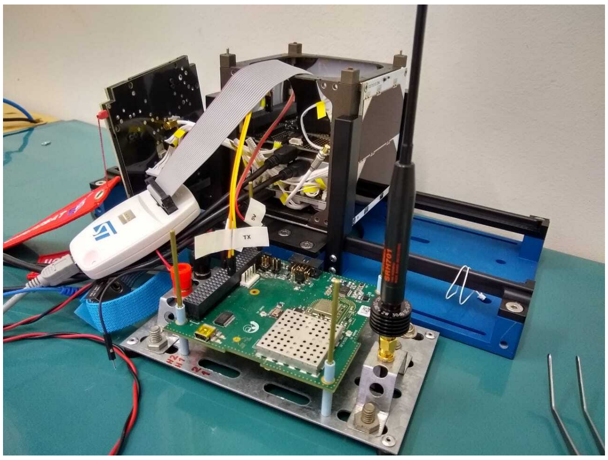

Figure 4: CONASAT-01 in test bench at INPE

4. OBC Project & Development

The First CubeSat of the CONASAT constellation has the following requisites:

1. 1U dimension;
2. No propulsion;
3. INPE's EDC as payload;
4. Omnidirectional antenna;
5. Parameters monitoring of the OBC and payload;
6. Low Earth orbit (below 700 km);

This work's objective is to propose an OBC to replace EnduroSat's OBC in the next CONASAT CubeSat. The requisites to the proposed OBC are:

1. To be completely compatible with CONASAT-01's hardware and software;
2. To use only COTS components;
3. To be robust to the radiation effect in LEO;
4. To be low cost;
5. To be ready for ADCS module inclusion and sensors filtering;
6. To be ready for new updates;

The low cost of the proposed OBC is related to the absence of royalties payments in the project. The solution by EnduroSat, for example, is also manufactured with COTS but the aggregated value due to flight heritage and the engineering project in general. This characteristic makes the Bulgarian manufacturer's onboard computer more expensive. Thus, in this work, we propose an Onboard Computer (OBC) to 1U CubeSat made of only COTS components, with an ARM processor as CPU (Central Processing Unit) and the FreeRTOS as an operational system.

The next subsection presents the OBC architecture, the component selection process description, and the basis for each project decision.

4.1. Architecture & Hardware Design

In component selection were considered low-power consumption, cost, communication interfaces, radiation influence, and compatibility with the CONASAT-01.

According to the OBC requirements, we propose the OBC architecture (See Figure 5), which uses as CPU an ARM-based 32-bit Cortex-M4 of the STM32 family. We chose this family to reuse the software and libraries developed for the CONASAT-01. To keep the hardware compatibilities, we adopt the STM32F427, which has a low-power consumption and frequency of up to 180MHz.

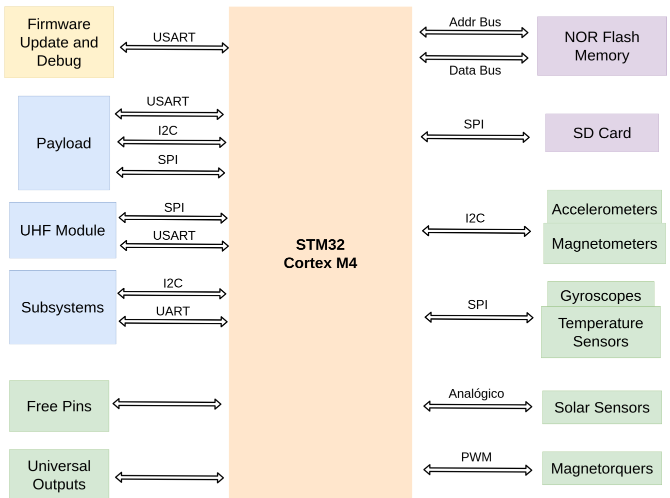

Figure 5: OBC Architecture

Beyond the processor, the OBC architecture defines all communication buses and the main peripherals. Based on Figure 5, it required:

- 4 SPIs;

- 3 I2Cs;
- 4 USARTs;
- Data and address buses for the 1GB NOR Flash memory;
- 6 analog inputs;
- 6 PWM outputs;
- 5 digital inputs/outputs;

With the processor unit defined, the selection of the other components was oriented by it, mainly the memory, sensor, and all COTS. Other factors also influenced the choice: cost, range, communication buses, and power consumption. The list of the selected components is in Table 1.

Table 1: Chosen Components for the OBC

Component	Reference
Microcontroller	STM32F427ZIT-LQFP144
1GB NOR Flash Memory	MT28EW01GABA
Accelerometer	LIS2MDL
Magnetometer	LIS2MDL
Channel-P MOSFET	FDG6316P
Channel-N MOSFET	DMN3270UVT-7
3.3V Voltage Regulator	MIC2920
5V Voltage Regulator	MIC2920

After the definition of the OBC's components, we need to place and route them. Then, we design a dual-layer PCB with dimensions and some connectors positions compatible with the CONASAT-01's OBC. The electronic schematic and PBC were designed with the assistance of a PCB software. Considering compatibility with CONASAT-01 as one of the main requirements, the essential external OBC interfaces must be defined by the INPE nanosatellite. This requirement will allow the board to be tested within the CONASAT-01. It also allows the launch of the proposed board in the next CONASAT constellation nanosatellite.

Hence, the dimension, perforation, and position of some connectors (PC/104, seven MOLEX 53398-1271, and a MOLEX 53398-0471) are the same as the CONASAT-01's OBC. The PC/104 allows the communication between the OBC and other subsystems from the CubeSat and provides 3.3V, 5V, and GND buses to the board. Named PAN-GT (from 1 to 6) are MOLEX 53398-1271, which, similar to the PC/104, allow communication with other nanosatellite modules. The sequence of PAN-GT-1 to PAN-GT-3 provides access to temperature sensors, gyroscopes, and solar sensors, while the sequence of PAN-GT-4 to PAN-GT-6 provides access to the PWM for the magnetorquers. The last MOLEX of this spec supports access to a MicroSD card by other subsystems. The same memory card is directly connected to the microcontroller by the SD connector. The placement of these connectors is presented in Figure 6.

The PC/104's pins, which are modular and shared with the entire nanosatellite, include: Communication with payload by USART, I2C and SPI; Communication with

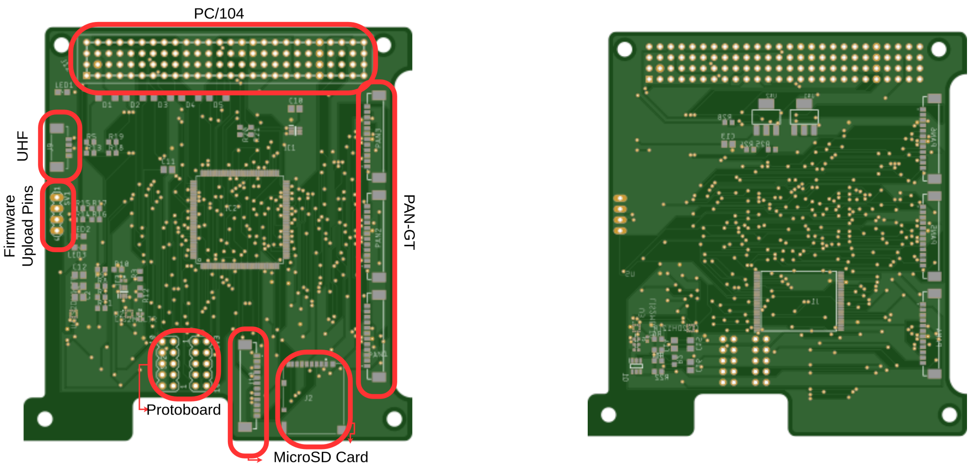

Figure 6: PCB with specified connectors

UHF module by SPI and USART; Communication with other subsystems by I2C and UART; OBC enable; 5 universal outputs;

Presented the required communication interfaces responsible for sensor data acquisition and control of the nanosatellite actuators, the ADCS sensoring, part of which is embedded on the board, is defined. Two accelerometers and two magnetometers are set on the board with cold redundancy, offering a strategy in case of LEO radiation damage.

The OBC was designed to allow only one of the redundant components to stay active. In this way, the power consumption does not increase because of the component duplicity. The component selection was implemented in hardware with two MOSFETs acting as switches.

Firmware upload will happen through a USART interface with an external FTDI (Future Technology Devices International). This OBC also has embedded non-volatile memory, 1GB NOR Flash. This type of storage is necessary to keep the telemetry and payload data before sending them to the earth station. NOR Flash memory has high access speed, and is resistant a radiation during the access [10].

There are two voltage regulators as well, for 3.3V and 5V. Lastly, a limited protoboard area with free pins, the possibility of connections with external clocks along with 3.3V and GND buses. The dimensions and perforations of the PCB were based on the EnduroSat structure to secure a perfect attachment on it.

After selecting the components and necessary circuits, the processor unit pins were singled out. Based on the microcontroller datasheet, the pins were chosen in this order of priority: Flexible Memory Controller (FMC) pins for the NOR Flash memory; I2C, SPI, USART, and UART interfaces; Analog inputs; PWM outputs; Universal pins;

4.2. Software Design

We propose the software architecture to repurpose some of the software routines and libraries developed for CONASAT-01. Thus, we keep the same real-time operating system (FreeRTOS) and the same hardware abstraction layer (HAL) of the CONASAT-01's OBC. Both FreeRTOS and HAL are provided by the microcontroller manufacturer (STMicroelectronics). The HAL is in the CMSIS (*Cortex Microcontroller Software Inter-*

face Standard) standard created by ARM, which defines an abstraction layer to access the hardware of Cortex-M processors.

To complete the OBC's software design, we propose new drivers, middleware, and some services.

The drivers serve to abstract the use and configuration procedure of several CubeSat peripherals. They are SD card memory, accelerometers, magnetometers, magnetorquers, gyroscopes, sensors of temperature, and solar panels.

The middleware is responsible for routines and the process of I/O CubeSat's data. The main routines are the management of ground station commands and file system management.

Finally, we use the services for the OBC's maintenance and mission tasks. About the tasks, we can highlight the telemetry and the payload management.

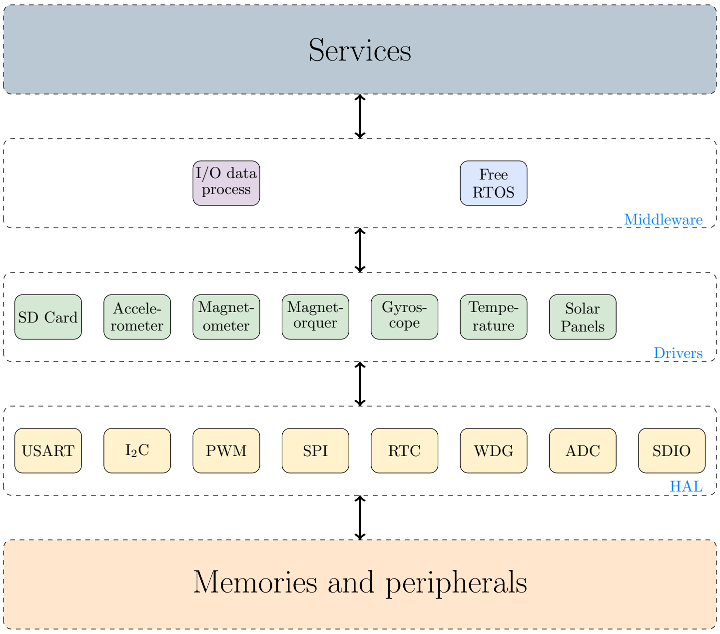

Figure 7: Software Architecture

5. Conclusion

This paper presented an onboard computer for an LEO CubeSat Nanosatellite. The proposed OBC was projected to be compatible with INPE's CONASAT-01. It also was designed aiming to be robust in the space environment, power-efficient, and mitigate the radiation effects in LEO.

Addressing these requisites and considering the space environment limitations, were projected an OBC electronic schema and printed circuit board. This OBC has an STM32 microcontroller, NOR Flash memory, and some embedded ADCS sensors.

Future works include PCB manufacture, new specific libraries development, and mission tasks for the CONASAT nanosatellite constellation.

Acknowledgments

This study was financed in part by the Coordenação de Aperfeiçoamento de Pessoal de Nível Superior - Brasil (CAPES) - Finance Code 001.

References

[1] U. of Concern Scientists, Ucs satellite database, 2021.
[2] C. F. de Melo, O. C. Winter, A era espacial, in: O. C. Winter, A. F. B. de Almeida Prado (Eds.), A Conquista do Espaço do Sputnik a Missão Centenário, Editora Livraria da Física, 2007, pp. 37–74.
[3] K. P. Queiroz, S. M. Dias, J. M. Duarte, M. M. Carvalho, Uma solução para o sistema brasileiro de coleta de dados ambientais baseada em nanossatélites, HOLOS 7 (2018) 132–142.
[4] C. L. G. Batista, A. C. Weller, E. Martins, F. Mattiello-Francisco, Towards increasing nanosatellite subsystem robustness, Acta Astronautica 156 (2019) 187–196.
[5] A. Poghosyan, A. Golkar, Cubesat evolution: Analyzing cubesat capabilities for conducting science missions, Progress in Aerospace Sciences 88 (2017) 59–83.
[6] A. Toorian, K. Diaz, S. Lee, The cubesat approach to space access, in: 2008 IEEE Aerospace Conference, pp. 1–14.
[7] M. Heidt, P. Puig-suari, P. Augustus, S. Moore, P. Nakasuka, P. Robert, J. Twiggs, Cubesat: A new generation of picosatellite for education and industry low-cost space experimentation, Small Satellite Conference (2000).
[8] ISIS, Cubesat information, 2021.
[9] E. Kulu, Nanosats database, 2021.
[10] E. Razzaghi, Design and Qualification of On-Board Computer for Aalto-1 CubeSat, Master's thesis, Lule University of Technology, 2012.
[11] ISIS, Isis on board computer, 2021.
[12] EnduroSat, Onboard Computer Type I - User Manual, EnduroSat, 1.0 edition, 2021.
[13] GomSpace, Gomspace — nanomind a3200, 2021.
[14] S. Vasudevan, Design and Development of a CubeSat Hardware Architecture with COTS MPSoC using Radiation Mitigation Techniques, Master's thesis, KTH, School of Electrical Engineering and Computer Science (EECS), 2020.
[15] E. Kulu, Nanosats database, 2021.
[16] L. T. Lumbwe, Development of an onboard computer (OBC) for a CubeSat, Master's thesis, Cape Peninsula University of Technology, Cidade do Cabo, África do Sul, 2013.
[17] J. Eickhoff, Onboard Computer Main Elements, Springer Berlin Heidelberg, Berlin, Heidelberg, pp. 51–69.
[18] V. Bostan, N. Secrieru, V. Ilco, V. Melnic, A. Martiniuc, V. Varzaru, Tumnanosat nanosatellite and kibocube program, 2020 13th International Conference on Communications, COMM 2020 - Proceedings (2020) 503–508.
[19] C. Nagarajan, R. G. D'souza, S. Karumuri, K. Kinger, Design of a cubesat computer architecture using cots hardware for terrestrial thermal imaging, in: 2014 IEEE International Conference on Aerospace Electronics and Remote Sensing Technology, pp. 67–76.
[20] S. Buckner, C. Carrasquillo, M. Elosegui, R. Bevilacqua, A novel approach to cubesat flight software development using robot operating system (ros), Small Satellite Conference (2020).
[21] A. C. R. Alves, Controle de Bordo para Nanossatélites: Desenvolvimento e Aplicação ao Projeto CONASAT, Master's thesis, Universidade Federal do Rio Grande do Norte (UFRN), Brasil, 2019.
[22] D. W. Coit, Cold-standby redundancy optimization for nonrepairable systems, IIE Transactions 33 (2001) 471–478.
[23] Hyunki Kim, Hyung-Joon Jeon, Keyseo Lee, Hyuntae Lee, The design and evaluation of all voting triple modular redundancy system, in: Annual Reliability and Maintainability Symposium. 2002 Proceedings (Cat. No.02CH37318), pp. 439–444.
[24] R. Barry, Mastering the FreeRTOS Real Time Kernel, Real Time Engineers Ltd., 2016.
[25] C. E. Gonzalez, C. J. Rojas, A. Bergel, M. A. Diaz, An architecture-tracking approach to evaluate a modular and extensible flight software for cubesat nanosatellites, IEEE Access 7 (2019).
[26] N. Chronas, UPSAT: a nanosatellite, Master's thesis, University of Patras, 2017.
[27] I. Latachi, T. Rachidi, M. Karim, A. Hanafi, Reusable and reliable flight-control software for a fail-safe and cost-efficient cubesat mission: Design and implementation, Aerospace 7 (2020).
[28] W. Yamaguti, V. Orlando, S. De, P. Pereira, Sistema brasileiro de coleta de dados ambientais: status e planos futuros, Anais XIV Simpósio Brasileiro de Sensoriamento Remoto (2009) p. 1633–1640.
[29] M. S. H. Gomes, Desenvolvimento de software para sistema de controle de bordo aplicado a nanossatélites de baixa órbita, Master's thesis, Universidade Federal do Rio Grande do Norte (UFRN), Natal, Brasil, 2021.

HARDWARE-IN-THE-LOOP SIMULATION OF AN ON-BOARD ENERGY-DRIVEN SCHEDULING ALGORITHM FOR CUBESATS

Vinícius P. Bernardo[(1)], Eduardo A. Bezerra[(2)], Laio O. Seman[(3)] Ramon Borba[(4)]

[(1)] Department of Electrical Engineering, Federal University of Santa Catarina (UFSC), Florianópolis 88040-900, SC, Brazil, vinicius.bernardo@posgrad.ufsc.br

[(2)] Department of Electrical Engineering, Federal University of Santa Catarina (UFSC), Florianópolis 88040-900, SC, Brazil, eduardo.bezerra@ufsc.br

[(3)] Department of Automation and Systems Engineering, Federal University of Santa Catarina (UFSC), Florianópolis 88040-900, SC, Brazil, laio@univali.br

[(4)] Department of Electrical Engineering, Federal University of Santa Catarina (UFSC), Florianópolis 88040-900, SC, Brazil, ramonborba97@gmail.com

Keywords: *Hardware-in-the-loop, task scheduling, CubeSat.*

Technological improvements and the miniaturization of components enabled a reduction on the average size of launched satellites, which started to contain many “commercial off the shelf” components, that are cheap, demand low power, and are widely available. This trend culminated in the development of the CubeSat standard, and in the fact that, nowadays, most satellite launches are in the “small-satellite” category (up to 180kg). As consequence of the reduced dimensions of most of the modern satellites, efforts arise on pursuing means to optimize energy management and consumption. Such efforts include evaluating which electrical power system architecture provides best overall efficiency, that often includes maximum power point tracking (MPPT) for harvesting energy using solar panels, which correspond to the most common primary source of power on small satellites. In this context, this work proposes the use of a knapsack task scheduling strategy aiming to maximize energy harvesting. An integrated thermal-electrical nanosatellite framework was used to test various priority functions and different heater activation strategies using tasks parameters of FloripaSat-1 and other randomly generated cases. Results shown that a saturating priority function presented the least amount of deadline losses. Although the different priority functions did not present significant influence in battery temperature, by allocating the remaining resources directly to the heater after selection phase of the tasks, an increase in correlation between ideal and achieved power generation from solar panels was obtained, and battery temperature operated closer to desired temperature range throughout the simulation. The control strategy was later implemented on an embedded environment, configuring a hardware-in-the-loop (HIL) simulation. The correctness of the algorithm was verified, along with its capabilities to fulfill the real time constraints. A speed analysis was conducted and verified a linear impact of the number of tasks on the computation time.

1. Introduction

Since the launch of the Sputnik 1 in 1957, hundreds of satellites have been launched. Technological improvements and the miniaturization of components enabled a reduction on the average size of launched satellites, which started to contain many “commercial off the shelf” (COTS) components, that are cheap, demand low power, and are widely available [1]. This trend culminated in the CubeSat concept. The CubeSat standard was created by the California Polytechnic State university (Cal Poly), and by the Stanford University in 1999 e defined as 1U the 10 cm x 10 cm x 10 cm cube with a maximum of 2kg [2]. Since then, most satellite launches are in the "small-sat" category (up to 180kg) and engulf nanosatellites (1 to 10kg) and the CubeSat standard [1] [3].

The Electrical Power System (EPS) is an essential subsystem of a nanosatellite that shall harvest from the surrounding space environment, store, and ultimately deliver power to other subsystems. The most common method for harvesting energy is through the photo-voltaic effect utilizing solar panels [4]. When operating a solar panel, to produce the highest possible amount of energy, it is desirable to stay as close as possible to the Maximum Power Point (MPP). With the decrease in embedded systems power consumption, the work by Fröhlich, Bezerra and Slongo [5] aimed to discover if Maximum Power Point Tracking (MPPT) circuits were still advantageous in low power applications considering their own consumption added to the system, and it found that a directly coupled circuit was able to extract more energy and is more efficient than using a dedicated MPPT circuit.

A study, by Slongo, Martínez, *et al.* [6] conducted a three-orbit experiment comparing four EPS architectures: the directly coupled, the very low dropout (VLDO) voltage regulator, the maximum power point tracking (MPPT) with an integrated circuit, and the MPPT with a discrete boost regulator. The study found that MPPT boost regulator architecture harvested more energy, but the VLDO voltage regulator architecture presented the best overall efficiency, and mathematically demonstrated that the latter architecture, along with the directly coupled architecture, could benefit from control of tasks execution.

Satellites may not receive continuous irradiance level along the entirety of the orbit. This, along with other factors related to conversion physics, makes this source of energy unstable. Therefore, energy storing devices are extremely common [6]. Current state-of-the-art energy storage systems use lithium ion (Li-ion) or lithium polymer (LiPo) secondary-type (rechargeable) batteries.

Lithium-ion batteries optimal temperature ranges from 15°C to 35°C, and the acceptable temperature ranges from -20°C to 70°C. Low temperature effects are much more related to the environment, usually happens in high-latitude areas and in space, and the effects involve slow down chemical reaction activity and charge-transfer velocity, resulting in reduction of energy and power capabilities. High temperature effects are not limited to environment and happen in a broader range of applications. Generally, lithium losses and active material degradation with result in capacity reduction, and the increase of internal resistance causes loss of power, and these effects happens in both low and high temperature with different causes [7].

With the increased use of small satellites, a high failure rate has been noticed [8]. Among the causes are hardware and software design mistakes along with failures in the integration process. In this bias, effectively predicting and testing the system can help discover and avoid failures that would otherwise compromise the mission. One effective method to model and simulate an engineering system, that consists of the combination of computer simulation and hardware in a single platform, is called hardware-in-the-loop (HIL). Due to the dynamics of batteries and photovoltaic panels regarding the effects of temperature, conducting a thermal simulation of these components is of great importance during development phases, for they can reduce costs of testing with physical components [9] and help predict temperature profiles in critical components on a dynamic environment [10] [11]. However, most work approaching thermal simulations lack active thermal management and do not integrate with the electrical models. Also, many unpredictable interactions between hardware can be detected, and many parameters such as signal noise, signal dropout, lag and others can be measured. Not only the real hardware can provide this unique response, but it can also be tested in different orbit conditions that are being virtually reproduced [12]- [13].

In the context of nanosatellites' limitations in terms of harvesting and storing energy, scheduling strategies can provide missions with a better quality of service, either as a planning tool – offline scheduling – or in real time – online algorithm, embedded in the satellite. In the field of task scheduling in nanosatellites, an exact approach is proposed by Pang *et al.* [14] for dealing with power and bandwidth limitations on nanosatellites. Online task scheduling algorithms based on "Earliest Deadline", "Earliest Arrival Time" and "Minimum Slack" ordering policies are proposed in [15], but power availability from primary and secondary sources of energy – i.e., solar panels and batteries – are not addressed in a quantified manner.

Zhang, Behbahani and Eltawil [16] address the inter-satellite communication problem between CubeSats. They propose to maximize transmission data rate based on online scheduling of operation frequencies and constrained by transmit power. An offline mixed integer formulation is described by Rigo, Seman, *et al.*, [17] for optimizing quality of service in nanosatellites missions through task scheduling. The model is energy constrained, provides exact optimal solutions, and implements Fuzzy constraints for considering battery usage. Only depth of discharge is considered for preserving battery lifetime, temperature analysis or constraints are not included.

Regarding online embedded optimization with constrained energy availability, Martínez and Slongo, in [6], [9], [18] and [19], research and analyze different MPPT architectures and task scheduling technics. Based upon these previous works, this research improves the scheduling algorithm proposed in [9] by reshaping the priority calculation of the satellite's tasks and changing its relation with the heater. Also, the control strategy is simulated in an embedded environment with much closer resemblance to the final application, in which the real time capability and performance of the control strategy can be accessed. The embedded algorithm is based on the 0-1 knapsack problem, which underlies Martínez [19] formulation and the present work.

2. Problem modeling

This Section presents the relevant equations to the model and the algorithms under study, as well as description of the hardware-in-the-loop tests configuration and setup. The model is used to simulate the thermal and electric dynamics of a nanosatellite and combines orbit, attitude, irradiance, thermal, and electrical models, including equivalent circuits that were used to represent the battery and solar panels. The model also and uses a directly coupled architecture. In this architecture, the solar panels, battery, load, and heater operation voltages are almost the same and are heavily influenced by the current drawn by the load and heater.

Given an initial SoC value, battery voltage, temperature, orbit inclination and altitude, the CubeSat parameters are calculated for each iteration, and the heater and load power are calculated considering a possible controller. A preliminary characterization of the satellite's tasks is necessary to use the proposed algorithm in orbit. Board 1 summarizes the notation of the variables that characterize the tasks, as well as model variables of the control strategy.

Board 1 - Tasks characterization variables

Notation	Description
n	Number of tasks. $n \in \mathbb{N}$.
P_L	Power consumed by the tasks. $P_L \in \mathbb{R}^+$.
P_{SP}	Power generated by the solar panels in Watts. $P_{SP} \in \mathbb{R}^+$.
W	Satellite's optimal power consumption in Watts. Output of MPPT algorithm. $W \in \mathbb{R}^+$.
$W_{eclipse}$	Satellite's constant consumption goal during eclipse. $W_{eclipse} \in \mathbb{R}^+$
T	Number of simulation steps. $T \in \mathbb{N}$.
J	The set of tasks. $J = \{j \mid j \in \mathbb{N}, j \leq n\}$.
r_j	Power consumption of task j in Watts. $r_j \in \mathbb{R}^+$.
c_j	Computing time of task j in seconds. $c_j \in \mathbb{N}, c_j \leq T$.
dl_j	Period of task j in seconds. $dl_j \in \mathbb{N}, dl_j \leq T$.
u_j	Priority of task j. $u_j \in \mathbb{N}$.
s_j	Submission time of task j in seconds. $s_j \in \mathbb{N}, s_j \leq T$.
d_j	Deadline j in seconds. $d_j \in \mathbb{N}, d_j \leq T$.
a_j	Executed time of task j in seconds. $a_j \in \mathbb{N}, a_j \leq T$.
rt_j	Remaining time of task j in seconds. $rt_j \in \mathbb{N}, rt_j \leq T$.
x_j	On-off status of task j. $x_j \in \{0,1\}$.
ex_j	Already executed flag of task j. $ex_j \in \{0,1\}$.

In this work, all tasks are periodic, so their submission times are always the same as their last deadlines. Tasks also are considered preemptive, and have the same amount of importance, having no intrinsic value that makes the execution of one task more valuable than another, leaving this decision entirely for the control strategy. In distributed computing systems, finding the best way to assign priorities poses great importance when implementing these systems.

The first part of the strategy used (represented by Algorithm 1) compares, for each task $j \in J$, the computation time c_j with the executed time a_j to know a task has ended, and if it has, sets the already executed ex_j value to 1. Then it checks it the time t already reached the task currently active deadline d_j, and if it has, calculates the new deadline as $d_j = d_j + dl_j$. Finally, the task priority is calculated, and is kept at a low value if it has already been executed for the current active deadline.

Vanderster, Dimopoulos, *et al.*, [20] presents a few common priority calculations policies used in distributed systems, some of which were used in this work. The first method of calculating priority is the Elapsed Time priority function (ET), which is calculated as follows (Equation 1) for each task $j \in J$:

$$u_j = 100\frac{t-\mathrm{s_j}}{dl_j} = 100\frac{t+\mathrm{dl_j}-\mathrm{d_j}}{dl_j} \tag{1}$$

This policy gives a normalized linear priority value from 0 to 100 between the last deadline (which is the same as the submission time) and the current active one. This amount of time between deadline is the period of the task. In order to reshape the priority function, it is possible to use another function as an activation function, such as the exponential and sigmoidal functions.

Algorithm 1: Dynamic priority calculation

```
for j = 0 … n:
    if c_j − a_j ≤ 0:
        x_j = 0
        a_j = 0
        u_j = 0
        ex_j = 1

    if t = d_j:
        d_j = d_j + dl_j
        ex_j = 0

    if x_j = 1:
        a_j = a_j + 1

    if ex_j = 1:
        u_j = 1
    else:
        u_j = priority function (j)
```

The calculation can be improved by finding a critical point in time in which the task must become active and stay active until it reaches its deadline in order to be able to satisfy its completion. This can be achieved by assigning a sufficiently big priority value M to a task once it reaches this critical point in time so that no other single task or combination of tasks takes priority over it. The priority calculation (which will be called Elapsed Time with M, or ET+M) then becomes (Equation 2):

$$u_j = \begin{cases} 100\frac{t+dl_j-d_j}{dl_j}, & d_j - t > c_j - a_j \\ M, & d_j - t \leq c_j - a_j \end{cases} \tag{2}$$

This calculation can be further iterated upon by taking into consideration the amount of computation time left for the task to finish in relation to its currently active deadline. This is done by adding the remaining time to the current time. The new calculation (Equation 3), which will be called Estimated Response Time (ERT) priority function, then becomes:

$$u_j = 100\frac{t-s_j+rt_j}{dl_j} = 100\frac{t+dl_j-d_j+c_j-a_j}{dl_j} \tag{3}$$

Another term that raises the priority of tasks that are close to completing can be added. This term is called Nearness to Completion Time and (NTCT) and is the ratio of the period dl_j of the task over the remaining time rt_j. Thus, the priority function of ERT+NTCT is (Equation 4):

$$u_j = 100\frac{t-s_j+rt_j}{dl_j} + \frac{dl_j}{rt_j} \tag{4.a}$$

$$u_j = 100\frac{t+dl_j-d_j+c_j-a_j}{dl_j} + \frac{dl_j}{c_j+a_j} \tag{4.b}$$

The goal of the scheduling algorithm is to seek the optimal amount of power that the satellites tasks should consume to achieve maximum power generation. When not in an eclipse situation, this optimal satellite consumption (W) is calculated using the solar panel power P_{SP} with the maximum power point tracking algorithm, and when it is, W is maintained at a fixed value $W_{eclipse}$ to prevent the MPPT algorithm form moving erratically. Once W is calculated, the algorithm needs to find which subset of tasks best fit this power consumption goal without exceeding it. One solution to this problem is formulated as a 0-1 knapsack problem, which can be described by (Equations 5):

$$Maximize: \sum_{j=1}^{n} u_j x_j \tag{5.a}$$
$$Subject\ to: \sum_{j=1}^{n} r_j x_j \leq W \tag{5.b}$$
$$x_j \in \{0, 1\} \tag{5.c}$$

The solution to each iteration of the simulation will dictate which tasks will stay active or not throughout its duration. The dynamic programming algorithm which was used to solve this problem has a time and space complexity of $O(n \cdot W)$. With the knowledge of which tasks remain active, the load power drawn by the tasks is calculated with (Equation 6):

$$P_L(t) = \sum_{j=1}^{n} r_j x_j \tag{6}$$

This value P_L is then fed into the model to calculate its parameters, directly affecting the solar panels operating point and consequently its generated power.

Implementing the presented control strategy presented in a microcontroller is a great way to further assess the feasibility of its real time capabilities in a much closer to the real scenario situation. In this settings, model and system variables are calculated and fed to the microcontroller on either digital or analog format and are used by the latter to generate the necessary control data. The computer is responsible to calculate the dynamics of the model, which are sent to the microcontroller using serial communication, and the final output of the control strategy, i.e., the tasks active status x_j is sent back to the computer, forming a closed loop (Figure 1-a). In order to satisfy the real time requirements of the problem, all communications and calculations must happen within time step frame of the simulation of 1 seconds. Figure 1-b shows the timing diagram for the system.

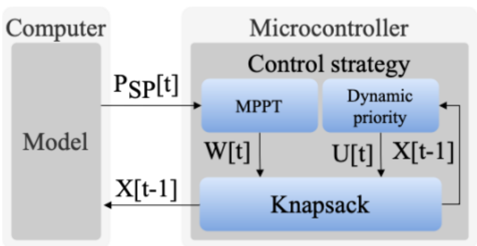

(a)

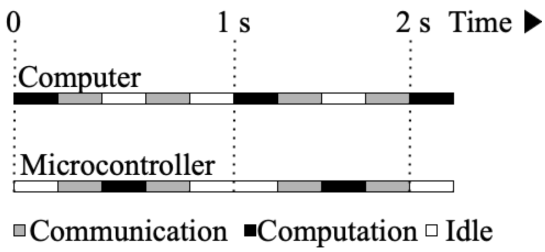

(b)

Figure 1 - Closed loop system (a) and HIL timing diagram (b).

3. Experimentation and Results

The integrated thermal-electrical framework was implemented using MATLAB, and the configuration used in this work is based on the 1U CubeSat FloripaSat-I [21], launched in December 2019. Its orbit is nearly circular and Sun-synchronous (SSO), represented as perfectly circular and with an inclination of 90º.

The different priority policies introduced in Section 2 were used in the aforementioned FloripaSat-I conditions in order to evaluate the impact on the number of missed deadlines. The total number of time steps was 70024, and each step represents 1 second, totaling 12 orbits. Each priority policy was treated as a different scenario s, with a total of $S = 6$ scenarios. After running the simulation for the different priority policies, the results were as following in Table 1.

Table 1 - Deadline misses with different priority policies.

Priority policy	Percentage of missed deadlines [%]
ET Linear + M (eq. 2)	0.23
ET Exponential + M	0.22
ET Sigmoid + M	0.17
ET Linear (eq.1)	0.23
ERT (eq. 3)	0.20
ERT + NTCT (eq. 4)	0.28

From the results, it can be observed that the number of missed deadlines was reduced when compared to the original control strategy presented by Vega Martínez [19]. The policies with linear shape (Linear + M, Linear, and ERT) had similar results, with the ERT performing better among those. The addition of the Nearness To Completion Time (NTCT) to the ERT policy worsened the result, while the Sigmoid + M presented the best result with the least amount of deadline misses.

Regarding the operating temperature of the battery, after normalizing the values of each scenario s as per Equation 7, it is possible to see that all simulations performed extremely similar, despite the difference in priority policies, as shown in Figure 2.

$$\text{normalized temperature}_s(t) = \frac{\text{temperature}_s(t)}{\left(\frac{\sum_{s=1}^{S} \text{temperature}_s(t)}{S}\right)} \text{ , } s \in [1, S] \tag{7}$$

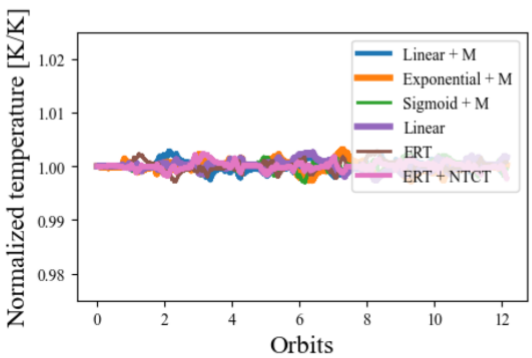

Figure 2 – Normalized battery operating temperature.

As for the MPPT performance, by calculating the Pearson's correlation coefficient between the desired and actual power generated from the solar panels throughout the simulation of each scenario, it was possible to observe that the overall performance was similar, and the difference in priority policies didn't influence in a significant way the individual results. The calculated correlation coefficient values for each scenario ranged from 0.9894 to 0.9974.

To try and improve the operating temperature of the battery and the amount of harvested energy the control strategy was changed by delivering the remainder of the MPPT algorithm output to the heater after allocating the tasks after each iteration. The correlation coefficient using this modified control strategy was $r = 0.9986$ compared to $r = 0.9934$. By plotting the ideal against the actual generated power throughout the 12 orbits, it is possible to observe the improvement in correlation in Figure 3(b) compared to Figure 3(a), indicating that the MPPT algorithm performed better. As for the battery operating temperature, the minimum temperature reached during the simulation increased from 242.0 K to 246.6 K, with the average temperature increasing by 2.5% (Figure 3(c).

Experiments were conducted using the hardware-in-the-loop setup previously described in the problem modeling section. After running the experiment with the hardware-in-the-loop setup, the results were compared with the simulation and the correctness of the algorithm implemented in the target language was verified. A performance analysis was conducted by varying the number of tasks from 1, up to 7, in different runs of the setup and measuring the time it took to complete a full loop iteration of the system for multiple time steps.

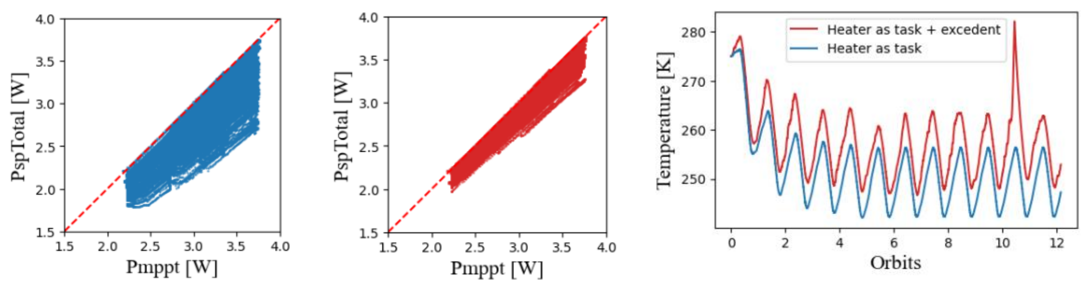

(a) (b) (c)

Figure 3 – Ideal against actual generated power from solar panels (a) without excedent power to heater, and (b) with excedent power to heater. Battery temperature during 12 orbits with different control strategies and Linear + M priority policy (c).

The results are shown in Figure 4, which shows the average time that the microcontroller takes to receive, compute, and answer the computer. It is possible to conclude that the implementation could satisfy the real time requirements of the system.

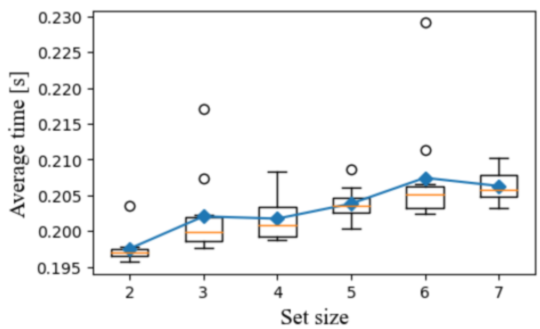

Figure 4 - Performance analysis of the hardware-in-the-loop simulation with different set sizes.

4. Conclusion

In this work an energy-driven scheduling algorithm was tested using an integrated thermal-electrical framework capable of representing the dynamics of important components like the battery and solar panels. It was shown that by shaping the priority function of the algorithm the number of missed deadlines was reduced by up to 26% in the simulation involving the FloripaSat-I real case scenario, and, by managing load power allocation to the heater, it was possible to improve the algorithm's harvested energy, as shown by the increase in correlation between actual and ideal solar panels power output. These improvements can lead to a reduction in unwanted low temperature effects on the battery, since its operating range increased by an average of 2.5%.

The integrated model framework was then expanded into a hardware-in-the-loop setup, which was used to implement the scheduling algorithm in the target language. A computation cycle of 1 second was used, and the behavior and real time capabilities of the algorithm was validated, and the control strategy calculations were performed by the microcontroller in under a quarter of a second.

References

[1] A. Poghosyan and A. Golkar, "CubeSat evolution: Analyzing CubeSat capabilities for conducting science missions," *Progress in Aerospace Sciences,* vol. 88, pp. 59-83, 2017.

[2] Cal Poly SLO and A. Johnstone, 2020. [Online]. Available: cubesat.org.

[3] NASA, State-of-the-Art: Small Spacecraft Technology, S. Weston, Ed., Mountain View, Califórnia: NASA, 2021.

[4] G. Galatis, J. Guo and J. Buursink, "Development of a solar array drive mechanism for micro-satellite platforms," *Acta Astronautica,* vol. 139, pp. 407-418, 2017.

[5] A. A. Fröhlich, E. A. Bezerra and L. K. Slongo, "Experimental analysis of solar energy harvesting circuits efficiency for low power applications," *Computers & Electrical Engineering,* vol. 45, pp. 143-154, 2015.

[6] L. Kessler Slongo, S. Vega Martínez, B. Vale Barbosa Eiterer and E. Augusto Bezerra, "Nanosatellite electrical power system architectures: Models, simulations, and tests," *International Journal of Circuit Theory and Applications,* vol. 48, pp. 2153-2189, 2020.

[7] S. Ma, M. Jiang, P. Tao, C. Song, J. Wu, J. Wang, T. Deng and W. Shang, "Temperature effect and thermal impact in lithium-ion batteries: A review," *Progress in Natural Science: Materials International,* vol. 28, pp. 653-666, 2018.

[8] J. Bouwmeester and J. Guo, "Survey of worldwide pico- and nanosatellite missions, distributions and subsystem technology," *Acta Astronautica,* vol. 67, pp. 854-862, 2010.

[9] S. Vega Martinez, E. M. Filho, L. O. Seman, E. A. Bezerra, V. d. P. Nicolau, R. G. Ovejero and V. R. Q. Leithardt, "An Integrated Thermal-Electrical Model for Simulations of Battery Behavior in CubeSats," *Applied Sciences,* vol. 11, 2021.

[10] S. Corpino, M. Caldera, F. Nichele, M. Masoero and N. Viola, "Thermal design and analysis of a nanosatellite in low earth orbit," *Acta Astronautica,* vol. 115, pp. 247-261, 2015.

[11] M. Bonnici, P. Mollicone, M. Fenech and M. A. Azzopardi, "Analytical and numerical models for thermal related design of a new pico-satellite," *Applied Thermal Engineering,* vol. 159, p. 113908, 2019.

[12] S. Corpino and F. Stesina, "Verification of a CubeSat via hardware-in-the-loop simulation," *IEEE Transactions on Aerospace and Electronic Systems,* vol. 50, pp. 2807-2818, 2014.

[13] N. R. Gans, W. E. Dixon, R. Lind and A. Kurdila, "A hardware in the loop simulation platform for vision-based control of unmanned air vehicles," *Mechatronics,* vol. 19, pp. 1043-1056, 2009.

[14] J. de Carufel, E. Martin and J.-C. Piedbœuf, "Control strategies for hardware-in-the-loop simulation of flexible space robots," *IEE Proceedings - Control Theory and Applications,* vol. 147, no. 6, pp. 569-579(10), November 2000.

[15] X. Wu and T. Vladimirova, "Hardware-in-Loop Simulation of a Satellite Sensor Network for Distributed Space Applications," in *2008 NASA/ESA Conference on Adaptive Hardware and Systems*, 2008.

[16] R. Finnset, S. K. Rao and J. Antonsen, "Real time hardware-in-loop simulation of ESMO satellite attitude control system," *Modeling, Identification and Control,* vol. 27, p. 125–140, 2006.

[17] C. K. Pang, A. Kumar, C. H. Goh and C. V. Le, "Design and robust scheduling of nano-satellite swarm for synthetic aperture radar applications," *2014 13th International Conference on Control Automation Robotics & Vision (ICARCV),* pp. 705-710, 2014.

[18] P. Dobiáš, E. Casseau and O. Sinnen, "Fault-Tolerant Online Scheduling Algorithms for CubeSats," *In Proceedings of the 11th Workshop on Parallel Programming and Run-Time Management Techniques for Many-core Architectures / 9th Workshop on Design Tools and Architectures for Multicore Embedded Computing Platforms (PARMA-DITAM'2020),* pp. 1-6, 2020.

[19] A. W. Zhang, A. S. Behbahani and A. M. Eltawil, "Joint frequency scheduling and power allocation for CubeSat communication," *38th International Communications Satellite Systems Conference (ICSSC 2021),* pp. 184-188, 2021.

[20] C. A. Rigo, L. O. Seman, E. Camponogara, E. M. Filho and E. A. Bezerra, "A nanosatellite task scheduling framework to improve mission value using fuzzy constraints," *Expert Systems with Applications, Volume 175,* 2021.

[21] L. K. Slongo, S. V. Martínez, B. V. B. Eiterer, T. G. Pereira, E. A. Bezerra and K. V. Paiva, "Energy-driven scheduling algorithm for nanosatellite energy harvesting maximization," *Acta Astronautica,* vol. 147, pp. 141-151, 2018.

[22] S. Vega Martínez, "Nanosatellite task scheduling algorithm for energy harvesting and QoS enhancement tested through a self-proposed thermal-electrical model," *Thesis,* p. 112, 2022.

[23] D. C. Vanderster, N. J. Dimopoulos, R. Parra-Hernandez and R. J. Sobie, "Resource allocation on computational grids using a utility model and the knapsack problem," *Future Generation Computer Systems,* vol. 25, pp. 35-50, 2009.

[24] G. M. Marcelino, S. Vega-Martinez, L. O. Seman, L. Kessler Slongo and E. A. Bezerra, "A Critical Embedded System Challenge: The FloripaSat-1 Mission," *IEEE Latin America Transactions,* vol. 18, pp. 249-256, 2020.

PDQSAT ELECTRIC POWER SUBSYSTEM CONTROL USING A DISCRETE EVENT SYSTEMS MODEL

Elder J. T. Santos(1), **Maria C. Pereira**(2), **Patrícia N. Pena**(3)
(1)Aerospace Engineering - Universidade Federal de Minas Gerais, e-mail: elderteves@gmail.com
(2)Department of Mechanics Engineering - Universidade Federal de Minas Gerais, e-mail: cecilia@demec.ufmg.br
(3)Department of Electronics Engineering - Universidade Federal de Minas Gerais, e-mail: ppena@ufmg.br

Keywords: *CubeSat, Electric Power Subsystem, Discrete Event Systems, Supervisory Control Theory, Simulation*

The PdQSat nanosatellite is the first academic CubeSat to be designed and built at the Federal University of Minas Gerais (UFMG) and aims to characterize commercial Lithium-Sulphur (Li-S) cells in a hostile environment. Li-S technology integrates the contemporary energy industry vanguard, making itself present in several sectors, such as automotive and aerospace. Its application potential, however, is not yet fully exploited, since some of its properties lack analysis and validation. The development of this mission, accordingly, has not only technical relevance, but also remarkable academic relevance, and may be used to qualify manpower in high-tech engineering, employing the best practices of the different areas involved. Therefore, in order to join Aerospace, Control and Automation, Electrical and Systems engineering around the context of a technological demonstration mission, controlling the Electric Power Subsystem (EPS) - vital for the space vehicle proper functioning - is regarded as an object of interest. In this work, in order to ensure the correct operation and integration of the photovoltaic panels pointing, power supply and the operating mode systems, the Supervisory Control Theory (SCT) of discrete event systems is used to model the subsystems and implement logical control with formal guarantees of control and non-blockingness. Thus, in order to validate its behavior, the subsystem was simulated under control of the obtained supervisors in orbit, allowing states assumed along the trajectory to be evaluated and validated.

1. Introduction

CubeSats have been created mainly as an educational tool, being a device that, while containing all subsystems of a traditional satellite, has a short lifecycle and a much smaller cost. Considering those features, it is a perfect tool for Engineering education, because undergraduate students can follow its design from conception to decomissioning. With further development of this technology, it was seen that CubeSats can be used as well as a utility spacecraft [1]. Commercial-Off-The-Shelf (COTS) components were made available and projects started to popularize. The Federal University of Minas Gerais (UFMG) is currently designing its first CubeSat, aiming to characterize a Lithium-Sulphur (Li-S) battery in a hostile environment. Such battery was already used in High Altitude Pseudo-Satellites (HAPS) and, if suitable for satellites, will represent a great achievement for space technology, considering it is much lighter than batteries available for such use. The Electrical Power Subsystem (EPS) is one of the most critical subsystems of a satellite and its proper design is very important for the mission. In this paper, we model and control the EPS using the Supervisory Control Theory (SCT), aiming to provide correct and nonblocking logical control for the pointing of the solar panels, switching energy sources and transitioning operation modes problems. In order to validate and illustrate the results, a simulation is developed in Matlab [2].

2. Preliminaries

The problem addressed in this paper is a multidisciplinary one, and requires understanding of different subjects to solve. In this Section, basic information on Orbital Mechanics, Electrical Power Systems and Discrete Events Systems are presented.

2.1. Orbital Mechanics

The movement of a body subject to a gravitational field is known since before the first satellite was launched. The physical laws being the same as the ones that natural bodies are subject to, centuries before the begin of space era it was well known that the Kepler laws were verified [3]. Considering the case where an artificial satellite orbits Earth, the First Kepler's Law states that such orbit is an ellipsis around Earth, that is located on one of the *foci* of it. Also taking into account the Third Kepler's Law, or Harmonic Law of planetary motion, it is known that the square of the period of the orbit (T) is proportional to the cubic of the semimajor axis (a) of the ellipsis, one can derive Kepler's Equation, that relates the satellite position to time [3]:

$$M = u - e \sin u, \tag{1}$$

in which M stands for mean anomaly (angle measured from *periapsis* direction in time t if the satellite was in a circular orbit with constant angular speed, being its *radius* equal to the semimajor axis):

$$M = \frac{2\pi}{T} t, \tag{2}$$

and u stands for eccentric anomaly (related to true anomaly - angle between *periapsis* direction and position vector of the satellite - and eccentricity of the orbit as:

$$\tan\left(\frac{u}{2}\right) = \sqrt{\frac{1-e}{1+e}} \tan\left(\frac{f}{2}\right). \tag{3}$$

Considering Equation 1 cannot be solved analytically, numerical methods have to be used to find the satellite's position in any time.

2.2. Electric Power System

All active spacecrafts need electrical power to operate. The Electrical Power Subsystem (EPS) is the system responsible for providing the energy to the other subsystems. EPS, then, has to convert and condition power, store energy, protect the system against overvoltage or overcurrent and distribute power to the spacecraft bus [4]. It has to provide energy to the mission under environmental constraints, and during all lifecycle of the spacecraft and also in all possible failure conditions, without control from ground (autonomously). An EPS, therefore, has mainly four functions: primary power source, energy storage, power management (power conditioning and charge and discharge control) and power distribution.

One of the most used methods to supply the spacecraft with electrical energy is to carry on-board an energy source (batteries) and recharge it with energy from outside environment, mainly from solar energy. In this case, photovoltaic effect of solar cells and chemical-electrical conversion in the battery [4].

Within this context, the assessment of the battery State-of-charge (SOC) plays an essential role, as well as in many other battery-powered applications. The State-of-charge of a cell denotes the capacity that is currently available as a function of the rated capacity. The value of the SOC varies between 0% and 100%, so if the SOC is 100%, the cell is said to be fully charged, whereas a SOC of 0% indicates that the cell is completely discharged [5].

2.3. Discrete Events Systems

Discrete event systems are dynamic systems that evolve with the occurrence of instantaneous events [6]. Traditional models, such as differential equations, cannot be used to express such behavior. Different models may be used, such as languages and automata, Petri nets, Max-plus algebra among others.

The Supervisory Control Theory is based on languages and automata. The finite and nonempty set of events is defined as Σ, a sequence of events is a string (with ϵ as the string of lenght zero). A set of strings is a language.

An automata is a quintuple $G = (Q, \Sigma, \hat{\delta}, q_0, F)$, where Q is the set of states, Σ is the set of events, $\hat{\delta}$ is the transition function, q_0 is the initial state and F is the set of final states. When an automaton is used to model a system, two languages describe the behavior of a system, the generated and the marked language. The generated language is the set of strings that can be executed from the initial state, until any state of the automaton. It models the set of all strings that are physically possible in the system. The other language, the marked language is the set of strings that are executed from the initial state reaching a marked state. It models the set of strings that complete tasks.

The parallel composition is an operation that synchronizes two automata, by simultaneously executing the events that occur in both automata. Events that are local to each automata is allowed when it is allowed in the original automaton [6].

The Supervisory Control Theory (SCT) is a formal method to design nonblocking supervisors that restrict the behavior of the system to follow restrictions (safe restrictions, justice, security and so on). SCT is implemented by means of the disablement of controllable events ($\Sigma_c \subseteq \Sigma$). The condition for the existence of a supervisor that restricts the plant to a desired language K is that K is controllable. The concept of being controllable is related the restriction of disabling only controllable events. The supervisor implements the minimally restrictive behavior.

In order to avoid large supervisors, an extension of the SCT is used, the Local Modular Supervisory Control [7]. The synthesis is done in the same way, but each supervisor has a partial view of the plant. In order to implement the same behavior of the classical SCT, a verification of nonconflict has to be performed.

3. Main Results

The PdQSat nano-satellite is a 3U model CubeSat, with dimensions following the standards defined in the CubeSat Design Specification Rev.14 [8].

In the following subsections, the modeling, supervisor design and simulation are briefly described.

3.1. Step 1 - Modeling

A model of the EPS was developed using automata. The physical states and events that involve the EPS were listed, as well as the transitions between these states and the specifications that relate the events of the various components, aiming to eliminate undesirable behaviors.

3.1.1. Photovoltaic Panels Pointing System

In addition to the solar incidence sensors attached to each of its six faces, the satellite has photovoltaic panels attached to three of its four 3U faces. Hence, the remaining faces are devoid of panel coverage. The states are: “Eclipse” state (E), in which no sensor is illuminated by the Sun, “Sunlight harnessed” state (H), in which one of the sensors belonging to panel-covered faces or a combination of them are sufficiently illuminated by the Sun, and “Sunlight available” state (A), in which only one of the sensors belonging to faces without panel coverage or a combination of them are sufficiently illuminated by the Sun.

The uncontrollable events, therefore, are: no sensor is receiving sunlight (β_0), at least one of the sensors belonging to panel-covered faces is receiving sufficient sunlight (β_1) and only one or more sensors belonging to faces without panel coverage is receiving sufficient sunlight (β_2). The Solar Incidence model is shown in Figure 1.

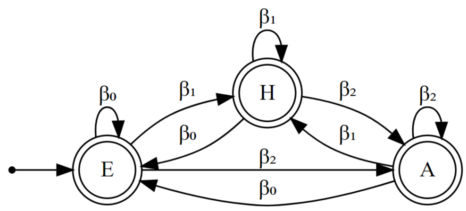

Figure 1: Solar incidence model.

To define the events of the satellite maneuver model, the attitudes that can be assumed by the CubeSat are limited to positions obtained by aligning a reference face to each direction of the $\hat{X}$, $\hat{Y}$ and $\hat{Z}$ axes. Therefore, it is assumed that the ADCS can move the satellite on any of the mentioned axes by increments of $+90°$ or $-90°$ in each axes, defining the controllable events as the set of possible maneuvers. The maneuvers model is shown in Figure 2.

The system specification implements the idea that the pointing system should act, by means of the described maneuvers, only when the satellite is exposed to sunlight but no panel is sufficiently illuminated, what is perceived by the occurrence of β_2. The system specification is shown in Figure 3.

A supervisor that implements such specification acts by defining which maneuver should be executed ($+-90X, Y, Z$) based on the incidence of sunlight in the sensors ($\beta_0, \beta_1, \beta_2$). The plant is obtained by the parallel composition of the the Solar incidence and Maneuvers models.

3.1.2. Power Supply System

The power supply can be provided by the photovoltaic panels and the battery. In this sense, the states defined for the model are the “Panel supply” (P) and the “Battery

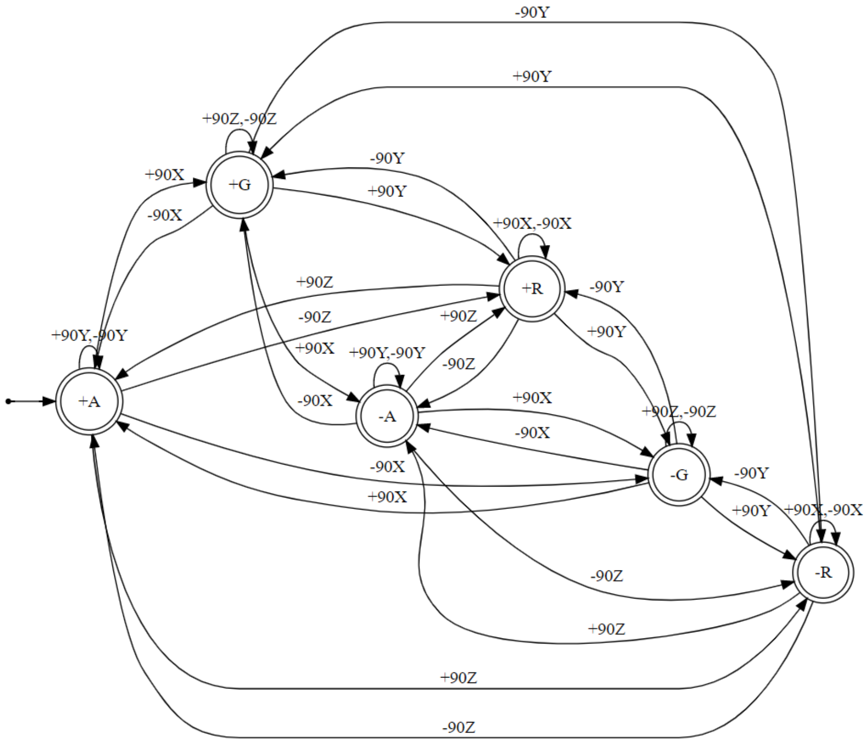

Figure 2: Maneuvers model.

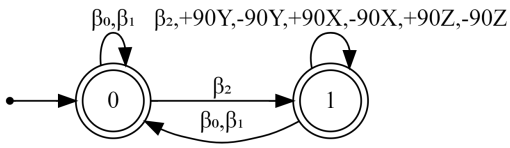

Figure 3: Photovoltaic Panels Pointing System Specification.

supply" (B) states. The controllable events, in this case, are switch to power supply by photovoltaic panels (γ_1) and switch to power supply by battery (γ_2). The supply model is shown in Figure 4.

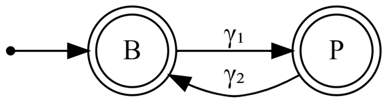

Figure 4: Supply model.

The system desired behavior consists of powering through the batteries while no panels are illuminated and powering through the panels if at least one panel receives sufficient sunlight. Thus, the specification only enables the switching for photovoltaic panels if at least one of them are illuminated. Similarly, the switching for battery power can only be enabled if no panels are sufficiently illuminated. The system specification is shown in Figure 5.

Therefore, a supervisor that implements such specification acts over the Solar incidence model and the Power Supply Switching model. The plant for such supervisor is obtained by doing the parallel composition of them.

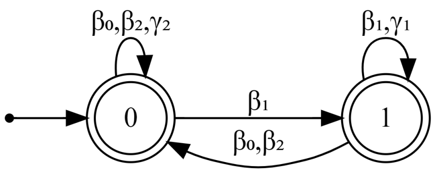

Figure 5: Power Supply System Specification.

3.1.3. Operating Mode System

In order to avoid considerable damage to the battery, it was defined that the system should go into emergency mode if the battery SOC is equal to or less than 25%, interrupting the power supply to non-critical components to reduce the energy consumption. The states of this plant consist of the two resulting operating modes: the "Nominal operating mode" (NO) and the "Emergency operating mode" (EM) states. The transitions between these states occur through the following controllable events: switch to nominal operating mode (ζ_1) and switch to emergency operating mode (ζ_2). The operating mode plant is shown in Figure 6.

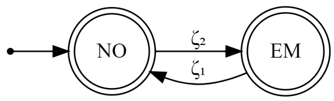

Figure 6: Operating Mode model.

In order to model the SOC variations that will occur while the satellite orbits Earth, the satellite's power budget and the panels power output were estimated.

The SOC of the battery can assume two different states, with reference to the safety limit: the "SOC over limit" (O) and the "SOC under limit" (U) states. The uncontrollable events are: battery SOC is at or below the safety limit (τ_1) and battery SOC is above the safety limit (τ_2). The SOC monitoring model is shown in Figure 7.

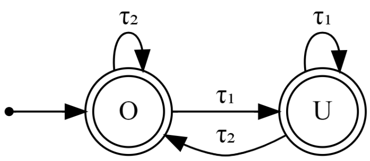

Figure 7: SOC monitoring model.

The system specification only enables the transition to the emergency operating mode if the battery SOC is equal or lower than the safety limit. On the other hand, enabling the transition to the nominal operating mode should only occur if the battery's SOC is higher than this limit. The system specification is shown in Figure 8.

Therefore, the global open loop behavior of the Operating Mode System is obtained by the parallel composition of the Operating Mode Switching and SOC Monitoring models. The supervisor will act over the composed system.

3.2. Step 2 - Supervisory Control

Based on the models and specifications presented earlier, the nonconflicting supervisors are calculated using the UltraDES library [9], an object-oriented library composed of data structures and algorithms intended for modeling, analyzing, and controlling discrete event systems. Three nonconflicting supervisors are obtained:

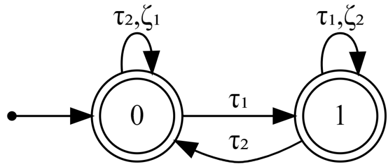

Figure 8: Operating Mode System Specification.

- Photovoltaic Panels Pointing System: 18 states and 90 transitions;
- Power Supply System: 6 states and 21 transitions;
- Operating Mode System: 4 states and 10 transitions;

The supervisors are not shown, but can be easily obtained using UltraDES [9].

3.3. Step 3 - Simulation

In this step, the entire system was simulated using MATLAB [2]. At each time step p, a set of uncontrollable events can occur as a function of the satellite position in the orbit, in order to reproduce the real behavior of the system's sensors. To simulate the operation of the system under control of the nonconflicting supervisors, the following logic was applied:

1. At time instant t_i, a controllable or uncontrollable event occurs;
2. Given the current state of the plant and the occurred event, the supervisor is queried for the corresponding transition. The system then assumes the state resulting from the transition. Moreover, in the query, it is verified if there is any controllable event enabled in the resulting state:
   a) If yes, the controllable event scheduled at the simulation level will occur in the next step;
   b) If no, no controllable event will occur in the next step;
3. Time evolves in one step p, i.e. $t_{i+1} = t_i + p$, and the described logic is repeated from the current state of the system;
4. The simulation is stopped when the time t_i equals the period T of the orbit.

In order to generate signals from sensors associated with the CubeSat illumination, a dynamic model of the satellite's orbit is necessary. Thus, a two-dimensional model was developed considering a low Earth orbit (LEO), so that the translation movement of the Earth can be neglected [10]. Two additional hypothesis were used: i) the Sun is at an infinite distance from the Earth (its light rays fall parallel over the entire orbit); ii) the position considered for the Sun in the plots to be presented will always be to the left of the Earth (Kepler's Equation is solved, obtaining the true anomaly of the satellite).

4. Results and Discussion

Three nonconflicting supervisors were obtained with UltraDES library [9]. In order to validate the operation of the obtained supervisors, the system behavior was simulated in a LEO ($z = 1000\ km$ and $e = 0.5$) similar to some of the orbits analyzed for the mission. The initial states configured in the simulation for the supervisors, therefore, were: Eclipse, Attitude 1, Battery supply, SOC over limit and Nominal operating mode.

Figure 9 presents the behavior of the Photovoltaic Panels Pointing System, graphically representing the evolution of its states during the orbit, whose period is 17,839 seconds. A step of 120 seconds was used, assuming that this is the time required for the ADCS to perform a unitary maneuver, favoring the visualization of the results.

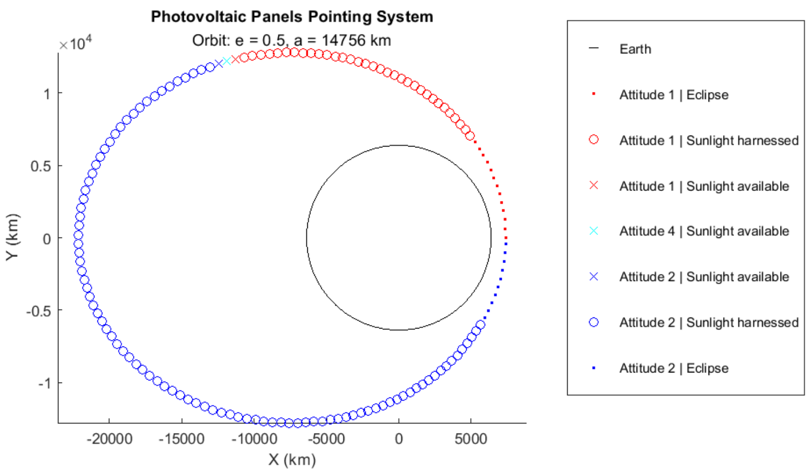

Figure 9: Behavior of the Photovoltaic Panels Pointing System in a full orbit.

From Figure 9, the CubeSat starts its trajectory with Attitude 1, maintaining it until leaving the eclipse zone and reaching $\theta \approx 130°$. In this position, the incidence of sunlight is considered null. Such information is obtained by the sensors and assimilated by the system, which performs a maneuver in one simulation step, assuming Attitude 4. The performed maneuver was not sufficient to ensure adequate illumination of the panels, so the process is repeated, achieving sufficient illumination over the panels in Attitude 2. Thus, it is attested that the system has presented the desired behavior.

Figure 10, in turn, presents the behavior of the Power Supply System over the orbit.

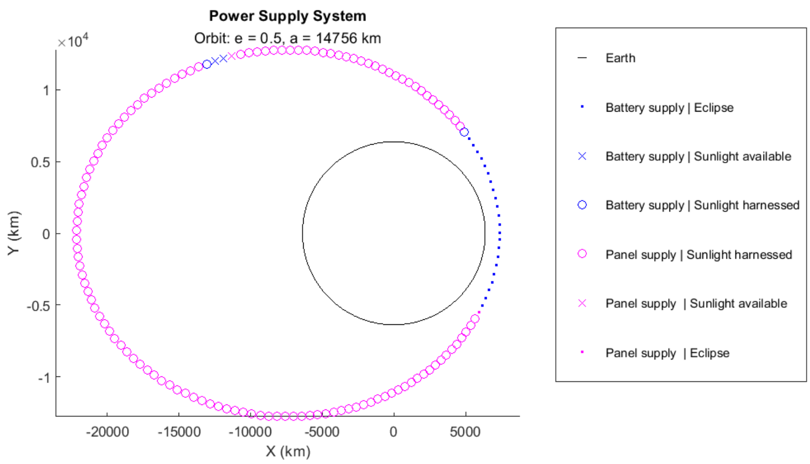

Figure 10: Behavior of the Power Supply System in a full orbit.

From Figure 10, it is observed that the Power Supply System presented the desired behavior, ensuring the power supply through battery during eclipse and also while the illumination on the panels was not sufficient. Finally, the behavior of the Operating Mode System and the variation of the battery SOC are displayed in figures 11 and 12, respectively.

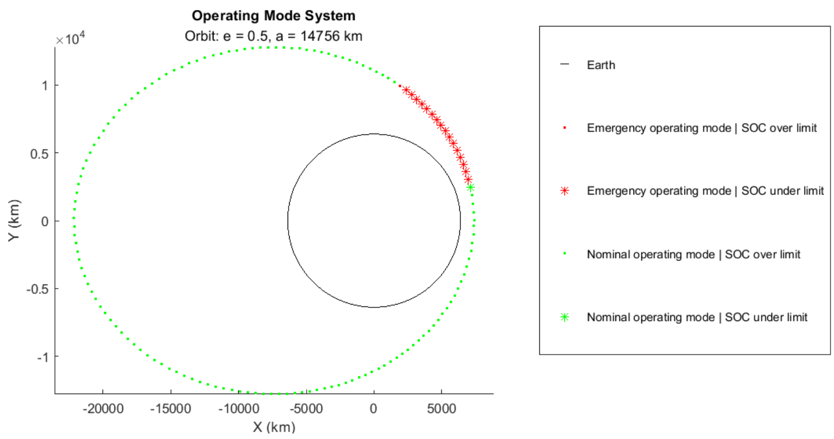

Figure 11: Behavior of the Operating Mode System in a full orbit.

From Figure 11, the system presented the desired behavior, ensuring that the EPS only operated in emergency mode as long as the SOC remained at or below the safety limit of 25%. Therefore, at all other times, the system operated in nominal mode.

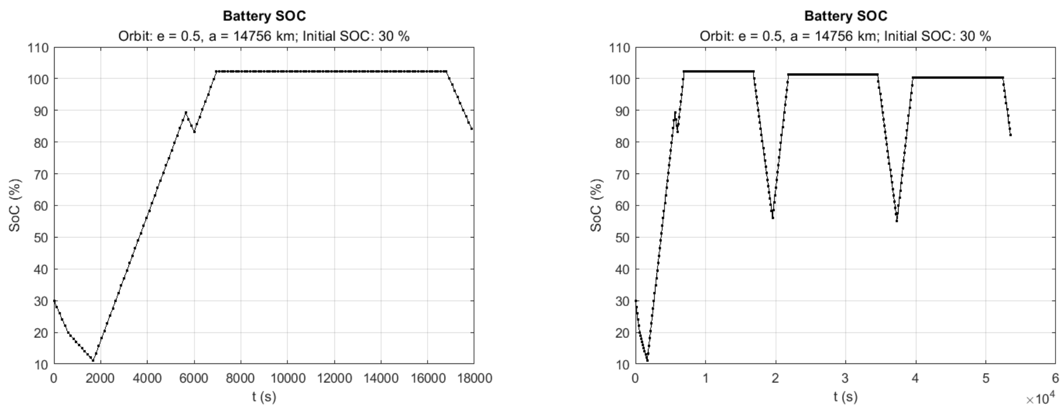

(1) **(2)**

Figure 12: Variation of the battery SOC in: (1) one full orbit; (2) three full orbits.

It is noteworthy that the change in the slope of the curve during the initial discharge easily seen in Figure 12(1) shows the reduction in energy consumption as an Emergency operating mode consequence. Also, is verified that the battery stops powering the system and starts being charged as soon as the CubeSat leaves the eclipse zone, powering it again during the interval in which no panel is sufficiently illuminated. Finally, the satellite enters the eclipse zone again switching once more to battery supply. The SOC behavior was also evaluated in three complete orbits, as seen in Figure 12(2).

From Figure 12(2), the satellite, after the maneuvers performed in the first orbit, does not need to act towards pointing its panels in the following orbits. The battery, therefore, continues powering the system during the eclipse and being charged during the illumination phases. Additionally, disregarding degradation effects, the battery charge and discharge cycles will be approximately 64% to 100% from the third orbit onwards.

5. Conclusion

This work proposed to solve a Power Supply Subsystem logical control problem in the context of the first academic satellite to be designed and built at UFMG, the PdQSat, through the Supervisory Control Theory of Discrete Event Systems.

The application of the SCT was appropriate to ensure the adequate control of the proposed models for the Photovoltaic Panels Pointing, Power Supply and Operating Mode systems, which presented their respective desired behaviors in the simulation performed. Furthermore, the use of this technique in the context of critical and hard-to-maintain applications where events shall not be missed is advantageous, since it allows one to formally guarantee the design of a system sensitive to the addressed events, while excluding any type of unwanted behavior.

In addition, the simulation of systems modeled by DES and controlled by means of SCT proved to be an useful tool to support the preliminary analysis, definition and design phases of a space mission, since it allows to manipulate, visualize and verify the behavior of a given system under several operational contexts in a simplified way, focusing on the states and events relevant to the analysis in question and reducing the demand for more complete and costly models.

The developed tool can be applied, for instance, to pre-dimension the battery capacity in view of the satellite's Power Budget, as well as the quantity, positioning and power output of the photovoltaic panels array. In addition, it is possible to verify the behavior of the integrated system by evaluating the interaction between panels, battery and load. Finally, it is also possible to evaluate the minimum and maximum SOC values expected for a given orbit, which is essential for battery degradation analysis.

References

[1] B. Shiotani, N. Fitz-Coy, S. Asundi, An end-to-end design and development life-cycle for cubesat class satellites.
[2] The MathWorks Inc., MATLAB R2020b version 9.9.0.1592791 (2020).
[3] H. Curtis, Orbital mechanics for engineering students, Butterworth-Heinemann, 2013.
[4] W. Ley, K. Wittmann, W. Hallmann, Handbook of space technology, John Wiley & Sons, 2009.
[5] G. Gharehpetian, S. M. M. Agah, Distributed Generation Systems, Butterworth-Heinemann, 2017.
[6] C. G. Cassandras, S. Lafortune, Introduction to Discrete Event Systems, Springer, 2nd edition, 2008.
[7] M. H. de Queiroz, J. E. R. Cury, Modular control of composed systems, Proceedings of the 2000 American Control Conference, 2000. 6 (2000) 4051–4055 vol.6.
[8] CalPoly, CubeSat Design Specification, Available at https://static1.squarespace.com/static/5418c831e4b0fa4ecac1bacd/t/5f24997b6deea10cc52bb016/1596234122437/CDS+REV14+2020-07-31+DRAFT.pdf (2021/11/07), 2020.
[9] L. V. R. Alves, P. N. Pena, L. R. R. Martins, UltraDES-A Library for Modeling, Analysis and Control of Discrete Event Systems, 20th World Congress of the International Federation of Automatic Control (2017) 5831–5836.
[10] K. R. Oliveira, Controle do Subsistema de Suprimento de Energia de um CubeSat em Órbita Baixa utilizando Sistemas a Eventos Discretos, Trabalho de Conclusão de Curso - Escola de Engenharia da Universidade Federal de Minas Gerais, Belo Horizonte (2021).

16

Poster Session

Assessing the Reliability of a Network-on-Chip through Physical Validation

Gustavo S. Mafra(1), **Thiago H. Rausch**(1), **Douglas A. Santos**(2), **Luigi Dilillo**(2), **Eduardo A. Bezerra**(3), **Douglas R. Melo**(1)
(1)LEDS, University of Vale do Itajaí, Brazil
(2)LIRMM, University of Montpellier, CNRS, France
(3)SpaceLab, Federal University of Santa Catarina, Brazil

Keywords: *Networks-on-Chip, Fault Tolerance, Neutron Radiation.*

Abstract

With the increased use of embedded computing and the number of cores in integrated systems, communication architectures more robust than the bus became necessary. Networks-on-chip are a solution proposed by academia and industry that makes systems more scalable with increased cores. The increase in cores is also observed in systems for use in critical environments, such as in space applications. However, architectures aimed at these applications suffer from radiation problems and extreme temperatures. Due to the flexibility and availability of logic elements, programmable logic devices are an attractive solution for developing embedded systems for space applications. However, these devices are sensitive to radiation, which makes fault tolerance techniques a requirement for their effective use in space and verification at the physical level since their circuit tends to suffer from radiation effects that cause error propagation. In this context, this work seeks to evaluate the reliability of a Network-on-Chip through physical prototyping tests. The solution employs traffic generators and meters to verify the correct functioning of the network with the complement traffic pattern. Thus, it becomes possible to certify that the behavior of the network in a physical device corresponds to the same presented in a simulation model. The network was first prototyped in the FPGA device Xilinx Zynq-7000 to obtain metrics from the network connected to the traffic components, then it was prototyped at the M2S010 FPGA for testing in a particle accelerator. The results obtained from the particle accelerator tests converge with those obtained in simulation, allowing an initial validation of the network's reliability.

1. Introduction

Currently, there is as increase necessity for devices with higher performance, but smaller area and with lower energy consumption [1]. Thus, components such as memories, controllers, and processors had to be miniaturized, making it possible to create Systems-on-Chip (SoCs). Recently, SoCs are incorporating a growing number of processing cores. In systems that integrate multiple cores, architectures more robust than the bus became necessary due mainly to the bus' lack of parallelism. Therefore, a solution proposed by academia and industry is the utilization of Networks-on-Chip (NoCs), which use integrated routers to make the systems more scalable by supporting a higher number of cores [2].

Email addresses: `gustavo_mafra@edu.univali.br` (**Gustavo S. Mafra**), `drm@univali.br` (**Douglas R. Melo**)

The continuous increase in the use of embedded computing and the number of cores in integrated systems is also observed in critical environments such as space and avionics applications. However, they suffer from the hostility of these environments, which subject electronic devices to effects from radiation and extreme temperatures. This hostility leads to temporary, permanent damages or intermittent failures that affect the behavior of computer systems [3].

Field Programmable Gate Array (FPGA) devices are an attractive solution for developing SoCs composed of multiple cores due to their high flexibility and availability of logic elements. However, as these devices are sensitive to radiation, the provision of fault tolerance techniques is required for their effective use in space applications [4].

Regarding the integration of multiple cores for critical environments, the work [5] proposes an NoC aiming at the physical implementation in a programmable logic device. The network uses finite state machines (FSMs) in the controller unit of the input flow regulation, packet routing, and channel arbitration structures, and applies triple modular redundancy (TMR) as a protection technique for these controllers. However, in that work, the architecture's reliability was validated only through simulation, not having obtained results in physical prototyping at the time.

In this context, we propose to prototype an NoC system to evaluate its reliability in harsh environments. We validated this system with a physical prototyping test in a particle accelerator, which exposed the system to neutron radiation.

2. Dependable Network-on-Chip

The NoC architecture developed by [5] aimed at space applications by implementing fault tolerance in its internal architecture elements. The designed architecture implemented triple modular redundancy in controllers and Hamming error correction code in buffers to ensure network reliability in critical environments. In addition, a set of architecture parameters were defined to evaluate the routers controllers' different implementation approaches, constituting Moore or Mealy state machines, in a standard or protected version.

The architecture of the router was designed with a focus on regularity, flexibility, and low area overhead. To fulfill these requirements, the authors used the wormhole switching technique since it provides lower latency for less cost. They also used input buffers capable of storing *n-words*. In addition, the router was conceived to integrate 2-D mesh topology networks.

The router is composed of five data ports, named *Local*, *North*, *East*, *South*, and *West*. The *Local* port is the terminal at which a processing core is attached, and the other ports connect the router to its neighbors. The input channels comprise controllers responsible for input flow regulation and packet routing, while the output channels include controllers performing channel arbitration and output flow regulation.

The controllers responsible for flow regulation implement a 4-stage handshake protocol for receiving and sending packet *flits* (a *flit* is the smallest piece of data over which is performed the flow regulation). The routing controller runs the *XY* algorithm to request an output channel to forward an incoming packet. The arbitration controller consists of a Round-Robin arbiter that schedules the use of the output channel by the packets in the router input channels.

The authors evaluated the architecture described using simulation, which consisted of simulating the traffic generation and the NoC operation with injection of single-event upset (SEU) faults in the registers using built-in commands of the ModelSim simulator that force bit-flips. The evaluation comprised measuring the throughput and error rate for different FSM combinations in the controllers of flow regulation, routing, and arbitration, resulting in eight different architectural configurations for each router evaluated in protected and standard forms.

3. Proposed evaluation platform

3.1. Test architecture

This work presents a solution for validating the reliability of the Network-on-Chip described above, using traffic generation (TG) and traffic meter (TM) components. Each router is connected to a TG component, responsible for generating and sending data packets to the network, and to a TM component that receives and validates the data by comparing it to the expected data. Figure 1 represents the structure adopted for the architecture validation. In this work, we used a 4x4 network with an 8-bit data width to perform the tests.

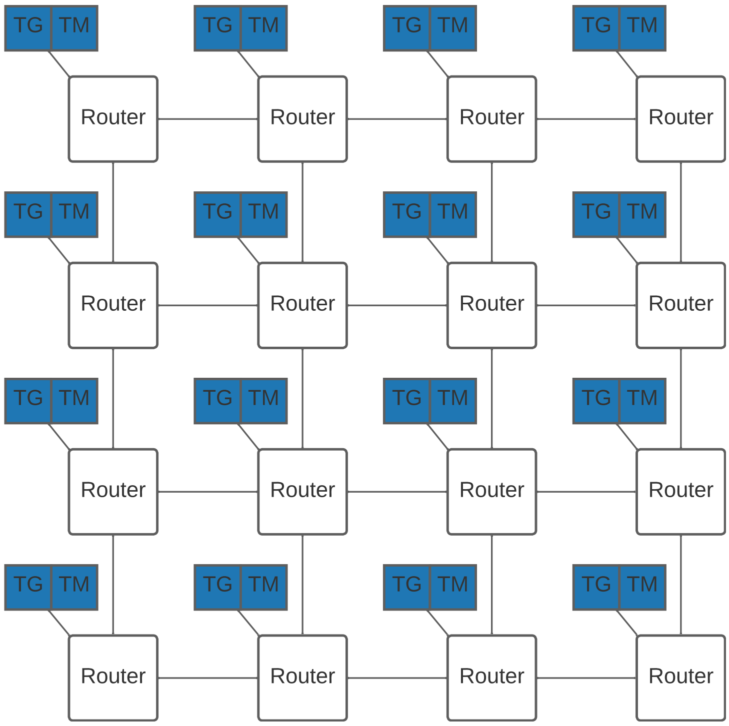

Figure 1: Proposed test architecture.

3.2. Traffic components

As previously described, the NoC flow regulation controller implements a 4-stage handshake protocol for receiving and sending packet *flits*. Thus, in order to send and receive data, we implemented a finite state machine (FSM) to send and receive the requests. Since the router was designed to enable the validation of different types of FSM (Moore or Mealy) for each controller, the components used for the network validation also allow FSM type switching.

Furthermore, the routing controller runs the *XY* algorithm to request an output channel to forward an incoming packet. The implemented traffic generator uses different traffic models to generate the packet header, constituted by the *X* and *Y* addresses of the receiver router. To evaluate the operation and reliability of the architecture, the complement traffic pattern was used.

Figure 2 shows the packet format used for the verification. The router's frame control is performed with one bit of data, and for sending a packet, only one of the *flits* will be the header, and only one will be the trailer, the others are payload *flits*. Both the header and the last payload *flit* (trailer) use '1' as the frame bit, while the regular payloads use '0'. To ensure the functioning of sending the packets, this principle presented was used in the generation of each *flit*, thus avoiding problems with misrouting or incomplete packets.

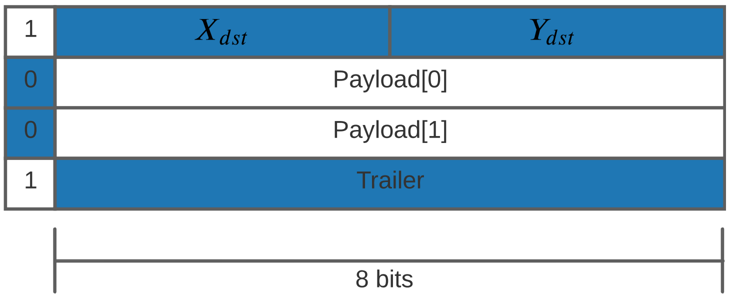

Figure 2: Packet format for verification.

The payload *flits* represent the useful data that will be forwarded by the processor cores connected to the NoC. Thus, in order to use random data for each message sent, the Linear-feedback shift register (LFSR) technique was used, given its application to generate pseudo-random numbers [6]. Thus, for each router, an initial value for the LFSR was defined based on its *XY* position in the network, this value is called a seed. Because the register has a finite number of possible states, it must eventually enter a repeating cycle. However, an LFSR with a well-chosen feedback function can produce a sequence of bits that appears random and which has a very long cycle [7].

To validate the received data on the router *Local* port, the traffic meter component performs a four-state handshake in order to work properly with the NoC flow regulation controller. The *flit* received by the component is compared with the expected *flit*, thus checking for possible errors in the received message.

The expected *flit* is generated using the LFSR technique. Thus the same polynomial is used in both components, ensuring that the sequence generated in the traffic meter component is the same as the traffic generator component. The seed used by the meter is defined with the first payload *flit* received, thereby the data comparison is performed only after receiving the first data packet.

The meter component is also responsible for measuring and storing the number of received packets and errors. Errors are incorrect data, such as bit-flips in the received *flit*. The number of received packets and identified errors from each router are stored in registers, which are accessible for further analysis.

4. Materials and methods

The traffic generators and traffic meter components were described using VHDL on a 4x4 NoC to generate and meter traffic through the *Local* port. Subsequently, the proposed test architecture was synthesized using Xilinx Vivado 2020 for cost and performance analysis. We selected the Zedboard Zynq-7000 development kit as the target device, and the synthesis tool's optimization options were kept at default.

To validate the generator and meter components implementation, we compared the meter's output to an equivalent implementation in testbench that used the same traffic pattern and traffic data. To generate traffic for the testbench, we used text files provided by a Python script that applied the same LFSR seed as the generator component, then compared both outputs via another Python script to check for mismatches.

4.1. Particle accelerator test

The hardware implementation was tested using neutron particles and the Microsemi SMF2000 FPGA, connected through a UART interface to output the data to a host computer. The tests developed in a particle accelerator seek to analyze the functioning of the network against neutron radiation. In this way, we carried out tests at Rutherford Appleton Laboratories – UK, more specifically at ChipIr beamline [8].

ChipIr, for Chip Irradiation, is an instrument designed to mimic the atmospheric neutron environment. Atmospheric neutrons are a major cause of Single Event Effects (SEE), which disrupt the correct operation of microelectronics devices and systems [8]. This instrument irradiates the device under test (DUT) with a flux up to 10^9 times greater than the natural radiation environment [9]. This high flux enables accelerated testing of electronic devices. According to [10], the average flux provided by this beamline is $5.6 \times 10^6 n/cm^2/s$ for energies above 10 MeV.

The test was set up so that, every 60 seconds, a reset signal is sent to the system to restart the test, so any possible errors wouldn't last over the run time. The output data received by the host computer consists of each router error and received packet counter, and also when the reset occurred. To analyze the data a Python script was used to count the errors and the number of received packets during the run period, and plot the values in two graphs for each router.

4.2. Traffic pattern

The work [11] presents different types of traffic patterns for the analysis of operation and performance in Networks-on-Chip. In this work, we chose to use the uniform traffic pattern named complement, where all routers have the same probability of being destinations. Since, in the study of data communication networks, uniform distribution is the most frequently used for NoC evaluations.

Figure 3 shows the complement traffic pattern, where each node is represented by its coordinates in binary format a_{n-1}, a_{n-2}, ..., a_1, a_0, and sends data to the node $\overline{a}_{n-1}$, $\overline{a}_{n-2}$, ..., $\overline{a}_1$, $\overline{a}_0$. This operation describes an inversion of the values of all bits in the address.

Origin	Destination
[0,0]=[0000]	[3,3]=[1111]
[0,1]=[0001]	[3,2]=[1110]
[0,2]=[0010]	[3,1]=[1101]
[0,3]=[0011]	[3,0]=[1100]
[1,0]=[0100]	[2,3]=[1011]
[1,1]=[0101]	[2,2]=[1010]
[1,2]=[0110]	[2,1]=[1001]
[1,3]=[0111]	[2,0]=[1000]
[2,0]=[1000]	[1,3]=[0111]
[2,1]=[1001]	[1,2]=[0110]
[2,2]=[1010]	[1,1]=[0101]
[2,3]=[1011]	[1,0]=[0100]
[3,0]=[1100]	[0,3]=[0011]
[3,1]=[1101]	[0,2]=[0010]
[3,2]=[1110]	[0,1]=[0001]
[3,3]=[1111]	[0,0]=[0000]

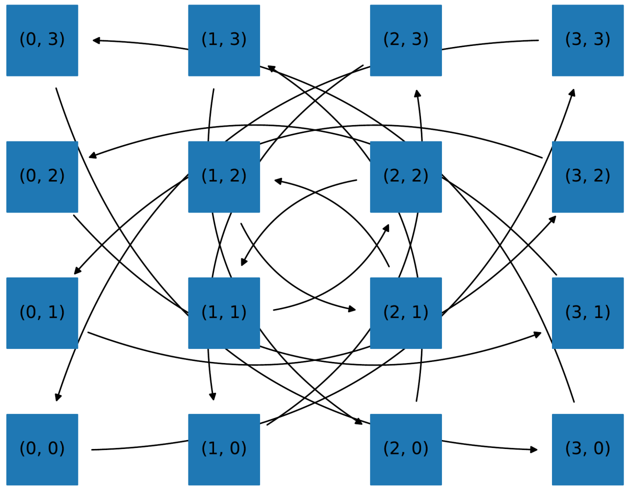

Figure 3: Complement traffic pattern.

5. Results

Table 1 presents the synthesis results for the NoC and traffic components, with the Zedboard Zynq-7000 development kit as the target device. As reported by the authors in [5], we see that the Mealy-based controllers require fewer FFs because the FSMs encode few states. Furthermore, using Mealy controllers implies a longer critical path and a lower operating frequency.

Table 1: NoC synthesis results with the traffic components on Zynq-7000.

Controllers FSM	LUTs	FFs	Fmax (MHz)
Moore	4386	4207	225.94
Mealy	3760	3841	160.78

Table 2 shows the increase in the use of LUTs and FFs, and the decrease in maximum frequency, caused by the insertion of traffic generator and traffic meter components in the *Local* port of the NoC for the physical tests.

Table 2: NoC synthesis overhead with traffic components.

Controllers FSM	LUTs	FFs	Fmax (MHz)
Moore	17.59%	19.00%	-29.12%
Mealy	21.41%	21.43%	-22.73%

The simulation with error insertion demonstrated equivalent results for the components described in the hardware and the testbench. It was observed that errors inserted into the network are measured by the meter's components, which subsequently increment the error counter of the router where the error was observed. Furthermore, the packet counter presented the expected operation, incrementing the counter whenever the *flit* trailer of a packet was received. With this validation, it was possible to start the test campaigns in particle accelerators.

5.1. Results obtained in particle accelerator

For the particle accelerator test, we used the M2S010 FPGA device from the Smartfusion2 family by Microsemi. This FPGA was chosen due to its reliable FPGA configuration memory, which is resistant to neutron radiation [12, 13]. Table 3 presents the synthesis results for the NoC with traffic components, and also the UART and the FSM used to control the experiment.

Table 3: NoC synthesis results with the traffic components on M2S010 FPGA.

Controllers FSM	LUTs	FFs	Fmax (MHz)
Moore	7074	4229	136.57
Mealy	7345	4217	79.30

In the first test campaign, we tested the Network-on-Chip with its controllers on Moore against neutron radiation. Furthermore, in the second test campaign, we redid the tests with the NoC using the controllers on Mealy. In both experiments, we estimate the delivery of packages and the incident of errors in 60 runs of 60 seconds.

5.1.1. Network controllers on Moore

Figure 4 demonstrates the router (0,0), which we consider to have an ideal operation since it has a very small variation in data throughput during the execution period, and errors weren't measured in the received packets. The variability in the number of received packets is observed in all routers, indicating normal variations due to the peripherals used to reset each run.

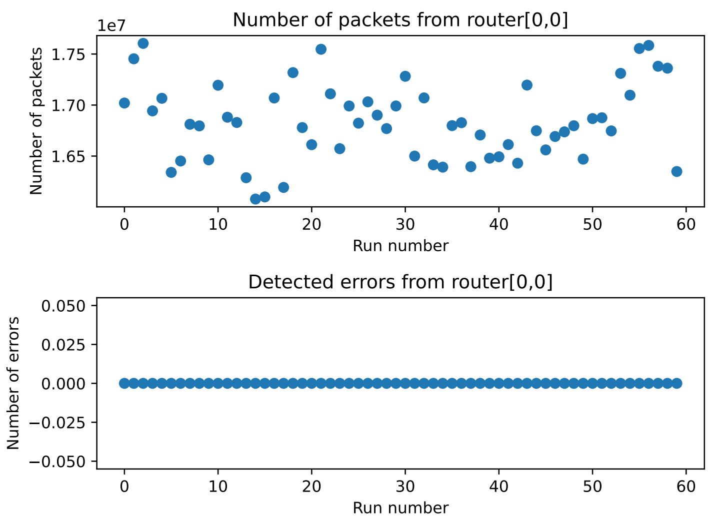

Figure 4: Router (0,0) results considered an ideal operation.

In Figure 5, we observe the occurrence of errors in the router (3,2). The error occurs in run 5, and errors are measured until the reset of this run. This error characterizes a bit-flip in the data buffer, thus affecting the data generated by the LFSR, causing a difference in the comparator present in the traffic meter component.

Figure 5: Router (3,2) results show errors in received data.

In Figure 6, it is possible to see misroutings occurring in run 6. This observation is based on the low number of packets received by the router in that run, indicating that the packets were lost before delivery. This decrease was not noticed on other routers during these runs, indicating that the problem occurred only when forwarding packets addressed to that router.

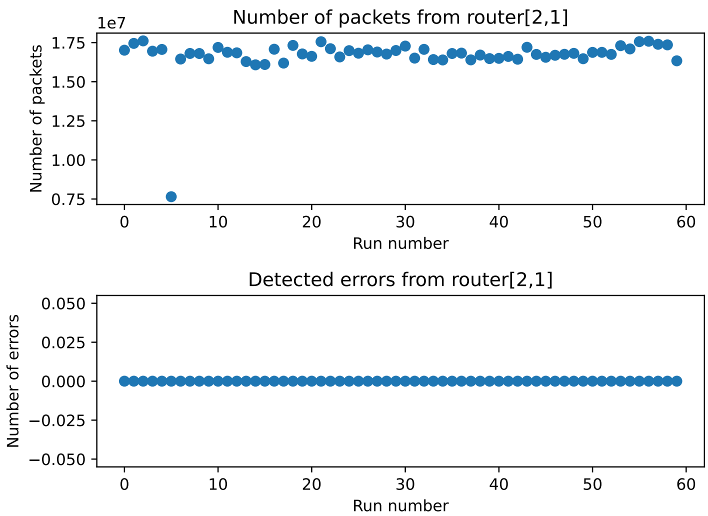

Figure 6: Router (2,1) results demonstrate misrouting.

5.1.2. Network controllers on Mealy

Figure 7 demonstrates the router (0,0) that we consider to have an ideal operation with Mealy controllers, i.e., errors weren't measured in the received packets. In addition, it is possible to observe the variation of packets received in each run. However, as previously mentioned, this variation occurs because the peripherals used to perform the resets interfere with the duration of each run.

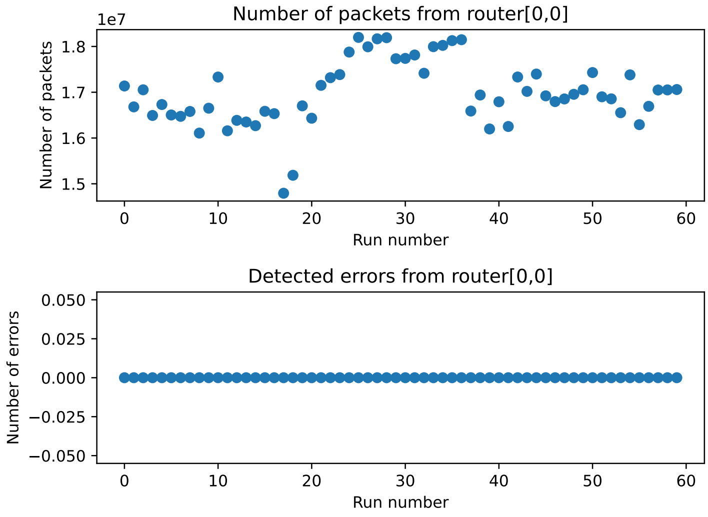

Figure 7: Router (0,0) results considered an ideal operation.

In Figure 8, it is possible to observe the occurrence of errors in the router (1,2). The error occurs in run number 2, and errors are measured until the reset of this run, the same type of error found with Moore controllers. Thus, we found that with Mealy controllers, errors occur less frequently than with the Moore FSM, but with the same consequences when they appear.

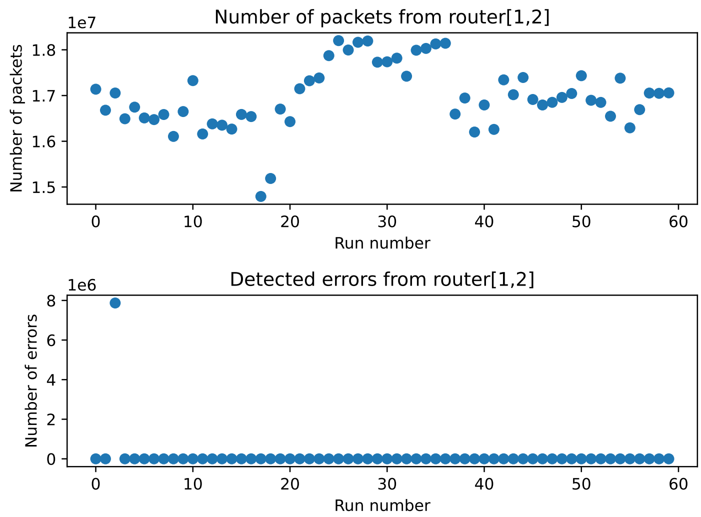

Figure 8: Router (1,2) results show errors in received data.

Tests with the controllers on Mealy didn't present any misrouting errors in the analyzed samples. In addition, errors were shown to be exceedingly rare in both Mealy and Moore controllers, but with the use of controllers on Mealy, there was a decrease in the occurrence of errors during the tests.

5.2. Discussion

In the 500 runs analyzed, 11 errors were observed using the controllers on Moore, 3 in the payload *flits*, and 8 in the header *flits*, which characterizes a misrouting. However, using controllers on Mealy only 1 error was observed on the packet payload, demonstrating a 91% increase in the network reliability.

The results obtained in physical prototyping and testing in particle accelerator converge with those obtained previously in simulation by the authors in the work [5], demonstrating that Mealy is the more reliable choice for the network controllers. However, further tests need to be conducted to accurately verify the reliability increase in the network using Mealy controllers.

6. Conclusion

The tests using the complement traffic pattern validate the operation of the NoC, thus enabling an understanding of the normal operating behavior of the network. Thereby, with the particle accelerator tests, it was possible to verify the behavior of the architecture in critical environments. The network proved to be tolerant most of the time, but it was also detected errors caused by the incidence of particles in the FPGA.

In future work, we intend to improve the evaluation in a particle accelerator by using other traffic models, in addition to a new test campaign with the reliable version of the network, in order to verify its operation and reliability in a hostile environment.

Acknowledgments

This work was supported by the Foundation for Support of Research and Innovation, Santa Catarina (FAPESC-2021TR001907), the Region d'Occitanie and the École Doctorale I2S from the University of Montpellier (20007368/ALDOCT-000932), and the RADNEXT EU project (Horizon 2020 - Grant Agreement no. 101008126).

References

[1] S. Pasricha, N. Dutt, On-chip communication architectures: system on chip interconnect, Elsevier, 2008.

[2] D. Jose, S. Yalamanchili, L. Ni, Interconnection Networks: an Engineering Approach, Morgan Kaufmann, 2003.

[3] M. Yang, G. Hua, Y. Feng, J. Gong, Fault-tolerance techniques for spacecraft control computers, John Wiley & Sons, 2017.

[4] F. Kastensmidt, P. Rech, FPGAs and Parallel Architectures for Aerospace Applications, Springer, 2016.

[5] D. Melo, C. Zeferino, L. Dilillo, E. Bezerra, Maximizing the inner resilience of a network-on-chip through router controllers design, Sensors (2019).

[6] M. Luby, Pseudorandomness and Cryptographic Applications, Princeton University Press, 1996.

[7] A. K. Panda, P. Rajput, B. Shukla, Fpga implementation of 8, 16 and 32 bit lfsr with maximum length feedback polynomial using vhdl, International Conference on Communication Systems and Network Technologies (2012).

[8] C. Cazzaniga, C. D. Frost, Progress of the scientific commissioning of a fast neutron beamline for chip irradiation, Journal of Physics: Conference Series (2018).

[9] C. Cazzaniga, M. Bagatin, S. Gerardin, A. Costantino, C. D. Frost, First tests of a new facility for device-level, board-level and system-level neutron irradiation of microelectronics, IEEE Transactions on Emerging Topics in Computing 9 (2021) 104–108.

[10] D. Chiesa, M. Nastasi, C. Cazzaniga, M. Rebai, L. Arcidiacono, E. Previtali, G. Gorini, C. D. Frost, Measurement of the neutron flux at spallation sources using multi-foil activation, Nuclear Instruments and Methods in Physics Research Section A: Accelerators, Spectrometers, Detectors and Associated Equipment 902 (2018) 14–24.

[11] L. P. Tedesco, Uma proposta para geração de tráfego e avaliação de desempenho para NoCs, Master's thesis, Pontifícia Universidade Católica do Rio Grande do Sul, 2005.

[12] Microsemi, IGLOO2 and SmartFusion2 Datasheet Version DS0128, 2018. Rev. 12.

[13] D. Dsilva, J.-J. Wang, N. Rezzak, N. Jat, Neutron SEE testing of the 65nm SmartFusion2 flash-based FPGA, in: 2015 IEEE Radiation Effects Data Workshop (REDW), pp. 1–5.

Payload-XL: A Subsystem to Validate FPGA-based Applications in Space Environment

Kleber Reis Gouveia Junior(1), **Edilberto Costa Neto**(1), **Márcio Hermany Gomes de Oliveira**(1), **Felipe Viel**(1),(2), **Miguel Boing**(1), **Gabriel Mariano Marcelino**(1), **André Martins Pio de Mattos**(1), **Laio Oriel Seman**(1),(2), **David Merodio Codinachs**(3), **Eduardo Augusto Bezerra**(1)

(1) Universidade Federal de Santa Catarina (UFSC), Brazil
(2) University of Vale do Itajaí (UNIVALI), Brazil
(3) European Space Agency (ESA), Netherlands

Keywords: *Radiation Tolerant FPGA, CubeSat, GOMX-5*

The advancement of processor and circuit technologies aimed at the space environment is vital to support new applications. Thus, those applications each day demand more and more resources and, simultaneously, are exposed to a critical environment. This work describes the BRAVE Application initiative, which results from a partnership between ESA and Spacelab-UFSC. It is conceived to evaluate the FPGA NG-Large device from the NanoXplore French company. This FPGA device is based on SRAM technology and is radiation hardened, being the target of experiments that seek to validate its ability to operate in a space environment, remaining responsive for the nine months of the GOMX-5 mission. The FPGA device is controlled via the MSP430FR6989 microcontroller, which controls the FPGA recording logic via bitstream configuration memory to carry out the experiments sent by the ground station. This satellite subsystem is planned to test the different components within the payload and monitor the functioning of the FPGA device and the experiments. The New File Reception application is the firmware responsible for receiving data and commands via the GR740 subsystem. The ground station sends data and commands to the Payload-XL control, where they are driven to the target destination, the MSP430 or the Fresh-MC softcore. The firmware Space Pods manages the execution of applications and process routines within the payload. The Space Pods is considered the control core and is executed on the MSP430. The firmware Housekeeping application monitors existing payload components, such as generating FPGA bitstream storage redundancy and safety checks on external FLASH memories. For embedded FPGA-based test applications, a softcore RISC-V running FreeRTOS, a UART-SpaceWire decoder, and a softcore Fresh-MC were tested to evaluate board operation. Payload-XL is an effort to globalize anti-radiation technology by conducting experiments with the BRAVE NG-Large in low earth orbit (LEO). To fulfill this objective, a robust, reconfigurable, secure system was created, capable of monitoring the operation of the FPGA device in detail and communicating with the ground stations. The system proved to be functional and ready to be used in space missions.

Email addresses: `kleber.gouveia@spacelab.ufsc.br` (**Kleber Reis Gouveia Junior**), `edilberto.costa.neto@posgrad.ufsc.br` (**Edilberto Costa Neto**), `eduardo.bezerra@ufsc.br` (**Eduardo Augusto Bezerra**)

1. Introduction

Small satellites have become increasingly common in many applications in the last decade. The application areas are diverse for this class of satellites, being seen in governmental, military, scientific, educational, and commercial applications [1, 2, 3]. This wide range of applications shows that the current space exploration scenario has been guided by the cost reduction of [4] space platforms, [5] miniaturization, use of radiation-hardened (rad-hard) components, and commercial components. off-the-shelf (COTS) combined with fault mitigation techniques [6, 7]. In addition to this movement, several studies have been carried out to characterize the radiation in the space environment, evaluate the effects of radiation on COTS commonly used in Cubesats, propose methodologies to increase the reliability of the systems and the radiation tolerance of small satellites [8][9].

There are several norms and manuals to guide satellite development, especially those defined by the European Cooperation for Space Standardization (ECSS) to guide space systems development. However, most of this material focuses on complex space systems requiring several steps in the development cycle that increase project duration and cost and require much time reviewing and preparing technical documentation. Combining these steps makes it unsuitable for developing low-cost missions such as the Cubesats. In this context, the ESA appears to define a guide for adapting the ECSS [10] standards to determine which standards must be followed and which parts of these standards must be adjusted for use in the development of Cubesats.

Several vision works bring new development methodologies, technologies, and equipment, focusing mainly on Cubesats. The works [4, 9, 11] bring evaluations, analyses, and methodologies that focus on the components that can integrate missions, bringing relevant information that helps designers to direct their choices for System-on-Chip (SoC), microcontrollers, FPGA, and memories on space missions. The works [12, 6] focus on presenting the development of subsystems and satellites of the Cubesat type to integrate and carry out missions that seek to validate integrated circuits (IC) technologies. Finally, in [13, 6] rules, techniques, and best practices are presented for the implementation of qualified boards for space applications.

Given the above, this work presents a flow based on standards and design techniques for the development and verification of Cubesats, combining agility, reliability, and low cost in the implementation of the Payload-XL subsystem that integrates the future GOMX-5 mission [14].

It also presents the development flow of applications, software, hardware, and software/hardware integration developed to validate the Payload-XL and executed in a space environment. The main contribution of this work is to present a satellite subsystem that will test the integration of a microcontroller with the Field-Programmable Gate-Array (FPGA) NG-Large. In addition, new application technologies will be tested, such as Housekeeping ManyCore (HK-MC) and a RISC-V-based core, both implemented in the NG-Large FPGA.

2. Board Organization and Architecture

The development of NG-Large is intended to demonstrate the FPGA NG-Large in orbit together with an FPGA reconfiguration mechanism that allows the remote update of the FPGA configuration bitstream to be performed. This reconfiguration mechanism, in conjunction with redundancy techniques, allows for greater system robustness and flexibility, as it is possible to send updates and new applications to Payload-XL throughout the life cycle of the GOMX-5 mission. Fig. 1 shows the complete flow.

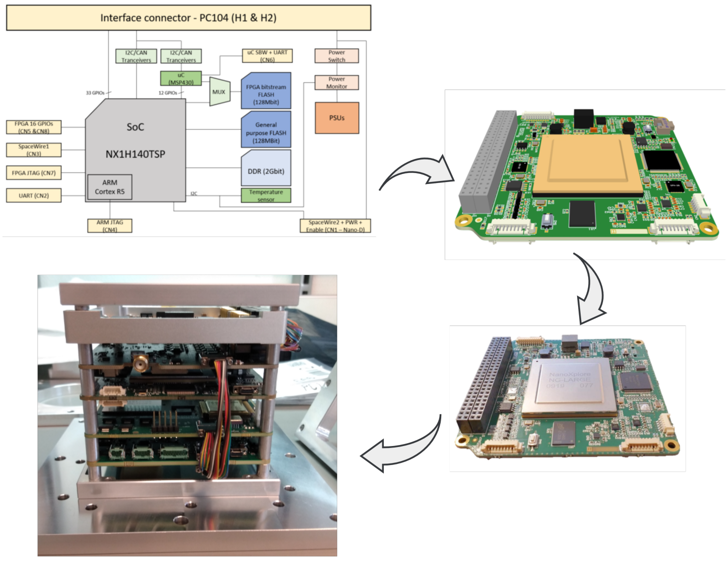

Figure 1: Design flow from block diagram to stacking on Cubesat GOMX-5.

The main component of Payload-XL is the FPGA NG-Large from the French company NanoXplore. Due to its manufacturing characteristics, it is intended for applications in critical environments, such as space.

2.1. Hardware development

The Payload-XL board hardware design is based on the ECSS-Q-ST-70-12C standard and [6]. Payload-XL is a system created in the modular PC104 standard, commonly used in Cubesats, and combines a COTS the radiation-tolerant FPGA NG-Large NXH140TSP, which has 140k LUTs, an ARM Cortex-R5 processor, has radiation tolerance for Total Ionizing Dose (TID), immunity to Single Event Latch-up (SEL), Linear Energy Transfer (LET) and Soft-Error Rate (SER). The Payload-XL architecture has NG-Large as the central processing block, which implements several communication interfaces through GPIO, UART, I2C, CAN, SpaceWire, and has access to Flash memories, RAM, temperature sensor, and voltage/current at the system power input. A Texas Instruments MSP430FR6989IPZR microcontroller is responsible for performing the FPGA reconfiguration.

The manufacturing of the Payload-XL focused on fast signal impedance, board layers, and signal impedance due to the end application of the board and the standards used as a basis. Impedance control in fast signals has received extra attention due to DDR2 and SpaceWire interface. For this, we adopted: (*i*) single-ended trails and differential pairs with impedances of 50 Ω and 100 $\Omega \pm 10\ \Omega$, respectively (*ii*) signals DQ/DM with timing differences less than 15 ps; (*iii*) route signals with the same length or by a group of bytes; (*iv*) The length difference between tracks for differential pair $<$ 3 mm and for data and strobe $<$ 5 mm. Figure 2 illustrates Payload-XL routing and layers.

The board project is designed using eight layers, where four were generated following [15] and four layers added to use DDR2. The materials used for the layers were combinations of Copper-PR2116 in layers 1, 3, 5, and 7 and Copper-FR4 in layers 2,

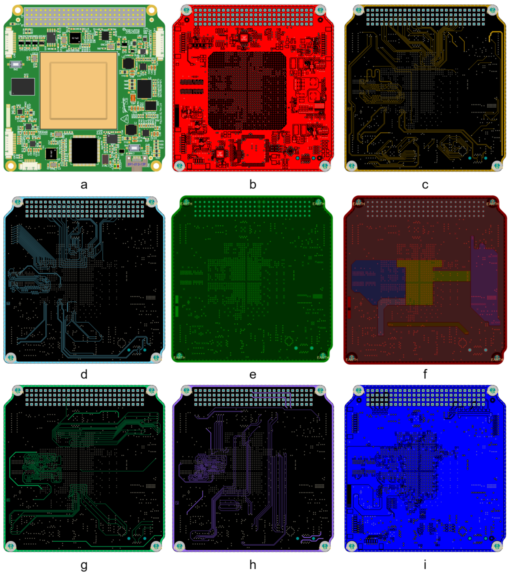

Figure 2: Layout details. Top view of 3D model (a), layer 1 (b), layer 2 (c), layer 3 (d), layer 4 (e), layer 5 (f), layer 6 (g), layer 7 (h), and layer 8 (i).

4, and 6. Layer 8 uses only copper. Finally, in terms of electromagnetic compatibility, the following was adopted: (*i*) single ground plane to avoid potential differences in the reference and coupling of external signals; (*ii*) ongoing plans to reduce the level of radiated emissions; (*iii*) adjacent layer power and ground planes for Ultra High Frequency (UHF) capacitors. (*iv*) circuit separation, avoiding crossing signals and separating tracks to prevent interference from different parts; (*v*) positioning and routing to reduce the critical signal length and loop area; and (*vi*) use of stripline track geometry that results in ≈20 dB lower radiated emissions than microstrip; and (*vii*) circuit ground connection via 1M Ω resistor at a single point following ECSS-E-ST-20-06C Rev.1.

2.2. Software Development

Software development at Payload-XL focuses mainly on implementing two components, tasks developed in C language for FreeRTOS running on μC MSP430 and firmware developed in Ruby language for a manycore architecture running on FPGA. The MSP430 operates at 16 MHz and has 2 KB of RAM and 128 KB of FRAM. FreeRTOS [16] was ported to operate on the MSP430 microcontroller to meet mission requirements and support external memory for expansion of storage capacity, but limiting μC to operate at 8 MHz. The tasks performed in FreeRTOS are: (*i*) *Startup*; (*ii*) *Heartbeat*; (*iii*) *Cubesat Protocol (CSP) Server*; (*iv*) *Watchdog Reset*; and (*v*) *Memory Management*. The task *FPGA Reconfiguration* is the main one running and allows the reconfiguration of the FPGA present in the Payload-XL. Figure 3 illustrates the operation of the main task of the system that configures the auxiliary components for direct access by the FPGA and, in the sequence, the communication of μC with the experiment in execution aiming at Telemetry, Tracking & Command (TT&C) with GroundStation.

With the development and design, it was necessary to develop additional tasks for maintaining the shared external memory, storage telemetry data such as boot count and failures, and identifying failures in the FPGA. Because μC also has R/W access to shared memory, it is possible to rearrange the order of execution of the experiments.

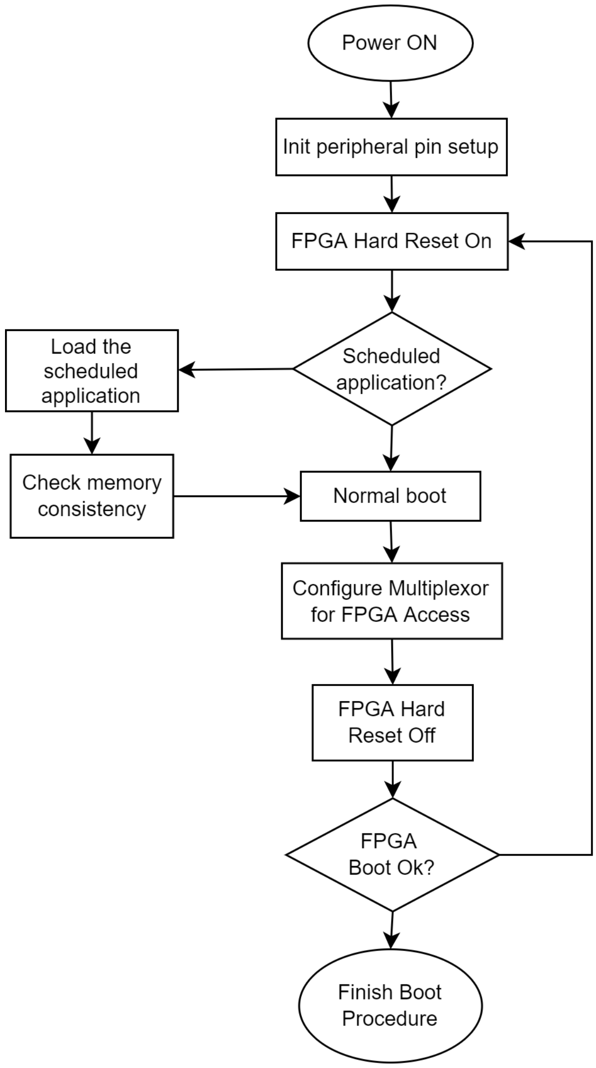

Figure 3: FPGA Reconfiguration algorithm.

The memory management routine acts according to the received TT&C commands, performing a memory reorganization. Figure 4 shows the application scheduling flow.

2.3. Digital Design Applications

The applications developed to run on the FPGA are the HK-MC, UART-SpaceWire Decoder (DU2SpW), and RISC-V with FreeRTOS Operating System. These applications make it possible to empirically evaluate the final concept of Payload-XL and assess whether the FPGA continues to have logical correctness in the processing. The HK-MC acts as an intermediary in the communication between the tasks that operate in μC and other subsystems of the Cubesat. This approach allows for responding to housekeeping requests from the Payload-XL subsystem to the Cubesat Onboard Computer (OBC) within 200 ms. The HK-MC has two processor nodes interconnected by a mesh interconnection infrastructure. One node is responsible for processing requests using CSP, and the other node supports communication via SpaceWire [17] and UART.

DU2SpW allows a UART communication to be translated to the SpaceWire protocol using the [17] interface and vice versa. This translation is necessary because μC uses UART and SpaceWire is the interconnect standard used in Cubesat. DU2SpW is

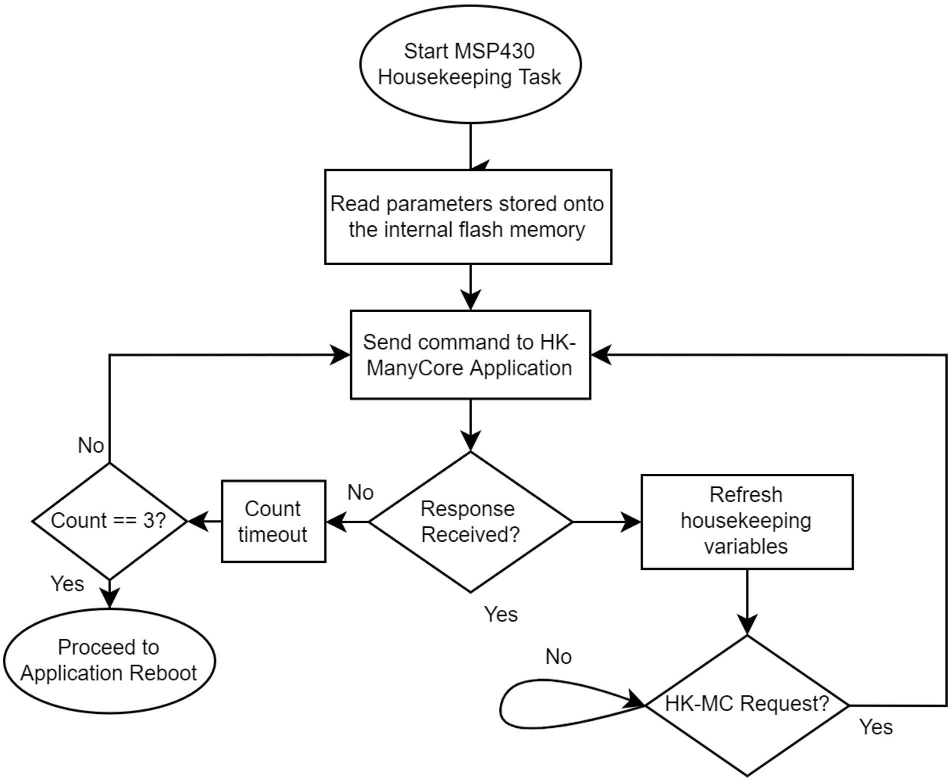

Figure 4: Application Scheduling Algorithm.

directly developed in hardware and focuses on interconnecting the Payload-XL with the rest of the Cubesat as an alternative to the HK-MC, allowing other experiments to use the FPGA logic. For the development of DU2SpW, the hardware description language VHSIC Hardware Description Language (VHDL) was used. The modular design allows the DU2SpW to be adapted for different mappings between different protocols. Finally, the implemented RISC-V focused on implementing applications with the potential to test the NG-Large FPGA and the ability to support a RISC-V RV32I softcore based on [18]. Ported FreeRTOS aims to evaluate a RISC-V with an operating system running on FPGA NG-Large. The adoption of FreeRTOS makes it possible for tasks executed in μC to be ported. In future missions, it is unnecessary to use μC.

3. Results

The Payload-XL was validated in different ways: (i) Compatibility, vibration, and operating energy tests; (ii) running tests of the software operating on μC; (iii) test run of the software on the HK-MC; and (iv) functional execution of applications running on the FPGA.

3.1. Hardware Results

The tests evaluate the hardware of external board communication, power-up, and communication between the integrated circuits present on the board, such as the FPGA, μC, and memories. In addition, vibration and stacking tests with the other GOMX-5 subsystems allowed us to evaluate, verify, and adjust the Payload-XL with others Cubesat subsystems. Fig. 5 shows a stacking test.

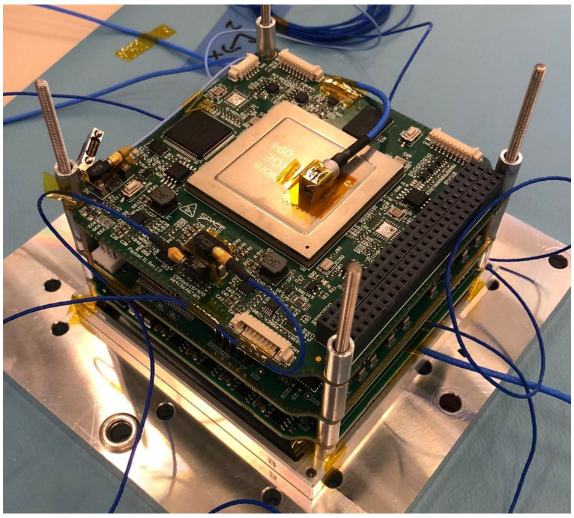

Figure 5: Operation test conducted in the Payload-XL laboratory.

These positive results show that the Payload-XL is functional and can integrate the mission. During the tests, adjustments were made in components and board structures, such as passive components and routing for the Payload-XL, to fully comply with the parameters and requirements of the GOMX-5 mission. These changes were influenced and made better integration of the Payload-XL into the mission. Table 1 demonstrate the accepted power dissipation of the Payload-XL to operate during the mission.

Table 1: Payload-XL power conniptions tests results.

Experiment	**Power**
Operations over FPGA and bitstream	8.35 W
FPGA reconfiguration	8.35 W
FPGA memory check	8.35 W
FPGA data encryption	8.35 W
Payload-XL and GR740 subsystem receiving samples	14.00 W

3.2. Software Results

The result from the developed software focused on verifying the tasks executed in μC and HK-MC. The metrics used to obtain the results form logical correctness in the execution and processing time. All tasks that ran on the FPGA were tested to ensure they fulfilled their roles. The execution of the main task *FPGA Reconfiguration* was 3 seconds. These metrics results show that the execution of the task can take 1 minute 20 seconds maximum but is entirely dependent on the size of the bitstream sent to experiment on the platform.

We also evaluated the firmware implemented on the HK-MC to a housekeeping request. Results show that the application needs only 680 microseconds to process the request and respond to the OBC with a positive confirmation that the Payload-XL is still operational using the 200 MHz transmission as a standard in communication via SpaceWire. Requests that depend on the μC response are sent at a rate of 115,200 bps via the UART protocol.

The HK-MC proved to be essential for Payload-XL because it does not allow the subsystem to be constantly reset due to the low processing capacity of the μC MSP430. This low processing capacity was mainly due to the CSP library used and necessary for processing requests. The average processing time of a CSP packet by μC is approximately 4 seconds, which makes it impossible to answer housekeeping.

3.3. FPGA Applications Results

As result metrics obtained with the digital projects mentioned before were: (*i*) frequency of operation; (*ii*) resource consumption; and (*iii*) bitstream size. This last metric is relevant because it directly impacts the execution of the *FPGA Reconfiguration* task. Tab. 2 summarizes the results obtained with initial experiments.

Table 2: FPGA Resources results from Payload-XL Applications

Application	Fmax	LUT	FF	Memory Bits	Bitstream Size
HK-MC	25 MHz	—	—	—	41kB
DU2SpW	25 MHz	346	336	48k	32kB
RISC-V	12.5 MHz	1,304	2,560	327.68k	1.32MB

The results obtained with digital designs were considered satisfactory for an FPGA that features radiation tolerance. An issue that aims to improve these results is, in the future, to design a board that seeks to optimize input and output signals that help the NG-Large synthesis tool to route and generate better resource consumption results, such as LUT, FF, and Memory Bits, and achieve higher operating frequency results. These optimizations will make it possible to improve processing capacity, such as that of RISC-V, and explore parallelism in the FPGA. The HK-MC resource results were not obtained due to the already synthesized IP and not being generated by us.

4. Conclusion

This paper presented Payload-XL, a radiation-hardened reconfigurable hardware architecture to implement a telecommand and telemetry module in Cubesats. The developed architecture consists of a PCB board designed to be radiation-hardened, an MCU to manage the reconfiguration process, and a radiation-hardened FPGA responsible for implementing the telecommand and telemetry module as main components.

The tests were performed to verify the capability of the FPGA reconfiguration. Also, the TC and TM flow were tested in order to test the implemented coding and decoding algorithms. While the imulatedesults showed efficiently, results in-orbit will be considered as the next step in the validation process. The architecture will be used for the in-orbit validation of two new technologies: the new BRAVE FPGA developed in France, FPGA reconfiguration by MSP430, and FPGA digital IPs. This process will be handled along with the GOMX-5 mission. Before launching the Payload-XL to space, close work will be directed to testing the developed Printed Circuit Board (PCB) to verify its endurance to protect from the radiation effects.

Future work will be concentrated on using the ARM R5 hardcore inside of NG-Large FPGA and integrating him with hardware accelerators IP in the logic area. The work is in progress with an Advanced Peripheral Bus (APB) protocol to/from the SpaceWire protocol interface.

Acknowledgments

The authors would like to thank the funding from Conselho Nacional de Desenvolvimento Científico e Tecnologico (CNPq) - Process 140368/2021-3 and Fundação Stremmer para Pesquisa, Desenvolvimento e Inovação (FEESC) - Process 23080.033 828/2021-30.

References

[1] G. M. Marcelino, et al., A critical embedded system challenge: The floripasat-1 mission, IEEE Latin America Trans. 18 (2020) 249–256.
[2] Y. Rahmat-Samii, V. Manohar, J. M. Kovitz, For satellites, think small, dream big: A review of recent antenna developments for cubesats., IEEE Antennas and Propagation Magazine 59 (2017) 22–30.
[3] J. C. McDowell, The low earth orbit satellite population and impacts of the spacex starlink constellation, The Astrophysical Journal Letters 892 (2020) L36.
[4] A. D. George, C. M. Wilson, Onboard processing with hybrid and reconfigurable computing on small satellites, Proceedings of the IEEE 106 (2018) 458–470.
[5] A. Gregorio, F. Alimenti, Cubesats for future science and internet of space: Challenges and opportunities, in: 2018 25th IEEE Inter. Conf. on Electronics, Circuits and Systems (ICECS), IEEE, pp. 169–172.
[6] C. A. Rigo, et al., Printed circuit board design methodology for embedded systems targeting space applications, IEEE Latin America Transactions 18 (2020) 257–264.
[7] A. Cristo, et al., Optimization of processor-to-hardware module communications on spaceborne hybrid fpga-based architectures, IEEE Embedded Systems Letters 5 (2013) 77–80.
[8] R. Secondo, et al., System level radiation characterization of a 1u cubesat based on cern radiation monitoring technology, IEEE Transactions on Nuclear Science 65 (2018) 1694–1699.
[9] G. Bonin, L. Stras, A new approach to radiation tolerance for high-orbit and interplanetary smallsat missions (2018).
[10] ESA, Tailored ECSS engineering standards for in-orbit demonstration cubesat projects, ESA, ESTEC: Noordwijk, The Netherlands (2016).
[11] B. Yost, et al., State-of-the-art small spacecraft technology (2021).
[12] R. Merl, P. Graham, A low-cost, radiation-hardened single-board computer for command and data handling, in: 2016 IEEE Aerospace Conference, IEEE, pp. 1–8.
[13] A. M. Hernandez, et al., Emc challenges for esa scientific missions, in: 2018 International Symposium on Electromagnetic Compatibility (EMC EUROPE), IEEE, pp. 34–39.
[14] ESA, ESA technology cubesats: Pushing the mission autonomy envelope (2021).
[15] R. D. Rules, Strategies for bga devices, user guide, 2016.
[16] FreeRTOS, 2020.
[17] 4Links, 2022.
[18] S. Nolting, The NEORV32 RISC-V processor, `https://github.com/stnolting/neorv32`, 2022.

INDIRECT GLOBAL MONITORING OF MINIMUM HABITAT CONDITIONS FOR THE LIFE OF BEES

Ana Carolina L. Oliveira(1), Ricardo V. M. Leite(2)
(1) Universidade Federal de Minas Gerais, Avenida Fleming 871, Ap 2 102, Belo Horizonte, Minas Gerais, Brazil, +5571999344126, acloliveira2001@gmail.com
(2) Senai CIMATEC, Estrada do coco km8 s/n. Condomínio Reserva Buscaville Q7 L8, Busca Vida, Camaçari, Bahia, Brazil, +5571987018635, ricardo.leite@aln.senaicimatec.edu.br

***Keywords**: Vegetation surveillance, Colony Collapse Disorder (CCD), Cubesats, Bees*

The bees are the main pollinating agents of the planet and so have key roles in the preservation of vegetation biodiversity and in the growth of many agricultural crops. In parallel, small satellites are being increasingly used in the agronomy, making the task of monitoring the plantation easier. In addition to the growing utilization of cubesats, its application in the vegetation surveillance for the aid of bee survival is still below its potential uses in solving or at least diminishing issues that contribute to the phenomenon known as Colony Collapse Disorder (CCD). Such phenomenon consists of a major population decline of bees, and it has been alerting the scientific community to the urgency of measures that contribute to the preservation of the honey producing species. Considering that the preservation of the natural habitat of bees is a fundamental activity for the process of protecting them and, consequently, solving problems of cultivation and production, this article has the general objective of monitoring, through small satellites, the conditions of vegetation cover that provide the survival of different species. As specific objectives, we have to capture and publish the local survival indexes; implementing a global routine for the dissemination of these indices to reduce the CCD, as well as the awareness of the need to maintain this anthropocentric attractor in the survival of these species, and the use of cubesats to achieve those objectives, by monitoring key regions for the proliferation of bees, determined from a pre-established database. To reach the objectives, a plant cover mapping routine by satellites seems necessary to collect and feed local and global databases with those equipment. This will guarantee the access to protective entities, government, academy and all research institutes. That action will alert about the areas that are below the acceptable threshold and allow the resolution of the problem, so that it doesn't reach critical levels and, consequently, the permanent extinction of bees. The authors believe that this project has a real potential to influence the run against the CCD, increase the levels of society awareness in the whole world about the importance of this complex nature chain, in addition to the real contribution of the proposal in a short, medium and long term.

1. Introduction

The bees are the main pollinating agents on the planet, with an incredible biodiversity of more than 25,000 species, they play a fundamental role in preserving the biodiversity of vegetation and are responsible for the growth of many agricultural crops. Thus, a world without bees, one of the main pollinating agents, is worrying, since an artificial substitute with similar performance to these beings is unknown [7].

In this sense, the contribution of bees to the continuity of the various forms of terrestrial life is crucial, however, those beings have not been treated with due relevance, causing a phenomenon known as "Colony Collapse Disorder" (CCD), which consists of in a sharp population decline that has been alarming the scientific community for the urgency of measures that contribute to the preservation of the species of these highly pollinating insects around the globe. This phenomenon is caused by bioinvasion, loss of habitat through fragmentation and degradation, climate change, decrease in the diversity of natural vegetation and exploitation [2], [7] and [12].

In this context, CUBESATs, satellites on a reduced scale resulting from a technological trend of the miniaturization of electronic components, stand out as a potential response to the CCD. Despite their reduced structure, such satellites have the ability to perform missions similar to large satellites, thus, with the reduction of the structure and popularization of the model, enabling the existence of commercial components, they present cost and manufacturing time lower when compared to large satellites, enabling its implementation in missions in different sectors.

Considering that the preservation of their natural habitat is a fundamental activity for protecting the bees, this project has the general objective of monitoring the existence and conditions of the vegetation cover that provide the survival of the different species. As specific objectives we have the definition of a governmental indicator of local survival index; implementation of a global routine for the dissemination of these indices in order to reduce the CCD, as well as the awareness of the need to maintain this anthropocentric attractor in the survival of these specimens.

2. Methodology

In order to develop the present work, a literature review was carried out, seeking to better understand the phenomenon of the CCD and its possible forms of mitigation, so that the most appropriate one could be applied, also covering its possible causes, the use of cubesats for plant monitoring and the relation between the behavior of bees in the face of adversities present in their territories.

Based on the results obtained, it was possible to determine the data necessary for the definition and calculation of ideal metrics for understanding the reality of bees in a given region and, then, to propose viable technologies for the use of remote sensing through the use of cubesats for the collection of these data.

3. Literature Review

3.1. Colony Collapse Disorder (CCD)

Bees, as pollinators, play an important role in the maintenance of wild plant life and the amount of food produced by crops, having an important role in the reproduction of approximately 80% of plant species [12]. However, there has been a population decline among bee populations, the so-called Colony Collapse Disorder (CCD).

The CCD is caused by several factors, and cannot explain its occurrence by just one bias. Among these, a significant example is the change in the temperature of the environment, since bees are ectothermic animals, which means they are unable to regulate their body temperature, so this phenomenon alters their behavior, generating an imbalance in the plant-pollinator relationship. In addition, it is also noticed the influence of contamination by pesticides both directly, pollination of plants with pesticides, and indirectly, a bee that was directly contaminated takes these substances to the hive.

Besides those, one of the biggest causes for their disappearance is the fragmentation of the territory, which triggers the isolation of species, and the degradation of their habitat, directly impacting the malnutrition of the bees present there [7]. In this way, the search for ideal and healthy vegetation for the installation of beehives becomes a crucial goal and inspiration for the development of this project.

3.2. Vegetation Cover Detection

In the discussion about reducing the effects that causes the CCD, it is clear that monitoring the vegetation cover of areas that contain bees is of paramount importance. Thus, the detection and classification of vegetation, as well as the evaluation of its health, with the use of a satellite can be done through the analysis of the reflectance of the visible and infrared light bands, which are reflected in a peculiar way for each species of plant.

In a study carried out at the University of Brasília [13], a classification system was created based on the level of photosynthetic activity and, because some spectral patterns are very similar, a junction with the histogrammatic analysis of the frequency of altimetric data by the Model Elevation Digital (AST14DEM) was made, so that different vegetation patterns could be better identified [5]. Other tools, such as Fragstats, were also used - to calculate area, density, size and variability metrics, nearest neighbor, among others, also used to identify vegetation - the Spectral Angle Mapper (SAM) - for the best classification spectral made by slicing the initial area for more focused analysis - and the decision tree, for joining the spectral and altimetric attributes, generating more homogeneous classifications [8] and [9].

3.3. CUBESATs

The CUBESATs are nanosatellites, generally with a mass between 1 and 10 kg divided into sections of basic dimension of 10x10x10 cm, configuring an 1U structure, which can be combined to form larger cubesats with, for example, 3Us (10x10x30cm), weighing between 3 and 4 kg [11]. This modality of satellites has a great advantage: the possibility of easy modulation of systems and subsystems, whose components can be easily found off the shelf (COTS), reducing their construction costs. In addition, CUBESATs, being small, can be launched together with other larger missions, reducing the high costs associated with launching satellites [11].

In this context, one of the sectors that began to be extensively explored by cubesats was agriculture, with the use of these models for mapping and monitoring plantations becoming increasingly common, such as the Planet's Dove constellation, composed of 3U-sized CUBESATs in Low Earth Orbit (LEO) capturing RGB wavelengths with a resolution of approximately 3 meters. Images captured in RGB are then translated into Normalized Difference Vegetation Index (NDVI) estimates. However, this translation is not something simple, so it becomes more feasible to apply technologies that directly capture the data necessary for the NDVI calculation. [10].

Furthermore, the possibility of using CUBESATs in this application becomes even more concrete since the use of large satellites for monitoring wild vegetation is already a well-documented reality. Since 1999, NASA has used a sensor present in the conventional satellite “Earth”, which has the function of particularizing the search conditions for vegetation cover [7] and [12]. In this scenario, in order to map the vegetation present in specific areas, the Advanced Spaceborne Thermal Emission and Reflection Radiometer (ASTER) could be used, by generating high spatial resolution multispectral images with stereo resources throughout its extension, which capture data through of 14 spectral bands, in which they pass between the visible spectrum and that of infrared waves [6]. Both technologies are already used in cubesats, as for example in the Planet constellation mentioned above.

This application is very similar to those necessary for the consolidation of the proposal in this article, becoming a precedent for its future execution.

4. CCD Response Proposal

Implementation a routine of plant cover mapping by cubesats and with the collection and feeding of data from those equipment with a view to monitoring and feeding a local (or distributed) database globally (via the web) for access by protective entities, governments, academies, research institutes in general, etc. This action will alert, applying the information compiled via satellite, about the areas that are below an acceptable value, making it possible to solve the problem in a timely manner so that the situation does not reach critical levels and, consequently, preserving the natural pollinating insects.

In addition to satellite data collection, there is a need to develop software that would be based on the use of general location information, plant diversity and natural habitat of bees in each region, present in a pre-existing database.

4.1 Control Metrics

Among the main causes of the CCD discussed earlier, the fragmentation of natural bee habitats stands out. In this sense, it is interesting to monitor plant coverage from two different perspectives: the distance between two planted areas and their health.

Thus, the establishment of control metrics is important so that it is possible to identify how isolated and healthy those areas are and whether this distance could cause isolation of bee species or expand in the near future, aggravating the disappearance of these insects.

4.1.1 Plant Health

While monitoring a specific area, parallel to the identification of plant species, there would also be monitoring and analyzing the health of the plants present in this location. This analysis can be done through the spectra of visible light and infrared waves, establishing the levels of radiation emitted by a healthy plant, since its health is directly linked with electromagnetic radiation (EMR).

The plant, in the process of photosynthesis performs absorptance (a), in which it absorbs blue and red bands; reflectance (b), the moment in which the infrared waves can be measured and transmittance (c). The more EMR (electromagnetic radiation) the plant is consuming, the less reflection, therefore, the lower the consumption, the greater the reflection [1].

Figure 1: Plant photosynthesis process [9].

With a focus on the reflectance, it is possible to analyze the spectral behavior and then monitor the health of the plant. This monitoring is possible since the vegetation absorbs sunlight in the red region proportionally to its activity and health, which can be perceived by the low digital values in the red channel detected by the satellites, at the same time, it presents strong reflection of sunlight in the infrared region, leaving high digital values in the infrared channel.

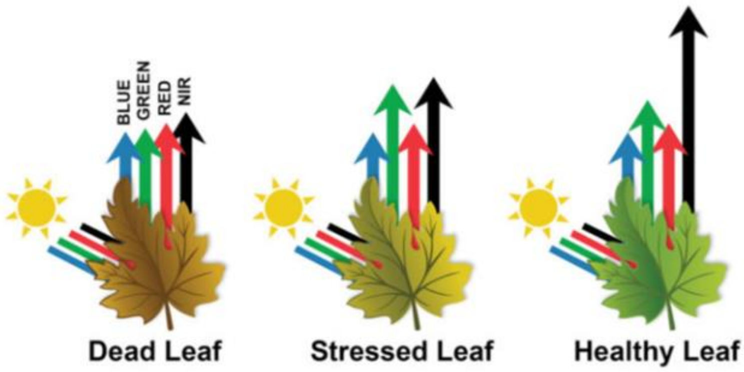

Figure 2: Spectral bands consumed by plants [9].

By not consuming the NIR band, also known as reflected infrared, the healthy plant has a higher reflectance, so to calculate the Normalized Difference Vegetation Index (NDVI) the formula below is used:

$$NDVI = \frac{NIR - Red}{NIR + Red}$$

Applying this formula to each pixel of the image to be analyzed, the resulting value will be between -1 and 1, so that the closer to 1, the greater the photosynthetic activity performed in that location, evidencing the presence of healthy vegetation and, similarly, the closer to -1, the lower photosynthetic activity, evidencing damaged vegetation or water bodies, buildings, exposed soil, among others [3].

The use of visible and near-infrared light bands for the NDVI calculation is widely used because it has been shown to be an adequate metric for the analysis of vegetation growth and distribution, stress and productivity [10].

4.1.2 Habitat Fragmentation

Moreover, regarding the spacing between bee colonies, Araújo et al (2003) describe that there is an intrinsic relationship between the necessary genetic heterogeneity in bee populations and the proximity of their colonies, so that the smaller the vegetation fragments and the density of these fragments, the greater the possibility of extinction of the species.

Thus, one way to monitor the cited aspect is based on the comparison between the spacing between regions and the average flight of bees in order to determine if the distance between portions of vegetation is compatible with the flight capacity of bees in the region. In this context, there is a linear correlation between the size of the bees' wings and their flight radius, considering the colony as the center, ranging from distances close to 600m for smaller species and even greater than 2km for larger species [4].

Along these lines, a possible metric for this parameter could be precisely the application of the correlation proposed by Araújo [4] to the average size of bees in a given study region. In this way, determining the maximum distance of vegetation spacing as well as the size of the vegetation portions, would make it possible to conclude whether that area is suitable for occupation, so that the comparison with the data obtained in the CUBESATs' monitoring can indicate the need for actions in that region.

4.2. Discussion

In this sense, by combining the data obtained from specific vegetation within larger biomes already classified in the database along with the location and understanding of the habitats of different bee species, it will be possible to identify favorable areas to the installation and development of colonies. Furthermore, with the analysis of the health of the plants present and of the area covered by such vegetations, it becomes possible to define which protection and maintenance measures should be carried out in these vegetations so that the bee habitat is preserved, thus reducing the force with which the CCD acts.

5. Conclusions

The research carried out for the making of this project made it possible to understand the importance of preserving bees across the planet, while also highlighting the importance of preserving and cultivating their natural habitats as crucial practices for preventing bee extinction. The authors believe that this project has real potential to positively influence the race against CDD, increase society's awareness levels across the planet about the importance of preserving nature's complex chains as well as having a real contribution in the short, medium and long term in said struggle. Therefore, the main legacy of this proposal is the accumulation of data for the purpose of implementing various public policies, in each country, on the actions of continuity of native vegetation cover, perhaps anthropocentric, with future developments in action plans with a view to preserving these environments and , therefore, multiple species of bees

In future projects, it is sought to refine the studies in the proposed metrics aiming to particularize them to each region of the planet, and so better meet the needs of the different bee species, which have several particularities among themselves, and to better define the relationship between the presence of bees and plant diversity.

Moreover, it is desirable to produce materials related to the ability to identify different vegetation through satellites and that provide data on climate change in order to more broadly and completely mitigate Colony Collapse Disorder.

Acknowledgments
We especially thank Gustavo R. Carvalho and João Gabriel C. S. Texeira and the professors Melina S. Lima and José Vicente C. Santos for their participation in the conception of the idea and in the initial development.

References

[1] A. B. Santos, Abelhas nativas: polinizadores em declínio. Natureza online, v. 8, p. 103-106, 2010.
[2] CETAPIS, Sem Abelhas Em Alimento, 2020.
[3] D. L. Souza, A. Evangelista-Rodrigues, M. S. C. Pinto, As Abelhas Como Agentes Polinizadores (The Bees Agents Pollinizer's). Revista electrónica de Veterinaria, v. 1695, p. 7504, 2007.
[4] E. D. Araújo, M. Costa, J. Chaud-Netto and H. G. Fowler, Body size and flight distance in stingless bees (HYMENOPTERA: MELIPONINI): Inference of flight range and possible ecological implications , Braz. J. Biol, 2004.
[5] J. P. Metzger, População em paisagens fragmentadas: da teoria das ilhas aos modelos atuais de metapopulação, Universidade de São Paulo, 2019.
[6] M. Abrams, The Advanced Spaceborne Thermal Emission and Reflection Radiometer (ASTER): Data products for the high spatial resolution imager on NASA's Terra platform, International Journal of Remote Sensing, Volume 21, Issue 5 (2000).
[7] M. J. F. Brown, R. J. Paxton, The conservation of bees: a global perspective, Apidologie, 2009.
[8] M. O. Oliveira, Declínio populacional das abelhas polinizadoras de culturas agrícolas. ACTA Apicola Brasilica, v. 3, n. 2, p. 01-06, 2015.
[9] Radiação eletromagnética x planta: saiba tudo, DRONENG DRONES E ENGENHARIA, 2018.
[10] R. Houborg and M. F. McCabe, High-Resolution NDVI from Planet's Constellation of Earth Observing Nano-Satellites: A New Data Source for Precision Agriculture, Remote Sensing, 2016.
[11] R. Walker, Technology CubeSats, ESA, 2022.
[12] S. C. Caires, D. Barcelos, Colapso das abelhas: Possíveis causas e consequências do seu desaparecimento na natureza, Acta Apicola Brasilica, 2017.
[13] W. P. Machado, R. F. Guimarães, O. A. de C. Júnior, R. A. T. Gomes, S. N. de Oliveira, R. V. R. Sodré, T. A. Chaves, Identificação de padrões de vegetação e análise dos fragmentos florestais a partir do processamento digital de análise morfométrica em imagens e análise morfométrica em imagens aster no município de cromínia-go. Revista Espaço e Geografia Universidade de Brasília, 2016

MBSE for modeling an Academic Satellite

Bruna S. Queiroz(1), **Maria C. Pereira**(2)
(1)*brunasq@ufmg.br*
(2)*cecilia@demec.ufmg.br*
Universidade Federal de Minas Gerais
Avenida Pres. Antonio Carlos, 6627 - EE/ DEMEC - Belo Horizonte, MG - Brazil

Keywords: *CubeSat, Aerospace Engineering, Systems Engineering, MBSE*

PdQSat is the first academic satellite to be designed and built in Federal University of Minas Gerais, UFMG. The University offers Aerospace and Systems Engineers degrees among others, making it an excellent environment for such a development. The CubeSat objectives are to characterize both a Li-S battery and a micro super capacitor that was designed and manufactured in UFMG Chemistry Department. Besides the technical objectives there are also educational ones, that are as important as the previous. For taking the most of learning oportunities, the team decided to go through the whole lifecycle of the product and for so, using Model Based Systems Engineering for modelling the satellite. So, the CubeSat is an excellent opportunity for Enginnering students as a PBL - Problem Based Learning. Here it was used Capella software to model the satellite and its interfaces. The work started with the basic definitions of the mission and its stakeholders. While discussing this matter we were able to find hidden stakeholders and details of the mission that impact the solution of the problem. The needs of the payloads were discussed and the model could be built. By knowing the subsystems and their roles to the design, and their interactions among themselves and with space environment – mechanical, electrical, information and others- the model was created. All stakeholders were identified and their roles in the project were well defined, so as to attribute them not only the work they are meant to do, but also the interfaces between their actions. This model is, for now, a functional model, i.e, the solution is not defined, but the characteristics the device shall have to be a solution for the given mission. The result is models to be used through all process for designing the CubeSat. This project aims to produce a documentation to be a guide to future academic satellites.

1. Introduction

The small satellites development allows university students participate in space vehicle projects. The CubeSat, a category of small satellites, is cheaper and has a shorter life cycle than conventional satellites [1]. In this context, Federal University of Minas Gerais (UFMG) students have been designing PdQSat [2], a system with technical and educational missions. In this context, the CubeSat arises as an opportunity for Problem Based Learning (PBL) techniques to be put in practice. PBL is a well known tool for active learning that consists of presenting a hands on activity, usually a real life problem, and having the students solving and/or helping to solve . During the development of the solution, the students develop the skills necessary to do so and experience a more solid and transferable knowledge than passive learning [3].

The technical missions of the CubeSat refer to the characterization a Li-S battery that will be manufactured in Minas Gerais and also the characterization of a micro super capacitor that was designed and manufactured by UFMG Chemistry Department.

Systems Engineering is a multidisciplinary subject with a holistic approach for complex systems life cycle design, planning and management [4]. This discipline has methods to work and manage the system emergent properties [5]. Thus, to achieve success in all life cycle phases, Systems Engineering characterize methods to allow the capture of the stakeholders interests, their needs and allow the system's capabilities to operate in its designed scenario [4].

These methods can also allow the understanding of consequences and the responses related to the actions applied in the system's project, both in short and long term. Them, it is possible to develop the capabilities for comprehension of all system perspectives and views [6]. Systems Engineering methods application earlier in the systems project is necessary to avoid unexpected behaviors. In the conceptual phase, the activities are characterized to map the capabilities, the system mission, the solution business and the needs that will be traced to the requirements and the system architecture. Applying the correct studies and synthesis early in the life cycle is possible to make a better comprehension about the motivation and process of the context for system deployment. Thus, these methods application enable the anticipation of problems, defects and risks and their mitigation actions design [7].

Systems Engineering practice must be tailored according to the context and the stakeholders involved on the project. The System Engineer must correctly capture the stakeholder's needs and demands while reflecting them into the technical objectives expected for the system. Thereafter, the boundary of the system is defined enabling trade-off analysis for the best solution that correspond the budget and needs. With the final solution, the System Engineer should apply decomposition methods to identify the emergent properties while relating them with the system's elements in order to guarantee the systems interaction effectiveness and increase the solution reliability [4].

Therefore, to achieve the PdQSat capabilities and mission requirements in the operational context, it is necessary to guarantee the components integration and the correct behavior of the CubeSat as a whole. Thus, Systems Engineering methodologies could be helpful to capture and manage correctly all the behaviors and avoid unexpected functions. These methodologies, associated with systems thinking, allows the correct PdQSat's life cycle management, conduction and development, enabling the comprehension of the students and others stakeholders needs through architecture and requirements decisions.

Studies related to Systems Engineering applications for CubeSat development are investigated since 2011 in the INCOSE's Space Systems Working Group [8]. The Model-Based Systems Engineering (MBSE) is the subject in one of these studies for CubeSats applications, with a methodology for using models through an architectural system view for all the life cycle, from capability views to functional views. MBSE provides support for requirements capture, design analyses and the traceability between the artifacts related to needs, requirements, logical components and functions. Through the design analyses it is possible to capture the interactions between the system parts and also between the system itself and the elements present in the environment context [9].

The MBSE project for the CubeSat domain presented by Kaslow [8] shows this methodology and provides a reference model for satellite's mission development. The study explores the definition related to the CubeSat as a system-of-interest and the main context for it, that is composed by stakeholders, external environment, external restrictions and organizational mission. Making the boundary for this domain, it is possible define the traceability between objectives, needs, requirements for each element and the system and define the measures of effectiveness. Thus, this artifacts will compose the system's functional architecture, with the traceability between the mission and domain elements.

2. Model-Based Systems Engineering

The construction of the architectural view for a system is important not just for traceability in the functional view, but for the system decomposition process. This process helps the problem identification between interfaces, the integration and interoperability of an item. Some kind of problems can be identified early in the development stage by architectural view and the mitigation actions can then be defined earlier.

For the MBSE in PdQSat context, it was used Capella software [10], version 5.1. Capella is a tool for systems projects based on Arcadia method. Arcadia method promotes model constructions through the development of view points for all life-cycle phases of the system, with the distinction of the space problem (where the objective is to understand the needs) and the solution space (the system itself) [11]. This method allows the models and diagrams production similarly to UML and SysML, as information diagrams, sequential diagrams, and class and interface diagrams. Whereas SysML and UML are modeling languages focusing on vocabulary and rules for diagrams construction, Arcadia method offers a structured approach with focus in engineering projects and systems architecture [12].

MBSE with Capella allows the construction of models through the life-cyle phases [11]. Thus, for PdQSat it was used the material prepared by Cerqueira [13] with instructions and explanations related to analysis for each system phase. The material prepared by Arikan and Jackson [14] was used for guidance and instructions about Capella utilization. The activities for each phase for model construction was:

- Operational analysis: identification of conditions, motivation, expectation and capabilities related to the stakeholders concerns and needs to reach the system's mission objectives. Thus, in this phase, it is necessary to identify the scenarios for the problem domain, including the risk factors, process opportunities and constraints. Other activity is the definition of the operational users (actors and organizations) of the future system and define their relationship in between the space-problem [13]. The diagrams for this phase are:
  - Operational entity breakdown
  - Operational capability diagram
  - Operational activities interaction diagram
  - Operational architecture diagram
  - Operational activity scenario
- System analysis: in this step, the system is analyzed as a black-box. So, with this perspective, it is not necessary to identify the physical characteristics. The

main focus is on the system's capabilities and functionalities that are traceable to the system's missions. In other words, the model's view-points of the system have the objective to answer and capture the needs expressed by the stakeholders. For the systems analysis, the system's boundary and its relation with the users and the environment context are defined, identifying the expected systems functions and the environment context functions [13]. The developed diagrams in this step are:

  – Contextual System Actors diagram
  – Mission diagram
  – Mission capabilities diagram
  – System Architecture
  – Functional Scenario
  – System Dataflow

- Logical Architecture: the operational components that compose the system is identified in this step. Defining these components the demonstration of how the interaction between the subsystems occurs is achieved. Therefore, these views are used to evaluate how the system functions is satisfying the stakeholders expectations (identified in the previous step). Then, it is necessary to define the subsystem functions traceable to the system's main functions through a structural and functional analysis [13]. One of the most important task in this step is to define more than one architecture to execute trade-off analysis and choose the most suitable candidate. The candidate will represent the solution that satisfy the expectation and constraints defined for the system, presenting the proposal with the greatest benefit for implementation [13]. When this step was executed for PdQSat, the definitions allowed the construction just for one solution candidate. Thus, the present document shows just one model for the system architecture for PdQSat. The diagrams produced in this step have the purpose to be a initial candidate, that must be incremented according to the decisions taken by the students in the project.
- Physical Architecture: the objective for this step is to define the physical properties expected for the system and how it will be built. The models should present details related to technical decisions and how the components executes the expected behaviors to achieve the functions defined in the previous step (through interfaces, inputs, outputs) [13]. The systems requirements must be defined for the accomplishment of this step. This work has models until the "Logical Architecture" step because of the amount of information available.

3. Results

This section presents the models developed for PdQSat project according to MBSE methodology. During the models' construction, many interactions with other students in PdQSat project were necessary to ensure that information reflects decisions and discussions with stakeholders. Thus, whether other decisions will be made or the stakeholders presents other needs, the models must be re-valuated to adapt according the new decisions or others functionalities.

The models produced in the Operational analyses are intended to build the understanding for problem context which the system will fulfill it capabilities.

- Operational Entity Breakdown (Figure 1): this model presents the operational entities and operational actors interested and related to the problems solution. Also, the diagram has the entities that set constraints or standards for the solution. The operational entities are social organizations or environment elements that interact with the system in all life cycle phases [13]. Furthermore, the operation actors are the “last level” of the entities and cannot be decomposed. Their interactions occur in the systems operational phase [13]. For this project, the hierarchical level for the entities is the CubeSat domain for the breakdown of all related entities for a CubeSat project, focused on the PdQSat reality. In the breakdown the entities related to project constraints or standards are presented: CubeSat.org (to represent the reference document CubeSat Design Specification [15]), Battery provider (the organization responsible for provide the battery cells for the payload). AEB (Brazilian Space Agency) is the entity related to the project financing and a stakeholder interested in the solution development. The entities for the academic development and for the solution operation are UFMG School of Engineering, launch segment and ground segment.

- Operational Capability Diagram (Figure 2): this model presents the expected capabilities for the operational entities that enables the operational objectives for the future system [13]. These capabilities are identified in the model with the letters “OC” for the Operational Capability term. For the PdQSat project, the operational entities and actors must perform the technology behaviors’ analysis in the space environment provided through data, mainly in the technologies related to the Li-S battery and super-capacitor. Besides, the operational entities with the academic purposes must enable the students development through the problem learning.

- Operational Architecture Diagram (Figure 3 and Figure 4): these models present the operational activities realized by the entities defined in the Operational Entity Breakdown. The activities performed by the entities occur to achieve the solution realization. The flows (i.e. the connections) between the activities are the operational process and contributes to operational capabilities (Figure 2) achievement. Figure 3 presents the activities and relations for the study and tests in the Li-S cell battery and super-capacitor candidates for the future solution. The figure also presents the activities for the students development and learning through the solution’s project. The Figure 3 shows the operational activities and the relations necessary between the entities for the technology demonstration in the space environment. These models have an architecture view-point to highlight how all the entities are connected.

In the next step, the models were developed considering the system as a black-box. The operational entities and actors are transferred to this phase into the Contextual System Actors diagram [16]. Besides, the models show the system missions, the traceability for the capabilities and the necessary system functions to achieve them. In this phase, it was decided to develop only the models related with the technology demonstration mission. Thus, the models for System analysis are:

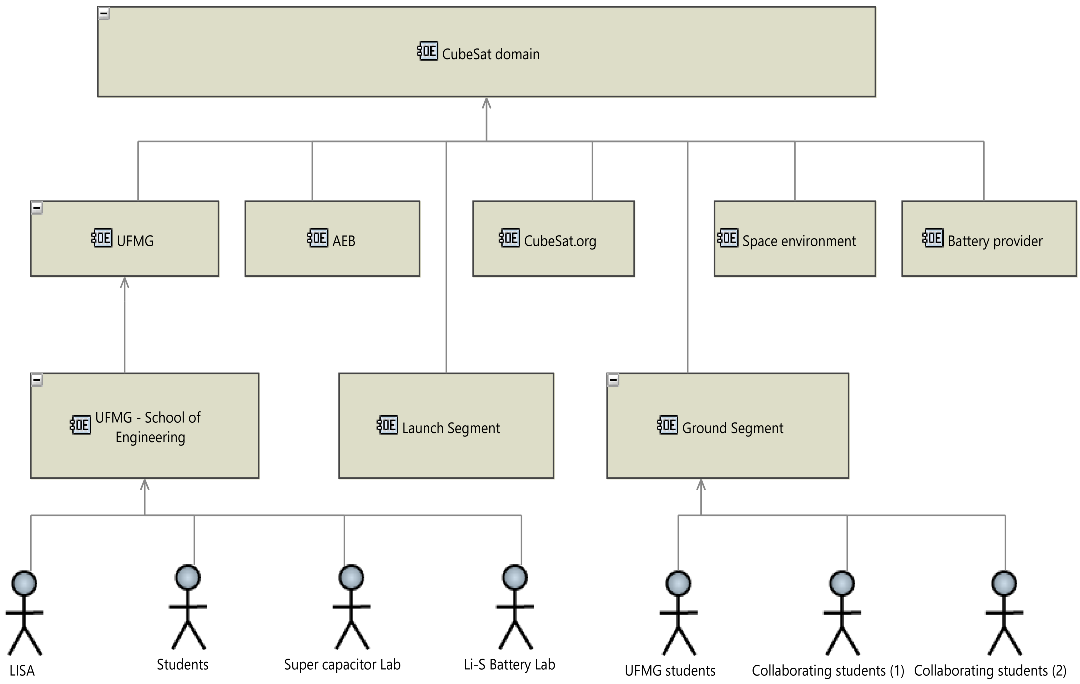

Figure 1: Operational Entity Breakdown.

- Mission capabilities diagram (Figure 5: the model shows the traceability between the capabilities expected for the solution and the system missions. The missions represented by the letter “M” are: Students development, Li-S battery technology demonstration and Super-capacitor technology demonstration.
- System Architecture (Figures 6 and 7): before the development of this model, it was necessary to define the functions and activities performed by the system to achieve the missions in a sequential form through the Functional Scenario. Thereafter, it was constructed a model to visualize the interaction between these activities to highlight the critical relations through the System Dataflow. The models in Figures 6 and 7 show the system as a whole and the internal and external necessary interactions to achieve the missions. Figure 7 has the focus on the activities and functions to achieve the Li-S technology demonstration and the Figure 6 to achieve the Super-capacitor technology demonstration.

The last models for this work are for the Logical Architecture. Figure 8 shows a proposal of the subsystems that could compose the PdQSat. The subsystems are divided by the payload, responsible for the mission achievement, and the spacecraft bus, that supports the payload. In the Logical Architecture (Figure 8), the expected functions for the system in the System Architecture model are allocated in their respective subsystems.

The other models developed for the project and all steps performed are described in [16].

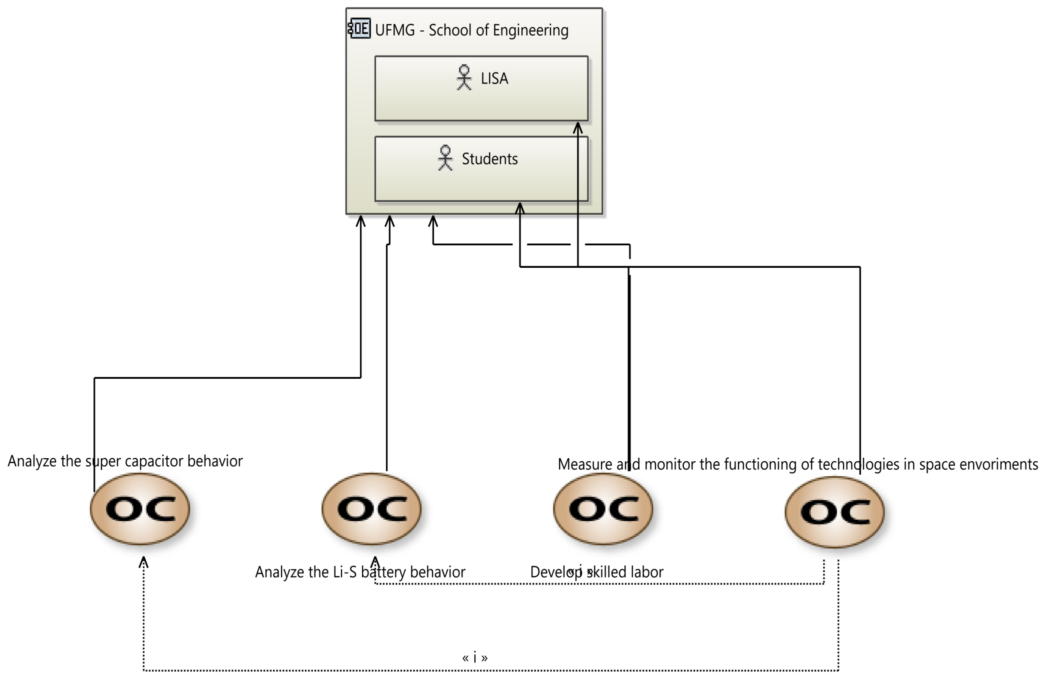

Figure 2: Operational Capability Diagram for PdQSat project

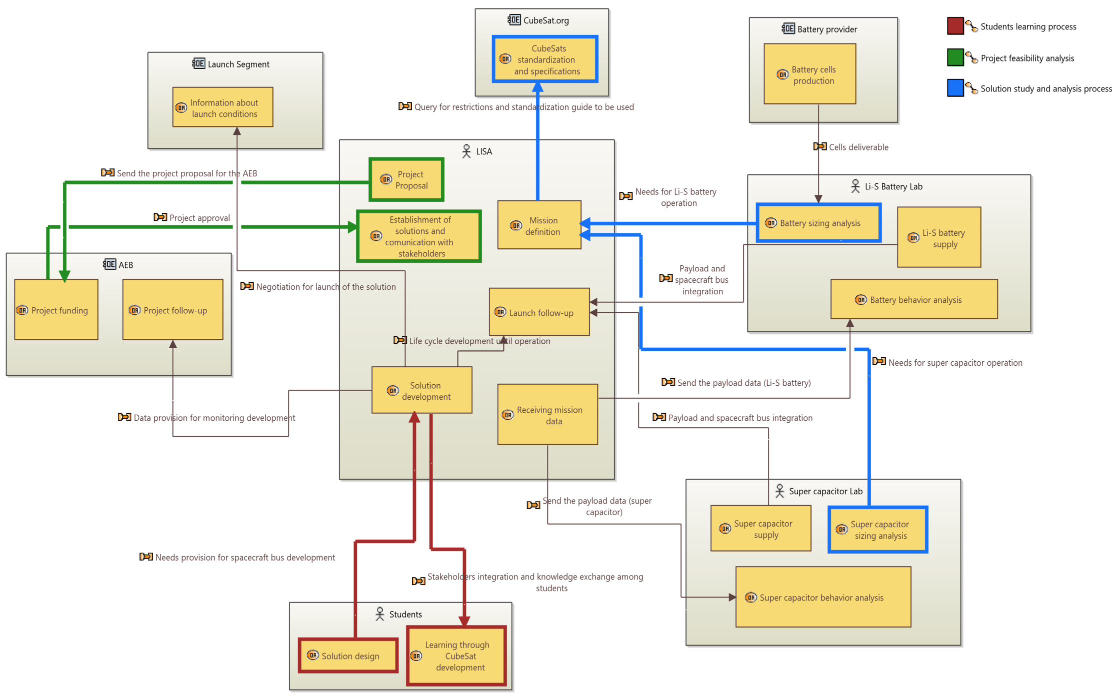

Figure 3: Operational Architecture Diagram for capabilities achievement.

4. Conclusion

This paper presented the use of the Systems Engineering discipline in complex systems, definitions and the related methodologies. Then, the document quote the MBSE use for CubeSat projects. With references about this methodology, it was pos-

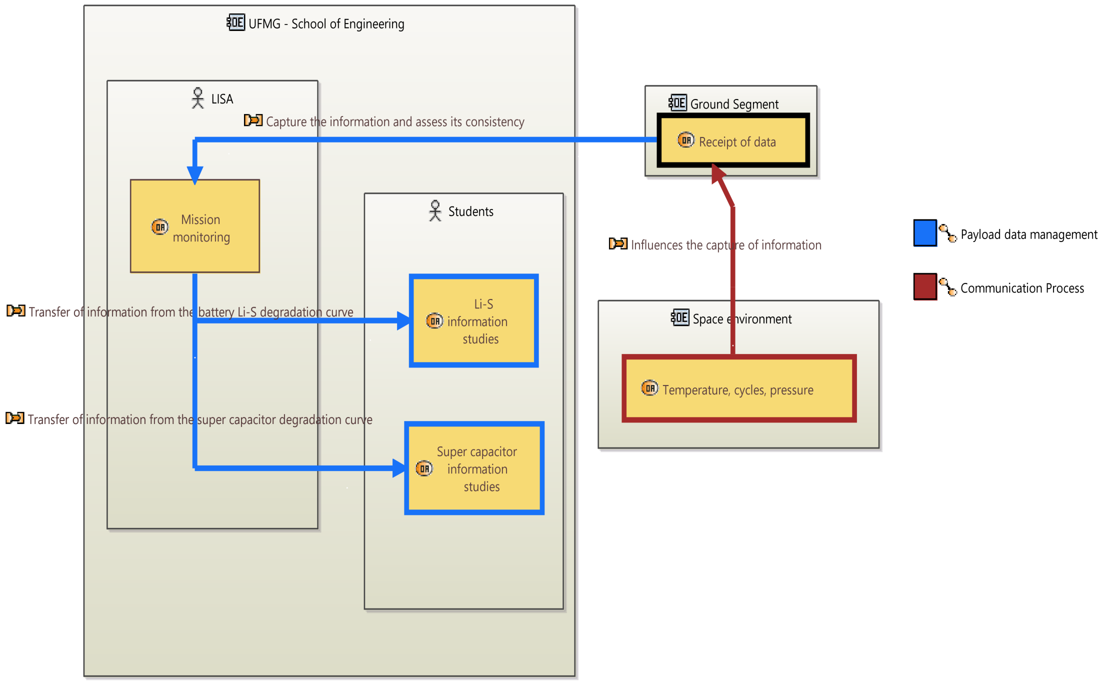

Figure 4: Operational Architecture Diagram for technology demonstration capabilities achievement.

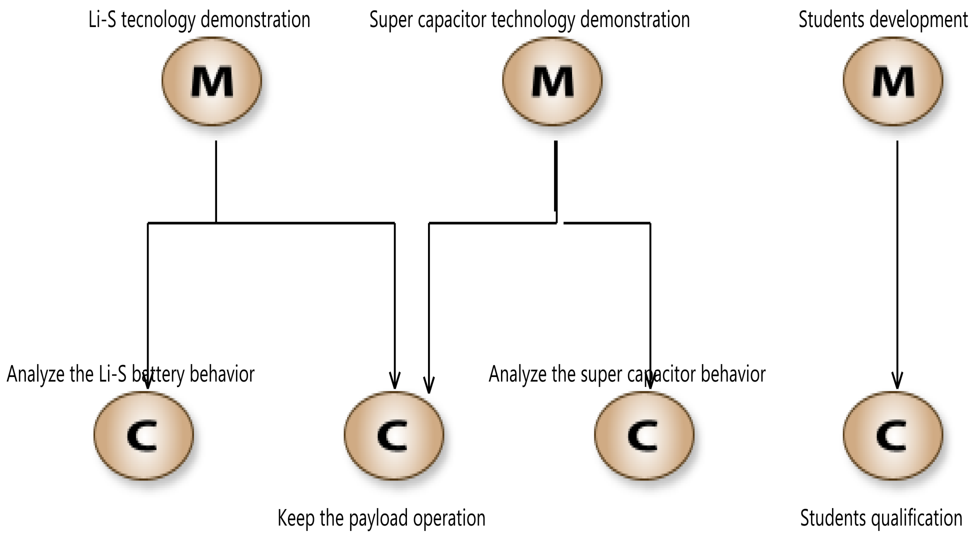

Figure 5: Mission capabilities diagram for PdQSat.

sible to show practical benefits related to Systems Engineering usage.

Lastly, it was presented the MBSE application result for the PdQSat project, containing the validated information with the stakeholders, to guarantee the correct capture of the needs and capabilities expected for the system. The results reflect the decisions taken at the beginning of the PdQSat's life cycle, with focus on the CubeSat's concept and operation, without the solution formalization. The use of MBSE aims the problem space and functional understanding, to identify the emergent properties.

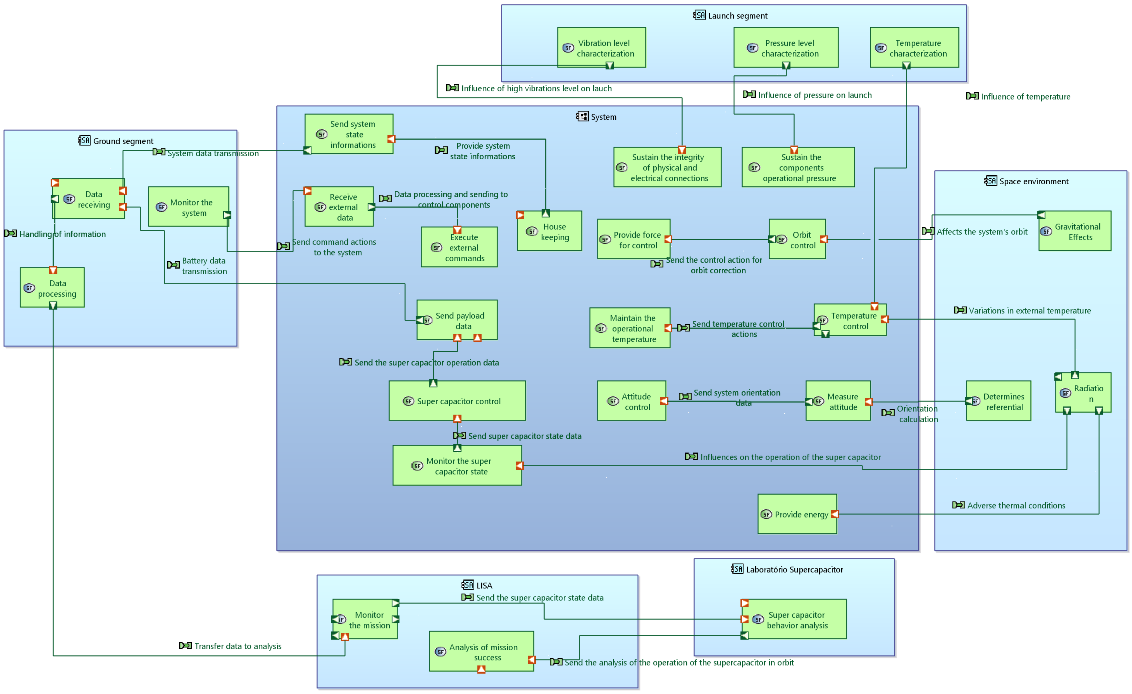

Figure 6: System Architecture for micro super capacitor technology demonstration.

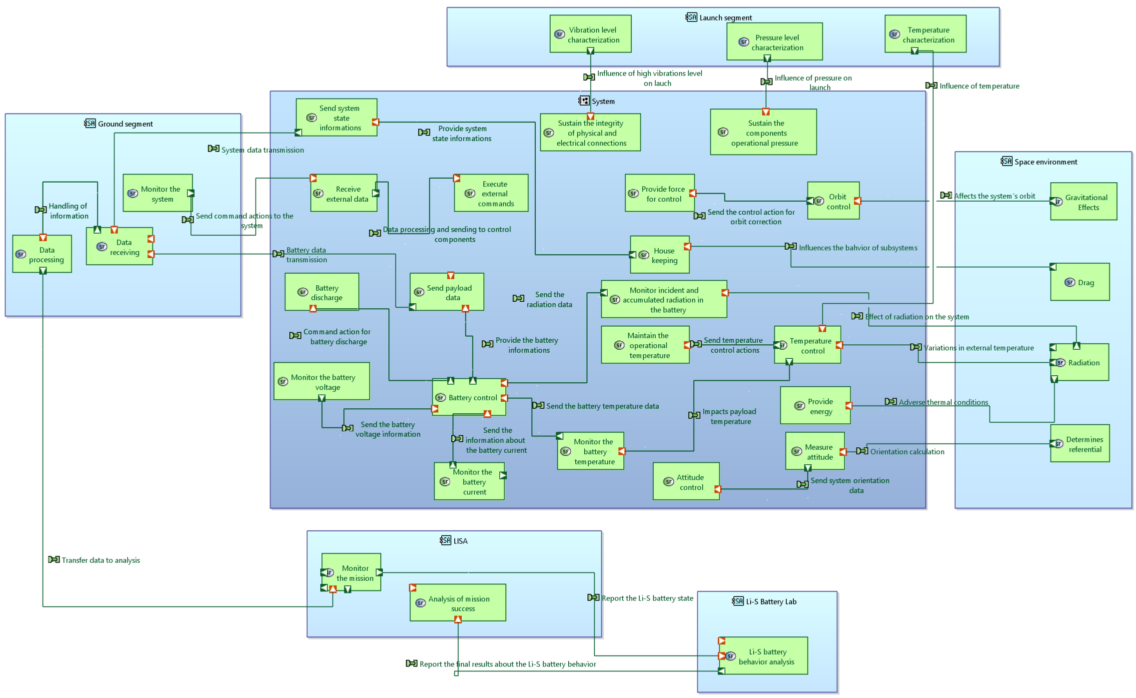

Figure 7: System Architecture for Li-S battery demonstration.

References

[1] C. NASA, 101: Basic concepts and processes for first-time cubesat developers, NASA and California Polytechnic State University (2017).

[2] M. C. Pereira, K. R. Marques, M. L. R. Fraga, P. H. C. Piçanco, Pdqsat i - projeto e construção de

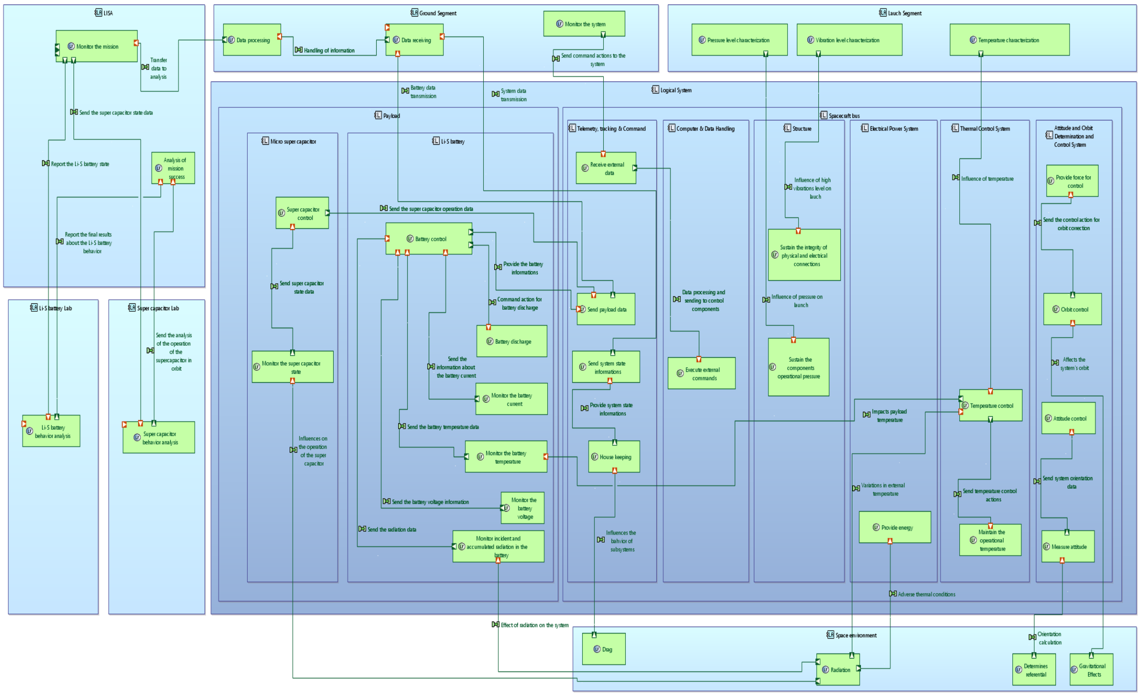

Figure 8: Logical Architecture for the PdQSat system.

um cubesat acadêmico para fins de demonstração tecnológica, 2020. Agência Espacial Brasileira 2020 - Proposta.

[3] C. Hsieh, L. Knight, Problem-based learning for engineering students: An evidence-based comparative study, The Journal of Academic Librarianship 34 (2008) 25–30.

[4] INCOSE, Systems Engineering Handbook: A Guide for System Life Cycle Processes and Activities, John Wiley and Sons, Inc., CA, USA, versão 4.0 edition, 2015.

[5] SEBoK-Authors, Systems engineering overview in sebok editorial board, 2021. BKCASE is managed and maintained by the Stevens Institute of Technology Systems Engineering Research Center, the International Council on Systems Engineering, and the Institute of Electrical and Electronics Engineers Systems Council.

[6] R. Adcock, J. Singer, D. Hybertson, H. Sillitto, B. Lawson, B. Wells, J. Martin, Overview of the systems approach, 2021.

[7] S. Cook, S. A. Wilson, et al., The case for investment in systems engineering in the early stages of projects and programs, in: Systems Engineering Test and Evaluation Conference 2018: Unlocking the Future Through Systems Engineering: SETE 2018, Engineers Australia Melbourne, pp. 82–95.

[8] D. Kaslow, B. Ayres, P. T. Cahill, M. J. Chonoles, L. Hart, C. K. Iwata, A. G. Levi, R. Yntema, Cubesat model-based systems engineering (mbse) reference model-development and distribution-interim status, in: AIAA SPACE 2016, 2016, p. 5551.

[9] A. Sousa-Poza, C. Keating, S. Kovacic, Systems engineering: evolution and challenges, International Journal of System of Systems Engineering 5 (2014) 379–399.

[10] Capella, Model based systems engineering - capella mbse tool, 2021.

[11] Capella, Capella mbse tool - arcadia, 2021.

[12] Capella, Is capella a sysml tool?, 2021.

[13] C. S. Cerqueira, Arcadia primer, 2021. Material Virtual.

[14] U. Arikan, P. Jackson, A capella tutorial, 2019. L.

[15] A. Johnstone, Cubesat design specification rev. 14, 2020.

[16] B. S. Queiroz, M. C. Pereira, Aplicação de metodologias de engenharia de sistemas para o ciclo de vida do pdqsat i - cubesat acadêmico, 2021.

Prevention and mitigation of the disaster cycle, as causes and effects of climate change, through the use of satellites and IT tools

B. Loretto Sanjines[(1)], Mateo Mercado[(2)]
[(1)] AIA Bolivian private University, 0000, Av. Ballivián, +59162645247, loresanjinesb@gmail.com [(2)] Bolivian private University, Av. Juan Pablo Segundo, +59174233064, matemerc@gmail.com

Keywords: *Natural disaster, satellite image, fire, remote sensing, early warning*

Earth observation satellites are a valuable tool for understanding dynamic phenomena in the environment. This work seeks to measure, justify, raise awareness and provide information on the causes and effects associated with climate change, approached from the respective satellite mapping, analyzing natural disasters, threats and risks that occur in various areas of the world, especially in fire situations in Bolivia, and South America. The study has evaluated the current situation with respect to satellites, assessing their detection of atmospheric, hydrological, volcanic disasters, and even some threats, as well as the problems that the general population currently faces to act at this time, due to the shortage of information in the region and in Bolivia, there is a need for satellite images, with the different bands, frequencies, colors, scale, patterns, texture, etc. Complementing projects, and working with specialized satellites, such as NOAA / NASA, NOAA-18, NOAA-19, GOES-16 and GOES-17. In order to provide data for the coherent detection of changes and daily interferometry, synthesize the information, launch an audible application that operates immediately, acquiring the information through remote sensing, collecting data from the earth's surface, it will provide the images in perceptible frequencies. Addition to geometric characteristics such as the wind vector, will show the classification of coverage in satellite images automatically, in real time, accurately and economically, in addition to saving the information on the situation. Remote sensing and early warning system, with monitoring and focus on the most recurrent fire places, such as fires in the Amazonas, Chiquitania, places with heat waves, droughts, prone to fires, will provide warning information together with the security system, that will to help both the different search, assistance, rescue and rescue groups, as well as the knowledge to the general public about their risk areas, areas of natural disasters, as an effective prevention, to avoid the depredation of the forests, the loss of lives and prevent other possible future disasters, thus achieving effective action in these scenarios, ensuring that in each emergency valuable seconds and resources are optimized with respect to the event.

1. Introduction

In recent years, satellite technology and remote sensing technology is developing rapidly. Image processing in remote sensing of the Earth. The application of satellite remote sensing to capture the Earth is increasing rapidly, so it plays an important role in monitoring the Earth's surface [1], environmental observation research is also essential in exploiting satellite image data. In the study of the environment, because the identifiable objects are in the large size group, we can use images of medium or low resolution to observe an object.

The Photogrammetry and Photointerpretation techniques helped in the Digital Elevation Models, risk maps and ground using development, these turned out thanks to the first images captured from Paris city by the hand of Gaspar Felix Torunachon when he was being the pioneer on Earth observation experience (1859).

Then, by the late fifties, with the investigation systems development, it was possible to get spatial wit. During Cold War, there was a competition between bands which made a deep investigation into it.
Also, Sputnik was launched in 1957, the first artificial satellite that helped with Earth, Moon and near planets exploration. In 1960, the first observation satellite from Earth, TIROS-1 was launched.

First spatial program in Bolivia Aerial photography in Bolivia
In Bolivia, a lot of aerial images were taken in La Paz and surroundings on July 11th of 1928 thanks to Braguet XIX plane and its photogrammetric cameras, these being controlled by Alfredo Santalla ang Cesar Gorriti.
During Chaco War (from 1932 to 1935), aerial photography helped a lot for the roads tracing in the unknown zones in Chaco Boreal. An important step for the use of this activity in national territory was the creation of Aerialphotography Section of Bolivian Airforce, with the help of this one last mentioned, some aerial photographies were obtained and these complemented the first topographic map of Bolivia (photogrammetric techniques were used in the development).

Bolivian satellite images
Bolivia had an early acquisition of satellite images with the US government collaboration. The first program that was installed in Bolivia was ERTS (Earth Resources Technology Satellite), which was sponsored by NASA, USGS, PNUD and USAD. Research was made in national territory about the making of a Hedge Map and actual use of Ground, and the additional data was used to analyze the distribution of field for the breeder use, forestall resources for wood extraction, recovery of saline soils, planning and agricultural activities, etc. In order to make the map, LANDSAT images, conventional aerial photographs and photo indexes were used.
It is important to mention that Bolivia was one of the pioneer countries in the application of Aerospace Technology. It was thanks to the sponsorship of countries like the United States that they experienced their new technologies in the national territory. Once the foreign collaboration was withdrawn, the country could no longer sustain projects of such magnitude, due to the lack of human and economic resources.

Spatial monitoring of disasters
Climate change, natural disasters, growth of the cities, glacier reductions are some of the variables that are able to monitor. The “Monitoreo Espacial de Desasatres y Riesgos a traves de imagenes de satelite” project proposed by UMSA (Universidad Mayor de San Andres) opened the line for the monitoring application in the country. The satellite images are able to measure the water pollution, duckweed and chlorophyll in the critic place of the zone. The study shows the urban spot over dangerous spots with warning disasters. For that, UMSA created ‘GeoVisor UMSA’, a geoportal that storage geographic information in standard format.

The objective of this study is to evaluate, alert and prevent through an application that will operate in real time, on the climatic situation that the region and Bolivia faces, through the use of satellites that operate and detect natural disasters and threats, an application that obtains, and provide detailed information to both first response teams and the general population, thus preventing future risks.

2. Antecedents

A. Forest fires in the region

Around the last few years, the fires in the region and in Bolivia have been worrying due to the increase over time. In Bolivia, from 2002 to 2021, Bolivia lost 3.31Mha of primary humid forest, the total area of primary humid forest in Bolivia decreased by 8.1% in this period of time. [2]

And from 2001 to 2021, 82% of forest loss occurred in areas where the dominant drivers of loss resulted in deforestation. [2]

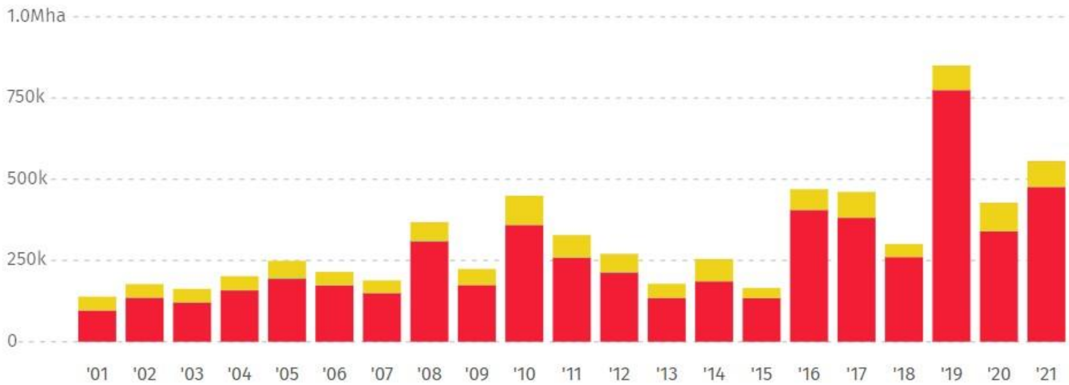

Fig. 1: GLOBAL FOREST WATCH. Since 2000 extension of tree cover | >30% tree canopy | These estimates do not take into account tree cover gain.

As for fires, in Bolivia, the peak fire season usually begins in early August, and lasts around 15 weeks. There were 18,429 VIIRS fire alerts reported between September 20, 2021 and September 12, 2022, considering only high confidence alerts. [2]

Between September 2, 2019 and August 29, 2022, Bolivia had a total of 261,320 VIIRS Alerts fire alerts, which are shown below. [2]

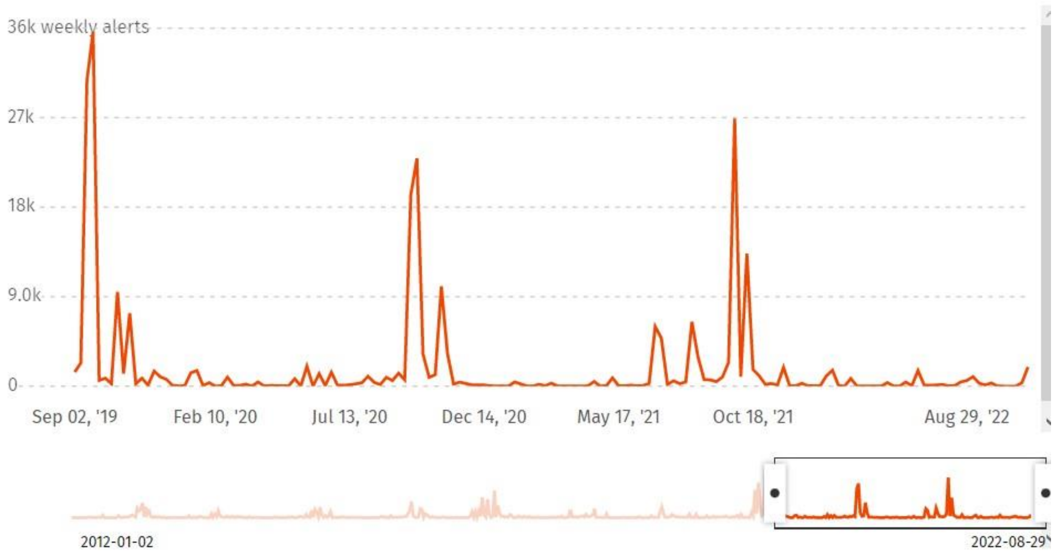

Fig. 2 Alerts from the Visible Infrared Imaging Radiometer Suite (VIIRS), about the time in which it occurred.

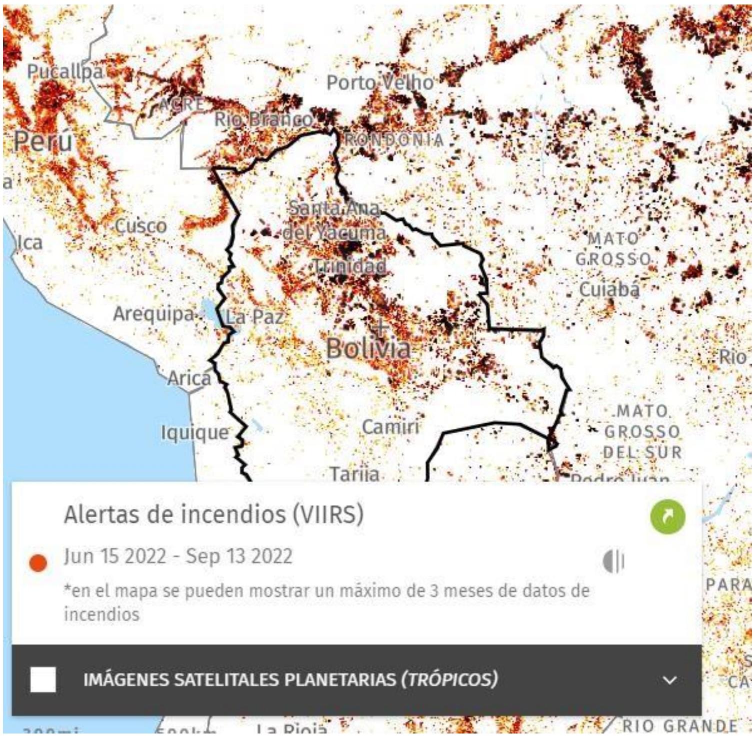

Fig. 3 Interplanetary satellite images, fire alerts (VIIRS) the map can display a maximum of 3 months of fire data

Being Santa Cruz one of the departments with the highest increase in forest fires, some data from 2020 are presented below [3].

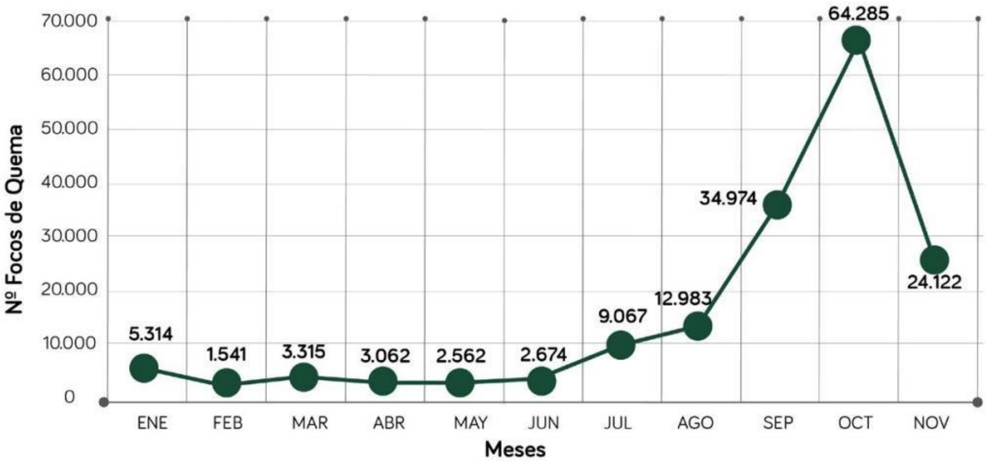

Fig. 4 Foci of burning, in the year 2020. Monthly distribution of burning sources for the year 2020, in the municipalities of the department of Santa Cruz.

B. Landslides and mud disasters in the region

The reliability of landslide susceptibility maps depends mainly on the quantity and quality of the data available, the scale of work and the selection of the appropriate analysis and modeling methodology. The process of creating these maps involves several qualitative or quantitative approaches (Soeters and van Westen 1996; Guzzetti et al. 1999). Much of the available literature on landslide assessment methodologies falls broadly into qualitative and quantitative approaches. In some similar methods to evaluate landslides, spatial risk is applied according to sensitivity analysis (Möderl and

Rauch 2011) [4]. On this basis, it is important to use a combination of several factor maps to produce the landslide susceptibility zonation by overlaying the calculated weight values for each of the nine factors and the subdata layers of the factor classes. Multi-criteria methods and the geographic information system (GIS) complement each other and allow building consensus and ensuring the sustainability of decision alternatives (Boroushaki and Malczewski 2010). Performing spatial analysis procedures using GIS allows the extraction of different factor maps from a Digital Elevation Model (DEM) such as elevation, slope, aspect, drainage and lineament characteristics.

As for the mud disaster, as a landslide mixed between land and water, which generates disasters in its path, as was the event that happened in 2018 in Ti-quipaya, Bolivia, below is the classification of mud disaster with Kanopus and Sentinel.

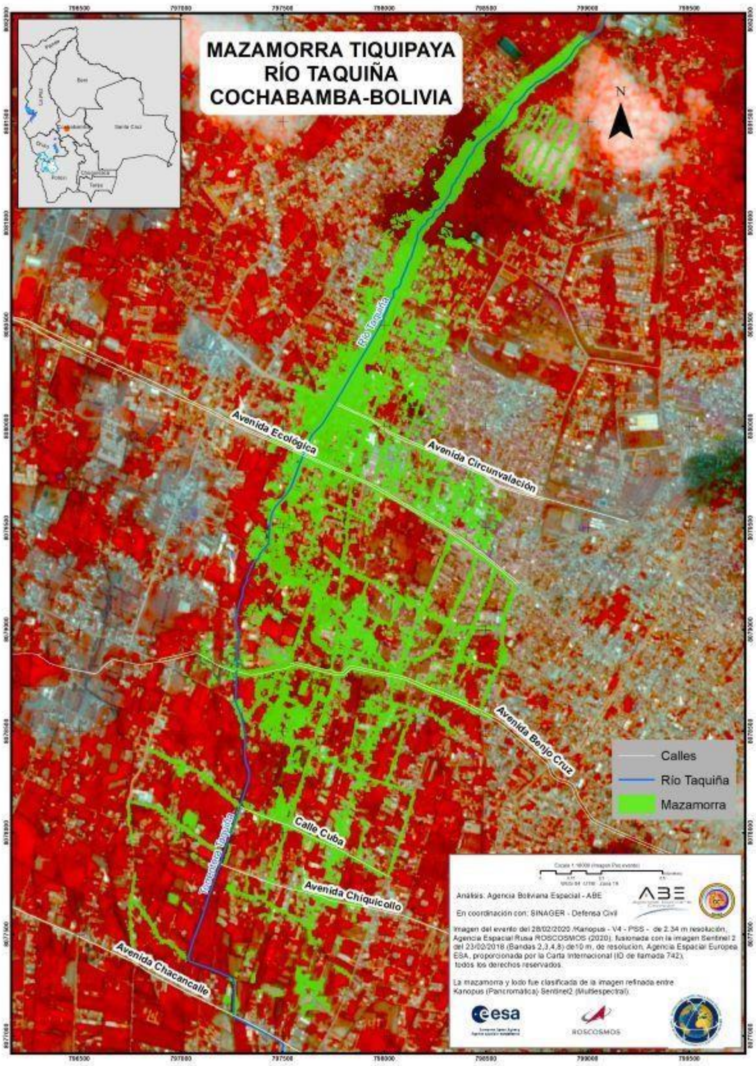

Fig. 5 Bolivian Space Agency, Satellite image of the mud disaster, Kanopus – V4 – 2.34 m PSS. and 10m Sentinel 2.

Landslide classification with TerraSAR-X.

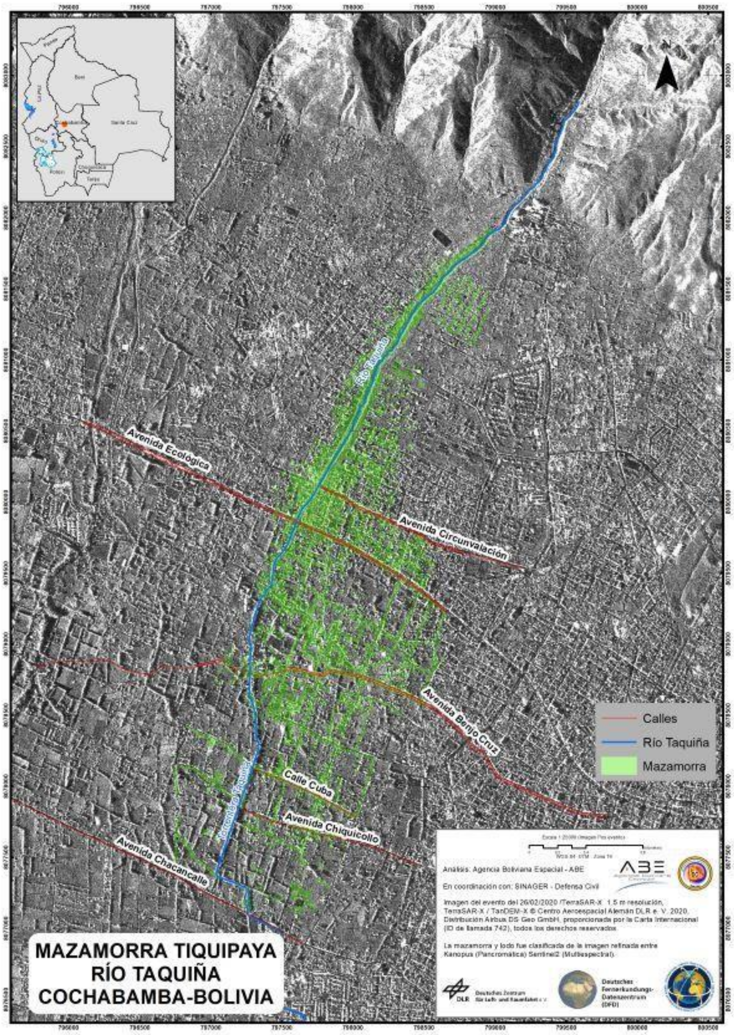

Fig. 6 Bolivian Space Agency (ABE), TerraSAR-X 1.5 m satellite image.

3. Types of sensors and satellite images

Table 1. Satellite data and details

Sensor	Spatial Resolution	Satellite image	Testing image
LANDSAT ETM	Panchromatic=15m Multispectral=30-60m N of Bands = 8 Vision field = 185*185km		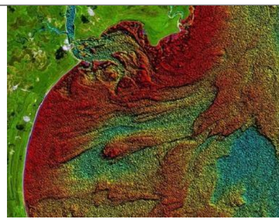

SPOT

Panchromatic=5m Multispectral=10m N of Bands = 5
Vision field =
60*60km

IKONOS

Panchromatic=1m Multispectral=4m N of Bands = 5
Vision field =
11*11km

**QUICKBIR
D**

Panchromatic=61cm Multispectral=2.44m N of Bands = 5
Vision field =
16.5*16.5km

EROS	Panchromatic=1.8m N of Bands = 1 Vision field = 60*60km		
NOAA	Multispectral=4000m N of Bands = 5 Vision field = 3000km		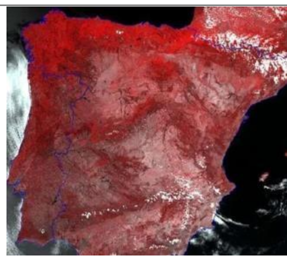
METEOSAT	Visible=2.5*2.5km Infrared Thermic y Medio=5*5km		

ERS	Resolution espacial:12.5m N of Bands = 5 Vision field = 5*5km25*25km-100*100km	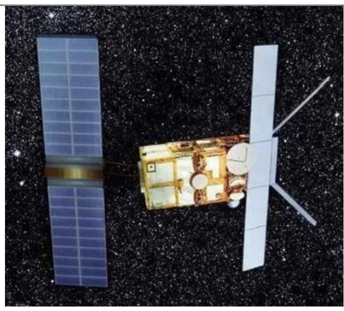	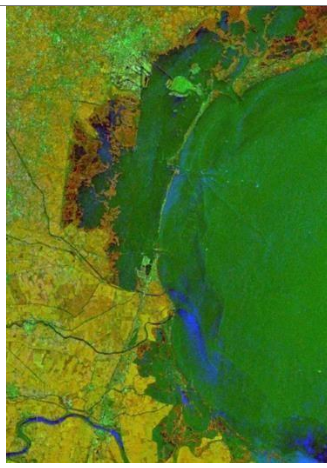
IRS	Panchromatic=5.8m N of Bands = 3 Vision field = 70*70km	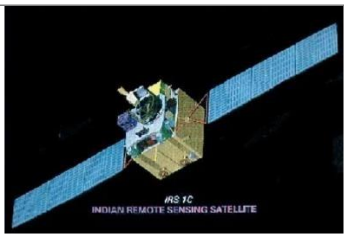	
ENVISAT	Depending on mode: 10-1530-1000m Vision field = 5*5-100*100-400*400km		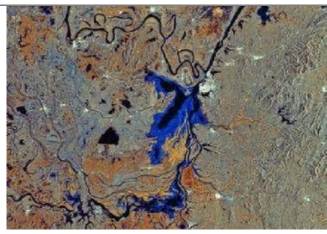

4. Application of Ground Stations in Bolivia

National Oceanic and Atmospheric Administration (NOAA) is a scientific agency to bring together the functions of several different agencies that focuses on the conditions of the weather and temperature. The main activities of the NOAA are:
- Monitoring and Earth systems with instruments and data collection networks.
- Understanding and describing Earth systems through research and analysis of data.
- Assessing and predicting the changes of these systems over time.

Every single day multiple NOAA weather satellites pass in orbit above us. NOAA's operational environmental satellite system is composed of two types of satellites: geostationary operational environmental satellites (GOES) for short-range warning and polar-orbiting environmental satellites (POES) for longer-term forecasting.
As discussed above, the classification of satellites overall, NOAA weather satellites is classified into two categories based on their orbit and life span (as shown in Fig. 7):

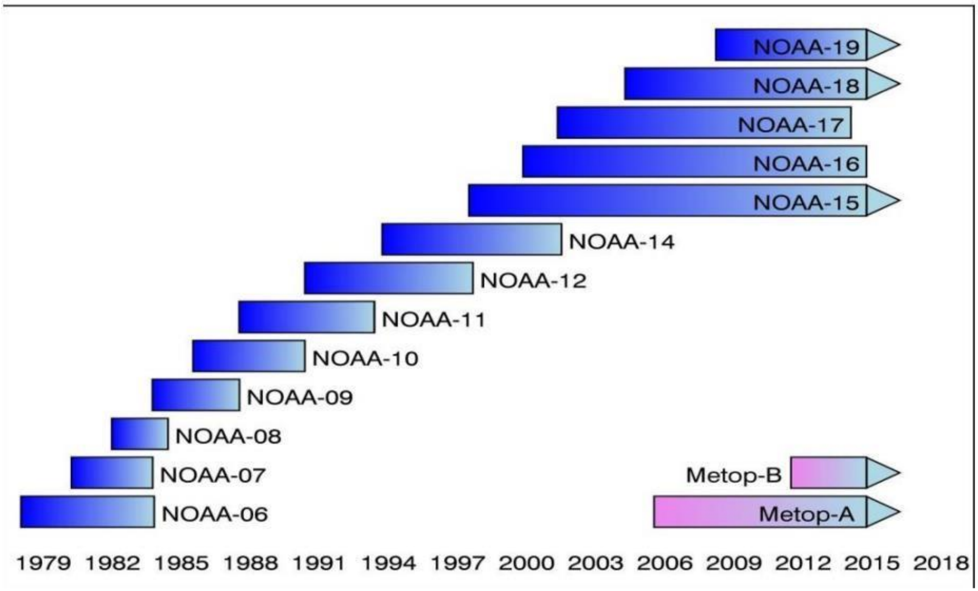

Fig. 7 Categories of NOAA satellites

Geostationary operational environmental satellites (GOES): GOES satellites provide continuous monitoring necessary for intensive data analysis as they orbit the Earth in a geosynchronous orbit (GEO) over the Equator with a speed matching the Earth's rotation.
Polar Operational Environmental Satellites (POES): NOAA POES are the fifth generation of polar satellites from the NOAA. These satellites have been developed together with NASA and the European organization EUMETSAT which build the MetOp satellites.

Applications satellites and remote sensing in disaster management
Tracking wind patterns. - Earthquakes can be predicted and sensed through the use of remote sensing. These sensors pass the warning to people who lives near affected area, then they will be able to relocate in a safe place or shelter.
Earthquake detection. - Remote sensing is able to detect an earthquake approach. Thus, provide useful information that helps on predict areas that could be damaged. This promotes the vulnerable groups relocation in order to save lives and its things.
Floods managements. - Through rain season, many places get flooded and immediately actions need to be done to support the situation. Remote sensing technique fits best, it captures an image of the ground so rescue mission can be started.
Drought prediction. - Remote sensing can be used to predict temperature rising. In case the temperature rises, a warning is passed to the vulnerable group and actions will be taken to reverse the situation.
Reconstruction of affected areas. - Many areas are affected during or after natural disasters, and there is a need for rebuild it. Remote sensing technique helps on simplify the process that is able to cover a bigger area in the same time.

The APT signal which can be accessed by the public makes NOAA weather satellite an alternative choice to get weather satellite image data. The NOAA weather satellite carries five types of sensors, one of which is the AVHRR (Advanced Very High-Resolution Radiometer) [6]. The AVHRR sensor has a function to detect the reflection of electromagnetic waves by clouds, objects on the surface of the earth. The APT

signals transmitted by NOAA satellites are RHCP (Right-Handed Circularly Polarized), so it takes an RHCP type antenna to produce a good signal reception [7][8][9].
The ideal antenna type for APT receiver at 137 MHz is the QFH antenna (Quadrifilar Helix) [9][10][11]. The QFH antenna we made using copper pipe with the proper dimensions. SDR is a key area for realizing a variety of software implementations that allow adaptive and reconfigurable communication systems [14]. Many SDR devices used as NOAA weather satellite receivers [13][14][15].

Method

In fig. 8, the process of getting the image is explained.

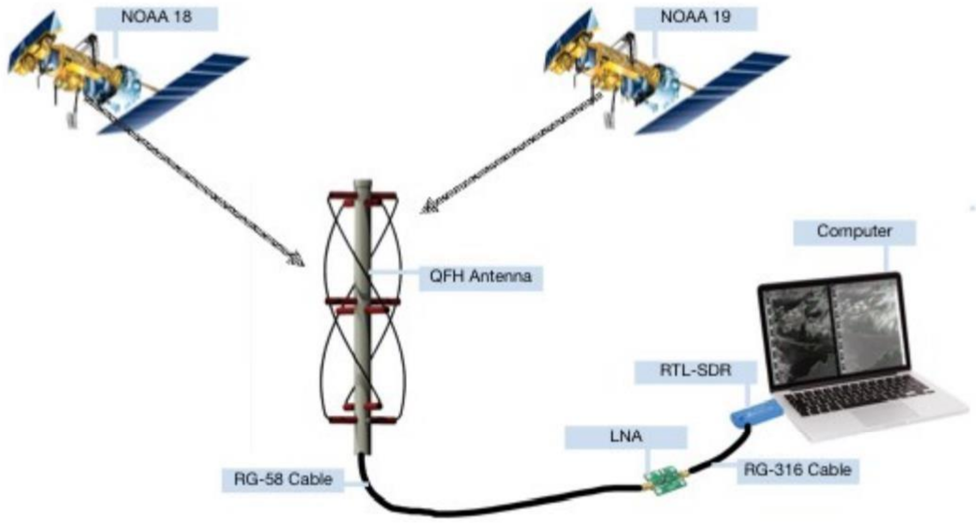

Fig 8. Summary of process made for getting an image.

In Fig. 9 there is a simplified Scheme of Satellite Image Data Acquisition System

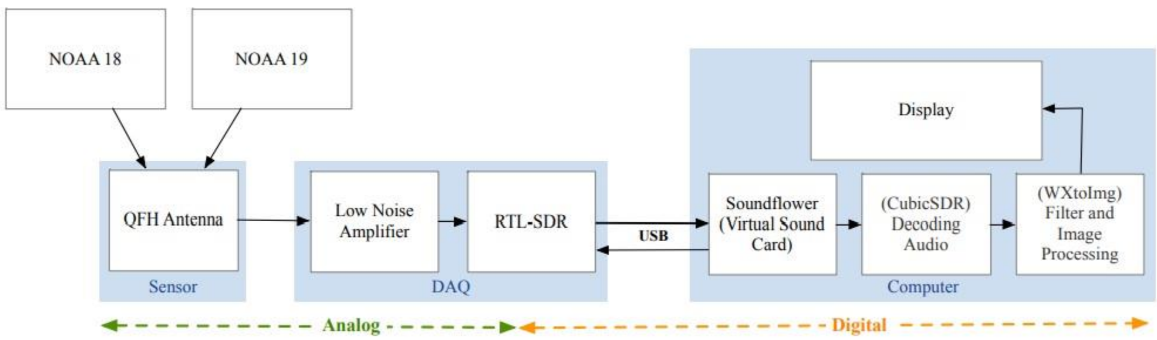

Fig. 9 Block Diagram of Satellite Image Data Acquisition System

Acquisition Result

Data acquisition process begins by sett center frequency on CubicSDR. The output from CubicSDR needs to be forwarded to WXtoImg so that the recording and decoding of APT signals can be done automatically. WXtoImg changed the recording of the wav file from the NOAA weather satellite APT signal to image data, which results can be instantly displayed on WXtoImg while still in the recording process. Figure 10. shows the sample acquisition of NOAA 19 satellite image data in real time on September 8, 2022 at 14:03 UTC. The satellite passes from south to north with a maximum elevation angle of 69 ° westward. The recording duration lasts for 11 minutes and 45 seconds.

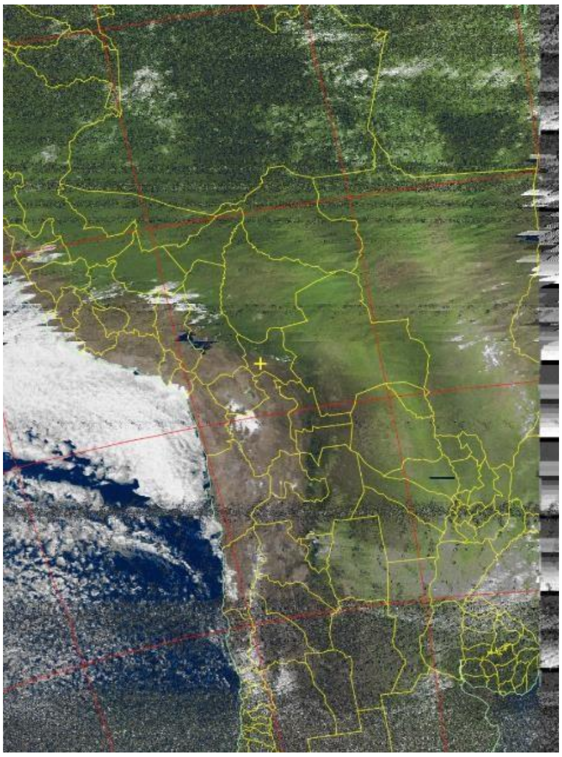

Fig.10. Screenshots of images obtained via Ground Station (UPB)

Next, the scheme of the application is presented, about the data input, the operation and the expected result of it.

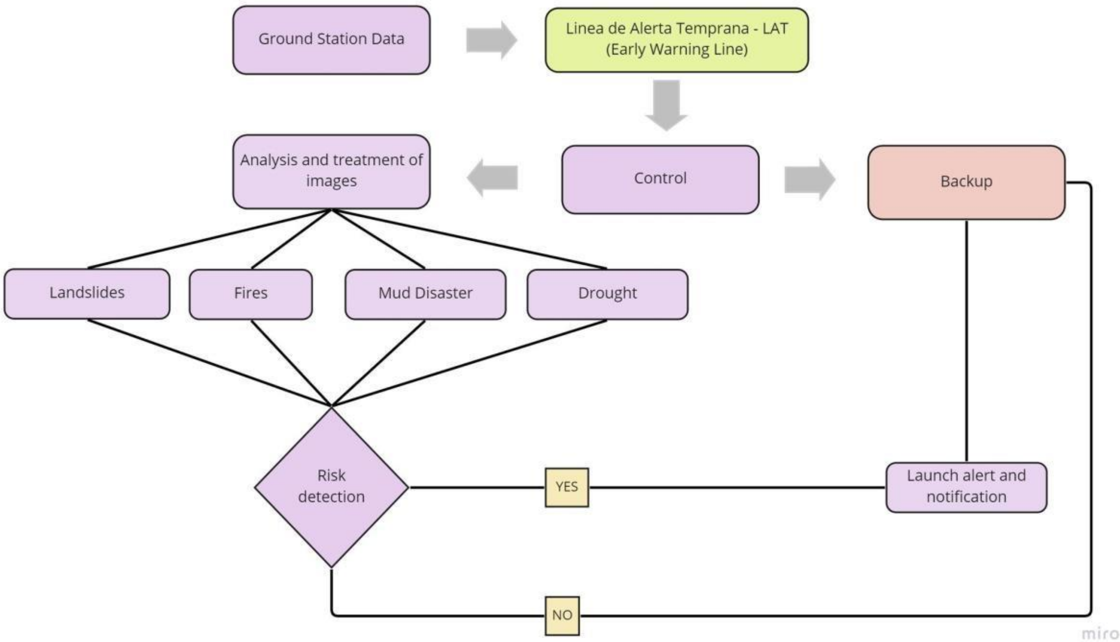

Fig. 11 Scheme of the application LAT

The application, which will have the name Early Warning Line (LAT in Spanish), will receive data from the ground station, after which, through a control center, it will analyze and interpret remote sensing data from satellites that operate open source in the region, after that it will identify the risks, if they exist, it will send an alert, and the data will be stored.

5. Conclusions

We have presented a possible solution to be able to prevent natural and human caused disasters in time, with the location of fires and landslides from satellite images. Our proposed application has demonstrated the combination between an image classification through the algorithm for image analysis and interpretation, in order to transmit this information to the general public, optimizing the data, and quick understanding, together with alerts, notifications for to be able to protect against future risks.

The results of the satellite images, which were shown by the earth station which operates with free source satellites, close to the region, in this study the need for said application in the Bolivian region is shown, due to the aforementioned disasters. in recent years, so we see convenient implementation in practice, remote sensing together with specific computer tools to be able to act, support and help first response teams, such as firefighters, red cross, police, population in general, and rescuers, who act at the moment to avoid damage, risks and future deaths.

Therefore, the latter being our concern. We continuously work to provide accurate identification and real-time detection by satellite, in order to cooperate and help, through computer and logical tools.

6. Future projects

This project is focused on prioritizing fires and landslides being the most frequent in the region, so in the first instance it will operate by identifying and interpreting satellite images that contain characteristics of this type of natural disaster, thus being a risk to living beings, and population.
In the future, it is proposed to add in the application, the interpretation and analysis of data about droughts and floods, this due to the data on dry lakes, managing to link with water preservation projects. Floods being a problem in the Latin American region, it is important to prevent them in order to help the vulnerable population.

References

[1] Deep Learning for Landslide Recognition in Satellite Architecture, Trong-An Bui; Pei-Jun Lee; KaiYew Lum; Clarissa Loh; Kyo Tan, 05 August 2020
[2] Global Forest Watch Data, Bolivia
[3] Chiquitano Forest Conservation Foundation Data
[4] Landslide susceptibility zonation using analytical hierarchy process and GIS for the Bojnurd region, northeast of Iran, Mohammad Reza Mansouri Daneshvar, December 2014
[5] National Oceanic and Atmospheric Administration, User's Guide for Building and Operating Environmental Satellite Receiving Stations, no. February. Suitland,: U.S. DEPARTMENT OF COMMERCE, (2009)
[6] "Design of a Ground Station to download images for Bolivia's environmental studies", J. Soliz, M. Lazarte, Puma.
[7] Gao S.S., Q. Luo, and F. Zhu, Circularly Polarized Antennas. Chichester: John Wiley & Sons, (2014)
[8] Stutzman W.L. and G. A. Thiele, Antenna Theory and Design 2nd edition. Hoboken: John Wiley & Sons, (1998)
[9] Balanis C.A. , Antenna Theory Analysis and Design 3rd Edition. Hoboken: John Wiley & Sons, (2005) [9] Hollander R.W., Resonant Quadrafilar Helical Antenna. Den Haag: Working Group Satellites, (1999)
[10] Fusco V.F., R. Cahill, and R. L. Li, "Quadrifilar loop antenna," IEEE Trans. Antennas Propag., vol. 51, no. 1, pp. 115–120, (2003)
[11] Govarthanam K.S., M. Abirami, and J. Kaushik, "Economical Antenna Reception Design for Software Defined Radio using RTL-SDR," in Proceedings of the International Conference on Innovative trends in Electronics Communication and Applications, 2014, pp. 185–190.
[12] Stewart R.W., K. W. Barlee, D. S. W. Atkinson, and L. H. Crockett, Software Definded Radio using MATLAB & Simulink and the RTL-SDR. Glasgow: Strathclyde Academic Media, (2015)
[13] Patil C., T. Chavan, N. Jhurani, D. Jethani, and M. Chaudhari, "Satellite Image Acquisition Using SDR," Int. J. Innov. Res. Comput. Commun. Eng., vol. 4, no. 6, pp. 2257–2263, (2016)
[14] Mahmood S., M. T. Mushtaq, and G. Jaffer, "Cost Efficient Design Approach for Receiving the NOAA Weather Satellites Data," in Proceedings of the IEEE Aerospace Conference, pp. 1–6, (2016)
[15] Hassini A. and A. H. Belbachir, "Hardware and software consideration to use near real time MSGSEVIRI and NOAA-AVHRR images," c, ISPS 2013, pp. 12–16, (2013)

17

Keynotes

17.1 The International Academy of Astronautics and its Activities

Speakers: Dr. Chantal Cappelletti

Dr. Chantal Cappelletti is currently an Assistant Professor at University of Nottingham (UK), where she is affiliated with the Nottingham Geospatial Institute (NGI) and Gas Turbine and Transmission Research Centre (G2TRC). Previously, she was an Assistant Professor at the University of Brasilia (Brazil) and a visiting researcher at Morehead State University (USA). She has led 6 satellite projects in Italy (UNISAT program and others) and in Brazil (SERPENS, TuPOD). Actually she is the leader of the Space Systems and CubeSat program at University of Nottingham (NottSpace) with several small satellite projects and international cooperation on going. She is author of several publications in the area of small satellites missions and applications, biomedical research in space and space debris. She is member of the International Academy of Astronautics and chairperson of the IAA Latin American CubeSat workshop since the first edition.

17.2 Enabling a new space ecosystem in Brazil: the role of nano and small sats

Speakers: Dr. Cristiano Trein

Civil Engineer (Federal University of Rio Grande do Sul (2002)), with a Master's degree in Structures from the Graduate Program in Civil Engineering at the Federal University of Rio Grande do Sul (2005) and a Ph.D. in Engineering from Kyoto University (2009) in Japan. Professional experience is divided between software development, structural engineering, research, and public administration. In the Federal Public Administration, he worked at the Ministry of Mines and Energy (MME) - Department of Energy Planning and Development, with the development of alternative energy sources. In this position, he participated in R&D boards at ANEEL, developed studies related to energy planning, proposed legal improvements related to alternative sources of generation, and conducted technical cooperation activities with universities in Brazil and abroad, among other activities. Currently, he is a permanent servant in the position of Technologist at the Brazilian Space Agency (AEB) and Director of Governance of the Space Sector (DAS 101.5). In this position, he is responsible for developing and promoting space activities in the country, whose base document is consolidated in the National Space Activities Program - PNAE of the Brazilian Space Agency. During his tenure at the head of the Space Sector Governance Board, he coordinated the Working Group that produced the PNAE 2022-2031; coordinates the Integrated Development Commission for the Alcântara Space Center (CDI-CEA); proposed and consolidated the Brazilian Space Sector Observatory (https://observatorio.aeb.gov.br/); established the Procedure for the Selection and Adoption of Space Missions (ProSAME) in the AEB; managed and coordinated the implementation of the Catarina Constellation; in addition to proposing several normative and legal instruments for the Brazilian Space Sector. It is active in the development of Brazilian infrastructure.

17.3 Aerospace Development from an Emerging Country Perspective: The case of Paraguay (First CubeSat mission-GuaraniSat-1

Speakers: Dr. Alejandro Molinas

Computer Programmer and Bachelor of Systems Analysis by the Polytechnic Faculty of the National University of Asunción with specializations and courses in prestigious Universities in technology, education, aviation systems, and Space. He Studied Civil Aviation Administration at the Singapore Civil Aviation Academy, has a master's in business administration (MBA), is a Specialist in Higher Education, is also a Specialist in Geographic Information Systems and Remote Sensing, and is currently pursuing a Doctorate in Education Sciences. With more than 25 years of professional experience in the public and private sectors, mainly in Information Technology, Education, Civil Aviation, and SPACE, Prof. Román was the Academic Coordinator of the three careers of Computer and Systems Engineering at the Faculty of Engineering of the University of the Integration of the Americas (UNIDA) for five years, Coordinator of the ICT Observatory of the Ministry of Technology of Paraguay. He was also elected Academician Full-Member of the International Academy of Astronautics (IAA) and Member of the International Astronautical Federation (IAF), where he is chairing the Developing and Emerging Countries committee. He is the Alternate Director for Paraguay and a Member of the Latin American and Caribbean Space Network (ReLaCa) board. He has given conferences and talks worldwide at several prestigious universities such as MIT, Kyushu Institute of Technology (Japan), and in Taiwan, France, Austria, England, Peru, Argentina, and others, with works presented at various international Congresses. He has received several recognitions and awards, such as the 2021 Technology Excellence Award in India, the Extraordinary Merit Award from the International Center for Land Policy Studies and Training (ICLPST) in Taiwan, and the Partnership Award from the Pacific Disaster Center in Hawaii. He currently serves as General Director of Execution and Aerospace Development of the Paraguayan Space Agency and as an Undergraduate and Graduate Professor at the University of the Integration of the Americas - UNIDA. He was recently appointed as GEO Principal for Paraguay.

17.4 Best Practices for the Development of Cubesat Missions

Speakers: Dr. Carlos Duarte

17.5 The Role and Value of Small Satellites for Research and Applications

Speakers: Dr. James Spann

Dr. James F. (Jim) Spann, Jr., is the Heliophysics Division Space Weather Lead at NASA Headquarters. During his 35-year NASA career, he developed and flew in space several auroral UV remote sensing instruments, managed the Marshall Space Flight Centers (MSFC) science research organization, which includes the disciplines of Astrophysics, Planetary Science, Heliophysics and Earth Science, and served as the MSFC Chief Scientist. A laboratory physicist by training, he earned his BS in mathematics and physics from Ouachita Baptist University (cum laude 1979) and his PhD in physics from the University of Arkansas (1985). He is the author or co-author of more than 70 peer reviewed journal articles primarily in space physics. He was the Principle Investigator of an international 6U CubeSat mission with the Brazilian space agency called SPORT that will investigate the conditions in Earths ionosphere, just above its upper atmosphere, that lead to disruptions in communication and GPS signals. He is actively engaged in defining science that exploration at NASA enables, the establishment of a NASA Space Weather Research Program and coordinating space weather activities with national and international partners. Furthermore, he is heading up the first Lunar Gateway science payload called HERMES that will study the solar wind and enable better space weather forecasting that enhances astronaut radiation protection for deep space human exploration. Dr. Spann grew up in Recife, Brazil from age 5, where his parents served as missionaries for over 33 years. He attended a Brazilian school (Colégio Americano Batista) though elementary, then a small international school (American School of Recife) before returning to the United States for college (Ouachita Baptist University and the University of Arkansas). He has two grown children (Hannah and Ben) and three grandchildren (Lyla, Lincoln, and William). He is an avid soccer fan, enjoys photography, on occasion relaxes with his guitar, and has a strong interest in the overlap of science and faith.

17.6 Amazonia 1 Mission From Design to In orbit Operation Technological and System Engineering Gains

Speakers: Dr. Adenilson Silva

He holds a degree in Mathematics from the Center for Development of Technology and Human Resources (1994), a master's degree in Space Engineering and Technology from INPE - National Institute for Space Research (1997), and a Ph.D. in Space Engineering and Technology from INPE - National Institute for Space Research / DLR - Deutsches Zentrum für Luft- und Raumfahrt (2001) (Germany). He is currently a senior technologist at the National Institute for Space Research, acting as the General Coordinator of the Coordination of Space Engineering, Technology, and Science and responsible for the satellite program based on the multi-mission platform (PMM) since 2011. He has experience in Satellite Project Management and the area of Aerospace Engineering, with emphasis on Mission Analysis, working mainly on the following topics: artificial satellites, optimization, systems control, attitude determination, and modeling.

17.7 The IAA's Handbook for Post-Mission Disposal of Satellites Less than 100 k

Speaker: Dr. Livio Gratton

Born in Buenos Aires, Argentina. He has a Master of Science and a Ph. D. In Aerospace Engineering from the Illinois Institute of Technology (Chicago, USA). Specialized in Aircraft Navigation Integrity using GNSS. Corresponding Member of the International Academy of Astronautics. Member of the Institute of Navigation. Chairman of Meeting on Space Product Assurance (Buenos Aires, 2016), 1st IAA Latin American Symposium on Small Satellites (Buenos Aires, 2017), and 2nd IAA Latin American Symposium on Small Satellites (Buenos Aires-Bariloche, 2019). Woks at CONAE since 2011, were he has been responsible for the propulsion subsystem, and member of the Coordination Committee leading the ISCUL project. After that, Director of the Gulich Institute (CONAE-UNC) and Responsible of CONAEs Higher Education Unit, leading the creation of 3 Master of Science programs. Currently dean of the Colomb Institute (CONAE-UNSAM). Army infantry officer from until 2001. Airborne and mountain troops specialist. UN Commendation during the Balkans conflict (1993) In recognition of exemplary performance and contribution to peacekeeping beyond the normal scope of duties, for showing outstanding bravery and attitude towards fellow human beings when penetrating a minefield to rescue an injured Dutch warrant officer and the mortal remains of a second one. Order of the Distinguished Services from the Argentine Army, and Decree of Recognition by the Argentine Congress for the same cause.

17.8 Small Sat Projects of ITA Space Center

Speaker: Dr. Luis Eduardo Vergueiro Loures da Costa

Prof. Loures is currently the Head of the Aerospace Systems Department in ITA. He is active in the Space Field for more than 36 years and has been the project manager of important Air Force projects like the Microsatellite Launch Vehicle (VLM), Atmospheric Reentry Satellite (SARA) and ITASAT. He was also the technical coordinator of the on-board electronics of the Satellite Launch Vehicle (VLS), version VSISNAV. His working area is Systems Engineering and Project Management.